JOHANNES GUTENBERG UNIVERSITÄT MAINZ

Max-Planck-Institut für Polymerforschung
Max Planck Institute for Polymer Research

Poly(phosphonate)s: Versatile Polymers for Biomedical Applications

Dissertation zur Erlangung des Grades eines

`Doktor rerum naturalium (Dr. rer. nat.)´

des Fachbereichs:

Chemie, Pharmazie und Geowissenschaften (FB 09),

der Johannes Gutenberg-Universität, Mainz

vorgelegt von

Thomas Wolf

Mainz 2017

The thesis was carried out from January 2015 until November 2017 in the department of [redacted] in the group of [redacted] at the Max Planck Institute for Polymer Research, Mainz.

Dekan: [redacted]

Prodekan: [redacted]

Gutachter 1: [redacted]

Gutachter 2: [redacted]

Date of oral examination:

I hereby declare that I wrote the dissertation submitted without any unauthorized external assistance and used only sources acknowledged in this work. All textual passages which are appropriate verbatim or paraphrased from published and unpublished texts, as well as all information obtained from oral sources, are duly indicated and listed in accordance with bibliographical rules. In carrying out this research, I complied with the rules of standard scientific practice as formulated in the statutes of Johannes Gutenberg-University Mainz to ensure standard scientific practice.

_____ _____

Thomas Wolf

Meiner Familie

„Das Schönste, was wir erleben können, ist das Geheimnisvolle. Es ist das Grundgefühl, das an der Wiege von wahrer Kunst und Wissenschaft steht. Wer es nicht kennt und sich nicht mehr wundern, nicht mehr staunen kann, der ist so gut wie tot und seine Augen erloschen."

Albert Einstein, *Mein Weltbild, 1934*.“

Danksagung

Im Laufe meiner Doktorarbeit und der Zeit davor haben mir viele Menschen auf unterschiedlichste Arten geholfen. Ohne sie wäre es mir nicht möglich gewesen, diese Arbeit in ihrer jetzigen Form präsentieren zu können. An dieser Stelle möchte ich mich explizit bei all diesen wichtigen Menschen bedanken.

Zuallererst bedanke ich mich bei [redacted]. Als direkter Betreuer meiner Arbeit bin ich ihm dankbar für die schöne Zeit, die ich in seiner Arbeitsgruppe verbringen durfte. Die vielen anregenden Ideen, konstruktive Kritik und freundlichen Gespräche waren maßgeblich daran beteiligt, dass ich meine Arbeit abschließen konnte. Ferner habe ich den kreativen Freiraum der mir gewährt wurde und die damit verbundene Freiheit in der Wahl meiner Forschungsthemen genossen und weiß dieses in mich gesetzte Vertrauen sehr zu schätzen.

Bei [redacted] möchte ich mich dafür bedanken, dass sie mich so freundlich in ihrem Arbeitskreis aufgenommen hat. Die vielen konstruktiven Diskussionen haben mich immer wieder dazu gebracht meine eigene Arbeit kritisch zu hinterfragen und haben meine Denkweise und meine Art wissenschaftlich zu arbeiten stark geprägt.

Herzlich danken möchte ich auch [redacted], der mich grade zu Beginn meiner wissenschaftlichen Karriere viel fachliches *know-how* gelehrt hat und mir immer mit gutem Rat zur Seite stand. Die zahlreichen Diskussionen und Hilfestellungen haben maßgeblich bei meiner Entwicklung, sowohl fachlich als auch persönlich, geholfen.

Meinen Kollegen [redacted] und [redacted] danke ich an dieser Stelle explizit für die schönen und angenehmen Kooperationsarbeiten und all die Mühen, die sie sich stehst beim Beantworten meiner Fragen zu biologischen Themen gegeben haben.

Dem gesamten [redacted] und insbesondere meinen direkten Kollegen aus der [redacted] danke ich für die wunderschöne Zeit die ich hier am Institut mit ihnen habe verbringen dürfen. All die Grillabende, Feiern, kreativen Mittagsrunden, Kaffeepausen und Gespräche haben den Arbeitsalltag aufgelockert und mir eine unvergessliche Zeit beschert.

Ein besonderer Dank geht dabei an [redacted], für all die spannenden Diskussionen, die schönen Unterhaltungen, jede Menge kreative Mittagspausen und ganz allgemein die tolle Zeit, die ich mit ihnen verbringen durfte.

Danken möchte ich auch meinen Bürokollegen [redacted] sowie meinen ehemaligen Laborpartnern [redacted] für die wunderbare Arbeitsatmosphäre und die schöne Zeit im Allgemeinen.

Dem von mir betreuten Dipmolanden [redacted], den Bachelor-/Master-Studenten [redacted] möchte ich mich ganz herzlich für all die Hilfe und die schöne Zeit danken. Ich hoffe, sie haben von mir mindestens genauso viel haben lernen können, wie ich von ihnen gelernt habe.

Ein ganz besonderer Dank geht an Frau [redacted] für die herzliche Aufnahme in ihrem Labor und die praktischen Hilfen, die sie mir mit all ihrer Erfahrung immer wieder gegeben hat. Ihre tatkräftige Unterstützung während zahlreicher Synthesen und Aufreinigung war eine unschätzbare Hilfe während meiner Arbeit, für die ich niemals dankbar genug sein kann.

Beim gesamten Team der Polymeranalytik, der Elektronenmikroskopie und der NMR Spektroskopie, namentlich [redacted], bedanke ich aufs tiefste für die unzähligen Messungen, die sie im Laufe der letzten Jahre für mich getätigt habe.

Im Speziellen danke ich [redacted] für die Hilfen beim Messen, Auswerten und Diskutieren der zahlreichen spezialisierten NMR Messungen.

[redacted] danke ich für ihre stete Hilfsbereitschaft, Freundschaft und Unterstützung bei der Betreuung der GPC Anlage.

Den noch nicht genannten Kooperationspartnern, mit denen ich unzählige kleine oder große Kooperationensarbeiten durchgeführt habe danke ich für die schöne und kreative Zeit. Dies sind im Speziellen [redacted] (*University of Nottingham*), [redacted] (*University of Bath*), [redacted] (*University of Stavanger*), [redacted] (MPIP), [redacted] (MPIP), [redacted] (Universität Halle) und [redacted] (Universität Potsdam).

Zu guter Letzt bedanke ich mich bei meiner Freundin [redacted], meinen Eltern, [redacted] und [redacted], sowie bei meiner Schwester [redacted] und meinem Schwager [redacted] dafür, dass sie immer in allem hinter mir stehen, mich unterstützen wo sie nur können und ich mich immer auf sie verlassen kann. Ohne sie wäre das Verfassen dieser Arbeit niemals möglich gewesen.

Table of Contents

Table of Contents

Table of Contents

Motivation and Objectives

Motivation

This thesis presents aliphatic poly(phosphonate)s (PPns) as degradable and polyfunctional polymers for biomedical applications. A library of novel cyclic phosphonate monomers has been designed and used in the ring-opening polymerization process. These poly(phosphoester)s (PPEs) bear a P-C bond in the side-chain and can be synthesized with high control. The obtained polymers are generally water-soluble, non-cell toxic materials with adjustable degradation rates. Previous studies from our group revealed that PPEs exhibit a "stealth effect" in *in vitro* studies for polymeric nanocarriers similar to that of PEG, making them promising candidates for biomedical applications in need of soluble and degradable polymers.

Synthetic PPEs are inspired by the DNA, the most essential natural PPE. DNA benefits from the unique properties of phosphorus as the PPE backbone provides stability, functional diversity (side-chains and charge), precise synthesis, and targeted degradation.

Compared to traditional poly(carboxylic acid ester)s synthetic PPEs provide several benefits: The pentavalent phosphorus contributes one bond per repetition unit for side-chain modifications. An additional modification of the phosphorus binding sphere gives access to an even more extensive chemical diversity (P-O, P-C, P-N, P-S). Finally, aside from the P-C bond, all P-X binding motives are hydrolytically cleavable, affording a completely biodegradable polymer backbone.

Since the pioneering works of Carraher *et al.* in the 1960s, synthetic PPEs have, apart from the use of ill-defined polycondensates as flame retardants, only found limited attention in academic and industrial research. This limited awareness was partially due to the problematic synthesis and moderate polymerizability of monomers required for a controlled synthesis via living polymerization techniques. However, PPEs experienced a comeback in the 21st century, when modern organocatalytic systems became available for polymer synthesis.

These catalysts, typically strong, non-nucleophilic organic bases, paved the way for the efficient ring-opening polymerization of the long known cyclic phosphoester monomers. As a living polymerization, the organocatalytic anionic ring-opening polymerization (oAROP) provides excellent control over the molecular weight by simple adjustment of the monomer to initiator ratio. Due to the absence of termination- and (under certain conditions) side-reactions, polymers with narrow molecular weight distributions and control over the end-groups are obtainable. Furthermore, the utilized organocatalysts are non-toxic, and the absence of metal ions facilitates purification of the final product and use in demanding medical applications.

The “gold standard” for soluble polymers in biomedical applications, even after 50 years of progress, is still poly(ethylene glycol) (PEG). PEG is non-toxic, biocompatible, does not show an acute immune response, and exhibits a distinct “stealth” behavior. The beneficial effect of PEGylation on the pharmacokinetics of drugs has been proven *in vitro*, *in vivo*, and in clinical applications. However, PEG has presented some disadvantages over the years. PEG is not hydrolytically degradable, leading to accumulation of high molecular weight material after repeated administration. Furthermore, PEG shows a distinct lack of functionality, limiting the variation of properties by chemical means. Finally, potentially owned to the constant exposure to PEG, anti-PEG antibodies have been detected in patients treated with PEGylated drugs on a regular basis and healthy blood donors, leading to accelerated blood clearance of the drug and decreasing its pharmacological efficacy.

As a consequence, polymer chemists have worked extensively on the development of polymers to complement the use of PEG in biomedical applications. Promising results are, upon others, shown by poly(glycerol)s, poly(2-oxazoline)s, and poly(saccharide)s which show excellent results under *in vitro*, and *in vivo* conditions. Importantly, no antibody formation was detected so far even though some formulations containing these polymers are already tested in clinical trials. However, it is only a matter of time until patients develop antibodies against these polymers when they are used on a larger scale. Therefore, the development of new polymer classes like PPEs is essential to provide complementary drug delivery systems for clinical use.

Motivation and Objectives

An increasing number of reports highlight the promising performances of PPEs and the previously hypothesized properties (e.g., degradability, chemical versatility, and control during the polymerization) were proven. Especially experiments aiming for drug delivery applications show encouraging results. Several groups report excellent biocompatibility and low cell toxicity. Just recently, our group was able to prove the reduced immune system recognition (“stealth effect”) of nanocarriers which are surface modified with PPEs. This demonstration of the “stealth effect” of PPEs marks an essential step towards their efficient use in biomedical applications.

However, poly(phosphate)s, the mainly used class of PPEs have a critical issue during their synthesis: the polymerization needs to be terminated at moderate conversions to prevent transesterification reactions in the backbone and side-chain. Alternatively, the use of co-catalysts is necessary, increasing the cost and the toxicity and impeding the purification process to meet the strict requirements for medical applications.

In our attempts to overcome the transesterification issue our group revived the long forgotten polymer class of poly(phosphonate)s (PPn) in 2014. These polymers bear a hydrolytically non-cleavable P-C bond in the side-chain. This small structural change efficiently suppresses transesterification reactions. The polymerization proceeds with unprecedented control, providing well-defined polymers even at high monomer conversions without the use of toxic co-catalysts. Additionally, the attachment of a non-cleavable side-chain prevents potential loss of functionality over time by hydrolysis. Furthermore, the investigated parental polymer was found to be non-toxic, water-soluble and degraded rapidly under slightly basic conditions.

Objectives

The primary objectives of the work presented herein are therefore as follows:

1. Increase the diversity of available PPns by the synthesis of new monomers, copolymerization, and side-chain variation/modification. Investigation of the respective PPn's (co-) polymer properties: particular focus is put on the solubility and stimuli responsiveness in water, the hydrolytic degradability, and the modification of fundamental polymer properties like the glass transition temperature. This objective is thoroughly discussed in the **Chapters 2**, **3**, **5**, **6**, and the first part of **Chapter 7**.

2. Transferring these stimuli-responsive poly(phosphonate)s into "smart" drug carriers for future use in biomedical applications. The focus on this part is put on aqueous UCST type stimuli responsiveness as this phenomenon is much less investigated in the literature compared to the LCST stimulus. This objective is dealt with in the second part of **Chapter 7**.

3. Evaluation of the *in vitro* "stealth" behavior of poly(phosphonate) against selected cells of the immune system with regard to future biomedical applications. Furthermore, fundamental investigation of the chemical origin of the "stealth effect" and which physical polymer properties induce or influence the protein corona formation associated the with "stealth effect". Special focus is put on model nanocarriers which were surface modified with PPns of different hydrophilicity. The influence of hydrophilicity on the "stealth effect" is investigated. This objective is debated in **Chapter 8**.

Chapter 2 covers the synthesis of cyclic phosphonate monomers with varying alkyl side-chain length. The polymerizability and polymerization behavior of the monomers as well as the solubility and degradation of the polymers in water is investigated. Furthermore, the toxicity towards HeLa cells and potential inhibition of the enzyme acetylcholine esterase is discussed.

Chapter 3 introduces a cycloalkyl-substituted phosphonate monomer and presents the first phosphonate copolymerization. The homopolymers are investigated regarding the thermal bulk properties. Copolymerization with a monomer from **Chapter 2**, known to produce water-soluble polymers with low glass transition temperature, is used to adjust the copolymers glass transition temperature and water-solubility. Finally, the copolymer toxicity towards the macrophage cell-line RAW 264.7 is evaluated.

Chapter 4 introduces the first side-chain crystalline poly(phosphonate) and afterward discusses the copolymerization behavior with known phosphonate monomers. Ring-opening copolymerization is utilized to vary the water-solubility and thermo-responsiveness of the non-cell toxic (RAW 264.7) copolymers. An LCST phase separation behavior with adjustable phase separation temperature is described and the phase transition mechanism thoroughly investigated on different length scales.

Chapter 5 presents a cooperative study with the University of Stavanger, Norway. The group of Prof. Dr. M. A. Kelland strongly focusses on the inhibition of gas hydrate formation in natural gas pipelines, a feat usually performed by polymers with a low LCST phase transition temperature. The goal of the cooperation is the evaluation of PPn copolymers previously introduced in **Chapter 3** and **Chapter 4** as gas hydrate inhibitors. Furthermore, to emphasize the value of using degradable polymers in an application that may easily leak material in the surrounding, the copolymers biodegradability is assessed. An OECD certificated biological oxygen demand (BOD) test is used, evaluating PPn microbial degradation in water of the North Sea.

Chapter 6 introduces the first side-chain modifiable phosphonate monomer and the subsequent co- and terpolymerization with phosphonate monomers from the previous chapters. The focus is again put on the water-solubility and thermal response of the copolymers. In addition to the variation of the copolymer composition, the polymer properties are altered by side-chain modifications via thiol-ene reaction.

The first part of **Chapter 7** presents the random copolymerization of monomers previously described in **Chapter 2** and **Chapter 6**. The non-cell toxic (RAW 264.7) pre-copolymers are side-chain modified via thiol-ene reaction to introduce UCST phase separation behavior in the copolymers, contrary to all previously discussed LCST copolymers. The UCST phase separation behavior and its dependency on copolymer composition, concentration, pH value and salt concentration in solution are thoroughly investigated.

Objective 2 is dealt with in the latter part of **Chapter 7**. After the investigation of the UCST behavior in the first part of the chapter, a UCST responsive carrier system is designed. Commercially available PEG is used as a macroinitiator for the ROP of phosphonates as a non-functional, permanently hydrophilic segment. The obtained block copolymers are side-chain modified to induce UCST behavior in the PPn block. These UCST block copolymers are investigated in regards to their aqueous self-assembly behavior as well as the thermo-responsiveness of the formed structures.

Objective 3 is discussed in a cooperation project with Johanna Simon from our group in **Chapter 8**. The influence of PPn hydrophilicity on the “stealth” behavior of PPn coated nanoparticles was investigated. First, the PPns with varying hydrophilicity introduced in **Chapter 4** are ω-functionalized in a one-pot reaction and grafted onto polystyrene nanoparticles. These PPn coated particles are analyzed regarding their protein adsorption in human plasma and subsequently to their uptake into macrophages.

Abstract

Chapter 1

Chapter 1 gives a general introduction to the field of poly(phosphoester)s (PPEs). As PPEs center around the medical field, first an introduction to the use of polymers in biomedical science is given, discussing the fundamental requirements for soluble polymers to be used in the human body. Afterwards, the more sophisticated properties of stimuli-responsive "smart" materials are discussed with a focus on thermoresponsive materials.

Afterwards, the current "gold standard", PEG, is introduced to determine the base of its success and its drawbacks, highlighting the need for complementary alternatives. The first part of **Chapter 1** closes with benefits and disadvantages of a selected few promising alternatives for PEG that are already used *in vivo* or clinical trials.

The second part of **Chapter 1** introduces poly(phosphoester)s. First, a short introduction of phosphorus, concerning its omnipresence and importance in nature, is given. This part is followed by a short historical background on the research of synthetic PPEs before summarizing some of the more recent literature on the controlled synthesis and applications of PPEs in the biomedical field.

Finally, poly(phosphonate)s (PPns) are introduced, which is the primary focus of the following (experimental) chapters. Based on a short historical background and a comprehensive review on synthetic PPns, this thesis is put in the right perspective and context.

Abstract

Chapter 2

Chapter 2 presents the synthesis and characterization of PPns carrying different alkyl side chains. Three novel cyclic monomers for the ring-opening polymerization (ROP) are introduced. The polymerization is promoted by the organocatalysts 1,8-diazabicyclo[5.4.0]undec-7-ene (DBU) and 1,5,7-triazabicyclo[4.4.0]dec-5-ene (TBD), proceeds with high control over molecular weight and produces polymers with narrow molecular weight distributions even at full monomer conversion. The polymers with methyl-, ethyl- and *i*-propyl- side chains are soluble in water without a temperature-dependent phase separation. They show no toxicity against HeLa cells at any tested concentration. Polymers with *n*-butyl side chains exhibit decreased solubility in water, concentration-dependent cloud point temperatures, and show increased toxicity against HeLa cells. All polymers exhibit significantly different degradation times under both neutral as well as basic conditions, enabling tuned degradation rates in water by side-chain variation. None of the polymers show inhibition of the enzyme acetylcholinesterase.

Chapter 3

2-Cyclohexyl-2-oxo-1,3,2-dioxaphospholane (^{CY}HexPPn), a new monomer for the ROP towards poly(phosphonate)s is presented in **Chapter 3**. The organo-catalyzed polymerization with TBD as catalyst produces homopolymers with good control over molecular weight and rather narrow molecular weight distributions. The homopolymer exhibits a glass transition 60 °C higher compared to all previously reported poly(phosphonate)s. Copolymerization with the water-soluble 2-isopropyl-2-oxo-1,3,2-dioxaphospholane (^{i}PrPPn) produces water-soluble, well-defined copolymers. The copolymer composition matches the theoretical value in all cases, and the T_g shows a linear correlation with the amount of ^{i}PrPPn incorporated. The copolymers exhibit only low cell-toxicity towards the sensitive murine macrophage-like cells RAW264.7.

Abstract

Chapter 4

Thermoresponsive polymers are promising materials for the development of drug carriers with a temperature-controlled release of the payload. Such “smart” polymers change their hydrophilicity upon a change in temperature and phase separate from aqueous solution. **Chapter 4** presents the design of random poly(phosphonate) copolymers with either high solubility in water or a finely tunable hydrophilic-to-hydrophobic phase transition upon heating (“LCST”). Polymerization via ROP provides high control over molecular weight and copolymer composition and produces polymers with narrow molecular weight distributions. The phase separation temperature can be adjusted in water and depends mainly on the copolymer composition. The phase transition mechanism was thoroughly investigated on different length scales via complementary methods: electron paramagnetic resonance spectroscopy (EPR), dynamic light scattering (DLS), UV-Vis spectroscopy, and confocal laser scanning microscopy (cLSM). The step-wise formation of aggregates near the cloud point temperature and subsequent growth up to macroscopic coacervates is proven.

Chapter 5

Chapter 5 presents a collaborative work with Prof. Dr. M Kelland from the University of Stavanger, Norway. The ability of PPn copolymers presented in **Chapter 3** and **Chapter 4** to inhibit gas hydrate formation is evaluated. The copolymers are investigated for their performance as kinetic methane hydrate inhibitors (KHIs) in high pressure rocking cells. All of the copolymers give better KHI activity than tests with no additive. However, none of the PPns give lower onset temperatures than the benchmark, poly(*N*-vinyl caprolactam), a well-known commercial KHI. Furthermore, the biodegradation of the copolymers is evaluated using the marine OECD306 test protocol, proving microbial degradation in seawater of PPns for the first time.

Abstract

Chapter 6

Coacervates are partially hydrated, colloidal polymer droplets in water held together by hydrophobic interactions and are considered promising candidates for drug delivery applications. **Chapter 6** presents the first simple coacervates made from temperature-induced phase separation of aqueous PPn terpolymer solutions. Such coacervates are interesting for drug carrier applications as they are non-toxic, fully biodegradable and form spontaneously upon heating above a threshold temperature (LCST). The investigated terpolymers are synthesized via the ROP of cyclic phosphonate monomers, ensuring high control over molecular weight, terpolymer composition, physical, and chemical properties, and providing polymers with rather narrow molecular weight distributions. Functional pendant groups for further modifications are randomly distributed over the whole chain to finely tune the balance of hydrophilic and hydrophobic side-chains. These functional terpolymers spontaneously phase separate into a polymer rich coacervate phase in water upon heating above the LCST, providing an elegant method to prepare degradable and non-toxic carrier system.

Chapter 7

Temperature-induced self-assembly of block copolymers allows the formation of smart nano-dimensional structures. Degradable UCST block copolymers that allow the swelling or even disassembly at elevated temperatures with eventual backbone hydrolysis have not been reported to date. **Chapter 7** first presents well-defined degradable PPns with adjustable UCST. The pre-copolymers obtained by ROP are modified by thiol-ene modification to introduce pendant carboxylic acids. By this means non-cell-toxic, degradable polymers exhibiting UCST behavior in water are produced. After a thorough investigation of the UCST behavior, block copolymers with PEG as a non-responsive water-soluble block are synthesized via the macroinitiator route. These block copolymers self-assemble into well-defined polymersomes with narrow size distribution. Depending on the block length ratio and degree of substitution, these structures either swell or disassemble entirely upon temperature increase.

Abstract

Chapter 8

Increasing the plasma half-time is an essential goal in the development and improvement of drugs and drug carriers. Attachment of polymer chains, especially poly(ethylene glycol) (PEG), the so-called PEGylation, is a well-established and effective method to increase the plasma half-time ("stealth effect"). However, the reasons for PEG's success are still widely unknown and are speculated to be the result of a decreased overall protein adsorption on the hydrophilic surface. **Chapter 8** presents a cooperative study with Johanna Simon from our group to investigate the influence of surface properties of PPn-coated nanocarriers on the "stealth" behavior. The focus is put especially on the protein adsorption behavior of carriers modified with PPns of different hydrophilicity to control the "stealth" properties. We combine the precision of ROP with the grafting-onto process to obtain nanocarriers with precise control over the surface hydrophilicity. We present that the overall protein amount is unchanged despite the different hydrophilicity of the investigated surfaces. However, the protein type is dramatically altered upon falling below a certain threshold hydrophilicity. This change in protein adsorption correlates well with the observed change of the interaction with immune cells *in vitro*.

Zusammenfassung

Kapitel 1

Kapitel 1 gibt eine allgemeine Einführung in das Gebiet der Poly(phosphoester) (PPEs). Da sich ein Großteil der Forschung rund um PPEs auf den medizinischen Bereich konzentriert, wird anfangs eine Einführung in die Verwendung von Polymeren in der biomedizinischen Forschung gegeben. Hierbei werden zunächst die grundlegenden Anforderungen an lösliche Polymere zur Verwendung im menschlichen Körper erörtert. Im Anschluss werden die spezialisierten Eigenschaften und Anforderungen von mittels eines Stimulus ansprechbaren, "intelligenten" Materialien mit Fokus auf temperatur-sensitiven Materialien diskutiert.

Danach wird der derzeitige „Gold-Standard“, PEG, diskutiert um die Grundlage für seinen Erfolg und seine Nachteile zu bestimmen und den Bedarf an komplementären, alternativen Polymeren hervorzuheben. Der erste Teil von **Kapitel 1** schließt mit Vor- und Nachteilen einiger aussichtsreicher Alternativen für PEG die bereits als komplementäre Polymere *in vivo* oder in klinischen Studien eingesetzt werden.

Der zweite Teil von **Kapitel 1** führt die Poly(phosphoester) ein. Zunächst wird eine kurze Erörterung des Elements Phosphor bezüglich seiner Allgegenwart und Wichtigkeit in der Natur gegeben. Auf diesen Teil folgt eine kurze Zusammenfassung über den historischen Werdegang der Forschung an synthetischen PPEs, bevor ein relevanter Teil der moderneren Literatur über die kontrollierte Synthese und Anwendung von PPEs im biomedizinischen Bereich zusammengefasst wird.

Abschließend werden Poly(phosphonate) (PPns) vorgestellt, die im Mittelpunkt der folgenden (experimentellen) Kapitel stehen. Ausgehend von einem kurzen historischen Hintergrund und einer umfassenden Übersicht über synthetische PPns wird diese Dissertation so in den richtigen Kontext gebracht.

Zusammenfassung

Kapitel 2

Kapitel 2 stellt die Synthese und Charakterisierung von PPns vor, die verschiedene Alkylseitenketten tragen. Drei neue cyclische Monomere für die Ringöffnungs-polymerisation (ROP) werden eingeführt. Die Polymerisation wird durch die Katalysatoren 1,8-Diazabicyclo [5.4.0] undec-7-en (DBU) und 1,5,7-Triazabicyclo [4.4.0] dec-5-en (TBD) katalysiert, verläuft mit hoher Kontrolle über das Molekulargewicht und es werden sogar bei vollem Umsatz Polymere mit engen Molekulargewichtsverteilungen erhalten. Die Polymere mit Methyl-, Ethyl- und *i*-Propyl Seitenketten sind ohne temperaturabhängige Phasenseparation in Wasser löslich. Sie zeigen keine Toxizität gegenüber HeLa-Zellen. Polymere mit *n*-Butylseitenketten zeigen eine verminderte Löslichkeit in Wasser mit konzentrationsabhängiger Phasenseparation und eine erhöhte Toxizität gegenüber HeLa-Zellen. Alle Polymere zeichnen sich sowohl unter neutralen als auch unter basischen Bedingungen durch signifikant unterschiedliche Abbauzeiten aus. Hierdurch wird eine genau abgestimmte Abbaurate in Wasser durch Variation der Seitenketten ermöglicht. Keines der Polymere zeigt eine Hemmung des Enzyms Acetylcholinesterase.

Kapitel 3

2-Cyclohexyl-2-oxo-1,3,2-dioxaphospholan (^{cy}HexPPn), ein neues Monomer für die ROP, wird in **Kapitel 3** vorgestellt. Die organokatalysierte Polymerisation mit TBD als Katalysator liefert Homopolymere mit guter Kontrolle über das Molekulargewicht und engen Molekulargewichtsverteilungen. Die Homopolymere zeigen einen um 60 °C höheren Glasübergang im Vergleich zu allen bisher beschriebenen Poly(phosphonaten). Die Copolymerisation mit 2-Isopropyl-2-oxo-1,3,2-dioxaphospholan (^{i}PrPPn) aus **Kapitel 2** ergibt wasserlösliche, wohldefinierte Copolymere. Die Copolymer-zusammensetzung stimmt in allen Fällen mit dem theoretisch ermittelten Wert überein und die Glasübergangstemperatur zeigt eine lineare Korrelation mit der Menge an eingebautem ^{i}PrPPn. Die Copolymere zeigen nur eine geringe Zelltoxizität gegenüber den empfindlichen murinen Makrophagen RAW264.7.

Zusammenfassung

Kapitel 4

Thermoresponsive Polymere sind vielversprechende Materialien für die Entwicklung von Wirkstoffträgern mit einer temperaturgesteuerten Freisetzung der eingeschlossenen Substanz. Solche "intelligenten" Polymere verändern ihre Hydrophilie beim Erhitzen und fallen aus wässriger Lösung aus. **Kapitel 4** stellt die Synthese von statistischen Poly(phosphonat) Copolymeren, entweder mit hoher Löslichkeit in Wasser oder einem fein einstellbaren Übergang von hydrophil zu hydrophob beim Erwärmen ("LCST"), vor. Die Polymerisation über ROP bietet hohe Kontrolle über das Molekulargewicht und die Copolymerzusammensetzung und stellt Polymere mit engen Molekulargewichts-verteilungen dar. Die Temperatur an der Phasenseparation auftritt, hängt hauptsächlich von der Copolymerzusammensetzung ab und kann in Wasser gezielt eingestellt werden. Der Phasenübergang wurde auf verschiedenen Längenskalen mit zueinander komplementären Methoden untersucht: Elektronenspinresonanzspektroskopie (EPR), dynamische Lichtstreuung (DLS), UV-Vis-Spektroskopie und konfokale Laser-Scanning-Mikroskopie (cLSM). Die stufenweise Bildung von Aggregaten nahe des Trübungspunktes und deren anschließendes Wachstum bis hin zur Bildung von makroskopischen Koazervaten werden gezeigt.

Kapitel 5

Kapitel 5 präsentiert eine gemeinschaftliche Arbeit mit Prof. Dr. M. A. Kelland von der Universität Stavanger, Norwegen. Die Fähigkeit von PPn Copolymeren, die in **Kapitel 3** und **Kapitel 4** vorgestellt wurden, die Gashydratbildung zu hemmen, wird untersucht. Die Copolymere werden auf ihre Leistung als kinetische Methanhydrat Inhibitoren (KHIs) in Hochdruck-Schwingzellen geprüft. Alle Copolymere ergeben eine bessere KHI-Aktivität als Tests ohne Additiv. Keines der PPns liefert jedoch niedrigere Start-Temperaturen als der *Benchmark* Vergleich, Poly(*N*-Vinylcaprolactam), ein bekannter kommerzieller KHI. Darüber hinaus wird der biologische Abbau der Copolymere anhand des marinen OECD306-Testprotokolls evaluiert. So wird zum ersten Mal der mikrobielle Abbau von PPns im Meerwasser nachgewiesen.

Zusammenfassung

Kapitel 6

Koazervate sind teilweise hydratisierte, kolloidale Polymer-Tröpfchen in Wasser, die durch hydrophobe Wechselwirkungen zusammengehalten werden. Sie werden als aussichtsreiche Kandidaten für Arzneimittelabgabeanwendungen angesehen. In **Kapitel 6** werden die ersten einfachen Koazervate aus der temperaturinduzierten Phasenseparation von wässrigen PPn-Terpolymerlösungen vorgestellt. Solche Koazervate sind als Arzneimittelträger interessant, da sie nicht toxisch und vollständig biologisch abbaubar sind und sich beim Überschreiten einer Schwellentemperatur (LCST) spontan bilden. Die untersuchten Terpolymere werden über die ROP von cyclischen Phosphonat-Monomeren synthetisiert, was eine hohe Kontrolle über Molekulargewicht, Terpolymer-Zusammensetzung, sowie physikalische und chemische Eigenschaften gewährleistet und Polymere mit engen Molekulargewichtsverteilungen erhalten werden. Um das Gleichgewicht von hydrophilen und hydrophoben Seitenketten fein abzustimmen, sind funktionelle Seitengruppen für weitere Modifikationen statistisch über die gesamte Kette verteilt. Die Mikrostruktur wird durch $^{31}P\{H\}$-NMR-unterstütze Kinetik Messungen untersucht und die Bildung von statistischen Copolymeren nachgewiesen. Diese funktionellen Terpolymere lagern sich beim Erhitzen über die LCST spontan in eine polymerreiche Koazervat-Phase in Wasser ab, wodurch ein elegantes Verfahren zur Herstellung eines abbaubaren und nicht toxischen Trägersystems bereitgestellt wird.

Kapitel 7

Die temperaturinduzierte Selbstorganisation von Blockcopolymeren ermöglicht die Bildung nanodimensionaler Strukturen. Abbaubare UCST-Blockcopolymere, die das Quellen oder sogar Auflösen der Überstrukturen bei erhöhten Temperaturen in Kombination mit eventueller Polymer-Hydrolyse erlauben würden, wurden bisher nicht berichtet. **Kapitel 7** stellt zunächst abbaubare PPns mit einstellbarer UCST vor. Die durch ROP erhaltenen Copolymere werden in thermoresponsive Polymere umgewandelt, indem Carbonsäure-Gruppen durch Thiol-En-Modifikation in die Seitenketten eingeführt werden. Auf diese Weise werden nicht zelltoxische, abbaubare Polymere erzeugt, die in Wasser ein UCST-Verhalten zeigen. Nach einer gründlichen Untersuchung des UCST-Verhaltens

werden Blockcopolymere mit PEG als nicht adressierbaren, wasserlöslichen Block hergestellt indem der Phosphonat-Block auf einen PEG-Makroinitiator auf polymerisiert wird. Diese Blockcopolymere ordnen sich selbst zu Polymersomen mit enger Größenverteilung an. Abhängig von Blocklängenverhältnis und Substitutionsgrad quellen oder zerfallen diese Strukturen bei einer Erhöhung der Temperatur.

Kapitel 8

Die Erhöhung der Plasmahalbwertszeit ist ein wichtiges Ziel in der Entwicklung und Verbesserung von Medikamenten und Wirkstoffträgern. Die Anlagerung von Polymerketten, insbesondere Poly(ethylenglykol) (PEG), die sogenannte PEGylierung, ist eine etablierte und effektive Methode zur Erhöhung der Plasmahalbwertszeit ("s*tealth*-Effekt"). Die Gründe für den Erfolg von PEG sind jedoch noch weitgehend unbekannt und es wird spekuliert, dass dies das Ergebnis einer verminderten Gesamtproteinadsorption an der hydrophilen Oberfläche ist. **Kapitel 8** stellt eine kooperative Studie mit Johanna Simon aus unserer Arbeitsgruppe vor, um den Einfluss von Oberflächeneigenschaften von PPn-beschichteten Nanoträgern auf den „*stealth*“ Effekt zu untersuchen. Der Fokus liegt insbesondere auf dem Proteinadsorptionsverhalten von Trägern, die mit PPns unterschiedlicher Hydrophilie modifiziert wurden, um die "*stealth*" -Eigenschaften zu kontrollieren. Wir kombinieren die Präzision von ROP mit dem Aufpfropfverfahren, um Nanoträger mit präziser Kontrolle der Oberflächenhydrophilie zu erhalten. Wir zeigen, dass die Gesamtproteinmenge trotz der unterschiedlichen Hydrophilie der untersuchten Oberflächen unverändert bleibt. Die Art der adsorbierten Proteine wird jedoch dramatisch verändert, wenn eine bestimmte Schwellen-Hydrophilie unterschritten wird. Diese Änderung der Proteinadsorption korreliert mit der *in vitro* beobachteten Veränderung der Wechselwirkung mit Immunzellen.

Graphical Abstract

Chapter 2: A library of well-defined and water-soluble poly(phosphonate)s with adjustable hydrolysis.

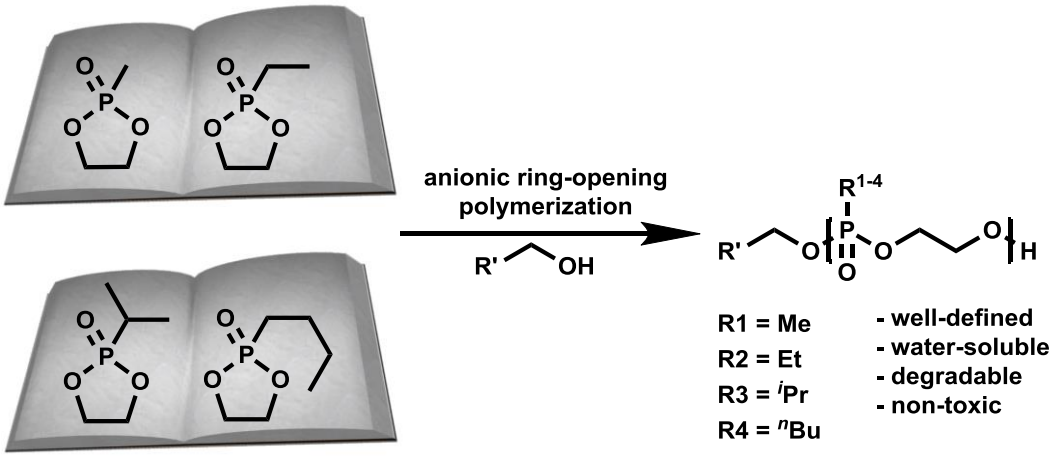

Chapter 3: Adjustable glass transition temperatures of poly(ethylene alkyl phosphonate) copolymers.

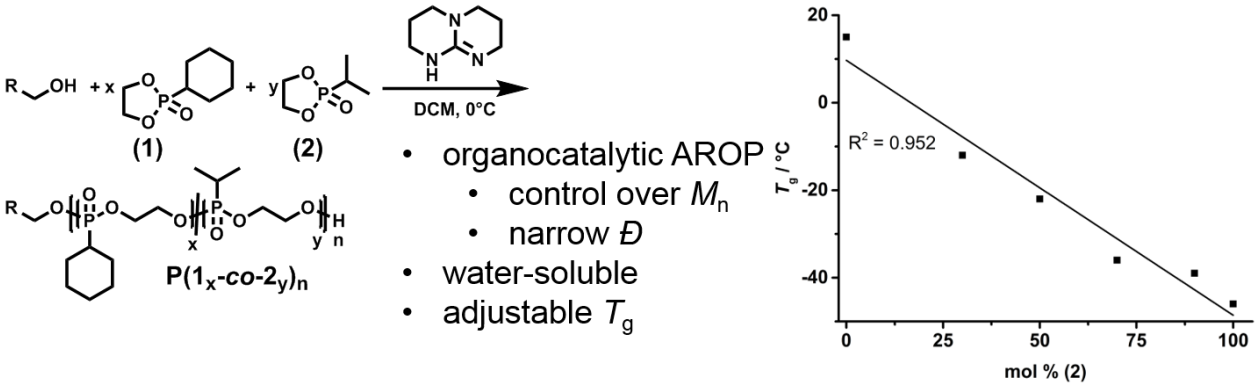

Graphical Abstract

Chapter 4: Poly(phosphonate) copolymers with lower critical solution temperatures: from single chains to macroscopic coacervates.

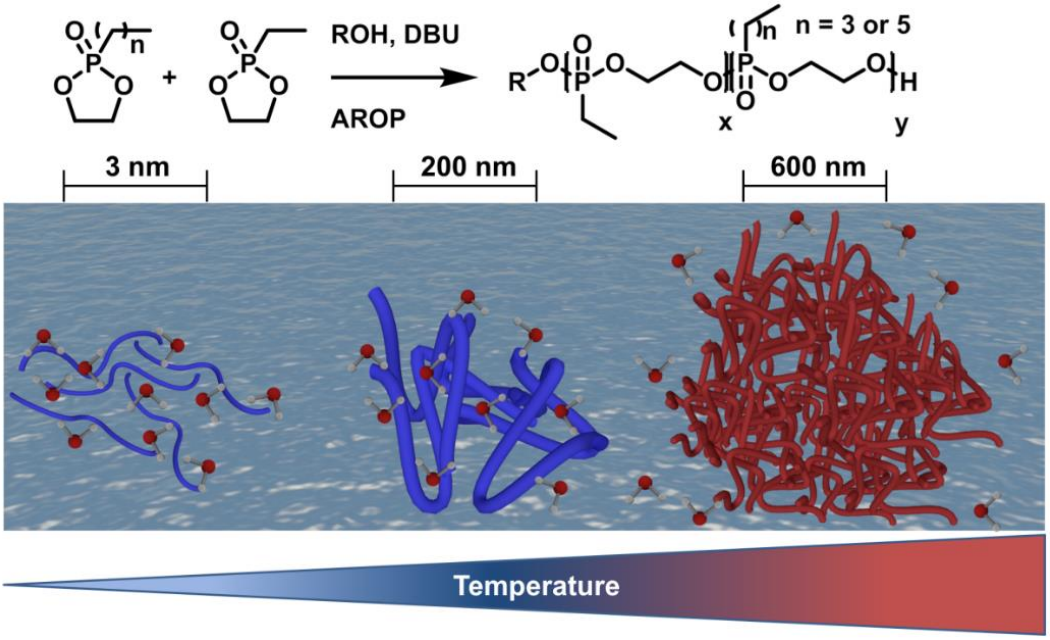

Chapter 5: Poly(alkyl ethylene phosphonate)s: A New Class of Non-amide Kinetic Hydrate Inhibitor Polymers.

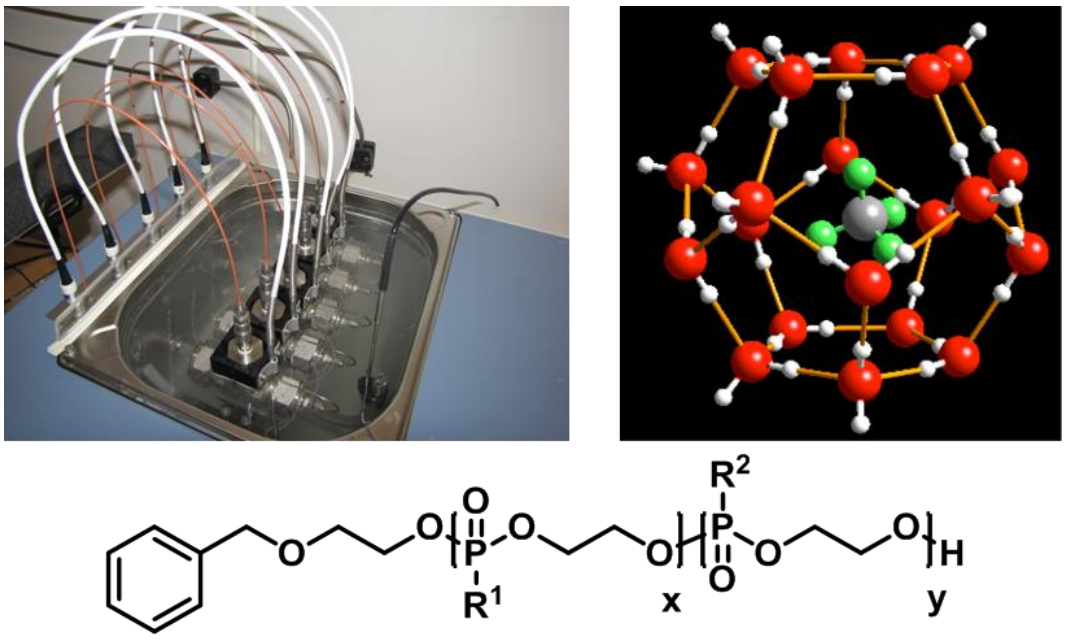

Graphical Abstract

Chapter 6: Thermoresponsive coacervate formation of random poly(phosphonate) terpolymers.

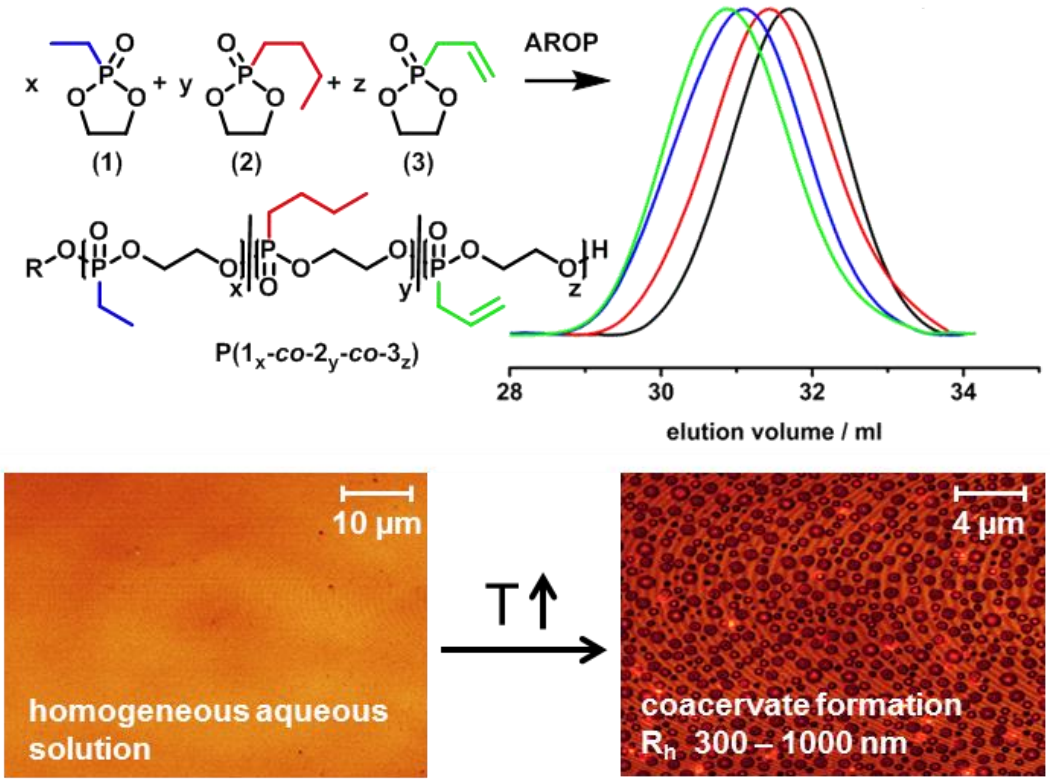

Chapter 7: Degradable Polymersomes with Upper Critical Solution Temperature - Induced Disassembly in Water.

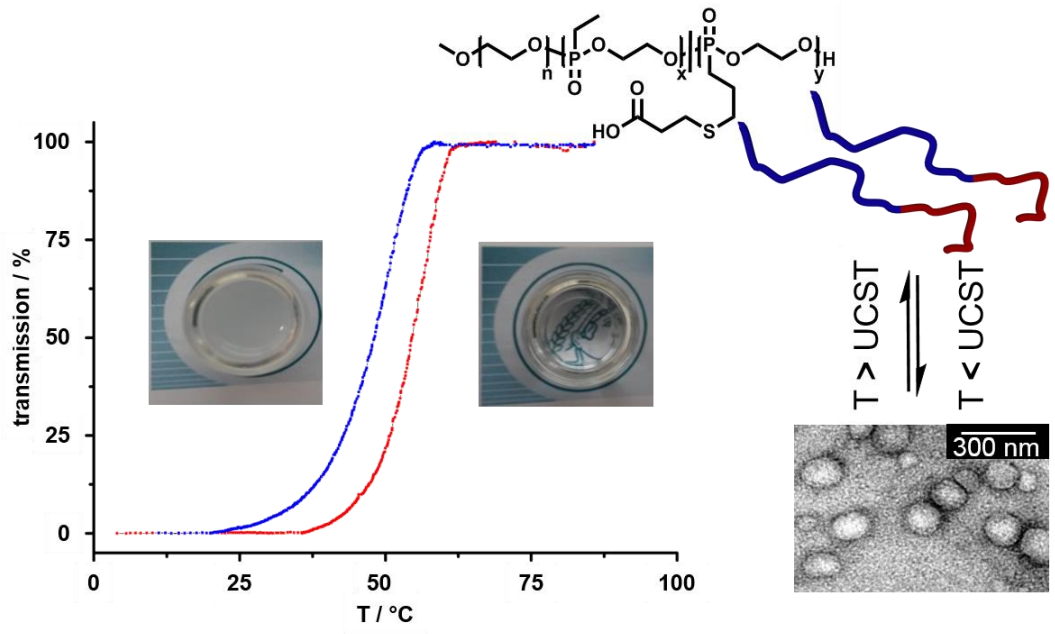

Graphical Abstract

Chapter 8: Hydrophilicity Regulates Specific Protein Adsorption on Poly(phosphoester) Coated Nanocarriers Controlling Uptake in Immune Cells.

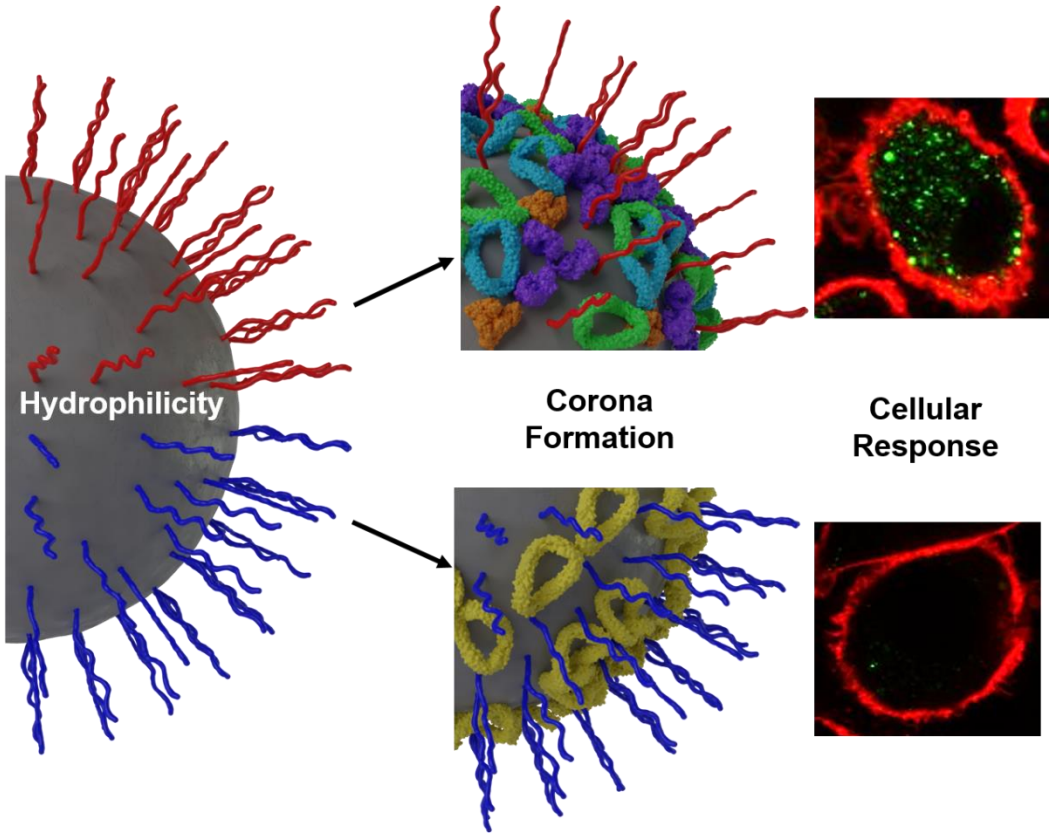

Chapter 1: Introduction

Polymers in Biomedical Applications

During the 50 years since the first use of synthetic polymers in biomedicine in the 1960's, the field has prospered tremendously from synthetic advances in polymer science as evidenced by the numerous polymer containing drug formulations in clinical trials or already available on the market by now (a few selected examples, Table 1.1).[1]

Table 1.1: Selected choice of some commercially available or clinically tested polymer-drug formulations.

formulation	drug	polymer	carrier type	status	reference
PEGasys	interferon alpha-2A	PEG	polymer-protein conjugate	market	4
Oncaspar	asparagase	PEG	polymer-protein conjugate	market	5
Krystexa	porcine-like uricase	PEG	polymer-protein conjugate	market	6
Genexol	paclitaxel	PEGylated PLA	AB type block copolymer micelle	market	7
POxsol	paclitaxel	poly(2-oxazoline)	ABA type triblock terpolymer micelle	pre-clinical	8
FCE28068	doxorubicin	HPMA	copolymer-drug conjugate	phase II	9
PG-TXL	paclitaxel	Poly(L-glutamic acid)	polymer-drug conjugate	phase II	9

The flexibility in polymer design, functionality, topology, and microstructures give rise to a great diversity of physical properties, which can be used in biomedical applications.[2,3] This enables fine tuning of each polymer to suit a selected application through sophisticated polymer synthesis and rational design of materials. Especially in the fields of surface coatings, drug delivery, and tissue engineering, polymers are an indispensable asset for many applications (Table 1.1).[1,3]

Advantages of polymer-conjugation

Attachment of polymers onto drug carriers or the drug itself provides significant advantages over the non-modified versions. Conjugation with a suitable polymer provides increased water-solubility and reduces the toxicity of many hydrophobic drugs.[1,3,10] The resulting steric shielding protects against hydrolytic and enzymatic degradation.[1,3,10] Furthermore, nonspecific interactions with or adsorption of blood components (so-called "opsonization") are significantly altered and in most cases reduced. This effectively prevents the uptake by cells of the immune system. Finally, the increased hydrodynamic radius of the conjugate reduces the renal excretion rate, as the glomerular filtration is size dependent. In total, all these factors amount to a significant increase in plasma half-time, increasing the pharmaceutical efficacy of the respective drug.[1,3,10]

The reduced recognition by the immune system and the slower blood clearance is referred to as "stealth effect". Previous studies attributed the effect solely to the observable reduced overall protein adsorption. However, recent studies from our department proved that reducing the protein adsorption alone is not sufficient to induce "stealth" properties. Rather, the specific adsorption of certain blood proteins (the so-called "dysopsonins") is necessary for a reduced cellular uptake.[11] Upon coming in contact with blood, proteins and other blood components adsorb on the surface of foreign objects like drug carriers, forming the so-called "protein corona".[12]

This protein layer alters the carrier's properties such as size, charge or aggregation and affects the body distribution, toxicity, and especially cellular interactions.[13,14] Today, controlling the protein corona in blood is considered to be crucial to design therapeutically effective nanocarriers. Specific corona proteins were identified as either opsonins (enhancing phagocytosis, e.g., immunoglobulins and complement proteins) or dysopsonins (decreasing phagocytosis, e.g., albumin, clusterin).[15] These dysopsonins were detected in high amounts on typical "stealth polymers" and are currently discussed as potential sources of the "stealth effect" (schematic representation in Figure 1.1).[11,16]

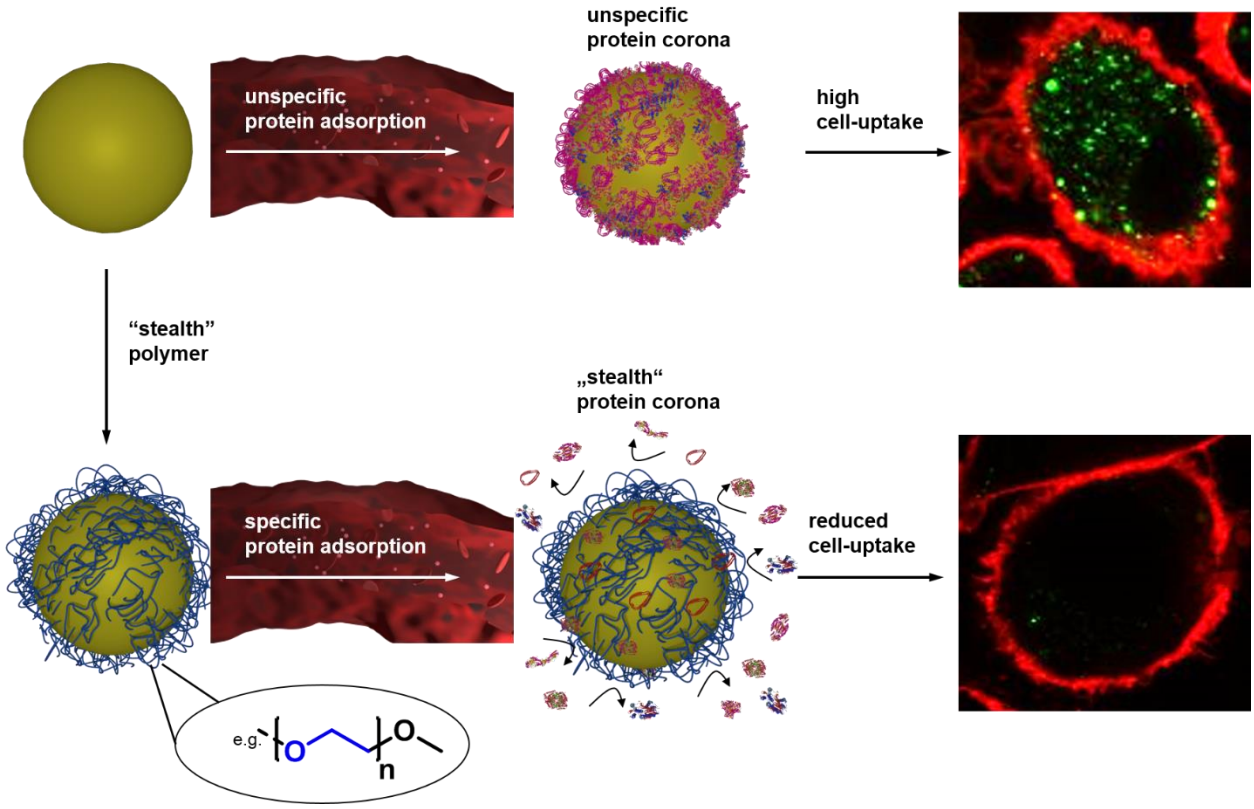

Figure 1.1: Schematic illustration of the formation of the protein corona from the bloodstream and the influence on the cellular uptake: Top row) "Non-stealth" surfaces adsorb large quantities of blood proteins non-specifically. This opsonization leads to an increased recognition and internalization by cells of the immune system. Bottom row: Modification of the surface with "stealth" polymers leads to a reduced overall and specific adsorption of blood proteins onto the surface. The adsorbed dysopsonins reduce the recognition and internalization by cells of the immune system.

The increased plasma half-time furthermore passively exploits the enhanced permeability and retention effect (EPR effect). This effect, first presented by Maeda *et al.* in 1984 describes the increased uptake of high molecular weight materials into cancerous and inflamed tissue.[17-19] These tissues are characterized by hyper-vascularization, and a leaky vasculature due to the tissues increased metabolic activity. This increased growth of blood vessels with leaky walls results in the passive accumulation of long-circulating, high molecular weight materials like drug conjugates. The EPR effect thus further increases the therapeutic efficacy of the drug by providing a passive targeting towards inflamed and cancerous tissue.[18,19]

Requirements for polymer applications *in vivo*

All polymers envisioned for use inside the body have to fulfill several requirements: The polymers have to be non-toxic; meaning cell-viability of the surrounding tissue must not suffer. Furthermore, the polymers must be non-immunogenic, hence not provoke a response of the immune system. Finally, the polymer synthesis has to provide control over molecular weight, and the polymers should have narrow molecular weight distributions. Molecular weight was found in many studies to strongly influence the biocompatibility and "stealth behavior".[20,21] Narrow molecular weight distributions are necessary to establish distinct structure-effect relationships.[22]

Depending on the specific applications additional properties are often demanded. In the case of drug delivery, the polymers need to be water-soluble or amphiphilic under physiological conditions. This prevents aggregation and increases the water-solubility of the drug. Degradability of the polymers may be desired to induce the timed release of cargo or prevent accumulation of polymeric material in the body after repeated administration. Especially accumulation is a significant issue for many currently used polymers due to potential damage to immune cells and excretory organs.

"Smart" stimuli-responsive polymers

More sophisticated carriers or coatings depend on the use of "smart" polymers. Such materials react to an external stimulus with a property change. Both the nature of the stimulus and the varied property can be addressed. Morphology, color, shape, hydrophilicity, solubility, conductivity, and redox potential are typically addressed. The most often used stimuli are pH[23-25,26], temperature[24,26,27], light[27], redox potential[25,26], application of an external electric/magnetic field[28], and the addition of small molecules[26]. Through the rational design of the polymer structure, more than one stimulus can be used. Two selected examples for multi stimuli-responsive materials (pH, T, and redox; T, and light) are shown in Figure 1.2. Due to the widespread success of such materials especially in biomedical applications, several excellent review articles are available today.[27,29,30]

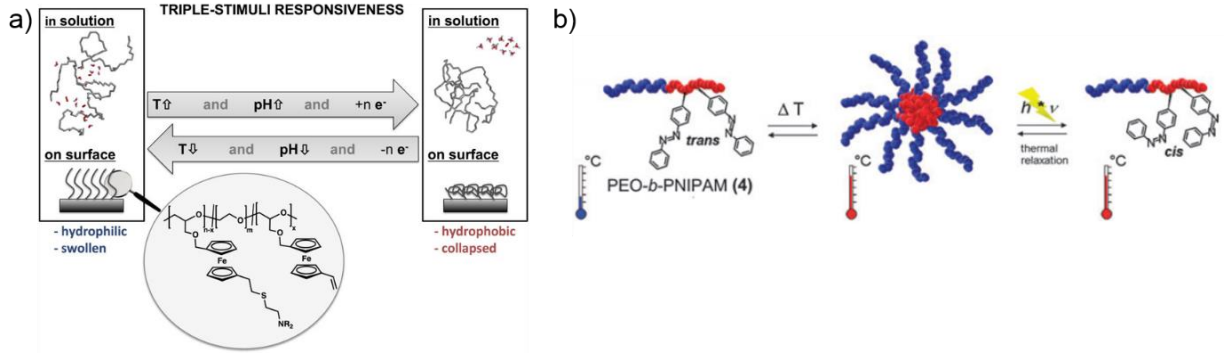

Figure 1.2: Selected examples of multi stimuli-responsive materials. a) pH, temperature and redox triple responsive polymers on the basis of ferrocene containing PEG. Copyright @ 2015 American Chemical Society. Reprinted with permission from ACS Applied Materials & Interfaces, free access Author Choice article.[25] b) Temperature and light dual responsive block copolymers on the basis of side-chain azobenzene containing P(NIPAM). Copyright @ 2010 The Royal Society of Chemistry. Reprinted with permission from Chemical Communications.[31]

The best understood and most often used stimulus is a change in temperature. Temperature can easily be varied from the outside, either by phototherapy or simple cooling. Additionally, inflamed or cancerous tissue intrinsically has an increased temperature due to the higher metabolic activity.[32] Typically, a temperature responsive polymer changes its solubility behavior upon the stimulus. Two cases are to be distinguished: decreased solubility and increased solubility (e.g., in water) at elevated temperature.

The first case describes the behavior of polymers showing a lower critical solution temperature (LCST), a temperature above which they become insoluble (Figure 1.3, top). The effect is widely observed for many water-soluble polymers with poly(*N*-isopropyl acrylamide) (P(NIPAM)) as the best-characterized example.[27, 29,33,34] The inverse case describes polymers that become insoluble in water below the critical temperature (upper critical solution temperature, UCST) (Figure 1.3, bottom). The UCST case, for aqueous systems, is much less frequently observed than the LCST case.[35] The schematic, idealized phase diagram (volume fraction *vs.* temperature) of a binary mixture for both cases are shown in Figure 1.3. When starting with a clear polymer solution, the chains are likely to exist in a random coil structure and be maximally solvated (middle of Figure 1.3). Upon crossing the coexisting curve (blue line) by heating (for LCST) or cooling (for UCST), respectively, the system becomes metastable. In this condition, minimal T-fluctuations can be tolerated without phase separation. Upon further T-change and crossing of the spinodal curve (brown line), phase separation is inevitable due to entropic (LCST) or enthalpy (UCST) reasons. The LCST and UCST are defined as the maxima or minima of the spinodal curves, respectively. Each other point in the phase diagrams on the spinodal curve is referred to as a composition dependent cloud point temperature (T_{cp}). Both phenomena have different physicochemical origins, which shall be briefly discussed in the following.[36]

To induce LCST behavior, usually, a balance of hydrophilic and hydrophobic segments in the polymer backbone is needed. Increasing the number of hydrophobic segments typically decreases the phase separation temperature. The process is mainly entropy driven. At low temperature, the polymer backbone is well-solvated, typically via H-bond interactions and the polymer-polymer interactions are shielded. As temperature increases, the H-bonding becomes weaker, and the T-dependency of the entropy term forces a release of polymer-bound (low degree of freedom) solvent into the bulk solvent (higher degree of freedom), resulting in a favorable gain of entropy. The hydrophobic polymer-polymer interactions, which tend towards polymer aggregation are less affected by temperature. As a combined result, the polymer chains undergo a coil-to-globule transition and precipitate from solution. This is accompanied by an increase of entropy of liberated water molecules previously bound to the polymer.[36,37,38]

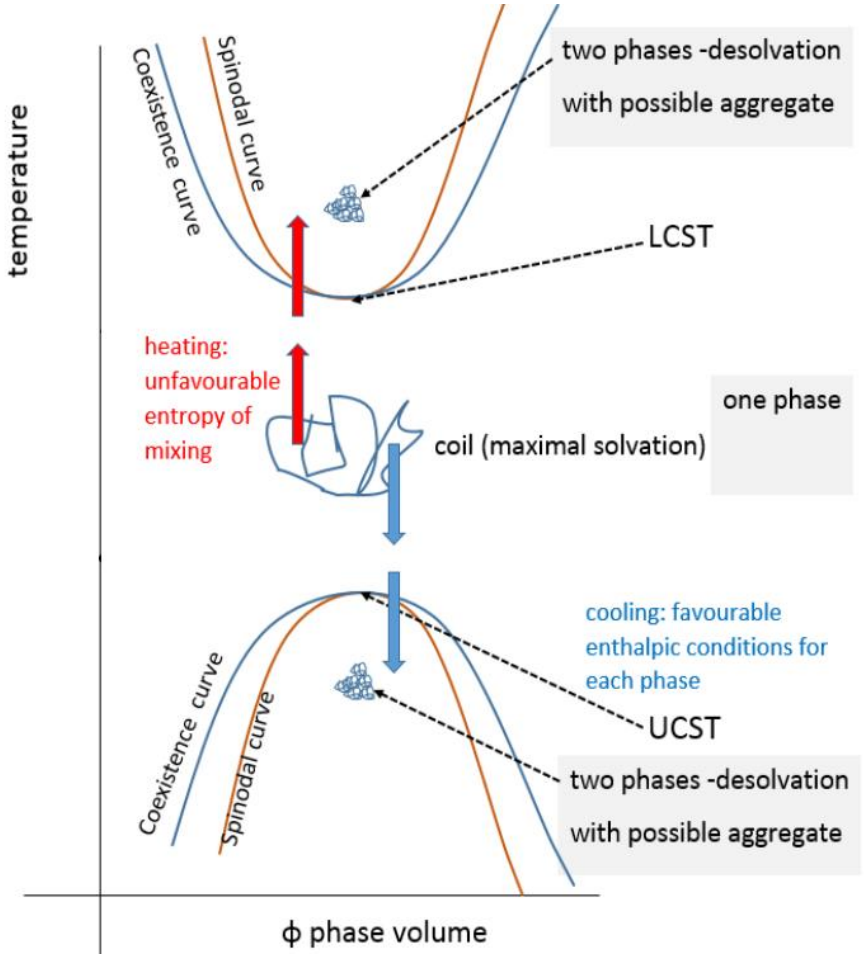

Figure 1.3: Schematic presentation of the phase diagrams of an LCST (top) and a UCST polymer (bottom). Blue lines represent the coexisting curves, brown lines the spinodal curves. Between the coexisting and the spinodal curve, the system is in a metastable condition in which minor T fluctuations are tolerated. Upon crossing the spinodal curve, phase separation is inevitable. Coil-to-globule phase separation and inverse case illustrated by stretched and collapsed "polymer" chain (blue coils). Copyright @ 2017 Multidisciplinary Digital Publishing Institute (MDPI). Reprinted and modified from Open Access journal Gels.[36]

To induce UCST behavior, temperature-sensitive intra- and inter-chain interactions are needed, which break upon heating of the solution, resulting in the solubilization of the polymer aggregates. Unlike the LCST-, the UCST phase separation is an enthalpy-driven process and typically relies on strong polymer-polymer and weak polymer-solvent interactions, respectively.[39] H-bond interactions are mostly utilized for temperature responsive aggregation/dissociation of the polymer chains. An increase in temperature decreases the effectiveness of inter- and intra-chain H-bonding and promotes interactions with the highly mobile solvent, thus solvatization of the polymer.[35,39]

The respective critical temperature (cloud point temperature T_{cp}) is easily obtained by UV-Vis turbidity measurements (Figure 1.4 and Figure 1.5). In these measurements, a light beam is passed through a cuvette, and the transmission is detected. For a clear solution (below LCST or above UCST, respectively) the transmission is 100%. Upon surpassing the critical temperature, transmission drops due to precipitation of the polymer from solution.

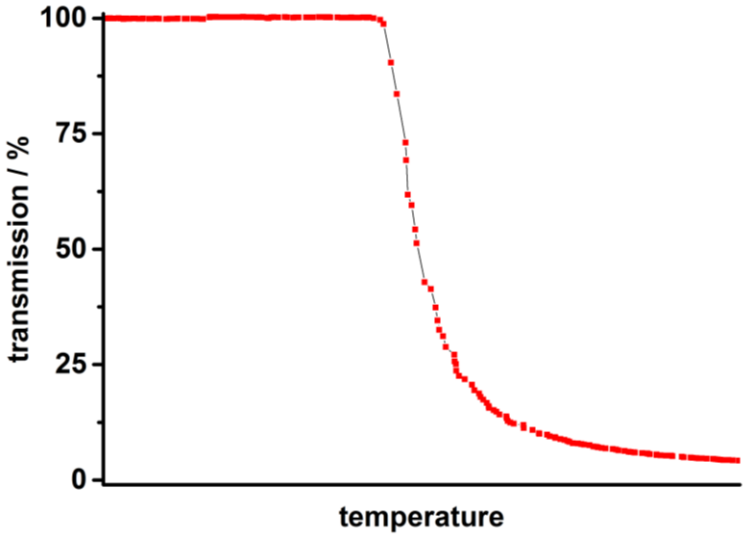

Figure 1.4: Schematic illustration of a UV-Vis turbidity measurement of an LCST polymer.

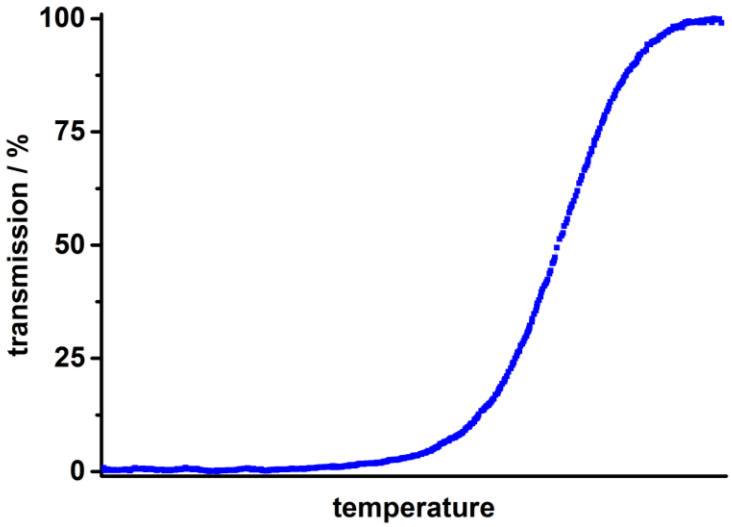

Figure 1.5: Schematic illustration of a turbidity measurement of a UCST polymer.

Poly(ethylene glycol): the "gold standard"

The benchmark polymer every new material needs to compete with is poly(ethylene glycol), PEG. Since its first use in the 1970's, the attachment of PEG to surfaces, carriers or drugs (a process nowadays termed "PEGylation") serves as the "gold standard" for hydrophilic polymers that are used in medicine today (Table 1.1).[1,10,40] The advantages of PEG are numerous. From the synthetic side, PEG is a low-cost material that is synthesized industrially on a large scale (~ 450 kt per year, 2016, Figure 1.6)[41] and pharmaceutical purity, as it is also used in cosmetics and as a food additive.[41,42]

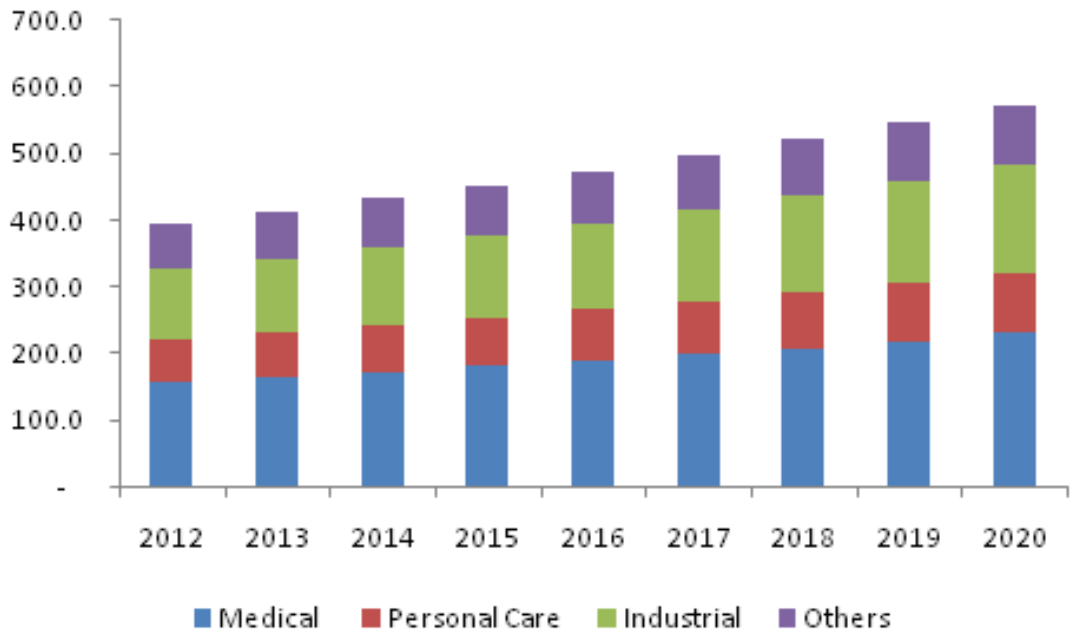

Figure 1.6: Global market production of PEG in kt per year and differentiation of PEG usage in different markets. Data collected till 2015, data from 2016 onwards predicted in 2015.[41]

The anionic ring-opening polymerization of ethylene oxide (Scheme 1.1) provides control over molecular weights ranging from 400 g mol^{-1} to about 50,000 g mol^{-1} and narrow molecular weight distributions ($Đ$ < 1.10).

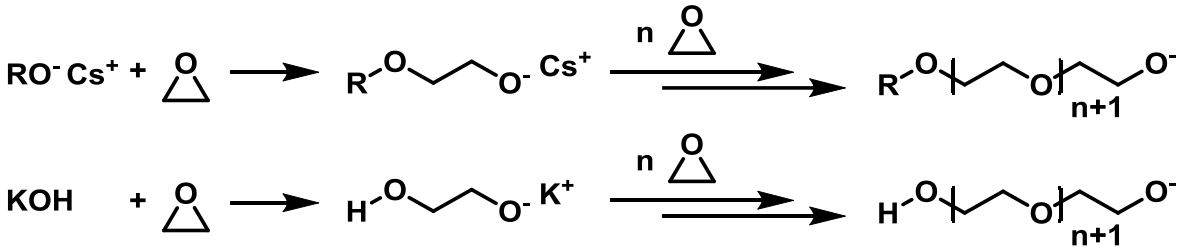

Scheme 1.1: The anionic ring-opening polymerization of ethylene oxide. Top: Initiated with cesium alkoxides as typically used in academics to produce α-functional PEG. Bottom: Initiated with potassium hydroxide as used in industrial synthesis to produce PEG-diol.

Despite its polyether structure, PEG is water-soluble due to H-bonding between the ethylene glycol units and water. Furthermore, it is soluble in a wide range of organic solvents, simplifying synthesis and end-group modification and it precipitates from solvents with low dielectric constants, facilitating purification. From the biological side, PEG is biocompatible, non-cell-toxic and triggers no acute immune-responds.[10] PEG also features a pronounced “stealth effect” when attached in sufficient amounts.[11,20] Consequently, many studies have shown the increased plasma half-time, decreased toxicity and improved pharmacokinetics of PEGylated substances, like drugs, proteins, micelles, and carriers.[6,9,21,43-45] All these assets have made PEG an indispensable polymer in biomedical applications and our daily life.

However, PEG still faces limitations: Regarding the synthesis and chemical structure of PEG, the lack of functionality is striking. Two functional groups, at the α- and ω-end of the polymer, but no further groups along the backbone are available for functionalization. The α-group is mostly a non-functional methoxy group originating from the synthesis. The ω-group is usually used for conjugation chemistry and blocked for sophisticated features like labeling, active targeting or stimuli responsiveness. Furthermore, the inherent stability of the polyether backbone towards hydrolysis and enzymatic degradation presents an issue concerning accumulations *in vivo*.[10]

Biodegradation of PEG was so far only demonstrated using sludge microbes in 2005 by Huang *et al.*[46] Consequently, the renal excretion limit determines the highest usable molecular weight. The exact value is difficult to determine, but studies suggest a suitable range of 20,000 g mol^{-1} to 60,000 g mol^{-1}.[22] This issue is being addressed by the rational incorporation of degradable linkers in the PEG chains.[47,48] However, the insertion of the cleavable sites needs to be carefully designed, as low M_n fragments of PEG (~ 400 g mol^{-1}) were found to be susceptible towards oxidation by the enzyme alcohol dehydrogenase forming toxic aldehyde products. This oxidative metabolism rate decreases significantly with increasing molecular weight.[49]

The final issue of PEG very likely arises due to the omnipresence of PEG in daily applications and drug formulations: despite the fact that PEG triggers no acute immune-responds, long-term exposure to PEG can lead to the formation of anti-PEG antibodies. First detected in 1983 by Richter *et al.* in rabbits, several studies report a change in the pharmacokinetics of the second injection of PEGylated carriers. These antibodies are today, upon others, accounted for hypersensitivity reactions observed in some patients treated with PEGylated formulations.[50,51]

Furthermore, the “accelerated blood clearance phenomenon” (ABC) is also suggested to occur due to anti-PEG antibody formation. This effect describes the drastic increase in blood clearance of PEGylated carriers after the first treatment. Rat models treated with PEGylated liposomes showed a 52% clearance 4h after the second injection (compared to 0.6% clearance 4h after the first injection, Figure 1.7).[52] However, also a growing amount of clinical studies struggle with the effects of this increased clearance. Importantly, recent studies identified anti-PEG antibodies in 22-25% of healthy blood donors that were not treated with PEGylated drugs. Two decades earlier, only 0.2% of healthy blood donors were found positive for anti-PEG antibodies. [53-56]

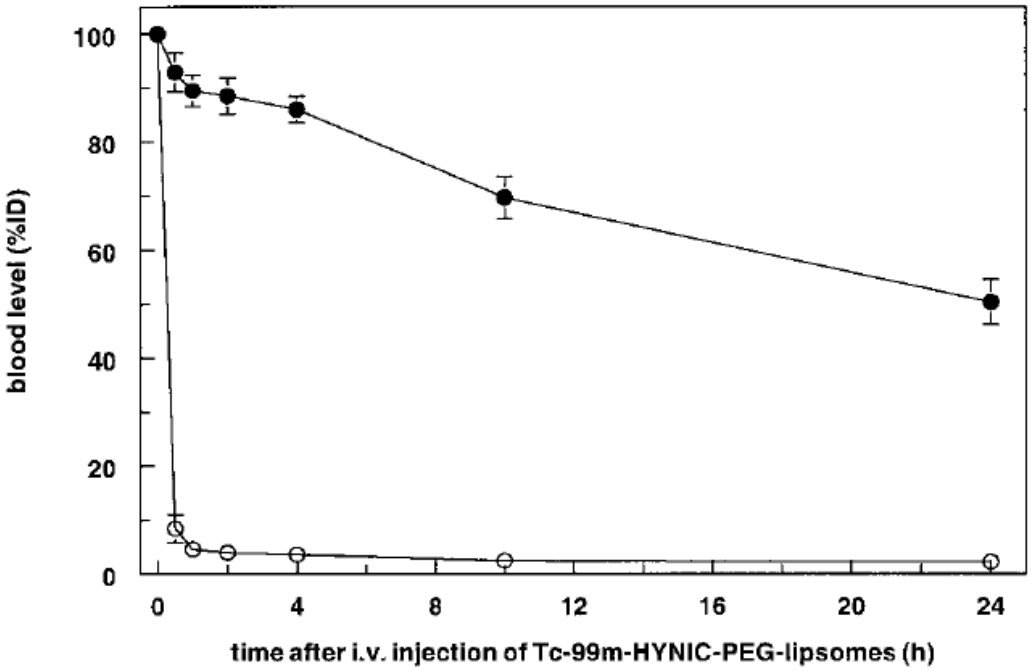

Figure 1.7: Blood clearance of PEG-liposomes in rats after the first (black dots) and second i.v. injection (open dots). The mean value of 6 rats presented. Copyright @ 2000 The American Society for Pharmacology and Experimental Therapeutics. Reprinted with permission from The Journal of Pharmacology and Experimental Therapeutics.[52]

As a consequence of the emerging issues of PEGylation and due to the wide variety of potential applications and obstacles to overcome in the field, it becomes apparent, that one polymer(class) is not enough to cover all applications. Therefore, synthetic chemists are continually being pressed to find complementary alternatives for PEG and novel, more specialized materials to improve existing and create new polymers for biomedical applications.[2,57]

Alternatives to PEG

Some of the most promising alternatives currently discussed are poly(glycerol)s (PG)[10], (modified) polysaccharides[10,16,58-60], poly(2-oxazoline)s (POx)[10,61,62], and poly(phosphoester)s (PPEs).[11,63] Possessing a similar polyether backbone as PEG with an additional hydroxyethyl side-chain at each repetition unit, linear and/or hyperbranched PG's share many beneficial traits of PEG (Scheme 1.2).[64]

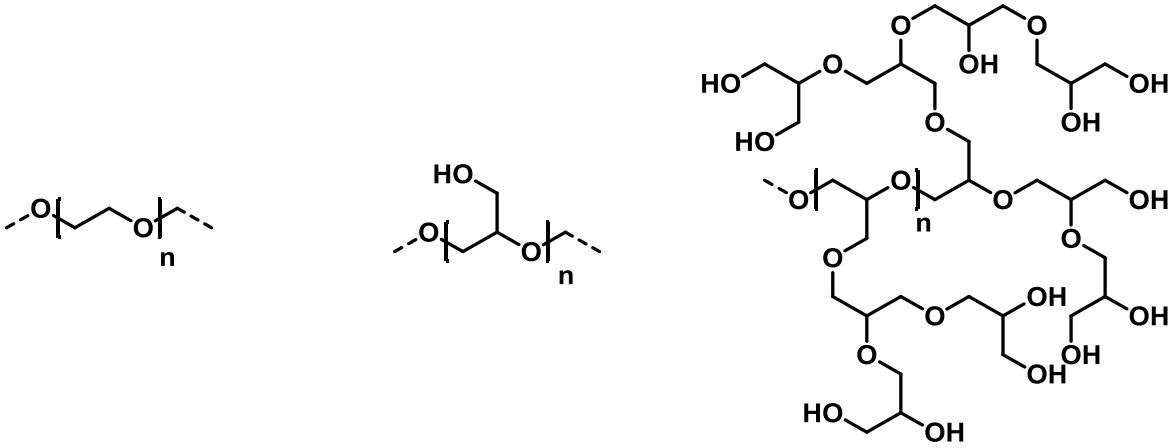

poly(ethylene glycol), PEG **linear poly(glycerol), linPG** **hyperbranched poly(glycerol), hbPG**

Scheme 1.2: Structures of PEG, linPG, and hbPG.

The biocompatibility of PG was found to be slightly superior to PEG[65,66], and no significant immunogenicity was detected.[65] The "stealth effect" is observed as expected[67], and the ABC phenomenon has not been reported for PG formulations, indicating no formation of anti-PG antibodies yet.[68] Furthermore, the side-chains enable polymer property variation and a high degree of diversity. This is usually achieved either by rational design of functional glycidyl ether monomers or by post-polymerization functionalization of the final polymer.[64,69]The anionic ring-opening polymerization of these glycidyl ether monomers offers the synthesis of "functional PEG" with excellent control over molecular weight, copolymer composition, knowledge of the microstructure, and narrow molecular weight distributions.[64,70] Still, PG's are non-degradable *in vivo*, as they are polyethers and especially high M_n PG's were found to accumulate in liver and spleen of treated mice.[71]

(Modified) polysaccharides bring the benefit of being derived from natural resources. Wholly natural saccharides like, e.g., dextrin or partially modified saccharides like hydroxyl ethyl starch (HES) have been used in biomedical applications for years. In addition to their inherent degradability and biocompatibility, they were found to efficiently induce a "stealth effect" and positively modify the pharmacokinetics of modified drugs.[72,73]

A class of fully synthetic polymers are the poly(2-oxazoline)s, which have been extensively investigated for the last 50 years.[74] These polymers can be synthesized with excellent control over molecular weight, copolymer composition, polymer microstructure, polymer topology, and narrow molecular weight distributions via the living cationic ring-opening polymerization (cROP, Scheme 1.3).

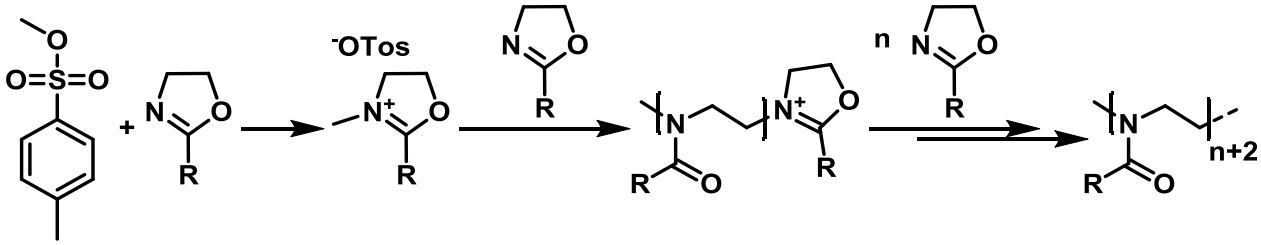

Scheme 1.3: Schematic living cationic ring-opening polymerization (cROP) of a 2-alkyl oxazoline initiated with methyl *p*-toluene sulfonic acid to form poly(2-alkyl oxazoline).

Exhaustive research has been done in the development of functional monomers and today, α, ω- and side-chain modifications make poly(2-oxazoline)s an impressively diverse polymer class, that is already commercially available (Aquazol®). Polymer properties concerning, e.g., solubility and functionality, are easily modified, enabling the design of "smart" polymers with, e.g., targeting or labeling units in the backbone.[10,62,75-77] A wide range of drug carriers, ranging from AB or ABA block-copolymer micelles (Figure 1.8) to "POxylated" liposomes, have been developed and show promising results, indicating excellent "stealth behavior" both *in vitro* and *in vivo*.[8,57,62,78-82] POx's are biocompatible, generally non-toxic and up to date, no anti-POx antibodies have been reported.[75,83,84] However, like PG's, POx's are non-degradable under physiological conditions and show a tissue accumulation similar to that of PEG in the liver, spleen, and kidney.[82]

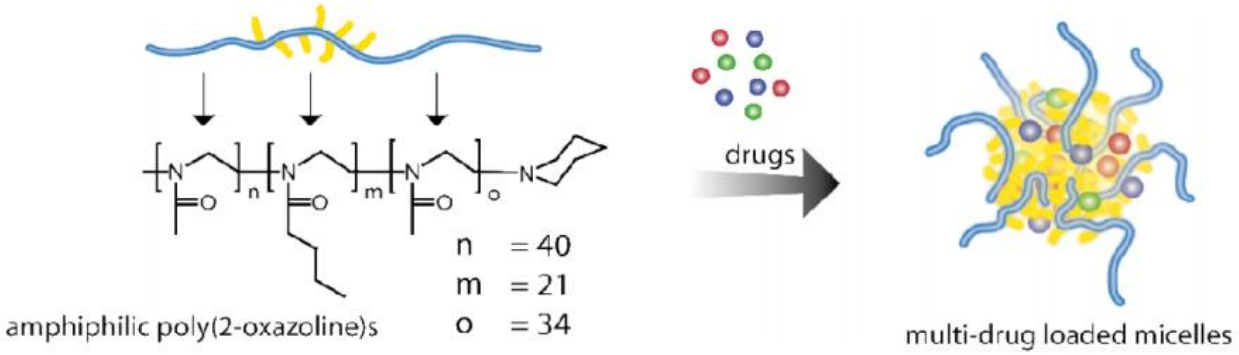

Figure 1.8: Structure of amphiphilic poly(2-oxazoline) ABA triblock copolymer and schematic formation of drug-loaded micelles for drug delivery. Copyright @ 2012 American Chemical Society. Reprinted with permission from Molecular Pharmaceutics.[8]

Despite the development of these and many more polymers used and discussed for biomedical applications, no polymer has been identified to perfectly fulfill all requirements. It stands to debate if a material like this will ever be designed. Furthermore, owning their more frequent use, it is only a matter of time until the inevitable discovery of the first antibodies against the polymer classes mentioned above. Therefore, the development of new polymers for biomedical applications needs to keep up with the rising demands on such materials.

One class of polymers, which was recently added to the portfolio of interesting materials in biomedicine are poly(phosphoester)s (PPEs). These polymers have been initially designed to mimic the most essential natural macromolecule, DNA. Consequently, they were expected to fulfill many requirements for use in biomedical applications: biocompatibility, non-toxicity, non-immunogenicity, water-solubility, and degradability. Furthermore, the pentavalent phosphorus offers a diverse synthetic platform for property modifications.

Phosphorus-Containing Polymers: Poly(phosphate)s

Phosphorus and Phosphates in nature

Phosphorus compounds are omnipresent in nature, either bound in inorganic salts, or organic compounds and Phosphorus is the 11th most abundant element on the planet. Without phosphoric acid esters, in particular, life as we know it, would not be possible.[85] The most fundamental requisites for life are all governed by or with the help of phosphoric acid derivatives:

The universal energy storage system preserved in all living organisms, ATP, is based on the potential energy stored in phosphoric acid anhydride bonds, i.e., pyrophosphates (Scheme 1.4, a). Cleavage of this bond provides energy for active biochemical synthesis, active transport through cells, nerve transport, growth mechanisms, and movement.[85,86]

Apart from energy storage, the activity of many enzymes is tightly regulated by active phosphorylation or dephosphorylation of crucial amino acids. In many, but not all, of these cases, ATP serves as a direct phosphorylation agent and simultaneously provides the necessary energy via anhydride cleavage.[85,86]

Furthermore, a large part of biological redox reactions depends on the redox potential of the NAD^+ / NADH coenzyme (Scheme 1.4, b, NAD^+ form). While not being involved in the redox reaction, phosphoric acid esters serve to enhance solubility and link two essential functional parts together in one molecule.[87]

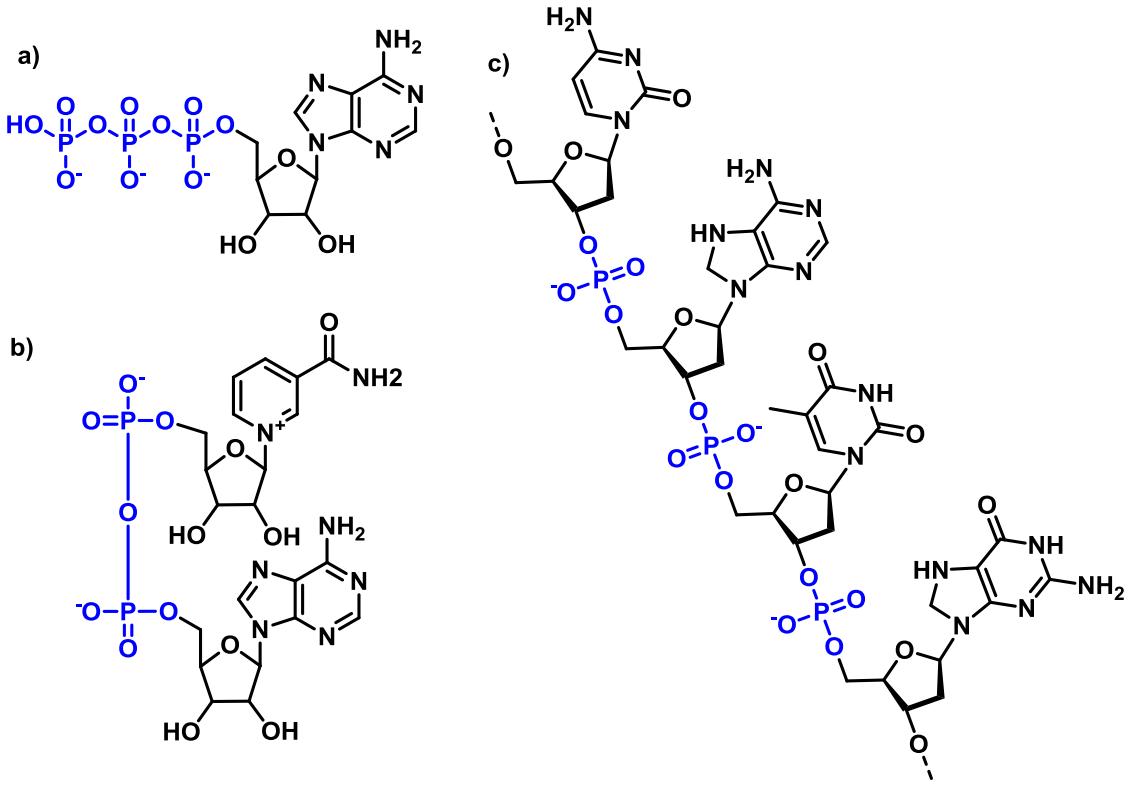

Scheme 1.4: Structures of the most important naturally occurring phosphoesters: a) Universal energy "currency" ATP. b) Redox-responsive system NAD^+. c) DNA, the only naturally occurring PPE.

Finally, probably the most essential phosphoric acid esters are DNA (Scheme 1.4, c) and RNA, respectively. The carriers of the genetic information are sequence defined polycondensates of phosphoric acid and substituted (deoxy-)ribose derivatives. Here, the PPE's perform several tasks. They serve as the backbone to retain the sequence definition and provide the necessary stability towards hydrolysis. Furthermore, the backbone can be cleaved on demand under enzymatic catalysis to repair, e.g., defects.[88] The negative charge distributed on the backbone prevents passive, undesired diffusion through membranes, and enables ionic complexation with components of the transcription apparatus necessary to "read" the genetic information, some enzymes of the DNA replication tools, and histones, positively charged proteins necessary for DNA storage and protein expression.[85]

Due to this omnipresence and significance in nature, chemists started to work on the development of synthetic poly(phosphoester)s. Their potential biodegradability, biocompatibility, and high structural diversity make them attractive especially in the field of biomedical applications. In comparison to poly(carboxylic acid ester)s, PPEs contain the pentavalent phosphorus atom, increasing the structural diversity by the addition of an additional side-chain. Different binding patterns can be incorporated in the backbone or side-chain (P-C, P-N), further broadening the property bandwidth of these materials (Scheme 1.5).

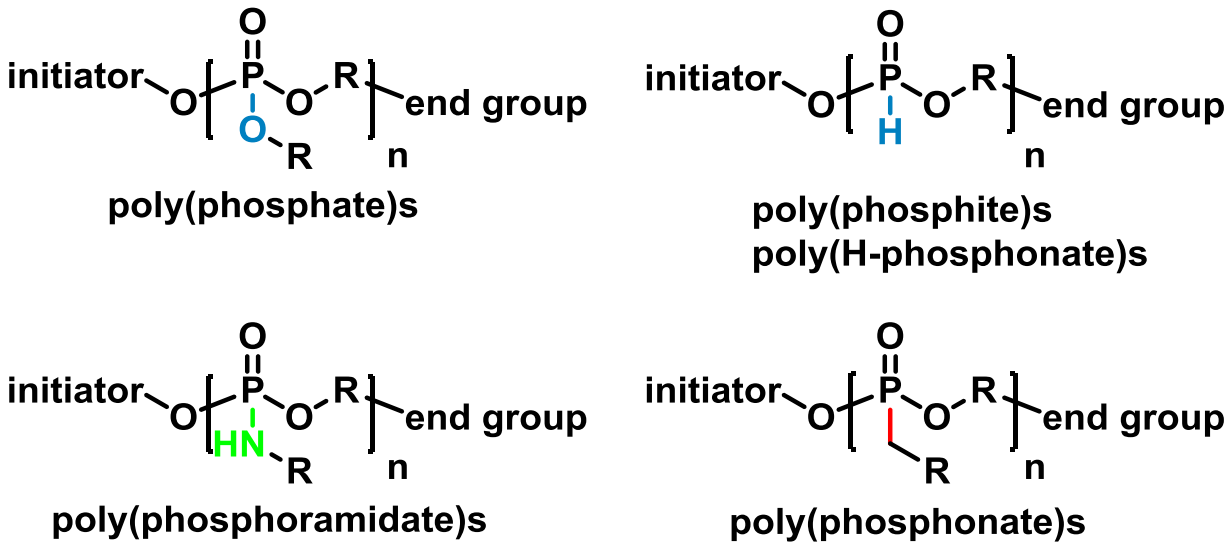

Scheme 1.5: Structures of the most commonly used PPEs with varying P-X bonds in the side-chain.

Today, several reviews concerning the different synthetic routes towards and applications of PPEs are available.[89-94] This chapter will give a short historical background regarding the synthesis of PPEs, but the primary focus will lie on the current organocatalytic ring-opening polymerization procedure.

Poly(phosphoric acid ester)s: Poly(phosphate)s

Phosphates are the most abundant phosphorus derivatives in nature. Also in synthetic polymers, poly(phosphate)s are by far the best-studied sub-class of all PPEs. While the first PPEs were synthesized via polycondensation reactions, the pioneering work on the ring-opening polymerization towards poly(phosphate)s has been conducted by Penczek *et al.* in the 1970s.[95] They focused their initial investigations on the cationic polymerization of 2-alkoxy-2-oxo-1,3,2-dioxaphosphorinanes, six-membered cyclic phosphates, to synthesize synthetic oligonucleotides via a controlled route (Scheme 1.6).

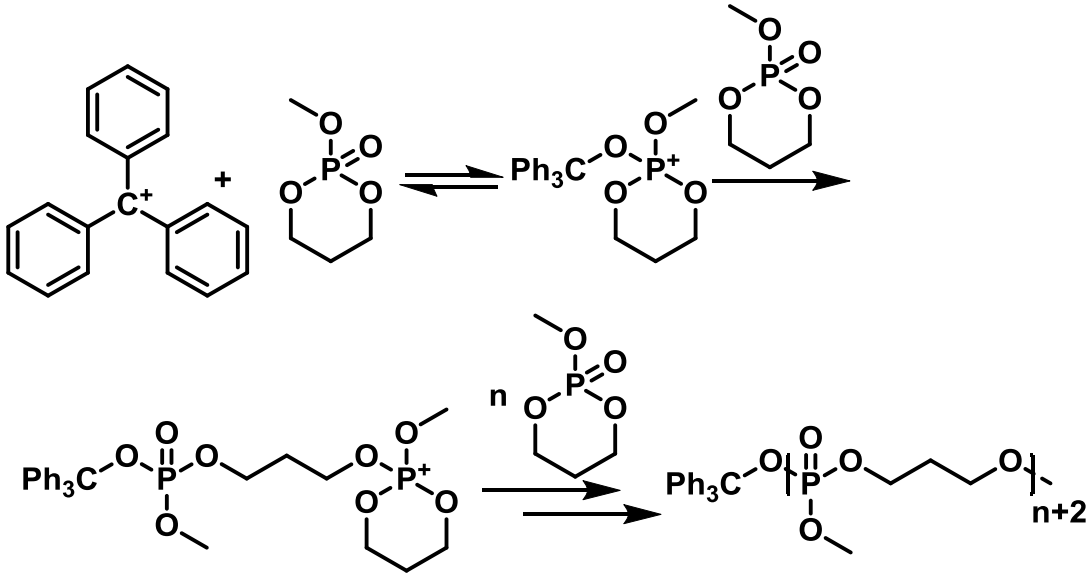

Scheme 1.6: Proposed cationic polymerization of 2-methoxy-2-oxo-1,3,2-dioxaphosphorinane initiated with the triphenyl methyl cation (anions omitted).[95]

ROP was carried out in the presence of triphenyl methyl salts and was prone to transesterification processes, thus resulting only in the formation of oligomers.[95] This work was complemented in 1977 by the detailed kinetic investigation of differently substituted monomers. The same anionic initiators as in the previous studies were used with a strong tendency towards chain-transfer reactions.[96] The anionic polymerization of these monomers initiated with sodium and potassium alkoxides, published in the same year, produced only low molecular weight compounds of around 1,000 g mol^{-1}. High degrees of transesterifications reactions limited the propagation, a result further confirmed by parallel work of Vogt *et al.*.[97,98]

Parallel to Penczeks work on six-membered monomers, Vogt *et al.* studied the polymerization of five-membered 2-alkoxy-2-oxo-1,3,2-dioxaphospholanes. Following the initial works of Munoz *et al.* they presented the alkoxide initiated ROP of these monomers. In contrast to the six-membered homologs, rapid monomer conversion was found at room temperature. However, kinetic studies pointed towards a pronounced tendency for transesterification reactions.[99]

Around the 1980s, a shift towards the use of the five-membered dioxaphospholane monomers occurred, and the six-membered rings vanished from the following literature, probably due to their lower ring-strain, making a controlled ROP without chain transfer difficult. In the following decades, several 5-membered cyclic monomers and detailed mechanistic studies were reported. (see Scheme 1.7).

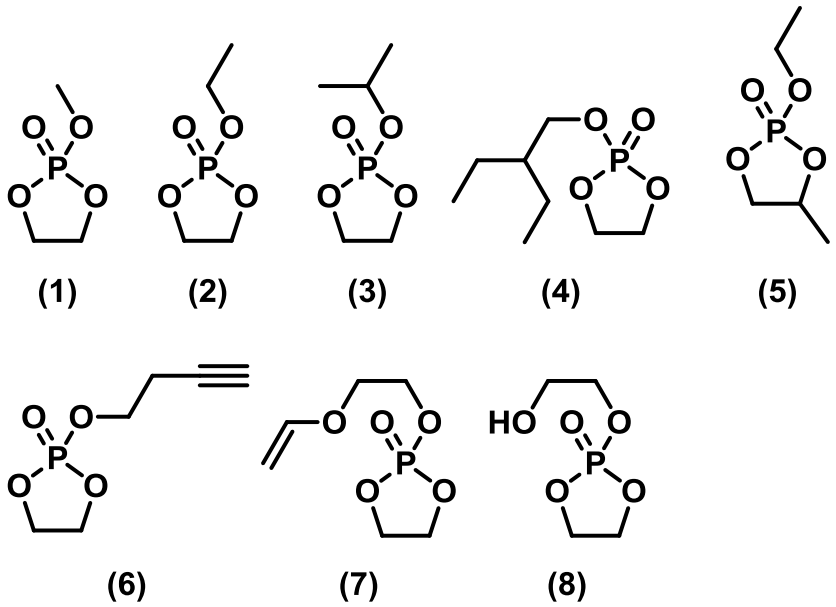

Scheme 1.7: Representative 2-alkoxy-2-oxo-1,3,2-dioxaphosphorinanes used in the ring-opening polymerization.

Polymerizations before 1998 were performed mainly with organo-aluminum or -magnesia reagents resulted in higher molecular weight polymers (M_n > 10,000 g mol^{-1}).[100] As a consequence the use of easy to synthesize organo-aluminum compounds dominated the field for many years.[101]

The first non-metal catalysis for PPE preparation was reported by Wen *et al*. in 1998 when they used lipase to polymerize 2-isopropoxy-2-oxo-1,3,2-dioxaphsopholane (Scheme 1.7, structure 3) enzymatically. Unlike the alkoxide or aluminum-catalyzed reactions, the polymerization needed high temperature and long reaction time (up to 170h) to proceed to high conversions (94%). Even then, materials with molecular weights below 2,000 g mol^{-1} were obtained.[102]

Wang *et al.* achieved higher degrees of polymerization (molecular weights up to 5,000 g mol-1) in 2006 when they utilized $Sn(Oct)_2$ as a catalyst for the insertion polymerization of 2-ethoxy-2-oxo-1,3,2-dioxaphsopholane (Scheme 1.7, structure 2; Scheme 1.8, proposed mechanism).[103]

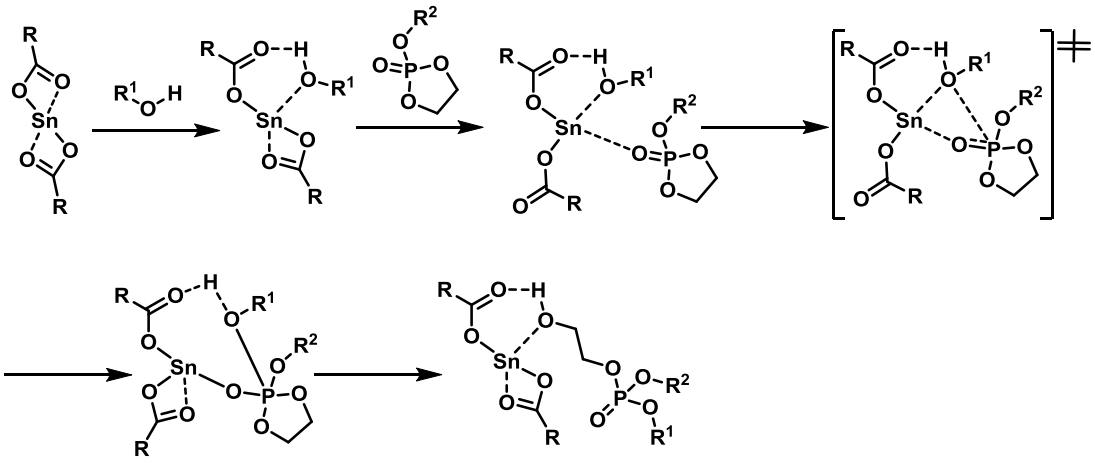

Scheme 1.8: Proposed mechanism of initiation and propagation of EEP polymerization with $Sn(Oct)_2$.[103]

The polymerization proceeded to high conversions (90%) within 30 min in THF at 40 °C. Only low conversion of less than 40% was achieved at 0 °C. However, a more detailed analysis of the polymerization and the resulting polymer showed that the reaction was prone to transesterification and depolymerization as side-reactions. The molecular weight distribution broadened significantly over time (1.31, 20 min to 1.69, 24h) and became bimodal after 4h of reaction (Figure 1.9). Furthermore, the apparent molecular weight deviated from the initial monomer to initiator feed ratio, indicating side-chain transesterifications and the formation of branched structures.[103]

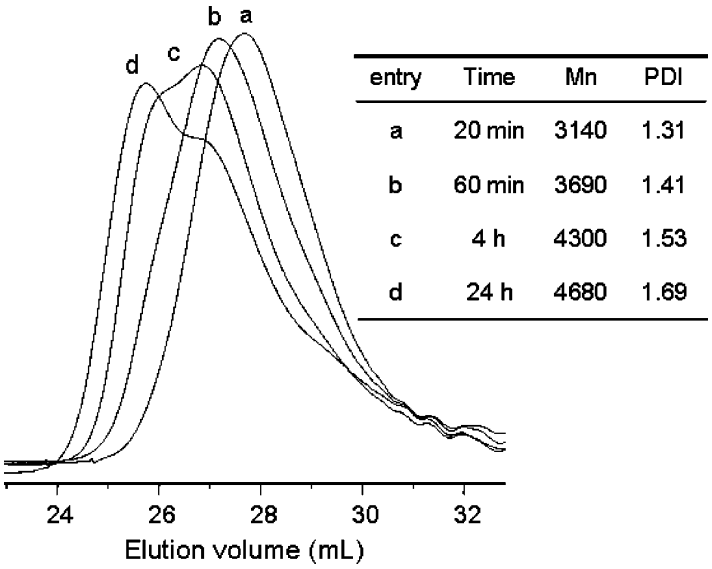

entry	Time	Mn	PDI
a	20 min	3140	1.31
b	60 min	3690	1.41
c	4 h	4300	1.53
d	24 h	4680	1.69

Figure 1.9: SEC elugrams of EEP polymerization with $Sn(Oct)_2$ in THF at 40 °C. Copyright @ 2006 American Chemical Society. Reprinted with permission from Macromolecules.[103]

Around that time, the first attempts to use well-defined PPEs as materials in biomedical applications were undertaken by Leong *et al.*. They synthesized copolymers composed of lactide and 2-ethoxy-2-oxo-1,3,2-dioxaphsopholane with yields of 70% and molecular weights of 10,000 g mol^{-1} to produce degradable, non-toxic drug carriers. However, no data concerning the microstructure of the polymer was shown. The copolymers showed little to no toxicity towards Hela-cells, indicating the biocompatibility of PPEs. Furthermore, they presented the diffusion-controlled release of a model compound, BSA, from porous microspheres made of their copolymer (Figure 1.10).[104]

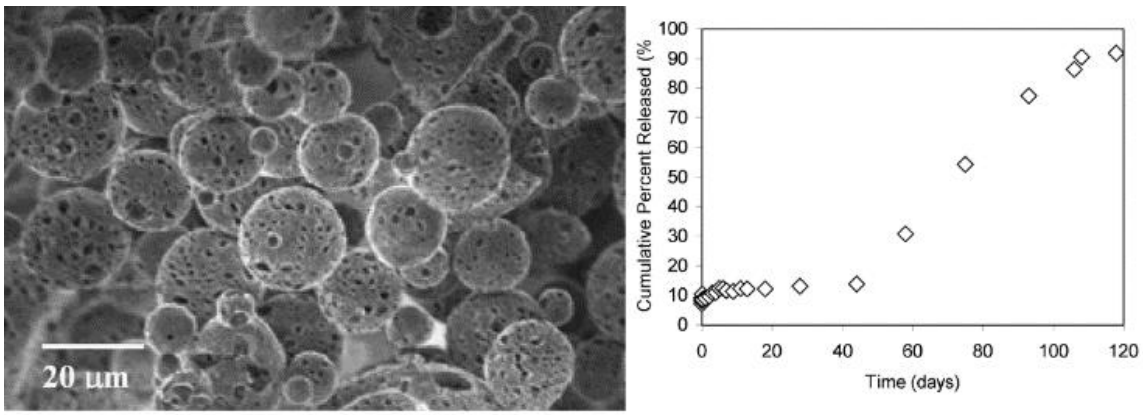

Figure 1.10: SEM image (left) and cumulative release profile of BSA from PLA-EEP microspheres in PBS (pH 7.4) at 37 °C. Copyright @ 2003 Elsevier. Reprinted with permission from Journal of Controlled Release.[104]

The first organocatalytic anionic ring-opening polymerization (oAROP) of cyclic phosphate esters was presented in 2010 by Iwasaki *et al.* They were the first to use the well-known organic bases DBU and TBD (Scheme 1.9, top and middle row) to polymerize 2-isopropoxy-2-oxo-1,3,2-dioxaphsopholane in the presence of a primary alcohol as an initiator.

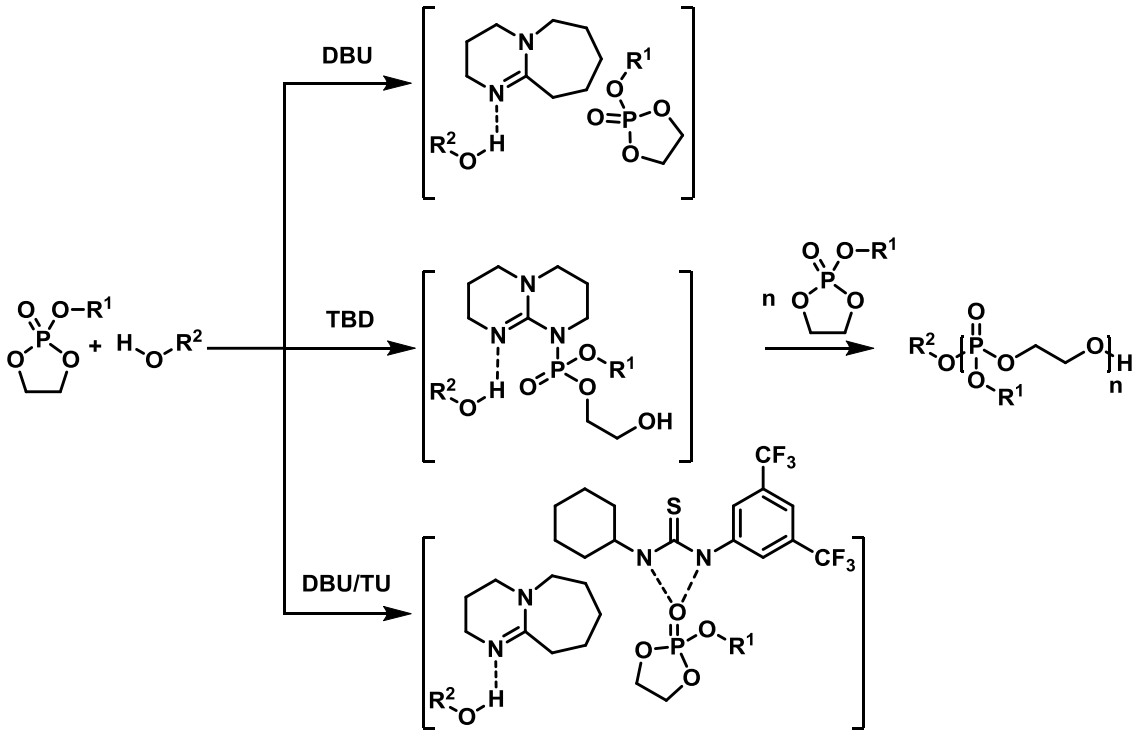

Scheme 1.9: Catalysts for the oAROP of cyclic phosphate monomers and their activation mechanism. Top: activation of initiator/active chain end ROH via DBU. Middle: Dual-activation of initiator/active chain end and monomer via TBD. Bottom: Activation of initiator/active chain end via DBU and activation of monomer via thiourea as a binary catalyst mixture.

Iwasakis investigations showed that this cyclic monomer can be rapidly polymerized with TBD to high conversions (90%) within 20 min at 0 °C. Exceptionally high control over molecular weight and narrow molecular weight distributions ($Đ$ < 1.10) were achieved. A linear dependence of the molecular weight evolution of the polymers to the monomer conversion indicated the absence of side-reactions like transesterifications and depolymerization, a further side-reaction not discussed in the synthesis of PPEs so far.[105]

The polymerization with DBU only gave moderate conversions (up to 60%) and needed reaction times up to 6h, especially for the high monomer to initiator ratios. Nonetheless, for 2-isopropoxy-2-oxo-1,3,2-dioxaphospholane, excellent control over molecular weight and narrow molecular weight distributions were obtained without the occurrence of side-reactions (Figure 1.11).[105]

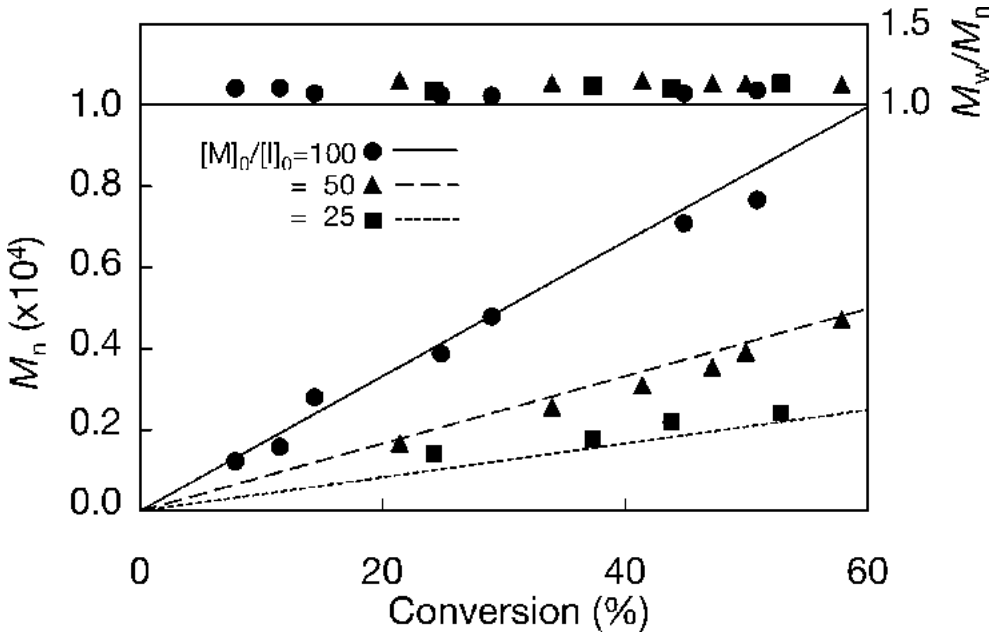

Figure 1.11: Plot of M_w / M_n and M_n versus monomer conversion for the polymerization of 2-isopropoxy-2-oxo-1,3,2-dioxaphospholane catalyzed with DBU for different $[M_0]$ / $[I_0]$ values. Copyright @ 2010 American Chemical Society. Reprinted with permission from Macromolecules.[105]

After this pioneering work on organocatalysis of phosphoesters, bases like DBU and TBD became the state of the art for the polymerization of cyclic phosphate monomers. In the same year, Liu et al. presented the synthesis of PPEs with varying topology, ranging from linear diblock copolymers over star diblock copolymers to hyperbranched PPEs by use of the inimer method (Scheme 1.7, structure 8, inimer).[106] While they synthesized their respective PPE macroinitiator conventional with $Sn(Oct)_2$, the second block was grown via modern DBU catalysis. This combination resulted in moderate molecular weight distributions ($Đ$ < 1.4) and yields (< 78%). Furthermore, they investigated the cell-toxicity of such polymers against NIH 3T3 fibroblasts. This cell line is much less resistant than HeLa cells, but still, no significant toxicity was observed for all copolymers.[106]

In 2012, Zhang *et al.* presented their DBU-catalyzed oAROP of an alkynyl functional phosphoester (Scheme 1.7, structure 6), offering the first side-chain modifiable PPE at that time (Figure 1.12). Polymerization was performed in dichloromethane and proceeded up to near quantitative conversion within 6 min following a first-order kinetic, despite the presence of the acidic alkynyl protons. However, using DBU as a base, molecular weight distributions broadened at conversions above 60%.[107]

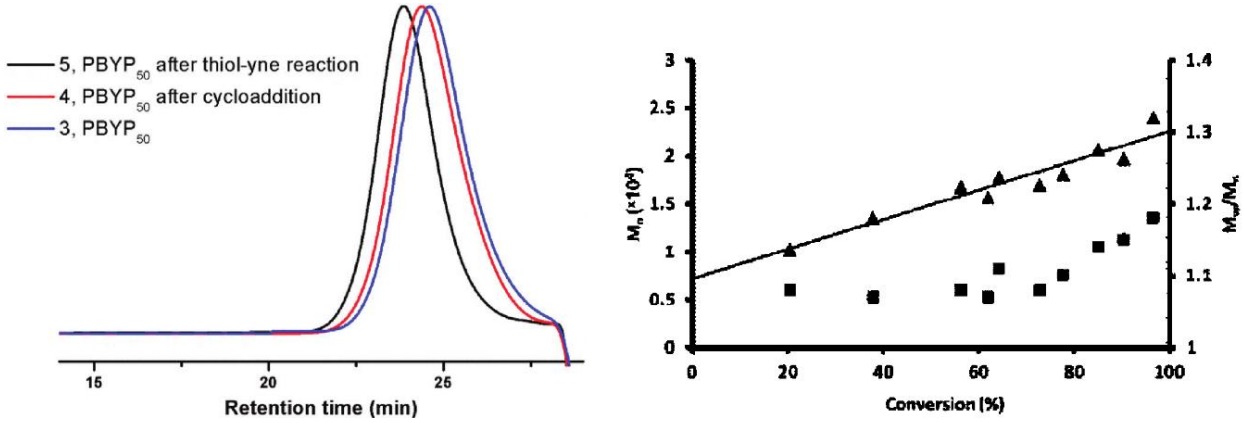

Figure 1.12: Left) SEC traces of alkynyl functional poly(phosphate) before (blue) and after modification via thio-yne (black) and Huisgen cycloaddition (blue). Right) Plot of M_n and M_w / M_n versus monomer conversion for the polymerization of alkynyl functional monomer catalyzed with DBU for $[M_0]$ / $[I_0]$ = 100. Copyright @ 2012 American Chemical Society. Reprinted with permission from ACS Macro Letters.[107]

An essential breakthrough in synthetic procedures was presented in the same year. Clement *et al.* published a detailed kinetic analysis of the oAROP of 2-ethoxy-, 2-isobutoxy-, and 2-butenoxy-2-oxo-1,3,2-dioxaphospholanes.[108] As catalysts, they used DBU, TBD, and a binary DBU / thiourea mixture, which has become popular for the ROP of lactones.[109] Here, the thiourea (Scheme 1.9, bottom row) activates the monomer via H-bonding interactions. They impressively show that these catalytic systems are able to polymerize a variety of dioxaphospholanes following first-order kinetics. However, only the DBU / thiourea mixture effectively suppresses transesterification reactions (Scheme 1.10) at high conversions leading to narrowly distributed ($Đ < 1.10$), high molecular weight (up to 70,000 g mol^{-1}) polymers for conversions above 90% (Figure 1.13).

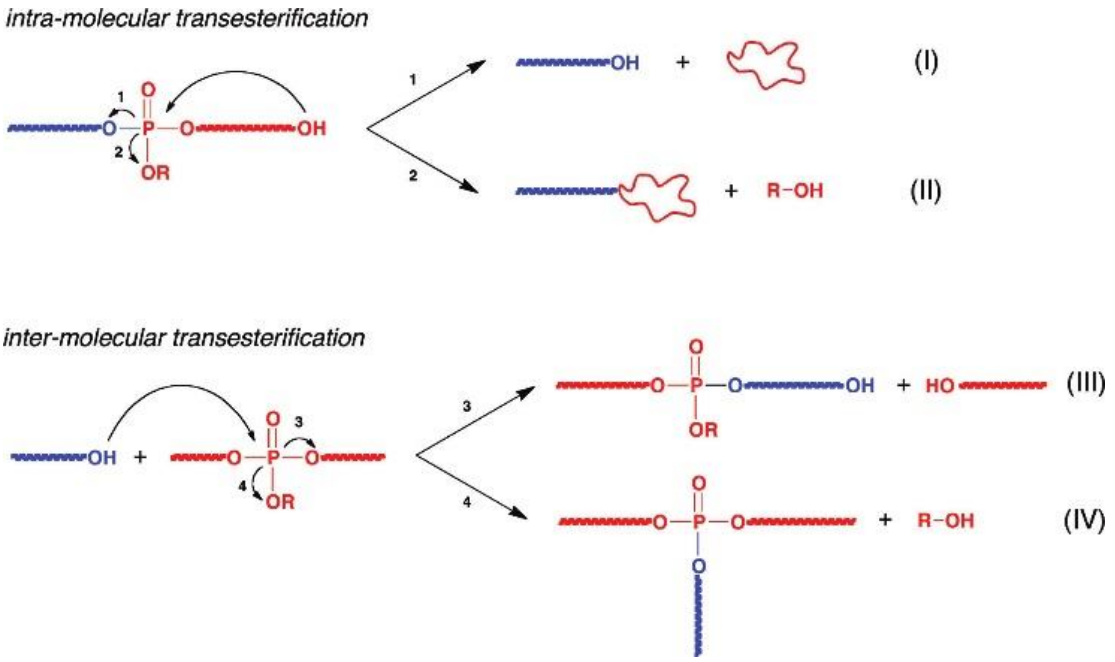

Scheme 1.10: Possible intra- and intermolecular transesterification reactions of poly(phosphoester)s during ROP. Copyright @ 2012 American Chemical Society. Reprinted with permission from Macromolecules.[108]

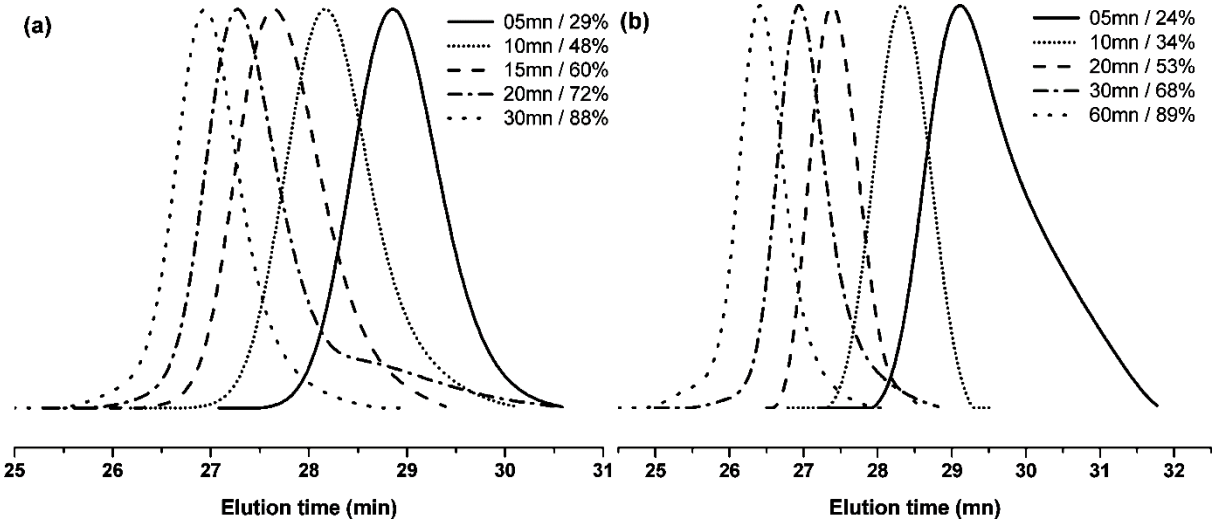

Figure 1.13: SEC traces of the polymerization 2-isobutyl-2-oxo-1,3,2-dioxaphospholane catalyzed with the binary DBU/TU mixture at 0 °C in toluene with $[M_0]$ / $[I_0]$ = 100 (left) and $[M_0]$ / $[I_0]$ = 400 (right). Copyright @ 2012 American Chemical Society. Reprinted with permission from Macromolecules.[108]

The TBD-catalyzed reactions were equally fast as the DBU/TU catalyzed reactions. However, all monomers tend towards transesterifications even after reaching nearly quantitative conversions over time in the presence of TBD (Figure 1.14).

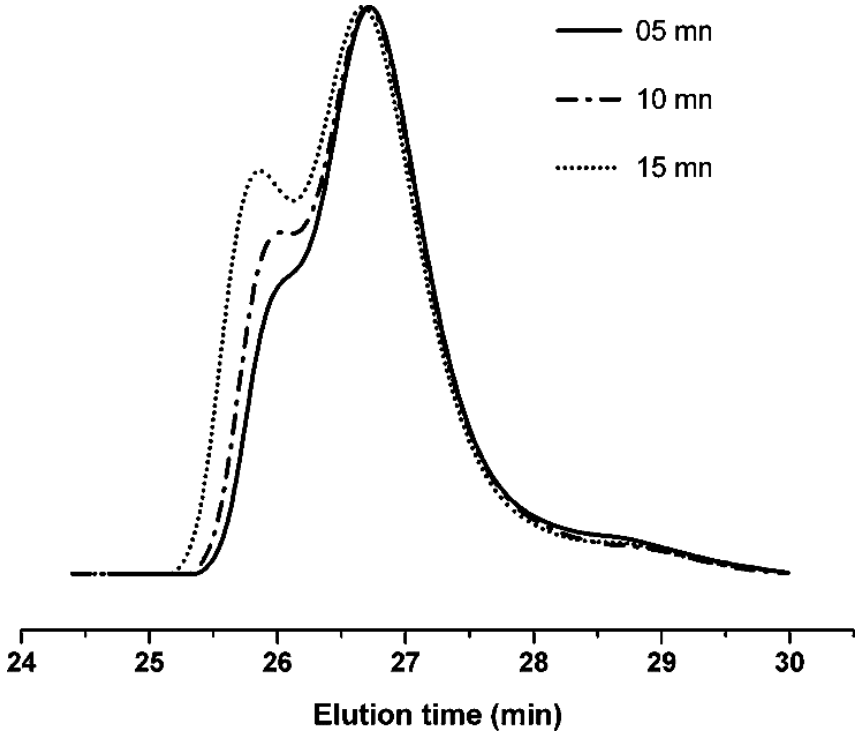

Figure 1.14: SEC traces of the polymerization 2-isobutyl-2-oxo-1,3,2-dioxaphospholane catalyzed with TBD at 0 °C in toluene with $[M_0]$ / $[I_0]$ = 200. Copyright @ 2012 American Chemical Society. Reprinted with permission from Macromolecules.[108]

The DBU catalyzed reactions, again, need to be terminated at low conversions (around 50 to 60%) to avoid side-reactions and broadening of the molecular weight distributions for all monomers (Figure 1.15).[108] Since the publishing of these results, several research groups have focused their work on the synthesis and biomedical applications of PPEs and have either used DBU, TBD or the binary DBU / thiourea (TU) mixture as the respective catalysts. In all cases the binary catalyst system or TBD have proven to be superior to the (much less expensive) DBU catalysis.

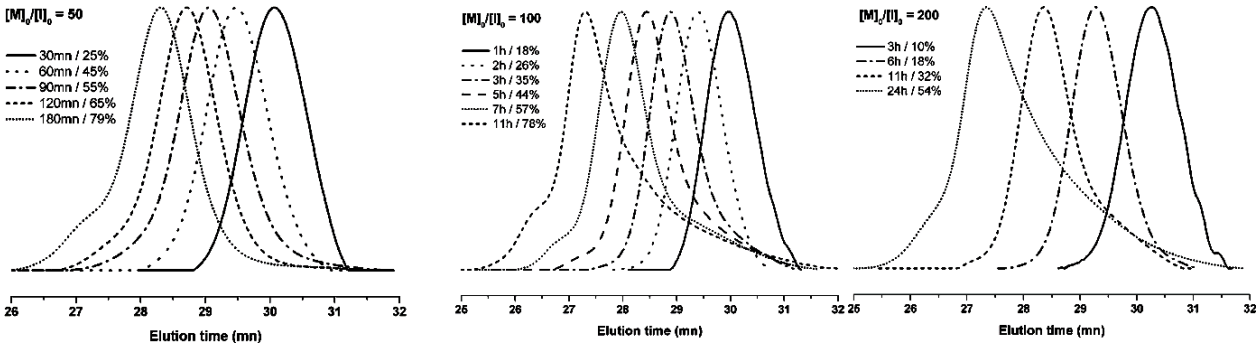

Figure 1.15: SEC traces of the polymerization 2-isobutyl-2-oxo-1,3,2-dioxaphospholane catalyzed with DBU at 0 °C in toluene with $[M_0] / [I_0] = 50$ (left), $[M_0] / [I_0] = 100$ (middle) and $[M_0] / [I_0] = 200$ (right). Copyright @ 2012 American Chemical Society. Reprinted with permission from Macromolecules.[108]

The following paragraphs feature and shortly discuss a few selected publications showing the potential of oAROP for PPE synthesis and respective applications:

In 2013, Steinbach *et al.* investigated the copolymerization behavior of dioxaphospholanes with 4-exo-substituted dioxaphospholanes via TBD catalysis to gain insight into the microstructure of such copolymers. A random incorporation of 2-ethoxy-2-oxo-1,3,2-dioxaphospholane and the 4-exo-substituted dioxaphospholane was proven.[110]

Lim *et al.* expanded the scope of side-chain functional PPEs by the DBU-catalyzed polymerization of a vinyl ether functional dioxaphospholane. They utilized different side-chain modifications, ranging from acetalization over thioacetalization to thiol-ene reactions. The polymers aggregation behavior into polymeric nanoparticles, their degradation in water and negligible cell-toxicity against RAW 264.7 macrophage cells as well as OVCAR-3 human ovarian adenocarcinoma cells was reported.[111]

An interesting work was presented in 2015 when Gao *et al.* used the DBU/TU mixture to catalyze the polymerization of 2-ethoxy-2-oxo-1,3,2-dioxaphospholane initiated from polyethylene-OH with a P_n of 680, showing the effectiveness of this catalytic mixture even for difficult initiator systems. In all cases molecular weight distributions below 1.15 and good control over the molecular weight up to 44,000 g mol^{-1} was achieved. The obtained polymers showed no cell-toxicity against HeLa-cells.[112]

Zhang *et al.* synthesized a block copolymer composed of an alkynyl substituted PPE and poly(lactic acid) by sequential polymerization. Their goal was the synthesis of an amphiphilic, degradable polymer with anionic charges in the side chain for complexation of antimicrobial active silver complexes (Figure 1.16).[113]

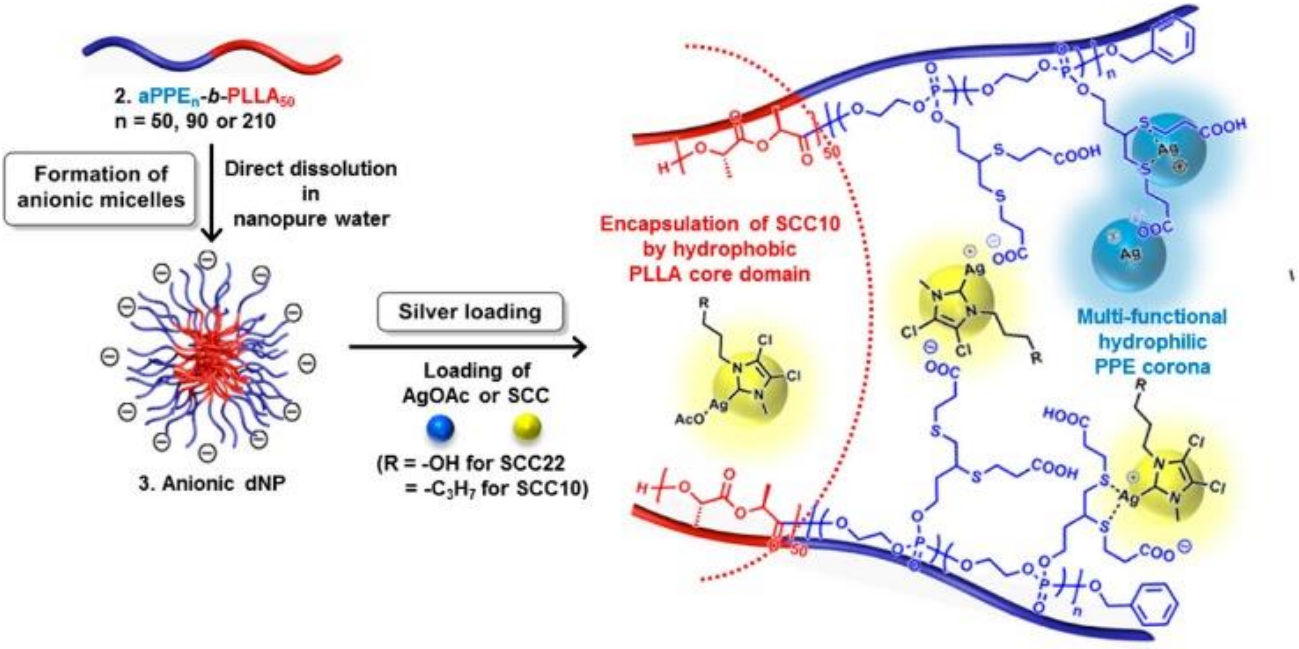

Figure 1.16: Schematic illustration of the work presented by Zhang *et al.*: Formation of PPE-b-PLLA block copolymer, the formation of micelles in solution and complexation of antimicrobial active silver complexes. Copyright @ 2015 American Chemical Society. Reprinted with permission from ACS Nano.[113]

In parallel, they presented the sequential synthesis of a PPE-*b*-PPE block copolymer with hydrophobic and alkynyl side-chains for paclitaxel incorporation and potential for click-side-chain modification. The high polymerization rate of the TBD catalyzed reaction made these polymers available within 10 min of total synthesis time.[114]

In 2016, Baeten *et al.* deviated from the traditional batch chemistry in glass reactors. They demonstrated dioxaphospholane polymerization either with the DBU/TU mixture or TBD and with subsequent thiol-ene reaction under continuous flow conditions (Figure 1.17).[115]

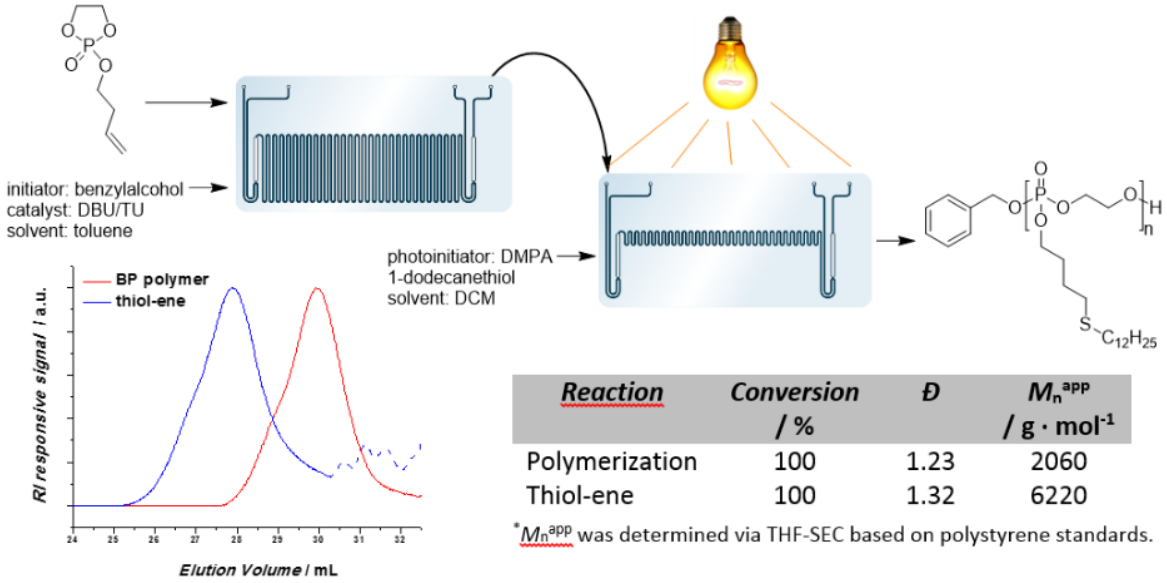

Reaction	Conversion / %	Đ	M_n^{app} / g · mol^{-1}
Polymerization	100	1.23	2060
Thiol-ene	100	1.32	6220

*M_n^{app} was determined via THF-SEC based on polystyrene standards.

Figure 1.17: Schematic representation of the microfluidic cascade consisting of a two-stage microreactor. First, polymerization of the alkene-functional cyclic phosphate with DBU/TU in toluene and subsequent photochemical thiol-ene reaction with 1-dodecane thiol. Copyright @ 2016 Elsevier. Reprinted with permission from European Polymer Journal.[115]

Wu *et al*. developed a tandem strategy to synthesize ABA triblock copolymers starting with the B block being synthesized by metal-catalyzed CO_2 / epoxide polymerization followed by DBU catalyzed oAROP of a dioxaphospholane.[116]

Schöttler *et al.* proved in 2016 that poly(2-ethoxy-2-oxo-1,3,2-dioxaphospholane) can be covalently attached to and stabilize polystyrene nanoparticles. Furthermore, they demonstrated that these polymers exhibit the same stealth behavior as poly(ethylene glycol), both regarding their cell-uptake and the protein adsorption in human blood plasma.[11] In a follow-up work, Müller *et al.* prepared PPE surfactants and similarly reduced the protein adsorption to the covalently attached PPEs.[117]

In 2017, Becker *et al*. introduced furfuryl containing dioxaphospholanes and used this platform for the first reversible PPE side-chain modification via *Diels-Alder* reaction. The hydrophilicity of the resulting polymers was analyzed via UV-VIS turbidity measurements regarding the attached side-chain. Furthermore, they presented the first detailed copolymerization online-NMR-kinetics of dioxaphospholanes, showing a preferred incorporation of the furfuryl monomer over the sterically less demanding ethyl monomer

(Figure 1.18). The formation of such a gradient microstructure needs to be considered during copolymerization as the microstructure greatly alters the polymer properties, such as solubility or distribution of reactive groups in the backbone.[118]

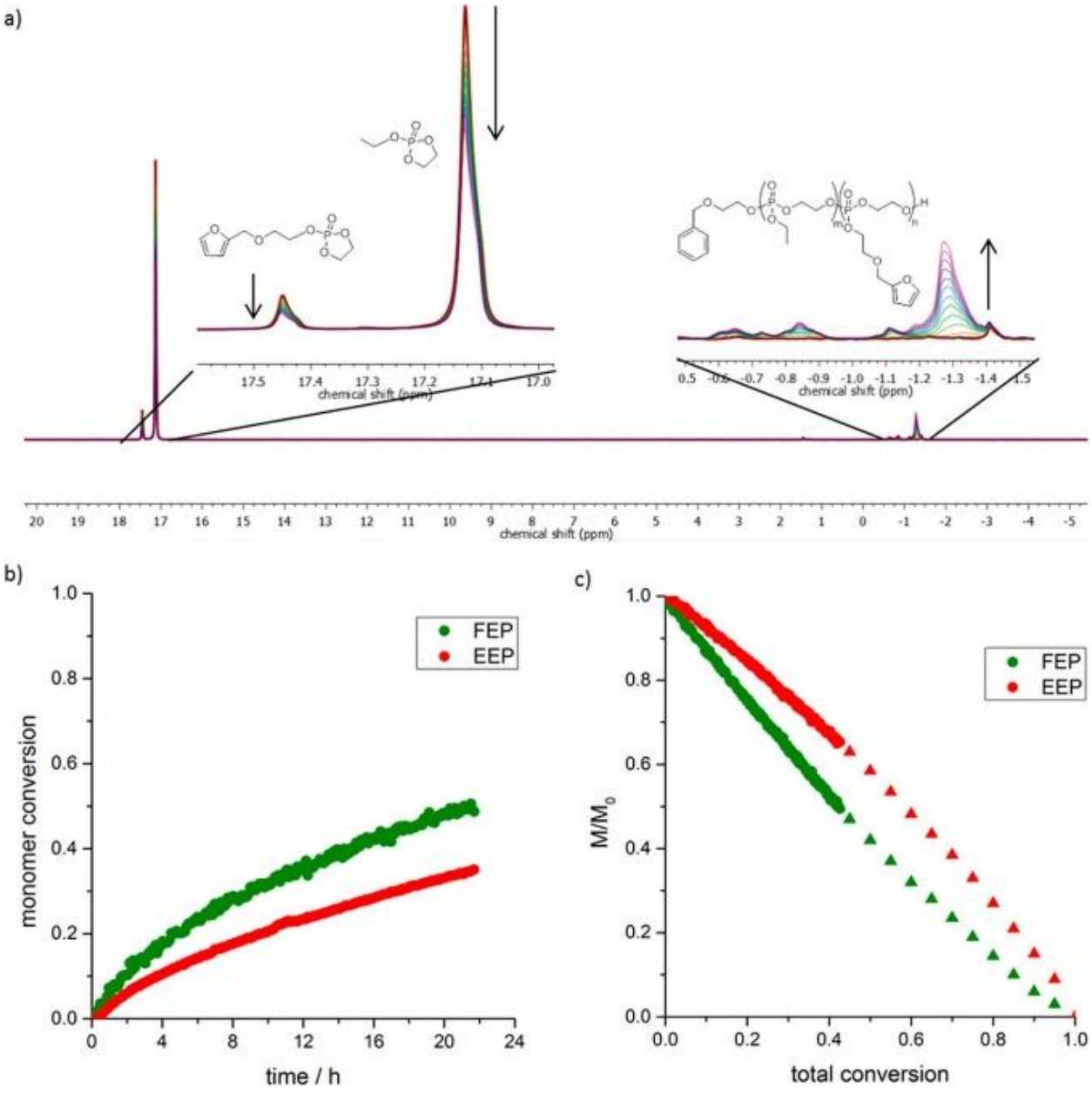

Figure 1.18: Real-time $^{31}P\{H\}$ NMR kinetics of the copolymerization of 2-ethoxy-2-oxo-1,3,2-dioxaphospholane (EEP, red) and the furfuryl functional cyclic phosphate (FEP, green): a) overlay and zoom-in into $^{31}P\{H\}$ NMR measurements, b) monomer conversion vs. time, and c) normalized monomer concentrations in the reaction versus total conversion. Copyright @ 2017 American Chemical Society. Reprinted with permission from Macromolecules.[118]

A potential alternative to the abovementioned catalysts DBU, TBD and DBU/TU was presented in 2014 by Stukenbroeker *et al.*. They reported the zwitterionic ring-opening polymerization of 2-isopropoxy-2-oxo-1,3,2-dioxaphospholane initiated with an *N*-heterocyclic carbene in the absence of alcohol initiators. Molecular weights up to 200,000 g mol^{-1} with moderate molecular weight dispersity ($Đ$ < 1.3) and mainly cyclic topology were obtained within minutes (Scheme 1.11).[119]

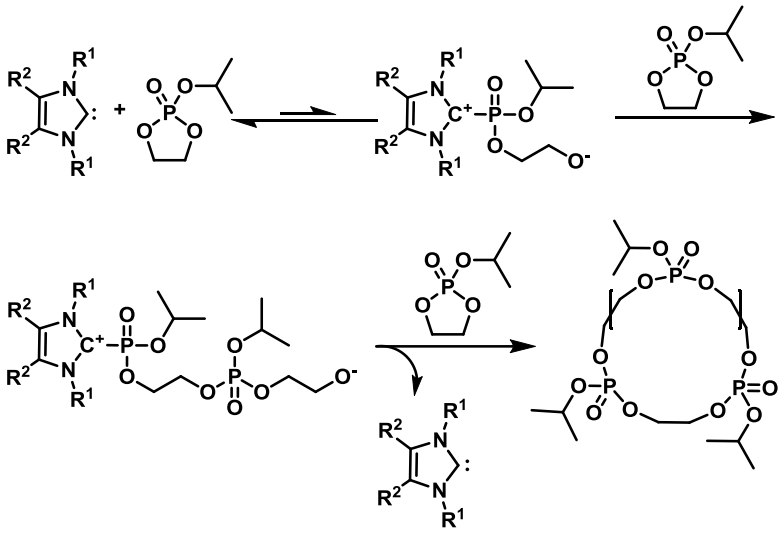

Scheme 1.11: Proposed mechanism for the zwitterionic ring-opening polymerization of 2-isopropoxy-2-oxo-1,3,2-dioxaphopspholane catalyzed with various N-heterocyclic carbenes. Copyright @ 2014 American Chemical Society. Adapted and reprinted with permission from Macromolecules.[119]

In conclusion, poly(phosphate)s are now a class of polymers that can be synthesized with excellent control over molecular weight, narrow molecular weight distributions, and a multitude of functional side-chains with varying topologies and microstructures. The polymerization catalyzed with TBD or the binary DBU/TU system proceeds within minutes to high conversions at low temperatures. Only the later binary system seems to be able to fully suppress side-reactions occurring at high conversions (as in the case of DBU) or longer reaction times (in the case of TBD). The use of an NHC catalysts provides access to the synthesis of high M_n cyclic polymers. A large quantity of different homo-, random-, or block copolymers has been synthesized for diverse applications in recent years. The overall low toxicity, degradability, and functionality makes poly(phosphate)s a seminal class of polymers, especially in the field of biomedical applications.

Alternative Phosphorus-Containing Polymers: Poly(phosphonates)s

Phosphonic acids and phosphonic acid esters in nature

Poly(phosphonic acid ester)s are a sub-class of poly(phosphoester)s, bearing a single P-C bond, instead of a third P-O bond (Scheme 1.12). The change from the electron withdrawing R-O-R group into an electron donor (R-CH_2-R, hyper-conjugation of the C-H σ-bonds with orbitals of the phosphorus) alters their reactivity significantly. The increased electron density at the phosphorous atom impedes nucleophilic attacks. Furthermore, unlike the P-O-R bond, the P-CH_2-R bond is not susceptible towards hydrolysis or transesterification reactions and only cleavable under harsh thermal, radical conditions.

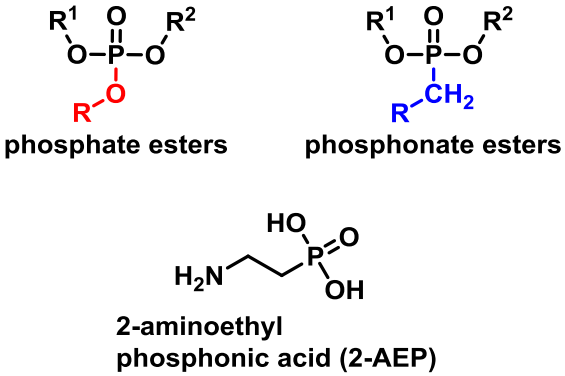

Scheme 1 .12: General structure of phosphoric acid esters (red) and the in the following discussed phosphonic acid esters (blue). Explicit structure of 2-aminoethyl phosphonic acid (2-AEP), the first isolated natural phosphonic acid).

In nature, phosphonic acids are not as wildly spread as phosphates but still present a significant phosphorus reservoir.[120] Recent ^{31}P NMR studies showed that 20-30% of the maritime phosphorus is bound in the form of phosphonic acid derivatives, making phosphonic acids an essential part of the maritime phosphorus cycle.[121] In some organisms phosphonates are even the dominant phosphorus species: 95% of phosphorus in the freshwater snail *Helisoma* is bound in the form of 2-aminoethyl phosphonic acid (2-AEP, Scheme 1.12) modified polysaccharides.[122]

2-AEP was also the first naturally occurring phosphonic acid to be discovered in 1959 in protozoa from sheep rumen.[123] Since then, phosphonates have been identified in many organisms in the form of phosphonylated polysaccharides, lipids, and low molecular weight compounds (Scheme 1.15).[120,124]

In the 60 years since the initial discovery, the biosynthetic pathways of 2-AEP and other phosphonates were elucidated. The pathways were found to be well conserved, centering around the building block phosphono acetaldehyde and the enzyme phosphoenolpyruvate phosphomutase (Ppm).[120] The enzyme catalyzes the isomerization of phosphoenolpyruvate, an essential part of primary metabolism, into the phosphonic acid derivative. *In vivo*, the equilibrium favors the phosphate form. However, the subsequent and irreversible decarboxylation reaction catalyzed by phosphonopyruvate decarboxylase (Ppd) shifts the equilibrium towards the phosphonate form and produces the desired phosphono acetaldehyde as building block for further biosynthesis.[120] (Scheme 1.13)

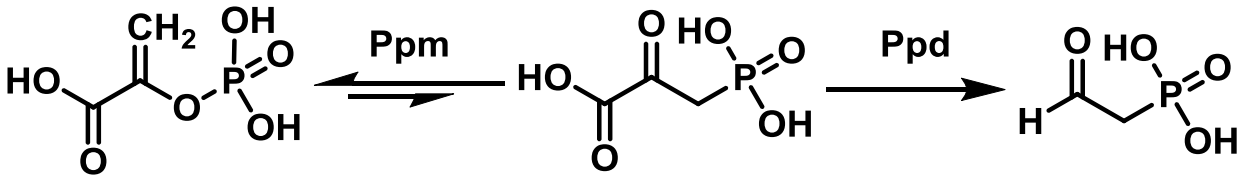

Scheme 1.13: Schematic biosynthetic pathway of the synthesis of phosphono acetaldehyde: Isomerization of phosphoenolpyruvate into phosphonopyruvate via the key enzyme, phosphoenolpyruvate phosphomutase (Ppm). Subsequent and irreversible decarboxylation into phosphono acetaldehyde by phosphonopyruvate decarboxylase (Ppd).

In the 1970s, the first biochemical phosphonate catabolism was discovered. Since then, different phosphonate catabolism pathways have been discovered. However, the first discovered pathway, the so-called C-P lyase pathway, has been studied in most detail as it is available in microorganism like *E. coli.* These bacteria have been found to catabolize methyl phosphonic acid under phosphate deficit conditions and produce methane in the process.[125]

The catabolic reaction is catalyzed by a multi-enzyme complex consisting of 14 (partially transmembrane, crystal structure elucidated in 2015) enzymes and the reaction mechanism has been elucidated only recently. The complex reaction involves the radical cleavage of the P-C bond (Scheme 1.14).[120]

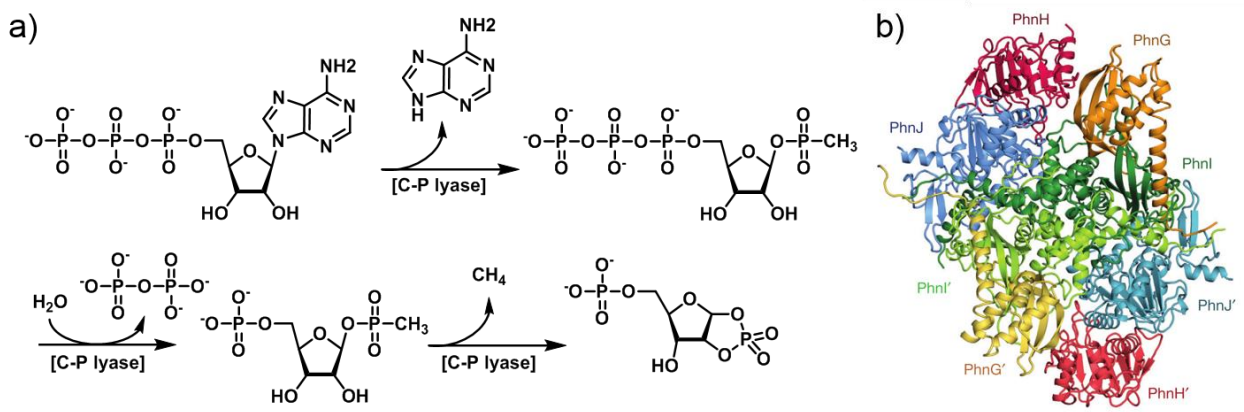

Scheme 1.14: a) Schematic presentation of the reaction catalyzed by the C-P lyase. Initial transfer of methyl phosphonic acid onto ATP, followed by hydrolysis of the tri-anhydride and finally radical P-C bond cleavage resulting in liberation of methane and the formation of a bicyclic phosphor-ribose. All schematically shown reactions are catalyzed by several enzymes and performed in multiple steps.[120] b) Crystal structure of the C-P lyase core complex with a molecular weight of 240KDa. Reprinted with permission from Nature Publishing Group.[125]

The exact reason for natures occasional use of phosphonates over phosphates is still unclear. It has been hypothesized that the chemical stability of the P-C bond towards hydrolysis and phosphatases enhances the stability of the respective lipids and sugars.[120,124] It was proven that phosphonates are directly involved in some signal transduction pathways, and that specific microorganisms can use phosphonates as phosphorus sources for their metabolism under phosphate deficit conditions.[120,124] Another hypothesis considers phosphonic acid as relics from an early earth with a more reductive and aggressive environment. This hypothesis is backed by the detection of various phosphonic acids brought to Earth on the *Murchison* meteorite in 1969, pointing towards a prebiotic origin of phosphonates.[120,124]

Most low molecular weight phosphonates possess a high biological activity. Prominent naturally occurring phosphonates are the anti-malaria drug fosmidomycin or the broad-band antibiotic fosfomycin, both of which are clinically used (Scheme 1.15).[126] The biological activity often originates from the high homology to phosphates but a slower rate of hydrolysis. This often results in the inhibition of a usually highly specific enzyme (Scheme 1.15) and makes phosphonates interesting candidates for the screening of new drugs.[127] The high activity is also used in the rational design of synthetic phosphonates. By far the most successful synthetic phosphonate is the broad-spectrum herbicide glyphosate, which was the most used herbicide (8.6 x 10^9 kg used worldwide since 1974, as of 2014) before falling into disrepute in 2015 (Scheme 1.15).[128]

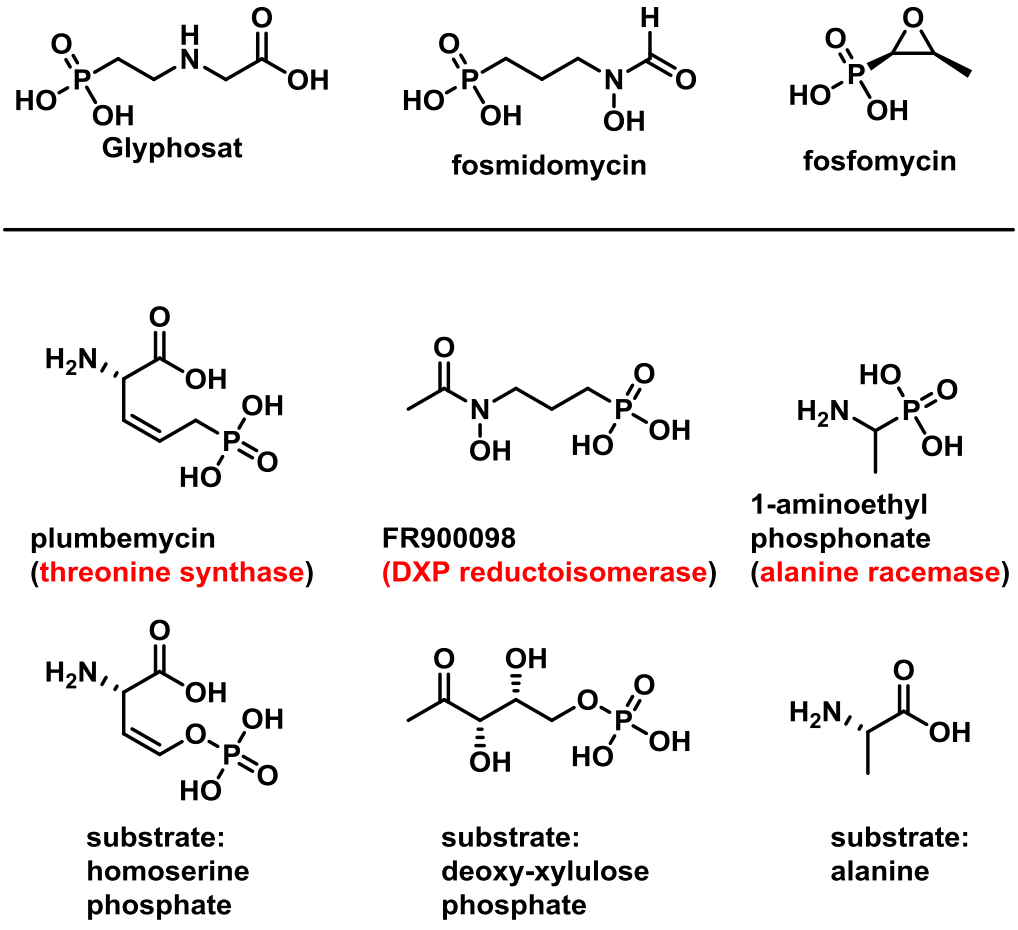

Scheme 1.15: Top: Structure of the naturally occurring phosphonic acid derivatives glyphosate (synthetic herbicide), fosmidomycin (natural anti-malaria drug), and fosfomycin (natural broad-band antibiotic). Bottom: Structure of some naturally occurring phosphonates and the enzyme (in red) they inhibit due to their resemblance of the natural enzyme substrate.[124]

Poly(phosphonic acid ester)s: Poly(phosphonate)s

In organic synthesis, phosphonic acid esters are known since the beginning of the 20th century, when *Arbuzov* and *Michaelis* first reported their synthesis from tri-*O*-alkyl phosphites. Due to their α-C-H acidity, they are used in organic synthesis, e.g., in the stereospecific synthesis of *E*-olefins (*Horner-Wadsworth-Emmons* Reaction) since the 1950s.[129,130] Furthermore, synthetic phosphonates are important ligands for metal ions and have become an indispensable asset in metal-catalytic chemistry.[131]

In macromolecular chemistry, especially for anionic polymerizations, the α-C-H acidity poses the potential issue and might induce side-reactions by deprotonation. However, the pK_a value of the α-proton of non-activated phosphonic acid esters is in the range of 30.[132,133] Significant deprotonations in the presence of typical organic bases for anionic polymerization ($21 < pK_a < 25$) is therefore unlikely. Additionally, these polymerizations are usually performed in the presence of an alcohol as an initiator, which possesses by far the most acidic proton in the mixture.

Still, the controlled synthesis of polymeric phosphonates was and still is a challenging topic in academic research. Consequently, the first synthetic poly(phosphonate)s were synthesized by polycondensation reactions of phosphonic acid esters/chlorides with the corresponding diols. Millich *et al.* has reported pioneering work in a series of publications describing the “Interfacial Synthesis of Polyphosphonate and Polyphosphate Esters” starting in 1969.[134-137] This lead to the development of mainly aromatic poly(phosphonate)s with excellent properties as flame retardant materials, a field in which they are being used as of today (e.g., FRX Polymers).[138] Research in more controlled synthetic pathways towards poly(phosphoester)s, however, was nearly exclusively being performed on poly(phosphate)s. A more comprehensive review concerning the history, synthesis, degradation, and applications of poly(phosphoester)s in general and poly(phosphonate)s, in particular, has recently been published by Bauer *et al*..[89]

The first synthesis of poly(phosphonate)s via ring-opening polymerization, while not finding much attention at the time, was reported in 1973 by Sharov *et al.*. They were the first to describe the thermal ring-opening polymerization of fluorinated cyclic alkylene alkyl(aryl) phosphonates with varying exocyclic side-chains (Scheme 1.16).[139] However, no detailed mechanistic investigations of the polymerization was presented.

Their goal was the investigation of the polymerizability of the monomers and compare the polymer properties with the respective poly(phosphate) derivatives. They report a reduced tendency towards ring-opening polymerization and a higher susceptibility to hydrolysis compared to the phosphate derivates. While not being investigated extensively, the use of sodium heptafluoro butylate was found to increase the propagation rates. Again, no mechanistic insights were presented as to whether the butylate functioned as initiator or catalysts. Still, this publication presents the first anionic ring-opening polymerization of cyclic phosphonate monomers.[139]

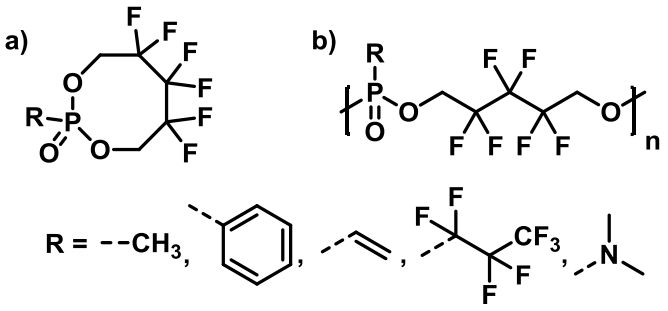

Scheme 1.16: a) structure of cyclic phosphonate and b) proposed structure of poly(phosphonate)s after thermal ring-opening polymerization by Sharov *et al.*.

In 1977, during their ongoing work on the polymerization of six-membered cyclic phosphoesters, Lapienis *et al*. published the polymerization of 2-hydro-2-oxo-1,3,2-dioxaphopsphorinane. Unlike six-membered phosphate monomers, this six-membered H-phosphonate polymerized readily in the presence of traditional anionic and cationic initiators. Yields up to 70% and molecular weights up to 10,000 g mol^{-1} were reported. The authors highlighted the polymers exceptionally high susceptibility to hydrolysis as well as the potential of the P-H bond being transformed into P-C, P-O and P-N derivatives.[140]

Apart from these pioneering works in the 1970's, however, the ring-opening polymerization of cyclic phosphonic acid esters did not receive any attention in academic or industrial research.

In 2014, Steinbach *et al.* revived the academic interest in poly(phosphonate)s by presenting the synthesis and polymerization of a five-membered cyclic methyl phosphonic acid ester: 2-methyl-2-oxo-1,3,2-dioxaphospholane (Scheme 1.17).[141] The idea was to eliminate the potential side-chain transesterification reactions occurring during the DBU catalyzed polymerization of 2-alkoxy-2-oxo-1,3,2-dioxaphospholane. To this end, the hydrolytically labile P-O-R side-chain was substituted by a hydrolytically stable P-CH_3 bond.

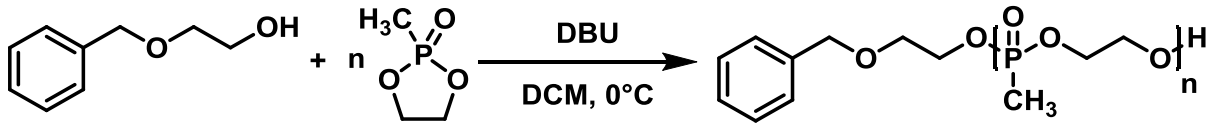

Scheme 1.17: First organocatalytic anionic ring-opening polymerization of five-membered 2-methyl-2-oxo-1,3,2-dioxophospholane with DBU catalysis.[141]

The polymerization proceeded under DBU catalysis by initiation with a primary alcohol in DCM at 0 °C in 30 min. However, propagation was considerably slower than the respective cyclic phosphate monomer. Degrees of polymerization of up to 200, resulting in polymers with molecular weights of 24,000 g mol^{-1}, were obtained. Narrow molecular weight distributions ($Đ$ < 1.10, Figure 1.19) were achieved even at high conversions up to 90%. Under the same reaction conditions, the respective phosphate polymerization needs to be terminated at 50-60% conversion to prevent transesterification reactions.[108] The polymerization follows linear first-order kinetics, without broadening of molecular weight distributions or loss of control at high conversions, indicating a living polymerization (Figure 1.19).

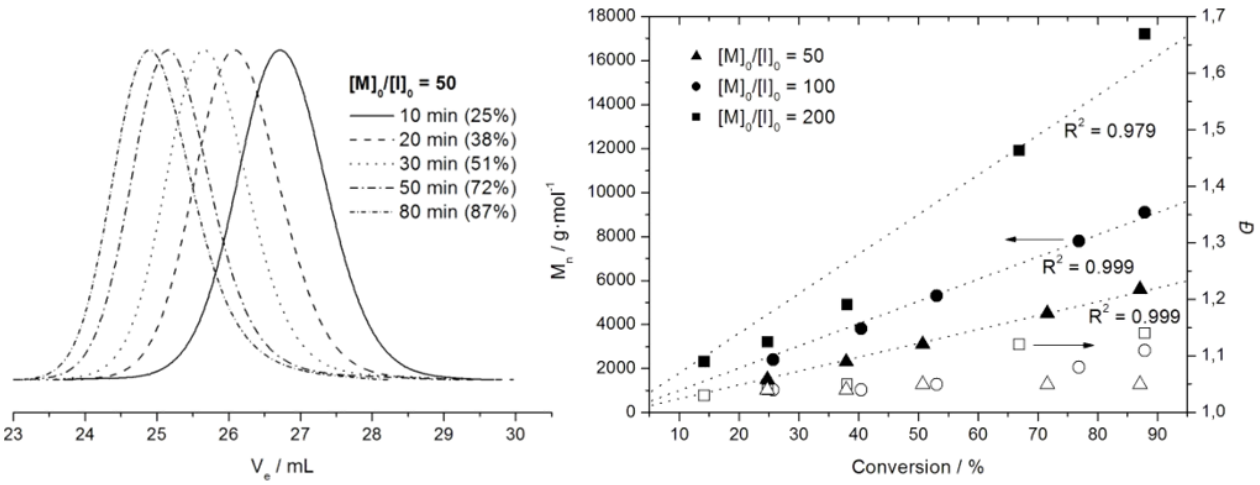

Figure 1.19: Left: Kinetic studies, the plot of M_n and $Đ$ versus the conversion of MeEP during the oAROP catalyzed with DBU in DCM at 0 °C. $[M_0]$ / $[I_0]$ varied from 50 to 200. Right: SEC analyses of the polymerization MeEP, catalyzed with the DBU at 0 °C in DCM with $[M_0]$ / $[I_0]$ = 50 at different times of the polymerization. Copyright @ 2014 American Chemical Society. Reprinted with permission from ACS Macro Letters.[141]

Furthermore, poly(2-methyl-2-oxo-1,3,2-dioxaphospholane) (PMeEP) was water soluble, non-cell toxic against HeLa-cells, and degraded hydrolytically. The degradation rate by hydrolysis was dependent on pH and faster under basic conditions.[141]

PMeEP was also the first poly(phosphonate) from AROP used in the field of biomedical science. Steinbach *et al.* presented the first protein-PMeEP conjugate in 2016.[142] The DBU catalyzed polymerization of 2-methyl-2-oxo-1,3,2-dioxoaphsopholane was terminated with *N,N'*-disuccinimidyl carbamate (DSC) to produce an active-ester functional poly(phosphonate) in one step with excellent yields, a high degree of ω-functionality and narrow molecular weight distribution. Two enzymes, BSA as a model compound and uricase as a medically relevant drug against gout, were modified with PMeEP and PEG. In a first study, the conjugation efficiency and residual enzyme activity were reported to be comparable to the PEG control model. A significant advantage over PEG, however, was the possibility to degrade the phosphonate backbone (Figure 1.20).[142] In a second study, the relaxation dynamics of the PMeEP-protein conjugates were analyzed by neutron scattering. Therefore, fully deuterated MeEP was synthesized an used for the polymerization and subsequent conjugation.[143]

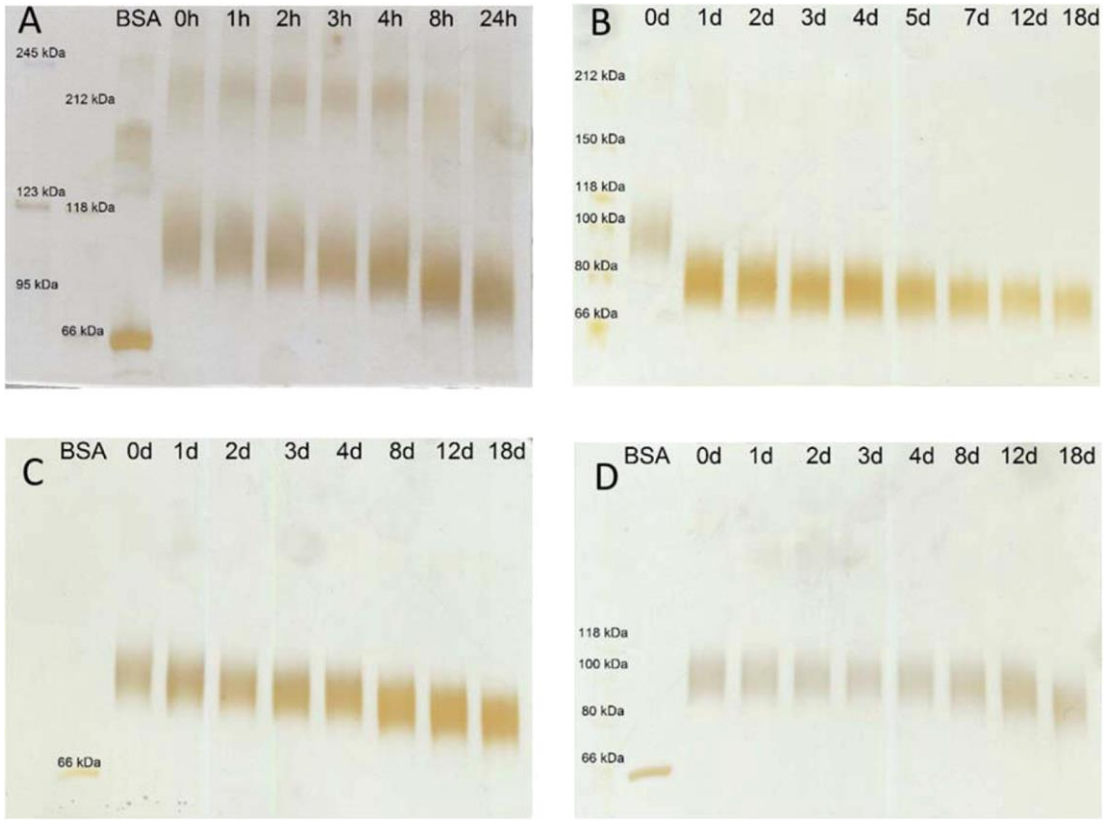

Figure 1.20: SDS-PAGE visualizing the degradation of the PPE conjugated to BSA incubated in aqueous buffer at pH 9.0 (a, b), pH 7.4 (c), and pH 5.0 (d). Copyright @ 2016 American Chemical Society. Reprinted with permission from Bio-macromolecules.[142]

Following these results, Wolf *et al*. presented a systematic investigation of the synthesis and polymerization of higher homologs of 2-alkyl-2-oxo-1,3,2-dioxaphospholanes.[144] In general, *n*-alkylated cyclic phosphonates readily polymerize under DBU catalysis (Scheme 1.18, top and middle row).

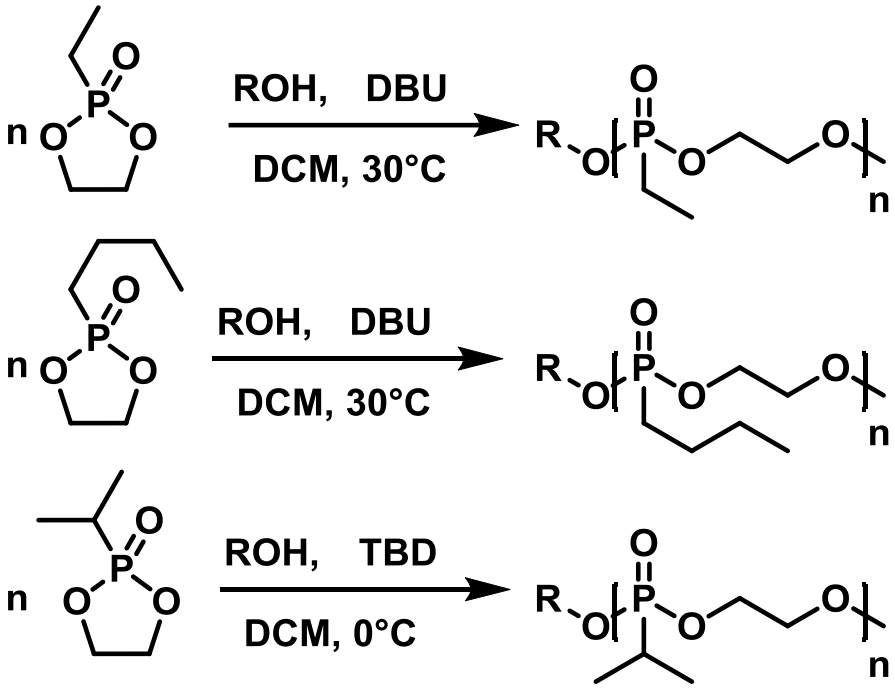

Scheme 1.18: DBU catalyzed anionic ring-opening polymerization of 2-alkyl-2-oxo-1,3,2-dioxaphospholanes.[144]

Due to the stronger inductive effect compared to the methyl derivative, both reaction time and temperature needed to be increased. Under optimized conditions (30 °C, 17h), however, well-defined polymers with excellent control over molecular weight (up to 6,000 g mol^{-1}) and rather narrow molecular weight distributions ($Đ$ < 1.25) were obtained. Again, no transesterification reactions were observed even at conversions above 90%. For the polymerization of 2-isopropyl-2-oxo-1,3,2-dioxaphospholane, the more reactive catalyst TBD was necessary to promote the polymerization (Scheme 1.18, bottom row). The need for a catalyst change could be attributed to steric hindrance as well as a more pronounced inductive effect of the secondary alkyl chain, increasing the electron density at the phosphorous thus impeding nucleophilic attacks.

Nonetheless, conversions above 90% were obtained, and the polymerization proceeded with excellent control over molecular weight and molecular weight distribution.

The ethyl and isopropyl substituted polymers were found to be water-soluble and non-cell toxic, whereas the *n*-butyl derivative was somewhat less water-soluble, showed LCST behavior in aqueous solution and a slight toxicity against HeLa-cells at high concentrations. Variation of the side-chain further altered the hydrolysis rate of the polymers significantly. While the methyl derivative hydrolyzed readily within hours at pH 9, the ethyl and isopropyl polymers remained stable for days to weeks under the same conditions, respectively.[144]

McDonald *et al.* published a comprehensive study of catalysts for the polymerization of cyclic phosphonate monomers.[145] They used the previously presented 2-methyl-2-oxo-1,3,2-dioxaphospholane as a model monomer. Concerning organic bases, under otherwise identical conditions, they observed a linear relationship between the pK_a of the base and the monomer conversion (Scheme 1.19).

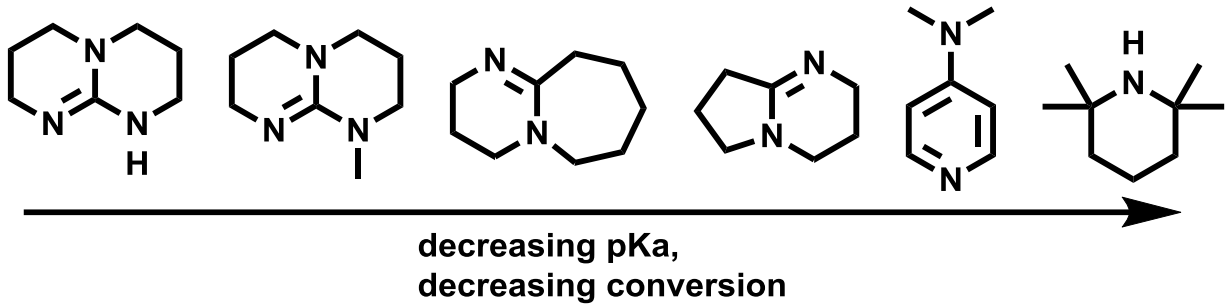

Scheme 1.19: Organocatalysts capable of polymerizing 2-methyl-2-oxo-1,3,2-dioxaphospholane in order of decreasing pK_a value.[145]

Only TBD, with its known dual-activation of chain-end and monomer, did not fit this linear trend as conversion was higher than expected from its pK_a value (Figure 1.21). Furthermore, a minimum pK_a of 14 was found to be necessary to initiate the polymerization, whereas high molar mass materials were only observed for catalysts with a pK_a of at least 19.

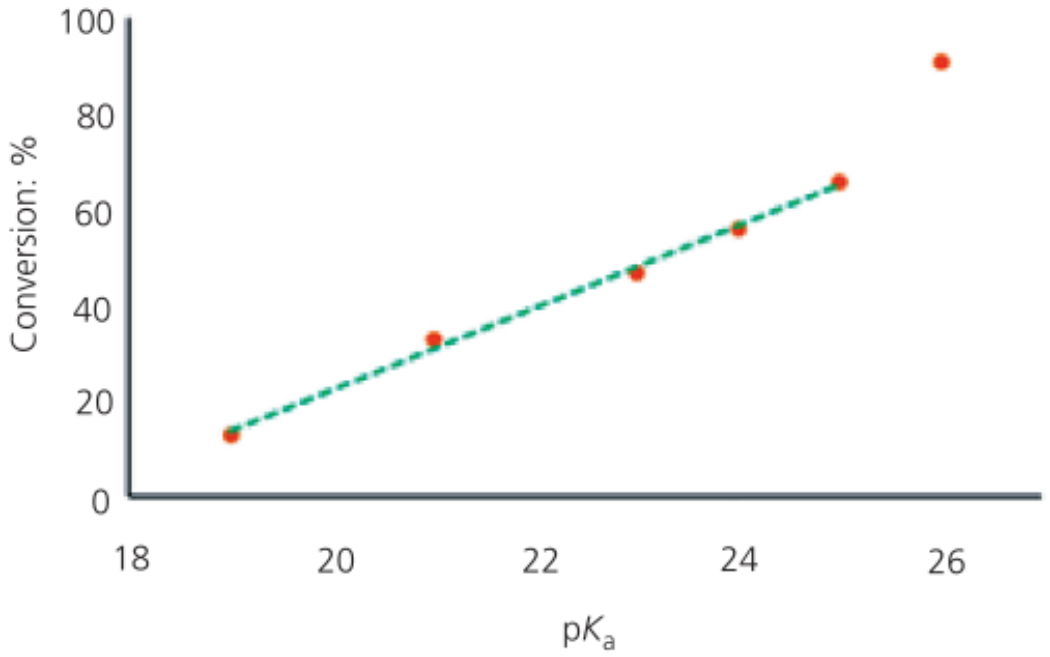

Figure 1.21: Plot of monomer conversion after 4h of polymerization versus pKa value of utilized catalyst for the polymerization of MeEP in DCM at 0 °C. Copyright @ 2016 ICE Publishing. Reprinted with permission from open access journal Green Materials.[145]

Interestingly, apart from slow initiation observed in the presence of DMAP, all able catalysts produced narrowly distributed polymers. This was attributed to the monomers low tendency towards transesterification reactions.[145]

Under the same reaction conditions (4h, room temperature, DCM), polymerization with $Sn(Oct)_2$ was not successful. However, the more reactive aluminum salen and salan complexes produced well-defined polymers with excellent yields and no loss of control. Finally, they tried to expand the monomer scope by synthesizing bicyclic and aromatic dioxaphospholane derivatives. However, these monomers did not polymerize under all investigated conditions.[145]

To increase the glass transition temperature of poly(ethylene alkyl phosphonate)s, inherently low T_g materials (T_g ~ -40 °C) a cyclohexyl substituted monomer was designed by Wolf *et al.* (Scheme 1.20).[146]

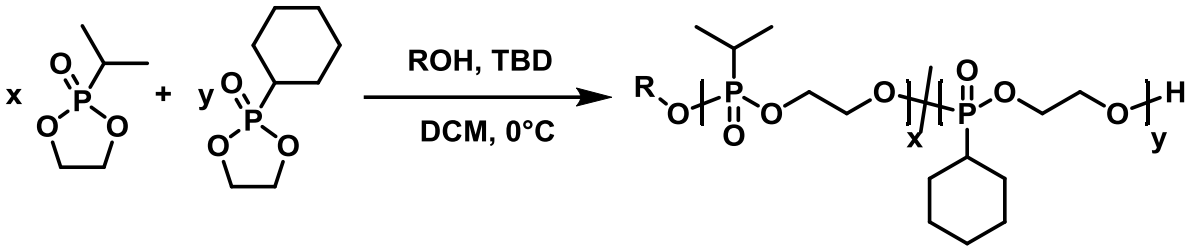

Scheme 1.20: Organocatalytic anionic ring-opening copolymerization of 2-isopropyl- and 2-cyclohexyl-2-oxo-1,3,2-dioxaphospholane catalyzed with TBD.

Homopolymerization as well as copolymerization with 2-isopropyl-2-oxo-1,3,2-dioxaphospholane was conducted with TBD as a catalyst and produced rather narrowly distributed polymers ($Đ$ < 1.5). The respective homopolymer showed a glass transition temperature 50 °C higher compared to *n*-alkylated poly(phosphonate)s. Statistical copolymerization was utilized to adjust the poly(phosphonate)s T_g's. The final copolymer composition matched the monomer feed ratio in all cases, and a linear trend between copolymer composition and T_g was observed, enabling a simple adjustment of the polymer properties (Figure 1.22).[146]

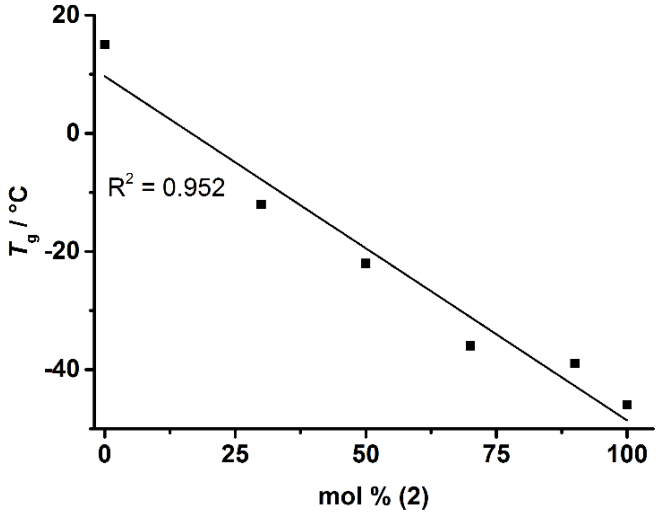

Figure 1.22: Correlation between the T_g's and the mol fraction of 2-isopropyl-2-oxo-1,3,2-dioxaphospholane (2) in copolymers with 2-cyclohexyl-2-oxo-1,3,2-dioxaphospholanes. Copyright @ 2016 The Royal Society of Chemistry. Reprinted with permission from Polymer Chemistry.[146]

In 2017, copolymerization of cyclic phosphonates was further extended to terpolymerization of 2-ethyl, 2-butyl, and 2-allyl-2-oxo-1,3,2-dioxaphospholanes by Wolf *et al.*. While again utilizing DBU as a single catalyst, the reaction temperature needed to be lowered to 0 °C to prevent isomerization reactions of the allyl side-chain. This effect is already known from the AROP of e. g. allyl glycidyl ether.[147] Kinetic investigations show that all monomers incorporated statistically in the polymer backbone, resulting in the formation of a random polymer. This work also presents the first side-chain modification by thiol-ene modification to alter the water-solubility and thermal phase separation behavior of poly(ethylene alkyl phosphonate)s (Scheme 1.21).[148]

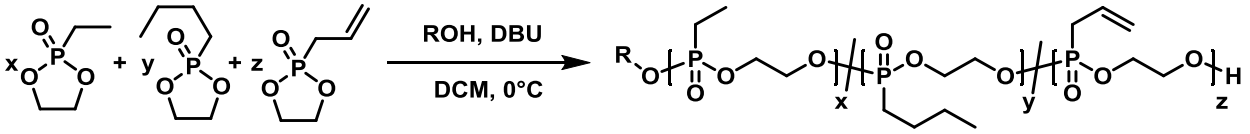

Scheme 1.21: DBU catalyzed terpolymerization towards side-chain reactive, random poly(phosphonate) terpolymers.

The synthesis of pendant carboxylic acid bearing poly(phosphonate)s showing UCST behavior in water was presented in the same year by Wolf *et al.*. Copolymerization of 2-ethyl and 2-allyl-2-oxo-1,3,2-dioxaphospholanes was conducted via DBU catalysis using either methoxy ethylene glycol or poly(ethylene glycol) as a macroinitiator (M_n = 5,000 g mol^{-1}) for the polymerization.[149] Narrowly distributed polymers with excellent control over molecular weight and molecular weight distributions were obtained. The resulting (block-) copolymers were side-chain modified with 3-mercapto propionic acid via thiol-ene reaction to produce UCST thermo-responsive polymers (Scheme 1.22).

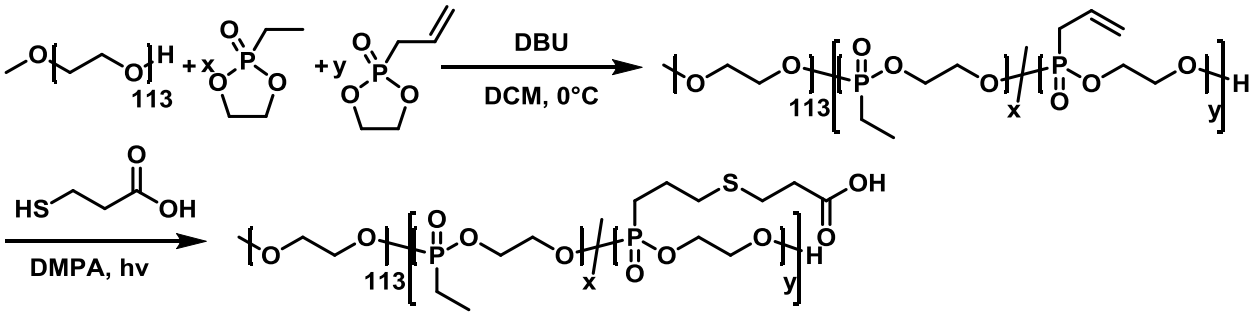

Scheme 1.22: Synthesis of UCST responsive amphiphilic block copolymers.

The amphiphilic PEG-*b*-poly(phosphonate) block copolymers assembled into vesicular structures of around 200 nm in diameter in water at room temperature. Increasing the temperature above the UCST type phase separation temperature resulted in a disassembling/swelling of the polymersomes, potentially releasing encapsulated cargo (Figure 1.23).

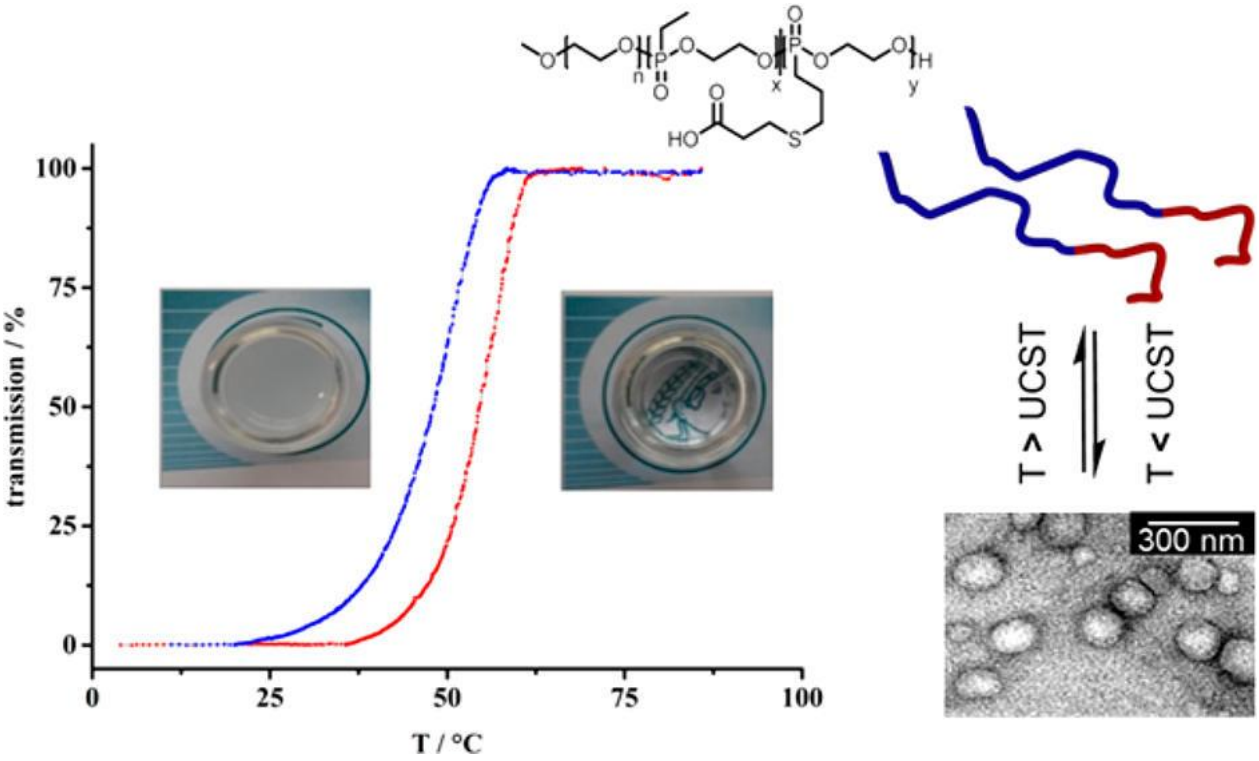

Figure 1.23: UV-Vis turbidity measurements of UCST thermo-responsive poly(phosphonate) copolymers (left) and self-assembling of UCST responsive block copolymers into polymersomes in water. Copyright @ 2017 American Chemical Society. Reprinted with permission from The Journal of the American Chemical Society.[149]

In the same year, Lin *et al.* published the first multi-gram scale synthesis of poly(ethylene alkyl phosphonate)s as well as their use as moderately active kinetic hydrate inhibitors in natural gas pipelines. Furthermore, they present the first evaluation of poly(phosphonate) biodegradation in seawater by bacteria. They show the degradation of up to 31% of polymeric material within 28 days under standardized conditions (OECD 306 protocol), proving poly(phosphonate)s microbial degradability in sea water.[150]

Lastly, Nifant'ev et al. presented their work on the magnesia catalyzed polymerization of dioxaphospholanes.[151] They compared the polymerizability of the ethyl- and a novel *t*butyl substituted dioxaphospholane with TBD and their magnesia catalysts. Using these magnesia catalysts, the ethyl dioxaphospholane monomer reached 89% (equaling 12,000 g mol^{-1}) conversion at -20 °C in 1h. However, molecular weight distributions of 1.46 indicated transesterification reactions. The *t*butyl dioxaphospholane did not polymerize with TBD even at 100 °C. Using the magnesia catalyst in bulk at 100 °C, however, the polymerization proceeded to 75% within 1h. Molecular weight distributions of 1.16 indicated the absence of transesterification reactions.

In conclusion, while being forgotten for nearly 40 years since its initial discovery, the ROP of cyclic phosphonate esters is experiencing a comeback since 2014 and mainly via organocatalysis so far. Catalysis via DBU is efficient for the polymerization of all reported *n*-alkylated 5-membered cyclic phosphonate derivatives in the presence of primary alcohols. Polymerization of *sec*-alkylated monomers typically proceed under TBD catalysis, and *tert*-alkylated monomers are unreactive in the presence of typical organocatalysts. Polymerization is slower than the respective phosphate polymerization due to the inductive effect of the alkyl side-chains. However, high conversions (> 95%) can be reached without transesterifications and molecular weight distribution broadening. Molecular weights up to 25,000 g mol^{-1} can be achieved and controlled by variation of the initiator to monomer ratio. Copolymerization generates random copolymers with good control copolymer composition. Due to the growing monomer variety, different chemical and physical polymer properties (e.g., T_g, solubility, thermal response) can be addressed and fine-tuned.

References

1. Duncan, R., *Nat. Rev. Drug Discov.,* **2003,** *2*, 347-60.
2. Ulery, B. D.; Nair, L. S.; Laurencin, C. T., *J. Polym. Sci. B: Polym. Phys.,* **2011,** *49*, 832-864.
3. Leader, B.; Baca, Q. J.; Golan, D. E., *Nat. Rev. Drug Discov.,* **2008,** *7*, 21-39.
4. Bailon, P.; Palleroni, A.; Schaffer, C. A.; Spence, C. L.; Fung, W.-J.; Porter, J. E.; Ehrlich, G. K.; Pan, W.; Xu, Z.-X.; Modi, M. W.; Farid, A.; Berthold, W.; Graves, M., *Bioconjugate Chem.,* **2001,** *12*, 195-202.
5. Graham, M., *Adv. drug deliv. rev.,* **2003,** *55*, 1293-1302.
6. Sherman, M. R.; Saifer, M. G.; Perez-Ruiz, F., *Adv. drug deliv. rev.,* **2008,** *60*, 59-68.
7. Kim, T. Y.; Kim, D. W.; Chung, J. Y.; Shin, S. G.; Kim, S. C.; Heo, D. S.; Kim, N. K.; Bang, Y. J., *Clin. Cancer Res.,* **2004,** *10*, 3708-3716.
8. Han, Y.; He, Z.; Schulz, A.; Bronich, T. K.; Jordan, R.; Luxenhofer, R.; Kabanov, A. V., *Mol. Pharm.,* **2012,** *9*, 2302-2313.
9. Mohanty, A. K.; Dilnawaz, F.; Mohanta, G. P.; Sahoo, S. K., *Targeted Drug Delivery : Concepts and Design*, Devarajan, P. V.; Jain, S., Eds. Springer International Publishing: Cham, **2015,** 389-407.
10. Knop, K.; Hoogenboom, R.; Fischer, D.; Schubert, U. S., *Angew. Chem. Int. Ed.,* **2010,** *49*, 6288-6308.
11. Schöttler, S.; Becker, G.; Winzen, S.; Steinbach, T.; Mohr, K.; Landfester, K.; Mailander, V.; Wurm, F. R., *Nat. Nanotechnol.,* **2016,** *11*, 372-377.
12. Lynch, I.; Salvati, A.; Dawson, K. A., *Nat. Nanotechnol.,* **2009,** *4*, 546-547.
13. Lee, Y. K.; Choi, E. J.; Webster, T. J.; Kim, S. H.; Khang, D., *Int. J. Nanomed.,* **2015,** *10*, 97-113.
14. Ritz, S.; Schöttler, S.; Kotman, N.; Baier, G.; Musyanovych, A.; Kuharev, J.; Landfester, K.; Schild, H.; Jahn, O.; Tenzer, S.; Mailander, V., *Biomacromolecules,* **2015,** *16*, 1311-1321.
15. Takeuchi, T.; Kitayama, Y.; Sasao, R.; Yamada, T.; Toh, K.; Matsumoto, Y.; Kataoka, K., *Angew. Chem. Int. Ed.,* **2017,** *56*, 7088-7092.
16. Kang, B.; Okwieka, P.; Schöttler, S.; Winzen, S.; Langhanki, J.; Mohr, K.; Opatz, T.; Mailander, V.; Landfester, K.; Wurm, F. R., *Angew. Chem. Int. Ed.,* **2015,** *54*, 7436-7440.
17. Maeda, H.; Matsumoto, T.; Konno, T.; Iwai, K.; Ueda, M., *J. Protein Chem.,* **1984,** *3*, 181-193.
18. Greish, K., *J. Drug Targe.,* **2007,** *15*, 457-464.
19. Haag, R.; Kratz, F., *Angew. Chem. Int. Ed.,* **2006,** *45*, 1198-1215.
20. Petersen, H.; Fechner, P. M.; Fischer, D.; Kissel, T., *Macromolecules,* **2002,** *35*, 6867-6874.
21. Suk, J. S.; Xu, Q.; Kim, N.; Hanes, J.; Ensign, L. M., *Adv. drug deliv. rev.,* **2016,** 28-51.
22. Pasut, G.; Veronese, F. M., *Progr. Polym. Sci.,* **2007,** *32*, 933-961.
23. Murthy, N.; Campbell, J.; Fausto, N.; Hoffman, A. S.; Stayton, P. S., *Bioconjug. Chem.,* **2003,** *14*, 412-419.
24. Schmaljohann, D., *Adv. drug deliv. rev.,* **2006,** *58*, 1655-1670.

25. Alkan, A.; Steinmetz, C.; Landfester, K.; Wurm, F. R., *ACS Appl. Mat. Interf.,* **2015,** *7*, 26137-26144.
26. Lu, Y.; Aimetti, A. A.; Langer, R.; Gu, Z., *Nature Rev. Mat.,* **2016,** *2*, 16075.
27. Jochum, F. D.; Theato, P., *Chem. Soc. rev.,* **2013,** *42*, 7468-7483.
28. Thevenot, J.; Oliveira, H.; Sandre, O.; Lecommandoux, S., *Chem. Soc. rev.,* **2013,** *42*, 7099-7116.
29. Wei, M.; Gao, Y.; Li, X.; Serpe, M. J., *Polym. Chem.,* **2017,** *8*, 127-143.
30. Bajpai, A. K.; Shukla, S. K.; Bhanu, S.; Kankane, S., *Progr. Polym. Sci.,* **2008,** *33*, 1088-1118.
31. Jochum, F. D.; Theato, P., *Chem. commun.,* **2010,** *46*, 6717-6719.
32. Stefanadis, C.; Chrysochoou, C.; Markou, D.; Petraki, K.; Panagiotakos, D. B.; Fasoulakis, C.; Kyriakidis, A.; Papadimitriou, C.; Toutouzas, P. K., *J. Clin. Oncol.* **2001,** *19*, 676-681.
33. Gibson, M. I.; O'Reilly, R. K., *Chem. Soc. rev.,* **2013,** *42*, 7204-7213.
34. Ward, M. A.; Georgiou, T. K., *Polymers* **2011,** *3*, 1215-1242.
35. Seuring, J.; Agarwal, S., *Acs Macro Lett.,* **2013,** *2*, 597-600.
36. Taylor, M.; Tomlins, P.; Sahota, T., *Gels,* **2017,** *3*, 4.
37. Heyda, J.; Soll, S.; Yuan, J.; Dzubiella, J., *Macromolecules,* **2014,** *47*, 2096-2102.
38. Meng, F.; Zhong, Z.; Feijen, J., *Biomacromolecules,* **2009,** *10*, 197-209.
39. Seuring, J.; Agarwal, S., *Macromol. Rapid Commun.,* **2012,** *33*, 1898-1920.
40. Davis, F. F., *Adv. drug deliv. rev.,* **2002,** *54*, 457-458.
41. *Market Research Report,* **2015,** report ID: 978-1-68038-353-9.
42. *The EFSA Journal* **2006,** *414*, 1-22.
43. Geng, S.; Yang, B.; Wang, G.; Qin, G.; Wada, S.; Wang, J. Y., *Nanotechnol.,* **2014,** *25*, 275103.
44. Zhang, F.; Zhang, S.; Pollack, S. F.; Li, R.; Gonzalez, A. M.; Fan, J.; Zou, J.; Leininger, S. E.; Pavia-Sanders, A.; Johnson, R.; Nelson, L. D.; Raymond, J. E.; Elsabahy, M.; Hughes, D. M.; Lenox, M. W.; Gustafson, T. P.; Wooley, K. L., *J. Am. Chem. Soc.,* **2015,** *137*, 2056-2066.
45. Christian, D. A.; Cai, S.; Bowen, D. M.; Kim, Y.; Pajerowski, J. D.; Discher, D. E., *Eur. J. Pharm. Biopharm.,* **2009,** *71*, 463-474.
46. Huang, Y.-L.; Li, Q.-B.; Deng, X.; Lu, Y.-H.; Liao, X.-K.; Hong, M.-Y.; Wang, Y., *Proc. Biochem.,* **2005,** *40*, 207-211.
47. Worm, M.; Leibig, D.; Dingels, C.; Frey, H., *ACS macro lett.,* **2016,** *5*, 1357-1363.
48. Dingels, C.; Muller, S. S.; Steinbach, T.; Tonhauser, C.; Frey, H., *Biomacromolecules,* **2013,** *14*, 448-459.
49. Herold, D. A.; Keil, K.; Bruns, D. E., *Biochem. Pharmacol.,* **1989,** *38*, 73-76.
50. Richter, A. W.; Åkerblom, E., *Int. Arch. Allergy Immun.,* **1983,** *70,* 124-131.
51. Szebeni, J.; Baranyi, L.; Savay, S.; Milosevits, J.; Bunger, R.; Laverman, P.; Metselaar, J. M.; Storm, G.; Chanan-Khan, A.; Liebes, L.; Muggia, F. M.; Cohen, R.; Barenholz, Y.; Alving, C. R., *J. Liposome Res.,* **2002,** *12*, 165-172.
52. Dams, E. T. M.; Laverman, P.; Oyen, W. J. G.; Storm, G.; Scherphof, G. L.; van der Meer, J. W. M.; Corstens, F. H. M.; Boerman, O. C., *J. Pharmacol. Exp. Ther.,* **2000,** *292*, 1071-1079.
53. Abu Lila, A. S.; Kiwada, H.; Ishida, T., *J. Control Release,* **2013,** *172*, 38-47.
54. Armstrong, J. K.; Hempel, G.; Koling, S.; Chan, L. S.; Fisher, T.; Meiselman, H. J.; Garratty, G., *Cancer,* **2007,** *110*, 103-111.

55. Garay, R. P.; El-Gewely, R.; Armstrong, J. K.; Garratty, G.; Richette, P., *Expert Opin. Drug Deliv.,* **2012,** *9*, 1319-1323.
56. Hashimoto, Y.; Shimizu, T.; Abu Lila, A. S.; Ishida, T.; Kiwada, H., *Biol. Pharm. Bull.,* **2015,** *38*, 417-424.
57. Pelegri-O'Day, E. M.; Lin, E. W.; Maynard, H. D., *J. Am. Chem. Soc.,* **2014,** *136*, 14323-13332.
58. Kang, B.; Opatz, T.; Landfester, K.; Wurm, F. R., *Chem. Soc. rev.,* **2015,** *44*, 8301-8325.
59. Besheer, A.; Vogel, J.; Glanz, D.; Kressler, J.; Groth, T.; Mader, K., *Mol. Pharm.,* **2009,** *6*, 407-415.
60. Baier, G.; Baumann, D.; Siebert, J. M.; Musyanovych, A.; Mailander, V.; Landfester, K., *Biomacromolecules,* **2012,** *13*, 2704-2715.
61. Bauer, M.; Lautenschlaeger, C.; Kempe, K.; Tauhardt, L.; Schubert, U. S.; Fischer, D., *Macromol. Biosci.,* **2012,** *12*, 986-998.
62. Bludau, H.; Czapar, A. E.; Pitek, A. S.; Shukla, S.; Jordan, R.; Steinmetz, N. F., *Eur. Polym. J.,* **2017,** *88*, 679-688.
63. Bauer, K. N.; Tee, H. T.; Velencoso, M. M.; Wurm, F. R., *Progr. Polym. Sci.,* **2017,** 73, 61-122.
64. Thomas, A.; Muller, S. S.; Frey, H., *Biomacromolecules,* **2014,** *15*, 1935-1954.
65. Kainthan, R. K.; Janzen, J.; Levin, E.; Devine, D. V.; Brooks, D. E., *Biomacromolecules,* **2006,** *7*, 703-709.
66. Imran ul-haq, M.; Lai, B. F.; Chapanian, R.; Kizhakkedathu, J. N., *Biomaterials,* **2012,** *33*, 9135-9147.
67. PY, J. Y.; Kainthan, R. K.; Zou, Y.; Chiao, M.; Kizhakkedathu, J. N., *Langmuir,* **2008,** *24*, 4907-4916.
68. Abu Lila, A. S.; Nawata, K.; Shimizu, T.; Ishida, T.; Kiwada, H., *Int. J. Pharm.,* **2013,** *456*, 235-242.
69. Herzberger, J.; Fischer, K.; Leibig, D.; Bros, M.; *J. Am. Chem. Soc.,* **2016,** *138*, 9212-9223.
70. Leibig, D.; Seiwert, J.; Liermann, J. C.; Frey, H., *Macromolecules,* **2016,** *49*, 7767-7776.
71. Kainthan, R. K.; Brooks, D. E., *Biomaterials,* **2007,** *28*, 4779-4787.
72. Noga, M.; Edinger, D.; Klager, R.; Wegner, S. V.; Spatz, J. P.; Wagner, E.; Winter, G.; Besheer, A., *Biomaterials,* **2013,** *34*, 2530-2538.
73. Noga, M.; Edinger, D.; Rodl, W.; Wagner, E.; Winter, G.; Besheer, A., *J. Control. Release,* **2012,** *159*, 92-103.
74. Hoogenboom, R., *Europ. Polym. J.,* **2017,** *88*, 448-450.
75. Luxenhofer, R.; Han, Y.; Schulz, A.; Tong, J.; He, Z.; Kabanov, A. V.; Jordan, R., *Macromol. Rapid Commun.,* **2012,** *33*, 1613-1631.
76. Kobayashi, S., *Progr. Polym. Sci.,* **1990,** *15* , 751-823.
77. Wiesbrock, F.; Hoogenboom, R.; Leenen, M. A. M.; Meier, M. A. R.; Schubert, U. S., *Macromolecules,* **2005,** *38*, 5025-5034.
78. Jaksch, S.; Schulz, A.; Di, Z.; Luxenhofer, R.; Jordan, R.; Papadakis, C. M., *Macrom. Chem. Phys.,* **2016,** *217*, 1448-1456.
79. Konradi, R.; Pidhatika, B.; Muhlebach, A.; Textor, M., *Langmuir,* **2008,** *24*, 613-616.
80. Mero, A.; Pasut, G.; Dalla Via, L.; Fijten, M. W.; Schubert, U. S.; Hoogenboom, R.; Veronese, F. M., *J. Control. Release,* **2008,** *125*, 87-95.

81. Pidhatika, B.; Möller, J.; Vogel, V.; Konradi, R., *CHIMIA Int. J. Chem.,* **2008,** *62*, 264-269.
82. Zalipsky, S.; Hansen, C. B.; Oaks, J. M.; Allen, T. M., *J. Pharm. Sci.,* **1996,** *85*, 133-137.
83. Luxenhofer, R.; Schulz, A.; Roques, C.; Li, S.; Bronich, T. K.; Batrakova, E. V.; Jordan, R.; Kabanov, A. V., *Biomaterials,* **2010,** *31*, 4972-4979.
84. Viegas, T. X.; Bentley, M. D.; Harris, J. M.; Fang, Z.; Yoon, K.; Dizman, B.; Weimer, R.; Mero, A.; Pasut, G.; Veronese, F. M., *Bioconjug. Chem.,* **2011,** *22*, 976-986.
85. Westheimer, F. H., *Science,* **1987,** *235*, 1173-1178.
86. Vella, F., *Biochem. Ed.,* **1997,** *25*, 49.
87. Canto, C.; Menzies, K. J.; Auwerx, J., *Cell Metab.,* **2015,** *22*, 31-53.
88. Lee, Y.; Klauser, P. C.; Brandsen, B. M.; Zhou, C.; Li, X.; Silverman, S. K., *J. Am. Chem. Soc.,* **2017,** *139*, 255-261.
89. Bauer, K. N.; Tee, H. T.; Velencoso, M. M.; Wurm, F. R., *Progr. Polym. Sci.,* **2017,** *73*, 61-122.
90. Steinbach, T.; Wurm, F. R., *Angew. Chem. Int. Ed.,* **2015,** *54*, 6098-6108.
91. Lapienis, G., Ring-Opening Polymerization of Cyclic Phosphorus Monomers. **2012**, 477-505.
92. Yilmaz, Z. E.; Jerome, C., *Macromol. Biosci.,* **2016,** *16*, 1745-1761.
93. Henke, H.; Bruggemann, O.; Teasdale, I., *Macromol. Rapid Commun.,* **2017,** *38,* 10.1002/marc.201600644.
94. Penczek, S.; Cypryk, M.; Duda, A.; Kubisa, P.; Slomkowski, S., *Progr. Polym. Sci.,* **2007,** *32*, 247-282.
95. Lapienis, G.; Penczek, S., *Macromolecules,* **1974,** *7*, 166-174.
96. Lapienis, G.; Penczek, S., *Macromolecules,* **1977,** *10*, 1301-1306.
97. Łapienis, G.; Penczek, S., *J. Polym. Sci.: Polym. Chem. Ed.,* **1977,** *15*, 371-382.
98. Vogt, W.; Siegfried, R., *Die Makromolekulare Chemie,* **1976,** *177*, 1779-1789.
99. Vogt, W.; Pflüger, R., *Die Makromolekulare Chemie.* **1975,** *1*, 97-110.
100. Libiszowski, J.; Kałużynski, K.; Penczek, S., *J. Polym. Sci.: Polym. Chem. Ed.,* **1978,** *16*, 1275-1283.
101. Sosnowski, S.; Libiszowski, J.; Słomkowski, S.; Penczek, S., *Die Makromolekulare Chemie, Rapid Commun.,* **1984,** *5*, 239-244.
102. Wen, J.; Zhuo, R.-X., *Macromol. Rapid Commun.,* **1998,** *19*, 641-642.
103. Xiao, C.-S.; Wang, Y.-C.; Du, J.-Z.; Chen, X.-S.; Wang, J., *Macromolecules,* **2006,** *39*, 6825-6831.
104. Wen, J.; Kim, G. J. A.; Leong, K. W., *J. Control. Release,* **2003,** 92, 39-48.
105. Iwasaki, Y.; Yamaguchi, E., *Macromolecules,* **2010,** *43*, 2664-2666.
106. Liu, J.; Pang, Y.; Huang, W.; Zhai, X.; Zhu, X.; Zhou, Y.; Yan, D., *Macromolecules,* **2010,** *43*, 8416-8423.
107. Zhang, S.; Li, A.; Zou, J.; Lin, L. Y.; Wooley, K. L., *ACS macro let.,* **2012,** *1*, 328-333.
108. Clément, B.; Grignard, B.; Koole, L.; Jérôme, C.; Lecomte, P., *Macromolecules,* **2012,** *45*, 4476-4486.
109. Lohmeijer, B. G. G.; Pratt, R. C.; Leibfarth, F.; Logan, J. W.; Long, D. A.; Dove, A. P.; Nederberg, F.; Choi, J.; Wade, C.; Waymouth, R. M.; Hedrick, J. L., *Macromolecules,* **2006,** *39*, 8574-8583.
110. Steinbach, T.; Schröder, R.; Ritz, S.; Wurm, F. R., *Polym. Chem.,* **2013,** *4*, 4469-4479.

111. Lim, Y. H.; Heo, G. S.; Rezenom, Y. H.; Pollack, S.; Raymond, J. E.; Elsabahy, M.; Wooley, K. L., *Macromolecules,* **2014,** *47*, 4634-4644.
112. Gao, H.; Tan, Y.; Guan, Q.; Cai, T.; Liang, G.; Wu, Q., *RSC Adv.,* **2015,** *5*, 49376-49384.
113. Lim, Y. H.; Tiemann, K. M.; Heo, G. S.; Wagers, P. O.; Rezenom, Y. H.; Zhang, S.; Zhang, F.; Youngs, W. J.; Hunstad, D. A.; Wooley, K. L., *ACS Nano,* **2015,** *9*, 1995-2008.
114. Zhang, F.; Zhang, S.; Pollack, S. F.; Li, R.; Gonzalez, A. M.; Fan, J.; Zou, J.; Leininger, S. E.; Pavia-Sanders, A.; Johnson, R.; Nelson, L. D.; Raymond, J. E.; Elsabahy, M.; Hughes, D. M.; Lenox, M. W.; Gustafson, T. P.; Wooley, K. L., *J. Am. Chem. Soc.,* **2015,** *137*, 2056-2066.
115. Baeten, E.; Vanslambrouck, S.; Jérôme, C.; Lecomte, P.; Junkers, T., *Europ. Poly. J.,* **2016,** *80*, 208-218.
116. Wu, G.-P.; Darensbourg, D. J., *Macromolecules,* **2016,** *49*, 807-814.
117. Muller, J.; Bauer, K. N.; Prozeller, D.; Simon, J.; Mailander, V.; Wurm, F. R.; Winzen, S.; Landfester, K., *Biomaterials,* **2017,** *115*, 1-8.
118. Becker, G.; Marquetant, T. A.; Wagner, M.; Wurm, F. R., *Macromolecules,* **2017,** 10.1021/acs.macromol.7b01716.
119. Stukenbroeker, T. S.; Solis-Ibarra, D.; Waymouth, R. M., *Macromolecules,* **2014,** *47*, 8224-8230.
120. McGrath, J. W.; Chin, J. P.; Quinn, J. P., *Nature rev. Microbiol.,* **2013,** *11*, 412-419.
121. L. L. Clark, E. D. I., R. Benner, *Am. J. Sci.,* **1999,** *299*, 724-737.
122. Miceli, M. V.; Henderson, T. O.; Myers, T. C., *Science,* **1980,** *209*, 1245-1247.
123. Horiguchi, M.; Kandatstu, M., *Nature,* **1959,** *184*, 901-902.
124. Metcalf, W. W.; van der Donk, W. A., *Annu. rev. biochem.,* **2009,** *78*, 65-94.
125. Seweryn, P.; Van, L. B.; Kjeldgaard, M.; Russo, C. J.; Passmore, L. A.; Hove-Jensen, B.; Jochimsen, B.; Brodersen, D. E., *Nature,* **2015,** *525*, 68-72.
126. P. Kafarski, B. L., *Curr. Med. Chem. Anticancer Agents,* **2001,** *1*, 301-312.
127. Cioni, J. P.; Doroghazi, J. R.; Ju, K. S.; Yu, X.; Evans, B. S.; Lee, J.; Metcalf, W. W., C, *J. Nat. Prod.,* **2014,** *77*, 243-249.
128. Benbrook, C. M., *Environ. Sci. Eur.,* **2016,** *28*, 3.
129. Maryanoff, B. E.; Reitz, A. B., *Chem. Rev.,* **1989,** *89*, 863-927.
130. Steinbach, T.; Wahlen, C.; Wurm, F. R., *Polym. Chem.,* **2015,** *6*, 1192-1202.
131. Albrecht-Schmitt, T.; Bujoli, B.; Cahill, C.; Murugavel, R.; Rocha, J.; Hix, G.; Shimizu, G.; Zubieta, J.; Zon, J.; Brunet, E., Royal Soc. Chem., **2011**, ISBN: 9781849733571.
132. Bordwell, F. G., *Acc. Chem. Res.,* **2002,** *21*, 456-463.
133. Qi, C.; Du, Y.; Lu, Y.; Sun, X.; Zhang, X. M., *J. Org. Chem.,* **2009,** *74*, 8078-8085.
134. Millich, F.; Carraher, C. E., *J. Polym. Sci. A1,* **1969,** *7*, 2669-2678.
135. Millich, F.; Carraher, C. E., *J. Polym. Sci. A1,* **1970,** *8*, 163-169.
136. Millich, F.; Carraher, C. E., *Macromolecules,* **1970,** *3*, 253-256.
137. Millich, F.; Carraher, C. E., *J. Polym. Sci. A1,* **1971,** *9*, 1715-&.
138. Chen, L.; Wang, Y. Z., Aryl *Materials (Basel),* **2010,** *3*, 4746-4760.
139. Sharov, V. N.; Klebanskii, A. L., *Polym. Sci. USSR,* **1973**, 2777-2782.
140. Kału??ynski, K.; Libiszowski, J.; Penczek, S., *Die Makromolekulare Chemie,* **1977,** *178*, 2943-2947.
141. Steinbach, T.; Ritz, S.; Wurm, F. R., Water-Soluble *Acs Macro Let.,* **2014,** *3*, 244-248.

142. Steinbach, T.; Wurm, F. R., *Biomacromolecules,* **2016,** *17*, 3338-3346.
143. Russo, D.; Plazanet, M.; Teixeira, J.; Moulin, M.; Hartlein, M.; Wurm, F. R.; Steinbach, T., *Biomacromolecules,* **2016,** *17*, 141-147.
144. Wolf, T.; Steinbach, T.; Wurm, F. R., *Macromolecules,* **2015,** *48*, 3853-3863.
145. Macdonald, E. K.; Shaver, M. P., *Green Materials,* **2016,** *4*, 81-88.
146. Wolf, T.; Nass, J.; Wurm, F. R., *Polym. Chem.,* **2016,** *7*, 2934-2937.
147. Obermeier, B.; Frey, H., *Bioconjug. Chem.,* **2011,** *22*, 436-444.
148. Wolf, T.; Rheinberger, T.; Wurm, F. R., *Europ. Poly. J.,* **2017,** 10.1016/j.eurpolymj.2017.05.048.
149. Wolf, T.; Rheinberger, T.; Simon, J.; Wurm, F. R., *J. Am. Chem. Soc.,* **2017,** *139*, 11064-11072.
150. Lin, H.; Wolf, T.; Wurm, F. R.; Kelland, M. A., *Energy & Fuels,* **2017,** *31*, 3843-3848.
151. Nifant'ev, I. E.; Shlyakhtin, A. V.; Bagrov, V. V.; Komarov, P. D.; Kosarev, M. A.; Tavtorkin, A. N.; Minyaev, M. E.; Roznyatovsky, V. A.; Ivchenko, P. V., Polym. Chem., **2017,** 10.1039/c7py01472d.

Chapter 2: A Library of Well-Defined and Water-Soluble Poly(phosphonate)s with Adjustable Hydrolysis.

Thomas Wolf[1], *Tobias Steinbach*[1], *and Frederik R. Wurm*[1]

[1]Max Planck-Institut für Polymerforschung, Ackermannweg 10, 55128 Mainz, Germany

Published in: Macromolecules, **2015,** 48, 3853-3863

Keywords: poly(phosphoester)s, poly(phosphonate)s, anionic ring-opening polymerization, degradable polymers

Chapter 2: A Library of Well-Defined and Water-Soluble Poly(phosphonate)s with Adjustable Hydrolysis.

Abstract

Poly(ethylene alkyl phosphonate)s with different alkyl side chains exhibit significant differences in their degradation behavior. Three different 2-alkyl-2-oxo-1,3,2-dioxaphospholanes, cyclic monomers for the ring-opening polymerization (ROP) towards poly(alkylene alkyl phosphonate)s, were synthesized by robust two- or three-step protocols in reasonable yields and high purity. The polymerization was promoted by the organocatalysts 1,8-diazabicyclo[5.4.0]undec-7-ene (DBU) and 1,5,7-triazabicyclo [4.4.0]dec-5-ene (TBD) and proceeded with high control over molecular weight and narrow molecular weight distributions ($Đ$ < 1.25) up to full conversion. The polymers with methyl, ethyl and isopropyl side chains were entirely soluble in water (up to 25 mg mL^{-1}) without a temperature-dependent phase separation. They showed no toxicity against HeLa cells after 24h of incubation at any tested concentration. Polymers with butyl side chains exhibited decreased solubility, concentration-dependent cloud point temperatures and showed toxicity against HeLa cells at concentrations above 25 µg mL^{-1}. The polymers showed no acetylcholinesterase inhibition properties. All polymers exhibited significantly different degradation times under both neutral as well as basic conditions (variation of the alkyl side chain allowed stabilities from 8h up to 6 days).

Introduction

Poly(ethylene glycol) (PEG) is today's "gold standard" polymer for many biomedical applications.[1] Its high water-solubility, low toxicity, and low immunogenicity have led to its success over the last decades, e.g., for the modification of surfaces, drugs, and nanocarriers. Its high stability in aqueous environment can be considered beneficial; however, accumulation, as well as uncontrolled and unwanted oxidative degradation of PEG into toxic byproducts has been reported.[2] Today several PEG-alternatives are discussed, however, the versatile poly(phosphoester)s (PPEs) are rarely investigated despite being biocompatible and biodegradable materials.[3-14]

PPEs are commonly divided into four sub-classes: poly(phosphate)s, poly(phosphite)s, poly(phosphoamidate)s and poly(phosphonate)s as shown in Scheme 2.1.

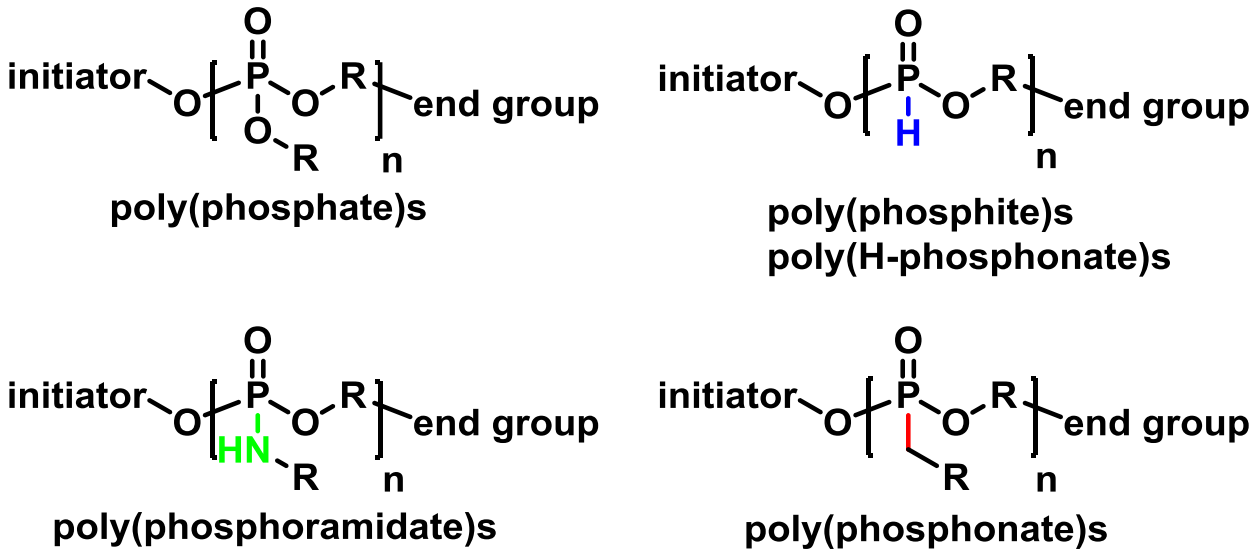

Scheme 2.1. Sub-classes of poly(phosphoester)s: a) poly(phosphate)s , b) poly-(phosphite)s, c) poly(phosphoramidate)s, and d) poly(phosphonate)s.

Currently, some researchers are interested in poly(phosphate)s and poly(phosphoamidate)s.[5-7,15-18] However, backbiting reactions during the polymerization have been reported due to the potentially cleavable side chains (ester or amide).

Poly(phosphonate)s, however, contain a chemically stable P-C bond which substitutes one of the P-(O/N)-C bonds and which is more resilient towards chemical hydrolysis, thermal decomposition and photolysis.[19] To the best of our knowledge, also no enzyme in the human body is capable of cleaving the P-C bond, and most natural occurring phosphatases are incapable of cleaving the other two ester groups (P-O-C bonds) of phosphonates.[20] Some microorganisms, however, are capable of metabolizing phosphonates as a nutrient source.[21] With these stable side chains, transesterification reactions have been successfully prevented.[22]

From a synthetic point of view, phosphonates are accessible by a variety of well-known chemical reactions like the *Michaelis-Arbuzov* or *Michaelis-Becker* reaction from commercially available starting materials.[23-27] Chemists are investigating other P-C bond formation reactions due to the high impact of phosphonates both in synthetic and coordinative chemistry.[28-30]

Phosphonates also play a specific role in living nature as hydrolytically stable phosphate analogs. Phosphonic acid derivatives have been found in various plants, fungi, bacteria, and in some vertebrates.[31] Recent ^{31}P NMR studies showed that up to 30% of phosphorus in the maritime phosphorous cycle is bound in phosphonic acid derivatives.[32]

In addition to these advantages, phosphonic acid esters are readily detectable in biological fluids which can be a significant advantage to determine biodistribution and clearance of polymeric samples and their degradation products. For most systems, elaborate labeling of the polymer is necessary to achieve detection in these fluids.[33-36] Phosphonates, however, can be detected in low concentrations via ^{31}P NMR spectroscopy. Due to the chemical shift difference between naturally occurring phosphoric acid esters and phosphonic acid esters of ca. 30 ppm, a differentiation between native and externally administered phosphorus species is considered possible.[37]

Despite the versatility, easy access, stability, natural abundance and potential detectability of phosphonic acid esters, poly(phosphonate)s have only been scarcely studied in modern polymer science since the early studies in the 1960s.[4] Initially, the polycondensation of diols and bisphosphonic acids has been reported and rather undefined, aromatic compounds have been prepared.[38,39] Today, these poly(phosphonate)s are commercialized as flame retardant additives. They receive increasing interest in recent years as halogenated flame retardants are being banned from the market.[40,41]

Recently, our group reported the synthesis of poly(phosphonate)s by acyclic diene metathesis polymerization (ADMET) and ring-opening metathesis polymerization (ROMP).[42-45] Simultaneously, 2-methyl-2-oxo-1,3,2-dioxaphospholane (MeEP) was used as the first cyclic phosphonate monomer for the anionic ring-opening polymerization (AROP) to synthesize well-defined ($Đ < 1.1$), water-soluble poly(ethylene methyl phosphonate)s with high degrees of polymerization.[22]

Chapter 2: A Library of Well-Defined and Water-Soluble Poly(phosphonate)s with Adjustable Hydrolysis.

Herein, we present the synthesis and polymerization of a series of new 2-alkyl-2-oxo-1,3,2-dioxaphospholanes. The monomer synthesis was performed in two to three robust steps with moderate to excellent yields. The organocatalytic AROP proceeded with high control over molecular weight, and narrow molecular weight distributions were obtained. The polymers showed high water-solubility and no cytotoxicity towards HeLa cells. Importantly, different degradation kinetics were observed depending on the side chains. This allows tailoring of the stability in aqueous solution at different pH values (from 8h up to 6 days without significant degradation). These polymers may be a potential substitute for PEG in biomedical applications as they are water-soluble, non-toxic and entirely degradable over a controlled period, and can easily be detected in biological fluids through ^{31}P NMR spectroscopy depending on the duration of their application and the amount administered.

Results and Discussion

Monomer Synthesis

Three novel monomers for the AROP of cyclic phosphonates have been developed: 2-alkyl-2-oxo-1,3,2-dioxaphospholanes bearing ethyl (**1**), isopropyl (**2**), or butyl (**3**) side chains were synthesized from easily accessible starting materials by a two or a three-step protocol in reasonable yields (Scheme 2.2). With this set of monomers, polymers with a different degree of hydrophobicity and steric shielding of the phosphonates centers were generated for the first time.

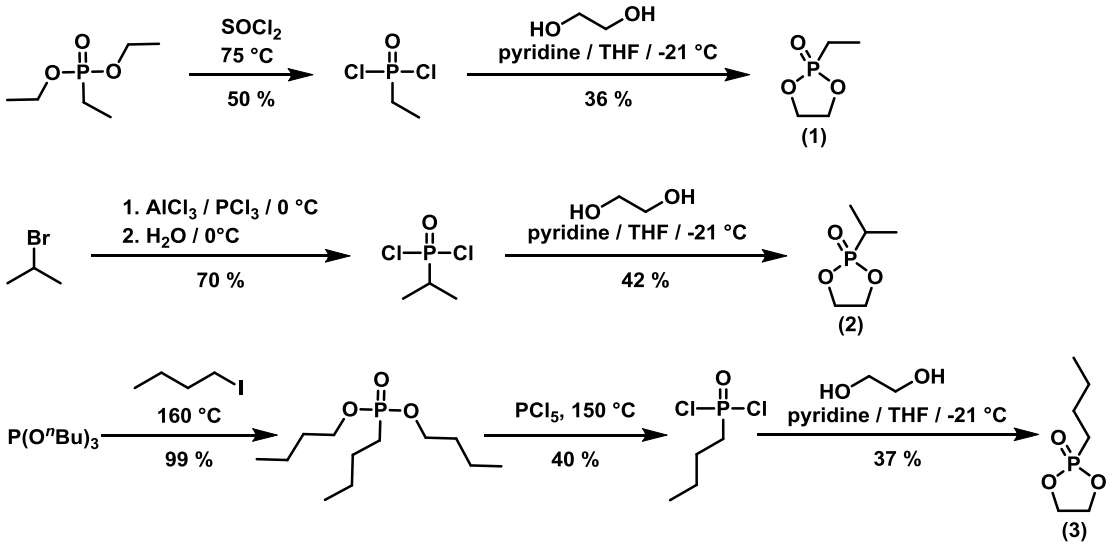

Scheme 2.2: Reaction Scheme for the synthesis of new 2-alkyl-2-oxo-1,3,2-dioxaphospholanes (1), (2) and (3).

2-Ethyl-2-oxo-1,3,2-dioxaphospholane (EtPPn, (**1**)) was synthesized starting from the commercially available *O, O*-diethyl ethyl phosphonate. Conversion into the corresponding phosphonic acid dichloride was performed with thionyl chloride. Cyclisation to the five-membered ring was achieved by esterification with ethylene glycol.

2-Isopropyl-2-oxo-1,3,2-dioxaphospholane (^{i}PrPPn, (**2**)) was obtained in a two-step synthesis starting from phosphorus trichloride, aluminum trichloride and 2-bromo propane followed by mild hydrolysis and subsequent ring-closing with ethylene glycol. The first step in the reaction proceeds via the formation of an anionic complex with the general structure of $[RPCl_3]^+[ALCl_4]^-$. Careful hydrolysis of this complex yields the phosphonic acid dichloride in excellent yields.

To receive the more hydrophobic 2-*n*-butyl-2-oxo-1,3,2-dioxaphospholane (^{n}BuPPn, (**3**)), first tri-*n*-butyl phosphite was reacted with 1-iodo-butane in a *Michaelis-Arbuzov* reaction. The obtained *O, O*-di-*n*-butyl *n*-butyl phosphonate was subsequently converted into the phosphonic acid dichloride by treatment with phosphorus pentachloride. The corresponding dichloride was reacted with ethylene glycol to obtain the monomer. The cyclic structure and purity of all compounds were confirmed by ^{1}H, ^{13}C{H}, and ^{31}P{H} NMR spectroscopy (Figures 2.1 - 2.5). Highest purity was aspired for successful AROP and achieved by double distillation of the monomers.

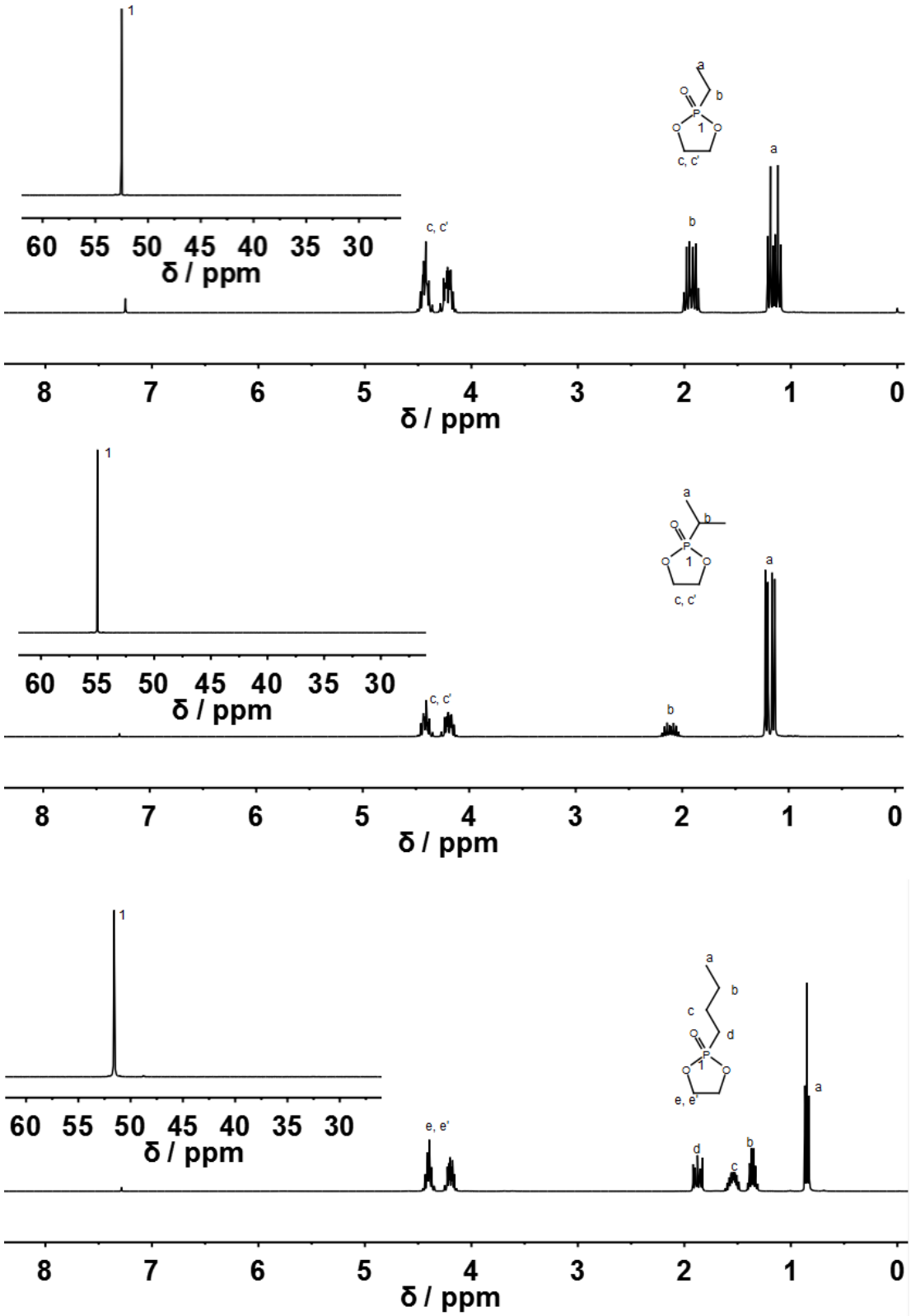

Figure 2.1: ^{1}H (300 MHz) and $^{31}P\{H\}$ (121 MHz) spectra of a) (1), b) (2), and c) (3) in $CDCl_3$ at 298K.

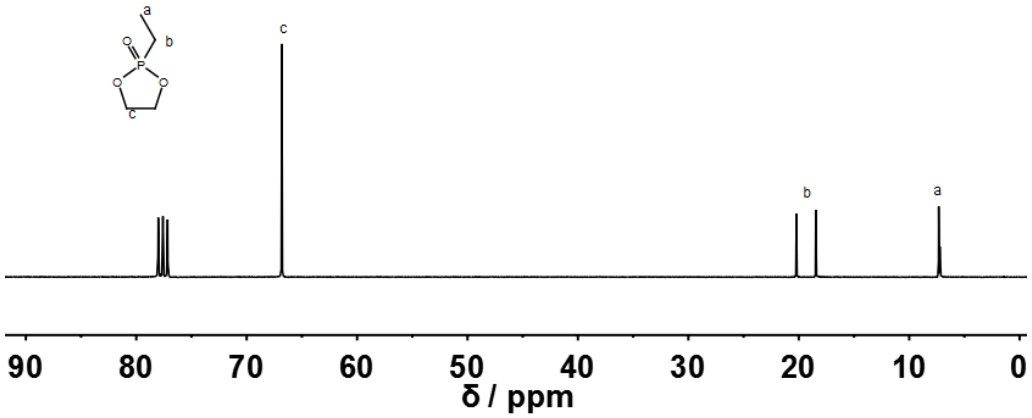

Figure 2.3: $^{13}C\{H\}$ NMR (75 MHz) of (1) in $CDCl_3$ at 298K.

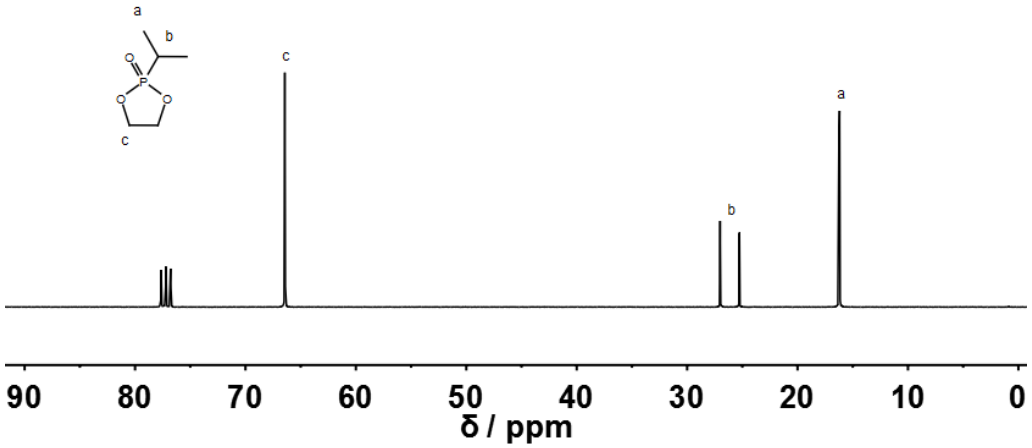

Figure 2.4: $^{13}C\{H\}$ NMR (75 MHz) of (2) in $CDCl_3$ at 298K.

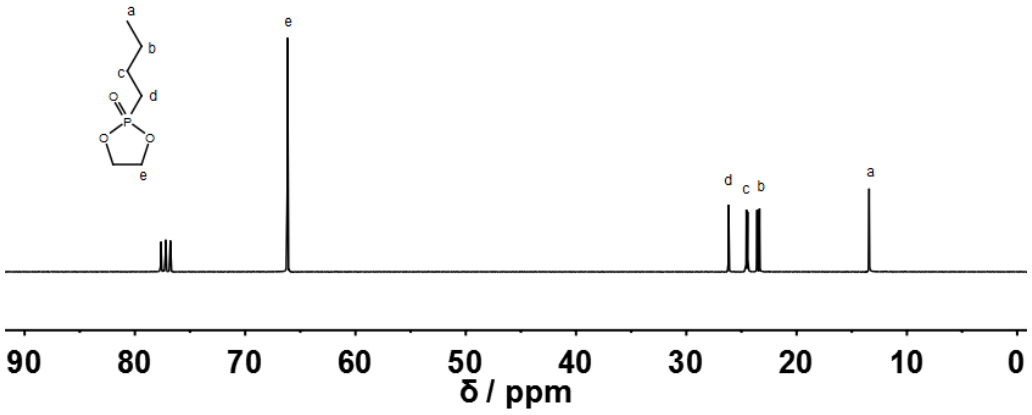

Figure 2.5: $^{13}C\{H\}$ NMR (75 MHz) of (3) in $CDCl_3$ at 298K.

The ^{1}H NMR spectra of all compounds exhibit two signals with a complex splitting pattern between 4.48 - 4.14 ppm indicating a chemical and magnetic inequality of the protons of the five-membered ring. This diastereotopy of the five-membered phosphonates, a result of the non-equivalence of two sides of the non-planar ring, was already observed in our previous work.[22] All aliphatic proton signals exhibit strong *J*-coupling to the phosphorus atom, resulting in a complex pattern of all resonances in the spectra (signal assignment Figure 2.1).

^{31}P{H} NMR spectroscopy proved to be highly sensitive towards the different phosphorus species as each different monomer exhibited a slightly different ^{31}P chemical shift despite the high homology of the compounds. (^{31}P{H} NMR ($CDCl_3$, ppm): 52.52 (**1**), 55.01 (**2**), 51.57 (**3**)) FTIR analysis was found to be sensitive to different P-C bond vibrations depending on the substitution pattern and can additionally be used to distinguish between the 2-alkyl-2-oxo-1,3,2-dioxaphospholane derivatives. (P-C vibration (cm^{-1}): 2917 (MeEP), 2868 (EtPPn, (**1**)), 2877 (*i*PrPPn, (**2**)), 2873 (*n*BuPPn, (**3**)) The fingerprint area showed strong homology between the different monomers. FTIR spectra of the respective monomers are shown in Figures 2.6 - 2.8.

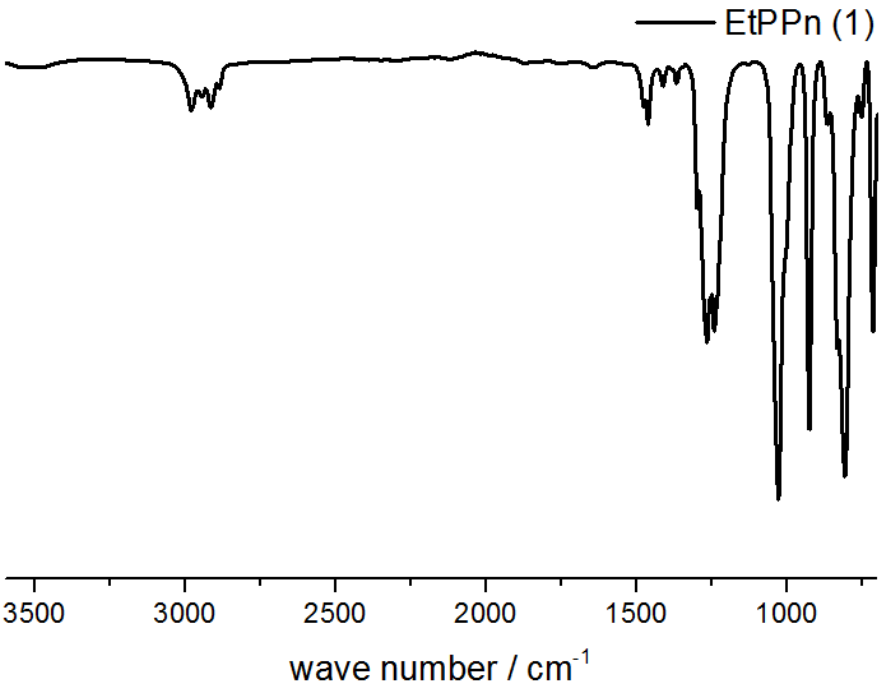

Figure 2.6: FTIR spectrum of (1) at 298K.

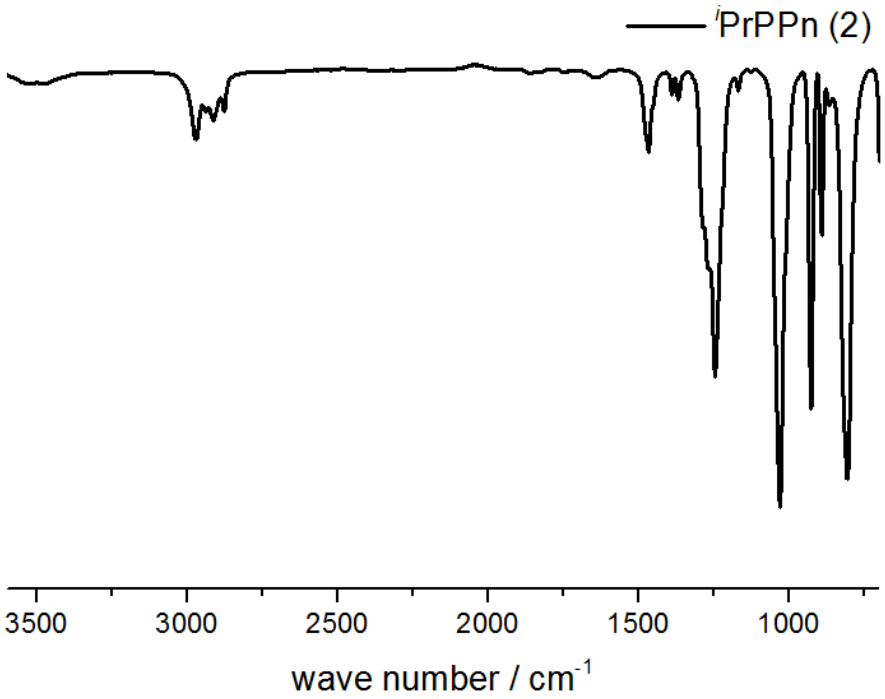

Figure 2.7: FTIR spectrum of (2) at 298K.

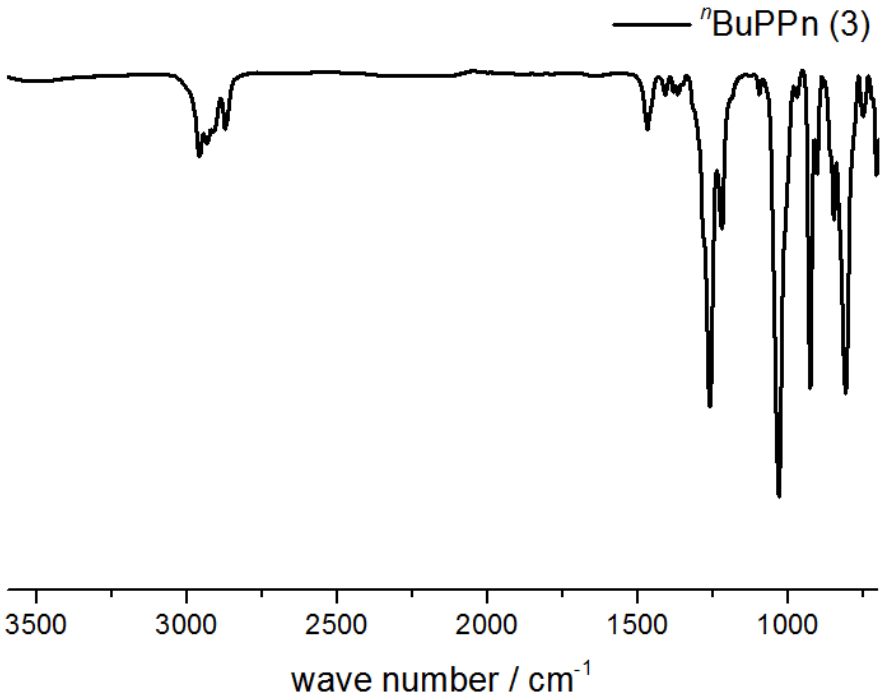

Figure 2.8: FTIR spectrum of (3) at 298K.

Polymer Synthesis

The 2-alkyl-2-oxo-1,3,2-dioxaphospholanes (**1**), (**2**) and (**3**) were polymerized via the organocatalytic AROP to ensure high control over molecular weight and molecular weight distribution. Both monomers (**1**) and (**3**), bearing a linear *n*-alkyl chain, polymerized readily with DBU as the catalyst and 2-(benzyloxy) ethanol as the respective initiator within 16h at 30 °C to conversions up to 98% (Scheme 2.3, a and c). The sterically more demanding (**2**) did not undergo polymerization under these conditions, however, polymerized with TBD at 0 °C within 20 min (Scheme 2.3, b). 2-(Benzyloxy) ethanol was chosen as the initiator to enable the ^{1}H NMR assisted the determination of the molecular weight, as well as to ensure a comparable reactivity of initiator and growing chain end.

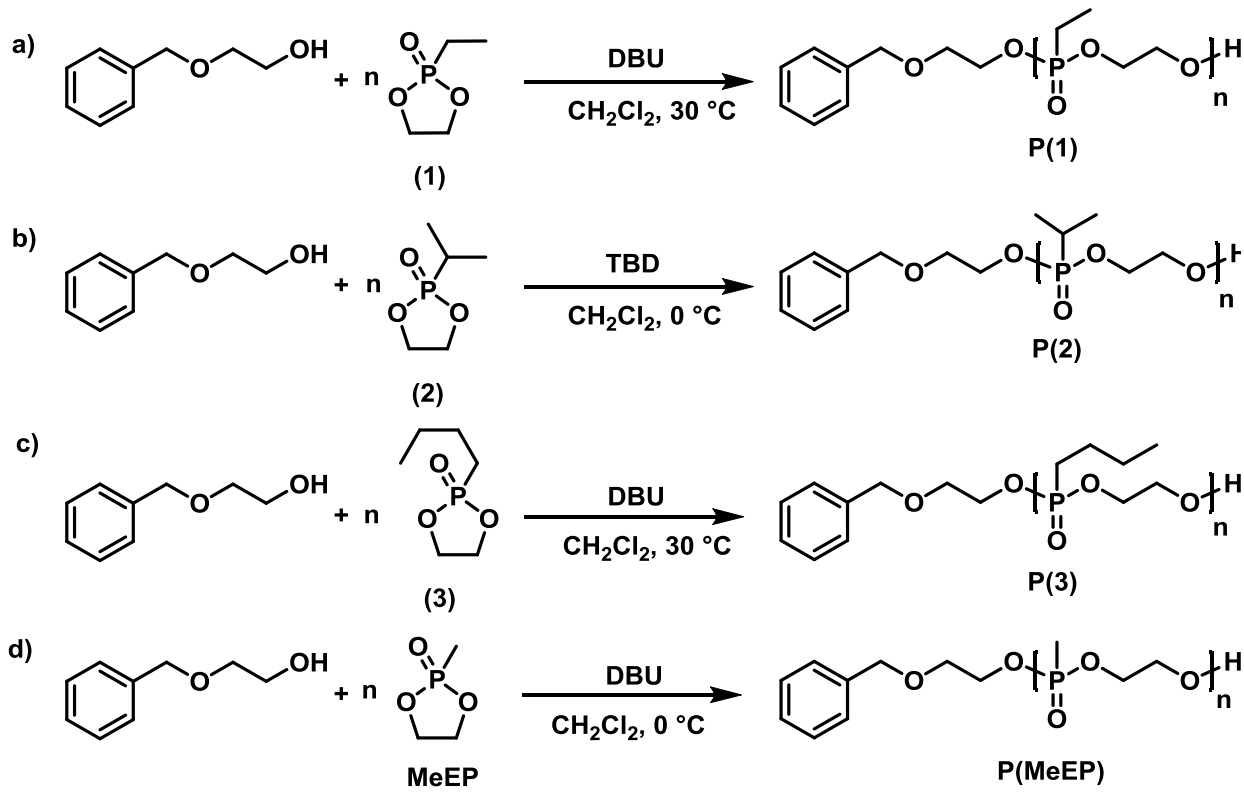

Scheme 2.3: DBU and TBD catalyzed AROP of a) (1), b) (2), c) (3), and d) MeEP.

Conversion of the monomer was followed by ^{31}P{H} NMR spectroscopy. A change in the chemical shift of the cyclic monomer (~ 50 ppm) to the linear phosphonic acid ester (~ 35 ppm) indicated the opening of the five-membered ring (Figure 2.9).

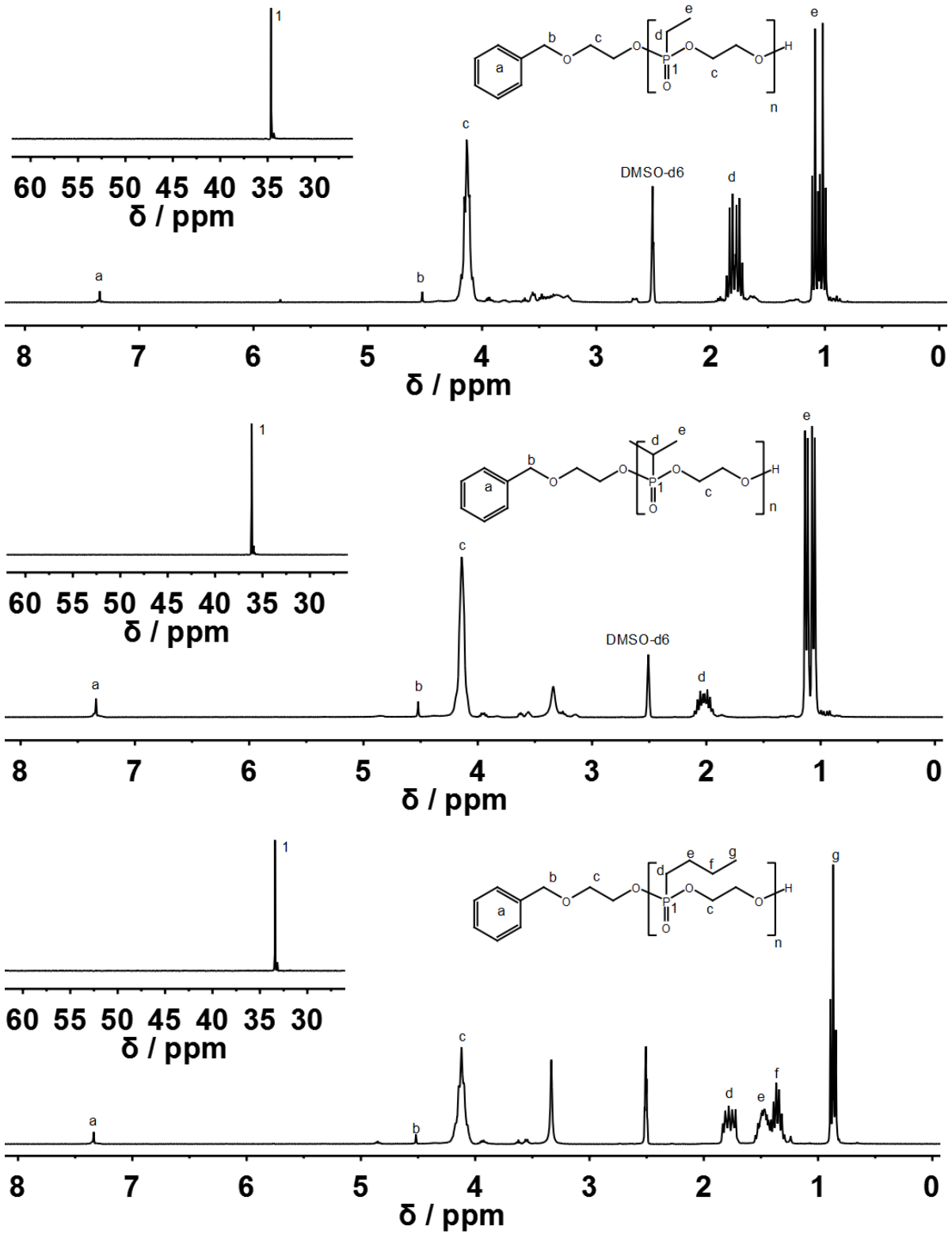

Figure 2.9: ^{1}H (300 MHz) and ^{31}P{H} (121 MHz) NMR spectra of a) P(1), b) P(2), and c) P(3) in DMSO-d_6 at 298K.

The molecular weight of the polymers was determined via ^{1}H NMR spectroscopy by comparing the integral of the aromatic signals of the initiator at 7.42 - 7.30 ppm with the backbone signal at 4.48 - 4.14 ppm. Polymers between 2,000 and 7,500 g mol^{-1} were obtained. The respective ^{1}H and $^{31}P\{H\}$ NMR spectra of **P(1)**, **P(2)** and **P(3)** are shown in Figure 2.9, $^{13}C\{H\}$ spectra are shown in Figures 2.10 - 2.12. Slight residues of catalysts were still present in the polymers even after repeated precipitation (Figure 2.9).

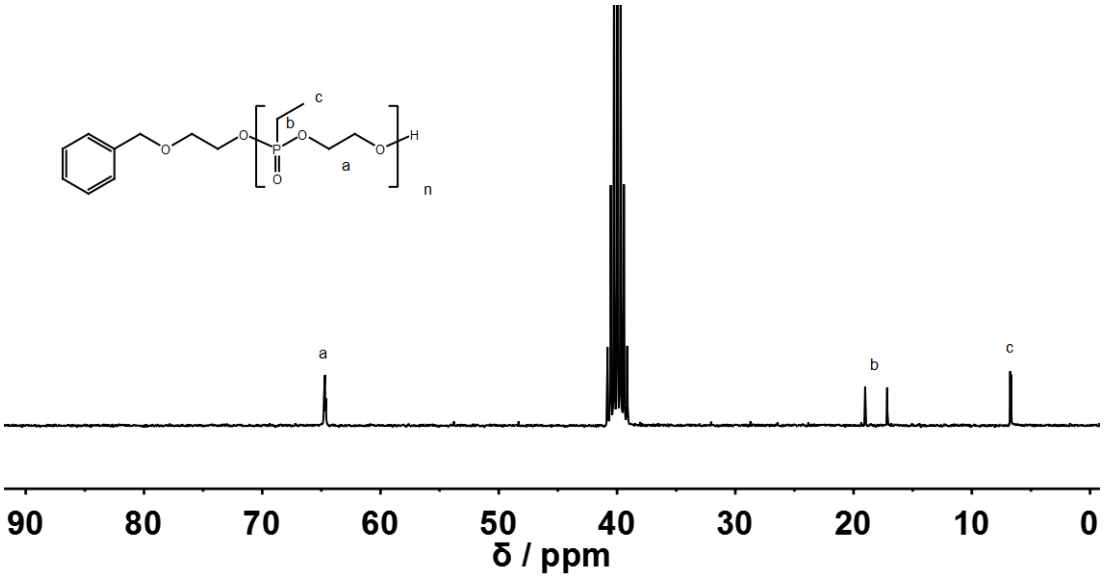

Figure 2.10: $^{13}C\{H\}$ NMR (75 MHz) of P(1) in DMSO-*d*$_6$ at 298K.

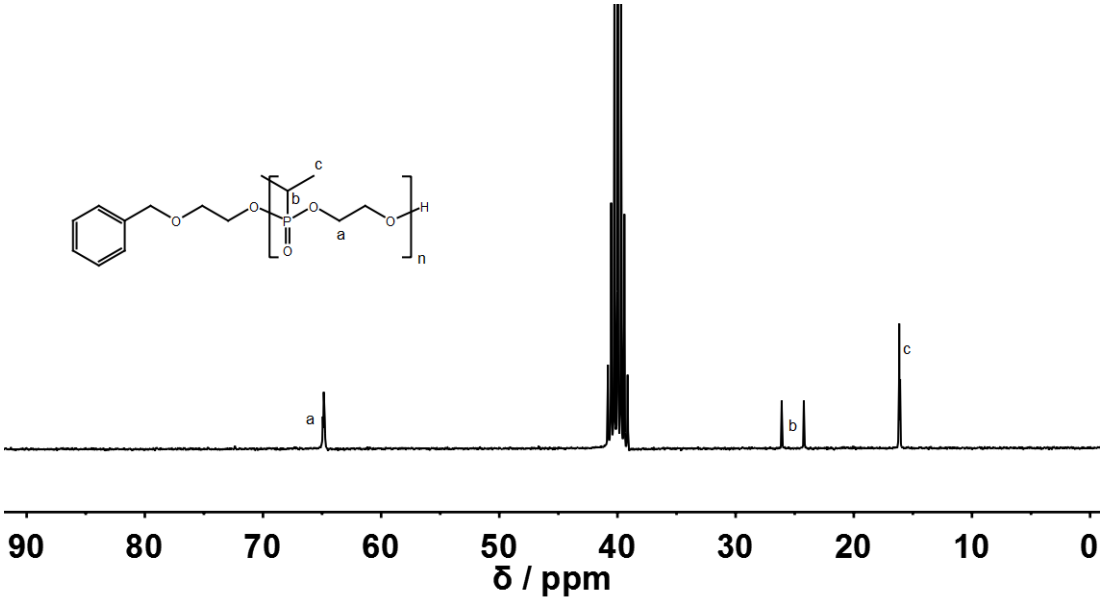

Figure 2.11: $^{13}C\{H\}$ NMR (75 MHz) of P(2) in DMSO-*d*$_6$ at 298K.

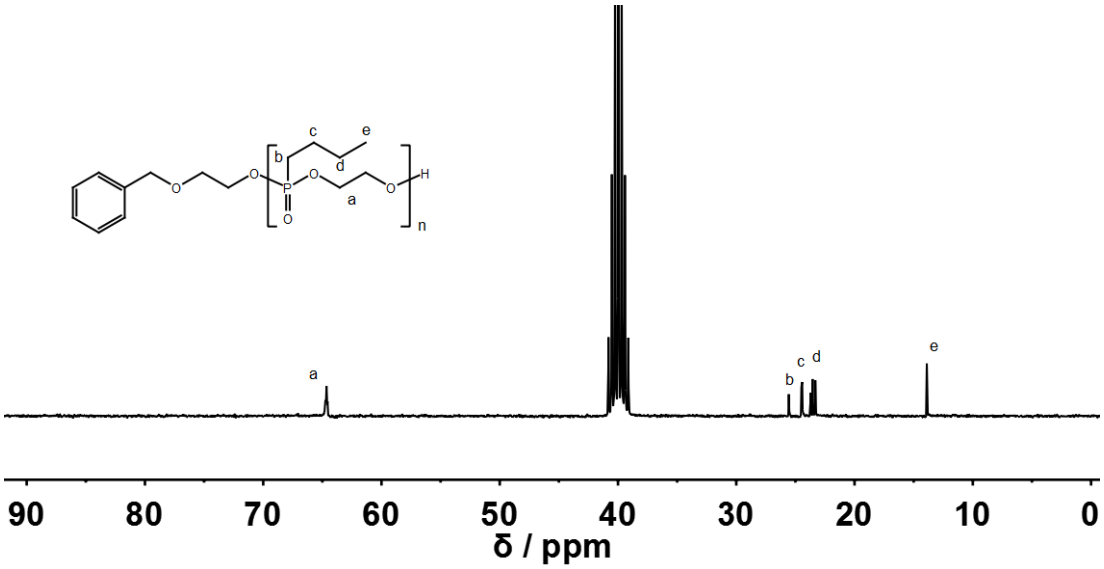

Figure 2.12: $^{13}C\{H\}$ NMR (75 MHz) of P(3) in DMSO-d_6 at 298K.

FTIR spectroscopy further demonstrated the incorporation of the initiator into the polymer sample. All FTIR spectra showed typical C(sp^2)-H vibrations at 1,600 cm^{-1}. No significant difference between the spectra of the polymers and the respective monomers were found except for a broadening of all signals. FTIR spectra of **P(1)**, **P(2)** and **P(3)** are shown in Figures 2.13 - 2.15.

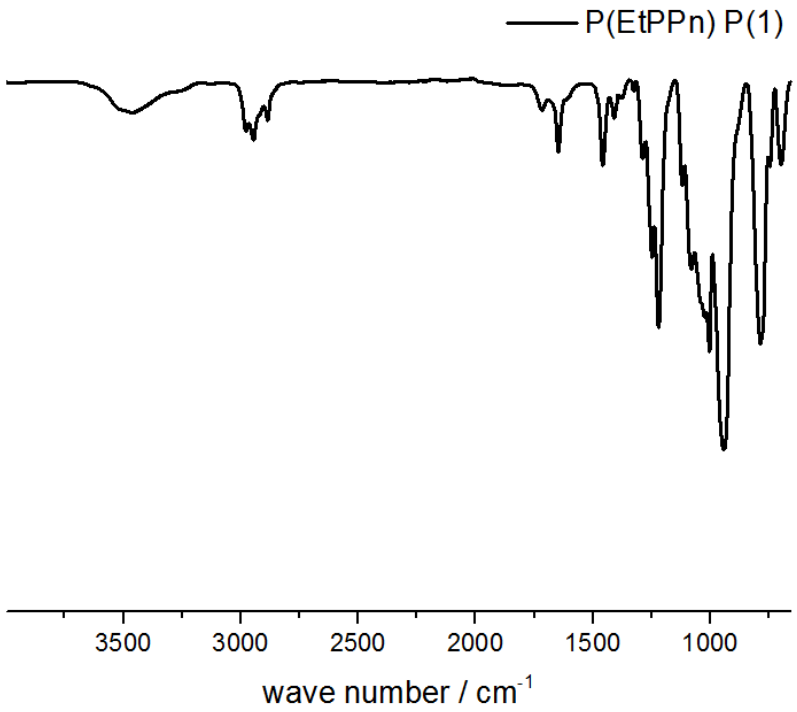

Figure 2.13: FTIR spectrum of P(1) at 298K.

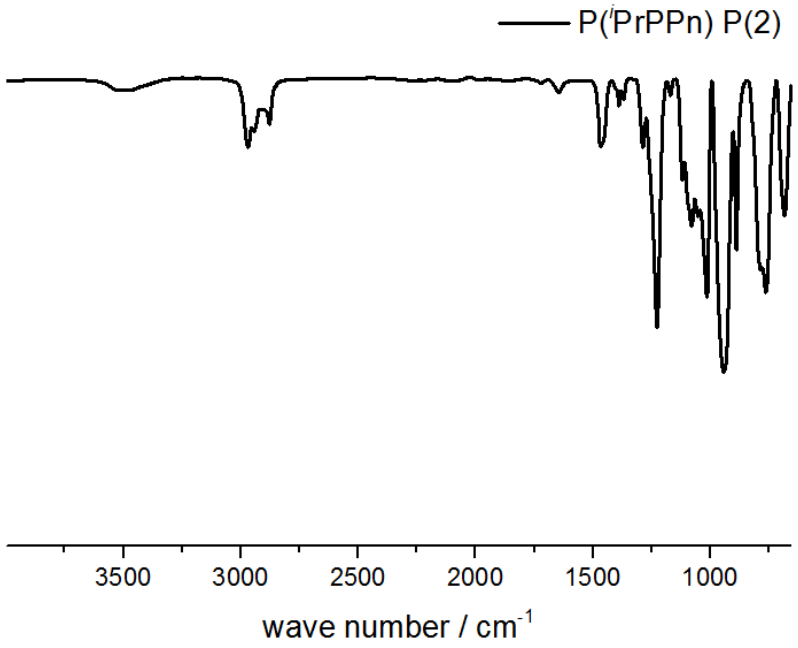

Figure 2.14: FTIR spectrum of P(2) at 298K.

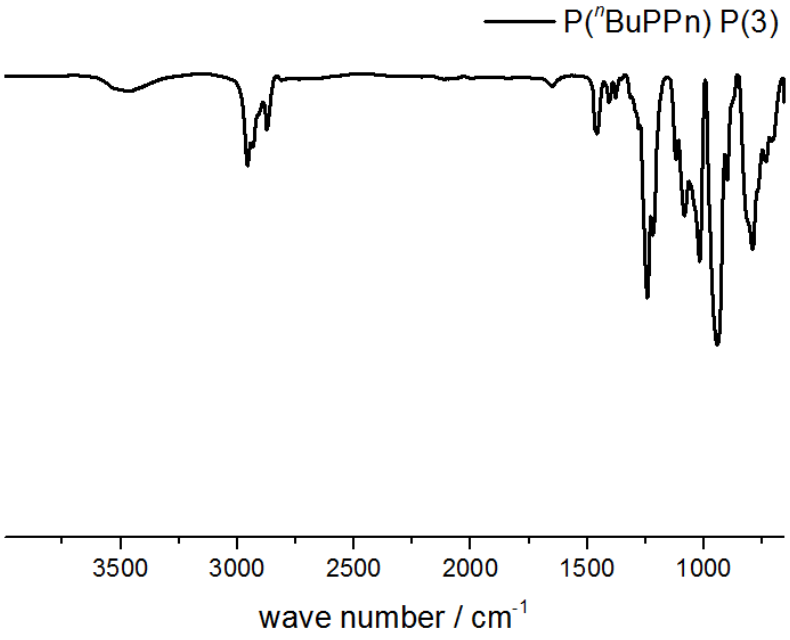

Figure 2.15: FTIR spectrum of P(3) at 298K.

Polymers exhibited monomodal SEC traces and were narrowly distributed ($Đ < 1.1$ for **P(1)** and **P(2)**). In some cases **P(3)** showed bimodal distributions. However, the overall molecular weight dispersity did not exceed $Đ = 1.25$ Representative SEC traces are shown in Figure 2.16.

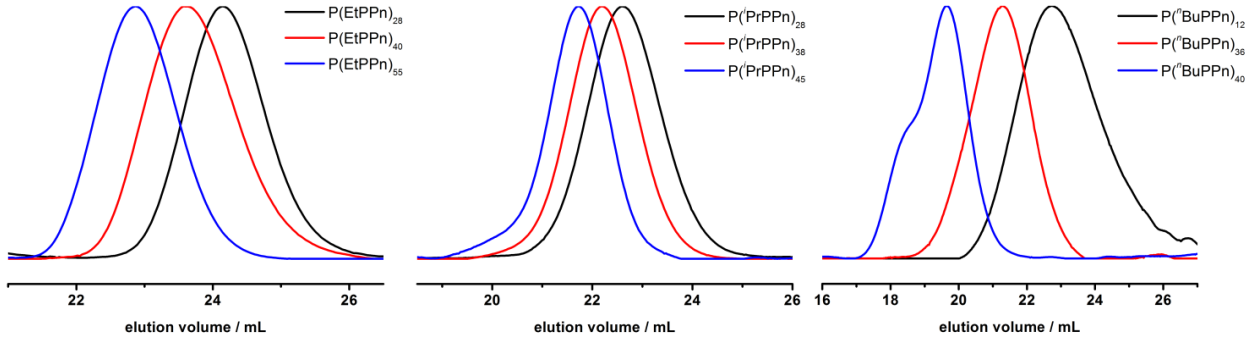

Figure 2.16: SEC traces (RI detection) of P(1) (left), P(2) (middle) and P(3) (right) in DMF at 50 °C.

Macroscopic Properties

All obtained polymers were amorphous materials with low glass transition temperatures around -45 to -50 °C. The chain length, as well as the side chain, had no significant effect on the glass transition temperature.

Polymers **P(1)** and **P(2)** were found to be water-soluble in all examined concentrations (up to 25 mg mL^{-1} in PBS 0.1 mol L^{-1} pH 7.4). No temperature dependency in their solubility was observed. This behavior is in sharp contrast to their phosphate homologs. Both poly(ethylene ethyl phosphate), as well as poly(ethylene isopropyl phosphate), show a lower critical solution temperature (LCST) at 38 °C and 5 °C respectively.[10, 46] The more hydrophobic polymers **P(3),** however, showed both a drastically decreased solubility as well as a strong concentration-dependent LCST behavior as shown in Figure 2.17.

P(3) became insoluble in PBS at concentrations higher than 0.1 mg mL^{-1} at room temperature. The complete polymer characterization is summarized in Table 2.1.

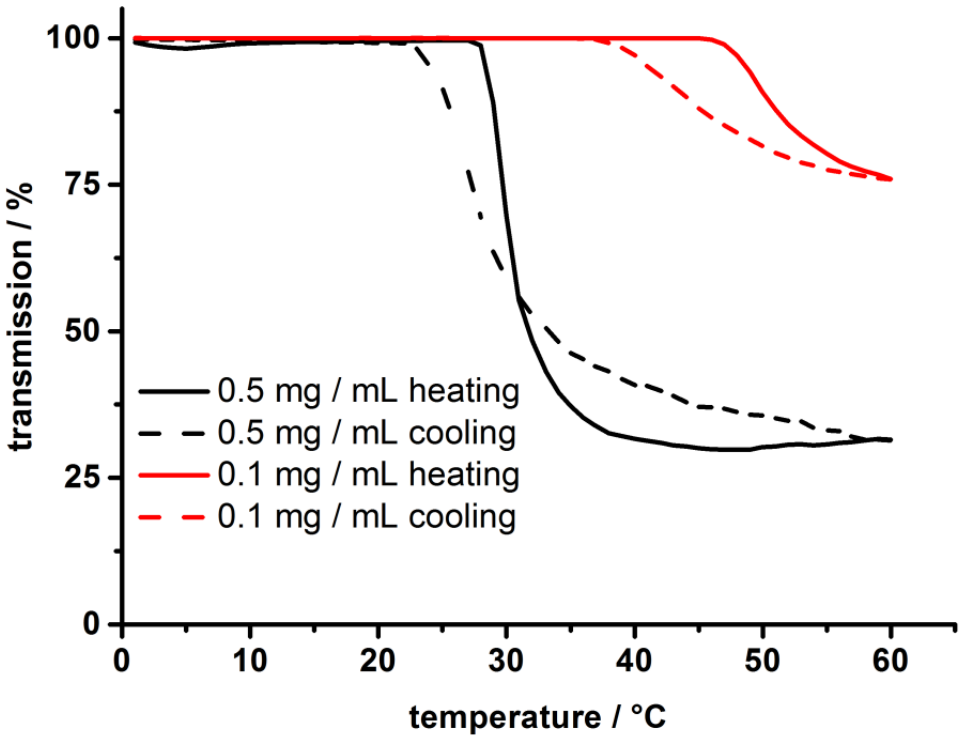

Figure 2.17: Turbidity measurements of $P(3)_{36}$ in PBS at a heating rate of 1 °C min^{-1}. The transmission was measured at 500 nm. Cloud point temperature (T_{cp}) was measured at the inflection of the heating curve. The occurrence of phase separation was observed at 31 °C (0.5 mg mL^{-1}) and 51 °C (0.1 mg mL^{-1}), respectively. Only a slight hysteresis was observed.

Table 2.1. Analytical results for all polymers.

polymer[a]	Y /%[b]	M_n / g mol^{-1}[b]	$Đ$[c]	T_g / °C[d]
P(1)$_{28}$	91	3,800	1.06	-49
P(1)$_{40}$	90	5,400	1.07	-45
P(1)$_{55}$	82	7,500	1.04	-46
P(*2*)$_{28}$	84	4,200	1.08	-42
P(2)$_{38}$	60	5,700	1.08	-44
P(*2*)$_{45}$	68	6,800	1.07	-41
P(*3*)$_{12}$	85	2,000	1.23	-61
P(*3*)$_{36}$	90	6,000	1.15	-48
P(*3*)$_{40}$	65	6,500	1.11	-50

[a] Type of monomer and degree of polymerization. [b] Conversion Y and M_n determined via ^{1}H NMR. [c] Determined via SEC in DMF at 50 °C (vs. PEG standards). [d] Determined by differential scanning calorimetry.

Biological Compatibility

Due to the high homology to other synthetic and naturally occurring PPEs, the abundance of phosphonic acid esters in living nature, and the studies previously reported by our group, the new poly(ethylene alkyl phosphonate)s were expected to be non-toxic.[22] The cytotoxicity of **P(1)$_{40}$** and **P(2)$_{38}$** was investigated *in vitro* against HeLa cells in a concentration range from 125 to 1,000 µg mL^{-1} after 24h of incubation at 37 °C in Dulbecco's modified eagle medium (DMEM), supplemented with 10% FCS. **P(3)$_{40}$** was tested under the same conditions at lower concentrations due to the lower solubility of the polymer. Cell viability was monitored as a function of ATP concentration which was dependent on the amount of living cells. PEG with a concentration of 1 mg mL^{-1} was used as the positive *benchmark*, and DMSO was used as negative control.

Both **P(1)$_{40}$**, as well as **P(2)$_{38}$** (Figures 2.18 and 2.19, respectively), showed no toxicity towards HeLa cells at the tested concentrations and viability was comparable with PEG. **P(3)$_{40}$** showed high toxicity against HeLa cells at concentrations of 100 µg mL^{-1} and 50 µg mL^{-1} (Figure 2.20). However, cell viability rose to 75% at a concentration of 25 µg mL^{-1} and was comparable with the control sample for concentrations equal and lower than 10 µg mL^{-1}.

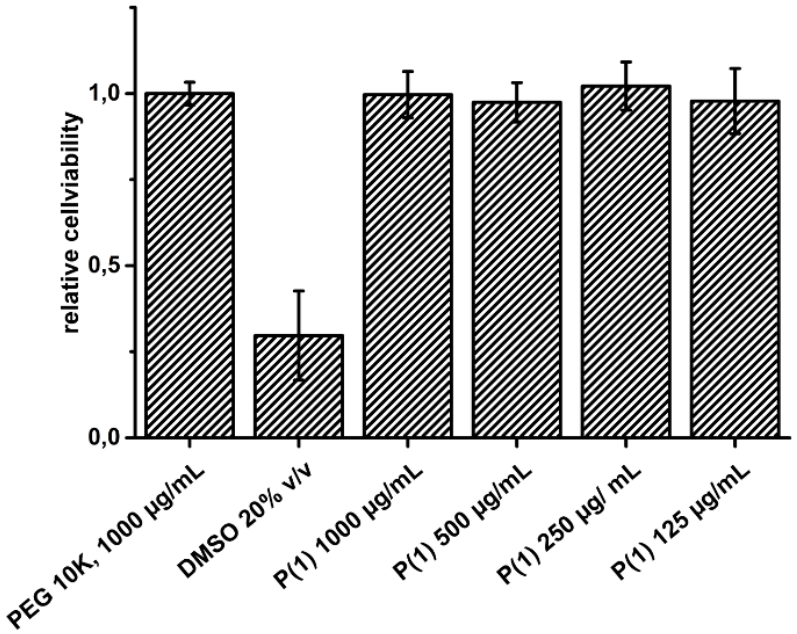

Figure 2.18: *In vitro* cell viability assay of HeLa cells treated with P(1)$_{40}$ after 24h of incubation. The experiments were carried out as three independent replicates.

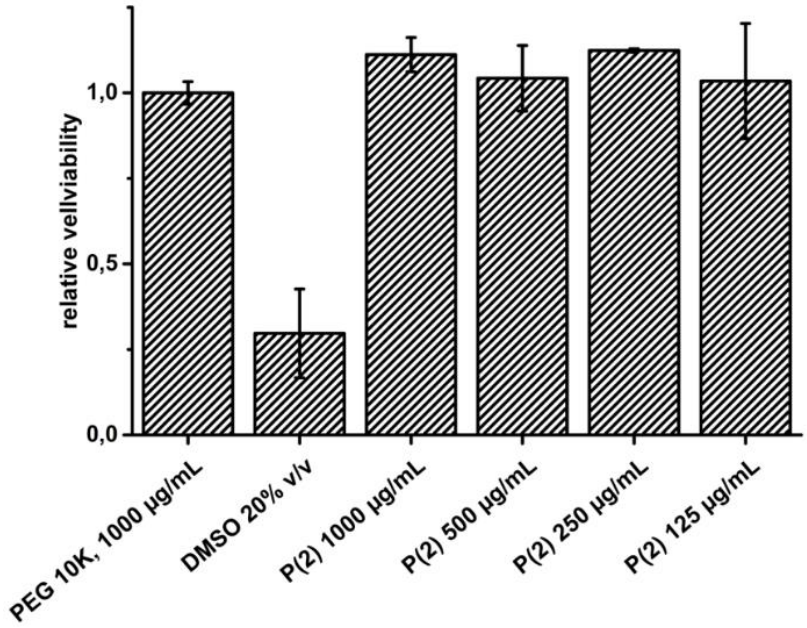

Figure 2.19: ***In vitro*** **cell viability assay of HeLa cells treated with $P(2)_{38}$ after 24h of incubation. The experiments were carried out as three independent replicates.**

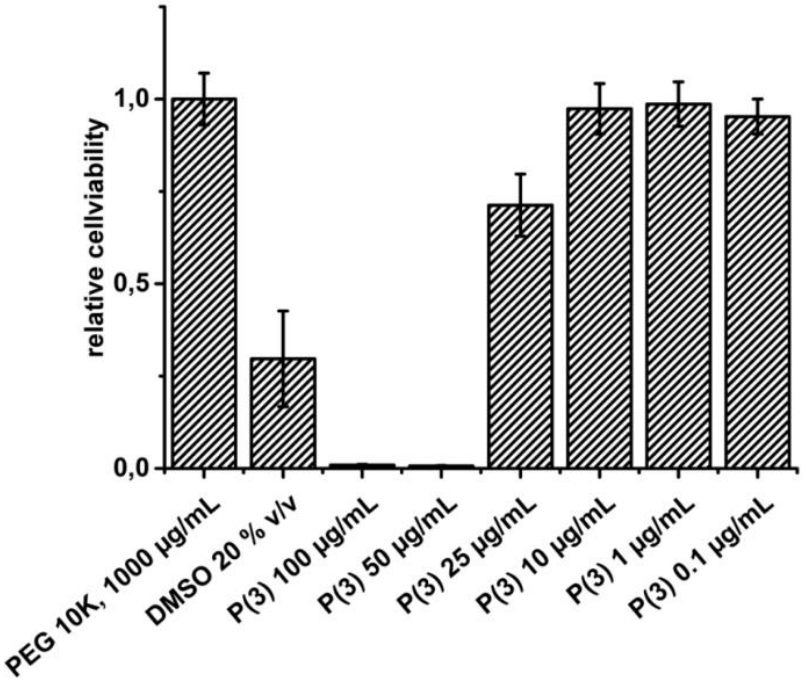

Figure 2.20: ***In vitro*** **cell viability assay of HeLa cells treated with $P(3)_{40}$ (c) after 24h of incubation. The experiments were carried out as three independent replicates.**

For further evaluation of the polymers biocompatibility, its effect on the enzyme acetylcholinesterase was analyzed. Acetylcholinesterase is a key enzyme in nerve transmission. It catalyzes the hydrolysis and deactivation of the neurotransmitter acetylcholine, terminating the incoming nervous signal. This preserves the well-defined equilibrium between activation and deactivation of the receiving nerve cells. Organophosphorus compounds with a well-solvated leaving group (-F, -O-Ph-NO_2) are known to show high toxicity by irreversibly inhibiting this enzyme through covalent modification of the catalytically active serine residue.[47] These “activated” phosphonic acid derivatives are used as toxins in pest control and agriculture but have also been used as chemical warfare agents. Therefore, the polymers herein presented with “non-activated” phosphonic acid esters needed to be studied in regards to their potential effect on acetylcholinesterase. The colorimetric assay used is based on the enzymatic cleavage of acetylthiocholine and the subsequent dithiol exchange reaction between the liberated thiocholine and the added 5,5’-dithio-3-bis-nitrobenzoic acid (DTNB) (Scheme 2.4).

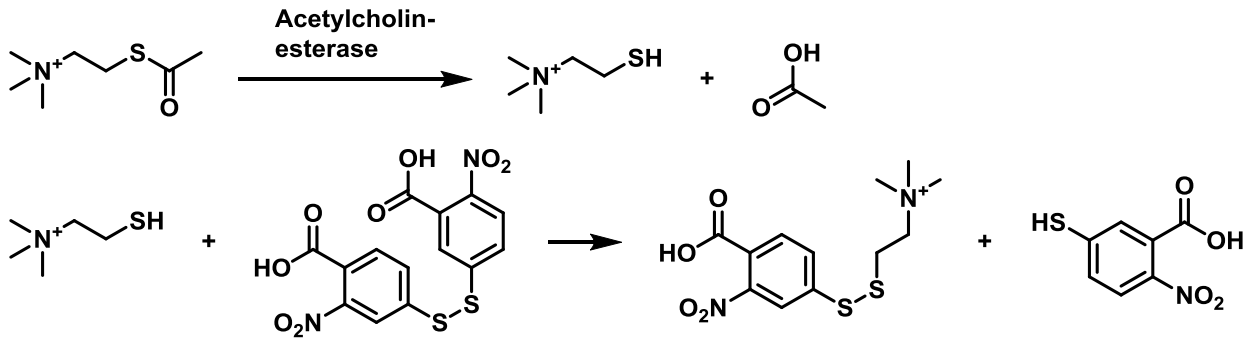

Scheme 2.4: Formation of 2-nitro-5-thiobenzoic acid used in the Amplite™ Colorimetric Acetylcholinesterase Assay.

The liberated 2-nitro-5-thiobenzoic acid shows a characteristic UV absorption at 410 nm which is proportional to the enzyme activity. 1,2,3,4-Tetrahydroacridin-4-amine (Tacrin), a known reversible acetylcholinesterase inhibitor, was used as a positive control. The reaction buffer without any further additive was used as a negative control (Figure 2.20). The tested polymers did not affect the enzymatic activity of acetylcholinesterase at the tested concentrations. Tacrine induced a nearly complete inhibition. An interference of the herein presented poly(phosphonate)s with acetylcholinesterase in future applications is therefore unlikely.

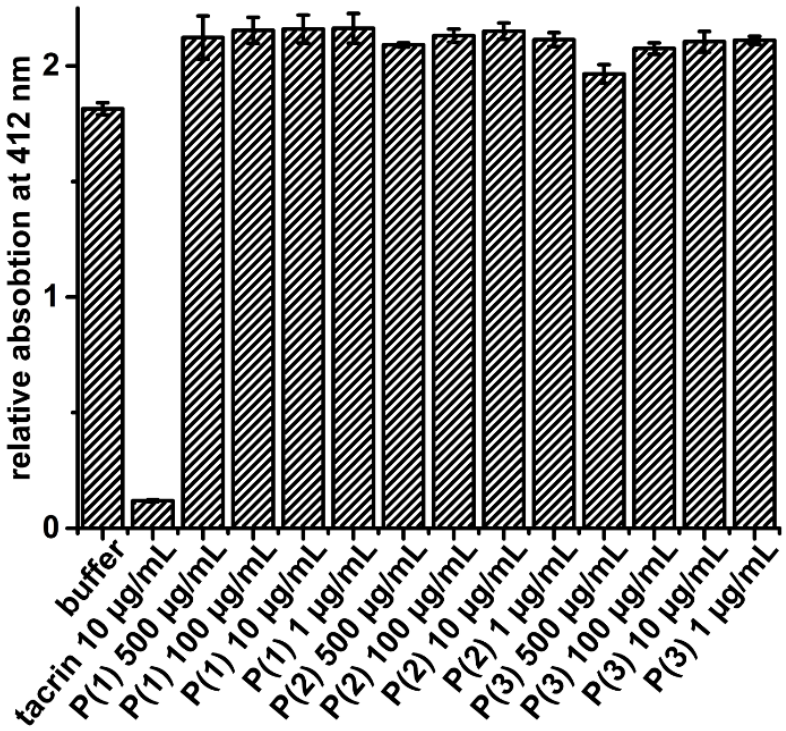

Figure 2.20: Results of the acetylcholinesterase assay of $P(1)_{40}$, $P(2)_{38}$ and $P(3)_{40}$ with tacrin as a positive control. The experiments were carried out as four independent replicates.

Degradation

The behavior of polymers in aqueous media in regards to their stability and degradation is an essential factor for many biomedical applications. The polymer is required to remain intact for a certain amount of time, e.g., to efficiently protect a conjugated material until the desired task is fulfilled. The eventual degradation, however, is essential for the excretion of the polymer and its degradation products from the body to avoid harmful accumulations or to provoke an immune response. Therefore, a precise knowledge of the degradation rate of polymeric material is of central importance for any biomedical application. Hydrolysis of phosphonate esters proceeds via a nucleophilic attack of water or hydroxyl ions to the phosphorus center.[48] The hydrolysis follows a second order kinetic and is dependent on the pH value. Therefore, degradation was performed at physiological pH of 7.4 as well as at pH 9 for enhanced degradation kinetics. The previously described poly(ethylene methyl phosphonate) was used as a reference to compare the stability of the herein presented polymers.[22]

In the case of $P(MeEP)_{21}$ at pH 7.4 (Figure 2.21, left) a significant decrease in signal intensity, as well as an apparent shift of the peak maximum to higher elution volumes, was observed within the first 4h. The distribution broadened over time, and monomodality was lost after 24h. Degradation proceeded considerably faster under basic conditions, and complete degradation was observed after 48h (Figure 2.21, right).

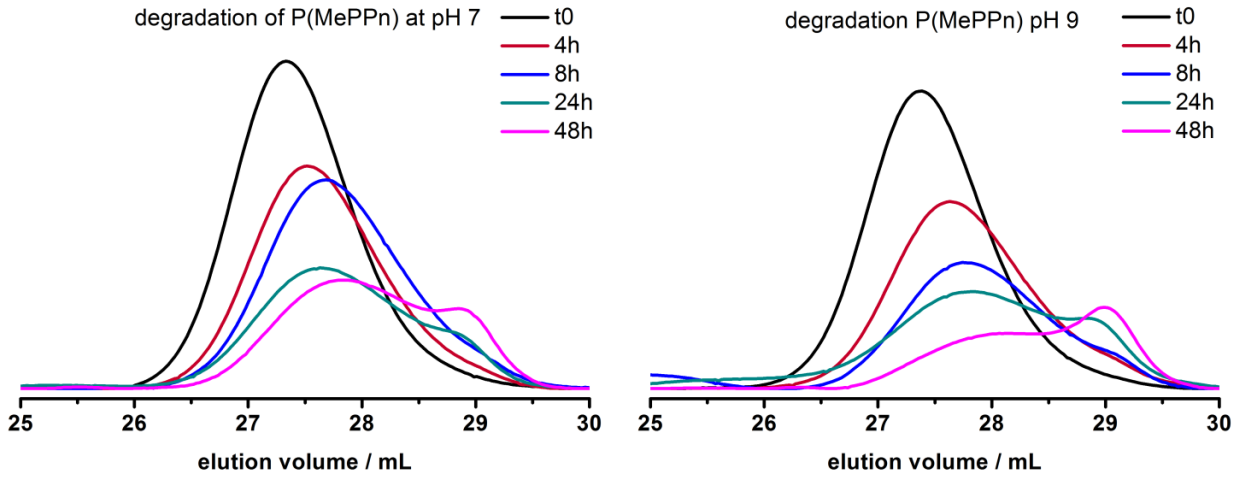

Figure 2.21: Degradation of $P(MeEP)_{21}$ monitored by SEC: at pH 7.4 (left) and pH 9 (right) in 0.1 M (NH4)2CO3 buffer at 37 °C. Refractive index measured in DMF at 50 °C.

Replacing the methyl side chain with ethyl groups increased the hydrolytic stability of the polymers dramatically: the degradation kinetics of **$P(1)_{40}$** are strongly reduced compared to $P(MeEP)_{21}$.

At pH 7.4 (Figure 2.22, left), no degradation was observed within the first 8h. Over the curse of two weeks, slight shifts in the elution volume were observed. Overall, the polymer remained stable over a period of 1 week without significant loss of molecular weight. Again, degradation rate increased at elevated pH values (Figure 2.22, right). Under these conditions, **$P(1)_{40}$** showed first signs of degradation within the first 8h. Strong broadening of the signal was observed within two weeks. Still, complete degradation, as observed for $P(MeEP)_{21}$ was not observed yet.

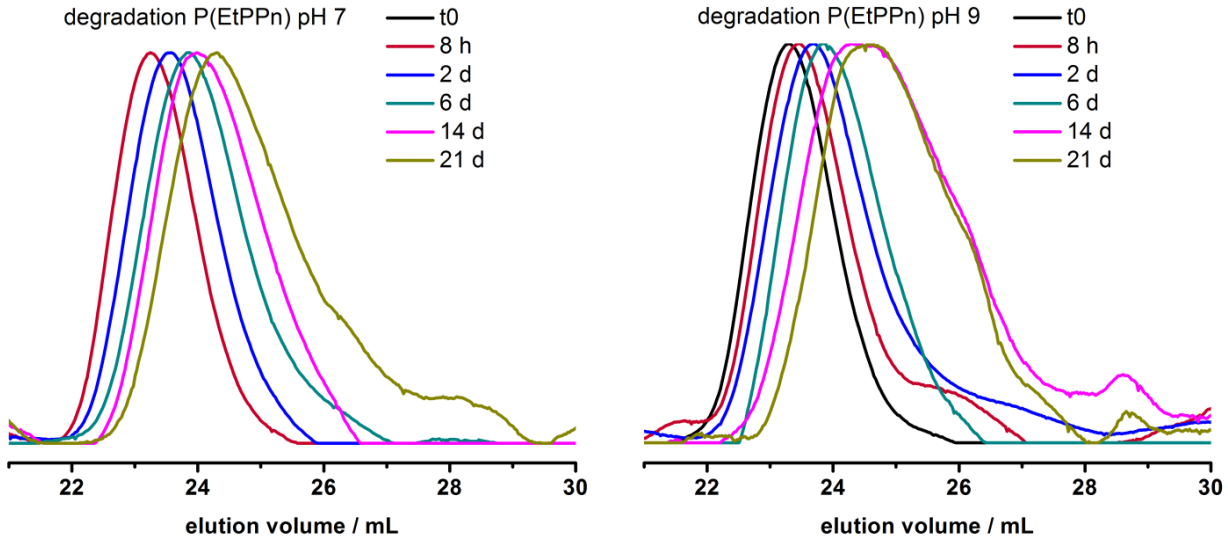

Figure 2.22: Degradation of $P(1)_{40}$ monitored by SEC: at pH 7.4 (left) and pH 9 (right) in 0.1 M $(NH_4)_2CO_3$ buffer at 37 °C. Refractive index measured in DMF at 50 °C.

Isopropyl groups shielded the phosphonate units even more while keeping a high solubility in aqueous medium. **$P(2)_{28}$** showed the highest hydrolytic stability (Figure 2.23):

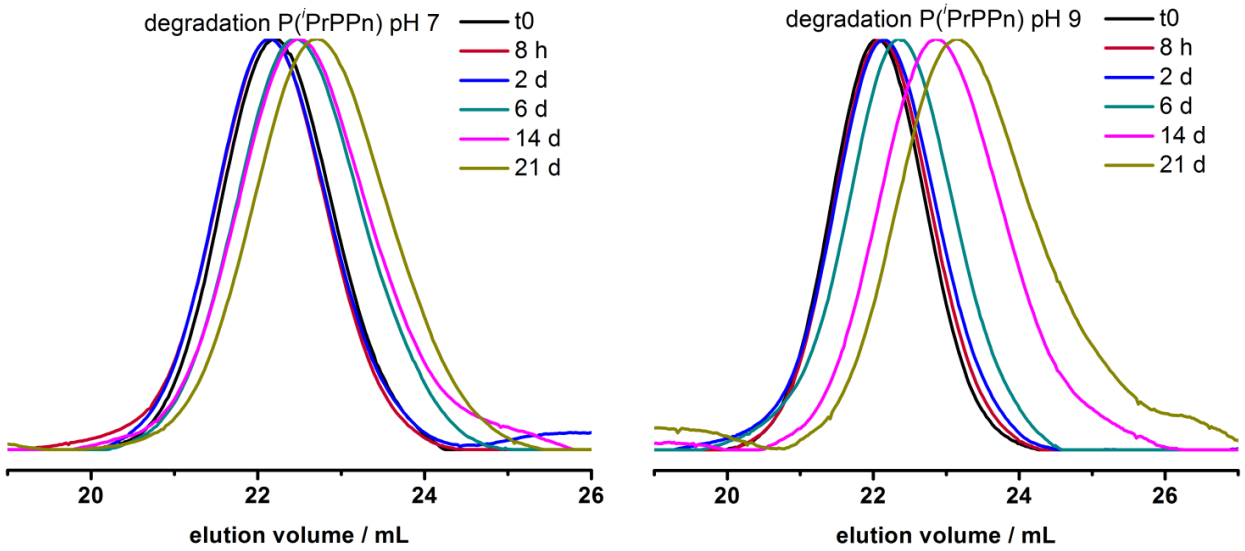

Figure 2.23: Degradation of $P(2)_{28}$ monitored by SEC: At pH 7.4 (left) and pH 9 (right) in 0.1 M $(NH_4)_2CO_3$ buffer at 37 °C. Refractive index measured in DMF at 50 °C.

At pH 7.4 (Figure 2.23, left), no change from the initial signal at t_0 was observed within the first two days. At the end of the experiment after three weeks only a slight change in elution volume, no broadening of the signal and no additional fragments were observed. At pH 9 (Figure 2.23, right) the first indications for degradation were detected within the first six days. However, a significant shift in elution volume was only observed after three weeks. Again, full degradation, as in the case of P(MeEP) was not observed. We showed a significant change in the degradation kinetics by variation of the reaction conditions and side chains. This allowed for stabilities from 8h up to 6 days without any significant degradation.

Summary and Conclusion

In summary, novel monomers for the AROP of poly(ethylene alkyl phosphonate)s have been synthesized and successfully polymerized. The AROP proceeded with excellent control both over molecular weight (between 2,500 g mol^{-1} and 7,500 g mol^{-1}) and molecular weight distribution ($Đ$ < 1.2). The obtained polymers deprived of **(1)** and **(2)** showed excellent water-solubility (up to 25 mg mL^{-1}) while **P(3)** exhibited a concentration-dependent LCST behavior. The viability of HeLa cells incubated for 24h with **P(1)** and **P(2)** was compatible with that of PEG even at high concentrations. **P(3)** showed toxicity at concentrations above 25 µg mL^{-1}. A considerable increase in hydrolytic stability was found through variation of the alkyl side chain: degradation times can be adjusted from 4h up to 6 days at physiological pH value. The presented monomers increase the toolbox for the synthesis of biocompatible, biodegradable poly(phosphoester)s with adjustable polymer properties such as aqueous stability and solubility. We thus believe that this class of polymers can complement the use of poly(ethylene glycol) in many bio applications due to these excellent properties.

Acknowledgements

The authors thank Prof. Dr. K. Landfester for continuous support. The authors acknowledge support from the “Deutsche Forschungsgemeinschaft” (DFG WU 750/ 6-1). The authors thank Johanna Simon for the cell culture and toxicity assays.

References

1. Knop, K.; Hoogenboom, R.; Fischer, D.; Schubert, U. S. *Angew. Chem. Int. Ed., Engl.* **2010,** 49, 6288-308.
2. Ulbricht, J.; Jordan, R.; Luxenhofer, R. *Biomaterials,* **2014,** 35, 4848-4861.
3. Wang, Y.-C.; Yuan, Y.-Y.; Du, J.-Z.; Yang, X.-Z.; Wang, J. *Macromol. Biosci.,* **2009,** 9, 1154-1164.
4. Kraicheva, I.; Vodenicharova, E.; Shenkov, S.; Tashev, E.; Tosheva, T.; Tsacheva, I.; Kril, A.; Topashka-Ancheva, M.; Georgieva, A.; Iliev, I.; Vladov, I.; Gerasimova, T.; Troev, K. *Bioorg. Med. Chem.,* **2014,** 22, 874-882.
5. Zhang, S.; Li, A.; Zou, J.; Lin, L. Y.; Wooley, K. L. *ACS Macro Lett.,* **2012,** 1, 328-333.
6. Clément, B.; Grignard, B.; Koole, L.; Jérôme, C.; Lecomte, P. *Macromolecules,* **2012,** 45, 4476-4486.
7. Zhang, S.; Zou, J.; Zhang, F.; Elsabahy, M.; Felder, S. E.; Zhu, J.; Pochan, D. J.; Wooley, K. L. *J. Am. Chem. Soc.,* **2012,** 134, 18467-18474.
8. Liu, J.; Pang, Y.; Huang, W.; Zhu, Z.; Zhu, X.; Zhou, Y.; Yan, D. *Biomacromolecules* **2011,** 12, 2407-2415.
9. Liu, J.; Huang, W.; Pang, Y.; Zhu, X.; Zhou, Y.; Yan, D. *Biomacromolecules,* **2010,** 11, 1564-1570.
10. Iwasaki, Y.; Yamaguchi, E. *Macromolecules,* **2010,** 43, 2664-2666.
11. Huang, S. W.; Wang, J.; Zhang, P. C.; Mao, H. Q.; Zhuo, R. X.; Leong, K. W. *Biomacromolecules,* **2004,** 5, 306-311.
12. Zhao, Z.; Wang, J.; Mao, H. Q.; Leong, K. W. *Adv. Drug Deliv. Rev.,* **2003,** 55, 483-499.
13. Mitova, V.; Slavcheva, S.; Shestakova, P.; Momekova, D.; Stoyanov, N.; Momekov, G.; Troev, K.; Koseva, N. *Eur. J. Med. Chem.,* **2014,** 72, 127-36.
14. Zhang, F.; Zhang, S.; Pollack, S. F.; Li, R.; Gonzalez, A. M.; Fan, J.; Zou, J.; Leininger, S. E.; Pavia-Sanders, A.; Johnson, R.; Nelson, L. D.; Raymond, J. E.; Elsabahy, M.; Hughes, D. M.; Lenox, M. W.; Gustafson, T. P.; Wooley, K. L. *J. Am. Chem. Soc.,* **2015,** 137, 2056-2066.
15. Ding, L.; Qiu, J.; Wei, J.; Zhu, Z. *Macromol. Rapid Commun.,* **2014,** 35, 1509-1515.
16. Lim, Y. H.; Heo, G. S.; Rezenom, Y. H.; Pollack, S.; Raymond, J. E.; Elsabahy, M.; Wooley, K. L. *Macromolecules,* **2014,** 47, 4634-4644.
17. Troev, K.; Naruoka, A.; Terada, H.; Kikuchi, A.; Makino, K. *Macromolecules,* **2012,** 45, 5698-5703.
18. Koseva, N.; Bogomilova, A.; Atkova, K.; Troev, K. *React. Funct. Pol.,* **2008,** 68, 954-966.
19. McGrath, J. W.; Chin, J. P.; Quinn, J. P. *Nature Rev. Microbiol.,* **2013**, 11, 412-419.
20. Kelly, S. J.; Dardinger, D. E.; Butler, L. G. *Biochemistry,* **1975,** 14, 4983-4988.
21. Huang, J.; Su, Z.; Xu, Y. *J. Mol. Evol.,* **2005,** 61, 682-690.
22. Steinbach, T.; Ritz, S.; Wurm, F. R. *ACS Macro Lett.,* **2014,** 3, 244-248.
23. Arbuzov, B. A. *Pure Appl. Chem.,* **1964,** 9, 307-336.
24. Michaelis, A.; Kaehne, R. *Ber. Dtsch. Chem. Ges.,* **1898,** 31, 1048-1055.
25. Kinnear, A. M.; Perren, E. A. *J. Chem. Soc. (Resumed),* **1952**, 3437-3445.
26. Meziane, D.; Hardouin, J.; Elias, A.; Guenin, E.; Lecouvey, M. *Heteroatom. Chem.,* **2009,** 20, 369-377.

27. Rajeshwaran, G. G.; Nandakumar, M.; Sureshbabu, R.; Mohanakrishnan, A. K. *Org. Lett.,* **2011,** 13, 1270-1273.
28. Fang, Y.; Zhang, L.; Li, J.; Jin, X.; Yuan, M.; Li, R.; Wu, R.; Fang, J. *Org. Lett.,* **2015,** 17, 798-801.
29. Wang, A. E.; Chang, Z.; Sun, W. T.; Huang, P. Q. *Org. Lett.,* **2015,** 17, 732-735.
30. Yang, J.; Chen, T.; Han, L. B. *J. Am. Chem. Soc.,* **2015,** 137, 1782-1785.
31. Metcalf, W. W.; van der Donk, W. A. *Annu. Rev. Biochem.,* **2009,** 78, 65-94.
32. L. L. Clark, E. D. I., R. Benner. *Am. J. Sci.,* **1999,** 299, 724-737.
33. Goddard, P.; Hutchinson, L. E.; Brown, J.; Brookman, L. J. *J. Control. Release,* **1989,** 10, 5-16.
34. Gaertner, F. C.; Luxenhofer, R.; Blechert, B.; Jordan, R.; Essler, M. *J. Control. Release,* **2007,** 119, 291-300.
35. Dams, E. T.; Laverman, P.; Oyen, W. J.; Storm, G.; Scherphof, G. L.; van Der Meer, J. W.; Corstens, F. H.; Boerman, O. C. *J Pharmacol. Exp. Ther.,* **2000,** 292, 1071-1079.
36. Allmeroth, M.; Moderegger, D.; Biesalski, B.; Koynov, K.; Rosch, F.; Thews, O.; Zentel, R. *Biomacromolecules,* **2011,** 12, 2841-2849.
37. Moedritzer, K.; Maier, L.; Groenweghe, L. C. D. *J. Chem. Eng. Data,* **1962,** 7, 307-310.
38. Iliescu, S.; Zubizarreta, L.; Plesu, N.; Macarie, L.; Popa, A.; Ilia, G. *Chem. Cent. J.,* **2012,** 6, 132-144.
39. Imai, Y.; Kamata, H.; Kakimoto, M.-A. *J. Pol. Sci.: Polym. Chem. Ed.,* **1984,** 22, 1259-1265.
40. Ranganathan, T.; Zilberman, J.; Farris, R. J.; Coughlin, E. B.; Emrick, T. *Macromolecules,* **2006,** 39, 5974-5975.
41. Steinbach, T.; Wurm, F. *Angew. Chem.,* **2015**, DOI: 10.1002/anie.201500147.
42. Steinbach, T.; Alexandrino, E. M.; Wurm, F. R. *Polym. Chem.,* **2013,** 4, 3800-3806.
43. Marsico, F.; Turshatov, A.; Weber, K.; Wurm, F. R. *Org. Lett.,* **2013,** 15, 3844-3847.
44. Steinbach, T.; Alexandrino, E. M.; Wahlen, C.; Landfester, K.; Wurm, F. R. *Macromolecules,* **2014,** 47, 4884-4893.
45. Marsico, F.; Wagner, M.; Landfester, K.; Wurm, F. R. *Macromolecules,* **2012,** 45, 8511-8518.
46. Iwasaki, Y.; Wachiralarpphaithoon, C.; Akiyoshi, K. *Macromolecules,* **2007,** 40, 8136-8138.
47. Sidell, F. R.; Borak, J. *Ann. Emerg. Med.,* **1992,** 21, 865-871.
48. Mabey, W.; Mill, T. *J. Phys.Chem. Ref. Data,* **1978,** 7, 383-415.
49. Maier, L. *Phosphorus, Sulfur, Silicon Relat. Elem.,* **1990,** 47, 465-470.

Supporting Information for

A library for well-defined and water-soluble poly(phosphonate)s with adjustable hydrolysis.

Materials

Solvents and chemicals were purchased from Acros Organics, Sigma Aldrich or Fluka and used as received unless otherwise stated. All chemicals were purchased in highest purities, dry and stored over molecular sieve (4Å), if possible. Ammonium bicarbonate was used as received from Fischer Scientific. Ultrapure water with a resistivity of 18 MΩ cm^{-1} (Milli-Q, Millipore®) was used to prepare buffers. Tetrahydrofuran (THF) was purchased from Sigma Aldrich and distilled from sodium before use. 2-(Benzyloxy)ethanol was purchased from ABCR, distilled from calcium hydride and stored over molecular sieve (4Å) and under argon before use. DBU was purchased from Sigma Aldrich, distilled before use and stored over molecular sieve (4Å) under argon. TBD was purchased from Sigma Aldrich and stored under argon. Deuterated solvents were purchased from Deutero GmbH (Kastellaun, Germany) and used as received.

Instrumentation and Characterization Techniques

Size exclusion chromatography (SEC) measurements were performed in DMF (containing 0.25 g L^{-1} of lithium bromide as an additive) at 50 °C and a flow rate of 1 mL min^{-1} with an Agilent 1100 Series as an integrated instrument, including a PSS HEMA column ($10^6/10^5/10^4$ g mol^{-1}), and a refractive index (RI) detector. Calibration was carried out using poly(ethylene glycol) standards provided by Polymer Standards Service. The ^{1}H, $^{13}C\{H\}$, and $^{31}P\{H\}$ NMR experiments were acquired on a 300 MHz Bruker AMX system. The temperature was kept at 298.3K and calibrated with a standard ^{1}H methanol NMR sample using the topspin 3.0 software (Bruker). $^{13}C\{H\}$ NMR spectra were referenced internally to solvent signals. $^{31}P\{H\}$ NMR spectra were referenced externally to phosphoric acid. The $^{13}C\{H\}$ NMR (75 MHz) and $^{31}P\{H\}$ NMR (121 MHz) measurements were obtained with a ^{1}H powergate decoupling method using 30 ° degree flip angle. All spectra were processed with the MestReNova 9.0.1-13254 software.

Differential Scanning Calorimetry (DSC) measurements were performed using a Perkin-Elmer 7 series thermal analysis system and a Perkin Elmer Thermal Analysis Controller TAC 7/DX in the temperature range from –100 to 80 °C under nitrogen with a heating rate of 10 °C min^{-1}. Cloud points were determined in Dulbecco's PBS (with 0.5 mmol L^{-1} $MgCl_2$ and 0.9 mmol L^{-1} $CaCl_2$, sterile filtered) from Sigma Aldrich and detected by the optical transmittance of a light beam (λ = 500 nm) through a 1 cm sample cell. The measurements were performed on a Jasco V-630 photo spectrometer with a Jasco ETC-717 Peltier element. The intensity of the transmitted light was recorded versus the temperature of the sample cell. The heating/cooling rate was 1 °C min^{-1} and values were recorded every 0.1 °C. Degradation of poly(ethylene alkyl phosphonate)s was performed in aqueous 0.1 M $(NH_4)_2CO_3$ buffer at 37 °C at a concentration of 10 mg mL^{-1}. After the appropriated degradation time 200 µL of the solution was diluted in 800 µL DMF and analyzed by SEC. Inhibition of acetylcholinesterase was tested with the Amplite™ Colorimetric Acetylcholinesterase Assay Kit from AAT Bioquest®, Inc.. The tests were performed according to the general protocol. Briefly, acetylcholine was incubated with the tested substance for 30 minutes at room temperature. Afterwards, the mixture of acetylthiocholine and DNTB was added and the reaction incubated for another 30 minutes at room temperature, protected from light. Afterwards, the absorbance at 412 nm was measured with a microplate reader.

HeLa cells were cultivated in Dulbecco's modified eagle medium (DMEM), supplemented with 10% FCS, 100 units penicillin and 100 mg mL^{-1} streptomycin (all from Invitrogen, Germany). Cells were grown in a humidified incubator at 37 °C and 5% CO_2. For determining cell-viability, HeLa cells were seeded at a density of 20.000 cells / cm^2 in 96-well plates. The polymers were dissolved in DMEM, and the indicated concentrations were produced by a serial dilution in DMEM. After 24h of incubation, the medium was replaced by the polymer supplemented medium (100 µL) and incubated for 24h.

The effect of poly(ethylene alkyl phosphonate)s on the viability of human cervical cancer cell line HeLa was measured with the commercially available CellTiter-Glo® Luminescent Cell-viability Assay (Promega). The assay was performed according to the provided protocol.

Experimental Part

Ethylphosphonic acid dichloride (EtPCl): The dichloride was synthesized according to literature.[49] *O,O*-Diethyl ethylphosphonic acid diester (100.0 g, 0.6 mol) and DMF (0.5 mL) was added drop wise to refluxing thionylchloride (180 mL, 1.5 mol). Strong gas evolution of methylene chloride and sulfur dioxide indicated the progress of the reaction. After 24h the gas evolution declined. Fractionated distillation of the raw product yielded the desired dichloride as a colorless liquid (47.5 g, yield: 53%, b.p. 92 °C / 6 mbar). ^{1}H NMR ($SOCl_2$, ppm): δ = 3.37 (dq, $^{2}J_{HP}$ = 15 Hz, $^{3}J_{HH}$ = 7.5 Hz, 2H), 2.18 (dt, $^{3}J_{HP}$ = 30 Hz, $^{3}J_{HH}$ = 7.5 Hz, 3H). ^{13}C{H} NMR ($SOCl_2$, ppm): δ = 37.42 (d, $^{1}J_{CP}$ = 98.3 Hz), 8.26 (d, $^{1}J_{CP}$ = 7.6 Hz). ^{31}P{H} NMR ($SOCl_2$, ppm): δ = 54.72.

2-Ethyl-2-oxo-1,3,2-dioxaphospholane (EtPPn, (1)): A flame-dried three-necked round-bottom flask, equipped with a magnetic stirring bar and two dropping funnels, was charged with 250 mL dry THF and cooled to -21 °C. Ethylphosphonic acid dichloride (46.8 g, 0.3 mol) was dissolved in dry THF (250 mL) and transferred into one dropping funnel via a flame-dried stainless steel capillary. A solution of dry ethylene glycol (19.8 g, 0.3 mol) and dry pyridine (50.6 g, 0.6 mol) in THF (250 mL) was transferred into the second dropping funnel via a flame-dried stainless steel capillary. Dropping speed was adjusted to be approximately equal for both mixtures. After complete addition the solution was stirred for 3h and kept over-night at -28 °C to facilitate the precipitation of the pyridinium hydrochloride byproduct. The precipitate was removed by filtration via a flame-dried Schlenk funnel, and the solvent was removed under reduced pressure. Fractionated distillation yielded the desired product as colorless oil (15.75 g, yield: 36%, b.p. 85 °C / 1x10^{-3} mbar). ^{1}H NMR ($CDCl_3$, ppm): δ 4.53 - 4.35 (m, 2H, -P-O-CH_2-), 4.29 - 4.15 (m, 2H, -P-O-CH_2-), 1.94 (dq, $^{2}J_{HP}$ = 17.5 Hz, $^{3}J_{HH}$ = 7.7 Hz, 2H, -P-CH_2-), 1.16 (dt, $^{3}J_{HP}$ = 21.0 Hz, $^{3}J_{HH}$ = 7.7 Hz, 3H, -CH_3). ^{13}C{H} NMR ($CDCl_3$, ppm): δ 66.86 (s, -P-O-C-), 19.34 (d, $^{1}J_{CP}$ = 132.9 Hz, -P-C-), 7.28 (d, $^{2}J_{CP}$ = 7.1 Hz, -C). ^{31}P{H} NMR ($CDCl_3$, ppm): δ 52.51. FTIR (cm^{-1}): 2979, 2944, 2919, 2886 (P-C), 1476, 1265 (P=O), 1241, 1027, 924, 806, 713.

Isopropylphosphonic acid dichloride (^{i}PrPCl): The dichloride was synthesized according to literature.[25] A flame-dried 1 L three-necked round-bottom flask was equipped with a dropping funnel and a mechanical stirrer. Freshly ground aluminum trichloride (137.3 g, 1 mol) was provided, and phosphorus trichloride (135.1 g, 1 mol) was added. The suspension was cooled to 5 °C and stirred vigorously. Isopropyl bromide (122.9 g, 1.2 mol) was added dropwise so that the temperature did not exceed 15 °C. During the addition, the suspension solidified, and stirring had to be discontinued. The mixture was left to stand at room temperature overnight. The solid was dissolved in dichloromethane (500 mL), the solution cooled to 0 °C by addition of $CO_{2(s)}$ and poured onto a mixture of 1500 g ice and 300 mL concentrated hydrochloric acid. The phases were separated and the aqueous phase extracted with dichloromethane. The combined organic phases were dried with $CaCl_2$ and evaporated to yield a black liquid. Fractionated distillation yielded the desired product as a colorless liquid (106.9 g, yield: 66%, b.p. 86 °C / 22 mbar). ^{1}H NMR ($CDCl_3$, ppm): δ 2.76 - 2.61 (m, 1H), 1.42 (dd, $^{3}J_{HP}$ = 27.0 Hz, $^{3}J_{HH}$ = 6.0 Hz, 6H). ^{13}C{H} NMR ($CDCl_3$, ppm): δ 41.83 (d, $^{1}J_{CP}$ = 94.6 Hz) 16.13 (d, $^{2}J_{CP}$ = 4.3 Hz). ^{31}P{H} NMR ($CDCl_3$, ppm): δ 61.90.

2-Isopropyl-2-oxo-1,3,2-dioxaphospholane (^{i}PrPPn, (2)): A flame-dried three-necked round-bottom flask, equipped with a magnetic stirring bar and two dropping funnels, was charged with 250 mL dry THF and cooled to -21 °C. Isopropylphosphonic acid dichloride (47.8 g, 0.3 mol) was dissolved in dry THF (250 mL) and transferred into one dropping funnel via a flame-dried stainless steel capillary. A solution of dry ethylene glycol (18.5 g, 0.3 mol) and dry pyridine (47.9 g, 0.6 mol) in THF (250 mL) was transferred into the second dropping funnel via a flame-dried stainless steel capillary. Dropping speed was adjusted to be approximately equal for both mixtures. After complete addition the solution was stirred for 5h and kept over-night at -28 °C to facilitate the precipitation of the pyridinium hydrochloride byproduct. The precipitate was removed by filtration via a flame-dried Schlenk funnel, and the solvent was removed under reduced pressure. Fractionated distillation yielded the desired product as colorless oil (18.3 g, yield: 42%, b.p. 85 °C / $1x10^{-3}$ mbar).

^{1}H NMR ($CDCl_3$, ppm): δ 4.49 - 4.32 (m, 2H, -P-O-CH_2-), 4.29 - 4.12 (m, 2H, -P-O-CH_2-), 2.11 (dp, $^{2}J_{HP}$ = 18.1 Hz, $^{3}J_{HH}$ = 7.2 Hz, 1H, -P-CH-), 1.18 (dd, $^{3}J_{HP}$ = 19.3 Hz, $^{3}J_{HH}$ = 7.2 Hz, 6H, -CH_3). ^{13}C{H} NMR ($CDCl_3$, ppm): δ 66.43 (d, $^{2}J_{COP}$ = 0.9 Hz, -P-O-C-), 26.14 (d, $^{1}J_{CP}$ = 131.9 Hz, -P-C-), 16.22 (d, $^{2}J_{CP}$ = 4.6 Hz, -C). ^{31}P{H} NMR ($CDCl_3$, ppm): δ 55.01. FTIR (cm^{-1}): 2970, 2912, 2877 (P-C), 1466, 1388, 1367, 1244 (P=O), 1026, 925, 890, 865, 804, 689.

***O,O*-di-*n*-Butyl-*n*-butylphosphonic acid diester (^{n}BuPPn):** Tri-*n*-butylphosphite (138.6 g, 0.5 mol) and 1-iodobutane (51.7 g, 0.25 mol) were refluxed in a 500 mL round-bottom flask equipped with a reflux condenser at 160 °C for 1.5 h. Fractionated distillation yielded the desired product as a colorless liquid (124.4 g, yield: 99%, b.p. 133 °C / 20 mbar). ^{1}H NMR ($CDCl_3$, ppm): δ 4.07 - 3.91 (m, 4H), 1.77 - 1.69 (m, 2H), 1.66 - 1.65 (m, 6H), 1.46 - 1.30 (m, 6H), 0.91 (t, 3JHH = 7.2 Hz, 9H). ^{13}C{H} NMR ($CDCl_3$, ppm): δ 65.15 (d, $^{2}J_{COP}$ = 5.3 Hz), 31.61 (s), 25.23 (d, $^{1}J_{CP}$ = 105 Hz), 24.48 (d, $^{2}J_{CP}$ = 3.7 Hz), 3.71 (d, $^{3}J_{CP}$ = 12.7 Hz), 18.80 (s), 13.70 (s). ^{31}P{H} NMR ($CDCl_3$, ppm): δ 32.72.

***n*-Butylphosphonic acid dichloride (^{n}BuPCl):** A 100 mL two-headed round-bottom flask was equipped with a reflux condenser and *O,O*-di-*n*-butyl-*n*-butylphosphonic acid diester (9.2 g, 0.04 mol) was provided. The flask was heated to 150 °C and phosphorus pentachloride (15.4 g, 0.08 mol) was added carefully in small portions. A vigorous gas and heat evolution indicated the progress of the reaction. After complete addition the reaction was heated for another 1 h. Fractionated distillation yielded the desired product as a colorless liquid (2.8 g, yield: 40%, b.p. 103 °C / 14 mbar). ^{1}H NMR ($CDCl_3$, ppm): δ 2.68 - 2.49 (m, 2H), 1.90 - 1.72 (m, 2H), 1.51 (h, $^{3}J_{HH}$ = 7.3 Hz, 2H), 0.96 (t, 3JHH = 7.3 Hz, 3H). ^{13}C{H} NMR ($CDCl_3$, ppm): δ 42.69 (d, $^{1}J_{CP}$ = 96.7 Hz), 24.87 (d, $^{2}J_{CP}$ = 6.6 Hz), 22.81 (d, $^{3}J_{CP}$ = 22.1 Hz), 13.41 (d, $^{4}J_{CP}$ = 1.5 Hz), 3.71 (d, $^{3}J_{CP}$ = 12.7 Hz), 18.80 (s), 13.70 (s). ^{31}P{H} NMR ($CDCl_3$, ppm): δ 51.56.

2-*n*-Butyl-2-oxo-1,3,2-dioxaphospholane (*n*BuPPn, (3)): A flame-dried three-necked round-bottom flask, equipped with a magnetic stirring bar and two dropping funnels, was charged with 250 mL dry THF and cooled to -21 °C. *n*-Butylphosphonic acid dichloride (15.9 g, 0.09 mol) was dissolved in dry THF (250 mL) and transferred into one dropping funnel via a flame-dried stainless steel capillary. A solution of dry ethylene glycol (5.6 g, 0.09 mol) and dry pyridine (14.4 g, 0.18 mol) in THF (250 mL) was transferred into the second dropping funnel via a flame-dried stainless steel capillary. Dropping speed was adjusted to be approximately equal for both mixtures. After complete addition the solution was stirred for 5h and kept over-night at -28 °C to facilitate the precipitation of the pyridinium hydrochloride byproduct. The precipitate was removed by filtration via a flame-dried Schlenk funnel, and the solvent was removed under reduced pressure. Fractionated distillation yielded the desired product as colorless oil (5.6 g, yield: 37%, b.p. 90 °C / 1x10^{-3} mbar). ^{1}H NMR ($CDCl_3$, ppm): δ 4.47 - 4.33 (m, 2H, -P-O-CH_2-), 4.27 - 4.14 (m, 2H, -P-O-CH_2-), 1.94 -1.80 (m, 2H), 1.63 - 1.47 (m, 2H), 1.36 (h, $^{3}J_{HH}$ = 7.3 Hz, 2H), 0.85 (t, $^{3}J_{HH}$ = 7.3 Hz, 3H, -CH_3). ^{13}C{H} NMR ($CDCl_3$, ppm): δ 66.16 (s, -P-O-C-), 25.40 (d, $^{1}J_{CP}$ = 117.0 Hz, -P-C-), 24.5 (d, $^{2}J_{CP}$ = 8.2 Hz), 23.47 (d, $^{3}J_{CP}$ = 16.7 Hz), 13.44 (s, -C). ^{31}P{H} NMR ($CDCl_3$, ppm): δ 51.64. FTIR (cm^{-1}): 2958, 2933, 2873 (P-C), 1467, 1407, 1380, 1365, 1259 (P=O), 1219, 1025, 925, 846, 807, 749, 704.

Representative procedure for the ROP of (1) and (3): The respective monomer was placed in a flame-dried Schlenk-tube, dissolved in dry benzene and dried by repeated lyophilization. The monomer was dissolved in dry dichloromethane at a concentration of 4 mol L^{-1}. A stock solution of initiator 2-(benzyloxy)ethanol in dry dichloromethane was prepared with a concentration 0.2 mol L^{-1}, and the calculated amount was added to the monomer solution via gas-tight syringe (Hamilton®). A stock solution of DBU in dry dichloromethane was prepared with a concentration of 0.2 mol L^{-1}. The monomer solution and the catalyst solution were adjusted to 25 °C. The polymerization was initiated by the addition of the calculated volume of the catalyst solution containing 3.0 equivalents of DBU concerning the initiator. Polymerization was terminated after 16h by the rapid addition of an excess of formic acid dissolved in dichloromethane with a concentration of

20 mg mL^{-1}. The colorless, amorphous polymers were purified by precipitation in cold diethyl ether for **P(1)** or hot water for **P(3)** and dried under reduced pressure.

Representative NMR data of P(1):

^{1}H NMR (DMSO-d_6 ppm): δ 7.37 - 7.29 (m, aromatic protons), 4.85 (t, terminal -O-H), 4.53 (s, aryl-CH_2-), 4.22 - 4.01 (m, backbone -CH_2-CH_2-), 3.63 (t, backbone terminal -CH_2-), 1.87 - 1.70 (m, side-chain -P-CH_2-), 1.14 - 0.98 (m, side-chain -CH_3). $^{13}C\{H\}$ NMR (DMSO-d_6, ppm): δ 133.78, 128.80, 127.97 (aromatic carbons), 64.56 (s, broad, backbone -CH_2-), 18.31 (d, $^{1}J_{CP}$ = 139.5 Hz, side-chain -P-CH_2-), 6.71 (d, $^{2}J_{CP}$ = 6.75 Hz, side-chain -CH_3). $^{31}P\{H\}$ NMR (DMSO-d_6, ppm): δ 34.63 (backbone), 34.38 (terminal).

Representative NMR data of P(3):

^{1}H NMR (DMSO-d_6,ppm): δ 7.37 - 7.29 (m, aromatic protons), 4.85 (t, terminal -O-H), 4.53 (s, aryl-CH_2-), 4.22 - 4.01 (m, backbone -CH_2-CH_2-), 3.63 (t, backbone terminal -CH_2-), 1.86 - 1.70 (m, side-chain -P-CH_2-), 1.65 - 1.24 (m, side-chain -CH_2-CH_2-), 0.88 (t, side-chain -CH_3). $^{13}C\{H\}$ NMR (DMSO-d_6, ppm): δ 133.78, 128.80, 127.97 (aromatic carbons), 64.56 (s, broad, backbone -CH_2-), 25.10 (d, $^{1}J_{CP}$ = 86.3 Hz, side-chain -P-CH_2-), 24.40 (d, $^{2}J_{CP}$ = 52.5 Hz, side-chain -CH_2-), 23.40 (d, $^{3}J_{CP}$ = 15.8 Hz, side-chain -CH_2-), 13.89 (s, side-chain CH_3). $^{31}P\{H\}$ NMR (DMSO-d_6, ppm): δ 33.39 (backbone), 33.15 (terminal).

Representative procedure for the ROP of (2): (2) was placed in a flame-dried Schlenk-tube, dissolved in of dry benzene and dried by repeated lyophilization. The monomer was dissolved in dry dichloromethane at a concentration of 4 mol L^{-1}. A stock solution of initiator 2-(benzyloxy)ethanol in dry dichloromethane was prepared with a concentration of 0.2 mol L^{-1}, and the calculated volume was added to the monomer solution via gas-tight syringe (Hamilton®). A stock solution of twice lyophilized TBD in dry dichloromethane was prepared with a concentration of 0.2 mol L^{-1}. The monomer- and catalyst solutions were cooled to 0 °C. The polymerization was initiated by addition of the calculated amount of the catalyst solution (1 equivalent of TBD with respect to the initiator). The polymerization was terminated after 20 min by the rapid addition of an excess of formic acid dissolved in

dichloromethane with a concentration of 20 mg mL^{-1}. The colorless, amorphous polymers were purified by precipitation in cold diethyl ether and dried under reduced pressure.

Representative NMR data of P(*3*):

^{1}H NMR (DMSO-d_6, ppm): δ 7.37 - 7.29 (m, aromatic protons), 4.85 (t, terminal -O-H), 4.53 (s, aryl-CH_2-), 4.22 - 4.01 (m, backbone -CH_2-CH_2-), 3.63 (t, backbone terminal -CH_2-), 2.12 - 1.94 (m, side-chain -P-CH-), 1.17 - 1.02 (m, side-chain -CH_3). $^{13}C\{H\}$ NMR (DMSO-d_6, ppm): δ 133.78, 128.80, 127.97 (aromatic carbons), 64.56 (s, broad, backbone -CH_2-), 25.22 (d, $^{1}J_{CP}$ = 141.4 Hz, side-chain -P-CH-), 16.12 (d, $^{2}J_{CP}$ = 4.9 Hz, side-chain -CH_3). $^{31}P\{H\}$ NMR (DMSO-d_6, ppm): δ 36.12 (backbone), 35.90 (terminal).

Chapter 2: A Library of Well-Defined and Water-Soluble Poly(phosphonate)s with Adjustable Hydrolysis.

Chapter 2 introduced the synthesis of three different 2-alkyl-2-oxo-1,3,2-dioxaphospholane monomers: ethyl-, *n*-butyl-, and isopropyl dioxaphospholane. Their homopolymerization and the respective homopolymer properties were discussed. The next consequent step in the development of functional poly(alkylene phosphonate) derivatives is the synthesis of monomers with functional groups as well as copolymerization of existing substances to varying the resulting copolymer properties. Therefore, the following chapters deal with the co-, and tertpolymerization behavior of dioxaphospholanes as well as with side-chain modifications after polymerization.

Chapter 3, in particular, discusses the synthesis of a cyclohexyl substituted monomer as well as the first copolymerization of dioxaphospholanes. This enables a precise adjustment of the respective copolymers glass transition temperature (T_g), a material property important for applications both in bulk as well as in solution.

Chapter 3: Adjustable Glass Transition Temperatures of Poly(ethylene alkyl phosphonate) Copolymers.

Thomas Wolf[1], Johannes Naß[1], and Frederik R. Wurm[1]

[1]Max Planck-Institut für Polymerforschung, Ackermannweg 10, 55128 Mainz, Germany

Published in: Polymer Chemistry, **2016,** 7, 2934-2937

Keywords: poly(phosphoester)s, poly(phosphonate)s, anionic ring-opening polymerization, copolymerization

Chapter 3: Adjustable Glass Transition Temperatures of Poly(ethylene alkyl phosphonate) Copolymers.

Abstract

2-Cyclohexyl-2-oxo-1,3,2-dioxaphospholane (^{Cy}HexPPn), a new monomer for the anionic ring-opening polymerization towards poly(ethylene alkyl phosphonate)s is presented. The organo-catalyzed polymerization produces homopolymers with excellent control over molecular weight and rather narrow molecular weight distributions. The homopolymer was found to exhibit a glass transition at 15 °C, which is 50 - 60 °C higher compared to all previously reported poly(ethylene n-alkyl phosphonate)s. Copolymerization with the water-soluble 2-isopropyl-2-oxo-1,3,2-dioxaphospholane (^{i}PrPPn) resulted in water-soluble, well-defined copolymers. The copolymer composition matched the theoretical value in all cases, and the T_g showed a linear correlation with the amount of ^{i}PrPPn incorporated. The copolymer was found to exhibit low cell-toxicity towards sensitive murine macrophage-like cells (RAW264.7).

Introduction

Poly(phosphonate)s (PPn's) are a relatively old polymer class known since the pioneering works of Carraher *et al*. on the polycondensation of phenyl phosphonic acid dichloride and aromatic diols.[1] Besides uses as flame retardant materials, however, this polymer class did receive only minor scientific or industrial attention.[2-4] Motivated by the properties of poly(phosphate)s as biodegradable polymers for drug delivery, Steinbach *et al*. developed the first living synthesis of poly(ethylene methyl phosphonate), a water-soluble, biocompatible poly(ethylene *n*-alkyl phosphonate), via organocatalytic anionic ring-opening polymerization (AROP).[5-7] Following these results, our group continued their research on the elucidation and variation of polymers based on this synthetic platform.[8] In contrast to the more prominent poly(phosphate)s, the phosphonate platform, which substitutes a hydrolytically labile phosphorous ester side chain to a chemically stable P-C bond, allows the precise adjustment of degradation rates and produces highly water-soluble polymers with low molecular weight dispersity up to full conversion.[5, 8]

Chapter 3: Adjustable Glass Transition Temperatures of Poly(ethylene alkyl phosphonate) Copolymers.

One crucial attribute to modify to broaden the potential field of applications of a polymer is its glass transition temperature (T_g). Whereas amorphous low T_g materials may exhibit elastic behavior, the incorporation of a high T_g segment, for example in a block-copolymer, could facilitate phase separation and hence facilitate self-aggregation behavior.[9] The glass transition temperature is heavily influenced by nature and especially steric demand of the polymer side-chain. The more rotational degrees of freedom available, the lower the glass transition temperature. Exceptionally rigid cyclic structures in the side-chain are therefore well-suited to increase the T_g of the material.

However, not many structures with cyclic aliphatic side-chains are known up to date. Hoogenboom et al. could demonstrate a significant increase in T_g of poly(2-oxazolines) by incorporation of a cyclopropyl side-chain and very recently presented three novel 2-cycloalkyl-2-oxazoline copolymers which showed high melting temperatures and a complex, non-linear dependence of the T_g with respect of the incorporated linear side-chain monomer.[10-11]

Here, we present the first synthesis of a new dioxaphospholane derivative, namely 2-cyclohexyl-2-oxo-1,3,2-dioxaphospholane (^{cy}HexPPn, **(1)**), bearing a cycloalkyl substituent and its well-controlled homo- as well as copolymerization with 2-isopropyl-2-oxo-1,3,2-dioxaphospholane (^{i}PrPPn, **(2)**) via organocatalytic AROP. The obtained polymers were thoroughly investigated via ^{1}H, ^{31}P{H} NMR, SEC, DSC and turbidity analysis. The T_g of the homopolymer was found to be around 15 °C, which is 50 - 60 °C higher than that of previously reported PPn's. A linear correlation between the T_g and the amount of **(2)** incorporated in the copolymer was found enabling fine tuning of the T_g to match future applications needs. Copolymerization further drastically improved the water-solubility of the polymers. Finally, cell-viability assays showed low cell-toxicity against the sensitive murine macrophage-like cells RAW 264.7.

Results and Discussion

Monomer Synthesis

(1) was synthesized via a two-step reaction (Scheme 3.1, a). In a first step, aluminium chloride, phosphorus(III)chloride and cyclohexyl bromide were converted to cyclohexyl phosphonic acid dichloride according to the literature protocol of Clay *et al*.[12] Ring-closing with ethylene glycol was conducted under high dilution according to a slightly modified literature protocol of Steinbach *et al.*[5] The monomer was received in acceptable yields and high purity as confirmed via ^{1}H, $^{31}P\{H\}$ and ^{13}C NMR spectroscopy.

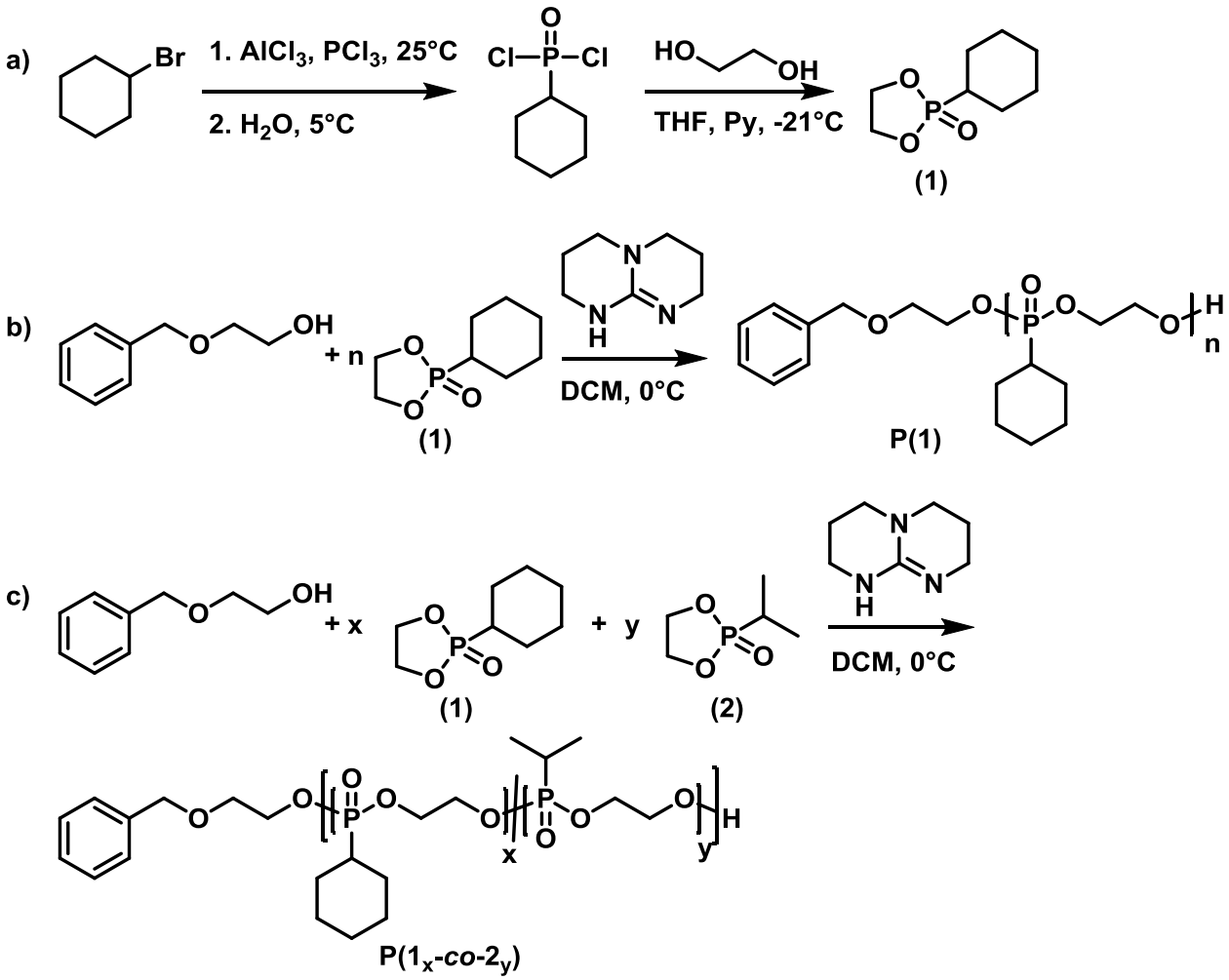

Scheme 3.1: a) Two-step synthesis of 2-cyclohexyl-2-oxo-1,3,2-dioxaphospholane (1); b) TBD-catalyzed and 2-(benzyloxy)ethanol-initiated anionic ring-opening polymerization of (1) in dichloromethane at 0°C to afford P(1)$_n$; c) TBD catalyzed and 2-(benzyloxy)ethanol initiated anionic ring-opening copolymerization of (1) and (2) in dichloromethane at 0°C to afford P(1$_x$-*co*-2$_y$).

The distinct multiplett of the intracyclic protons in the ^{1}H NMR spectrum between 4.54 and 4.19 ppm as well as the characteristic shift in ^{31}P{H} NMR spectroscopy (47.5 ppm) confirmed the success of the reaction (Figure 3.1, a and Figure S3.4).

The protons of the cyclohexane ring showed a complex J-splitting pattern due to the influence of the non-planarity of the cyclohexane ring and strong J_{HP} coupling (Scheme 3.2).

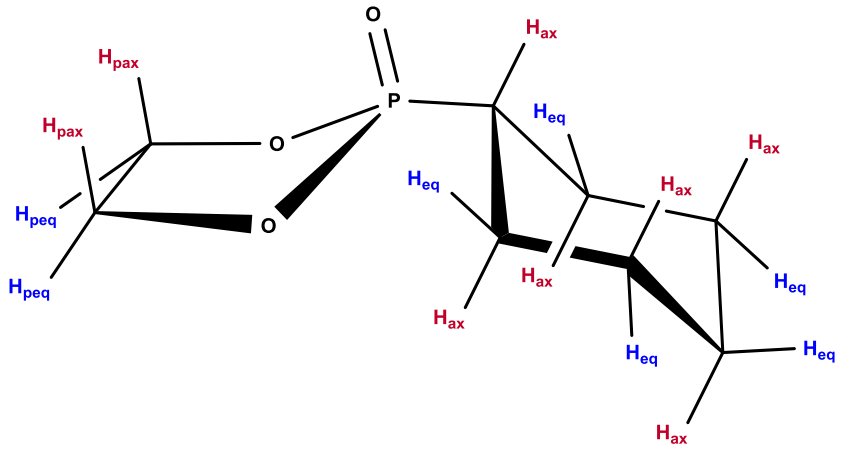

Scheme 3.2: Assumed conformation of (1). The equatorial (H_{eq}), axial (H_{ax}) protons of the six-membered ring, as well as the pseudo-equatorial (H_{peq}) and the pseudo-axial (H_{pax}) protons of the five-membered ring, are marked.

Polymer Synthesis

The organocatalytic AROP of the new monomer **(1)** proceeded in analogy to the previously reported polymerization of dioxaphospholanes with secondary alkyl side-chains.[8] 1,5,7-Triazabicyclo[4.4.0]dec-5-ene (TBD) was used as base in the presence of a primary alcohol at 0 °C and proceeded to high conversions (> 90%) within 2h (Scheme 3.1, b). The obtained polymers were thoroughly characterized via ^{1}H, ^{31}P{H}, and ^{13}C NMR spectroscopy as well as SEC and DSC analysis. The ^{1}H NMR spectrum showed the disappearing of the characteristic monomer multiplets (4.54 - 4.19 ppm) and the emerging of a broad backbone signal from 4.22 to 4.05 ppm. Accurate determination of M_n was possible via ^{1}H NMR assisted end-group analysis by comparing the integrals of the aromatic initiator (7.26 ppm) with the above-mentioned backbone resonance (Figure 3.1, b).

The polymers were synthesized with good control over molecular weights up to 20,000 g mol^{-1}. ^{31}P{H} analysis showed a significant shift from 47.57 ppm of the monomer to a broad signal at 33.12 ppm for the polymer. The end-group phosphorous was visible as the low-intensity signal at 32.96 ppm (Figure S3.6).

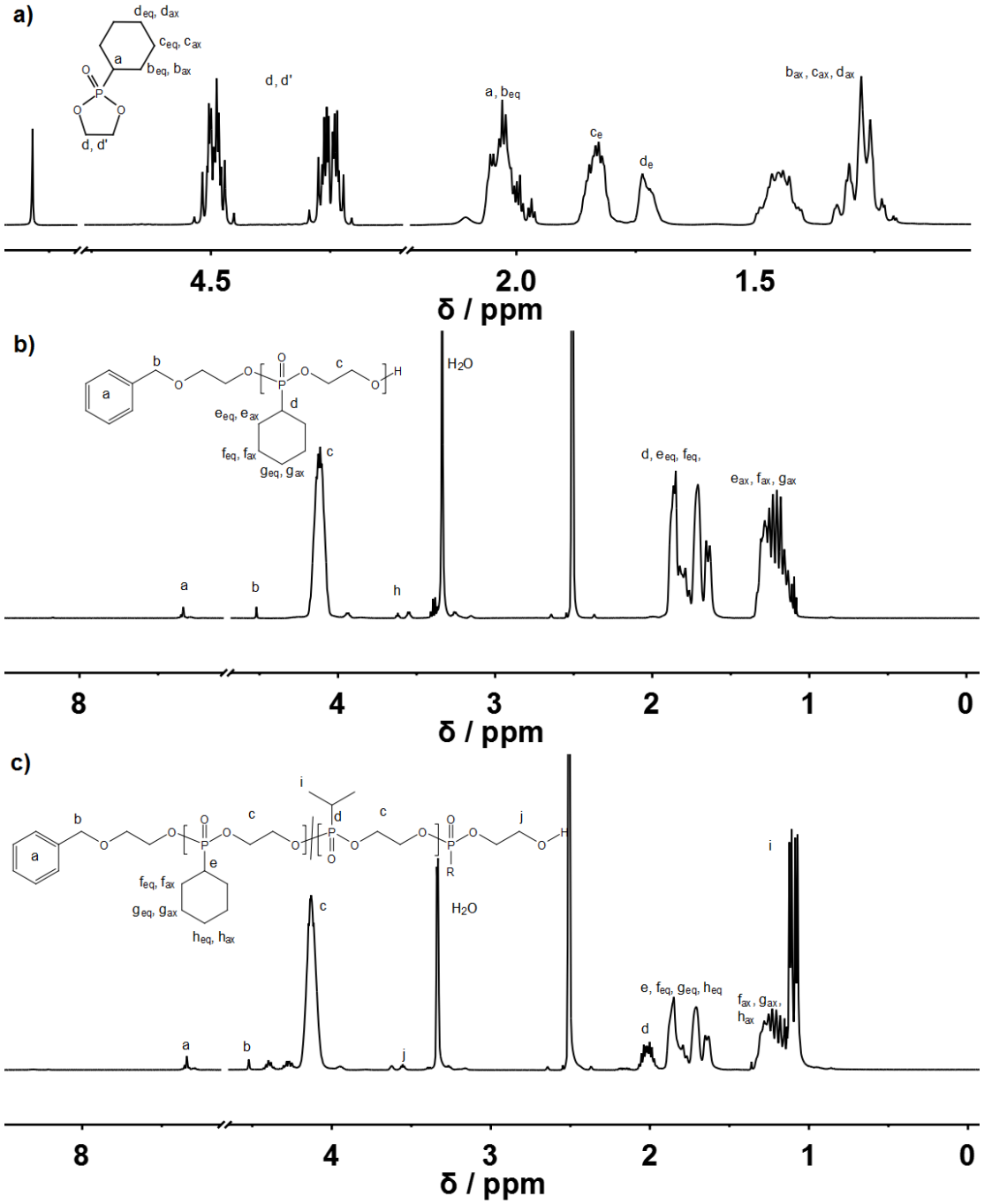

Figure 3.1: a) ^{1}H (500 MHz) NMR spectrum of (1) in $CDCl_3$ at 298K; b) ^{1}H (500 MHz) NMR spectrum of P(1)$_n$ in DMSO-d_6 at 298K; c) ^{1}H (500 MHz) NMR spectrum of P(1$_{30}$-*co*-2$_{30}$) in DMSO-d_6 at 298K.

The obtained polymers were well-defined with a rather narrow molecular weight distribution (*Đ*) (Figure 3.2, left). The glass transition temperature (T_g) of **P(1)$_x$** was found to be around 15 °C, 50-60 °C higher than that of previously reported poly(ethylene alkyl phosphonate)s.[5,8] This comparatively high T_g further enlarges the toolbox of potential applications of poly(ethylene alkyl phosphonate)s. The complete polymer characterization is summarized in Table 3.1.

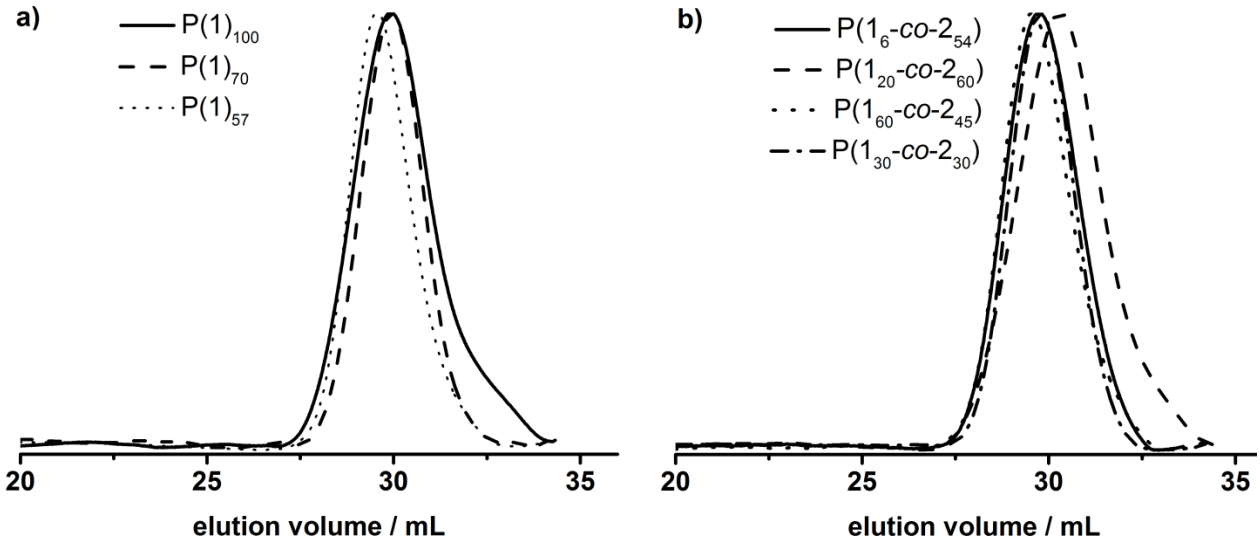

Figure 3.2: SEC traces (RI detection) of a) P(1)$_n$ and b) P(1$_x$-*co*-2$_y$) in DMF at 333K.

As the homopolymers of **(1)** are hydrophobic materials, copolymers with 2-isopropyl-2-oxo-1,3,2-dioxaphospholane (^{i}PrPPn, **(2)**) were prepared. The homopolymer of **(2)** is known to be highly water-soluble (> 10 g L^{-1}), with a T_g at ca. -40 °C and polymerizes under the same conditions as **(1)**, allowing the copolymerization to proceeded under the same conditions as the homopolymerization (Scheme 3.2, c).[8] **(2)** was synthesized according to a literature protocol.[8] The incorporation of the hydrophilic comonomer produced water-soluble poly(ethylene alkyl phosphonate) copolymers and allowed a graduate adjustment of the copolymer's T_g.

The success of the copolymerization was observed by the vanishing of the monomer resonances in the $^{31}P\{H\}$ NMR spectra at 47.5 ppm (**(1)**) and 50.45 ppm (**(2)**), respectively, as well as the emerging of the polymer resonances at 32.96 ppm (**P(1)**) and 29.88 ppm (**P(2)**), respectively (Figure 3.3).

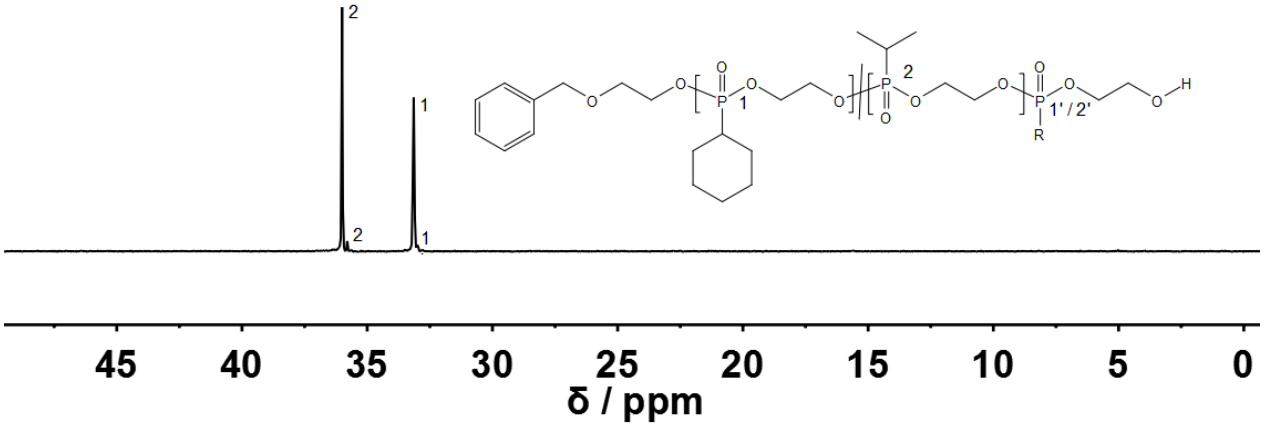

Figure 3.3: ^{31}P (202 MHz) NMR spectrum of P(1_x-*co*-2_y) in DMSO-d_6 at 298K.

The broad backbone signal in the ^{1}H NMR spectrum from 4.21 to 4.02 ppm further confirmed the polymerization (Figure 3.1, c). The end-group analysis in ^{1}H NMR spectroscopy enabled accurate determination of M_n (*vide supra*). Both ^{1}H NMR as well as $^{31}P\{H\}$ NMR spectroscopy was used to calculate the copolymer composition. In the $^{31}P\{H\}$ NMR spectrum comparison of the well-separated resonances at 32.96 ppm (**P(1)**) and 29.88 ppm (**P(2)**) was used to determine the copolymer composition. In ^{1}H NMR the resonances of the respective side-chains at 1.92 to 1.60 ppm (**P(1)**) and 2.09 to 1.94 ppm (**P(2)**), respectively, were used to determine an accurate copolymer composition. Both methods of calculation gave the same results, and the copolymer composition matched the theoretical values in all cases.

^{1}H DOSY NMR spectroscopy was used to ensure the successful synthesis of a copolymer (Figure 3.4). Both the backbone signals (4.21 to 2.02 ppm), as well as all signals originating from the respective side-chains and the initiator, show the same diffusion coefficient (black box) suggesting the formation of a copolymer. The molecular weight distribution was found to be rather narrow and monomodal. Precise control over molecular weight up to 15,000 g mol^{-1} was achieved. (Figure 3.2, b).

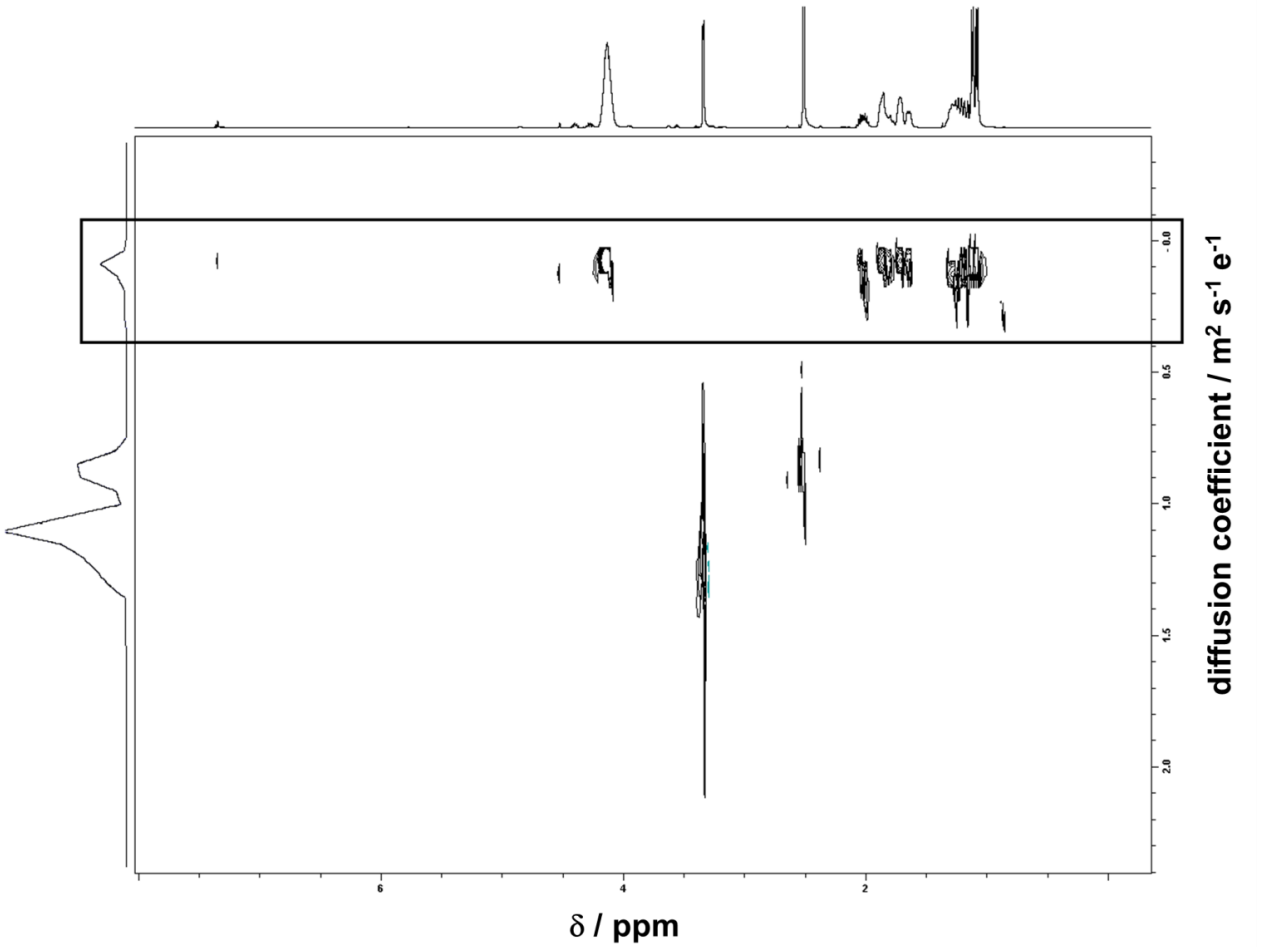

Figure 3.4: ^{1}H DOSY (500 MHz) NMR spectrum of P(1_x-*co*-2_y) in DMSO-d_6 at 298K. All copolymersignals of backbone and side-chains show a diffusion coefficient of 0.15 m^2 s^{-1} (black box) whereas the solvent DMSO-d_6 and H_2O show a significantly higher diffusion coefficient.

Analytical data of all polymers are summarized in Table 3.1.

Table 3.1: Analytical results of the AROP of (1) and (2).

sample	theo. ration (1) / (2) [a]	M_n / g mol^{-1} [b]	$Đ$ [c]	T_g / °C [d]
P(1)$_{57}$	-	10,800	1.28	16.1
P(1)$_{70}$	-	13,300	1.20	16.3
P(1)$_{100}$	-	19,100	1.36	15.5
P(1$_6$-*co*-2$_{54}$)	0.11 / 0.91	9,100	1.31	-39.2
P(1$_{20}$-*co*-2$_{60}$)	0.25 / 0.75	12,700	1.49	-26.4
P(1$_{20}$-*co*-2$_{45}$)	0.31 / 0.69	10,500	1.35	-26.9
P(1$_{30}$-*co*-2$_{30}$)	0.47 / 0.53	10,100	1.24	-21.8
P(1$_{44}$-*co*-2$_{23}$)	0.65 / 0.35	11,800	1.26	-14.1
P(1$_{56}$-*co*-2$_{29}$)	0.66 / 0.34	15,000	1.40	-15.1

a) Monomer composition at t = 0, determined via ^{1}H NMR spectroscopy in DMSO-D_6 at 298K. b) Determined via ^{1}H NMR spectroscopy in DMSO-d_6 at 298K. c) Determined via SEC in DMF (60°C) (PEG standard). d) Determined via DSC at a heating rate of 10 °C min^{-1}.

Macroscopic Properties

The water-solubility of the copolymers was dramatically enhanced by the incorporation of **(2)**. Copolymers with up to 50 mol% of **(1)** were soluble at concentrations of 1 g L^{-1}, compared to the insoluble **P(1)**. Further decrease of the amount of **(1)** in the copolymer resulted in a gradual increase of water-solubility. These water-soluble copolymers exhibited LCST like phase separation at elevated temperatures. Consequently, the cloud point temperature increased with decreasing amount of incorporated hydrophobic comonomer **(1)**, indicating a higher hydrophilicity of the copolymer. The turbidity measurements are shown in Figure 3.5.

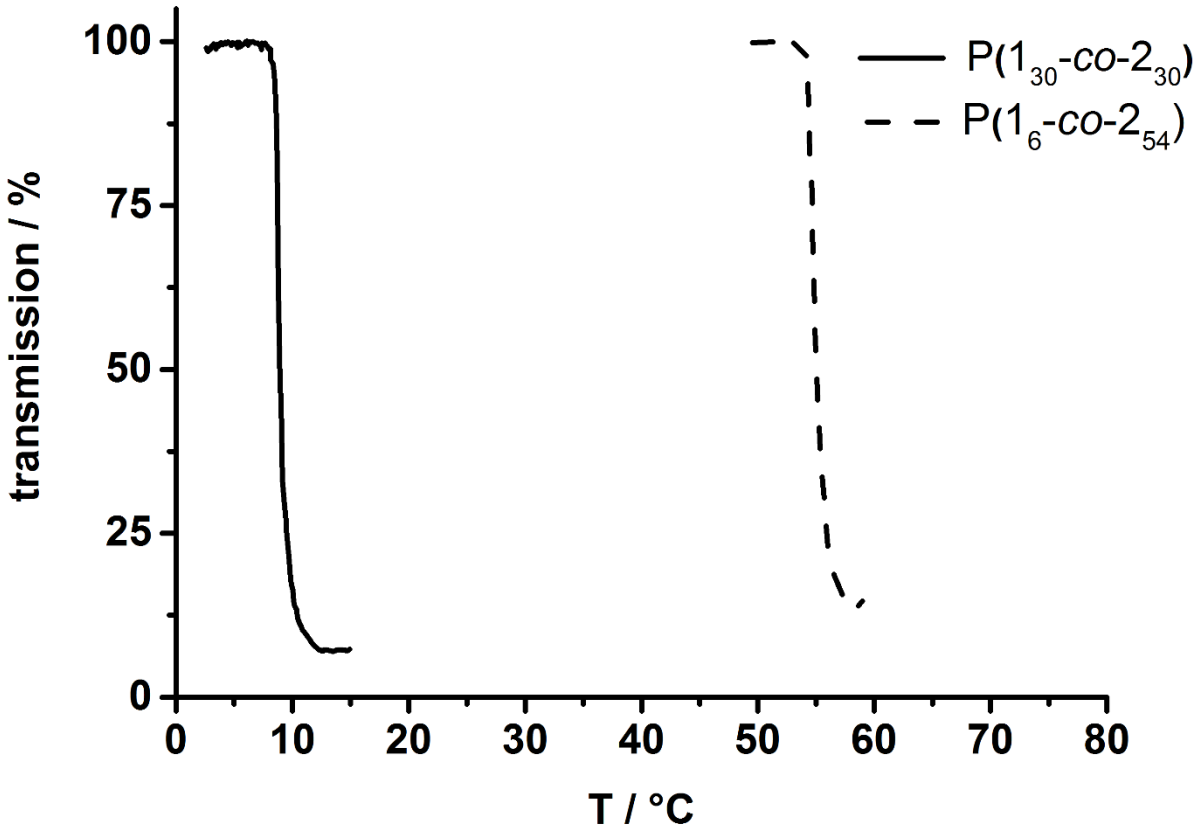

Figure 3.5: Turbidity measurements (heating curves) of P(1_6-*co*-2_{54}) (dashed curve) and P(1_{30}-*co*-2_{30}) (black line) in PBS at a concentration of 1 g L^{-1} and a heating rate of 1 °C min^{-1}. The transmission was measured at 500 nm. A significant increase of cloud point temperature observed upon increasing the amount of (2) in the polymer chain.

DSC measurements revealed a single T_g for the copolymers. This indicated the formation of a random copolymer, as a block-copolymer is expected to show two distinct glass transition temperatures as long as phase separation occurs.

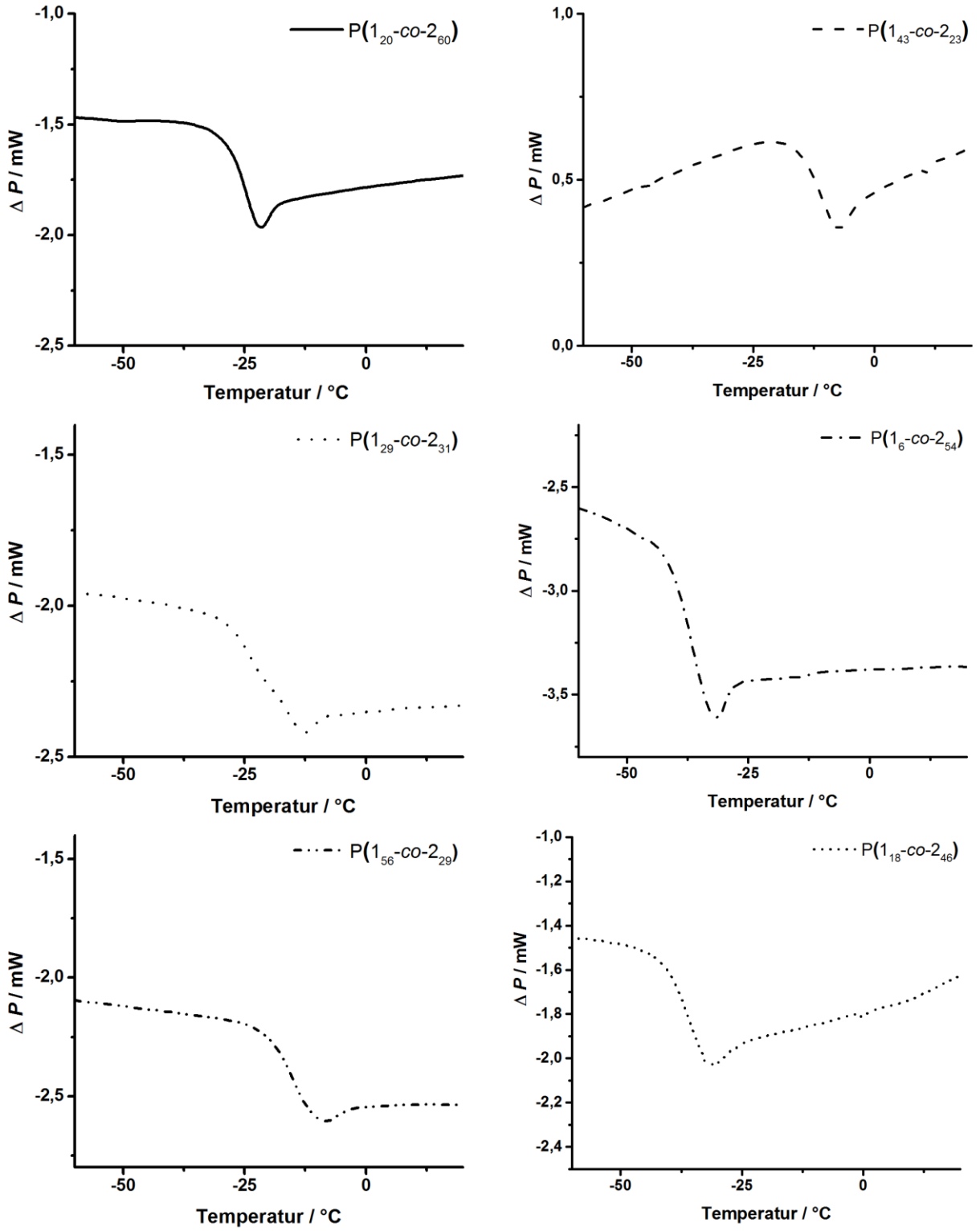

Figure 3.6: DSC thermograms of P(1$_x$-*co*-2$_y$) with different copolymer compositions at a heating range of 10 °C in the range from -60 °C to 20 °C. The increase of T_g with the incorporation of (1) visible.

A linear correlation between the measured T_g and the amount of **(2)** incorporated in the polymer was found (Figure 3.6).

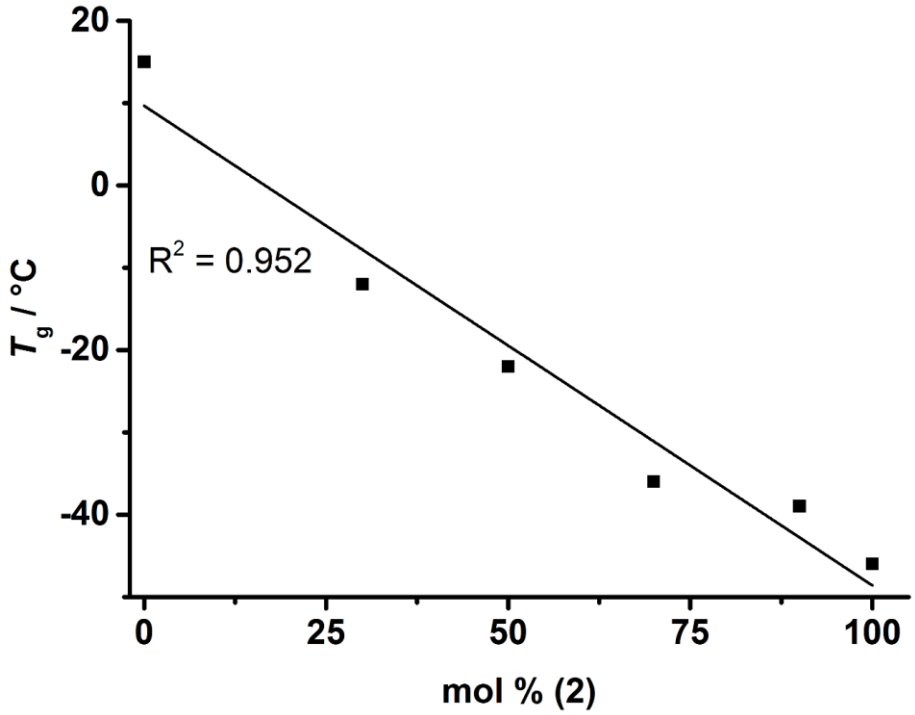

Figure 3.7: Linear correlation between the measured T_g's (from DSC) and the mol fraction of (2) in the copolymers P(1_x-*co*-2_y).

Hence, an adjustment of the T_g of the copolymers in the range from -45 to 15 °C is possible.

This makes **P(1_x-*co*-2_y)** the first known water-soluble poly(ethylene alkyl phosphonate)s with adjustable T_g over a broad temperature range.

Biological Compatibility

Finally, to elucidate the biocompatibility of the newly synthesized materials, a representative *in vitro* cell-toxicity test of **P(1_{20}-*co*-2_{45})** was performed with the sensitive murine macrophage-like cells RAW 264.7 (Figure 3.8). The cells were incubated with a solution of **P(1_{20}-*co*-2_{45})** in medium (+10% FBS) at the respective concentration for 24h. Afterwards, cell viability was determined via the commercially available CellTiterGlo® Luminescent Cell-Viability Assay (Promega) according to the delivered protocol. No cytotoxicity was detected at pharmaceutically relevant concentrations. However, a significantly reduced viability was found for concentrations exceeding concentrations of 200 µg mL^{-1}.

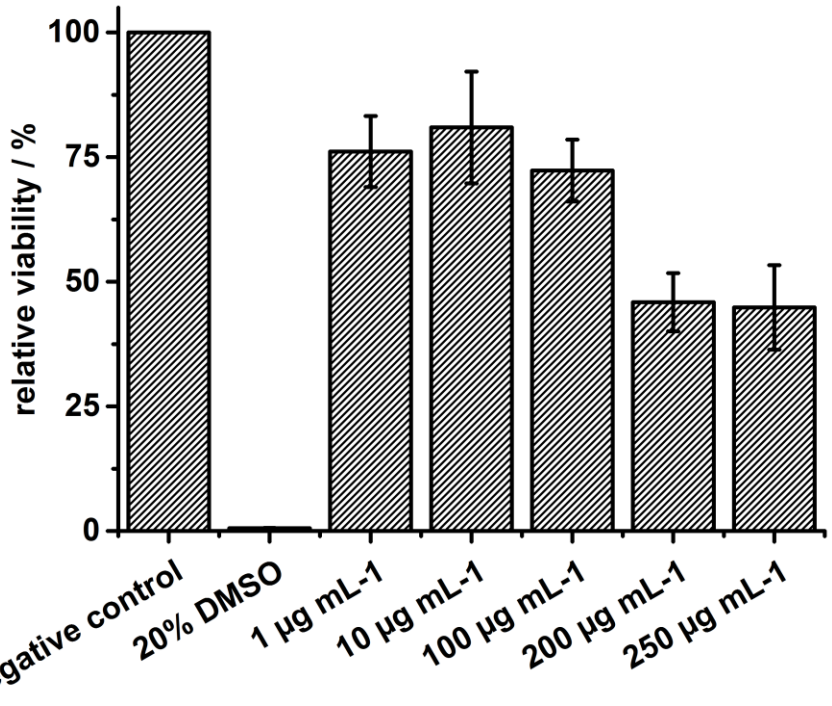

Figure 3.8: In vitro cell-viability assay against murine macrophage-like cells (RAW 264.7). 24h incubation of P(1_{20}-*co*-2_{45})at 37°C with the pure medium as a negative control and 20% DMSO as a positive control. All experiments were performed in triplicates (performed by Johanna Simon).

Summary and Conclusion

To conclude, the successful synthesis of the novel dioxaphospholane monomer 2-cyclohexyl-2-oxo-1,3,2-dioxaphospholane, the first phosphonate monomer for the anionic ring-opening polymerization carrying a cycloalkyl side-chain, is reported. The cyclic monomer polymerized via organocatalytic anionic ring-opening polymerization with TBD to afford well-defined polymers with good control over molecular weight and T_g of ca. 15 °C, i.e., 50 - 60 °C higher than previously reported poly(ethylene *n*-alkyl phosphonate)s. The T_g of these water-insoluble materials was further adjusted by copolymerization with 2-isopropyl-2-oxo-1,3,2-dioxaphospholane **(2),** and a linear correlation between the T_g and the incorporated amount of **(2)** was found.

Water-soluble copolymers with low cell-toxicity against macrophage-like cells (RAW 264.7) and T_g's in the range from +15 to -40 °C were obtained. This makes P(1_x-*co*-2_y) the first known water-soluble poly(alkylene alkyl phosphonate)s with adjustable glass transition temperature. Future studies for the preparation of biodegradable nanocarriers with similar systems are on the way and will be reported in due course.

Acknowledgements

The authors thank Prof. Dr. K. Landfester for continuous support. The authors acknowledge support from the "Deutsche Forschungsgemeinschaft" (DFG WU 750/ 6-1). The authors thank Johanna Simon for the cell culture and toxicity assays.

References

1 Millich, F.; Carraher, C. E., *J. Polym. Sci.* A1, **1969,** 7, 2669-2678.
2 Kim, K.-S., *J. Appl. Polym. Sci*., **1983,** 28, 1119-1123.
3 Ranganathan, T.; Zilberman, J.; Farris, R. J.; Coughlin, E. B.; Emrick, T., *Macromolecules,* **2006,** 39, 5974-5975.
4 Steinbach, T.; Wurm, F. R., *Angew. Chem. Int. Ed.*, **2015,** 54, 6098-108.
5 Steinbach, T.; Ritz, S.; Wurm, F. R., *ACS Macro Lett.*, **2014,** 3, 244-248.
6 Lim, Y. H.; Tiemann, K. M.; Heo, G. S.; Wagers, P. O.; Rezenom, Y. H.; Zhang, S.; Zhang, F.; Youngs, W. J.; Hunstad, D. A.; Wooley, K. L., *ACS Nano*, **2015,** 9, 1995-2008.
7 Schöttler, S.; Becker, G.; Winzen, S.; Steinbach, T.; Mohr, K.; Landfester, K.; Mailander, V.; Wurm, F. R., *Nat. Nanotechnol.*, **2016,** DOI: 10.1038/nnano.2015.330.

8 Wolf, T.; Steinbach, T.; Wurm, F. R., *Macromolecules*, **2015,** 48, 3853-3863.
9 Nardin, C.; Hirt, T.; Leukel, J.; Meier, W., *Langmuir*, **2000,** 16, 1035-1041.
10 Bloksma, M. M.; Weber, C.; Perevyazko, I. Y.; Kuse, A.; Baumgartel, A.; Vollrath, A.; Hoogenboom, R.; Schubert, U. S., *Macromolecules*, **2011,** 44, 4057-4064.
11 Jerca, V. V.; Lava, K.; Verbraeken, B.; Hoogenboom, R., *Polym. Chem.Uk.*, **2016,** 7, 1309-1322.
12 Clay, J. P., *J. Org. Chem*., **1951,** 16, 892-894.

Supporting Information for

Adjustable glass transition temperatures of poly(ethylene alkyl phosphonate) copolymers.

Materials

Solvents and chemicals were purchased from Acros Organics, Sigma Aldrich or Fluka and used as received unless otherwise stated. All chemicals were purchased in highest purities, dry and stored over molecular sieve (4Å), if possible. 2-(Benzyloxy)ethanol was purchased from ABCR, distilled from calcium hydride and stored over molecular sieve (4Å) and under argon before use. TBD was purchased from Sigma Aldrich and stored under argon. Deuterated solvents were purchased from Deutero GmbH (Kastellaun, Germany) and used as received. Dulbecco's Modified Eagle Medium (DMEM), fetal bovine albumin (FBS penicillin and streptomycin were purchased from Invitrogen, Germany.

Instrumentation and Characterization Techniques

Size exclusion chromatography (SEC) measurements were performed in DMF (1 g L^{-1} LiBr added) at 60°C and a flow rate of 1 mL min^{-1} with a PSS SECcurity as an integrated instrument, including a PSS GRAM 100-1000 column and a refractive index (RI) detector. Calibration was carried out using poly(ethylene glycol) standards provided by Polymer Standards Service. The ^{1}H, $^{13}C\{H\}$, and $^{31}P\{H\}$ NMR experiments were acquired on a Bruker 500 AMX system. The temperature was kept at 298.3K and calibrated with a standard ^{1}H methanol NMR sample using the topspin 3.0 software (Bruker). $^{13}C\{H\}$ NMR spectra were referenced internally to solvent signals. $^{31}P\{H\}$ NMR spectra were referenced externally to phosphoric acid. The $^{13}C\{H\}$ NMR (125 MHz) and $^{31}P\{H\}$ NMR (201 MHz) measurements were obtained with a 1H powergate decoupling method using 30 ° degree flip angle. 2D NMR experiments (^{1}H DOSY (Diffusion ordered spectroscopy)) were measured on a Bruker 500 AMX NMR spectrometer under the same conditions as mentioned above. All spectra were processed with the MestReNova 9.0.1-13254 software. Differential Scanning Calorimetry (DSC) measurements were performed using

a Mettler-Toledo DSC823 thermal analysis system in the temperature range from -80 to 50 °C under nitrogen with a heating rate of 10 °C min^{-1}. Cloud points were determined in Dulbecco's phosphate buffered saline (no Ca^{2+}, no Mg^{2+}) from Thermo Fischer scientific and detected by the optical transmittance of a light beam (λ = 500 nm) through a 1 cm sample cell. The measurements were performed on a Jasco V-630 photo spectrometer with a Jasco ETC-717 Peltier element. The intensity of the transmitted light was recorded versus the temperature of the sample cell. The heating/cooling rate was 1 °C min^{-1} and values were recorded every 0.1 °C.

Murine macrophage-like cells (RAW 264.7) were cultivated in DMEM supplemented with 10% FBS, 100 units of penicillin, and 100 mg mL^{-1} streptomycin. Cells were grown in a humidified incubator at 37°C and 5% CO_2. The effect of **P(1$_x$-*co*-2$_y$)$_n$** on cell viability of RAW 264.7 cells was measured by CellTiter-Glo Luminescent Cell Viability Assay (Promega) according to the manufacturer. Luminescent signals were measured with a Tecan infinite M1000. RAW 264.7 cells were seeded at a density of 15 000 cell per cm^2 in 96-well plates (100 µL per well). The polymers were dissolved in DMEM (stock concentration: 1 mg/mL) and further diluted to the indicated concentrations. After 24h of incubation, the cell culture medium was replaced by the polymer supplemented medium, and cells were incubated for 24h.

Experimental

Cyclohexyl phosphonic acid dichloride: The dichloride was synthesized according to literature.[1] A flame-dried 1 L three-necked round-bottom flask was equipped with a dropping funnel, a thermometer, and a mechanical stirrer. Freshly ground aluminum trichloride (133 g, 1.0 mol) was provided, and phosphorus trichloride (137 g, 1.0 mol) was added. The suspension was cooled to 5 °C and stirred vigorously. Cyclohexyl bromide (81 g, 0.5 mol) was added dropwise so that the temperature did not exceed 10 °C. The mixture was stirred for another 20 minutes at 5 °C and for further 30 min at 25 °C. The formed solid was dissolved in dichloromethane, the solution cooled to -20 °C by addition of $CO_{2(s)}$ and hydrolyzed with 185 mL water while keeping the temperature below 0 °C.

The precipitated solid was filtered off, and the organic phase was evaporated *in vacuo*. Fractionated distillation yielded the desired product as a colorless powder (71 g, 0.36 mol, yield: 67%, b.p. 75 °C / 5x10^{-2} mbar). ^{1}H NMR (500MHz, $CDCl_3$-*d*, ppm): δ 2.43-2.33 (m, 1H), 2.24-2.16 (m, 2H), 1.95-1.86 (m, 2H), 1.77-1.69 (m, 1H), 1.55-1.43 (m, 2H), 1.37-1.17 (m, 3H). ^{13}C NMR (125 MHz, $CDCl_3$-*d*, ppm): δ 51.00 (d, 1C, P-**C**H-, $^{1}J_{CP}$ = 91.3 Hz), 25.90 (d, 2C, P-CH-**C**H_2, $^{2}J_{CP}$ = 5.0 Hz), 25.58 (d, 2C, P-CH-CH_2-**C**H_2- $^{3}J_{CP}$ = 20.0 Hz), 25.18 (d, 1C, P-CH-CH_2-CH_2-**C**H_2- $^{4}J_{CP}$ = 2.5 Hz) . ^{31}P NMR (201 MHz $CDCl_3$-*d*, ppm): δ 58.28.

2-cyclohexyl-2-oxo-1,3,2-dioxaphospholane (*^{cy}*HexPPn, (1)): The ring-closing reaction was performed according to a slightly altered literature protocol.[2] A flame-dried three-necked round-bottom flask, equipped with a magnetic stirring bar and two dropping funnels, was charged with 250 mL dry THF and cooled to -21°C. Cyclohexyl phosphonic acid dichloride (30 g, 0.15 mol) was dissolved in dry THF (250 mL) and transferred into one dropping funnel via a flame-dried stainless steel capillary. A solution of dry ethylene glycol (9 g, 0.15 mol) and dry pyridine (23 g, 0.30 mol) in THF (250 mL) was transferred into the second dropping funnel via a flame-dried stainless steel capillary. Dropping speed was adjusted to be approximately equal for both mixtures. After complete addition the solution was stirred for 3h and kept over-night at -28°C to facilitate the precipitation of the pyridinium hydrochloride byproduct. The precipitate was removed by filtration via a flame-dried Schlenk funnel, and the solvent was evaporated under reduced pressure. The obtained solid was dissolved in dichloromethane and washed three times with brine. The organic phase was dried over sodium sulfate and evaporated in vacuo. Fractionated distillation yielded the desired product as colorless solid (9 g, 0.05 mol yield: 33%, b.p. 115°C / 9x10-3 mbar). ^{1}H NMR (500MHz, CDCl3-d, ppm): δ 4.51-4.40 (m, 2H, P-O-CH2), 4.28-4.15 (m, 2H, P-O-CH2), 2.07-1.90 (m, 3H) 1.88-1.74 (m, 2H), 1.74-1.62 (m, 1H), 1.50-1.33 (m, 2H), 1.33-1.14 (m, 3H). ^{13}C NMR (125 MHz, CDCl3-d, ppm): δ 66.39 (d, 2C, P-O-CH2-CH2-, 2JCP = 2.5 Hz), 31.22 (d, 1C, P-CH-, 1JCP = 130.0 Hz), 21.36 (d, 2C, P-CH-CH2, 2JCP = 3.8 Hz), 21.18 (d, 2C, P-CH-CH2-CH2- 3JCP = 16.3 Hz), 20.84 (d, 1C, P-CH-CH2-CH2-CH2- 4JCP = 1.3 Hz). ^{31}P NMR (201 MHz CDCl3-d, ppm): δ 47.50.

Representative procedure for the ROP of (1) and (2): The respective monomer(s) was/were placed in a flame-dried Schlenk-tube, dissolved in dry benzene and dried by repeated lyophilization. The monomer was dissolved in dry dichloromethane at a concentration of 4 mol L^{-1}. A stock solution of initiator 2-(benzyloxy)ethanol in dry dichloromethane was prepared with a concentration of 0.2 mol L^{-1}, and the calculated volume was added to the monomer solution via gas-tight syringe (Hamilton®). A stock solution of twice lyophilized TBD in dry dichloromethane was prepared with a concentration of 0.2 mol L^{-1}. The monomer- and catalyst solutions were cooled to 0°C. The polymerization was initiated by addition of the calculated amount of the catalyst solution (1 equivalent of TBD with respect to the initiator). The polymerization was terminated after 2h by the rapid addition of an excess of formic acid dissolved in dichloromethane with a concentration of 20 mg mL^{-1}. The colorless, amorphous polymers were purified by precipitation in cold diethyl ether and dried under reduced pressure.

Representative NMR data for P(1): ^{1}H NMR (500MHz, DMSO-d_6, ppm): δ 7.37-7.26 (m, aromatic protons), 4.22-4.02 (m, polymer backbone), 3.61 (m, 2H, terminal), 4.50 (m,benzylic protons) 1.92-1.02 (m, side-chain). ^{13}C NMR (125 MHz, DMSO-d_6, ppm): δ 128.19 und 127.45 (aromatic protons), 64.32 (polymer backbone), 34.50 (d, side-chain), $^{1}J_{CP}$ = 141.3 Hz), 25.50-25.27 (m, side-chain). ^{31}P NMR (201 MHz DMSO-d_6, ppm): δ 33.11 (polymer backbone), 32.98 (terminal group).

Representative NMR data for P(1_x-*co*-2_y)$_n$: ^{1}H NMR (500MHz, DMSO-d_6, ppm): δ 7.38-7.27 (m, aromatic protons), 4.22-4.07 (m, polymer backbone), 3.65-3.61 (m, terminal group), 4.52 (m, benzylic protons) 2.08-1.95 (m, isopropyl side-chain), 1.92-1.02 (m, cyclohexyl side-chain), 1.14-1.05 (m, isopropyl side-chain). ^{13}C NMR (125 MHz, DMSO-d_6, ppm): δ 128.19 und 127.45 (aromatic protons), 64.32 (polymer backbone), 34.50 (d, cyclohexyl side-chain, $^{1}J_{CP}$ = 141.3 Hz), 25.50-25.27 (m, cyclohexyl side-chain), 25.22 (d, $^{1}J_{CP}$ = 141.4 Hz, isopropyl side-chain), 16.12 (d, $^{2}J_{CP}$ = 4.9 Hz, isopropyl side-chain). ^{31}P NMR (201 MHz DMSO-d_6, ppm): δ 36.12 (isopropyl backbone), 35.90 (isopropyl terminal groups), 33.11 (cyclohexyl backbone), 32.98 (cyclohexyl terminal groups).

Supporting Figures

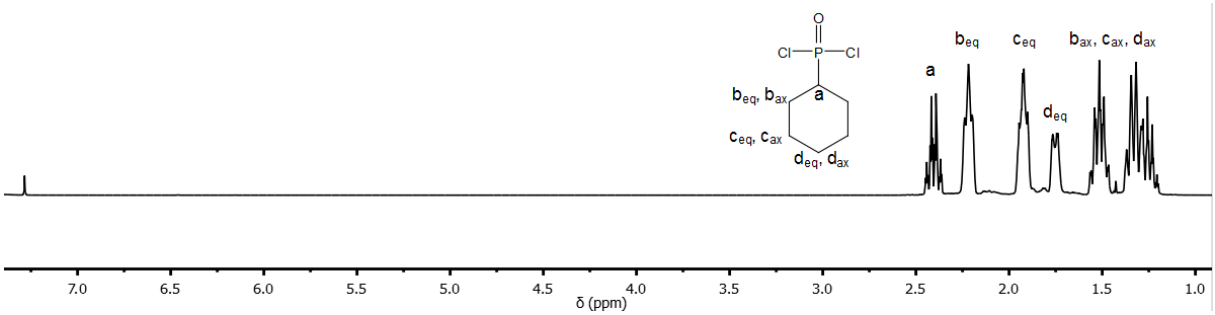

Figure S3.1: ^{1}H (500 MHz) NMR spectrum of cyclohexyl phosphonic acid dichloride in $CDCl_3$ at 298K.

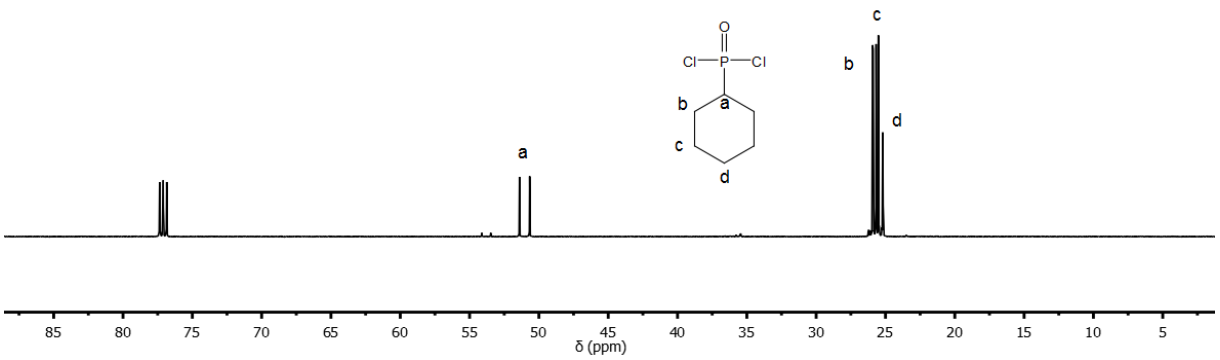

Figure S3.2: ^{13}C (125 MHz) NMR spectrum of cyclohexyl phosphonic acid dichloride in $CDCl_3$ at 298K.

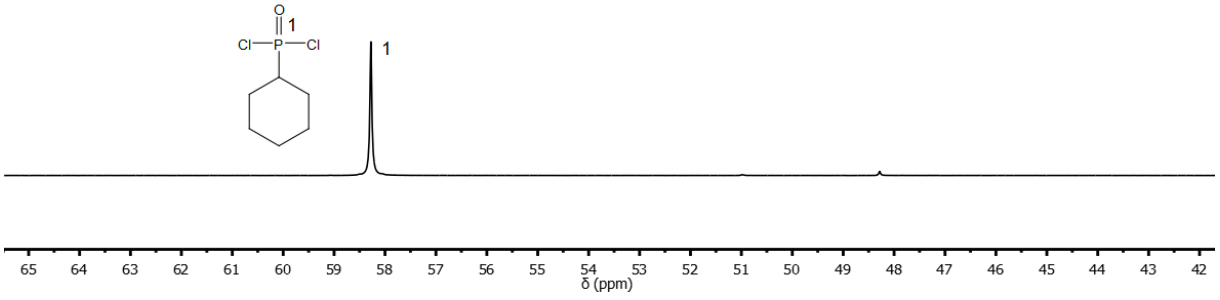

Figure S3.3: ^{31}P (202 MHz) NMR spectrum of cyclohexyl phosphonic acid dichloride in $CDCl_3$ at 298K.

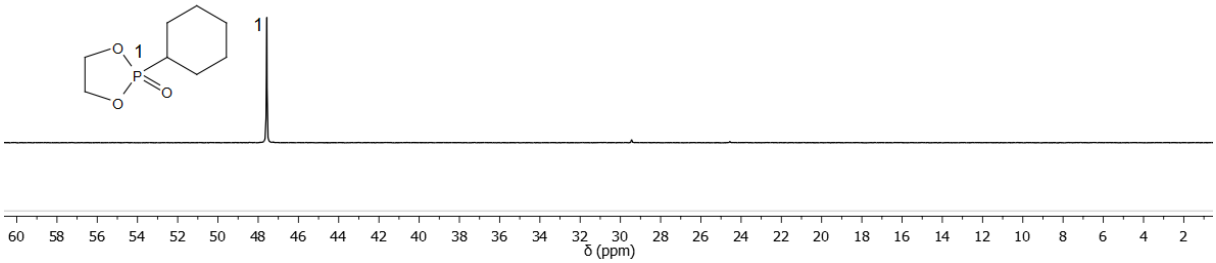

Figure S3.4: ^{31}P (202 MHz) NMR spectrum of (1) in $CDCl_3$ at 298K.

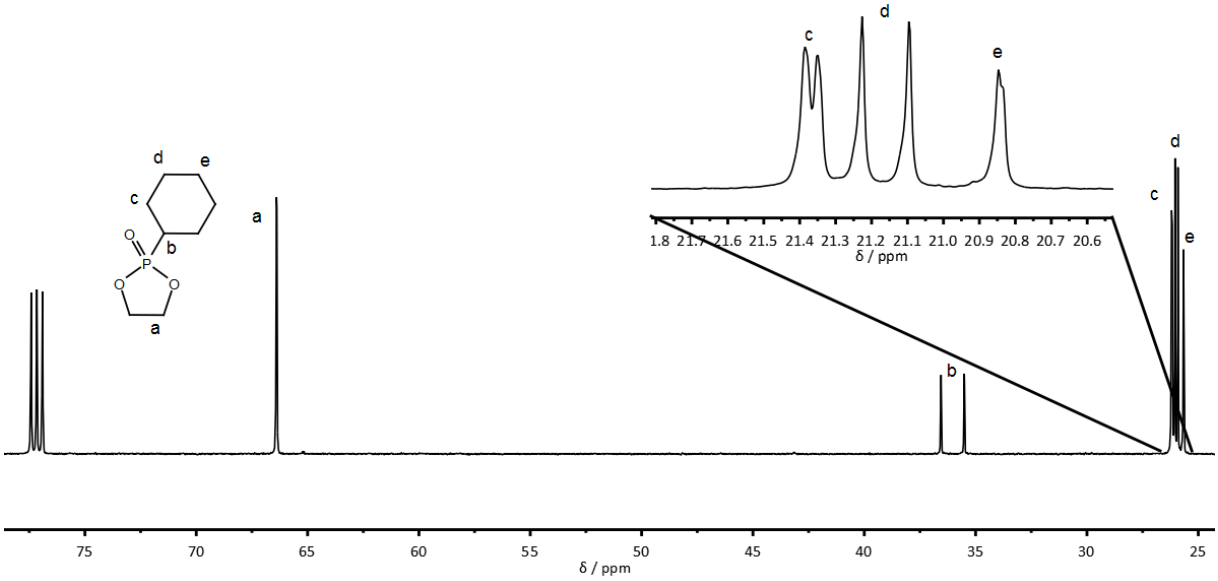

Figure S3.5: ^{13}C (125 MHz) NMR spectrum of (1) in $CDCl_3$ at 298K.

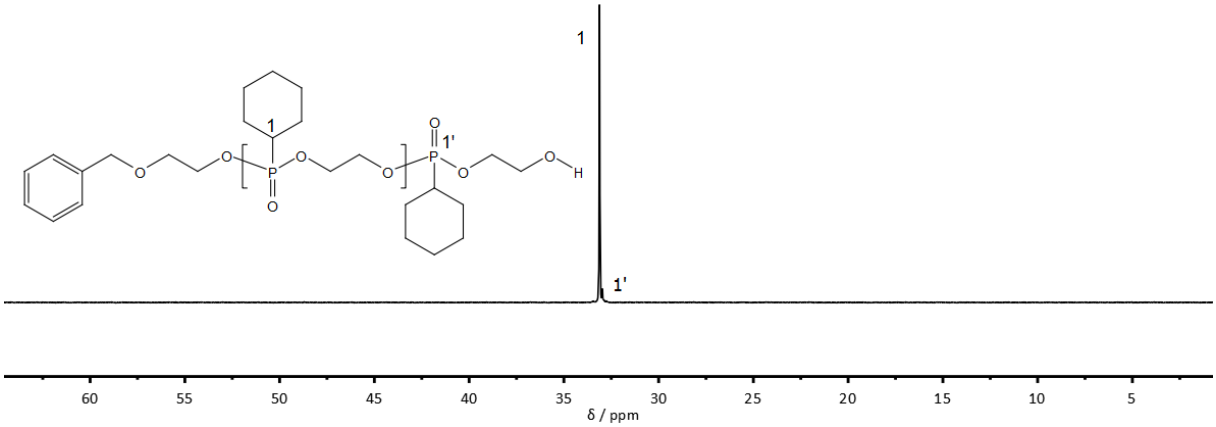

Figure S3.6: ^{31}P (202 MHz) NMR spectrum of P(1) in DMSO-d_6 at 298K.

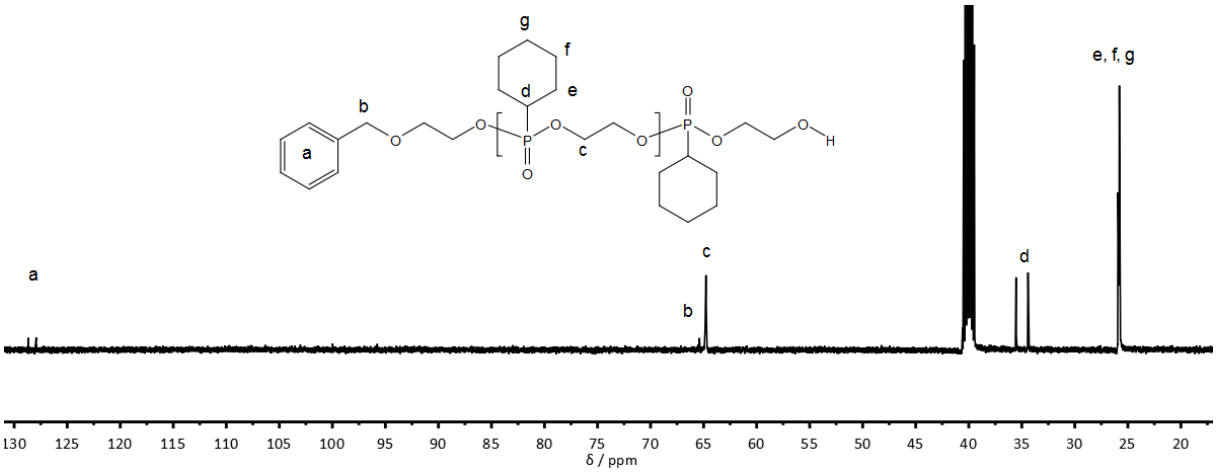

Figure S3.7: ^{13}C (125 MHz) NMR spectrum of P(1) in DMSO-d_6 at 298K.

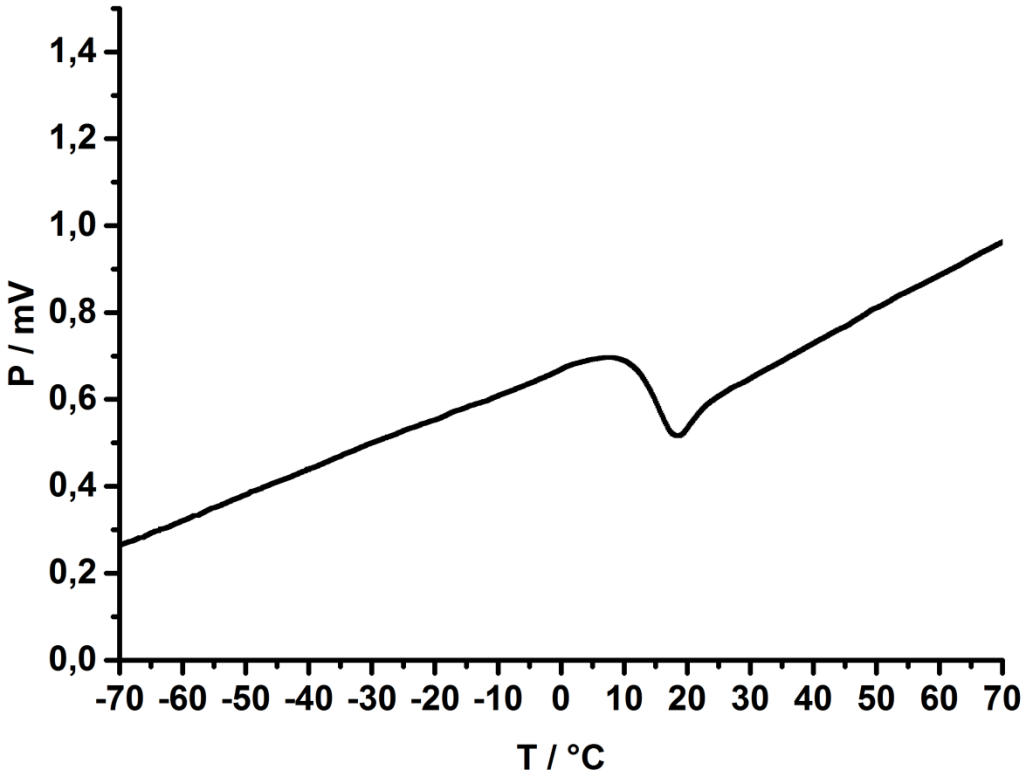

Figure S3.8: DSC thermogram of P(1) at a heating rate of 10 °C min^{-1} in the temperature range from -70 °C to 70 °C.

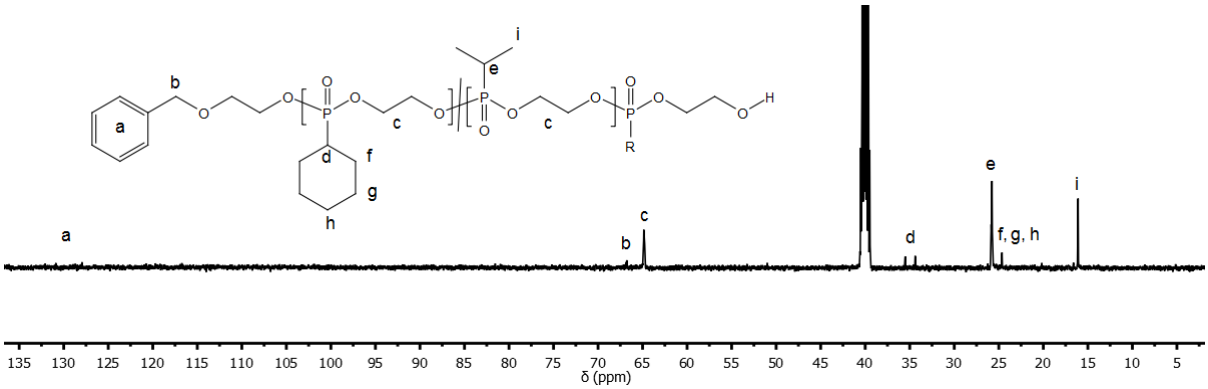

Figure S3.9: ^{13}C (125 MHz) NMR spectrum of P(1_x-*co*-2_y)$_n$ in DMSO-d_6 at 298K.

References:

1. Clay, J. P., *J. Org. Chem.,* **1951,** *16*, 892-894.

2. Steinbach, T.; Ritz, S.; Wurm, F. R., *ACS Macro Lett.,* **2014,** *3*, 244-248.

Chapter 3: Adjustable Glass Transition Temperatures of Poly(ethylene alkyl phosphonate) Copolymers.

Chapter 3 discussed the first copolymerization of dioxaphospholanes and adjustment of the copolymer T_g in a broad temperature range. An important matter not yet discussed, however, is the copolymerization behavior of the dioxaphospholanes. Different microstructures, ranging from perfectly alternating, over random, and gradient structures up to block copolymers are possible and these microstructures will alter the final polymer properties.

Furthermore, novel monomers are needed to vary the polymer properties in a broader range and finally, the already observed LCST behavior of poly(ethylene alkyl phosphonate copolymer)s needs more precise investigation.

Therefore, **Chapter 4** starts with the synthesis of a new, side-chain crystalline poly(ethylene alkyl phosphonate), followed by analysis of the copolymerization kinetics of dioxaphospholanes. Copolymerization is then used to produce temperature responsive LCST PPns, whose phase separation behavior is thoroughly investigated on several length scales using complementary techniques.

Chapter 4: Temperature-Responsive Poly(phosphonate) Copolymers: from Single Chains to Macroscopic Coacervates

Thomas Wolf[1], Johannes Hunold[2], Johanna Simon[1], Christine Rosenauer[1], Dariush Hinderberger[2], and Frederik R. Wurm[1]

[1]Max Planck-Institut für Polymerforschung, Ackermannweg 10, 55128 Mainz, Germany

[2]Martin-Luther-Universität Halle-Wittenberg, Institut für Chemie, Von-Danckelmann-Platz 4, 06120 Halle (Saale), Germany

Submitted to: Polymer Chemistry, **October 2017**

Keywords: poly(phosphoester), ring-opening polymerization, thermoresponsive polymers, turbidity measurements, continuous wave electron paramagnetic resonance spectroscopy, dynamic light scattering, confocal laser scanning microscopy

Chapter 4: Temperature-Responsive Poly(phosphonate) Copolymers: from Single Chains to Macroscopic Coacervates.

Abstract

Thermoresponsive polymers are promising materials for the development of “smart” devices like drug carriers with a temperature-controlled release of the payload. Such polymers change their hydrophilicity upon heating and phase separate from aqueous solution. Especially in sophisticated biomedical applications, a detailed understanding of the different stages of the phase separation is essential to prevent, e.g., premature release of cargo or the formation of large aggregates. We present the first series of random poly(ethylene alkyl phosphonate) copolymers with either high solubility in water or a finely tunable hydrophilic-to-hydrophobic phase transition upon heating (“LCST”). Polymerization via the organocatalytic anionic ring-opening polymerization provided high control over molecular weight (up to 23,000 g mol^{-1}), copolymer composition, and resulted in narrow molecular weight distributions ($Đ < 1.3$). The phase separation temperature was precisely adjusted in a range from 60 °C to 6 °C in water, depending on the copolymer composition. The phase transition was thoroughly investigated on different length scales via electron paramagnetic resonance spectroscopy (EPR), dynamic light scattering (DLS), UV-Vis spectroscopy and confocal laser scanning microscopy (cLSM)s, proving the step-wise formation of aggregates close to the cloud point temperature up to macroscopic coacervates.

Introduction

Responsive materials, which are substances showing a property change upon an external stimulus, are of interest for a variety of applications. They are exceptionally well-studied in the field of “smart“ drug carrier development.[1-5] Here, polymers have to be water-soluble, biocompatible, non-toxic, preferably degradable, and also are responsive towards specific triggers. One interesting stimulus is temperature, as it is easily applied with good spatial and temporal control. A detailed understanding of the underlying mechanisms of these triggers is essential to prevent, e.g., premature release of cargo.

Most temperature responsive polymers exhibit a hydrophilic-hydrophobic phase transition upon heating (lower critical solution temperature, LCST) in a defined solvent (water in most cases). The phase separation occurs due to a loss of solvent-polymer hydrogen

bonding at elevated temperatures.[6-8] As a result, the inter- and intra-chain hydrophobic-hydrophobic interactions dominate and the polymer chain collapses. This is accompanied by an increase of entropy of liberated water molecules previously bound to the polymer. These polymers are often proposed for "smart" delivery systems in biomedical applications.[9-10]

In addition to the abovementioned criteria, a sharp, reversible and hysteresis-free phase transition is desirable to guarantee a fast and precise response of the material. To prevent premature reactions to the wrong or insufficient stimulus, a precise adjustment of the phase separation temperature and detailed understanding of the underlying mechanism is essential. To this end elaborated analytical techniques (e.g., UV-Vis, EPR spectroscopy, DLS, cLSM) can be used to gain a better understanding of these mechanisms on different length scales.[11-12]

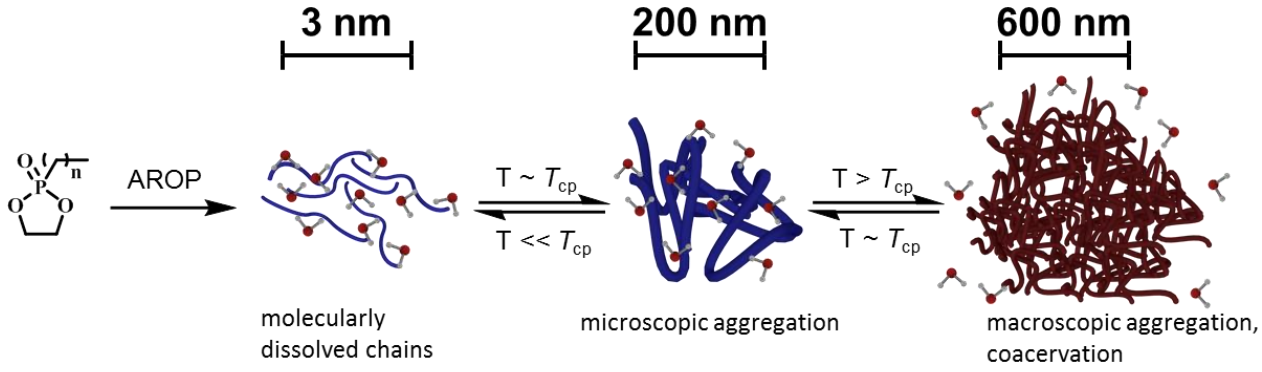

Scheme 4.1: Schematic presentation of this study: Anionic ring-opening copolymerization produces well-defined, water-soluble random copolymers. Phase separation behavior of the copolymers in the aqueous medium is investigated through various methods. Formation of nano-inhomogeneities and microscopic aggregates close to the cloud point temperature (T_{cp}) observed via CW EPR and DLS measurements, respectively. Macroscopic aggregation above T_{cp} and formation of coacervates visualized via turbidity measurements and confocal laser scanning microscopy.

One class of polymers receiving increased attention as candidates in biomedical applications are poly(phosphoester)s (PPEs).[13-17] The phosphoric acid ester bonds can be cleaved hydrolytically, eliminating the threat of accumulation of polymeric material in the body.[18-22] Via different chemistries polymers with adjustable hydrophilicity are accessible, and due to the pentavalent phosphorus additional chemical functionality can be installed into every repeat unit.[16,17,23]

Chapter 4: Temperature-Responsive Poly(phosphonate) Copolymers: from Single Chains to Macroscopic Coacervates.

The anionic ring-opening polymerization (AROP) of cyclic phosphates give fast access to water-soluble PPEs with a high control over molecular weight. However, transesterification reactions need to be considered.[24-25] Still, today, a variety of different PPEs are have been reported exhibiting LCST behavior.[26-28]

Recently, we have developed poly(ethylene alkyl phosphonate)s (PPns), that are aliphatic poly(phosphoester)s with a phosphorus-carbon bond in the side-chain, which might be of interest for biomedical applications. These polymers are accessible via the organocatalytic ROP of 2-alkyl-2-oxo-1,3,2-dioxaphospholanes providing excellent control over molecular weight, copolymer composition, and narrow molecular weight distributions.[20,21,29] First studies have shown that PPns are water-soluble, non-toxic and their properties can be finely tuned by variation of the pendant side-group.[20,21] In contrast to poly(phosphate) synthesis, transesterification side-reactions during the synthesis of poly(phosphonate)s are less pronounced, allowing living polymerization up to high conversions.[15,20,21] Copolymerization of 2-alkyl-2-oxo-1,3,2-dioxaphospholanes was shown to produce random copolymers with material properties (solubility, T_g) dependent on the copolymer composition.[29,30]

In this work, we study the LCST behavior of a series of novel copolymers of poly(ethylene alkyl phosphonate)s. Polymers with molecular weights between 7,700 and 23,000 g mol^{-1}, narrow molecular weight distributions, and adjustable copolymer compositions were prepared. The phase separation temperature of the resulting copolymers was dependent on the copolymer composition. Copolymers with less than 50mol% or 30mol% of the two hydrophobic co-monomers, respectively, were water-soluble and non-thermoresponsive. Above these values phase transitions upon heating an aqueous solution was observed with adjustable macroscopic cloud points between 6 °C to 55 °C in the current set of polymers. A combination of electron paramagnetic resonance spectroscopy (EPR), dynamic light scattering (DLS), UV-Vis spectroscopy, and confocal laser scanning microscopy (cLSM) were used to analyze the phase transition of these copolymers and get a deeper understanding of the phase transition of these polymers. The results of this study will allow the future design of fully degradable nano- or microcarrier devices based on PPEs.

Results and Discussion

Monomer synthesis

Three different five-membered cyclic phosphonates for the AROP were synthesized to generate a library of temperature-responsive poly(ethylene alkyl phosphonate)s (Scheme 4.2, a). Monomers **(1)** and **(2)** were synthesized according to the literature.[20] Monomer **(3)** with a hydrophobic *n*-hexyl side-chain was newly developed for the current study (Scheme 4.2, b): The *Michaelis-Arbuzov* reaction of *n*-hexyl bromide and triethyl phosphite yielded *O, O*-diethyl *n*-hexyl phosphonic acid diethyl ester. Conversion to the corresponding phosphonic acid dichloride was achieved by chlorination with thionyl chloride. Finally, condensation with ethylene glycol provided the cyclic monomer **(3)**. Detailed experimental description, as well as analytical data, can be found in the Supporting Information.

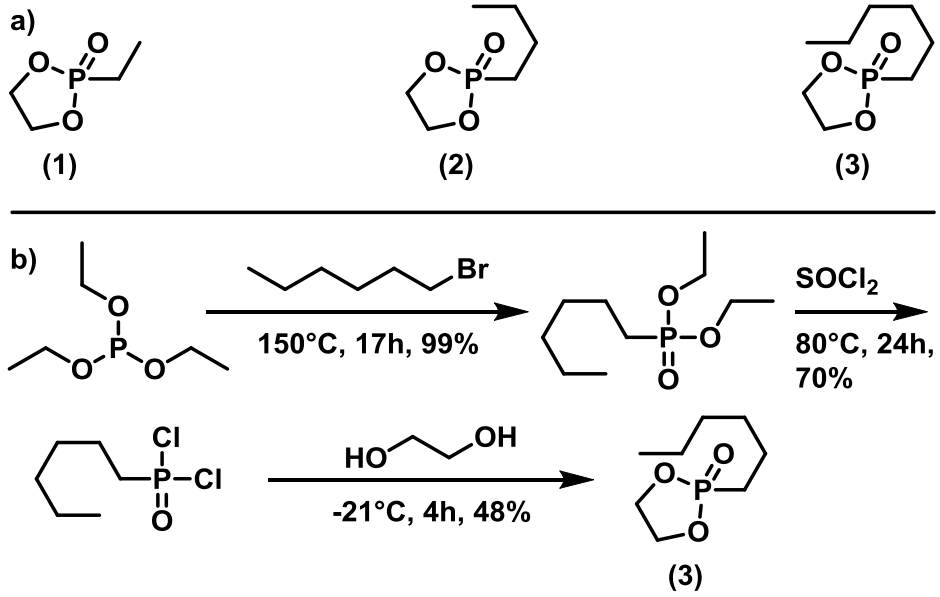

Scheme 4.2: a) Structure of the 2-alkyl-2-oxo-1,3,2-dioxaphospholane monomers used in this study. b) Synthesis Scheme of 2-*n*-hexyl-2-oxo-1,3,2-dioxaphospholane (3), starting with the *Michaelis-Arbuzov* reaction between triethyl phosphite and *n*-butyl bromide, followed by chlorination with thionyl chloride, and ring-closing with ethylene glycol.

Homopolymerization

First, the homopolymerization behavior of 2-*n*-hexyl-2-oxo-1,3,2-dioxaphospholane **(3)** as well as the respective properties of **P(3)$_n$** was investigated. Following previously reported results regarding the AROP of dioxaphospholanes, ^{n}HexPPn was polymerized in dichloromethane (DCM) with 1,8-diazabicyclo[5.4.0]undec-7-en (DBU) as the catalyst at 30 °C with 2-(benzyloxy)ethanol as an initiator, which allowed end-group analysis via ^{1}H NMR spectroscopy (Scheme 4.3).[20]

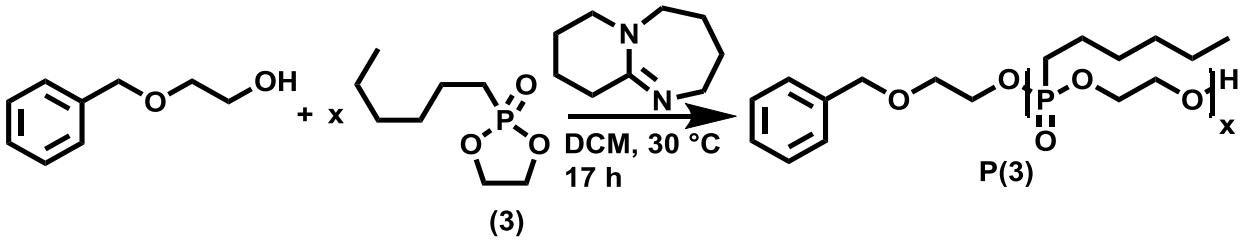

Scheme 4.3: Reaction Scheme for the 2-(benzyloxy)ethanol-initiated and DBU-catalyzed AROP of (3).

Successful polymerization is indicated from the ^{1}H NMR spectra by the broad resonance of the backbone protons ranging from 4.22 to 4.01 ppm after 17h of polymerization time (Figure 4.1, a, signal c). Determination of M_n was conducted via end-group analysis, by comparison of the initiator signals at 7.26 ppm with the backbone resonances. The ^{31}P{H} spectrum (Figure 4.1, a, inset) reveals a distinct shift from the monomer (51.4 ppm) to a polymer with two phosphorus signals originating from the backbone (Figure 4.1, signal 1, 33.5 ppm) and the terminal phosphorus (Figure 4.1, signal 1', 32.9 ppm). SEC analysis (Figure 4.1, b) shows symmetrical monomodal molecular weight distributions ($Đ$ ~ 1.20; *vs*. PEG standards). The polymer is insoluble in water but can be readily dissolved in organic solvents such as diethyl ether, dichloromethane, chloroform, dimethyl sulfoxide, or dimethylformamide.

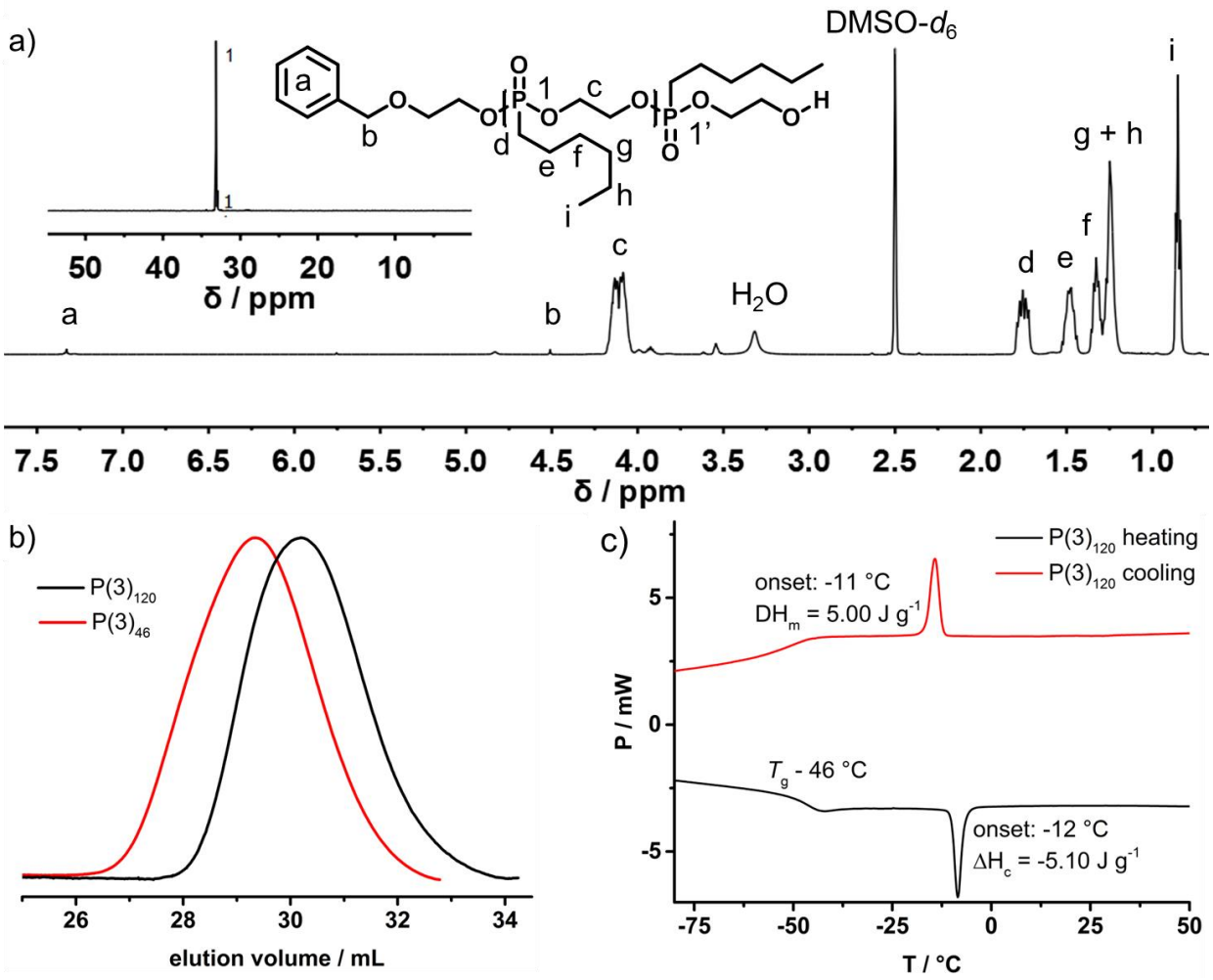

Figure 4.1: a) ^{1}H NMR (500 MHz) ^{31}P{H} NMR (201 MHz) (inset) spectra of $P(3)_{120}$ in DMSO-d_6 at 298K. b) SEC elugrams (RI detection) of $P(3)_{120}$ and $P(3)_{46}$ in DMF at 333K. c) DSC thermogram of $P(3)_{120}$ at a heating rate of 10 °C min^{-1} in the temperature range from -80 °C to 50 °C (second heating and cooling curves shown).

Thermal analysis via DSC (Figure 4.1, c) reveals a low glass transition temperature (T_g = - 46 °C) similar to previously reported poly(alkylene alkyl phosphonate)s. Additionally, a melting signal with onset at -10 °C and an enthalpy of fusion of 5 J g^{-1} is observed, indicating the first side-chain crystallization observed for poly(ethylene alkyl phosphonates)s from AROP.[20,21] With the polymerizability of monomer **(3)** ensured we proceeded with the synthesis of the thermoresponsive poly(ethylene alkyl phosphonate) copolymers **P(1$_x$-*co*-2$_y$)** and **P(1$_x$-*co*-3$_y$)**.

Copolymerization

The organocatalytic anionic ring-opening copolymerization of the monomer **(1)**, resulting in hydrophilic repeat units, with either monomer **(2)** or **(3)** (each producing hydrophobic units) was performed at 30 °C with DBU as the respective catalyst as a one-pot reaction for 17h (Scheme 4.4).

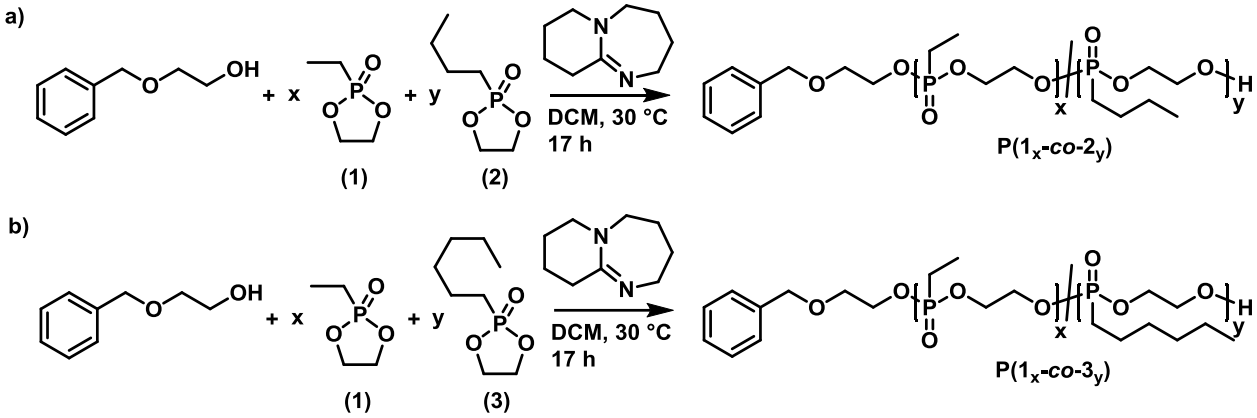

Scheme 4.4: Reaction Scheme for the 2-(benzyloxy)ethanol-initiated and DBU catalyzed anionic ring-opening copolymerization of (1) with a) (2) to form P(1_x-*co*-2_y) and b) with (3) to form P(1_x-*co*-3_y).

The representative ^{1}H and ^{31}P{H} NMR spectra of **P(1_x-*co*-2_y)** and **P(1_x-*co*-3_y)** are shown in Figure 4.2. Molecular weights can be determined by end-group analysis from the ^{1}H NMR spectra (*vide supra*). Polymers with molecular weights ranging from 7,700 to 23,000 g mol^{-1} were obtained. ^{1}H NMR spectroscopy further provided information on the copolymer composition of the final material.

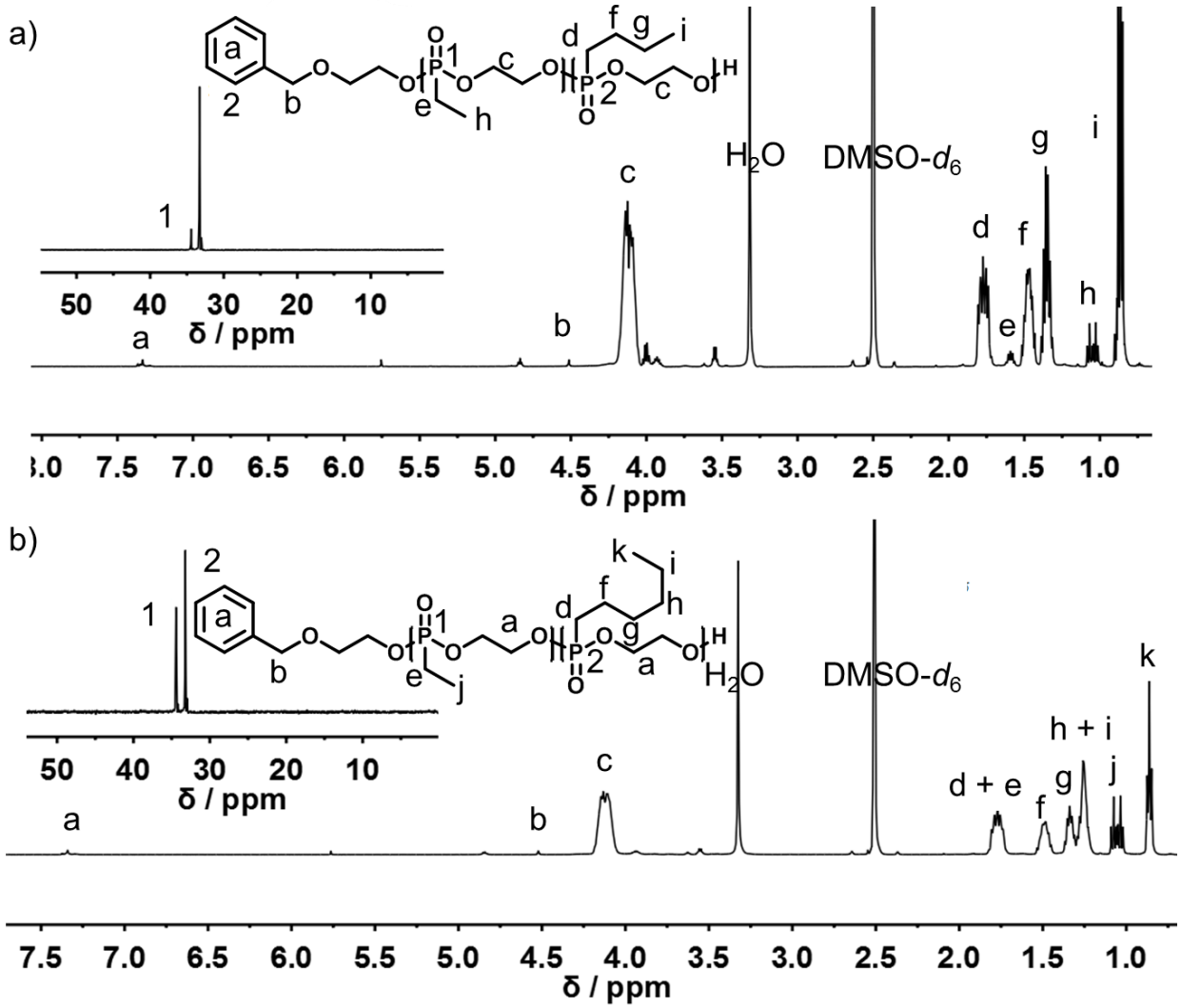

Figure 4.2: ^{1}H NMR (500 MHz) and ^{31}P{H} NMR (201 MHz, inset) spectra of a) P(1_{15}-*co*-2_{118}) and b) P(1_{62}-*co*-3_{56}) in DMSO-d_6 at 298K.

The resonance of the terminal -CH_3 side-chains of **(1)** at 1.06 ppm is well separated from the respective terminal -CH_3 group resonances of **(2)** and **(3)** at 0.86 ppm allowing the calculation of the copolymer composition. In addition to ^{1}H NMR spectroscopy, the comparison of the relative intensities of the backbone resonances in the ^{31}P{H} NMR spectra at 34.4 ppm for **(1)**, 33.2 ppm for **(2)** and **(3)**, respectively also reveals the copolymer composition (Figure 4.2, insets). The experimentally found polymer composition matched the monomer feed ratios in all cases, both from ^{1}H or ^{31}P NMR analysis.

^{1}H DOSY NMR spectra (Figure 4.3) further prove a successful copolymerization, as all relevant resonances, i.e., backbone and respective side-chains, have the same diffusion coefficient and are part of the same molecule.

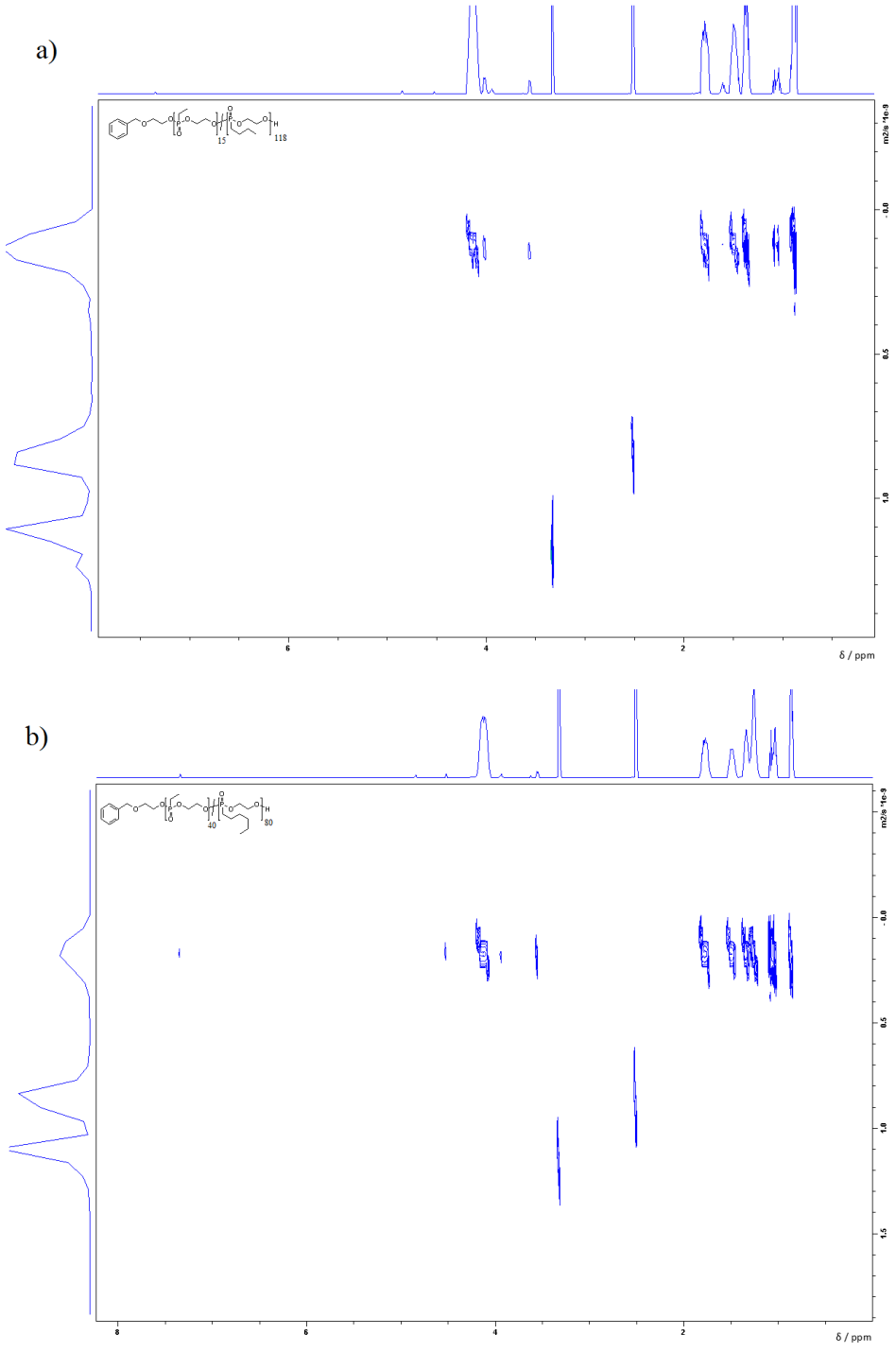

Figure 4.3: ^{1}H DOSY NMR (500 MHz) spectra of a) P(1_{15}-*co*-2_{118}) and b) P(1_{40}-*co*-3_{80}) in DMSO-d_6 at 298K.

All polymers regardless of molecular weight or copolymer composition showed a symmetrical monomodal SEC traces with rather narrow molecular weight distributions ($1.18 < Đ < 1.30$; vs. PEG standard) (Figure 4.4, a, b).

The microstructure of the copolymers is expected to have a significant influence on the solubility and phase separation behavior. Therefore, the copolymerization kinetics of **(1)** with **(2)** and **(3)**, respectively, were analyzed via $^{31}P\{H\}$ NMR spectroscopy. Figure 4.4, c shows the molar fraction of **(1)** integrated into the respective copolymer at different times during the copolymerization. Starting from the initial 1 to 1 ratio of the monomer feed ([A] / ([A] + [B]) = 0.5), the copolymer composition remains constant for the whole time of both copolymerizations.

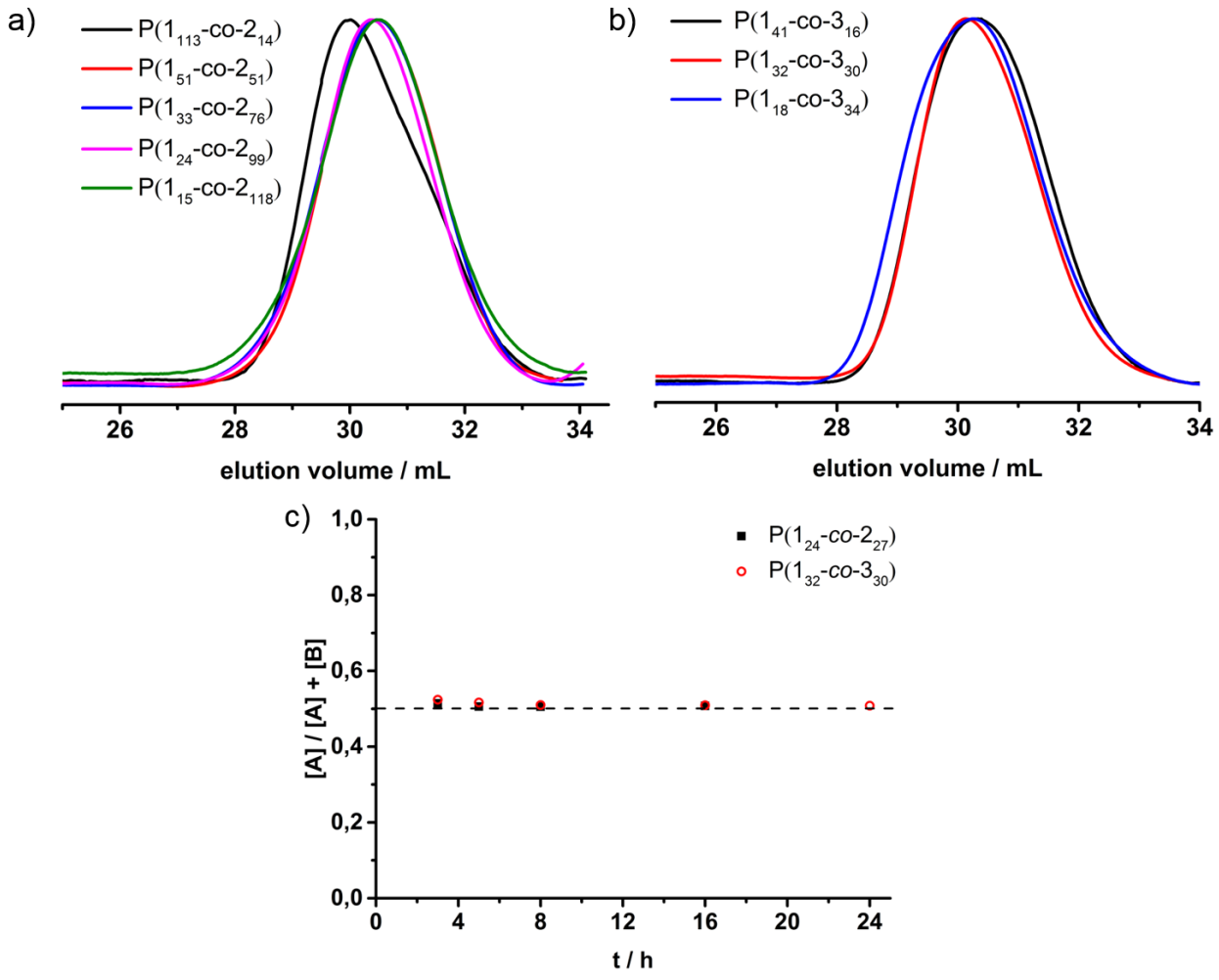

Figure 4.4: SEC traces (RI detection) of a) P(1_x-*co*-2_y) and b) P(1_x-*co*-3_y) with different copolymer compositions measured in DMF at 333K (RI detection). c) The molar fraction of (1) plotted against the reaction time: copolymerization of (1) and (2) (black squares) and copolymerization of (1) and (3) (red circle).

This indicates that all co-monomers are incorporated in the polymer at the same rate and have the same reactivity, thus resulting in the formation of a random copolymer without any detectable gradients.

DSC analysis shows the T_g for all copolymers between -55 and -42 °C and that the side-chain crystallinity observed for **P(3)$_{120}$** vanishes for the copolymers resulting in entirely amorphous materials (Figure 4.5).

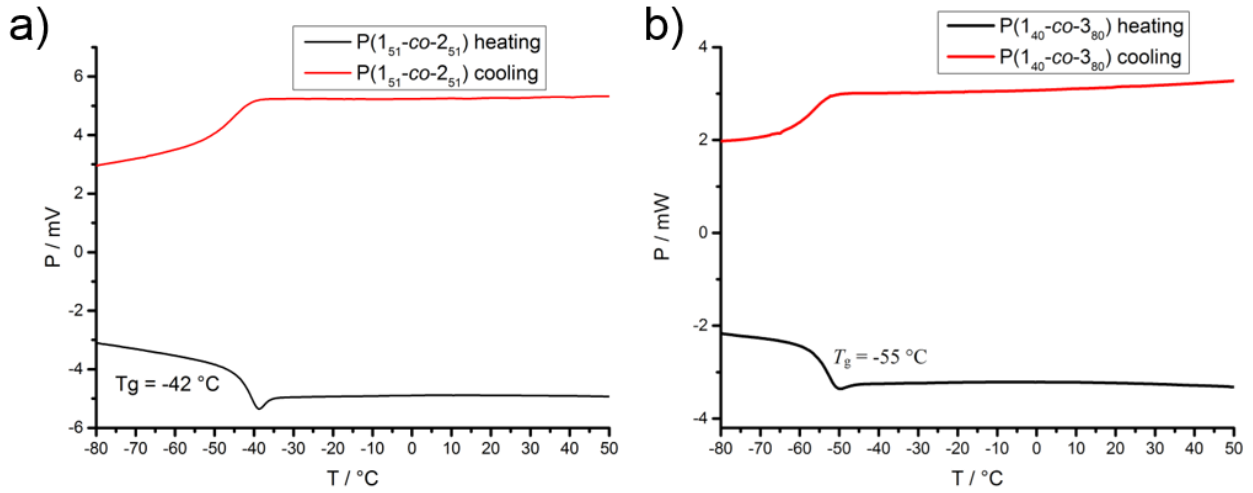

Figure 4.5: DSC measurement at a heating rate of 10 °C min^{-1} in the temperature range from -80 °C to 50 °C: a) P(1$_{51}$-*co*-2$_{51}$) and b) P(1$_{40}$-*co*-3$_{80}$).

Cell-toxicity measurements against the macrophage cell-line RAW 264.7 showed a concentration-dependent cell-toxicity for **P(1$_{51}$-*co*-2$_{51}$)** and **P(1$_{41}$-*co*-3$_{16}$)**. The toxicity was negligible at pharmaceutically suitable concentrations (< 100µg mL^{-1}). Above 250 µg mL^{-1}, a reduction in the viability is observed (Figure S4.10). The effect was more pronounced for the more hydrophobic copolymers **P(1$_{41}$-*co*-3$_{16}$)**. A similar trend was previously reported for other poly(ethylene alkyl phosphonate)s with hydrophobic side-chains.[20] Analytical data of all copolymers are summarized in Table 4.1 and Table 4.2.

Table 4.1: Characterization data of the copolymers of (1) and (2).

polymer [a]	monomer feed [b]	copolymer composition [c]	M_n / g mol^{-1} [c]	Y / %[c]	$Đ$ [d]	T_g / °C [e]	T_{cp} / °C [f]
P(1$_{113}$-*co*-2$_{47}$)	0.70 / 0.30	0.70 / 0.30	23,000	89	1.18	-55	> 100
P(1$_{51}$-*co*-2$_{51}$)	0.50 / 0.50	0.50 / 0.50	15,000	83	1.30	-55	50
P(1$_{24}$-*co*-2$_{27}$)	0.46 / 0.54	0.47 / 0.53	7,700	79	1.29	-42	51
P(1$_{33}$-*co*-2$_{76}$)	0.29 / 0.71	0.30 / 0.71	17,000	82	1.30	-44	26
P(1$_{24}$-*co*-2$_{99}$)	0.19 / 0.81	0.19 / 0.81	19,500	72	1.26	-46	16
P(1$_{15}$-*co*-2$_{118}$)	0.12 / 0.88	0.11 / 0.89	21,000	74	1.21	-45	8

a: Type of polymer and degree of polymerization as determined by ^{1}H NMR spectroscopy. b: Monomer feed ratio. c: M_n and conversion Y determined via ^{1}H NMR spectroscopy. d: Determined via SEC in DMF at 333K (vs. PEG standard). e: Determined via DSC measurements. f: Determined via UV Vis spectroscopy.

Table 4.2: Characterization data of the copolymers of (1) and (3).

polymer [a]	monomer feed [b]	copolymer composition [c]	M_n / g mol^{-1}[c]	Y / %[c]	$Đ$ [d]	T_g / °C [e]	T_{cp} / °C [f]
P(3)$_{120}$	-	-	23,000	74	1.20	-46	-
P(3)$_{46}$	-	-	8,800	86	1.30	-40	-
P(1$_{41}$-*co*-3$_{16}$)	0.71 / 0.29	0.71 / 0.29	8,600	93	1.19	-43	55
P(1$_{62}$-*co*-3$_{56}$)	0.52 / 0.48	0.52 / 0.48	19,000	68	1.20	-50	56
P(1$_{32}$-*co*-3$_{30}$)	0.49 / 0.51	0.52 / 0.48	10,000	80	1.28	-54	26
P(1$_{40}$-*co*-3$_{80}$)	0.30 / 0.70	0.33 / 0.67	21,000	70	1.30	-53	-
P(1$_{18}$-*co*-3$_{43}$)	0.29 / 0.71	0.29 / 0.71	10,000	75	1.25	-54	-

a: Type of polymer and degree of polymerization as determined by ^{1}H NMR spectroscopy. b: Monomer feed ratio. c: M_n and conversion Y determined via ^{1}H NMR spectroscopy. d: Determined via SEC in DMF at 333K (vs. PEG standard). e: Determined via DSC measurements. f: Determined via UV Vis spectroscopy.

Thermal behavior in solution

The solubility and thermal behavior of the copolymers in water were thoroughly investigated. First, turbidity measurements were performed to investigate the macroscopic solution behavior. Copolymers with low amounts of the hydrophobic comonomer exhibited high solubility in water (> 10 g L^{-1}), however, polymers containing more than 50 mol% of **(2)** or 30 mol% of **(3)**, respectively undergo a phase separation upon heating. The cloud point temperatures (T_{cp}) were tailored over a broad temperature range from 6 °C to 55 °C in the current copolymer set (Figure 4.6, a, b).

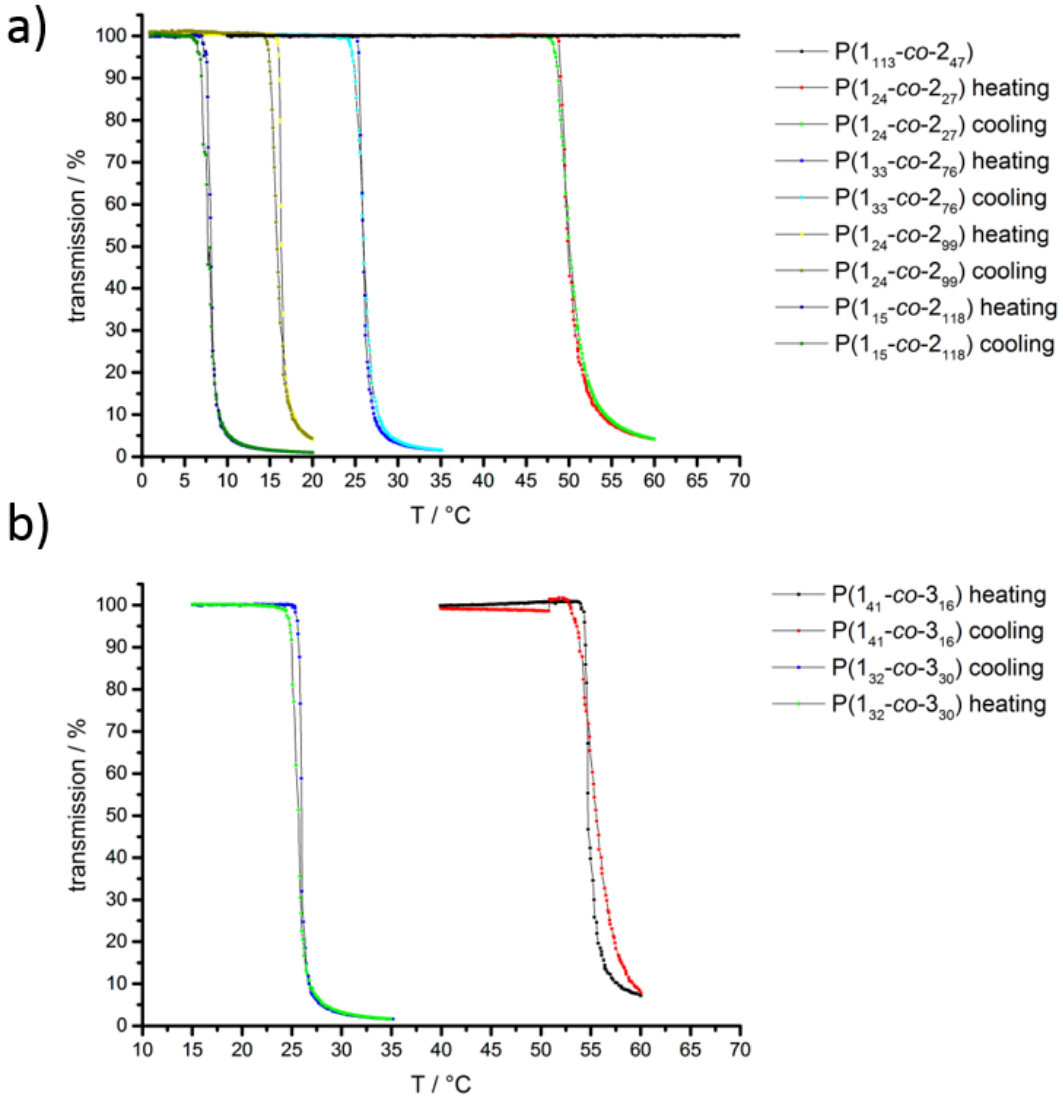

Figure 4.6: Thermal response of poly(ethylene alkyl phosphonate) copolymers: Turbidity measurements (heating and cooling curves) of a) P(1_x-*co*-2_y), b) P(1_x-*co*-3_y) in ultrapure water at a concentration of 10 g L^{-1} and a heating/cooling rate of 1 °C min^{-1}. The transmission was measured at 500 nm.

A linear dependency between the T_{cp} and the number of hydrophobic side-chains incorporated in the copolymer was found (Figure 4.7). In all cases, little to no hysteresis occurred during the cooling of the samples, indicating a well-reversible phase transition.

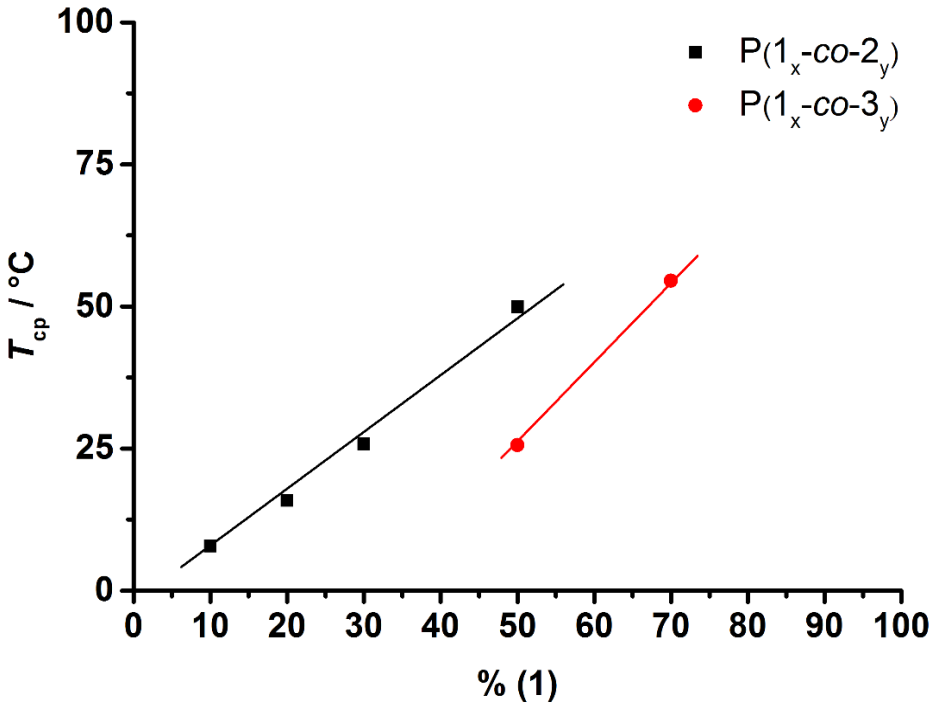

Figure 4.7: Linear correlation between comonomer ratio and T_{cp}.

In accordance with the literature, the LCST cloud point temperatures were found to be dependent on the ionic strength of the solution.[31] Addition of sodium phosphate (0.1 M PBS, pH 7.4) shifted the phase transition by 6 °C to lower temperatures (Figure 4.8). Addition of calcium ions at the same osmolarity further decreased T_{cp}, indicating interactions between the phosphonate backbone and the Ca^{2+} ions. This is in good accordance with the theory of Hofmeister *et al.* regarding the antichaotropic effect of sodium ions.[31]

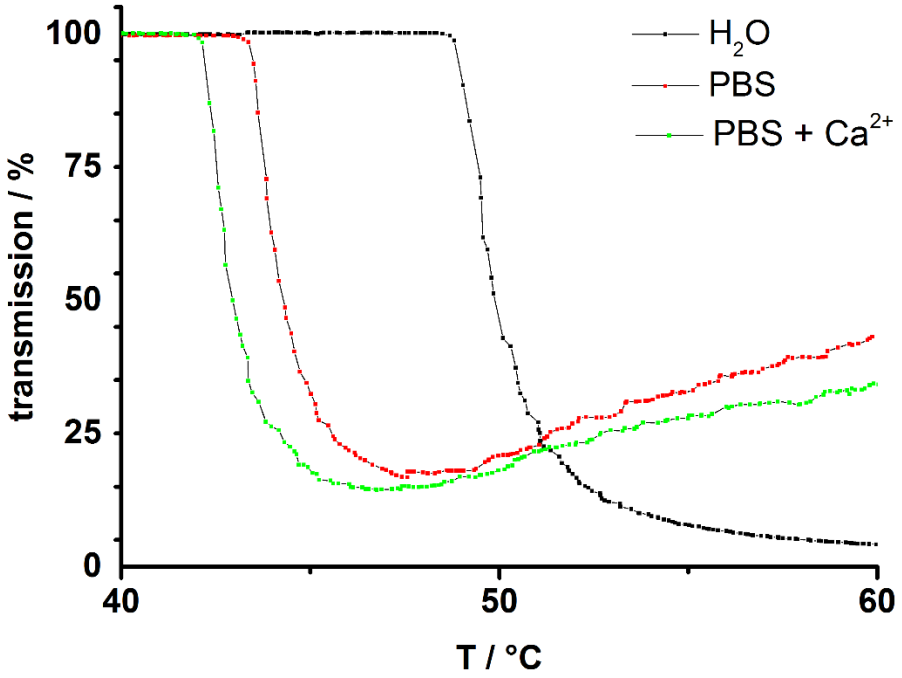

Figure 4.8: Turbidity measurements of P(1_{51}-*co*-2_{51}) in ultrapure water (black), in the presence of monovalent ions (red) and divalent ions (green), respectively. Measurements were performed at a concentration of 10 g L^{-1} and a heating rate of 1 °C min^{-1}. The transmission was measured at 500 nm. Cloud point temperature (T_{cp}) was measured at the inflection of the heating curve.

Three complementary methods, each observing different length scales during the phase separation process, were used to gain a more detailed understanding of the phase separation behavior of poly(ethylene alkyl phosphonate)s: EPR spectroscopy was employed to detect the formation of nano-dimensional structural inhomogeneities. Then, dynamic light scattering was employed to analyze the formation of larger aggregates before the macroscopic precipitation of the solution visible by UV-Vis turbidity measurements. Finally, confocal laser scanning microscopy visualized the macroscopic aggregates and analyzed their structure.

The CW EPR spectra recorded during the heating of an aqueous solution of 15 mg mL^{-1} of **P(1_{33}-*co*-2_{76})** with 0.2 mM 2,2,6,6,-tetramethylpiperidine-1-oxiyl (TEMPO) in DPBS buffer are shown in Figure 4.10. Under these conditions, which were optimized for the CW EPR measurements, macroscopic phase separation occurred at 25 °C and no macroscopic aggregation is visible in dynamic light scattering at 20 °C (Figure 4.9).
The sample was chosen due to the convenient position of the phase separation temperature for the measurements.

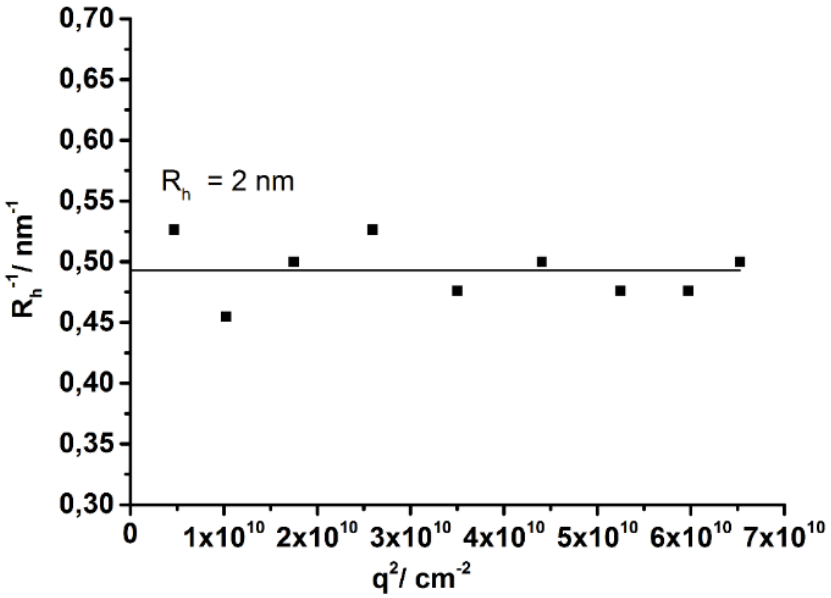

Figure 4.9: Dynamic light scattering results of P(1_{33}-co-2_{76}) at 15 mg mL^{-1} in DPBS.

It can be seen, that the intensity and line shape of the high-field peak changes with increasing temperature. In the range between 10 and 16 °C, the intensity of the high-field line first decreases slightly when the temperature increases, which could, e.g., indicate a slight rise in viscosity or a slight decrease in polarity in the spin probe environment experienced by some of the spin probes.

If, however, the temperature is only increased further by just 2 °C (from 16 to 18 °C), the signal intensity maximum decreases significantly. The reason for the observed intensity decrease of the high-field line is the simultaneous occurrence of a second, slightly less polar solvated, probe species at 18 °C. This spin probe species shows a slightly smaller hyperfine splitting constant A (i.e., its high-field line appears at slightly lower magnetic field values) indicating a lower spin probe environmental polarity. Since the hyperfine coupling

values of this second, “hydrophobic”, species (~47 MHz) are still very high compared to these species in other, more conventional LCST type polymers (~44-45 MHz), we can conclude that the less polar polymer-rich regions, probed by the appearance of the second spin probe species, are still water swollen (A in bulk water: ~48 MHz).[11, 32-34]

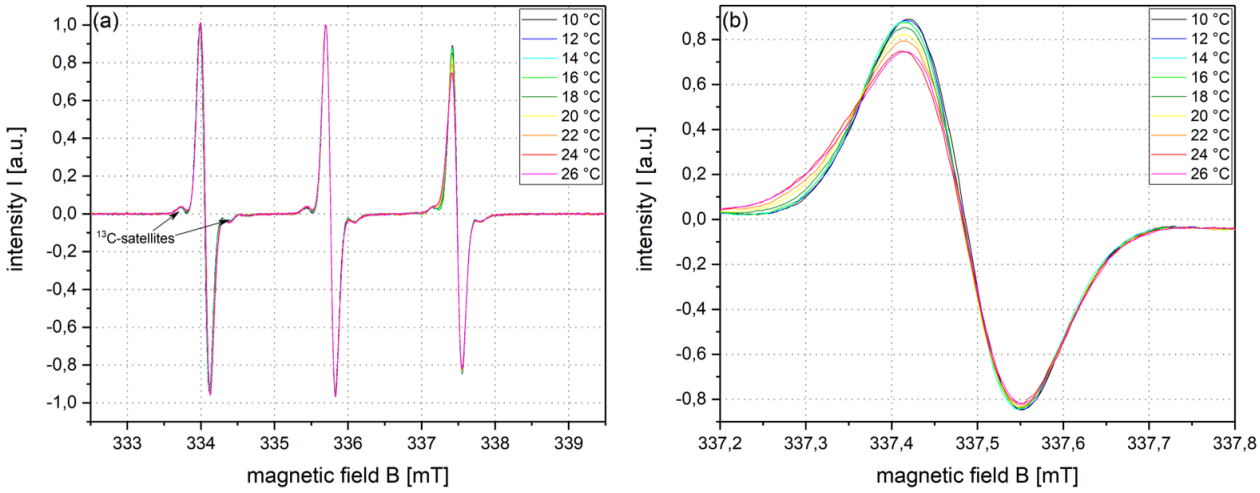

Figure 4.10: CW EPR spectra of an aqueous solution of 15 mg mL^{-1} P(1_{33}-*co*-2_{76}) with 0.2 mM TEMPO in DPBS buffer. a) full spectra and b) enlarged high-field region.

In these LCST polymers, we can distinguish two types of water: On the one hand bulk water with the relatively freely tumbling hydrophilic probe species with comparatively high environmental polarity. On the other hand, polymer-associated water that forms the hydration shell around the polymer chains where the more hydrophobic probe species with a reduced environmental polarity is located. Thus, already 6 - 7 °C below the macroscopic cloud point temperature T_{cp} of about 25 °C a phase separation between still fully solvated and less solvated yet still water-swollen polymer regions on the nanoscale could be observed by EPR spectroscopy.

These nanoscopic inhomogeneities continue to grow at a further temperature increase so that the polymer chains are more and more dehydrated (and yet still water swollen in comparison to conventional LCST polymers). As an additional result of this dehydration process, the environmental viscosity of the hydrophobic probe species increases and also their mobility is reduced. Both effects together lead to a steady signal intensity decrease of the high-field peak, until it reaches its minimum at 24 - 26 °C, which corresponds quite well with T_{cp}.

To further investigate aggregation during the phase separation process, temperature-dependent DLS measurements were performed. **P(1_{24}-*co*-2_{27})** with a T_{cp} at 50 °C (10 g L^{-1}, H_2O) was exemplarily chosen for these experiments due to the convenient phase separation temperature for the experiment. Figure 4.11, a) shows the hydrodynamic radii measured in the light scattering experiment (left, black) and the relative intensities (right, red) of the observed processes as a function of temperature.
At 27 °C, below the T_{cp}, the majority of the polymers are molecularly dissolved with a small fraction of aggregates only. This can be concluded as there are only two processes observed: One with a hydrodynamic radius of 1.5 nm corresponding to 70% of the total scattering intensity (molecularly dissolved polymer, circles) and one process with a hydrodynamic radius of 50 nm corresponding to 30% of the scattering intensity (aggregates, triangles). Due to the high size dependence of scattering intensity ($I \propto r^3$), the later process scatters nearly 40,000 times stronger than the 1.5 nm process. Therefore, below T_{cp}, an only negligible fraction of the polymer is already present in an aggregated state while the majority is molecular dissolved. Upon heating, the relative scattering intensities of these processes change when approaching the phase separation temperature: While keeping a constant radius, the scattering intensity of the 1.5 nm process drops to 12% at 50 °C. The radius and scattering intensity of the second process, however, gradually increases to120 nm and 88%, respectively at 50 °C. Upon surpassing the T_{cp} a sharp and fast increase of the radius is observed up to large aggregates of R_h > 250 nm.

Such large structures are readily observed by confocal laser scanning microscopy (cLSM). The respect cLSM pictures of **P(1_{15}-*co*-3_{118})** at different temperatures are shown in Figure 4.11, b). The investigated polymer was switched to a more hydrophobic polymer with a T_{cp} of 8 °C for more convenient measurements as the microscope could not be heated. In addition to conventional transmission spectroscopy to observe the structure of the aggregates the fluorescence of Nile Red, a solvatochromic dye with weak fluorescence in hydrophilic medium and high fluorescence in the more hydrophobic environment was measured. For this purpose, Nile red was co-dissolved in the aqueous polymer solution below T_{cp} and heated during the measurement.

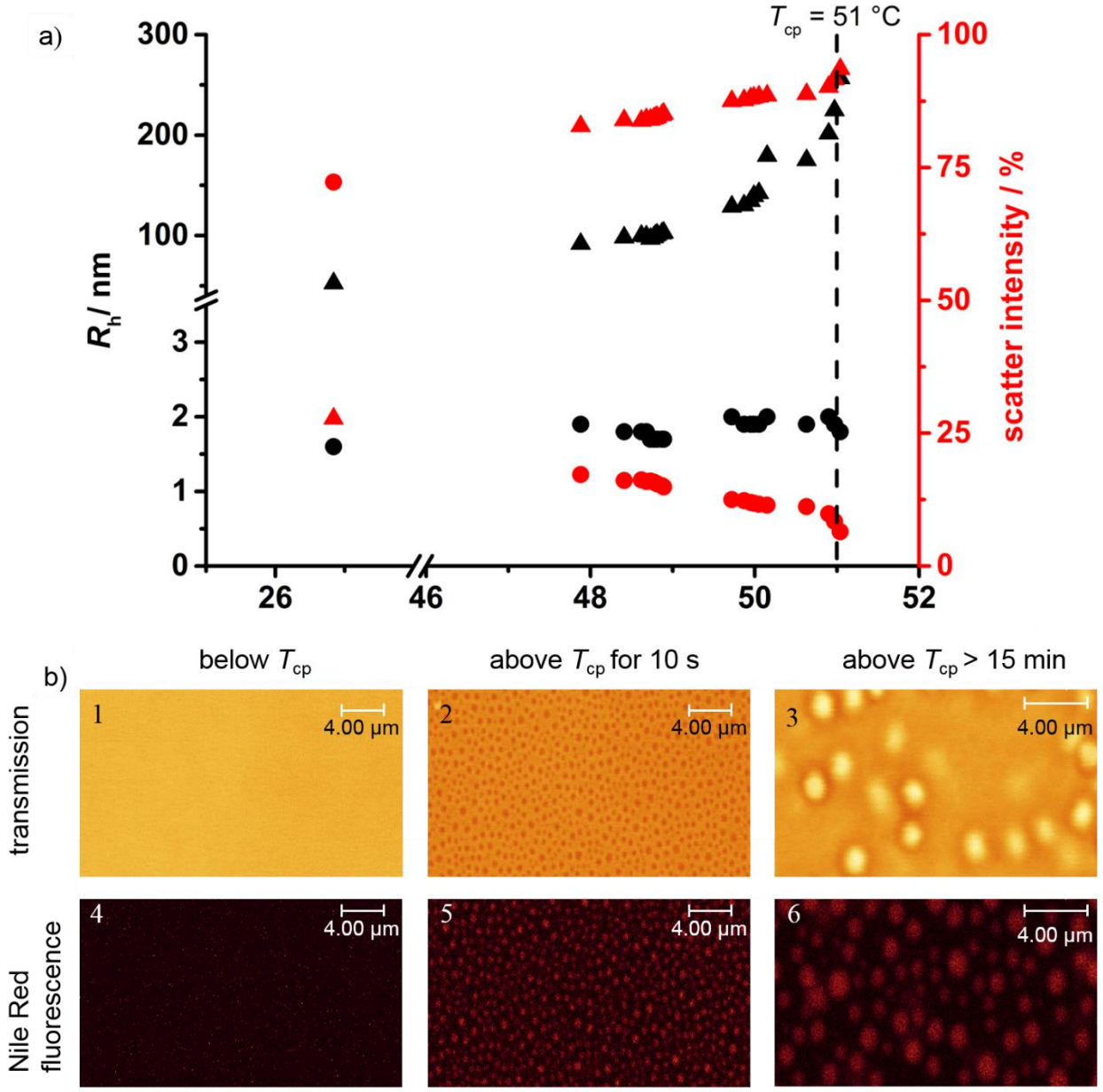

Figure 4.11: a) Temperature-dependent DLS measurements of P(1_{24}-*co*-2_{27}). b) Confocal laser scanning microscopy pictures of P(1_{15}-*co*-3_{118}) (T_{cp} = 8 °C) top row: transmission channel below T_{cp} (1), immediately after surpassing T_{cp} (2) and above T_{cp} (3), bottom row: respective Nile Red fluorescence channel below (4), immediately after surpassing (5) and above T_{cp} (6).

Below the T_{cp} of the copolymer, a clear solution with little fluorescence was observed in the transmission and Nile Red channel, indicating a homogeneous hydrophilic environment under this resolution. This indicates that the subtleties of pre-collapsed dehydration as seen in CW EPR are not detectable with the much larger and more

hydrophobic probes. This method complements the few nm scale characterizations of EPR spectroscopy and characterizes the formed large aggregates. If the temperature is raised above T_{cp} of the polymer well-defined spherical structures with diameters of ca. 600 nm abruptly become visible. These structures show strong Nile Red fluorescence indicating a less hydrophilic environment compared to the surrounding water phase. This is in excellent accordance with the observation of R_h = 250 nm aggregates observed in DLS measurements. These aggregates grew in size over time due to coalescence and eventually formed perfectly spherical coacervate droplets with a diameter of ca. 2,000 nm, as already observed for a related system.[30]

With these results, we can propose a mechanism for the LCST phase separation of these poly(ethylene alkyl phosphonate) copolymers: At low temperatures, the major fraction of the copolymer is molecularly dissolved in water as unimers. Upon increasing the temperature, the steadily decreasing polymer-water hydrogen bond interaction results in the formation of nanoscopic polymer inhomogeneities, as visualized by CW EPR spectroscopy. Further increase in temperature leads to complete dehydration of the polymer and formation of aggregates (R_h < 100 nm) were detectable in DLS. These slowly increase in size till a threshold temperature is reached upon which a rapid phase separation occurs into a polymer free water-phase and large polymer aggregates (R_h ~ 250 nm). Macroscopically, this results in a clouding of the solution and the detection of T_{cp} in transmission spectroscopy. Over time, coalescence of the aggregates results in the formation of large macroscopic droplets and complete phase separation.

Summary and Conclusion

In summary, we studied the hydrophilic-to-hydrophobic phase transition of thermo-responsive aliphatic poly(phosphonate)s on different length scales: the nanometer-sized regime was studied by CW EPR spectroscopy, revealing two types of water: first, bulk water with the freely tumbling hydrophilic probe and second, polymer-associated water that forms the hydration shell around the polymer chains where the more hydrophobic probe species with a reduced environmental polarity is located. Upon reaching/exceeding a critical temperature, fast aggregate growth and the formation of macroscopic droplets

was observed (by dynamic light scattering and confocal microscopy) resulting in clouding of the solution (quantified by turbidity measurements). The LCST behavior was studied based on a series of poly(ethylene alkyl phosphonate) copolymers, which were prepared by the ring-opening polymerization of 2-alkyl-2-oxo-1,3,2-dioxaphospholanes with ethyl, butyl, and hexyl side chains. Random copolymers with molecular weights between 7,700 and 23,000 g mol^{-1} and molecular weight distributions between 1.18 and 1.30 were prepared, which exhibited thermo-responsive behavior over a broad temperature range depending on the copolymer composition. The results of this study give a deeper insight into the LCST phase transition in PPE-copolymers and will allow the future design of fully degradable thermo-responsive materials based on PPEs.

Acknowledgment

The authors thank Angelika Manhart (MPIP) for synthetic assistance, Johanna Simon (MPIP) for the cell culture and toxicity assays, and Christine Rosenauer (MPIP) for DLS measurements. The authors acknowledge support from the "Deutsche Forschungsgemeinschaft" (DFG WU 750/ 6-1).

References:

1. Ratner, B. D.; Bryant, S. J., *Annu. Rev. Biomed. Eng.,* **2004,** *6*, 41-75.
2. Meyers, S. R.; Grinstaff, M. W., *Chem. Rev.,* **2012,** *112*, 1615-32.
3. Anastase-Ravion, S.; Ding, Z.; Pelle, A.; Hoffman, A. S.; Letourneur, D., *J. Chromatogr. B.,* **2001,** *761*, 247-254.
4. Kanazawa, H.; Yamamoto, K.; Matsushima, Y.; Takai, N.; Kikuchi, A.; Sakurai, Y.; Okano, T., *Anal. Chem.,* **1996,** *68*, 100-5.
5. de Las Heras Alarcon, C.; Pennadam, S.; Alexander, C., *Chem. Soc. Rev.,* **2005,** *34*, 276-85.
6. Nayak, S.; Lee, H.; Chmielewski, J.; Lyon, L. A., *J. Am. Chem. Soc.,* **2004,** *126*, 10258-9.
7. Hoogenboom, R., *Angew. Chem. Int. Ed.,* **2009,** *48*, 7978-94.
8. Sahn, M.; Yildirim, T.; Dirauf, M.; Weber, C.; Sungur, P.; Hoeppener, S.; Schubert, U. S., *Macromolecules,* **2016,** *49*, 7257-7267.
9. Schmaljohann, D., *Adv. Drug Deliv. Rev.,* **2006,** *58*, 1655-70.
10. Jochum, F. D.; Theato, P., *Chem. Soc. Rev.,* **2013,** *42*, 7468-83.
11. Kurzbach, D.; Junk, M. J.; Hinderberger, D., *Macromol. Rapid Commun.,* **2013,** *34*, 119-34.
12. Herzberger, J.; Kurzbach, D.; Werre, M.; Fischer, K.; Hinderberger, D.; Frey, H., *Macromolecules,* **2014,** *47*, 7679-7690.

13. Steinbach, T.; Wurm, F. R., *Biomacromolecules,* **2016,** *17*, 3338-3346.
14. Zhang, F.; Zhang, S.; Pollack, S. F.; Li, R.; Gonzalez, A. M.; Fan, J.; Zou, J.; Leininger, S. E.; Pavia-Sanders, A.; Johnson, R.; Nelson, L. D.; Raymond, J. E.; Elsabahy, M.; Hughes, D. M.; Lenox, M. W.; Gustafson, T. P.; Wooley, K. L., *J. Am. Chem. Soc.,* **2015,** *137*, 2056-66.
15. Steinbach, T.; Wurm, F. R., *Angew. Chem. Int. Ed.,* **2015,** *54*, 6098-108.
16. Becker, G.; Marquetant, T. A.; Wagner, M.; Wurm, F. R., *Macromolecules,* **2017**.
17. Bauer, K. N.; Tee, H. T.; Velencoso, M. M.; Wurm, F. R., *Progr. Polym. Sci.,* **2017,** *73*, 61-122.
18. Knop, K.; Hoogenboom, R.; Fischer, D.; Schubert, U. S., *Angew. Chem. Int. Ed.,* **2010,** *49*, 6288-308.
19. Lin, H.; Wolf, T.; Wurm, F. R.; Kelland, M. A., *Energy & Fuels,* **2017,** *31*, 3843-3848.
20. Wolf, T.; Steinbach, T.; Wurm, F. R., *Macromolecules,* **2015,** *48*, 3853-3863.
21. Steinbach, T.; Ritz, S.; Wurm, F. R., *Acs Macro Lett.,* **2014,** *3*, 244-248.
22. Wang, H.; Su, L.; Li, R.; Zhang, S.; Fan, J.; Zhang, F.; Nguyen, T. P.; Wooley, K. L., *ACS Macro Lett.,* **2017**, 219-223.
23. Becker, G.; Ackermann, L. M.; Schechtel, E.; Klapper, M.; Tremel, W.; Wurm, F. R., *Biomacromolecules,* **2017**.
24. Dove, A. P., *ACS Macro Lett.,* **2012,** *1*, 1409-1412.
25. Nuyken, O.; Pask, S. D., *Polymers,* **2013,** *5*, 361-403.
26. Steinbach, T.; Schroder, R.; Ritz, S.; Wurm, F. R., *Polym. Chem.,* **2013,** *4*, 4469-4479.
27. Wang, Y.-C.; Li, Y.; Yang, X.-Z.; Yuan, Y.-Y.; Yan, L.-F.; Wang, J., *Macromolecules,* **2009,** *42*, 3026-3032.
28. Iwasaki, Y.; Kawakita, T.; Yusa, S.-i., *Chem. Lett.,* **2009,** *38*, 1054-1055.
29. Wolf, T.; Nass, J.; Wurm, F. R., *Polym. Chem.-Uk,* **2016,** *7*, 2934-2937.
30. Wolf, T.; Rheinberger, T.; Wurm, F. R., *Europ. Polym. J.,* **2017**.
31. Hofmeister, F., *Archiv für Experimentelle Pathologie und Pharmakologie,* **1888,** *24*, 247-260.
32. Junk, M. J.; Li, W.; Schluter, A. D.; Wegner, G.; Spiess, H. W.; Zhang, A.; Hinderberger, D., *Angew. Chem. Int. Ed.,* **2010,** *49*, 5683-7.
33. Kurzbach, D.; Reh, M. N.; Hinderberger, D., *Chem. Phys. Chem.,* **2011,** *12*, 3566-72.
34. Junk, M. J. N.; Li, W.; Schlüter, A. D.; Wegner, G.; Spiess, H. W.; Zhang, A.; Hinderberger, D., *Macromol. Chem. Phys.,* **2011,** *212*, 1229-1235.

Supporting Information for:

Temperature-Responsive Poly(phosphonate) Copolymers: from Single Chains to Macroscopic Coacervates

Materials

Solvents and chemicals were purchased from Acros Organics, Sigma Aldrich or Fluka and used as received unless otherwise stated. All chemicals were purchased in highest purities, dry and stored over molecular sieve (4Å), if possible. 2-(Benzyloxy)ethanol and DBU were distilled from calcium hydride and stored over molecular sieve (4Å) under argon prior to use. Deuterated solvents were purchased from Deutero GmbH (Kastellaun, Germany) and used as received. Ultrapure water with a resistivity of 18.2 MΩ cm^{-1} (Milli-Q, Millipore®) was used to prepare buffers. Dulbecco's Modified Eagle Medium (DMEM), fetal bovine albumin (FBS penicillin and streptomycin were purchased from Invitrogen, Germany.

Instrumentation and Characterization Techniques

Size exclusion chromatography (SEC) measurements were performed in DMF (1 g L^{-1} LiBr added) at 60 °C and a flow rate of 1 mL min^{-1} with a PSS SECcurity as an integrated instrument, including a PSS GRAM 100-1000 column and a refractive index (RI) detector. Calibration was carried out using poly(ethylene glycol) standards provided by Polymer Standards Service. All NMR experiments were acquired on a Bruker 500 AMX system. The temperature was kept at 298.3K and calibrated with a standard ^{1}H methanol NMR sample using the topspin 3.0 software (Bruker). $^{13}C\{H\}$ NMR spectra were referenced internally to solvent signals. $^{31}P\{H\}$ NMR spectra were referenced externally to phosphoric acid. The $^{13}C\{H\}$ NMR (125 MHz) and $^{31}P\{H\}$ NMR (201 MHz) measurements were obtained with a 1H powergate decoupling method using 30 ° degree flip angle. 1D NMR spectra were processed with the MestReNova 9.0.1-13254 software whereas ^{1}H DOSY (diffusion orientated spectroscopy) NMR spectra were processed with the TopSpin 3.0 software. Differential Scanning Calorimetry (DSC) measurements were performed using a Mettler-Toledo DSC823 thermal analysis system in the temperature range from -100 to

100 °C under nitrogen with a heating rate of 10 °C min^{-1}. Cloud points were determined either in ultrapure water with a resistivity of 18.2 MΩ cm^{-1} (Milli-Q, Millipore®) or in otherwise stated salt solutions and detected by the optical transmittance of a light beam (λ = 500 nm) through a 1 cm sample cell. The measurements were performed on a Jasco V-630 photo spectrometer with a Jasco ETC-717 Peltier element. The intensity of the transmitted light was recorded versus the temperature of the sample cell. The temperature ramp was 1 °C min^{-1} and values were recorded every 0.1 °C. Murine macrophage-like cells (RAW 264.7) were cultivated in DMEM supplemented with 10% FBS, 100 units of penicillin, and 100 mg mL^{-1} streptomycin. Cells were grown in a humidified incubator at 37 °C and 5% CO_2. The effect of P(1_n-*co*-2_m) and P(1_n-*co*-2^{COOH}_m) on cell viability of RAW 264.7 cells were measured by CellTiter-Glo Luminescent Cell Viability Assay (Promega) according to the manufacturer. Luminescent signals were measured with a Tecan infinite M1000. RAW 264.7 cells were seeded at a density of 15 000 cells cm^{-2} in 96-well plates (100 µL per well). The polymers were dissolved in DMEM (stock concentration: 1 mg mL^{-1}) and further diluted to the indicated concentrations. After 24h of incubation, the cell culture medium was replaced by the polymer supplemented medium, and cells were incubated for 48h.

Experimental

***O,O*-diethyl *n*-hexyl phosphonic acid diester:** Triethylphosphite (198.00 g, 1.19 mol) and *n*-hexyl bromide (106.00 g, 0.64 mol) were heated at 150 °C for 17 h in a round-bottom flask equipped with a dean-stark receiver to collect the formed bromoethane. Fractionated distillation of the mixture yielded the desired phosphonic acid diester as a colorless liquid. (126.53 g, 0.63 mol, yield: 99%, bp 72-80 °C / 4 mbar). ^{1}H NMR ($CDCl_3$, 500 MHz, 298K, ppm): δ = 4.12 - 4.00 (m, 4H, -O-O-C**H$_2$**-), 1.74 - 1.66 (m, 2H, -P-C**H$_2$**-), 1.60 - 1.52 (m, 2H, -P-CH2-C**H$_2$**-), 1.38 - 1.21 (m, 6H, -P-CH_2-CH_2-C**H$_2$**-C**H$_2$**-C**H$_2$**-), 0.86 (t, 3H, -C**H$_3$**, $^{3}J_{CH}$ = 6.9 Hz). ^{13}C{H} NMR ($CDCl_3$, 125 MHz, 298K, ppm): δ = 61.44 (d, -P-O-**C**-, $^{2}J_{CP}$ = 6.5 Hz), 31.38 (s, P-**C**-), 30.38 (d, -P-C-**C**-, $^{2}J_{CP}$ = 16.9 Hz), 25.81 (d, -P-C-C-**C**-, $^{3}J_{CP}$ = 140.4 Hz), 22.50 (d, -P-C-C-C-**C**-, $^{4}J_{CP}$ = 2 Hz), 22.45 (s, -P-C-C-C-C-**C**-), 16.58 (d, -**C**, $^{5}J_{CP}$ = 2 Hz), 14.11 (s, -P-O-C-**C**). ^{31}P{H} NMR ($CDCl_3$, 201 MHz, 298K, ppm): δ = 32.61

***N*-hexyl phosphonic acid dichloride**: *O,O*-Diethyl *n*-hexyl phosphonic acid diester (100.00 g, 0.49 mol) and DMF (0.70 mL) was added drop wise to refluxing thionylchloride (139.00 g, 1.17 mol). Strong gas evolution of methylene chloride and sulfur dioxide indicated the progress of the reaction. After 24h the gas evolution declined. Fractionated distillation of the raw product yielded the desired dichloride as a colorless liquid (69.61 g, yield: 36%, b.p. 130-135 °C / 60 mbar). ^{1}H NMR ($CDCl_3$, 500 MHz, 298K, ppm): δ = 2.61 - 2.50 (m, 2H, -P-C**H$_2$**-), 1.87 - 1.76 (m, H, -P-CH_2-C**H$_2$**-), 1.50 - 1.42 (m, 2H, -P-CH_2-CH_2-C**H$_2$**-), 1.33 - 1.27 (m, 4H, -P-CH_2-CH_2-CH_2-C**H$_2$**-C**H$_2$-**), 0.88 (t, 3H, -CH3, $^{3}J_{HH}$ = 10 Hz). ^{13}C{H} NMR ($CDCl_3$, 125 MHz, 298K, ppm): δ = 42.98 (d, -P-**C**-, $^{1}J_{CP}$ = 96.3 Hz), 31.04 (d, -P-C-**C**-, $^{2}J_{CP}$ = 1.6 Hz), 29.24 (d, -P-C-C-**C**-, $^{3}J_{CP}$ = 21.5 Hz), 22.87 (d, -P-C-C-C-**C**-, $^{4}J_{CP}$ = 6.5 Hz), 22.25 (s, -P-C-C-C-C-**C**-), 13.91 (s, -**C**). ^{31}P{H} NMR ($CDCl_3$, 201 MHz, 298K, ppm): δ = 51.27

2-*n*-Hexyl-2-oxo-1,3,2-dioxaphospholane (3): A flame-dried three-necked round-bottom flask, equipped with a magnetic stirring bar and two dropping funnels, was charged with 250 mL dry THF and cooled to -21 °C. *N*-hexyl phosphonic acid dichloride (30.18 g, 0.15 mol) was dissolved in dry THF (250 mL) and transferred into one dropping funnel via

a flame-dried stainless steel capillary. A solution of dry ethylene glycol (19.33 g, 0.15 mol) and dry pyridine (23.51 g, 0.30 mol) in THF (250 mL) was transferred into the second dropping funnel via a flame-dried stainless steel capillary. Dropping speed was adjusted to be approximately equal for both mixtures. After complete addition, the solution was stirred for 3h and kept over-night at 4 °C to facilitate the precipitation of the pyridinium hydrochloride byproduct. The precipitate was removed by filtration via a flame-dried Schlenk funnel, and the solvent was removed under reduced pressure. Fractionated distillation yielded the desired product as colorless oil (13.61 g, yield: 48%, b.p. 90 °C / $4x10^{-2}$ mbar). ^{1}H NMR ($CDCl_3$, 500 MHz, 298K, ppm): δ = 4.46 - 4.36 (m, 2H, -P-O-C**H$_2$**-), 4.35 – 4.14 (m, 4H, -P-O-C**H$_2$**-), 1.88 (dt, 2H, -P-C**H$_2$**-, $^{2}J_{HP}$ = 17.1 Hz, $^{3}J_{HH}$ = 8.0 Hz), 1.56 (dp, 2H, -P-CH_2-C**H$_2$**-, $^{3}J_{HP}$ = 20.8 Hz, $^{3}J_{HHb}$ = 7.9 Hz, $^{3}J_{HHc}$ = 6.6 Hz), 1.33 (p, 2H, -P-CH_2-CH_2-C**H$_2$**-, $^{3}J_{HH}$ = 7.4 Hz), 1.27 – 1.17 (m, 4H, -P-CH_2-CH_2-CH_2-C**H$_2$**-C**H$_2$**-), 0.81 (t, 3H, -C**H$_3$**, $^{3}J_{HH}$ = 6.6 Hz). ^{13}C{H} NMR ($CDCl_3$, 125 MHz, 298K, ppm): δ = 66.15 (s, -P-O-**C**-), 31.15 (s, -P-**C**-), 30.03 (d, -P-C-**C**-), $^{2}J_{CP}$ = 16.4 Hz), 25.61 (d, -P-C-C-**C**-, $^{3}J_{CP}$ = 130.4 Hz), 22.54 (d, -P-C-C-C-**C**-, $^{4}J_{CP}$ = 5.4 Hz), 22.28 (s, -P-C-C-C-C-**C**-), 13.91 (s, -**C**). ^{31}P{H} NMR ($CDCl_3$, 201 MHz, 298K, ppm): δ = 51.42

Representative procedure for the (co-)polymerization of (1) with (2) or (3): The respective monomers were weighed into a flame-dried Schlenk-tube, dissolved in dry benzene and dried by repeated lyophilization. The monomers were dissolved in dry dichloromethane at a total concentration of 4 mol L^{-1}. A stock solution of initiator 2-(benzyloxy)ethanol in dry dichloromethane was prepared with a concentration 0.2 mol L^{-1}, and the calculated amount was added to the monomer solution via gas-tight syringe (Hamilton®). A stock solution of DBU in dry dichloromethane was prepared with a concentration of 0.2 mol L^{-1}. The monomer solution and the catalyst solution were adjusted to 30 °C. The polymerization was initiated by the addition of the calculated volume of the catalyst solution containing 3.0 equivalents of DBU concerning the initiator. Polymerization was terminated after 16h by the rapid addition of an excess of formic acid dissolved in dichloromethane with a concentration of 20 mg mL^{-1}.

The colorless, amorphous polymers were purified by precipitation in cold diethyl ether or petrolether (for **(2)** content above 70% and **(3)** content above 50%), dialyzed against Milli-Q (Millipore®) water and dried at reduced pressure.

Representative NMR data of P(3)$_{120}$: ^{1}H NMR (DMSO-d_6, 500 MHz, 298K, ppm): δ = 7.37 - 7.29 (m, aromatic C**H**), 4.85 (t, terminal -O-**H**), 4.53 (s, aryl-C**H$_2$**-), 4.22 - 4.01 (m, backbone -C**H$_2$**-C**H$_2$**-), 3.63 (t, backbone terminal -C**H$_2$**-OH), 1.80 - 1.71 (m, side-chain -P-C**H$_2$**-), 1.53 - 1.43 (m, side-chain -P-CH$_2$-C**H$_2$**-), 1.37 - 1.30 (m, side-chain -P-CH$_2$-CH$_2$-C**H$_2$**-), 1.29 - 1.19 (m, side-chain -P-CH$_2$-CH$_2$-CH$_2$-C**H$_2$**-C**H$_2$**-), 0.88 - 0.82 (m, side-chain -C**H$_3$**). ^{13}C{H} NMR (DMSO-d_6, 125 MHz, 298K, ppm): δ 133.78, 128.80, 127.97 (s, aromatic **C**), 64.56 (s, broad, backbone -**C**H$_2$-), 60.85 (s, aryl-**C**-), 31.29 (s, -P-**C**-), 30.06 (d, -P-C-**C**-, $^{2}J_{CP}$ = 16.7 Hz), 25.03 (d, -P-C-C-**C**-, 3JCP = 140.0 Hz), 22.41 (d, -P-C-C-C-**C**-, $^{4}J_{CP}$ = 3.7 Hz), 22.35 (s, -P-C-C-C-C-**C**-), 14.17 (s, -**C**). ^{31}P{H} NMR (DMSO-d_6, 201 MHz, 298K, ppm): δ 33.51 (backbone), 32.95 (terminal).

Representative NMR data of P(1$_{15}$-*co*-2$_{118}$): ^{1}H NMR (DMSO-d_6, 500 MHz, 298K, ppm): δ = 7.37 - 7.29 (m, aromatic C**H**), 4.85 (t, terminal -O-**H**), 4.53 (s, aryl-C**H$_2$**-), 4.22 - 4.01 (m, backbone -C**H$_2$**-C**H$_2$**-), 3.63 (t, backbone terminal -C**H$_2$**-OH), 1.84 - 1.70 (m, side-chain -P-C**H$_2$**-), 1.63 - 1.56 (m, side-chain -P-C**H$_2$**-), 1.54 - 1.41 (m, side-chain -P-CH$_2$-C**H$_2$**-), 1.40 - 1.29 (m, side-chain -P-CH$_2$-CH$_2$-C**H$_2$**-), 1.05 (dt, side-chain -P-CH$_2$-C**H$_3$**, $^{3}J_{HP}$ = 20.1 Hz, $^{3}J_{HH}$ = 7.6 Hz), 0.86 (t, side-chain -P-CH$_2$-CH$_2$-CH$_2$-C**H$_3$**, $^{3}J_{HH}$ = 7.3 Hz). ^{13}C{H} NMR (DMSO-d_6, 125 MHz, 298K, ppm): δ 133.78, 128.80, 127.97 (s, aromatic **C**), 64.56 (s, broad, backbone -**C**H$_2$-), 60.85 (s, aryl-**C**-), 24.66 (d, side-chain -P-**C**-, $^{1}J_{CP}$ = 145.0 Hz), 24.42 (d, side-chain –P-C-**C**-, $^{2}J_{CP}$ = 5 Hz), 23.41 (d, side-chain -P-C-C-**C**-, $^{3}J_{CP}$ = 16.3 Hz), 18.06 (d, side-chain -P-**C**-, $^{1}J_{CP}$ = 138.8 Hz), 13.90 (s, side-chain -P-C-C-C-**C**), 6.68 (d, side-chain -P-C-**C**, $^{2}J_{CH}$ = 6.3 Hz). ^{31}P{H} NMR (DMSO-d_6, 201 MHz, 298K, ppm): δ = 34.43 (backbone), 34.18 (terminal), 33.28 (backbone), 33.04 (terminal).

Representative NMR data of P(1_{32}-*co*-3_{30}): ^{1}H NMR (DMSO-d_6, 500 MHz, 298K, ppm): δ = 7.37 - 7.29 (m, aromatic C**H**), 4.85 (t, terminal -O-**H**), 4.53 (s, aryl-C**H$_2$**-), 4.22 - 4.01 (m, backbone -C**H$_2$**-C**H$_2$**-), 3.63 (t, backbone terminal -C**H$_2$**-OH), 1.83 - 1.69 (m, side-chain -P-C**H$_2$**-), 1.55 - 1.41 (m, side-chain -P-CH$_2$-C**H$_2$**-), 1.38 - 1.31 (m, side-chain, -P-CH$_2$-CH$_2$-C**H$_2$**-), 1.30 - 1.1.19 (m, side-chain -P-CH$_2$-CH$_2$-CH$_2$-C**H$_2$**-C**H$_2$**-), 1.05 (dt, side-chain -P-CH$_2$-C**H$_3$**, $^{2}J_{HP}$ = 20.1 Hz, $^{3}J_{HH}$ = 7.6 Hz), 0.86 (t, side-chain -P-CH$_2$-CH$_2$-CH$_2$-CH$_2$-CH$_2$-C**H$_3$**, $^{3}J_{HH}$ = 6.8 Hz). ^{13}C{H} NMR (DMSO-d_6, 125 MHz, 298K, ppm): δ 133.78, 128.80, 127.97 (s, aromatic **C**), 64.56 (s, broad, backbone -**C**H$_2$-), 60.85 (s, aryl-**C**-), 31.29 (s, -P-**C**-), 30.06 (d, -P-C-**C**-, $^{2}J_{CP}$ = 16.7 Hz), 25.03 (d, -P-C-C-**C**-, 3JCP = 140.0 Hz), 22.41 (d, -P-C-C-C-**C**-, $^{4}J_{CP}$ = 3.7 Hz), 22.35 (s, -P-C-C-C-C-**C**-), 18.06 (d, side-chain -P-**C**-, $^{1}J_{CP}$ = 138.8 Hz), 14.17 (s, -**C**), 6.68 (d, side-chain -P-C-**C**, $^{2}J_{CH}$ = 6.3 Hz). ^{31}P{H} NMR (DMSO-d_6, 201 MHz, 298K, ppm): δ = 34.44 (backbone), 34.20 (terminal), 33.21 (backbone), 33.01 (terminal).

Supporting figures

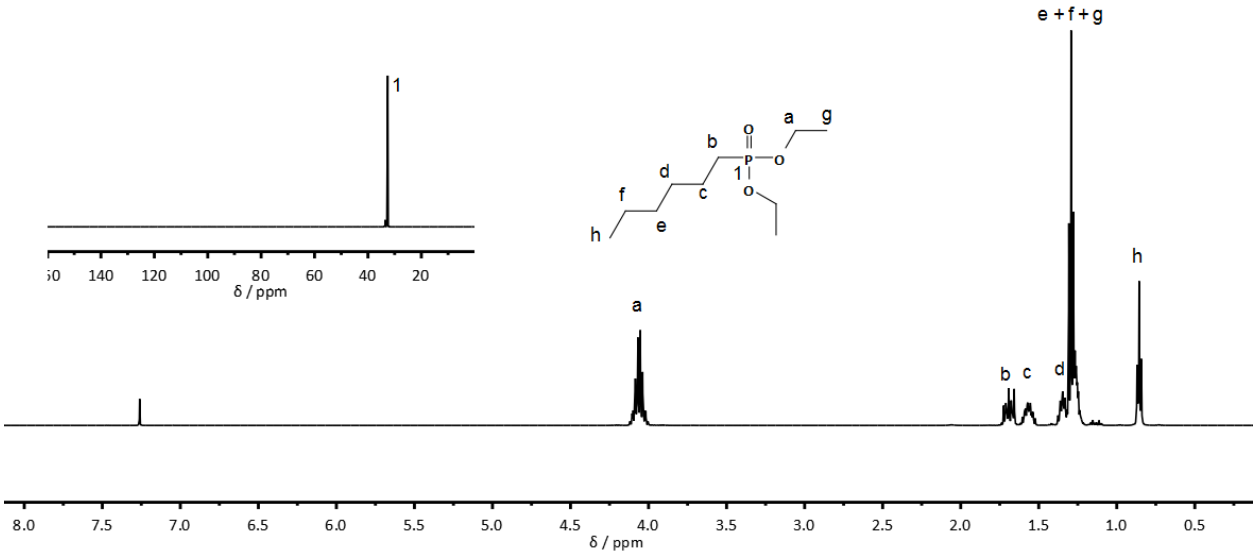

Figure S4.1: ^{1}H (500 MHz) and ^{1}P{H} (201 MHz) NMR spectra of O, O-diethyl n-hexyl phosphonic acid diester in $CDCl_3$ at 298K.

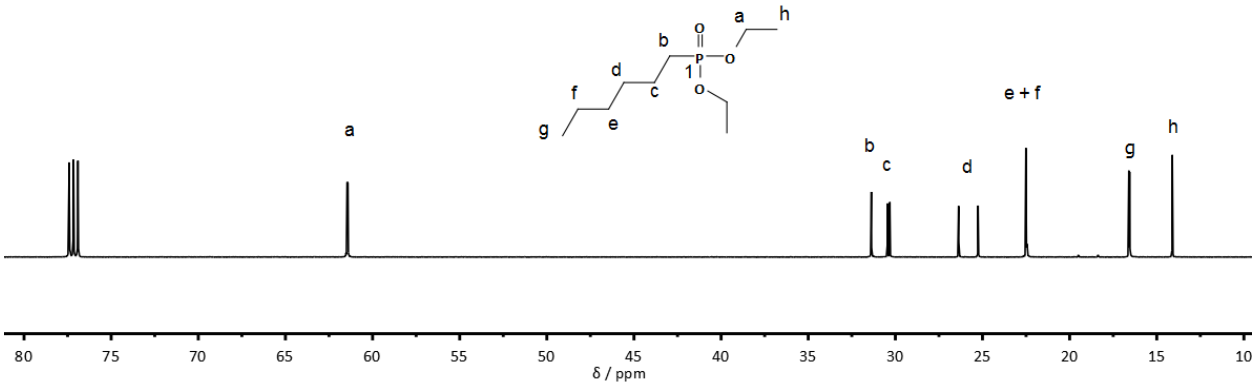

Figure S4.2: ^{13}C (125 MHz) NMR spectrum of O, O-diethyl n-hexyl phosphonic acid diester in $CDCl_3$ at 298K.

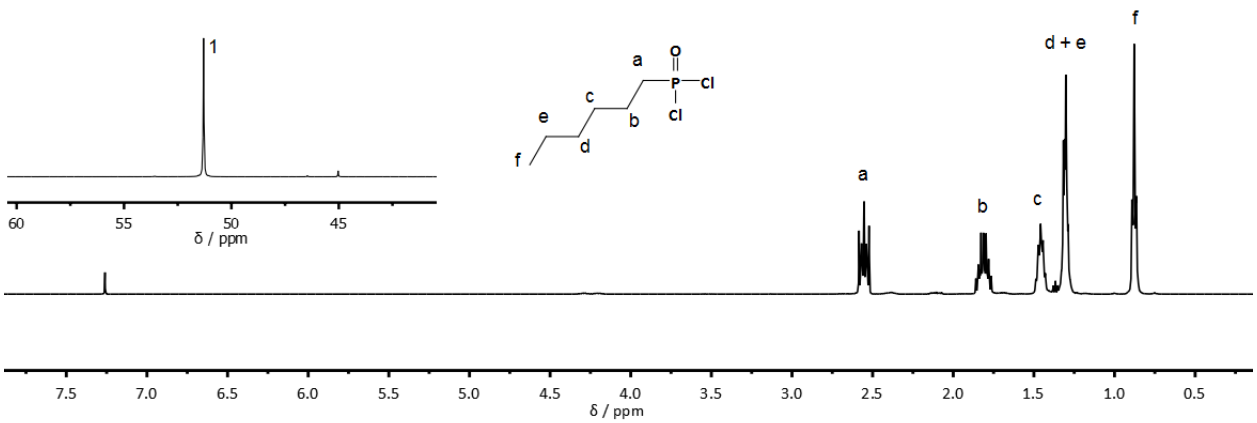

Figure S4.3: ^{1}H (500 MHz) and $^{31}P\{H\}$ (201 MHz) NMR spectra of *n*-hexyl phosphonic acid dichloride in $CDCl_3$ at 298K.

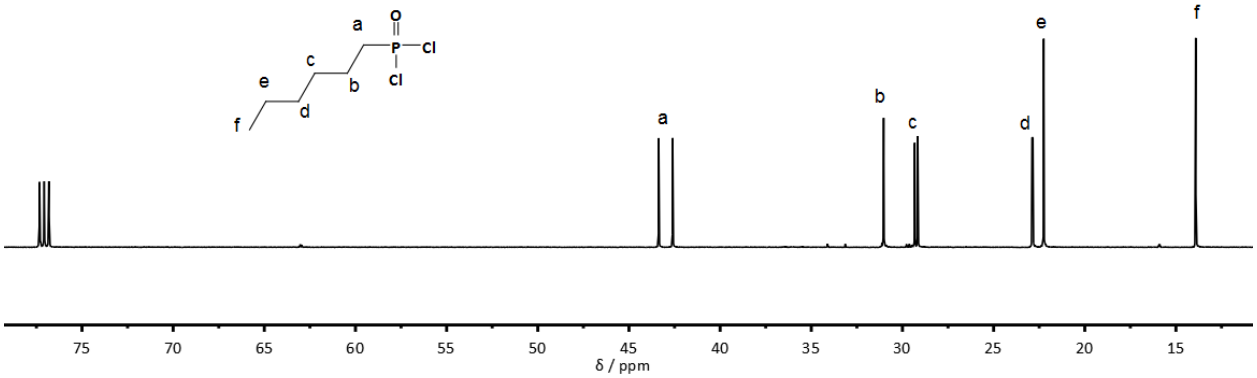

Figure S4.4: ^{13}C (125 MHz) NMR spectrum of *n*-hexyl phosphonic acid dichloride in $CDCl_3$ at 298K.

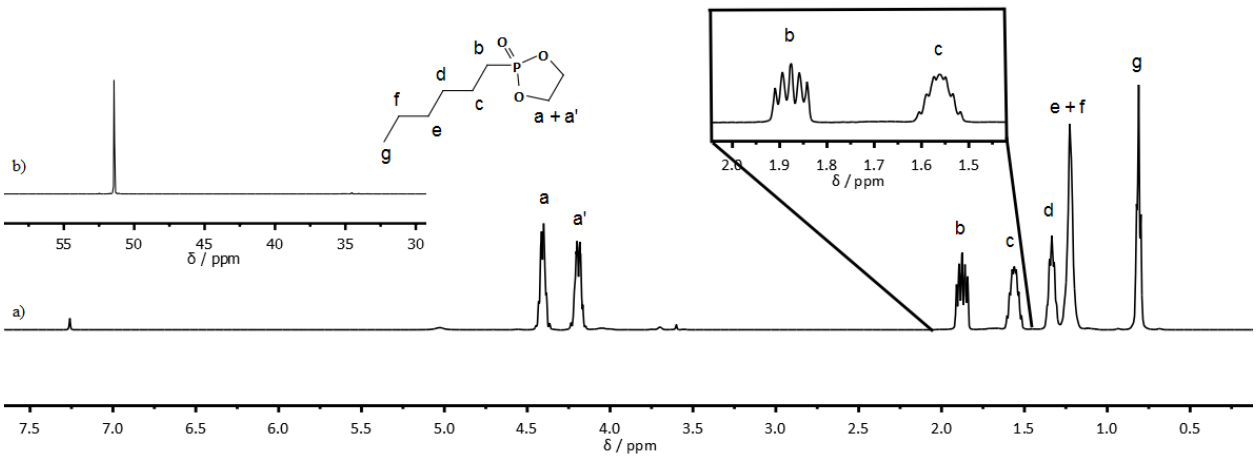

Figure S4.5: a) ^{1}H NMR (500 MHz) and b) $^{31}P\{H\}$ NMR (201 MHz) spectra of (3) in $CDCl_3$ at 298K. Region from 2.05 - 1.42 ppm magnified for clarification of J_{HP} coupling.

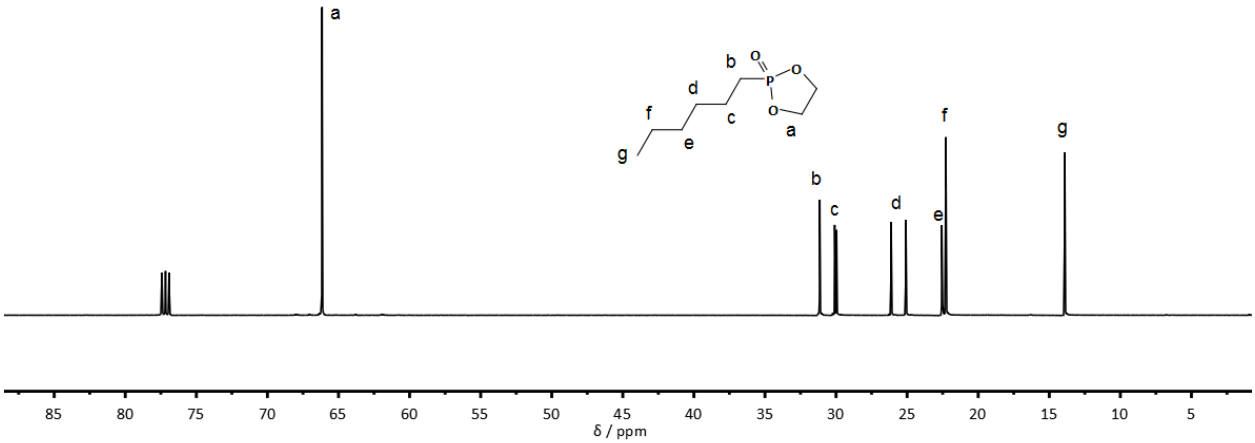

Figure S4.6: ^{13}C (125 MHz) NMR spectrum of 2-*n*-hexyl-2-oxo-1,3,2-dioxaphospholane (*n*HexPPn, (3)) in $CDCl_3$ at 298K.

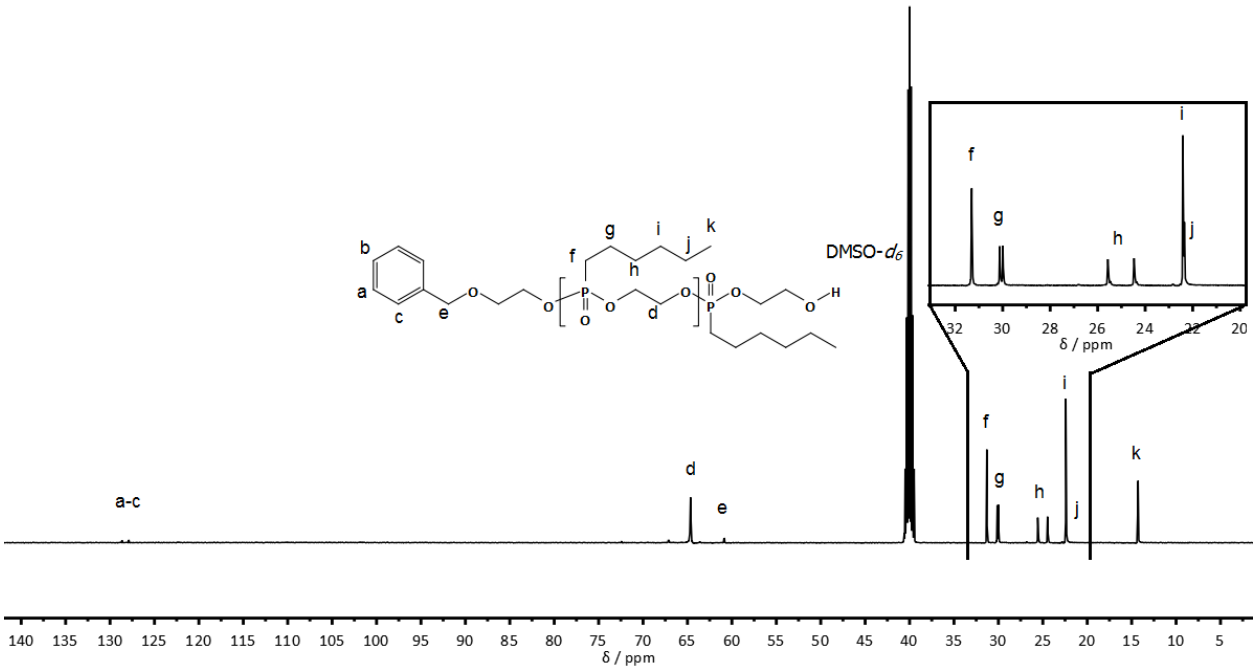

Figure S4.7: ^{13}C (125 MHz) NMR spectrum of P(3)120 in DMSO-d_6 at 298K. The region from 32 to 20 ppm is magnified for clarification.

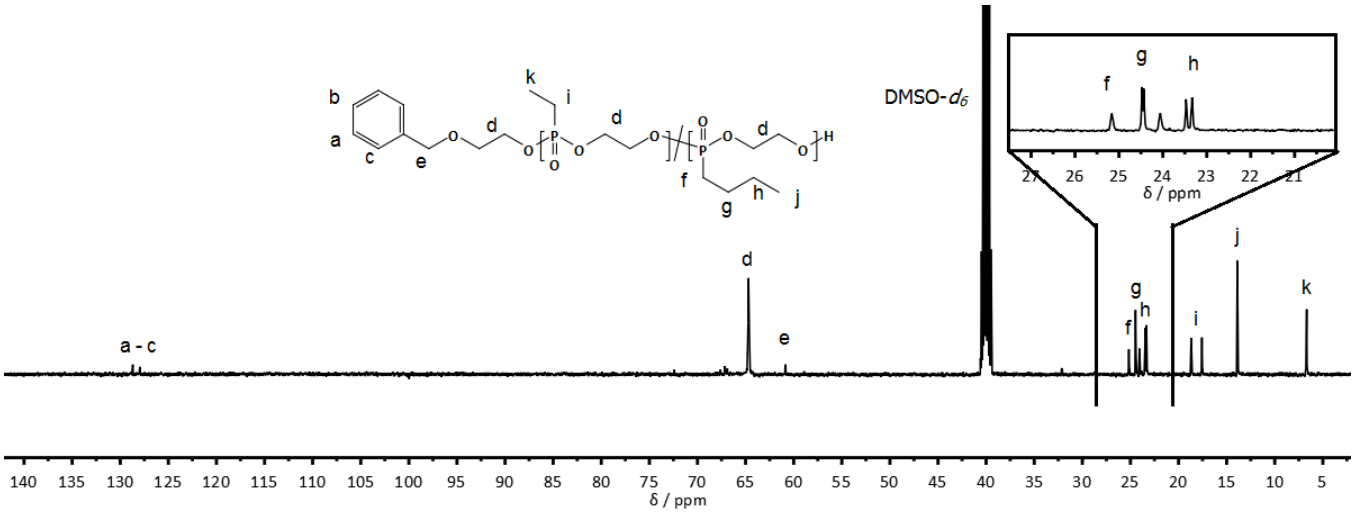

Figure S4.8: ^{13}C (125 MHz) NMR spectrum of P(1_{15}-*co*-2_{118}) in DMSO-d_6 at 298K. The region from 27 to 20 ppm is magnified for clarification.

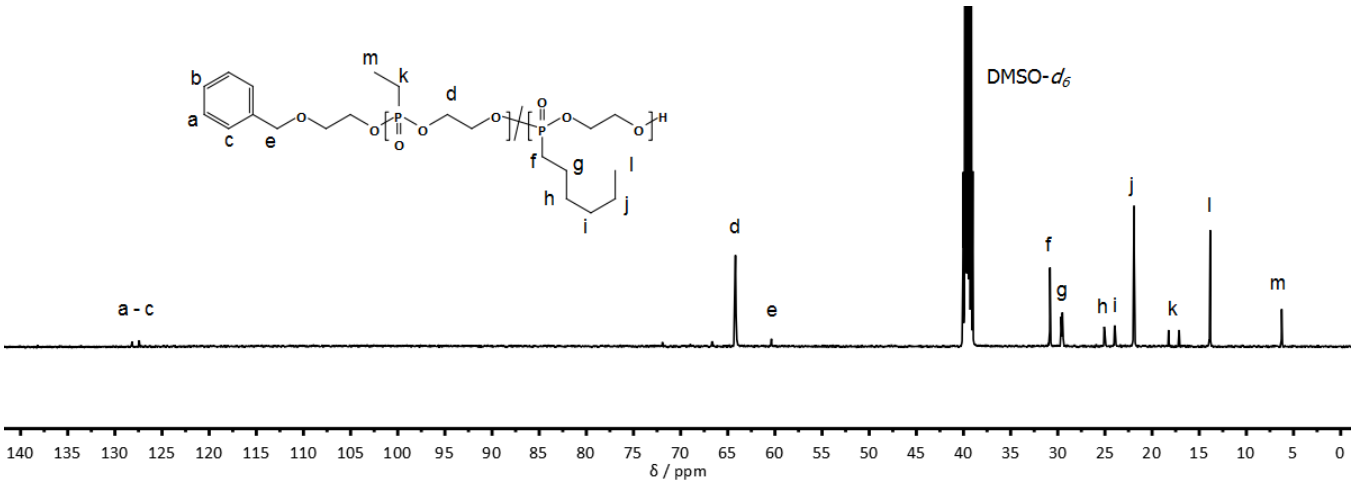

Figure S4.9: ^{13}C (125 MHz) NMR spectrum of P(1_{62}-*co*-3_{56}) in DMSO-d_6 at 298K.

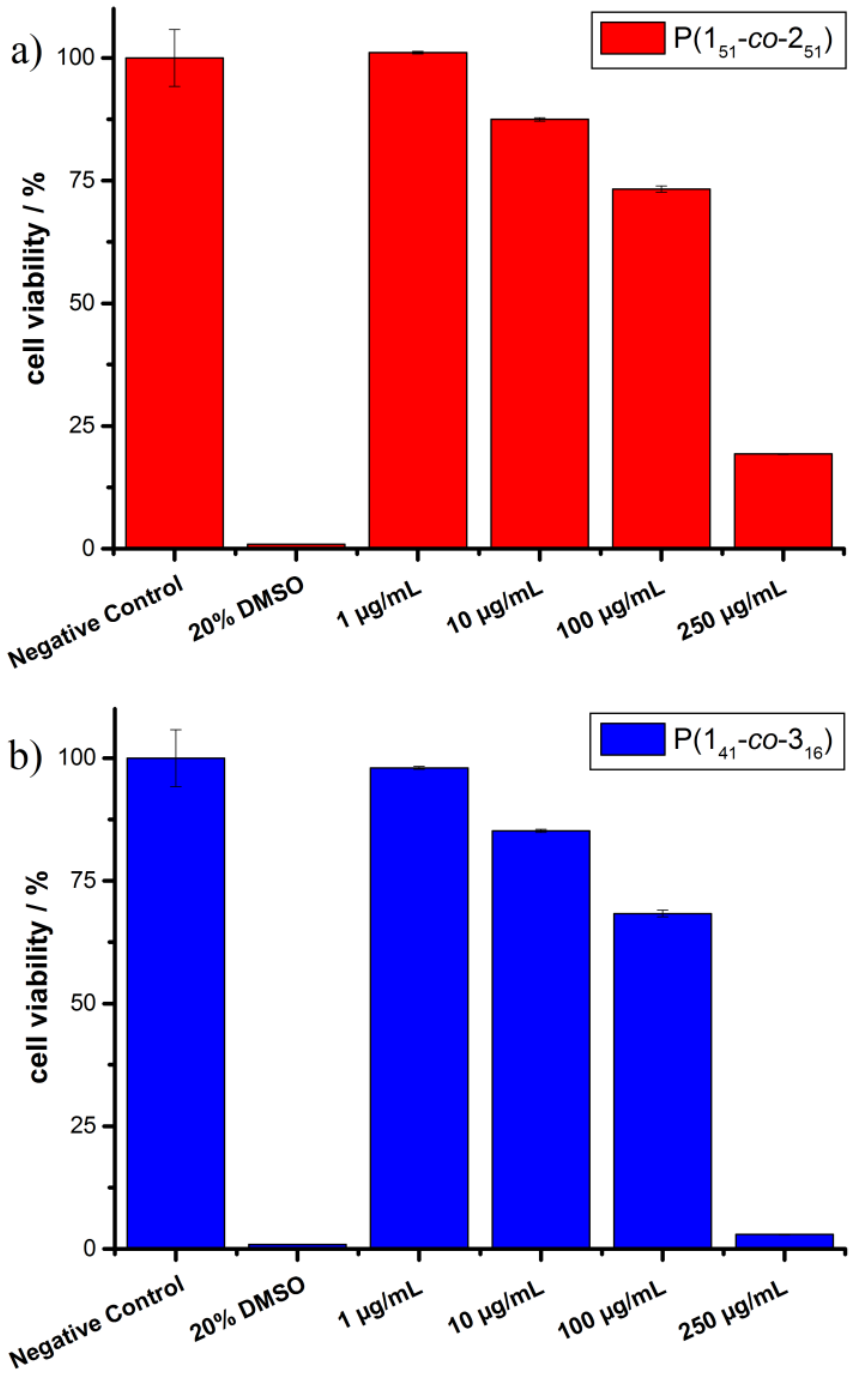

Figure S4.10: ***In vitro*** **cell viability assay of RAW264.7 cell-line treated with a) P(1$_{51}$-*co*-2$_{51}$) and b) P(1$_{41}$-*co*-3$_{16}$) after 24h of incubation. The experiments were carried out as three independent replicates (performed by Johanna Simon).**

Chapter 4: Temperature-Responsive Poly(phosphonate) Copolymers: from Single Chains to Macroscopic Coacervates.

Chapter 3 and **Chapter 4** laid the synthetic foundation for the use of poly(ethylene alkyl phosphonate) copolymers in various applications. The flexibility of the used chemistry, as well as the resulting material's properties, were shown. This diversity opens up for a broad variety of potential applications due to the ease of property variation. Polymers with high water solubility, adjustable hydrophilicity, hence LCST phase separation temperature, or varying glass temperatures were synthesized.

Chapter 5 presents the cooperative study with Prof. Dr. M. A. Kelland at the University of Stavanger, Norway. The polymers presented in **Chapter 3** and **Chapter 4** were tested for their ability to inhibit the formation of gas hydrates in natural gas pipelines, a vital application to prevent plugging of pipelines and potential environmental hazard due to pipeline leakage. Furthermore, the copolymers biodegradation behavior by microbial oxidative degradation is presented.

Chapter 5: Poly(alkyl ethylene phosphonate)s – A New Class of Non-Amide Kinetic Hydrate Inhibitor Polymers

Hong Lin[1], Thomas Wolf[2], Frederik R. Wurm[2], and Malcolm A. Kelland[1]

[1]Department of Mathematics and Natural Science, Faculty of Science and Technology, University of Stavanger, N-4036 Stavanger, Norway

[2]Max-Planck-Institute for Polymer Research, Ackermannweg 10, D-55128 Mainz, Germany

Published in: Energy&Fuels, **2017,** 31, 3873-3848

Thomas Wolf performed the polymer synthesis and characterization. **Hong Lin** performed the polymer evaluation for KHI applications as well as BOD biodegradation testing.

Keywords: poly(phosphoester)s, poly(phosphonate)s, anionic ring-opening polymerization, biodegradable polymers, KHI inhibitors

Chapter 5: Poly(alkyl ethylene phosphonate)s – A New Class of Non-Amide Kinetic Hydrate Inhibitor Polymers.

Abstract

All commercial kinetic hydrate inhibitor (KHI) formulations are based on polymers with an amide (or imide) functional groups. In our continuing work to explore non-amide based KHI polymers, a series of poly(ethylene alkyl phosphonate)s (PPns) has been synthesized. These polymers were investigated for their performance as KHIs in high pressure rocking cells using a Structure II-forming gas mixture and the slow constant cooling test method over 24h. All of the PPns gave better KHI activity than tests with no additive. However, despite several of the polymers being designed to have low cloud points, a factor that is often used for good KHI performance, none of the PPns gave lower onset temperatures than poly(*N*-vinyl caprolactam), a well-known commercial KHI with low cloud point. A random PPn copolymer with eight ethyl and eight *n*-hexyl groups gave a biodegradation of about 31% using the marine OECD306 test protocol.

Introduction

Kinetic hydrate inhibitors (KHIs) are a class of chemicals used primarily to prevent gas hydrate plugging of oil and gas production lines.[1-3] KHIs are a class of low dosage hydrate inhibitor since they are dosed at much lower concentrations (usually 0.1-1.0 wt.% active material) compared to thermodynamic inhibitors such as methanol or monoethylene glycol (MEG). As far as we are aware, all commercial KHIs are based on polymers containing amide or imide groups. These include homopolymers and copolymers of *N*-vinyl pyrrolidone (VP) and *N*-vinyl caprolactam (VCap), *N*-isopropyl methacrylamide copolymers, hyperbranched poly(ester amide)s, and polyester pyroglutamates. A wide range of other amide-containing polymers have also been investigated as KHIs, including, maleimide copolymers, poly(aspartamide)s, *N*-vinyl amides, proteins and peptides, poly(citramide)s, ring-opened poly(oxazoline)s, poly(glycine)s and amide derivatives of oligoethylene amines and poly(ethylene amine)s.[4,5]

The amide or imide groups in all these classes of polymers are used to keep the polymers water-soluble via hydrogen-bonding, as well as participating in the hydrate nucleation and crystal growth inhibition processes. Recently, we have turned our attention to alternative classes of KHIs without amide groups. We did this for several reasons: Firstly, to determine whether non-amide polymers could be found with similar or even higher efficacy than the amide polymers. Secondly, to find more biodegradable alternatives, particularly to the polyvinyl-based KHI amide polymers. Thirdly, to shed light on the mechanisms of KHIs, and as to whether amide or imide groups are essential for either good hydrate nucleation or growth inhibition.

Regarding non-amide/imide polymers as KHIs, we have investigated hyperbranched polyamine oxides and shown that they still show remarkably good KHI performance even when oligomers are used with only a few amine oxide groups (Scheme 5.1, a).[6-7] Like amides, amine oxides have strong H-bonding groups with water molecules and with the correct alkyl groups on the nitrogen atom, they also show excellent crystal growth inhibition properties.[8] We also investigated a series of polymers of ring-closed isopropenyl oxazoline as KHIs (Scheme 5.1, b).[9] Hydrogen-bonding is also possible between the oxazoline groups and water molecules either in the water phase or on hydrate particles. Reasonable KHI performance was shown for the poly(isopropenyl oxazoline) homopolymer, but the effect was significantly enhanced by copolymerization with the amide-containing monomer *N*-isopropyl methacrylamide.

Even more relevant to the present study, we investigated the performance of a series of poly(vinyl phosphonate) diesters (Scheme 5.1, c).[10] The best polymers in this class gave fairly god KHI performance if the cloud point of the polymer was low (ca. 18 - 20^{o}C). However, based on past research with many other classes of polymers with polyvinyl backbones it is very probably they will exhibit poor seawater biodegradability.[11]

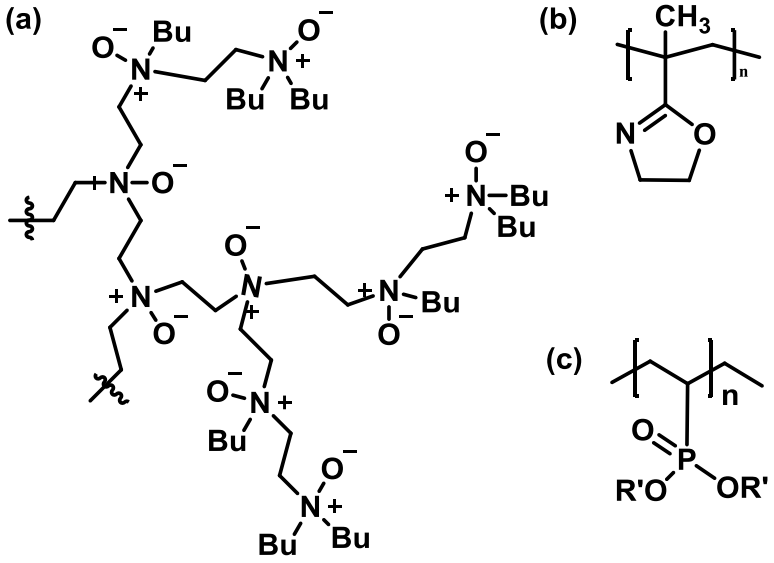

Scheme 5.1: General structures of a) hyperbranched polyamine oxides, b) poly (isopropenyl oxazoline)s and c) poly(dialkyl vinyl phosphonate)s.

We wondered whether another class of phosphonate ester polymers, i.e., with the phosphonic acid esters within the polymer backbone, PPns would show any KHI performance and additionally offering the possibility for biodegradation in seawater. Recently, Wolf *et al*. developed a library of aliphatic poly(ethylene alkyl phosphonate)s (PPn's) by living ring-opening polymerization of cyclic phosphonates. These polymers have been proposed for use in medical applications, are non-cytotoxic, and may show thermoresponsive behavior in aqueous solution at physiological temperatures.[12] With the phosphonate esters in the polymer backbone, a potentially degradable material is accessible with the additional possibility to tune the stability by adjusting the nature of the pendant P-alkyl group.[13] Interestingly, some marine microorganisms, however, are capable of metabolizing phosphonates as a nutrient source, which might be an ideal prerequisite for their use as KHIs.[14,15] This paper explores for the first time the KHI performance and proves the seawater biodegradability of a range of PPns.

Experimental Conditions

Polymer Synthesis

The comparative polymers used in this study were poly(*N*-vinyl caprolactam) (PVCap) and poly(*N*-vinyl pyrrolidone) (PVP). The PVCap was obtained from BASF as Luvicap EG as a 41.1 wt.% solution in monoethyleneglycol with M_w of 2,000-4,000 g mol^{-1}. The PVP was obtained as 100% powder from Ashland Chemical with M_w of 4,000 g mol^{-1}.

The 2-alkyl-2-oxo-1,3,2-dioxaphospholanes for this study were synthesized by the literature procedures.[16,17] This included monomers with ethyl, isopropyl, *n*-butyl, *n*-hexyl and cyclohexyl groups. The different 2-alkyl-2-oxo-1,3,2-dioxaphospholanes were copolymerized to form PPns via the organocatalytic AROP to ensure high control over molecular weight and molecular weight distribution (Figure 5.2). Details of the polymerization procedure have been reported previously.[16,17] The structures of the poly(alkyl ethylene phosphonate)s (PPns) synthesized are summarized in Scheme 5.3.

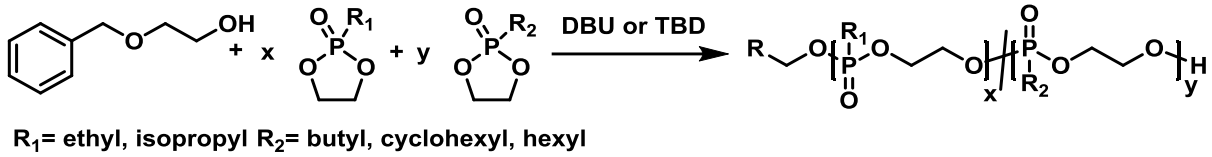

R_1= ethyl, isopropyl R_2= butyl, cyclohexyl, hexyl

Scheme 5.2: Polymerization of 2-alkyl-2-oxo-1,3,2-dioxaphospholanes by organocatalyzed AROP to form PPn's (herein a mixture of two monomers was copolymerized).

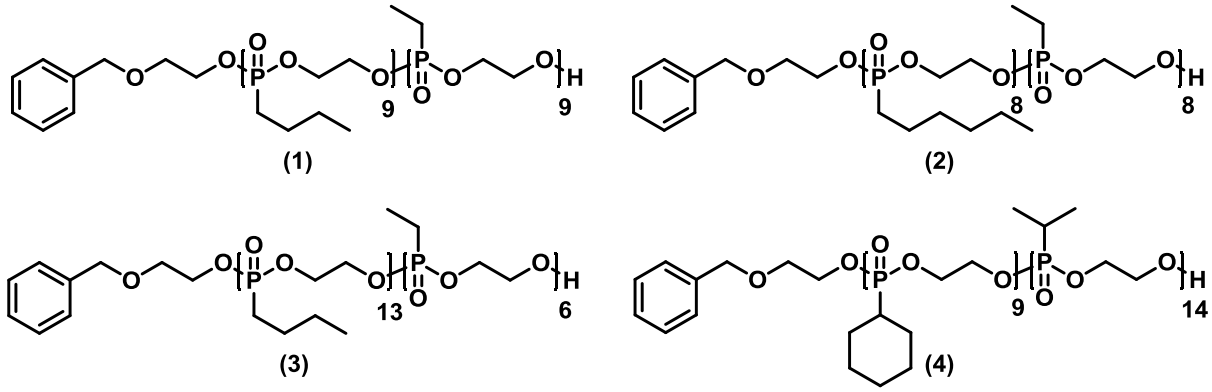

Scheme 5.3: Structures of poly(alkyl ethylene phosphonate)s (PPns) synthesized in this study.

Cloud points (T_{cp}) of the PPns were determined either in ultrapure water with a resistivity of 18.2 MΩ cm^{-1} (Milli-Q, Millipore®) or in otherwise stated salt solutions and detected by the optical transmittance of a light beam (λ = 500 nm) through a 1 cm sample cell. The measurements were performed on a Jasco V-630 photo spectrometer with a Jasco ETC-717 Peltier element. The intensity of the transmitted light was recorded versus the temperature of the sample cell. The temperature ramp was 1 °C min^{-1} and values were recorded every 0.1 °C. The results are given in Figure 5.1 and summarized in Table 5.1.

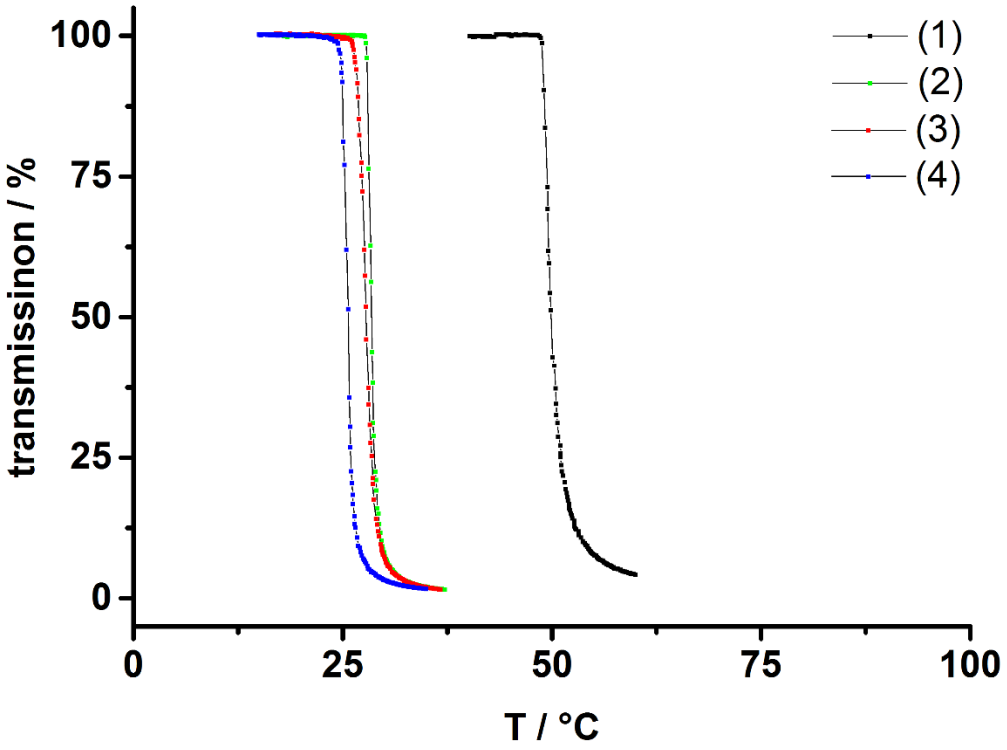

Figure 5.1: Polymer cloud point measurements (performed by Thomas Wolf).

Table 5.1: Poly(alkyl ethylene phosphonate)s (PPns) synthesized in this study and their cloud points.

polymer	polymer composition[a]	M_n / g mol^{-1} [a]	$Đ$ [c]	T_{cl} / °C[b]
(1)	ethyl : ^{n}butyl 9:9	2,700	1.61	48
(2)	ethyl : ^{n}hexyl 8:8	2,600	1.59	28
(3)	ethyl : ^{n}butyl 6:13	3,500	1.57	27
(4)	^{i}propyl : ^{cy}hexyl 14:9	3,800	1.50	25

[a] Comonomer ratio and molecular weight determined from ^{1}H NMR.[b] Cloud point temperature determined by turbidity measurements.[c] Determined by SEC (DMF, against PEG)

High-Pressure KHI Equipment and Test Methods

All polymers were investigated for their kinetic hydrate inhibition performance using a set of five parallel high-pressure steel rocking cells.[18] The equipment was manufactured and supplied by PSL Systemtechnik, Germany (Figure 5.2). Each cell is 40 mL and contains a steel ball which causes extra agitation of the fluids during rocking. The gas composition used was a hydrocarbon gas mixture with some CO_2 and N_2, typical of a North Sea natural gas (Table 5.2). The gas mixture preferentially forms Structure II gas hydrates.

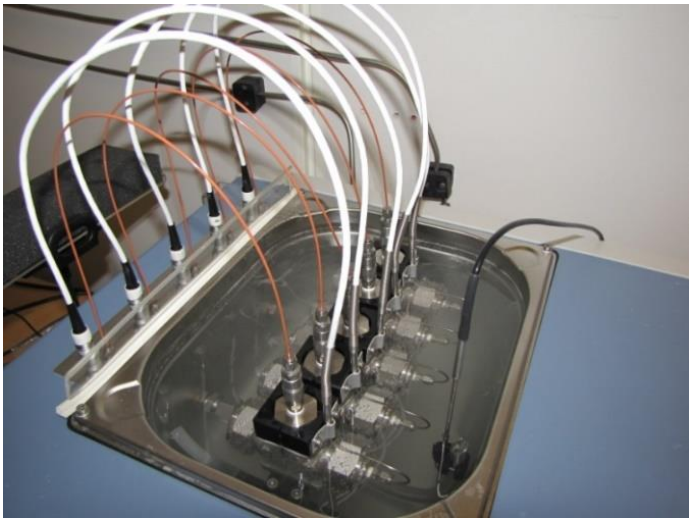

Figure 5.2: The rocker rig with the five steel rocking cells positioned in the cooling bath.

Table 5.2: Composition of Synthetic Natural Gas (SNG).

component	mol%
methane	80.67
ethane	10.20
propane	4.90
isobutane	1.53
n-butane	0.76
N_2	0.10
CO_2	1.84

The test method used was the slow "constant cooling" (CC) method. At the start of each experiment, the pressure was approximately 76 bar. The equilibrium temperature (T_{eq}) at this pressure has been determined by standard laboratory dissociation experiments, warming at 0.025 °C h^{-1} for the last 3 - 4 °C.[19-20] Five repeated equilibrium tests were carried out, which gave T_{eq} = 20.2 ± 0.5 °C. This value is in good agreement with the calculated T_{eq} value of 20.5 °C using Calsep's PVTSim software.

The CC test procedure for evaluating KHI performance was as follows:

1. Each cell was filled with 20 mL of deionized water in which the various polymers had been dissolved to the desired concentration.
2. Air in the cells was removed by a combination of vacuum pumping and filling with SNG to 3-5 bar and then a repeated step of vacuum pumping.
3. The cells were pressurized to 76 bar and rocked at 20 rocks min^{-1} at an angle of 40°.
4. The cells were cooled from 20.5 °C to 2.0 °C at a rate of 1.0 °C h^{-1}.
5. The pressure and temperature of each cell, as well as the temperature of the cooling bath, were logged on a computer.

An example of the pressure and temperature data recorded is given in the graph in Figure 5.3. As the cell is a closed system, a linear pressure decrease is seen due to the reduction in temperature. The first deviation from this linear pressure decrease is defined as the observed onset temperature for hydrate formation, T_o, even though nucleation may have occurred earlier on an undetectable scale. At some time after this initial hydrate formation temperature, a rapid pressure decrease is seen indicating rapid hydrate growth. The temperature, T_a, at which the hydrate growth is at its most rapid is determined at the steepest part. In Figure 5.3 the T_o and T_a values are very close, which is an indication that the KHI has only a minor effect on the hydrate crystal growth processes. The overall results show that the temperatures are homogeneous for all cells in the water bath and none of the cells contains any systematic errors that lead to consistently better or worse results.

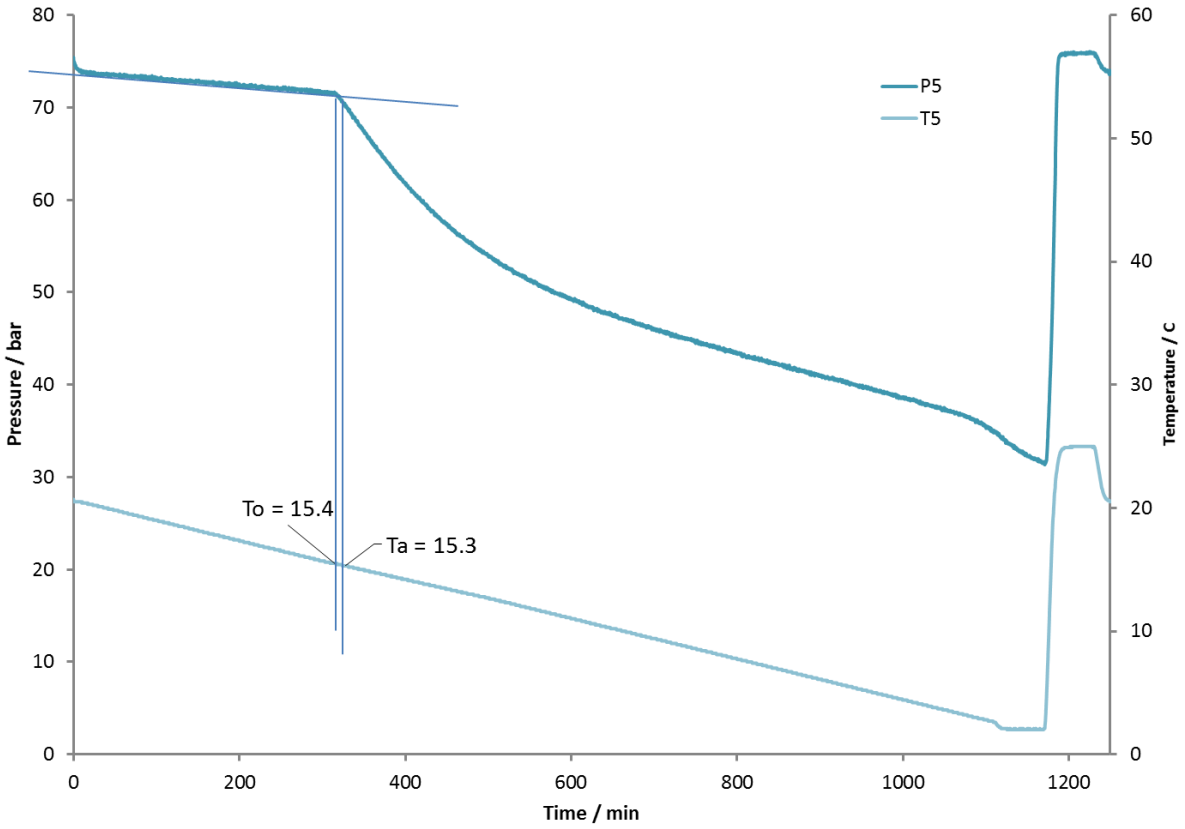

Figure 5.3: Pressure and temperature data analysis for a single CC KHI test (performed by Hong Lin).

Marine Biodegradation Studies

Marine biodegradability was determined using the method based on OECD 306 guidelines.[21,22] In summary, biological oxygen demand (BOD) for each chemical was measured using the OxiTop® Control manometric closed system (WTW, Germany) over 28 days. The percentage biodegradability was determined based on comparing the measured BOD and the calculated theoretical oxygen demand (ThOD) values. The test medium was seawater without inoculum, but nutrients were added to ensure non-limiting conditions for microbial activity and growth.

The test flasks contained seawater, nutrients and the test chemicals. Three different types of control flasks were also used:

(1) seawater "blanks" with nutrients only added,

(2) negative controls with autoclaved seawater (killing any organisms present), nutrients and the test chemicals at 60 mg L^{-1} concentration,

(3) positive seawater controls with nutrients and a readily biodegradable chemical, sodium benzoate, at 100 mg L^{-1}.

Each chemical, positive control and blank were tested in triplicate, while only one flask was used as a negative control for each tested chemical. The seawater sample used in all studies was from the same batch of 20 l collected at the International Research Institute of Stavanger (IRIS), Mekjarvik, Norway. Seawater is available at this institute from Byfjorden, pumped via a pipeline system at a depth of 70 m and temperature 12 °C. The seawater was stored in the dark at 20 °C overnight before being used in the test bottles the next day. Seawater (297 mL) was added to 510 mL amber bottles, and nutrient solutions were added as described earlier by our group.[23]

After incubation of the OxiTop® control flasks, 1.8 mL of a 1.0 w/w % solution (in distilled water) of each test chemical was added to the test and negative control flasks, while 1.0 mL of a 30 g L^{-1} sodium benzoate solution was added to the positive control flasks. Magnetic stirrer bars were also added. The screw-top measuring heads, containing sodium hydroxide pellets to adsorb produced carbon dioxide, were replaced.
The flasks were stirred on magnetic stirrers in an incubator cabinet in the dark at 20 °C. Oxygen consumption data via measurement of pressure loss was recorded over a 28 days period. At this time the ThOD of each polymer was calculated as described in the OECD 306 guidelines, taking into account complete nitrification. Blank oxygen consumption values (BOD values representing background respiration in seawater) were deducted from each test compound's BOD before determining the percentage biodegradability.

Results and Discussion

Polymer synthesis

2-methyl-2-oxo-1,3,2-dioxaphospholane (MeEP) was used as the first cyclic phosphonate monomer for the anionic ring-opening polymerization (AROP) to synthesize well-defined ($Đ$ < 1.1), water-soluble poly-(ethylene methyl phosphonate)s with high degrees of polymerization.[24] This polymer is readily water-soluble and shows no cloud point temperature. Based on other KHI studies we have conducted with water-soluble polymers with pendant alkyl groups we were reasonably sure that this PPn with pendant methyl groups and high cloud point would be a poor KHI. As main-chain poly(phosphonate), PMeEP slowly hydrolyzes even at neutral pH, which would be detrimental for KHI use. For example, it has been shown that for the PPn P(MeEP)$_{21}$ at pH 7.4, the molecular weight distribution broadened over time and monomodality was lost after 24h. However, replacing the methyl side chain with ethyl or isopropyl groups, the hydrolytic stabilities of the polymers increased significantly to days or weeks, respectively.[24]

Novel copolymers have been prepared by statistical copolymerization of two monomers (Table 5.1). The 2-alkyl-2-oxo-1,3,2-dioxaphospholanes used in this study were polymerized via the organocatalytic AROP to ensure high control over molecular weight and molecular weight distribution. By adjusting the comonomer ratio, also the hydrophilicity of the copolymers was adjusted, and cloud point temperatures in the range between 25 and 48 °C were prepared.

Cloud Point Studies

The ethyl and isopropyl-substituted PPn homopolymers are known to show no cloud point (T_{cp}) (or lower critical solution temperature (LCST)) up to 100 °C even at high concentrations. The more hydrophobic *n*-butyl-substituted poly(phosphonate) exhibits a cloud point depending on the polymer concentration, while the *n*-hexyl- or the cyclohexyl-substituted PPns are insoluble in water. In comparison, the phosphate (and not phosphonate) ester homopolymers, poly(ethylene ethyl phosphate) and poly(ethylene isopropyl phosphate) are known to show cloud points at 38 °C and 5 °C respectively.[25,26]

For this KHI study, we were interested in keeping the cloud point reasonably low as there is increasing evidence that this may aide kinetic hydrate inhibition.[3,5] Therefore, all the PPn polymers listed in Table 5.1 have cloud points in the range 25-48ºC. The *n*-butyl PPn homopolymer has a cloud point lower than 10 °C, so therefore we made and tested PEAP (**3**), which is a copolymer of the *n*-butyl and ethyl phosphonate monomers. It exhibited a cloud point as a 1 wt.% solution of 27 °C which guaranteed solubility through the whole range of KHI test temperatures from 20.5 °C down to 2 °C. Since the isopropyl homopolymer has no cloud point, we additionally prepared copolymers of the isopropyl monomer with the cyclohexyl monomer giving a copolymer with a cloud point of 25 °C.

KHI Test Results

Table 5.3 summarizes the CC KHI test results for all the PPns at various concentrations and with the two comparative well-known KHI polymer additives PVP and PVCap. All polymers at all concentrations gave significantly lower T_o values than no additive indicating that they all have KHI activity. However, none of the new PPns showed better KHI performance than the two lactam-based polymers PVP and PVCap. Since all four of the PPns have low cloud points (T_{cl} = 25 - 48 ºC), this shows clearly that low cloud point is not a prerequisite for high KHI performance, although it can be a factor for other classes of polymers. These polymers are capable of forming hydrogen-bonds between the phosphonate oxygen atoms and water molecules in either free water or gas hydrate particles. However, the mediocre KHI performance of these polymers is not due to the lack of hydrogen-bonding from hydrogen atoms in the polymer, as seen for example in poly(*N*-monoalkyl acrylamides) because polymers without such hydrogen atoms can show high KHI performance. Examples are (PVCap), used in this study, or poly(acryloyl pyrrolidine).[27-28]

Table 5.3: KHI constant cooling test results for poly(alkyl ethylene phosphonate)s (PPns) and comparative additives (performed by Hong Lin).

additive	concentration	T_o / ºC	T_a / ºC
no additive	-	18.3	16.7
PVP	2,500	11.3	10.5
PVCap	2,500	9.5	8.4
	5,000	7.4	6.6
(1)	2,500	14.3	14.0
	5,000	13.6	13.1
(2)	2,500	15.1	14.9
	5,000	15.0	14.8
(3)	2,500	13.5	12.6
	5,000	12.7	11.7
(4)	2,500	12.6	11.5
	5,000	12.1	11.7
	7,500	12.3	11.4

Another feature of the PPns was the small decrease in T_o values when increasing the test concentration from 2,500 ppm to 5,000 ppm and even as high as 7,500 ppm. The most significant decrease observed was 0.8 ºC from 2500 to 5000ppm for PPn (**3**). Usually, under the same test conditions, we have seen T_o values drop by 2 - 3 ºC across this range of concentrations for other polymer classes as summarized in Table 5.4. Interestingly, this also includes non-amide based polymers such as the ring-closed poly(isopropenyl oxazoline)s. However, occasionally we do encounter polymer classes that do not show large performance increases when raising the KHI concentration from 2,500 ppm upwards. An example is poly(ethylene citramide)s which only showed a T_o drop of about 0.5 ºC (in the T_o range of 11 - 9 ºC, similar to that of the PPns) from 2,500 to 5,000 ppm. There may be several reasons for this behavior, including polymer solubility and changes in polymer-polymer interactions.

The difference between T_o and T_a values for the PPns in Table 5.3 was in line with expected values from previous studies, such as those referenced in Table 5.4. This suggests that the PPns, especially polymers (**3**) and (**4**), have some effect on crystal growth.

Table 5.4: Maximum decrease in T_o value observed for various polymer classes.

polymer class	**T_o decrease**
PPns (this work)	0.8
PVCap (this work)	2.1
poly(*N*-alkylacrylamide)s[29]	2.0
poly(2-vinyl-4,4-dimethylazlactone)s[30]	2.1
ring-closed poly(isopropenyloxazoline)s[9]	2.9
poly(*N*-alkylglycine)s[31]	2.6
poly(hydroxyl-*N*-alkylcarbamate)s[32]	2.6
poly(ethylene citramide)s[33]	0.5

Biodegradation activities

As poly(phosphonate)s may undergo backbone degradation, we evaluate their seawater biodegradation for the first time. This is also the first report on the biodegradation of such polymers in general; previously only hydrolytic degradation under artificial conditions was reported by our group.[16] We chose copolymers (**2**) and (**4**) and studied their degradation behavior. It was expected that **4** with the bulkier isopropyl and cyclohexyl groups is less prone to degradation, compared to **2**, carrying *n*-alkyl substituents.

The biodegradation activities were measured according to the OECD306 test protocol and compared to sodium benzoate as the biodegradable reference. All tests were carried out in triplicate, and the maximum error was ±15%. Table 5.5 summarizes the biological oxygen demand (BOD) for the calibration standard (seawater only), sodium benzoate, PVCap and PPns (**2**) and (**4**).

Sodium benzoate gave the expected rapid and full degradation with no significant lag time, giving a 28 days biodegradation of about 87% without assimilation included in the calculation. PVCap showed negligible biodegradation. A similar value has been reported previously for a VP: VCap copolymer.[34] The biological oxygen demand (BOD) of (**2**) showed a reasonable biodegradation of about 31% in 28 days while (**4**) proved higher stability with a detectable biodegradation of about 13% in the same time. Neither polymer showed “ready biodegradability”, a term usually considered for chemicals with higher than 60% biodegradation in 28 days. However, reaching the threshold value of 20% biodegradation is useful with regards to obtaining an approved ecotoxicological category for offshore use in the North Sea, an area considered to have the strictest offshore environmental regulations.[11] A possible reason for the higher biodegradation of PPn (**2**) compared to (**4**) may be due to both the pendant groups of the backbone in (**2**) (i.e., ethyl and *n*-hexyl groups) being linear. Secondary and especially tertiary carbon atoms, such as found in the *iso*propyl and cyclohexyl groups of PPn (**4**) tend to be more slowly biodegraded.[11] Despite the amide nitrogen being part of the backbone several poly(2-alkyl-2-oxazoline)s with high or low cloud points in water were shown to have negligible biodegradation in 28 days.[35]

Table 5.5. Average biodegradability activity (triplicate tests) measured by the OECD 306 procedure over 28 days (performed by Hong Lin).

Inhibitor	% BOD by OECD 306
seawater	0
sodium benzoate	87
PVCap	2
(2)	31
(4)	13

Summary and Conclusion

To determine the significance of the amide or imide group in KHI polymers, we have recently endeavored to investigate other polymers with alternate functional groups. These groups provide good water-solubility even in the presence of hydrophobic groups which are essential for KHI performance.

In this study, we prepared a series of well-defined poly(ethylene alkyl phosphonate)s (PPns) with adjustable hydrophilicity and studied their performance as KHIs. Copolymers with predefined low cloud point temperatures have been prepared, but only mediocre performance as KHI in high pressure rocking cells using a Structure II-forming gas mixture was found. Nevertheless, we were able to show for the first time, that poly(phosphonate)s undergo biodegradation in seawater. A copolymer with eight ethyl and eight *n*-hexyl groups gave a reasonable biodegradation of about 31% using the marine OECD306 test protocol. Also, the degree of degradation could be adjusted by the copolymer structure. This study was the first foray into poly(phosphonate)s as KHIs. The proven biodegradation of these poly(phosphonate)s renders them interesting for their use in the marine environment as they will ultimately fully degrade, either by biodegradation and additional hydrolysis. We are exploring the possibility of other related PPns to optimize the KHI performance and biodegradability.

Acknowledgements

We thank Lilian Ree for a repeat KHI test on one of the polymers and to Dr. Andrea Bagio for help with the biodegradation tests. F.R.W. thanks the Deutsche Forschungsgemeinschaft (DFG WU750/6-1) for funding.

References

1. Kelland, M.A., *Energy Fuels,* **2006**, 20, 825-847.
2. Sloan Jr., E.D.; Koh, C.A., Third Ed. CRC Press, Taylor & Francis Group, Boca Raton, FL, **2008**.
3. Kelland, M.A., Materials Science Research, Vol.8. Nova Science Publishers Inc., New York (Chapter 5), **2011**.
4. Perrin, A.; Musa, O.M.; Steed, J.W. *Chem. Soc. Rev.,* **2013,** 42, 1996-2015.
5. Ke, W.; Kelland, M.A. *Energy Fuels,* **2016,** 30, 10015−10028.
6. Kelland, M.A.; Magnusson, C.D.; Lin, H.; Abrahamsen, E.; Mady, M.D. *Energy Fuels,* **2016**, 30, 5665−5671.
7. Magnusson, C.D.; Kelland, M.A. *Energy Fuels,* **2015,** 29, 6347−6354.
8. Kelland, M.A.; Mady, M.F. *Energy Fuels,* **2016,** 30, 3934−3940.
9. Reyes, F.T.; Malins, E.L.; Becer, C.R.; Kelland, M.A., *Energy Fuels,* **2013,** 27, 3154−3160.
10. Magnusson, C.D.; Liu, D.; Eugene Y.-X. Chen, E. Y.-X.; Kelland, M.A. *Energy Fuels,* **2015,** 29, 2336–2341.
11. Kelland, M. A. Production Chemicals for the Oil and Gas Industry; 2nd Ed., CRC Press (Taylor & Francis Group): Boca Raton, FL, **2014**.
12. Steinbach, T.; Ritz, S.; Wurm, F. R. *ACS Macro Lett*., **2014,** 3, 244−248.
13. McGrath, J. W.; Chin, J. P.; Quinn, J. P. *Nat. Rev. Microbiol.,* **2013,** 11, 412−419.
14. Huang, J.; Su, Z.; Xu, Y. *J. Mol. Evol.,* **2005,** 61, 682−690.
15. Kim, A.; Benning, M. M.; OkLee, S.; Quinn, J.; Martin, B. M.; Holden, H. M.; Dunaway-Mariano, D. *Biochemistry,* **2011,** 50, 3481−3494.
16. Wolf, T.; Steinbach, T.; Wurm, F.R. *Macromolecules,* **2015,** 48, 3853−3863.
17. Wolf, T.; Naß, J.; Wurm, F.R. *Polym. Chem*., **2016,** 7, 2934-2937.
18. Chua, P. C.; Kelland, M. A.. *Energy Fuels,* **2012,** 26, 1160-1168.
19. Gjertsen, L. H.; Fadnes, F. H., **2000**; 912, 722-734.
20. Tohidi, B.; Burgass, R. W.; Danesh, A.; Ostergaard, K. K.; Todd, A. C., Eds. **2000**; 912, 924-931.
21. OECD Guideline for testing of chemicals, Biodegradability in Seawater, **2002**. Adopted by the Council on 17th July, p. 27.
22. Mady, M.F.; Bagi, A.; Kelland, M.A.; *Energy Fuels,* **2016,** 30, 9329−9338.
23. Jensen, M. K.; Kelland, M. A, *J. Petrol. Sci. Eng.,* **2012,** 66, *94-95*.
24. Steinbach, T.; Ritz, S.; Wurm, F. R. *ACS Macro Lett.,* **2014,** 3, 244−248.
25. Iwasaki, Y.; Wachiralarpphaithoon, C.; Akiyoshi, K. *Macromolecules,* **2007,** 40, 8136−8138.

26. Iwasaki, Y.; Yamaguchi, E. *Macromolecules,* **2010,** 43, 2664−2666.
27. Chua, P.C.; Kelland, M.A. *Energy Fuels,* **2010,** 26, 4481−4485.
28. Del Villano, L.; Kelland, M.A.; Miyake, G.M.; Chen, E.Y.-X. *Energy Fuels,* **2010,** 24, 2554–2562.
29. Mady, M.F.; Bak, J.B.; Lee, H.; Kelland, M.A. *Chem. Eng. Sci*., **2014,** 119, 230-235.
30. Ree, L.H.S.; Kelland, M.A.; Roth, P.J.; Batchelor, R. *Chem. Eng. Sci*., **2016,**152, 248–254.
31. Reyes, F.T.; Guo, L.; Hedgepeth, J.W.; Zhang, D.; Kelland, M.A. *Energy Fuels,* **2014,** 28, 6889−6896.
32. Abrahamsen, E.; Kelland, M.A. *Energy Fuels,* 30, **2016,** 8134−8140.
33. Reyes, F.T.; Kelland, M.A.; Sun, L.; Jian Dong, J. *Energy Fuels,* **2015,** 29, 4774−4782.
34. Del Villano, L.; Kommedal, R.; Kelland, M.A. *Energy Fuels,* **2008,** 22, 3143-3149.

Chapter 5: Poly(alkyl ethylene phosphonate)s – A New Class of Non-Amide Kinetic Hydrate Inhibitor Polymers.

Chapter 3 and **Chapter 4** discussed the copolymerization as well as copolymerization kinetics of dioxaphospholanes. The polymer properties were adjusted via copolymerization to vary bulk properties and solubility behavior. **Chapter 5** presented a potential application of PPn copolymers outside of the field of biomedical applications.

Apart from copolymerization, polymer properties can be altered by post-polymerization modifications and the introduction of functional groups. Therefore, **Chapter 6** introduces a new monomer, the prop-2-en ("allyl-") substituted dioxaphospholane derivative to enable a variety of different side-chain modifications. The terpolymerization of three different dioxaphospholanes as well as the first thiol-ene modification on poly(phosphonate)s to vary the polymers solubility behavior is presented.

Chapter 6: Thermoresponsive Coacervate Formation of Random Poly(phosphonate) Terpolymers.

Thomas Wolf[1]*, Timo Rheinberger*[1]*, and Frederik R. Wurm*[1]

[1]Max Planck-Institut für Polymerforschung, Ackermannweg 10, 55128 Mainz, Germany

Published in: European Polymer Journal, **2017,** 10.1016/j.eurpolymj.2017.05.048

Keywords: anionic ring-opening polymerization, random terpolymerization, poly(phosphoester)s, poly(ethylene alkyl phosphonate)s, thiol-ene, LCST-type phase separation, simple coacervates

Chapter 6: Thermoresponsive Coacervate Formation of Random Poly(phosphonate) Terpolymers.

Abstract

Coacervates are partially hydrated, colloidal polymer droplets in water held together by hydrophobic interactions and are considered promising candidates for drug delivery applications. We present the first simple coacervates made from temperature-induced phase separation of aqueous poly(phosphoester) terpolymer solutions. Such coacervates are interesting for drug carrier applications as they are non-toxic, fully biodegradable and form spontaneously upon heating above a threshold temperature (lower critical solution temperature, LCST). The investigated poly(ethylene alkyl phosphonate) terpolymers are synthesized via the organocatalytic anionic ring-opening polymerization of cyclic phosphonate monomers. This way polymers with high control over molecular weight, terpolymer composition (and hence physical and chemical properties) and rather narrow molecular weight distributions ($Đ < 1.30$) are produced. The terpolymers bear functional pendant groups for further modifications and have a finely tunable balance of hydrophilic and hydrophobic side-chains randomly distributed over the whole chain, as proven by $^{31}P\{H\}$ NMR polymerization kinetics. These functional terpolymers spontaneously phase separate into a polymer rich coacervate phase in water upon heating above the LCST, providing an elegant method to prepare degradable and non-toxic carrier system.

Introduction

The precise synthesis of polymers for the preparation of nanometer- or micrometer-sized carriers is a relevant field of current research. The entrapment of reactive or labile drugs inside a polymeric carrier reduces adverse or systemic reactions and prevents their premature exclusion and degradation in the body.[1-4] One of the many systems discussed for these applications are coacervates, liquid-liquid phase separated polymer solutions which form spontaneously upon specific stimuli and are known to have exceptionally high loading-capacities.[5-8]

One such stimulus can be temperature to induce the desolvatisation and subsequent phase separation into a polymer-poor aqueous phase and a polymer-rich coacervate phase. Polymers showing such phase separation behavior are called LCST (lower critical solution temperature) polymers and are extensively studied in literature for many

applications.[9-13] LCST-induced coacervate formation, however, is far less often observed in synthetic polymers as most synthetic polymer form ill-defined precipitates upon phase separation.[6,14-17]

Some of the primary requirements for polymers to be used as carrier systems are biocompatibility, low toxicity, solubility in water, the potential to induce a release mechanism and degradability. Today, even though there are a growing number of polymer-drug formulations being approved by the FDA, poly(ethylene glycol) (PEG) is still considered as *the* gold standard for water-soluble, biocompatible polymers.[18-21] Despite its many assets, however, PEG suffers from several drawbacks: the polyether backbone is non-degradable under biological conditions which might lead to accumulation of high molecular weight PEG. Due to its abundance in many formulations, a significant percentage of people have developed “anti-PEG” antibodies over the past decades. This reduces the efficacy of PEG-based drug formulations in many cases.[21-25] Finally, chemical modification of PEG is usually only possible at the $\alpha-$ and $\omega-$ end of the polymer, restraining the adjustment of PEG properties towards specific needs.

To overcome some of these shortcomings of PEG, several research groups have suggested various synthetic or natural polymers as PEG-alternatives.[20, 26-29] One class receiving growing attention in recent years are poly(phosphoester)s (PPEs) based on the pioneering works of Penczek *et al*. and Carraher *et al*. in the 1970’s as they mimic the natural poly(phosphoester)s found ubiquitous in nature: DNA and RNA.[30-32]

Today, the majority of these PPEs are produced via the organocatalytic anionic ring-opening polymerization (AROP) of cyclic phosphoester. This provides excellent control over molecular weight and narrow molecular weight distributions. Furthermore, several functional groups have been introduced to the pendant ester to date.[28,33-45] However, if well-defined PPEs are demanded, the polymerization needs to be terminated at moderate conversions (50-70%) or special, toxic, and expensive catalysts need to be added to prevent excessive transesterification reactions that would broaden the molecular weight distribution. Our group recently presented another strategy to well-defined PPEs: the preparation of poly(alkylene alkyl phosphonate)s (PPn)s, aliphatic PPEs with a

hydrolytically stable P-C bond in the side chain. We found that this small structural change successfully prevents transesterification even at high conversions (> 95%). The AROP of 2-alkyl-2-oxo-1,3,2-dioxaphospholanes, the respective cyclic monomers, was already performed with methyl-, ethyl- and isopropyl-side-chains resulting in non-toxic and still fully degradable polymers with excellent control over molecular weight and narrow molecular weight distributions.[40,42] Copolymers of 2-alkyl-2-oxo-1,3,2-dioxaphospholanes bearing an isopropyl and a cyclohexyl group showed a linear correlation between the glass transition temperature (T_g) and the copolymer composition.[43]

In this work, we extend the scope of poly(ethylene alkyl phosphonate)s with the new side-chain functional monomer 2-allyl-2-oxo-1,3,2-dioxaphospholane **(3)**. For the first time, we study the terpolymerization behavior of three different dioxaphospholane monomers. The thermoresponsive behavior of the obtained terpolymers in aqueous solution, as well as the temperature, triggered the formation of simple coacervates is presented. In combination with previous studies investigating the hydrolytic and microbial (seawater) degradation of PPn's, this straightforward preparation of degradable coacervates might be beneficial for future degradable drug delivery or self-healing applications.[40,42,46]

Results and Discussion

Monomer synthesis

Anionic ring-opening polymerization produces polymers with high control over molecular weight and copolymer composition as well narrow molecular weight distributions. A broad range of different cyclic monomers producing various polymer classes, ranging from poly(carbonate)s over poly(ester)s to PPEs, as well as many different catalyst systems are known.[45,47-50] In the case of the poly(ethylene alkyl phosphonate) synthesis, the necessary cyclic phosphonate monomers are the 2-alkyl-2-oxo-1,3,2-dioxaphospholanes. These monomers can be polymerized under organocatalytic conditions and produce poly(ethylene alkyl phosphonate)s with adjustable physical and chemical properties (e.g., hydrolysis rate, solubility) depending on the monomer design.[40,42,45] To synthesize polymers that further exhibit a thermoresponsive behavior in water, a combination of hydrophilic and hydrophobic side-chains can be used.[9] Furthermore, the addition of

reactive groups in the side-chain enables post-polymerization modifications for further variation of the properties (e.g., cross-linking, reactive pendant groups).

For this purpose, we synthesized three cyclic monomers for the AROP, namely the hydrophilic 2-ethyl-2-oxo-1,3,2-dioxaphospholane **(1)**, the hydrophobic 2-*n*-butyl-2-oxo-1,3,2-dioxaphospholane **(2)** and the functional 2-allyl-2-oxo-1,3,2- dioxaphospholane **(3)**. **(1)** and **(2)** were prepared according to literature while monomer **(3)** was prepared as described in Scheme 6.1, c.[42]

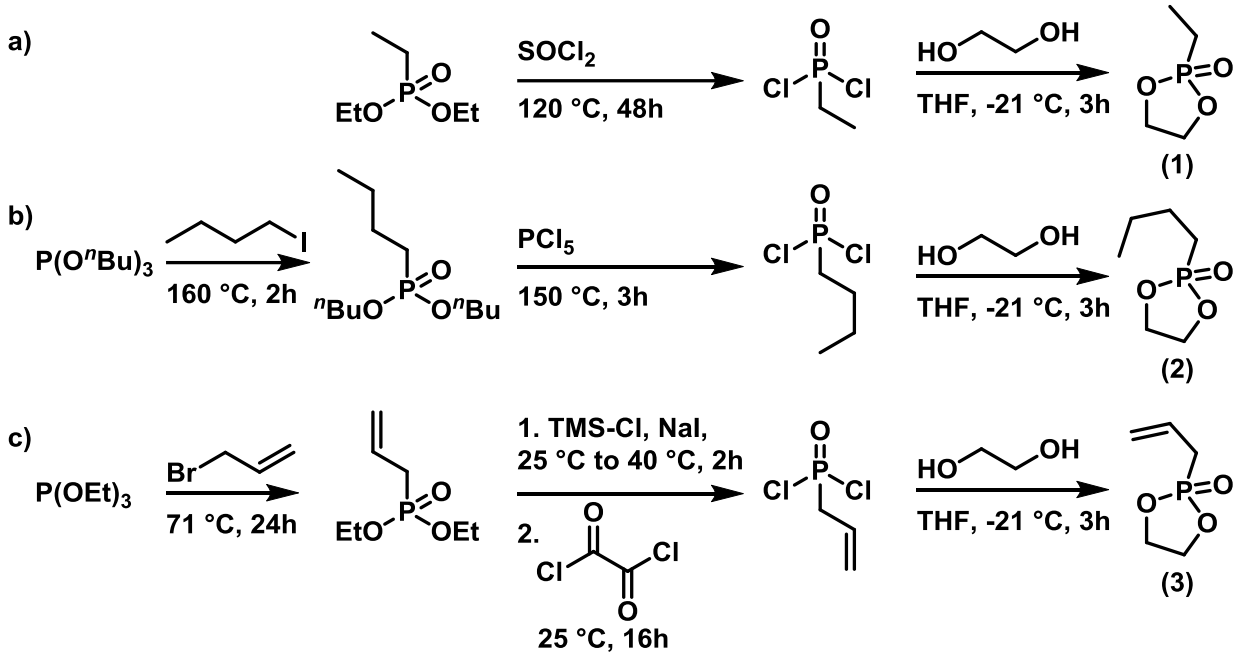

Scheme 6.1: Synthesis Scheme of the monomers: a) Chlorination of commercially available *O, O*-diethyl ethyl phosphonate with thionyl chloride and subsequent ring-closing reaction with ethylene glycol to produce monomer (1). b) *Michaelis-Arbuzov* reaction of tri-*n*-butyl phosphite with *n*-butyl iodide yields *O,O*-di-*n*-butyl *n*-butyl phosphonate. Chlorination with phosphorus pentachloride (PCl_5) and subsequent ring-closing reaction with ethylene glycol produces monomer (2). c) Synthesis of *O, O*-diethyl allyl phosphonate via *Michaelis-Arbuzov* reaction of triethyl phosphite and allyl bromide. Conversion into *O, O*-di(trimethylsilyl) allyl phosphonate with trimethylsilyl chloride (TMS-Cl) and subsequent chlorination with oxalyl chloride. Ring-closing reaction with ethylene glycol produces monomer (3).

In general, the corresponding phosphite is converted into the *O, O*-dialkyl alkyl phosphonate via a *Michaelis-Arbuzov* reaction. Chlorination of the dialkyl esters proceeds under various conditions and is dependent on the steric hindrance of the ester and the sensitivity of the side-chains. Therefore, the non-hindered and commercially available *O, O*-diethyl ethyl phosphonate is readily converted into the respective dichloride via chlorination with thionyl chloride. The more hindered *O, O*-di-*n*-butyl *n*-butyl phosphonate only forms the dichloride by reaction with PCl_5 in good yields.[42] The double bond of *O, O*-diethyl allyl phosphonate, however, is susceptible to side-reactions under both conditions mentioned above and hence chlorination with the milder reagent oxalyl chloride at room temperature is necessary to ensure acceptable yields (60%) and prevent side-reactions. The additional formation of the reactive *O, O*-di(trimethylsilyl) ester intermediate is, however, necessary.

^{1}H, $^{31}P\{H\}$ (Figure 6.1) and ^{13}C NMR spectroscopy were used to confirm the structure of the monomers and all intermediates. The ^{1}H NMR spectrum of all monomers shows the characteristic strongly split multiplet from 4.53 to 4.10 ppm of the ring-protons as well as all ^{1}H resonances of the respective side-chains. $^{31}P\{H\}$ NMR spectroscopy shows one sharp signal at 52.2, 51.7 and 45.9 ppm for the three monomers **(1)**, **(2)** and **(3)**, respectively.

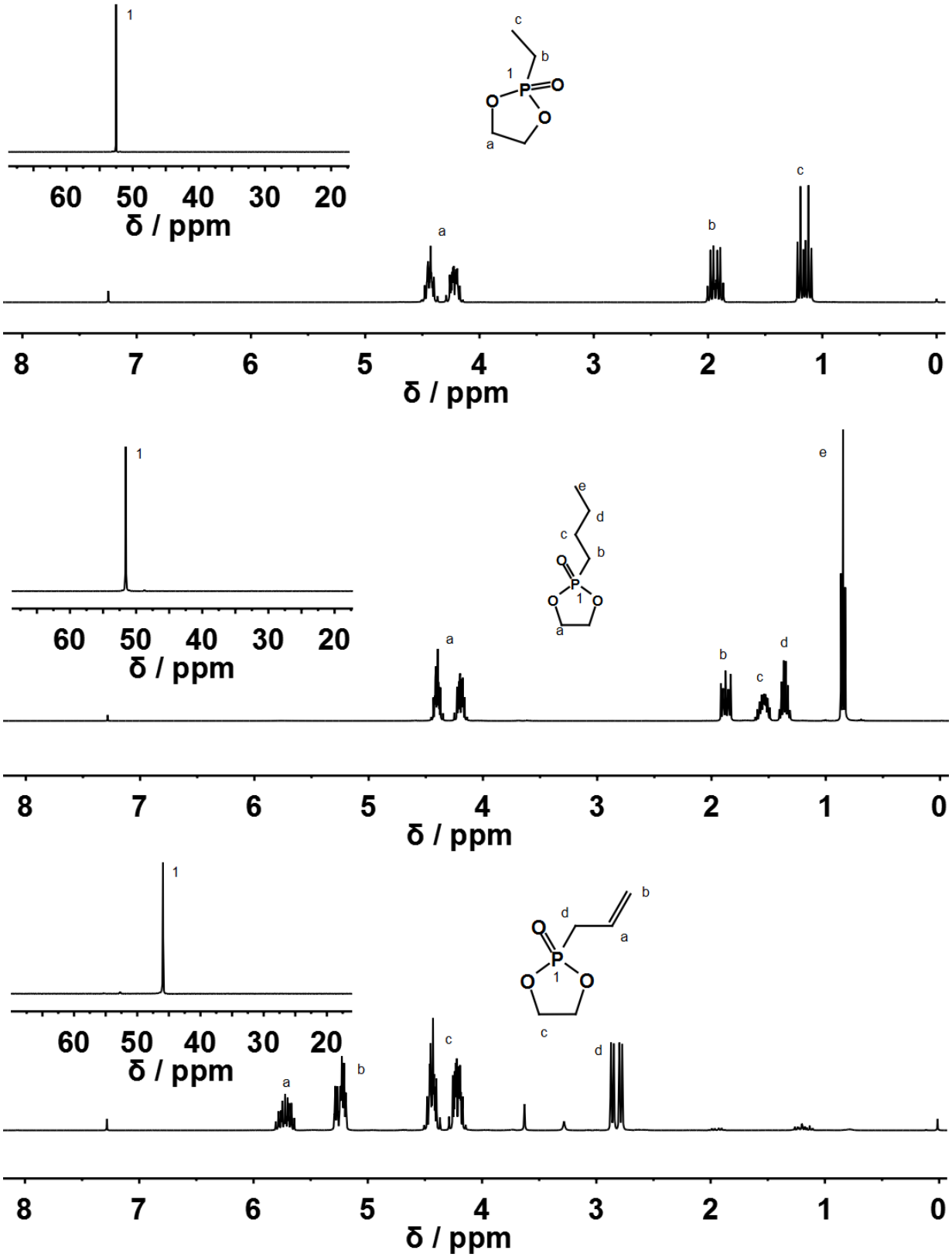

Figure 6.1: NMR characterization: ^{1}H 500 MHz, $^{31}P\{H\}$ 201 MHz, inset, 298K, $CDCl_3$ of cyclic monomers (1), (2) and (3).

Polymer Synthesis

Polymerization was performed under the established conditions for the respective homo polymerizations.[42] 2-(Benzyloxy)ethanol was used as an initiator to enable end-group analysis for subsequent molecular weight determination via ^{1}H NMR spectroscopy. 1,8-diazabicyclo-[5.4.0]undec-7-en (DBU) was used as an organic catalyst base as schematically shown in Scheme 6.2.

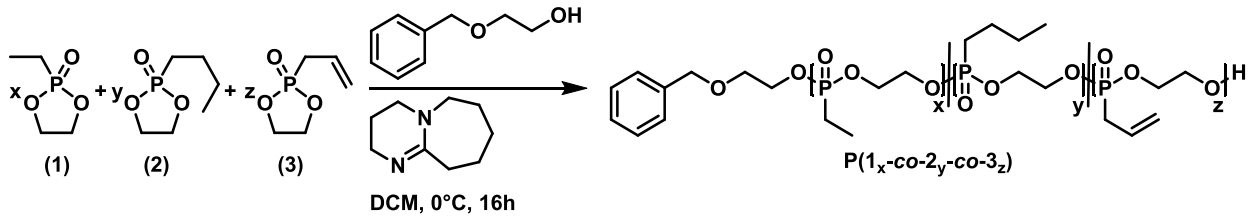

Scheme 6.2: Anionic ring-opening terpolymerization of 2-oxo-2-alkyl-1,3,2-dioxaphospholane monomers (1), (2) and (3) catalyzed with the organic base 1,8-diazabicyclo[5.4.0]undec-7-en (DBU) and initiated with the 2-(benzyloxy)ethanol in dichloromethane (DCM) to produce P(1x-co-2y-co-3z).

Polymerization proceeded to high conversions (>90%) within 16hours. All polymers were analyzed via ^{1}H and ^{31}P{H} NMR spectroscopy. Representative NMR spectra are shown in Figure 6.2, a. The ^{31}P{H} NMR spectrum shows three distinct resonances at 34.5, 33.3 and 28.1 ppm, respectively, indicating ring-opening of the cyclic monomers (monomer resonances at 52.2, 51.7 and 45.9 ppm, respectively).

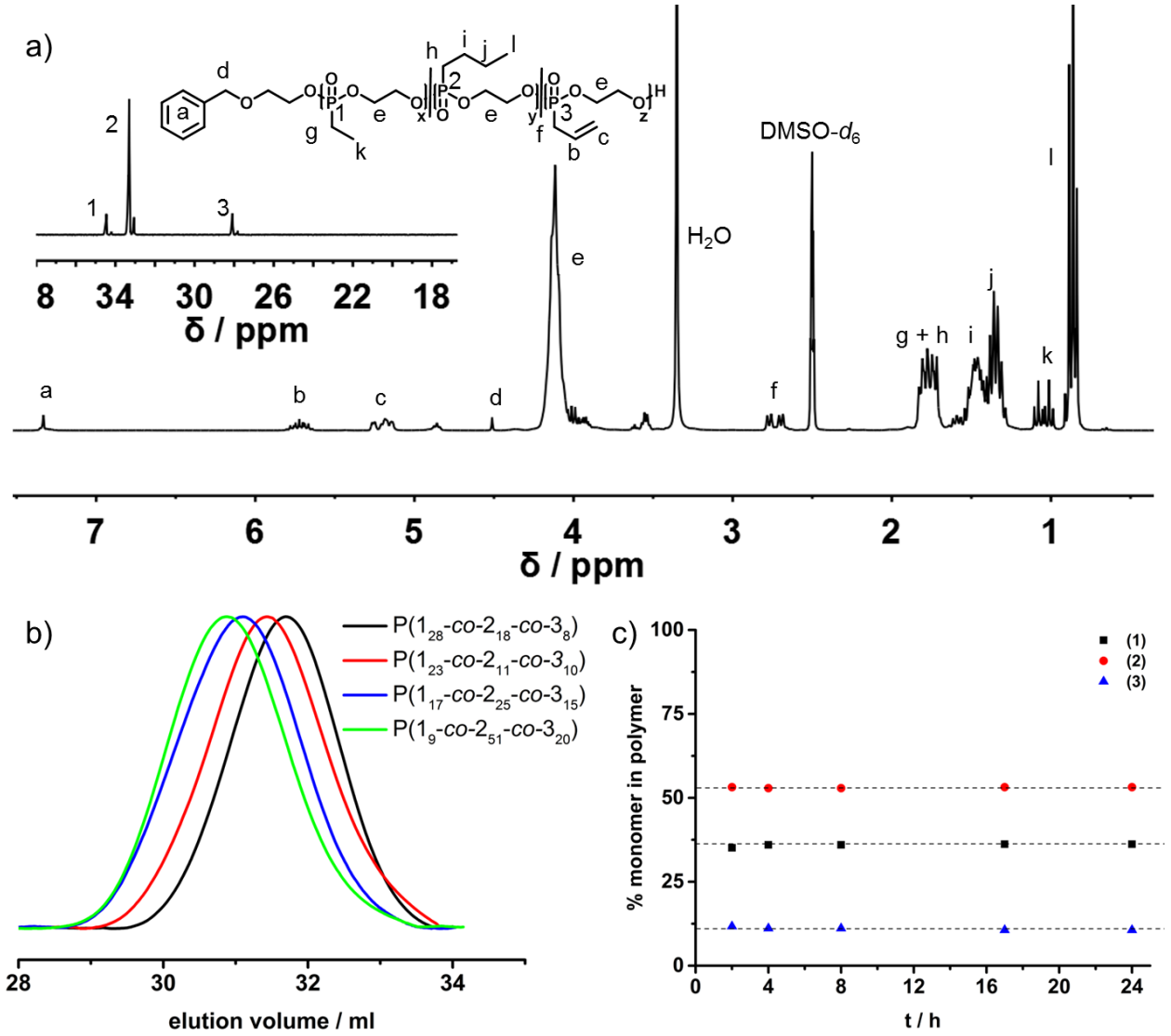

Figure 6.2: Characterization of terpolymers synthesized via anionic ring-opening terpolymerization: a) Representative ^{1}H NMR (500 MHz, DMSO-d_6, 298K) and ^{31}P{H} NMR (201 MHz, DMSO-d_6, 298K, inset) spectrum of P(1_x-*co*-2_y-*co*-3_z). b) Representative SEC elugrams (DMF, 333K, RI detection) of P(1_x-*co*-2_y-*co*-3_z). c) Terpolymerization kinetics of AROP of three monomers at the same time: plot of each monomer incorporated into the polymer backbone over time.

These resonances were assigned to the three monomers **(1)**, **(2)** and **(3)** via ^{1}H^{31}P{H} HMBC 2D NMR measurements through correlation of the phosphorus resonances and the characteristic side-chain resonances (Figure 6.3).

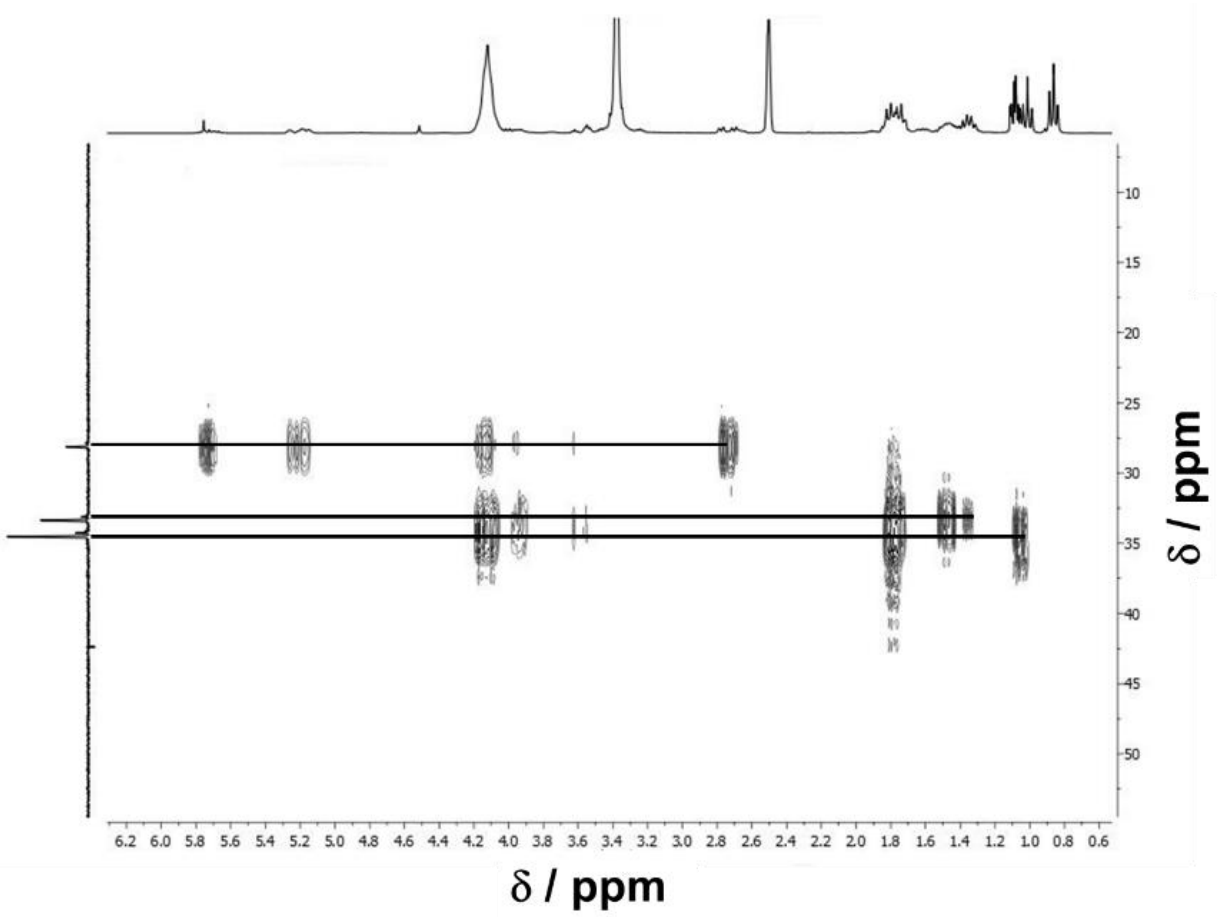

Figure 6.3: $^{1}H^{31}P$ HMBC (500 MHz) NMR spectrum P(1_x-*co*-2_y-*co*-3_z) in DMSO-d_6 at 298K.

The relative intensity of these three resonances matched the monomer feed ratio in all cases and was used to determine the exact terpolymer composition. The ^{1}H NMR spectrum shows all resonances expected from the respective monomer spectra. The broadening of the resonance at 4.14 ppm from the backbone indicates successful polymerization. The signals of the terminal -CH_3 groups from monomer **(1)** (signal k) and **(2)** (signal l) are well-separated as are all signals from monomer **(3)** (signals b, c, and f). This enabled determination of the terpolymer composition via ^{1}H NMR spectroscopy. Furthermore, these signals are well-resolved, and even the respective J-coupling is observed, indicating a high degree of mobility of the side-chains (Figure 6.2). In all cases, this matched the results obtained from $^{31}P\{H\}$ NMR spectroscopy. ^{1}H NMR spectroscopy was used to determine the degree of allyl-group isomerization to be less than 5% in all cases (signal at 4.85 ppm originating from the prop-2-ene group). Furthermore, the

resonance of the aromatic initiator at 7.34 ppm was used to determine the degree of polymerization and molecular weight (M_n) of the polymer.

Finally, to ensure the formation of an actual terpolymer, ^{1}H DOSY NMR spectroscopy was performed (Figure 6.4). All resonances (backbone and all side-chains) have the same diffusion-coefficient and are hence part of the same molecule.

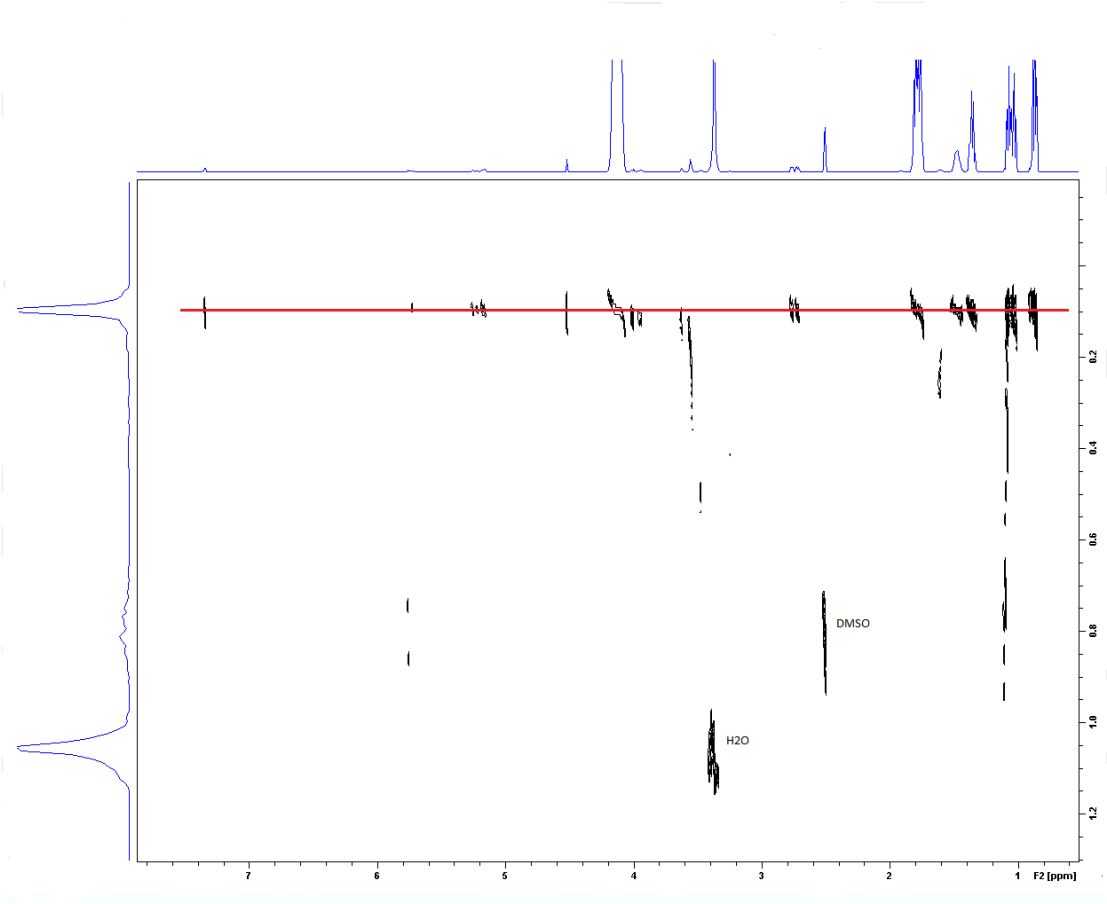

Figure 6.4:^{1}H DOSY (500 MHz) NMR spectrum P(1_x-*co*-2_y-*co*-3_z) in DMSO-d_6 at 298K.

Analysis via SEC (DMF, 333K, RI detection, Figure 6.2, b) shows a narrow, monomodal molecular weight distribution without tailing for all polymers, further proving the existing of one distinct polymer species and not three independent homopolymers. To get more insight on the microstructure of the terpolymer, ^{31}P{H} NMR assisted polymerization kinetics were performed. The relative ratios of the ^{31}P{H} NMR signals already incorporated in the polymer backbone were observed over the course of the polymerization and compared with the initial monomer feed.

As seen in Figure 6.2, c, the relative ratio of all monomers incorporated into the polymer backbone stays constant over the whole time. This shows that all monomers have the same rate of polymerization. We hence conclude that the organocatalytic AROP of three different 2-alkyl-2-oxo-1,3,2-dioxaphospholanes results in the formation of random terpolymer without any detectable gradient structures.

Thermal analysis in bulk via differential scanning calorimetry shows a single glass transition temperature at ca. -40 °C for all examples of our terpolymer library. This is in good accordance with previous studies on the respective homopolymers.[40, 42] Detailed analytical data of all terpolymers synthesized and used in this study are summarized in Table 6.1.

Table 6.1: Characterization data of the PPn terpolymers prepared in this study.

sample[a,b]	M_n theo. / g mol^{-1}[c]	M_n / g mol^{-1}[a]	$Đ$[d]	Y / %[a,b]	T_g / °C[e]
P(1$_{23}$-*co*-2$_{11}$-*co*-3$_{10}$)	6,500	6,600	1.25	92	-40.7
P(1$_{11}$-*co*-2$_{31}$-*co*-3$_{11}$)	8,000	8,000	1.20	93	-54.2
P(1$_{28}$-*co*-2$_{18}$-*co*-3$_{8}$)	8,200	8,100	1.19	90	-44.9
P(1$_{17}$-*co*-2$_{25}$-*co*-3$_{15}$)	9,000	8,800	1.21	96	-43.2
P(1$_{9}$-*co*-2$_{51}$-*co*-3$_{20}$)	14,000	12,700	1.24	92	-45.4
P(1$_{10}$-*co*-2$_{57}$-*co*-3$_{19}$)	13,500	13,700	1.15	90	-47.7
P(1$_{10}$-*co*-2$_{60}$-*co*-3$_{10}$)	14,200	14,000	1.14	92	-47.3
P(1$_{29}$-*co*-2$_{111}$-*co*-3$_{22}$)	21,500	21,000	1.10	91	-45.2

a) M_n, copolymer composition and conversion Y determined via ^{1}H NMR spectroscopy. b) Determined via ^{31}P{H} NMR spectroscopy. c) According to monomer feed ratio. d) Determined via size exclusion chromatography (SEC) (DMF, RI detection, 333K vs. PEG standard). e) Determined via differential scanning calorimetry (DSC).

Post-polymerization modification reaction

The accessibility of the pendant double bonds for further side-chain modifications was assessed. The radical thiol-ene reaction was chosen as this reaction can proceed under mild conditions and is very efficient. The reaction was performed with the photo-catalyst 2,2-dimethoxy-2-phenyl acetophenone (DMPA) and cysteine as thiol to exemplarily introduce a zwitterionic moiety in the side-chain (Figure 6.5, a). A UV lamp (365 nm) was used, and full conversion was reached after 30 min of irradiation. $^{31}P\{H\}$ NMR spectroscopy proved to be very sensitive to follow the reaction. Figure 6.5, b shows the $^{31}P\{H\}$ NMR spectra of **P(1_{10}-*co*-2_{60}-*co*-3_{10})** before (bottom) and after (top) irradiation. The allyl-P resonance at 28.1 ppm vanishes and a new resonance at 32.7 ppm arises, indicating a change in the chemical environment of the former allyl-P towards an aliphatic system.

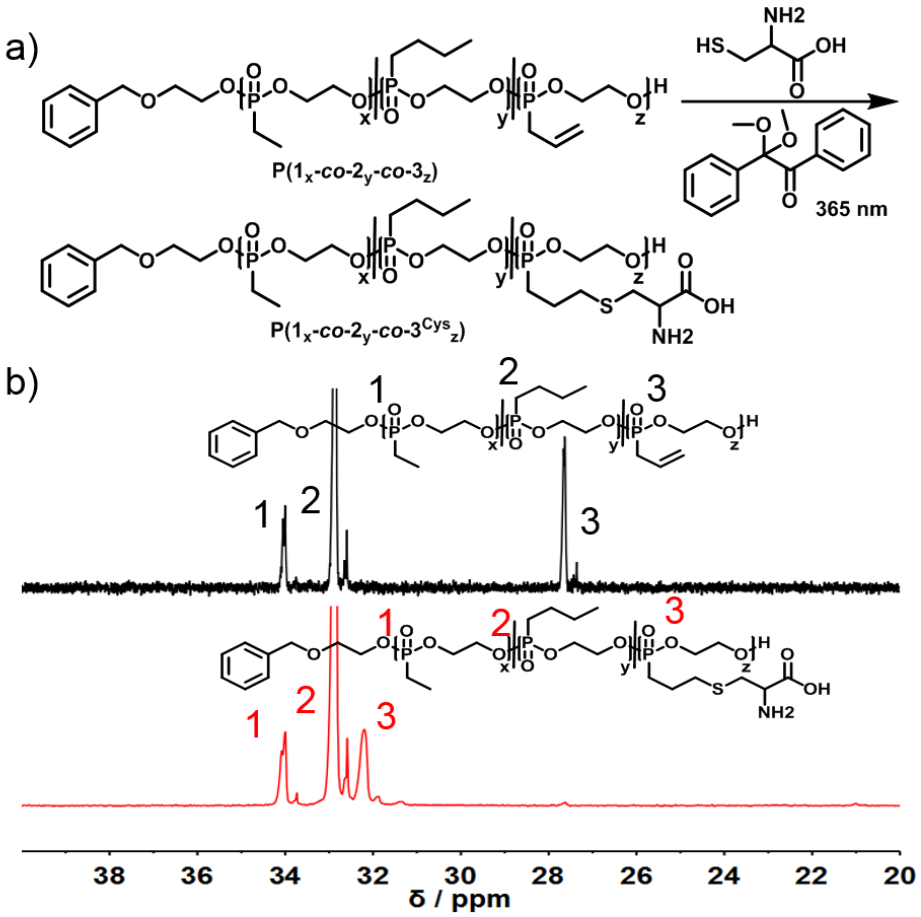

Figure 6.5: a) Schematic post-polymerization reaction via UV initiated radical thiol-ene modification with cysteine. b) $^{31}P\{H\}$ (201 MHz, 298K, DMSO-d_6) NMR spectra comparison of cysteine-modified (top) and unmodified (bottom) terpolymer.

The same conclusion can be drawn from the vanishing ^{1}H NMR resonances of the double bonds (Figure 6.6) as well as the emerging -COOH resonance (170 ppm) in ^{13}C NMR spectroscopy (Figure 6.7).

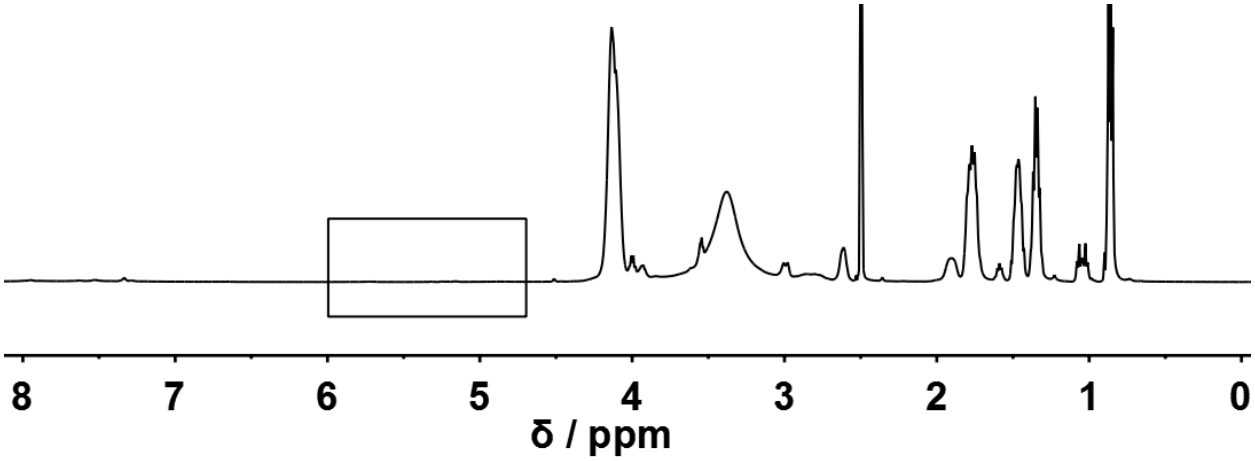

Figure 6.6: ^{1}H (500 MHz) NMR spectrum of P(1_x-*co*-2_y-*co*-3^{Cys}_z) in DMSO-d_6 at 298K. The region of former double bond resonances marked.

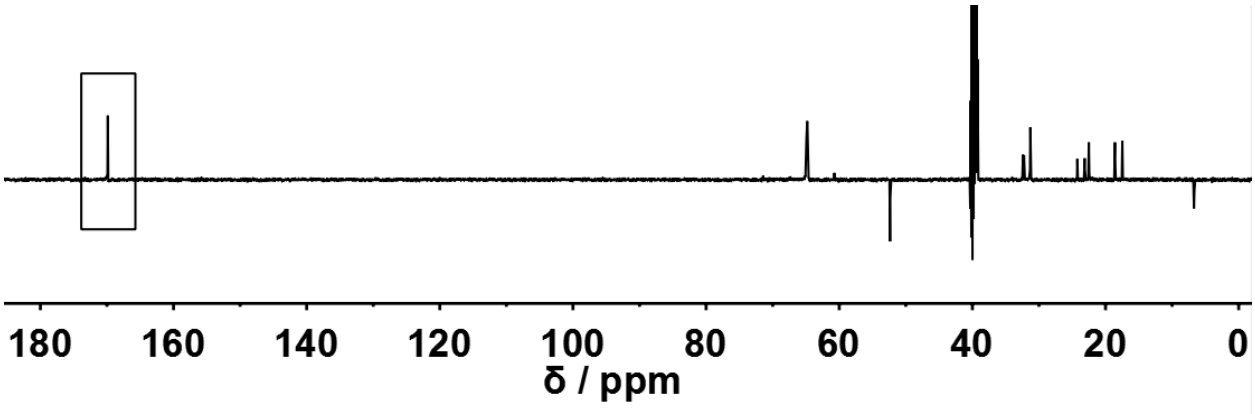

Figure 6.7: ^{13}C (125 MHz) NMR spectrum of P(1_x-*co*-2_y-*co*-3^{Cys}_z) in DMSO-d_6 at 298K. The region with the novel -COOH ^{13}C resonance marked.

Thermal behavior in solution

All terpolymers were soluble in water up to concentrations of 10 g L^{-1} at low temperatures. Increasing the temperature resulted in phase separation and polymer precipitation in the case of all unmodified polymers. In contrast, the cysteine modified polymer stayed water-soluble even at elevated temperatures due to the anionic (pH 8) or cationic (pH 3) character of the side-chains. At pH 5, around the isoelectric point of the cysteine groups, a 10% drop in transmission is observed above 80 °C, indicating a cloud point just outside the measurable range.Turbidity measurements at three different pH values are shown in Figure 6.8.

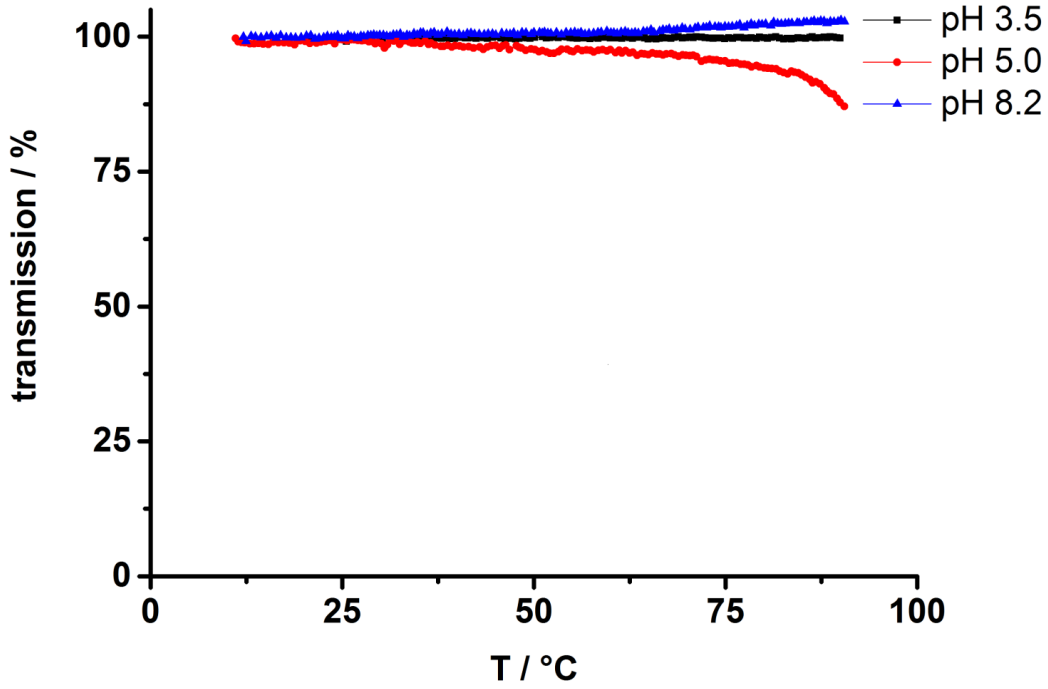

Figure 6.8: UV-VIS transmission turbidity measurements of P(1_{10}-*co*-2_{60}-*co*-3^{Cys}_{10}) (10 g L^{-1}, water, heating 1 °C min^{-1}, 500 nm) at different pH values.

The thermal behavior of the unmodified terpolymers in pure water was investigated via turbidity measurements (Figure 6.9). Rapid phase separation at elevated temperature was observed with little to no hysteresis upon cooling, indicating a fast and reversible phase separation. The phase separation temperature, i.e., the cloud point temperature (T_{cp}) was dependent on the molecular weight and terpolymer composition. Incorporation of more hydrophobic *n*-butyl moieties resulted in a shift of T_{cp} towards lower temperatures.

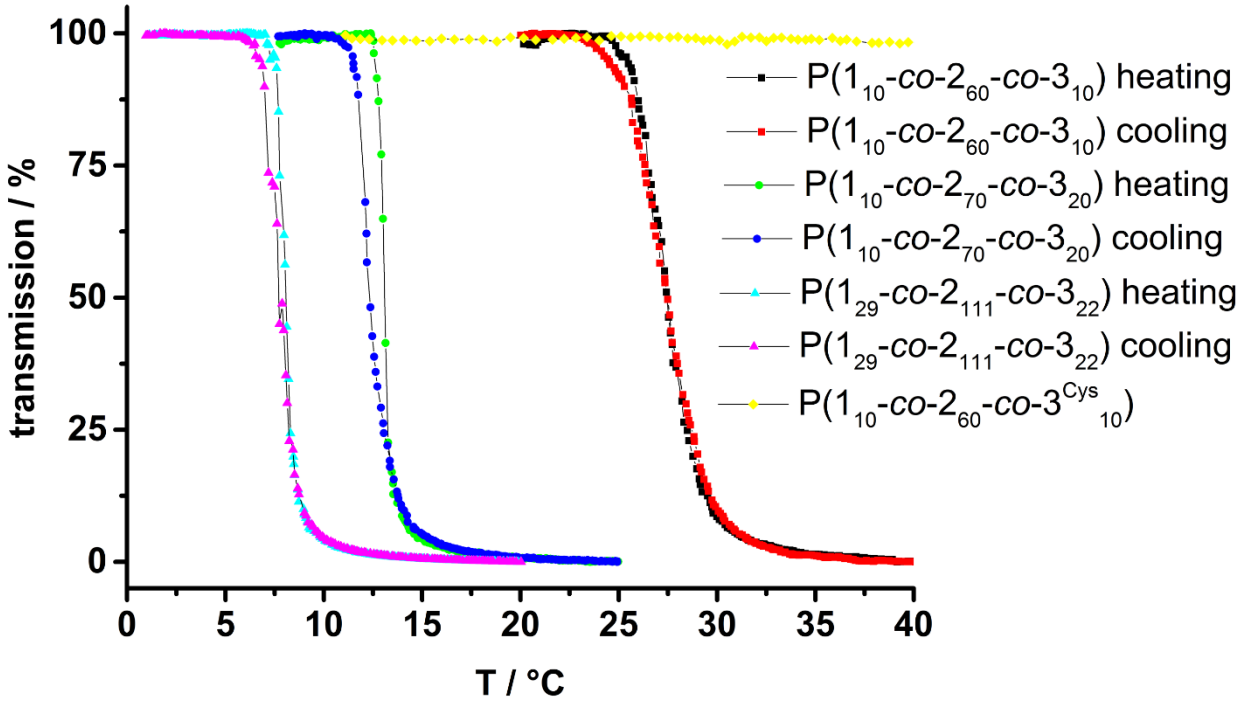

Figure 6.9: Representative UV-VIS transmission turbidity measurements of P(1_x-*co*-2_y-*co*-3_z) (10 g L^{-1}, water, heating/cooling rate 1 °C min^{-1}, 500 nm).

The resulting mixture consisting of water and phase separated polymer was analyzed via confocal laser scanning microscopy. Figure 6.10 shows the reflection channel of an aqueous solution (10 g L^{-1}, T_{cp} = 7 °C) of **P(1_{29}-*co*-2_{111}-*co*-3_{22})** below (left) and above (right) phase separation temperature. The spherical shape of the formed aggregates with diameters of 600 to 2,000 nm is visible as well as a bright spot at the center of the aggregate.

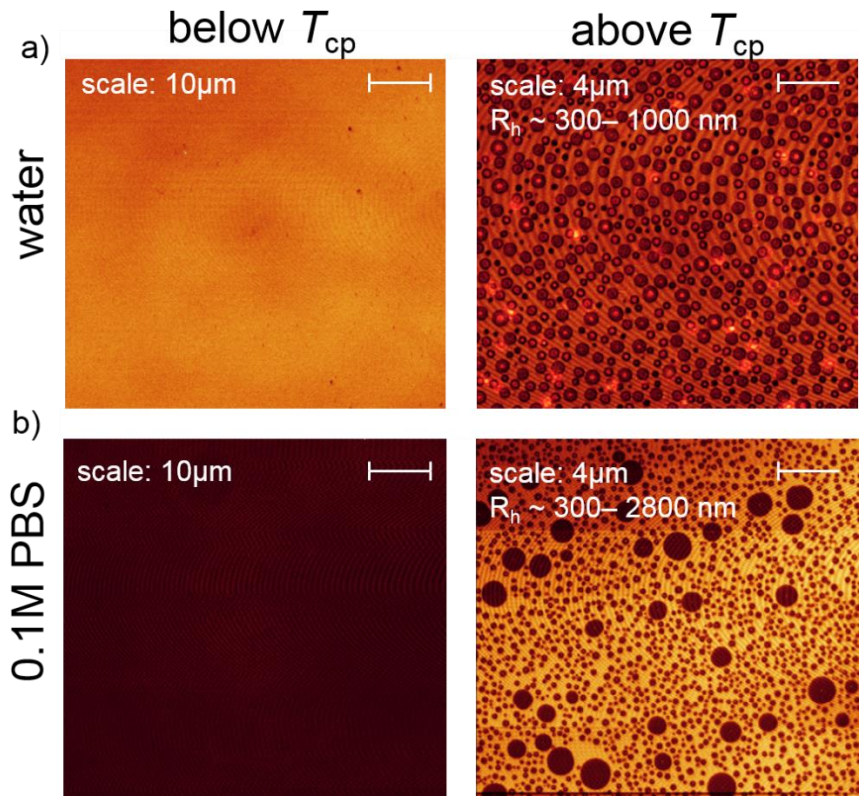

Figure 6.10: a) Confocal laser scanning microscopy (cLSM) pictures of P(1_{29}-*co*-2_{111}-*co*-3_{22}) in water below and above T_{cp} (7 °C), reflection channel shown. b) Confocal laser scanning microscopy (cLSM) pictures of P(1_{29}-*co*-2_{111}-*co*-3_{22}) in 0.1 M PBS buffer below and above T_{cp} (7 °C), transmission channel shown.

Therefore, an aqueous solution of **P(1_{29}-*co*-2_{111}-*co*-3_{22})** phase separates into a phase consisting of perfectly spherical droplets, a so-called coacervate phase, and a polymer poor aqueous phase upon heating. This is in sharp contrast to known systems such as P(NIPAM) which precipitates upon heating into solid particles of irregular form and size.[6] Performing the same experiment again in 0.1 M PBS buffer further supports the thesis of the coacervate formation. Figure 6.10, c shows the transmission picture of a solution of **P(1_{29}-*co*-2_{111}-*co*-3_{22})** in 0.1 PBS (10 g L^{-1}) again below and above T_{cp}. Under these conditions, the formed droplets show a strong tendency to coagulate due to the higher interfacial energy created by the more hydrophilic aqueous environment.

Summary and Conclusion

To conclude, we successfully performed the first organocatalytic anionic ring-opening terpolymerization of 2-alkyl-2-oxo-1,3,2-dioxaphospholanes. The terpolymerization proceeded randomly with excellent control over molecular weights (6,600 g mol^{-1} up to 21,000 g mol^{-1}), terpolymer composition and rather narrow molecular weight distributions. This lays the foundation for even more sophisticated polymer architectures and functionalities without loss of control over the polymerization. Radical thiol-ene modification of the pendant double bonds proceeded within 30 min to full conversion. All unmodified terpolymers were water-soluble even at high concentrations (up to 10 g L^{-1}) and showed phase separation at elevated temperatures (6 - 30 °C), whereas the cysteine-modified terpolymers stayed soluble even at high temperatures. The phase separation temperature was adjustable by variation of the molecular weight and the terpolymer composition. The terpolymers formed a polymer rich coacervate phase upon phase separation which is a prominent candidate for future applications as fully degradable carrier systems. Further studies investigating this interesting phase-separation behavior are currently in progress to elucidate the influence of several external and intrinsic parameters on the phase separation.

Acknowledgment

The authors acknowledge support from the “Deutsche Forschungsgemeinschaft” (DFG WU 750/ 6-1). The authors thank Angelika Manhart for synthetic assistance.

References:

1 H. Maeda, J. Wu, T. Sawa, Y. Matsumura, K. Hori, *J. Control. Release, **2000,** 65, 271-84.*
2 B. Kang, T. Opatz, K. Landfester, F.R. Wurm, *Chem. Soc. Rev.*, **2015,** 44, 8301-25.
3 M. Karimi, P. Sahandi Zangabad, A. Ghasemi, M. Amiri, M. Bahrami, H. Malekzad, H. Ghahramanzadeh Asl, Z. Mahdieh, M. Bozorgomid, A. Ghasemi, M.R. Rahmani Taji Boyuk, M.R. Hamblin, ACS Appl. Mater. Interfaces, **2016,** 8, 21107-33.
4 F. Meng, Z. Zhong, J. Feijen, *Biomacromolecules*, **2009,** 10, 197-209.
5 R. Arshady, Polym. Engin. Sci., **1990,** 30, 905-914.
6 X.C. Yin, H.D.H. Stover, *Macromolecules,* **2003,** 36, 9817-9822.
7 X. Yang, N. Gao, L.D. Hu, J.L. Li, Y.B. Sun, *J. Food Engin.*, **2015,** 161, 87-93.
8 L. Muthuselvi, A. Dhathathreyan, B., *Biointerfaces,* **2006,** 51, 39-43.
9 H. Feil, Y.H. Bae, J. Feijen, S.W. Kim, *Macromolecules*, **1993,** 26, 2496-2500.

10 C. de Las Heras Alarcon, S. Pennadam, C. Alexander, *Chem. Soc. Rev*., **2005,** 34, 276-85.
11 D. Schmaljohann, *Adv. drug deliv. rev*., **2006,** 58, 1655-70.
12 Y. Lu, A.A. Aimetti, R. Langer, Z. Gu, *Nature Rev. Mat.*, **2016,** 2, 16075.
13 W. Park, S.J. Park, S. Cho, H. Shin, Y.S. Jung, B. Lee, K. Na, D.H. Kim, *J. Am. Chem. Soc*., **2016,** 138, 10734-7.
14 J.P. Swanson, L.R. Monteleone, F. Haso, P.J. Costanzo, T.B. Liu, A. Joy, *Macromolecules,* **2015,** 48, 3834-3842.
15 F. Ramirez-Crescencio, A.E. Enciso, M. Hasan, V.C. da Costa, O. Annunziata, R. Redon, J.L. Coffer, E.E. Simanek, *Molecules,* **2016,** 21, 599.
16 T. Maeda, M. Takenouchi, K. Yamamoto, T. Aoyagi, Polymers **2009,** 41, 181-188.
17 J.P. Swanson, M.R. Martinez, M.A. Cruz, S.G. Mankoci, P.J. Costanzo, A. Joy, *Polym. Chem*., **2016,** 7, 4693-4702.
18 W.B. Liechty, D.R. Kryscio, B.V. Slaughter, N.A. Peppas, *An. rev. chem. biomol. engin.*, **2010,** 1, 149-73.
19 F.M. Veronese, G. Pasut, *Drug Discov. Today*, **2005,** 10, 1451-8.
20 E.M. Pelegri-O'Day, E.W. Lin, H.D. Maynard, T, *J. Am. Chem. Soc.*, **2014,** 136, 14323-32.
21 K. Knop, R. Hoogenboom, D. Fischer, U.S. Schubert, *Angew. Chem. Int. Ed.*, **2010,** 49, 6288-308.
22 R.P. Garay, R. El-Gewely, J.K. Armstrong, G. Garratty, P. Richette, *Expert Opin. Drug Deliv.*, **2012,** 9, 1319-23.
23 J.J. Verhoef, J.F. Carpenter, T.J. Anchordoquy, H. Schellekens, *Drug Discov. Today*, **2014,** 19, 1945-52.
24 J.K. Armstrong, G. Hempel, S. Koling, L.S. Chan, T. Fisher, H.J. Meiselman, G. Garratty, *Cancer*, **2007,** 110, 103-11.
25 N.J. Ganson, S.J. Kelly, E. Scarlett, J.S. Sundy, M.S. Hershfield, *Arthritis Res. Ther.*, **2006,** 8, R12.
26 M. Bauer, C. Lautenschlaeger, K. Kempe, L. Tauhardt, U.S. Schubert, D. Fischer, *Macromol. Biosci.*, **2012,** 12, 986-98.
27 R. Luxenhofer, Y. Han, A. Schulz, J. Tong, Z. He, A.V. Kabanov, R. Jordan, *Macromol Rapid Commun*, **2012,** 33, 1613-31.
28 T. Steinbach, F.R. Wurm, *Biomacromolecules*, **2016,** 17, 3338-3346.
29 R. Duncan, M.J. Vicent, *Adv. drug deliv. rev.*, **2013,** 65, 60-70.
30 G. Łapienis, S. Penczek, *J. Polym. Sci.: Polyme. Chem. Ed.*, **1977,** 15, 371-382.
31 G. Lapienis, S. Penczek, J. Pretula, *Macromolecules*, **1983,** 16, 153-158.
32 S. Penczek, A. Duda, K. Kaluzynski, G. Lapienis, A. Nyk, R. Szymanski, *Makromolekulare Chemie. Macromolecular Symposia*, **1993,** 73, 91-101.
33 F. Zhang, S. Zhang, S.F. Pollack, R. Li, A.M. Gonzalez, J. Fan, J. Zou, S.E. Leininger, A. Pavia-Sanders, R. Johnson, L.D. Nelson, J.E. Raymond, M. Elsabahy, D.M. Hughes, M.W. Lenox, T.P. Gustafson, K.L. Wooley, *J. Am. Chem. Soc.*, **2015,** 137, 2056-66.
34 Y.H. Lim, K.M. Tiemann, G.S. Heo, P.O. Wagers, Y.H. Rezenom, S. Zhang, F. Zhang, W.J. Youngs, D.A. Hunstad, K.L. Wooley, ACS Nano **2015,** 9, 1995-2008.
35 S. Zhang, H. Wang, Y. Shen, F. Zhang, K. Seetho, J. Zou, J.S. Taylor, A.P. Dove, K.L. Wooley, *Macromolecules*, **2013,** 46, 5141-5149.
36 S. Zhang, A. Li, J. Zou, L.Y. Lin, K.L. Wooley, *ACS macro lett.*, **2012,** 1, 328-333.

37 Y. Iwasaki, E. Yamaguchi, *Macromolecules*, **2010,** 43, 2664-2666.
38 A. Tamura, M. Tokunaga, Y. Iwasaki, N. Yui, *Macromol. Chem. Phys.*, **2014,** 215, 648-653.
39 T. Steinbach, R. Schröder, S. Ritz, F.R. Wurm, *Polym. Chem.*, **2013,** 4, 4469.
40 T. Steinbach, S. Ritz, F.R. Wurm, *ACS macro lett.*. **2014,** 3, 244-248.
41 T. Steinbach, C. Wahlen, F.R. Wurm, *Polym. Chem.*, **2015,** 6, 1192-1202.
42 T. Wolf, T. Steinbach, F.R. Wurm, *Macromolecules*, **2015,** 48, 3853-3863.
43 T. Wolf, J. Nass, F.R. Wurm, *Polym. Chem.*, **2016,** 7, 2934-2937.
44 G. Becker, L.M. Ackermann, E. Schechtel, M. Klapper, W. Tremel, F.R. Wurm, *Biomacromolecules*, **2017**.
45 T. Steinbach, F.R. Wurm, *Angew. Chem. Int. Ed.*, **2015,** 54, 6098-108.
46 H. Lin, T. Wolf, F.R. Wurm, M.A. Kelland, *Energy & Fuels*, **2017**.
47 S. Cho, G.S. Heo, S. Khan, A.M. Gonzalez, M. Elsabahy, K.L. Wooley, *Macromolecules*, **2015,** 48, 8797-8805.
48 K.V. Fastnacht, S.S. Spink, N.U. Dharmaratne, J.U. Pothupitiya, P.P. Datta, E.T. Kiesewetter, M.K. *ACS macro lett*., **2016,** 5, 982-986.
49 A.P. Dove, *ACS macro lett*., **2012,** 1, 1409-1412.
50 N.E. Kamber, W. Jeong, R.M. Waymouth, R.C. Pratt, B.G. Lohmeijer, J.L. Hedrick, *Chem. Rev.*, **2007,** 107, 5813-40.

Supporting Information for

Thermoresponsive coacervate formation of random poly(phosphonate) terpolymers

Materials

Solvents and chemicals were purchased from Acros Organics, Sigma Aldrich or Fluka and used as received unless otherwise stated. All chemicals were purchased in highest purities, dry and stored over molecular sieve (4Å), if possible. 2-(Benzyloxy)ethanol was purchased from ABCR, distilled from calcium hydride and stored over molecular sieve (4Å) and under argon before use. DBU was purchased from Sigma Aldrich, distilled before use and stored over molecular sieve (4Å) under argon. Deuterated solvents were purchased from Deutero GmbH (Kastellaun, Germany) and used as received.

Instrumentation and Characterization Techniques

Size exclusion chromatography (SEC) measurements were performed in DMF (1 g L^{-1} LiBr added) at 60 °C and a flow rate of 1 mL min^{-1} with a PSS SECcurity as an integrated instrument, including a PSS GRAM 100-1000 column and a refractive index (RI) detector. Calibration was carried out using poly(ethylene glycol) standards provided by Polymer Standards Service. The ^{1}H, $^{13}C\{H\}$, and $^{31}P\{H\}$ NMR experiments were acquired on a 500 MHz Bruker AMX system. The temperature was kept at 298.3K and calibrated with a standard ^{1}H methanol NMR sample using the topspin 3.0 software (Bruker). $^{13}C\{H\}$ NMR spectra were referenced internally to solvent signals. $^{31}P\{H\}$ NMR spectra were referenced externally to phosphoric acid. The $^{13}C\{H\}$ NMR (125 MHz) and $^{31}P\{H\}$ NMR (201 MHz) measurements were obtained with a ^{1}H powergate decoupling method using 30 ° degree flip angle. 2D NMR experiments (^{1}H DOSY (Diffusion ordered spectroscopy)) were measured on a Bruker 500 AMX NMR spectrometer under the same conditions as mentioned above. All spectra were processed with the MestReNova 9.0.1-13254 software. Differential Scanning Calorimetry (DSC) measurements were performed using a Mettler-Toledo DSC823 thermal analysis system in the temperature range from -80 to 50 °C under nitrogen with a heating rate of 10 °C min^{-1}. Cloud points were determined in

ultrapure water with a resistivity of 18 MΩ cm^{-1}, or Dulbecco's phosphate buffered saline, respectively and detected by the optical transmittance of a light beam (λ = 500 nm) through a 1 cm sample cell. The measurements were performed on a Jasco V-630 photo spectrometer with a Jasco ETC-717 Peltier element. The intensity of the transmitted light was recorded versus the temperature of the sample cell. The heating/cooling rate was 1 °C min^{-1} and values were recorded every 0.1 °C. Confocal laser scanning microscopy was performed with an LSM SP5 STED Leica Laser Scanning Confocal Microscope (Leica, Germany), consisting of an inverse fluorescence microscope DMI 6000 CS equipped with a multi-laser combination and five detectors operating in the range of 400-800.

Experimental

Ethylphosphonic acid dichloride: The compound was synthesized according to literature protocol.[42] Briefly, *O,O*-diethyl ethylphosphonic acid diester (100.0 g, 0.6 mol) and DMF (0.5 mL) was added drop wise to refluxing thionylchloride (180 mL, 1.5 mol). Strong gas evolution of methylene chloride and sulfur dioxide indicated the progress of the reaction. After 24h the gas evolution declined. Fractionated distillation of the raw product yielded the desired dichloride as a colorless liquid (yield: 80%, b.p. 92 °C / 6 mbar). ^{1}H NMR ($SOCl_2$, ppm): δ = 3.37 (dq, $^{2}J_{HP}$ = 15 Hz, $^{3}J_{HH}$ = 7.5 Hz, 2H), 2.18 (dt, $^{3}J_{HP}$ = 30 Hz, $^{3}J_{HH}$ = 7.5 Hz, 3H). $^{13}C\{H\}$ NMR ($CDCl_3$, ppm): δ = 37.42 (d, $^{1}J_{CP}$ = 98.3 Hz), 8.26 (d, $^{1}J_{CP}$ = 7.6 Hz). $^{31}P\{H\}$ NMR ($SOCl_2$, ppm): δ = 54.72.

2-Ethyl-2-oxo-1,3,2-dioxaphospholane (1): The compound was synthesized according to literature protocol.[42] Briefly, a flame-dried three-necked round-bottom flask, equipped with a magnetic stirring bar and two dropping funnels, was charged with 250 mL dry THF and cooled to -21 °C. Ethyl phosphonic acid dichloride (46.8 g, 0.3 mol) was dissolved in dry THF (250 mL) and transferred into one dropping funnel via a flame-dried stainless steel capillary. A solution of dry ethylene glycol (19.8 g, 0.3 mol) and dry pyridine (50.6 g, 0.6 mol) in THF (250 mL) was transferred into the second dropping funnel via a flame-dried stainless steel capillary. Dropping speed was adjusted to be approximately equal for both mixtures. After complete addition the solution was stirred for 3h and kept over-night

at -28 °C to facilitate the precipitation of the pyridinium hydrochloride byproduct. The precipitate was removed by filtration via a flame-dried Schlenk funnel, and the solvent was removed under reduced pressure. Fractionated distillation yielded the desired product as colorless oil (yield: 71%, b.p. 85 °C / 1x10^{-3} mbar). ^{1}H NMR ($CDCl_3$, ppm): δ 4.53 - 4.35 (m, 2H, -P-O-CH_2-), 4.29 - 4.15 (m, 2H, -P-O-CH_2-), 1.94 (dq, $^{2}J_{HP}$ = 17.5 Hz, $^{3}J_{HH}$ = 7.7 Hz, 2H, -P-CH_2-), 1.16 (dt, $^{3}J_{HP}$ = 21.0 Hz, $^{3}J_{HH}$ = 7.7 Hz, 3H, -CH_3). ^{13}C{H} NMR ($CDCl_3$, ppm): δ 66.86 (s, -P-O-C-), 19.34 (d, $^{1}J_{CP}$ = 132.9 Hz, -P-C-), 7.28 (d, $^{2}J_{CP}$ = 7.1 Hz, -C). ^{31}P{H} NMR ($CDCl_3$, ppm): δ 52.2.

***O,O*-di-*n*-Butyl-*n*-butyl phosphonic acid diester:** The compound was synthesized according to literature protocol.[42] Briefly tri-*n*-butyl phosphite (138.6 g, 0.5 mol) and 1-iodobutane (51.7 g, 0.25 mol) were refluxed in a 500 mL round-bottom flask equipped with a reflux condenser at 160 °C for 1.5 h. Fractionated distillation yielded the desired product as a colorless liquid (yield: 99%, b.p. 133 °C / 20 mbar). ^{1}H NMR ($CDCl_3$, ppm): δ 4.07 - 3.91 (m, 4H), 1.77 - 1.69 (m, 2H), 1.66 - 1.65 (m, 6H), 1.46 - 1.30 (m, 6H), 0.91 (t, 3JHH = 7.2 Hz, 9H). ^{13}C{H} NMR ($CDCl_3$, ppm): δ 65.15 (d, $^{2}J_{COP}$ = 5.3 Hz), 31.61 (s), 25.23 (d, $^{1}J_{CP}$ = 105 Hz), 24.48 (d, $^{2}J_{CP}$ = 3.7 Hz), 3.71 (d, $^{3}J_{CP}$ = 12.7 Hz), 18.80 (s), 13.70 (s). ^{31}P{H} NMR ($CDCl_3$, ppm): δ 32.72.

***n*-Butyl phosphonic acid dichloride:** The compound was synthesized according to literature protocol.[42] Briefly, a 100 mL two-headed round-bottom flask was equipped with a reflux condenser and *O,O*-di-*n*-butyl-*n*-butyl phosphonic acid diester (9.2 g, 0.04 mol) was provided. The flask was heated to 150 °C and phosphorus pentachloride (15.4 g, 0.08 mol) was added carefully in small portions. A vigorous gas and heat evolution indicated the progress of the reaction. After complete addition the reaction was heated for another 1 h. Fractionated distillation yielded the desired product as a colorless liquid (yield: 60%, b.p. 103 °C / 14 mbar). ^{1}H NMR ($CDCl_3$, ppm): δ 2.68 - 2.49 (m, 2H), 1.90 - 1.72 (m, 2H), 1.51 (h, $^{3}J_{HH}$ = 7.3 Hz, 2H), 0.96 (t, 3JHH = 7.3 Hz, 3H). ^{13}C{H} NMR ($CDCl_3$, ppm): δ 42.69 (d, $^{1}J_{CP}$ = 96.7 Hz), 24.87 (d, $^{2}J_{CP}$ = 6.6 Hz), 22.81 (d, $^{3}J_{CP}$ = 22.1 Hz), 13.41 (d, $^{4}J_{CP}$ = 1.5 Hz), 3.71 (d, $^{3}J_{CP}$ = 12.7 Hz), 18.80 (s), 13.70 (s). ^{31}P{H} NMR ($CDCl_3$, ppm): δ 51.5.

2-*n*-Butyl-2-oxo-1,3,2-dioxaphospholane (2): The compound was synthesized according to literature protocol.[42] Briefly, a flame-dried three-necked round-bottom flask, equipped with a magnetic stirring bar and two dropping funnels, was charged with 250 mL dry THF and cooled to -21 °C. *n*-Butyl phosphonic acid dichloride (15.9 g, 0.09 mol) was dissolved in dry THF (250 mL) and transferred into one dropping funnel via a flame-dried stainless steel capillary. A solution of dry ethylene glycol (5.6 g, 0.09 mol) and dry pyridine (14.4 g, 0.18 mol) in THF (250 mL) was transferred into the second dropping funnel via a flame-dried stainless steel capillary. Dropping speed was adjusted to be approximately equal for both mixtures. After complete addition the solution was stirred for 5h and kept over-night at -28 °C to facilitate the precipitation of the pyridinium hydrochloride byproduct. The precipitate was removed by filtration via a flame-dried Schlenk funnel, and the solvent was removed under reduced pressure. Fractionated distillation yielded the desired product as colorless oil (yield: 77%, b.p. 90 °C / 1x10^{-3} mbar). ^{1}H NMR ($CDCl_3$, ppm): δ 4.47 - 4.33 (m, 2H, -P-O-CH_2-), 4.27 - 4.14 (m, 2H, -P-O-CH_2-), 1.94 -1.80 (m, 2H), 1.63 - 1.47 (m, 2H), 1.36 (h, $^{3}J_{HH}$ = 7.3 Hz, 2H), 0.85 (t, $^{3}J_{HH}$ = 7.3 Hz, 3H, -CH_3). ^{13}C{H} NMR ($CDCl_3$, ppm): δ 66.16 (s, -P-O-C-), 25.40 (d, $^{1}J_{CP}$ = 117.0 Hz, -P-C-), 24.5 (d, $^{2}J_{CP}$ = 8.2 Hz), 23.47 (d, $^{3}J_{CP}$ = 16.7 Hz), 13.44 (s, -C). ^{31}P{H} NMR ($CDCl_3$, ppm): δ 51.7.

***O,O*-diethyl Allyl phosphonic acid diester:** Triethyl phosphite (194.50 g, 1.17 mol) and allyl bromide (173.00 g, 1,43 mol) were heated at 71 °C for 23h in a round-bottom flask equipped with a dean-stark receiver to collect the formed bromoethane. Fractionated distillation of the mixture yielded the desired phosphonic acid diester as a colorless liquid. (yield: 93%, bp 60-62 °C / 4 mbar). ^{1}H NMR ($CDCl_3$, 500 MHz, 298K, ppm): δ = 5.82 – 5.66 (m, 1H, -C**H**=CH_2), 5.22 – 5.08 (m, 1H, -CH=C**H$_2$**), 4.13 – 43.97 (m, 4H, -P-O-C**H$_2$**-), 2.55 (ddt, 2H, $^{2}J_{HP}$ = 21.9 Hz, $^{2}J_{HH}$ = 7.4 Hz, $^{3}J_{HH}$ = 1.3 Hz, -P-C**H$_2$**-), 1.26 (t, 6H, $^{3}J_{HH}$ = 7.1 Hz, -O-CH_2-C**H$_3$**). ^{13}C{H} NMR ($CDCl_3$, 125 MHz, 298K, ppm): δ = 127.49 (s, -C=**C**), 119.73 (d, $^{2}J_{CP}$ = 16.5 Hz)-**C**=C), 61.79 (s, -P-O-**C**-), 31.66 (d, 1JCP = 137.5 Hz, P-**C**-), 16.27 (s, -O-C-**C**). ^{31}P{H} NMR ($CDCl_3$, 201 MHz, 298K, ppm): δ = 26.90

Allyl phosphonic acid dichloride: In a flame-dried 100 mL Schlenk-flask under argon, *O, O*-diethyl allyl phosphonic acid diester (50.00 g, 0.30 mol) was dissolved in acetonitrile (400 mL). Dry sodium iodide (84.00 g, 0.60 mol) was added. The Schlenk-flask was equipped with a dropping funnel, and chloro trimethyl silane (136.00 g, 1.20 mol) was added dropwise at room temperature. After complete addition, the reaction was heated to 40 °C for 2h. $^{31}P\{H\}$ NMR analysis of the crude reaction mixture confirmed the formation of *O, O*-bis(trimethyl)silyl allyl phosphonic acid diester. $^{31}P\{H\}$ NMR ($CDCl_3$, ppm): δ 22.07. Excess of chloro trimethyl silane and solvent were evaporated *in vacuo*. The crude ester was used without further purification. It was dissolved in dichloromethane (100 mL), and DMF (0.5 mL) was added. Oxalyl chloride (102.00 g, 1.20 mol) was added drop-wise at room temperature. After complete addition, the reaction was stirred for 16h. Fractionated distillation yielded the desired product as a colorless liquid (yield: 60%, b.p. 100 °C / 40 mbar). ^{1}H NMR ($CDCl_3$, ppm): δ 5.29 - 5.73 (m, 1H, -C**H**=CH_2), 5.53 - 5.37 (m, 2H, -CH=C**H$_2$**), 3.37 (ddt, $^{2}J_{HP}$ = 19.0 Hz, $^{3}J_{HH}$ = 7.3 Hz, $^{4}J_{HH}$ = 1.1 Hz, 2H, P-C**H$_2$**-). $^{13}C\{H\}$ NMR ($CDCl_3$, ppm): δ 124.57 (d, $^{2}J_{CP}$ = 19.5 Hz, -C=**C**), 124.02 (d, $^{3}J_{CP}$ = 14.7 Hz, -**C**=C), 47.58 (d, $^{1}J_{CP}$ = 97.5 Hz, P-**C**-). $^{31}P\{H\}$ NMR ($CDCl_3$, ppm): δ 46.02.

2-Allyl-2-oxo-1,3,2-dioxaphospholane (4): The cyclic monomer was synthesized according to a modified literature procedure.[40] A flame-dried three-necked round-bottom flask, equipped with a magnetic stirring bar and two dropping funnels, was charged with 250 mL dry THF and cooled to -21 °C. Allyl phosphonic acid dichloride (29.2 g, 0.20 mol) was dissolved in dry THF (250 mL) and transferred into one dropping funnel via a flame-dried stainless steel capillary. A solution of dry ethylene glycol (11.0 g, 0.20 mol) and dry pyridine (29.0 g, 0.40 mol) in THF (250 mL) was transferred into the second dropping funnel via a flame-dried stainless steel capillary. Dropping speed was adjusted to be approximately equal for both mixtures. After complete addition the solution was stirred for 5h and kept over-night at -28 °C to facilitate the precipitation of the pyridinium hydrochloride byproduct. The precipitate was removed by filtration via a flame-dried Schlenk funnel, and the solvent was removed *in vacuo*. Fractionated distillation yielded the desired product as colorless oil (yield: 51%, b.p. 86 °C / $1x10^{-3}$ mbar). ^{1}H NMR ($CDCl_3$, ppm): δ 5.81 - 5.65 (m, 1H, -C**H**=CH_2), 5.33 - 5.17 (m, 2H, -CH=C**H$_2$**), 4.52 - 4.37

(m, 2, H-P-O-C**H$_2$**-), 4.30 - 4.11 (m, 2H, -P-O-C**H$_2$**-), 2.82 (ddt, $^2J_{HP}$ = 22.0 Hz, $^3J_{HH}$ = 7.4 Hz, $^4J_{HH}$ = 1.2 Hz, 2H, -P-C**H$_2$**-). ^{13}C{H} NMR ($CDCl_3$, ppm): δ 126.46 (d, $^2J_{CP}$ = 12.1 Hz, -**C**=C), 121.02 (d, $^3J_{CP}$ = 14.3 Hz, - C=**C**), 66.72 (s, -P-O-**C**-), 31.15 (d, $^1J_{CP}$ = 129.5 Hz, -P-**C**-). ^{31}P{H} NMR ($CDCl_3$, ppm): δ 45.9.

Representative procedure for the terpolymerization of dioxaphospholanes: The respective monomers were weighed into a flame-dried Schlenk-tube, dissolved in dry benzene and dried by three times lyophilization. The monomers were dissolved in dry dichloromethane at a total concentration of 4 mol L^{-1}. A stock solution of the initiator in dry dichloromethane was prepared with a concentration 0.2 mol L^{-1}, and the calculated amount was added to the monomer solution via gas tight syringe (Hamilton®). A stock solution of DBU in dry dichloromethane was prepared with a concentration of 0.2 mol L^{-1}. The monomer solution and the catalyst solution were adjusted to 0 °C. The polymerization was initiated by the addition of the calculated volume of the catalyst solution containing 3.0 equivalents of DBU with respect to the initiator. Polymerization was terminated after 16h by the rapid addition of an excess of formic acid dissolved in dichloromethane with a concentration of 20 mg mL^{-1}. The colorless, amorphous polymers were purified by precipitation in cold diethyl ether, dialyzed against Milli-Q (Millipore®) water and dried at reduced pressure.

Representative NMR data of P(1$_{10}$-*co*-2$_{60}$-*co*-3$_{10}$): ^{1}H NMR (DMSO-d_6, 500 MHz, 298K, ppm): δ = 7.37 - 7.29 (m, aromatic CH), 5.81 - 5.64 (m, side-chain -CH=C**H$_2$**), 5.30 - 5.11 (m, -C**H**=CH_2), 4.85 (t, terminal -O-H), 4.53 (s, aryl-CH_2-), 4.22 - 4.01 (m, backbone -CH_2-CH_2-), 3.63 (t, backbone terminal -CH_2-OH), 2.84 – 2.62 (dd, side-chain, -P-CH_2-C=, $^2J_{HP}$ = 22.0 Hz, $^3J_{HH}$ = 7.4 Hz), 1.84 - 1.70 (m, side-chain -P-CH_2-), 1.63 - 1.26 (m, side-chain -P-CH_2-C**H$_2$**-C**H$_2$**-CH_3), 1.05 (dt, side-chain -P-CH_2-C**H$_3$**, $^3J_{HP}$ = 20.1 Hz, $^3J_{HH}$ = 7.6 Hz), 0.86 (t, side-chain -P-CH_2-CH_2-CH_2-C**H$_3$**, $^3J_{HH}$ = 7.3 Hz). ^{13}C{H} NMR (DMSO-d_6, 125 MHz, 298K, ppm): δ 133.78, 128.80, 127.97 (s, aromatic C), 127.05 (s, side-chain, P-C-**C**=C), 120.88 (s, side-chain, P-C-C=**C**), 64.56 (s, broad, backbone -CH_2-), 60.85 (s, aryl-C-), 30.99 (d, side-chain, P-**C**-C=C, $^1J_{CP}$ = 171,2 Hz), 24.66 (d, side-chain -P-C-, $^1J_{CP}$ = 145.0 Hz), 24.42 (d, side-chain –P-C-**C**-, $^2J_{CP}$ = 5 Hz), 23.41 (d, side-chain -P-C-**C**-**C**-,

$^{3}J_{CP}$ = 16.3 Hz), 18.06 (d, side-chain -P-C-, $^{1}J_{CP}$ = 138.8 Hz), 13.90 (s, side-chain -P-C-C-C-**C**), 6.68 (d, side-chain -P-C-**C**, $^{2}J_{CH}$ = 6.3 Hz). ^{31}P{H} NMR (DMSO-d_6, 201 MHz, 298K, ppm): δ = 34.5, 33.3, 28.1.

Representative thiol-ene modification of P(1_x-*co*-2_y-*co*-3_z) with cysteine: The terpolymer (1 eq in respect to the allyl-groups) was dissolved in DMF (5 mL) and 10 eq of cysteine and 0.3 eq of 2,2-Dimethoxy-2-phenyl acetophenone (DMPA) was added. The mixture was degassed by three freeze-pump-thaw cycles, transferred into an argon flushed quartz-glass cuvette (1 cm x 1 cm), stirred and irradiated at 365 nm at room temperature via a conventional UV lamp for TLC plates for 30 min. Afterwards, the polymer was precipitated three times in cold diethyl ether, dialyzed against Milli-Q (Millipore®) water and dried at reduced pressure.

Representative NMR data of P(1_x-*co*-2_y-*co*-3^{Cys}_z): ^{1}H NMR (DMSO-d_6, 500 MHz, 298K, ppm): δ = 7.37 - 7.29 (m, aromatic CH), 2.94 - 2.69 (m, -S-C**H$_2$**-C**H**-), 4.53 (s, aryl-CH_2-), 4.22 - 4.01 (m, backbone -CH_2-CH_2-), 3.63 (t, backbone terminal -CH_2-OH), 1.84 - 1.70 (m, side-chain -P-CH_2-), 1.63 - 1.26 (m, side-chain -P-CH_2-C**H$_2$**-C**H$_2$**-CH_3), 1.05 (dt, side-chain -P-CH_2-C**H$_3$**, $^{3}J_{HP}$ = 20.1 Hz, $^{3}J_{HH}$ = 7.6 Hz), 0.86 (t, side-chain -P-CH_2-CH_2-CH_2-C**H$_3$**, $^{3}J_{HH}$ = 7.3 Hz). ^{13}C{H} NMR (DMSO-d_6, 125 MHz, 298K, ppm): δ 170.11 (s, -**C**OOH), 133.78, 128.80, 127.97 (s, aromatic C), 64.56 (s, broad, backbone -CH_2-), 60.85 (s, aryl-C-), 24.66 (d, side-chain -P-C-, $^{1}J_{CP}$ = 145.0 Hz), 24.42 (d, side-chain –P-C-**C**-, $^{2}J_{CP}$ = 5 Hz), 23.41 (d, side-chain -P-C-**C**-**C**-, $^{3}J_{CP}$ = 16.3 Hz), 18.06 (d, side-chain -P-C-, $^{1}J_{CP}$ = 138.8 Hz), 13.90 (s, side-chain -P-C-C-C-C), 6.68 (d, side-chain -P-C-C, $^{2}J_{CH}$ = 6.3 Hz). ^{31}P{H} NMR (DMSO-d_6, 201 MHz, 298K, ppm): δ = 34.5, 33.3, 32.69.

Supporting Figures

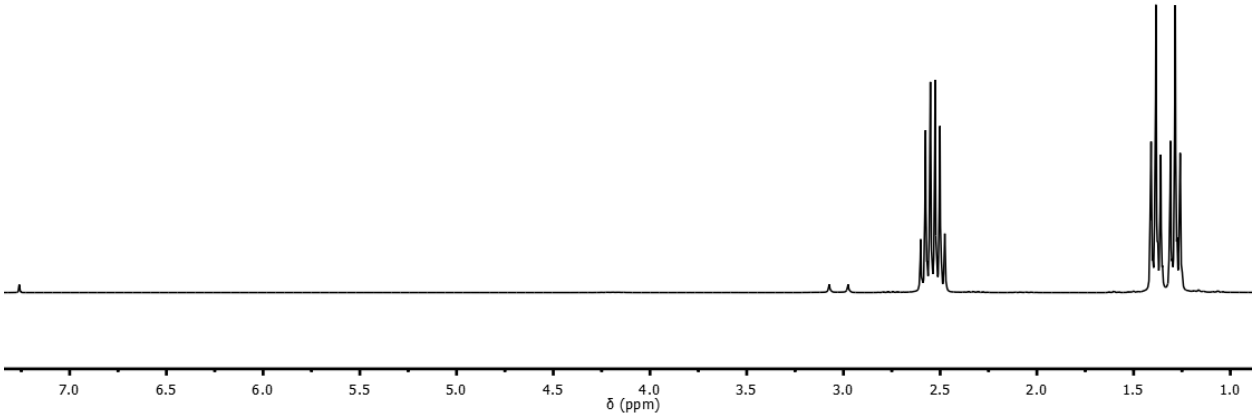

Figure S6.1: ^{1}H NMR (500 MHz) spectrum of ethyl phosphonic acid dichloride in $CDCl_3$ at 298K.

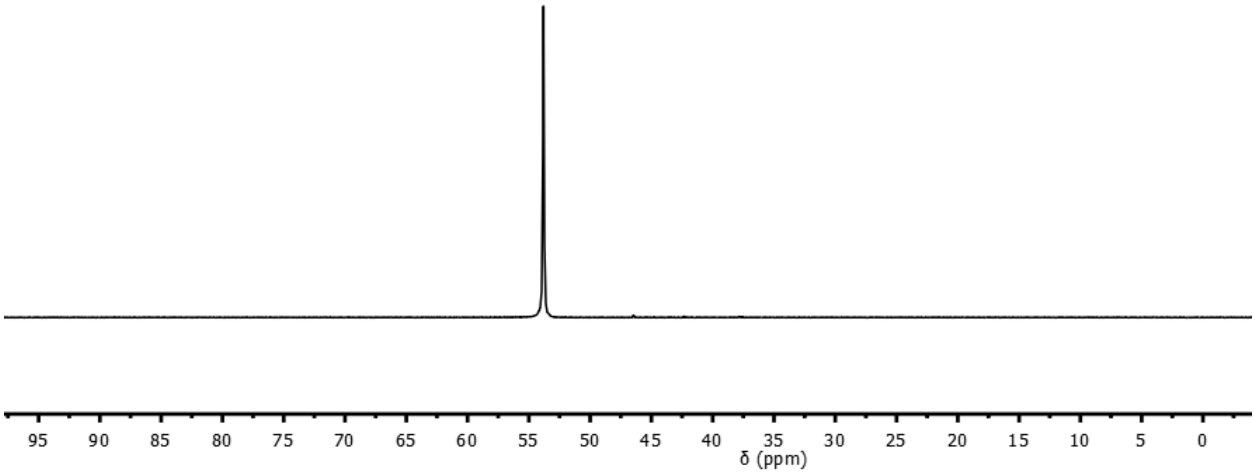

Figure S6.2: ^{31}P NMR (201 MHz) spectrum of ethyl phosphonic acid dichloride in $CDCl_3$ at 298K.

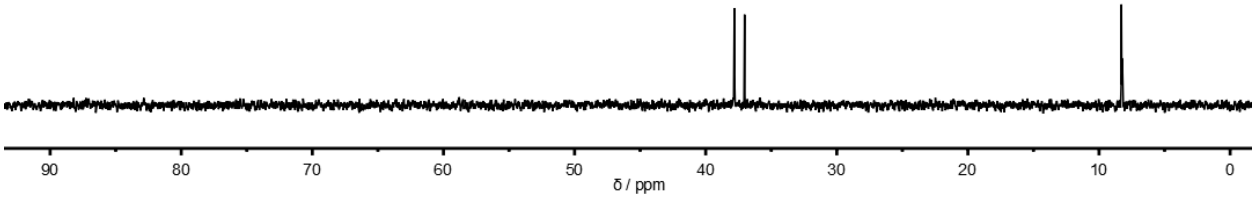

Figure S6.3: ^{31}C NMR (125 MHz) spectrum of ethyl phosphonic acid dichloride in thionyl chloride at 298K.

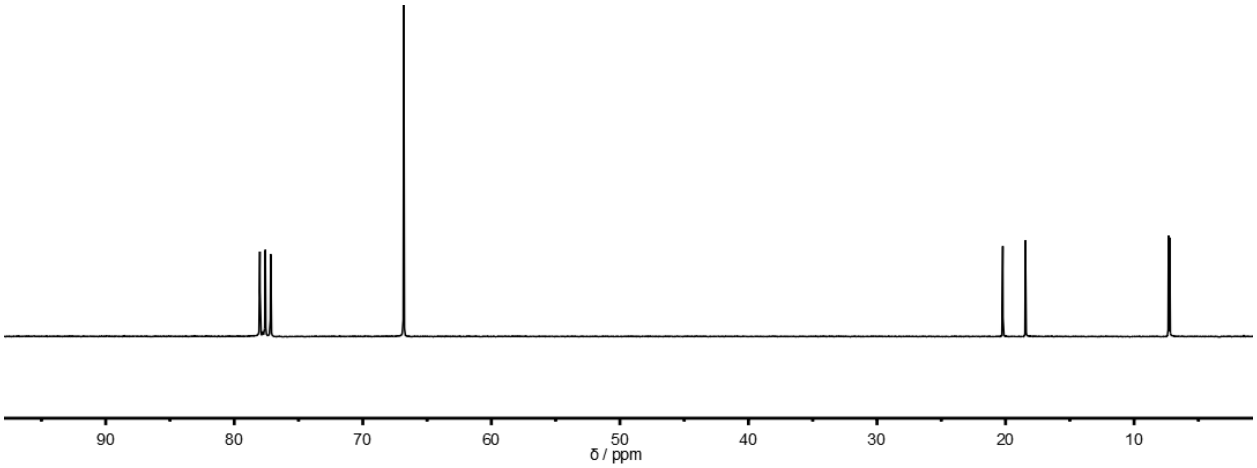

Figure S6.4: ^{13}C NMR (125 MHz) spectrum of 2-ethyl-2-oxo-1,3,2-dioxaphospholane (1) in $CDCl_3$ at 298K.

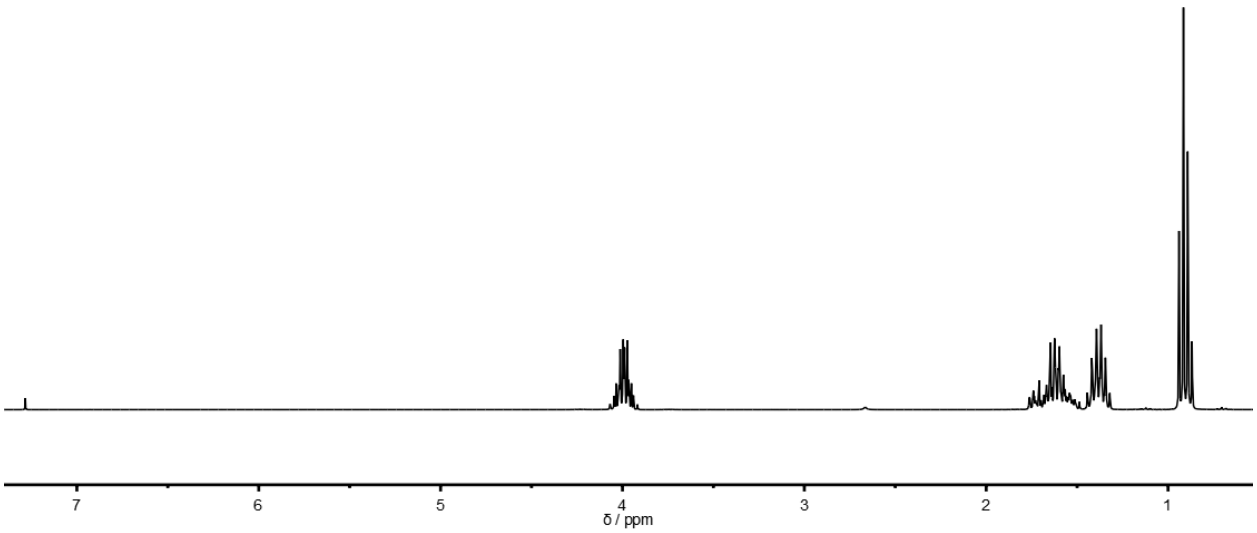

Figure S6.5: ^{1}H NMR (500 MHz) spectrum of *O, O*-di-*n*-butyl *n*-butyl phosphonic acid diester in $CDCl_3$ at 298K.

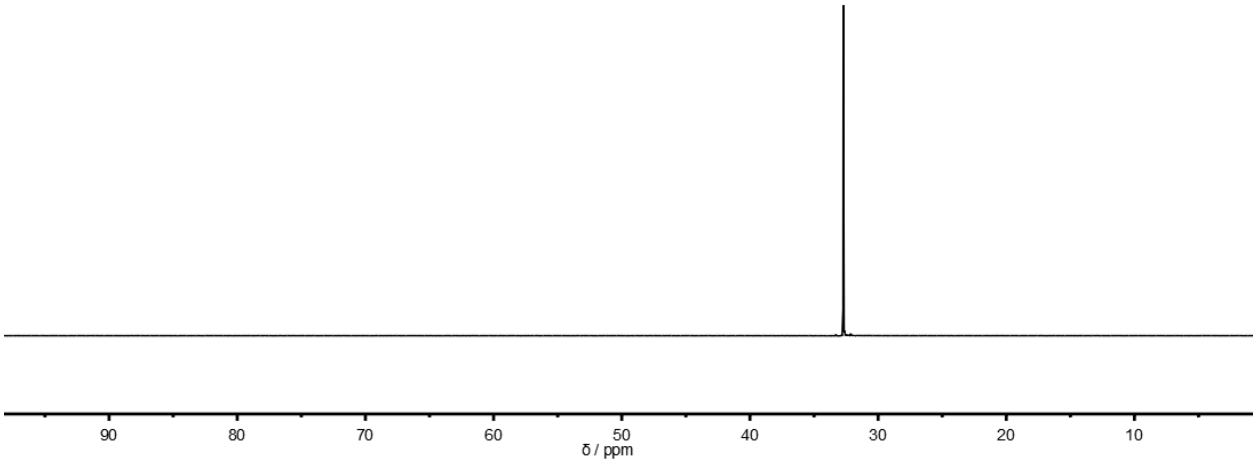

Figure S6.6: ^{31}P NMR (201 MHz) NMR spectrum of *O*, *O*-di-*n*-butyl *n*-butyl phosphonic acid diester in $CDCl_3$ at 298K.

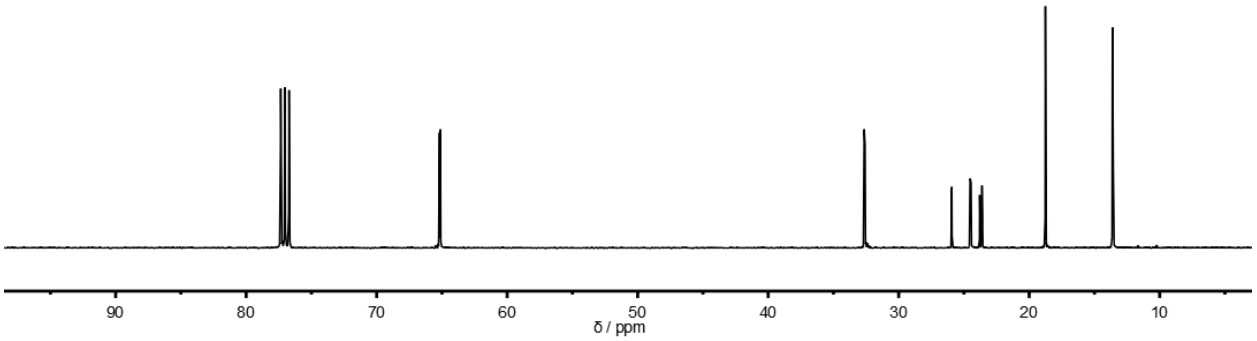

Figure S6.7: ^{13}C (125 MHz) NMR spectrum of *O*, *O*-di-*n*-butyl *n*-butyl phosphonic acid diester in $CDCl_3$ at 298K.

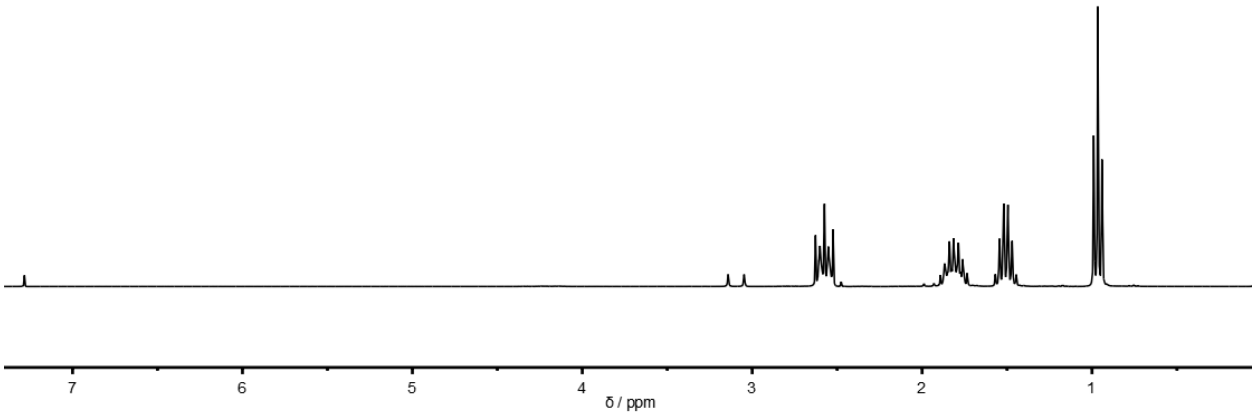

Figure S6.8: ^{1}H (500MHz) NMR spectrum of *n*-butyl phosphonic acid dichloride in $CDCl_3$ at 298K.

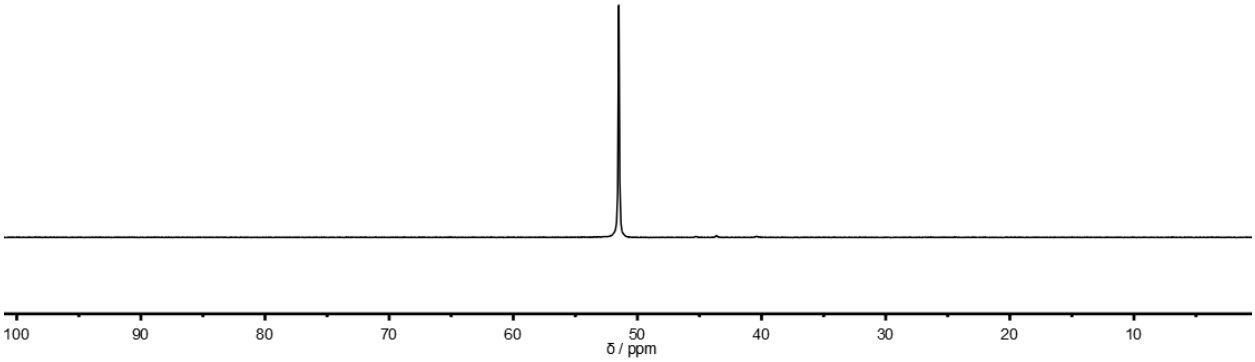

Figure S6.9: ^{31}P (201 MHz) NMR spectrum of *n*-butyl phosphonic acid dichloride in $CDCl_3$ at 298K.

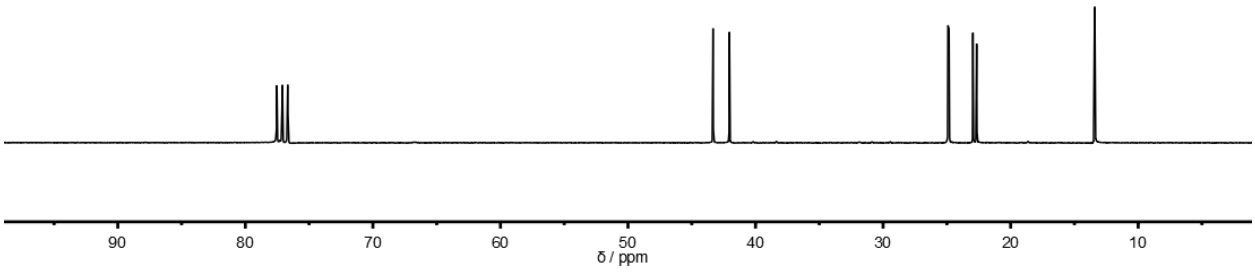

Figure S6.10: ^{13}C (125 MHz) NMR NMR spectrum of *n*-butyl phosphonic acid dichloride in $CDCl_3$ at 298K.

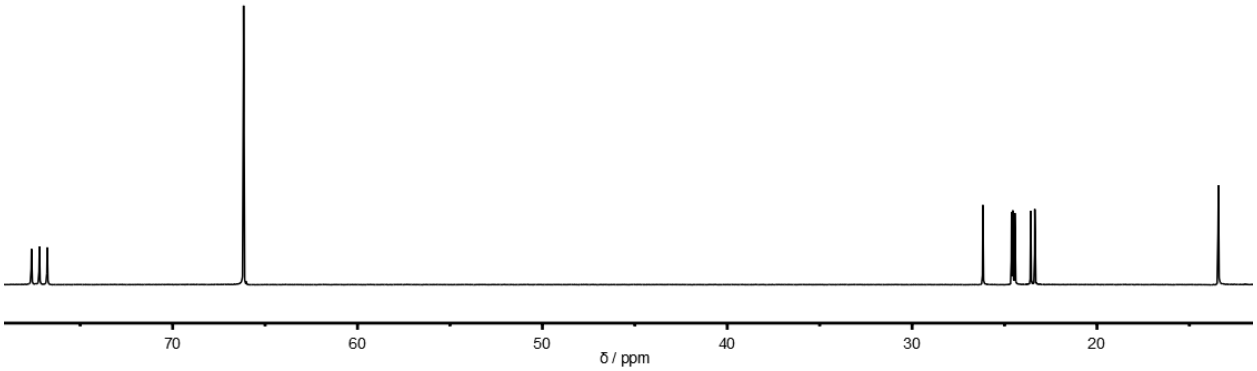

Figure S6.11: ^{13}C (125 MHz) NMR spectrum of 2-*n*-butyl-2-oxo-1,3,2-dioxaphospholane (2) in $CDCl_3$ at 298K.

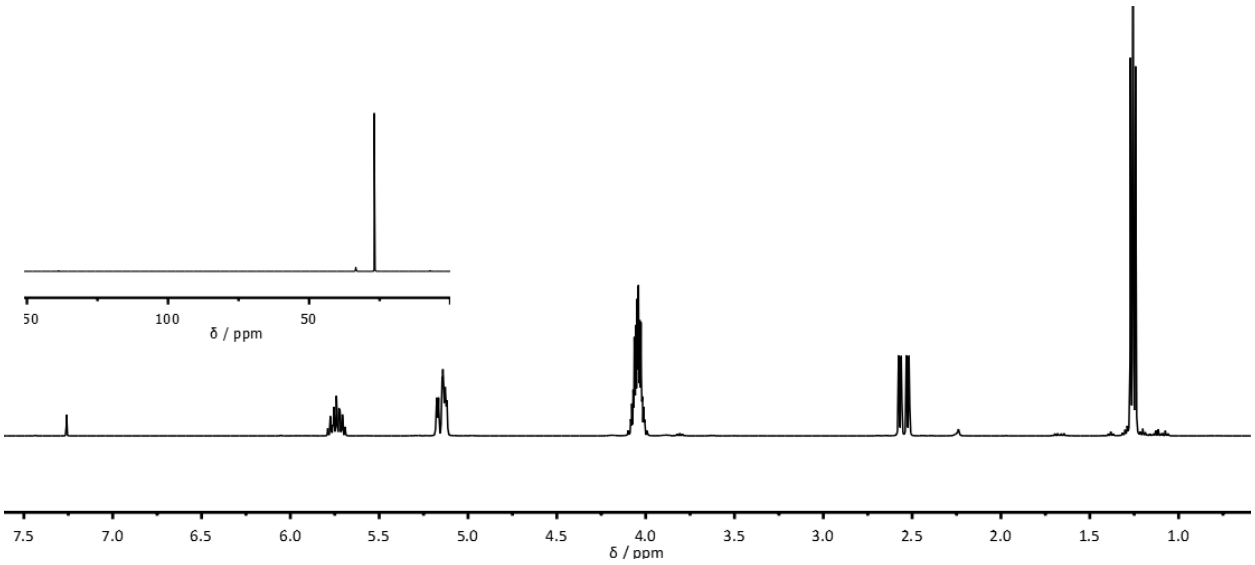

Figure S1.12: ^{1}H NMR (500 MHz) and $^{31}P\{H\}$ NMR (201 MHz) spectra of allyl phosphonic acid diethyl ester in $CDCl_3$ at 298K.

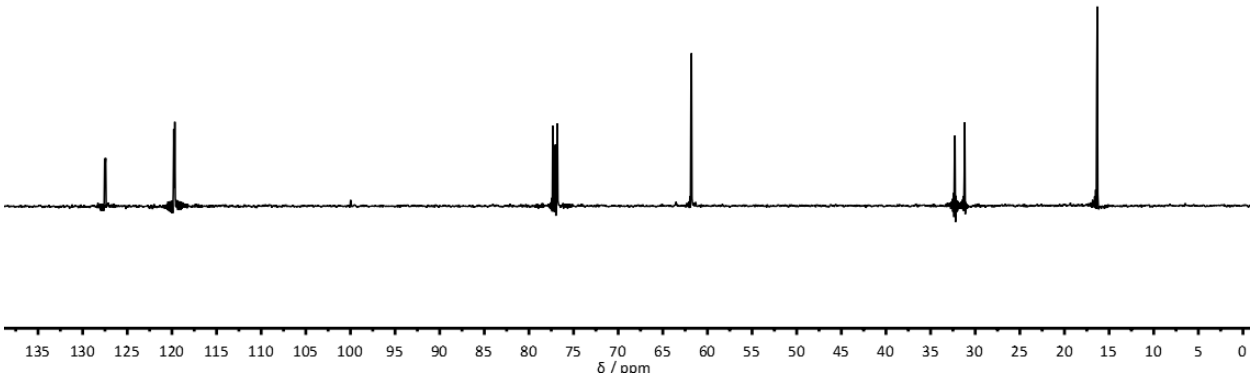

Figure S6.13: ^{13}C NMR (125 MHz) spectra of allyl phosphonic acid diethyl ester in $CDCl_3$ at 298K.

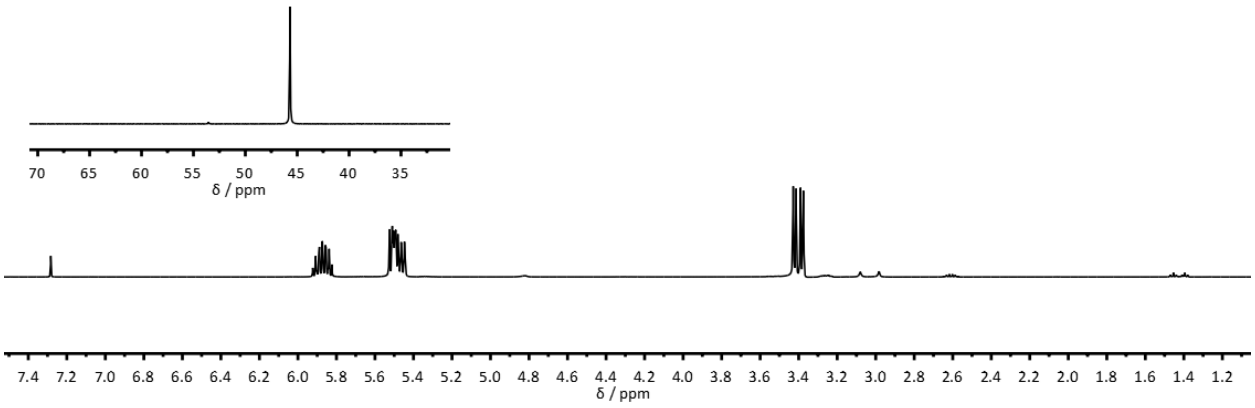

Figure S6.14: ^{1}H NMR (500 MHz) and $^{31}P\{H\}$ NMR (201 MHz) spectra of allyl phosphonic acid dichloride in $CDCl_3$ at 298K.

.

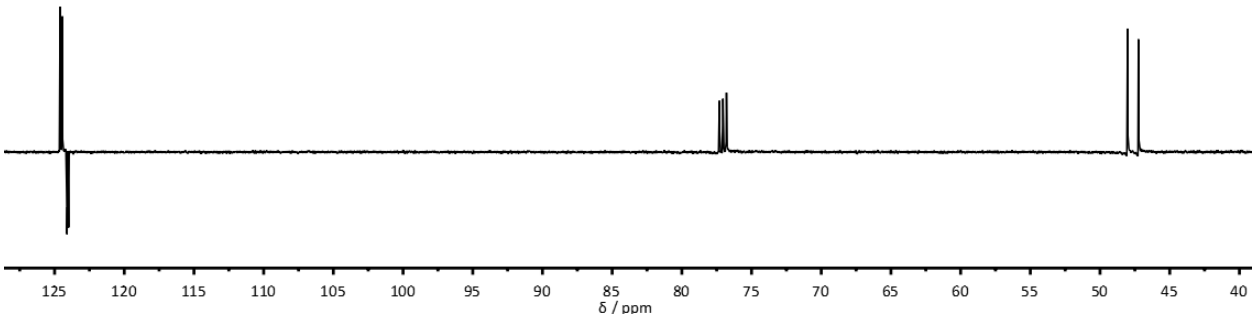

Figure S6.15: ^{13}C NMR (125 MHz) NMR spectrum of allyl phosphonic acid dichloride in $CDCl_3$ at 298K.

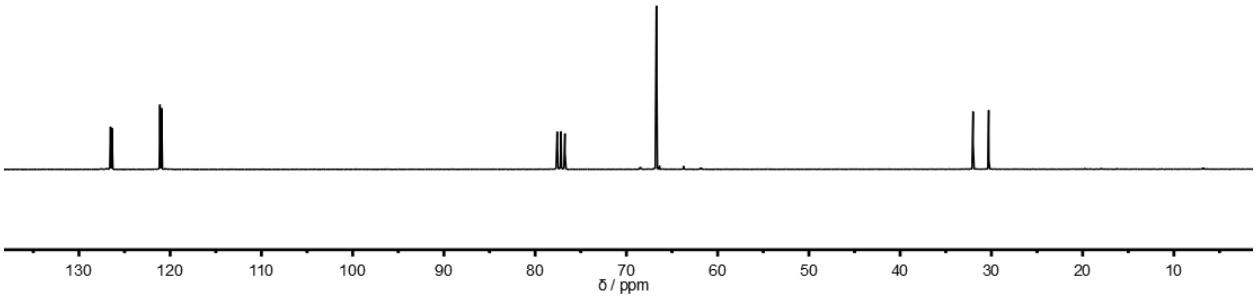

Figure S6.16: ^{13}C NMR (125 MHz) NMR spectrum of 2-allyl-2-oxo-1,3,2-dioxaphospholane (3) in $CDCl_3$ at 298K.

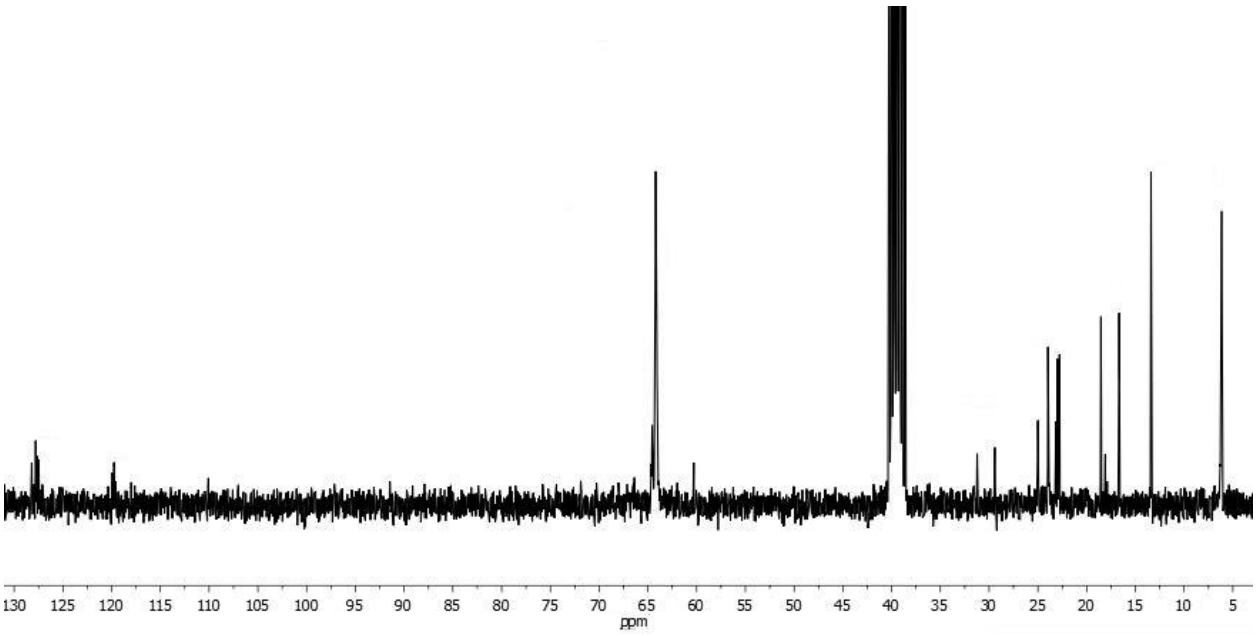

Figure S6.17: ^{13}C NMR (125 MHz) spectrum of P(1_x-*co*-2_y-*co*-3_z) in DMSO-d_6 at 298K.

Chapter 6: Thermoresponsive Coacervate Formation of Random Poly(phosphonate) Terpolymers.

Chapter 6: Thermoresponsive Coacervate Formation of Random Poly(phosphonate) Terpolymers.

The previous chapters introduced the copolymerization of dioxaphospholanes as well as the radical thiol-ene side-chain modification of PPns and focused strongly on the LCST behavior and variation of the LCST phase separation temperature of aqueous solutions of PPn co- and terpolymers. The opposite case of thermal response, UCST behavior in aqueous solutions, is much less frequently observed in the literature but very interesting for biomedical applications.

Therefore, **Chapter 7** combines most of the previously discussed methods (copolymerization, kinetics analysis, side-chain modification and degradation studies), to present amphiphilic, temperature responsive UCST block-copolymer polymersomes. These structures spontaneously assemble at room temperature and disassemble/swell upon increasing the temperature as a model drug delivery system towards regions of elevated temperature, like inflamed or cancerous tissue.

Chapter 7: Degradable Polymersomes with Upper Critical Solution Temperature - Induced Disassembly in Water.

Thomas Wolf[1], Timo Rheinberger[1], Johanna Simon[1], and Frederik R. Wurm[1]

[1]Max Planck-Institut für Polymerforschung, Ackermannweg 10, 55128 Mainz, Germany

Published in: Journal of the American Chemical Society, **2017,** 139, 11064-11072

Keywords: anionic ring-opening polymerization, random copolymerization, block-copolymerization, poly(phosphoester)s, poly(ethylene alkyl phosphonate)s, thiol-ene, UCST-type phase separation, polymersomes, UCST-polymersomes

Chapter 7: Degradable Polymersomes with Upper Critical Solution Temperature Induces Disassembly in Water.

Abstract

Temperature-induced self-assembly of block copolymers allows the formation of smart nano-dimensional structures. Mostly, non-degradable LCST segments are applied to prepare such dynamic aggregates. However, degradable UCST block copolymers that would allow the swelling or even disassembly at elevated temperatures with eventual backbone hydrolysis have not been reported to date. We present the first well-defined degradable poly(phosphonate)s with adjustable UCST. The organocatalytic anionic ring-opening copolymerization of 2-alkyl-2-oxo-1,3,2-dioxaphospholanes provided functional polymers with excellent control over molecular weight and copolymer composition. The pre-polymers were turned into thermoresponsive polymers by thiol-ene modification to introduce pendant carboxylic acids. By this means non-cell-toxic, degradable polymers exhibiting UCST behavior in water between 43 °C and 71 °C were produced. Block copolymers with PEG as a non-responsive water-soluble block can self-assemble into well-defined polymersomes with narrow size distribution. Depending on the responsive block, these structures either swell or disassemble entirely upon an increased temperature.

Introduction

Thermoresponsive polymers change their properties upon a temperature change and typically undergo phase separation from solution. Such materials are currently discussed for the preparation of temperature responsive surfaces, purification procedures or smart drug carriers that release their cargo upon a temperature stimulus.[1-4] To date, polymers with lower critical solution temperature (LCST), such as poly(*N*-isopropyl acrylamide), P(NIPAM), rule the field.[5-9] These polymers phase separate from (aqueous) solution upon heating. Inflamed as well as cancerous tissue, however, exhibits temperatures several degrees above body temperature due to an increased metabolic rate. Therefore, polymers increasing their water-solubility above a specific temperature are of much interest for biomedical applications like drug delivery towards tissue with increased temperature.[10]

However, compared to LCST polymers, fewer polymers have been reported that undergo the opposite upper critical phase separation (UCST) in which a hydrophobic to hydrophilic change occurs upon heating in water. While many systems have been

presented that exhibit UCST behavior in organic solvents or in polymer blends, UCST behavior in water is more uncommon.[11-13]

Temperature sensitive intra- and inter-chain interactions, which break upon heating of the solution, resulting in solubilization of the polymer aggregates, are needed to induce UCST behavior,. Typically, strong H-bonding or Coulomb interactions are utilized for this. Zwitterionic poly(sulfobetaine)s, most commonly poly(sulfobetaine methacrylate, (PSBMA) are examples with UCST in water due to their Coulomb interactions.[14] UCST phase separation on the basis of hydrogen-bond interactions has mainly been investigated in two complementary systems: carboxylic acid bearing polymers like poly(acrylic acid) derivatives and polymers with amide- / urea groups like poly(*N*-acryloyl glycinamide) (PNAGA).[15-25] The latter polymer has already been studied for biomedical applications by several groups.[26,27]

In both cases, H-bond interactions are responsible for temperature responsive aggregation/dissociation of the polymer chains. An increase in temperature decreases the effectiveness of inter- and intra-chain H-bonding and promotes interactions with the highly mobile solvent. In the case of carboxylic acid dimerization, the UCST depends on salt concentration, and pH value as the dissociation state of the acid and electrolyte interactions influence the overall H-bonding.[28-29] In addition to polymers showing either LCST of UCST behavior in water, there are some that show both transitions which are termed “schizophrenic polymers”. They usually combine a fine hydrophilic-hydrophobic balance of side-chains needed for LCST behavior together with electrostatic or H-bonding interactions used to induce UCST behavior.[30-31] A recent example by Zhang *et al*. presented block copolymers with a P(NIPAM) block and a multi-responsive block containing, among others, H-bond forming *p*oly(N-acryloyl glycine) groups providing UCST properties.[32] This is a wonderful example of H-bonding dependent schizophrenic polymers forming complex structures in water depending on the temperature.

A significant disadvantage of most presented UCST (and LCST) polymers is, however, their inherent non-degradability. To date, most of the presented polymers are based on polymerization of vinyl monomers resulting in a non-hydrolysable and mostly non-biodegradable backbone. One exception was presented by Loh *et al*. in the form of supramolecular UCST hydrogels composed of bio-degradable polyglycerol sebacate

backbone from which acrylic monomers were grafted via ATRP which makes the majority of the polymer material non-degradable.[33] A fully degradable UCST polymer was presented by Wang *et al*., who synthesized bio-degradable poly(vinyl acetate-co-vinyl alcohol) backbones and grafted degradable poly(*p*-dioxanone) onto the backbone.[34] While being fully bio-degradable, however, the degradation of PVA is known to be very slow as no hydrolysis of the C-C backbone can take place. Adequately fast degradation in aqueous medium is essential to reduce the risk of accumulation of polymeric material, either in the body after repeated administrations or in the environment. Consequently, only a few systems are known that utilize UCST phase separation behavior for smart drug carriers.[32, 35-37]

To overcome this disadvantage, we chose poly(phosphoester)s as a platform for our system due to their inherent hydrolytic- and bio-degradability as well as diversity in pendant groups.[38,39] The organocatalytic anionic ring-opening polymerization (AROP) of 2-alkyl-2-oxo-1,3,2-dioxaphospholanes allowed us to synthesize well-defined, hydrolytically degradable poly(ethylene alkyl phosphonate)s.[40-42] In this work, we expand this platform towards the side-chain functional cyclic phosphonate monomer, 2-allyl-2-oxo-1-3-2-dioxaphospholane **(2)**. AROP and copolymerization with 2-ethyl-2-oxo-1,3,2-dioxaphospholane provided excellent control over molecular weight, copolymer composition, and narrow molecular weight distributions. These poly(ethylene alkyl phosphonate)s are water-soluble and have an adjustable number of allylic double bonds along the polymer backbone. In analogy to the work of Tunca *et al.* a simple, fast and efficient radical post-polymerization thiol-ene reaction was used to introduce further functionality into the polymer backbone.[43] 3-Mercaptopropionic acid was used introduce carboxylic acid groups for H-bonding interactions to produce polymers with UCST. Finally, by using monofunctional *m*-PEG as an initiator for the AROP, we prepared UCST-type thermoresponsive block copolymers that self-assemble into polymersomes in water and either irreversibly swell, or reversibly disassemble and reassemble upon temperature change.

Results and Discussion

Monomer Synthesis

The cyclic monomer for the AROP, 2-ethyl-2-oxo-1,3,2-dioxaphospholane **(1)** was synthesized according to literature.[41] The comonomer 2-allyl-2-oxo-1,3,2-dioxaphospholane **(2)** was synthesized via a three-step synthesis starting with the *Michelis-Arbuzov* reaction of triethyl phosphite and allyl bromide. The allyl phosphonic acid diethyl ester was converted to allyl phosphonic acid di(trimethylsilyl) ester with TMS-Cl and subsequently chlorinated with oxalyl chloride. The obtained allyl phosphonic acid dichloride was converted into the cyclic monomer by ring-closing condensation with ethylene glycol (Scheme 7.1, a). Both monomers were obtained in high purity after distillation at reduced pressure. ^{31}P NMR spectroscopy showed a single sharp resonance at 52.5 ppm for monomer **(1)** and at 45.9 ppm for monomer **(2)** (Supporting Information for synthetic details and characterization data).

Polymer Synthesis

Monomers **(1)** and **(2)** were polymerized via organocatalytic AROP to produce the respective copolymers **P(1$_x$-*co*-2$_y$)** as shown in Scheme 7.1, b. In analogy to the homopolymerization of 2-alkyl-2-oxo-1,3,2-dioxaphospholanes, 1,8-diazabicyclo-[5.4.0]undec-7-ene (DBU) was used as the catalyst and 2-(methoxy)ethanol or poly(ethylene glycol) monomethyl ether (P_n = 113) as the respective initiators.[40,41] Under these conditions, well-defined copolymers with molecular weights between 5,300 and 14,000 g mol^{-1} and different copolymer composition were obtained; the base-catalyzed allyl-propenyl isomerization during the polymerization was kept below 5% by performing the polymerization at 0 °C.

^{1}H NMR spectroscopy was used to assess the composition and the molecular weight of the polymers (Figure 7.1, a). The degree of polymerization was determined by comparing the resonances originating from the initiator (signal a, 3.37 ppm) with the backbone methylene protons (signal b, 4.35 - 4.06 ppm).

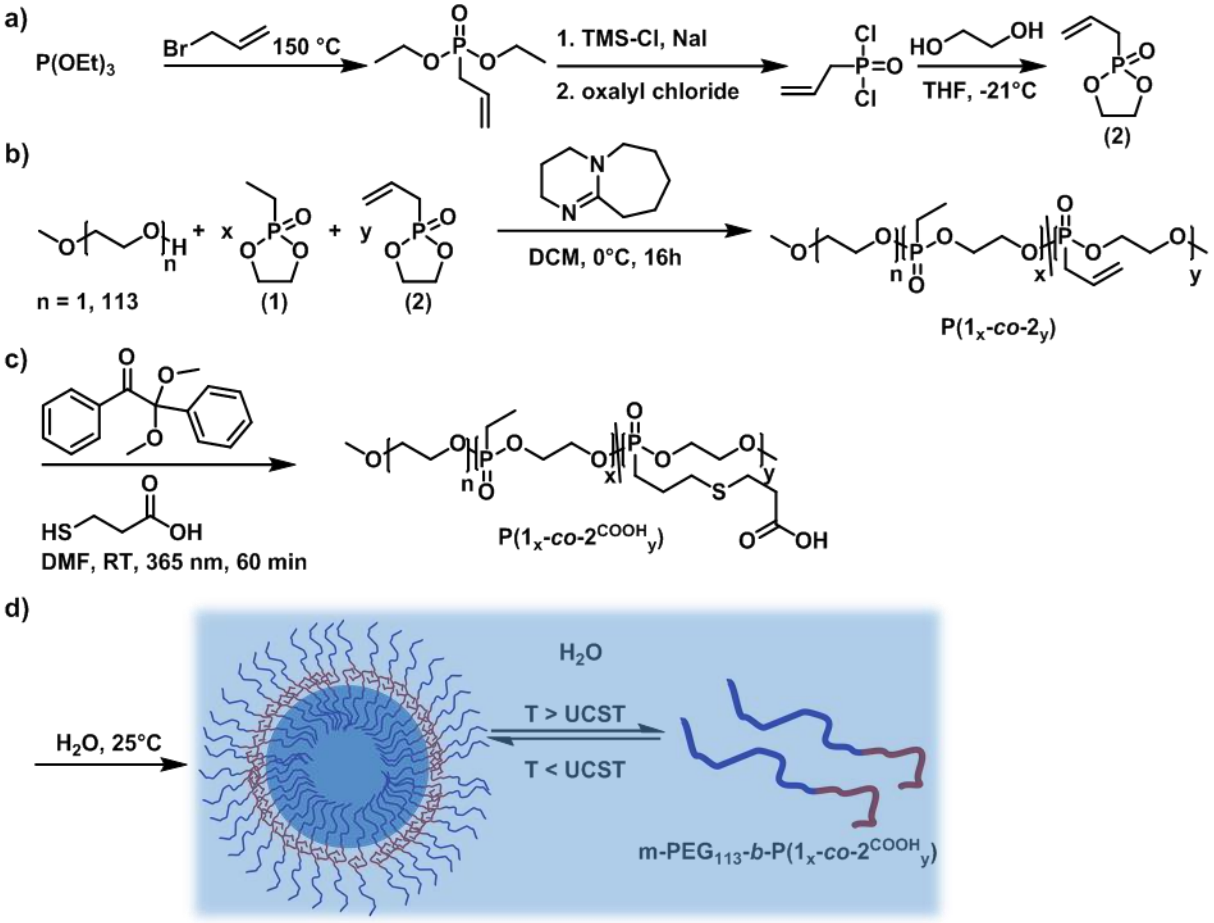

Scheme 7.1: a) Synthesis of 2-allyl-2-oxo-1,3,2-dioxaphospholane (2). b) Anionic ring-opening copolymerization of (1) and (2) using DBU as a catalyst to produce P(1_x-*co*-2_y). c) Photochemical post-polymerization modification of P(1_x-*co*-2_y) with 3-mercaptopropionic acid to produce P(1_x-*co*-2^{COOH}_y). d) Temperature-dependent (UCST) aggregation of thermoresponsive block copolymers m-PEG_{113}-*b*-P(1_x-*co*-2^{COOH}_y).

Furthermore, integration of the signals of the side-chains protons (signals c to j) enabled precise determination of the copolymer composition and the degree of isomerization. ^{31}P NMR spectroscopy proved to be a sensitive probe to the copolymer composition and gave access to the comonomer and isomerization ratio by integration of the particular ^{31}P NMR resonances (Et-P, 35.2 ppm; Allyl-P, 28.5 ppm; propenyl-P, 19.6 ppm) (Figure 7.1, a, inset). The observed copolymer composition matched the monomer feed ratio in all cases.

To further investigate the structure and composition of the copolymers, we analyzed the copolymerization kinetics by taking samples during the polymerization of a 1 to 1 mixture of monomers. The copolymer composition was then determined via ^{31}P NMR spectroscopy. Figure 7.1, c shows the plot of the mol fraction of **(1)** incorporated into the polymer during the polymerization. As the plot resulted in a horizontal line, no preferred incorporation of the two monomers occurred, indicating the formation of random copolymers of **(1)** and **(2)**.

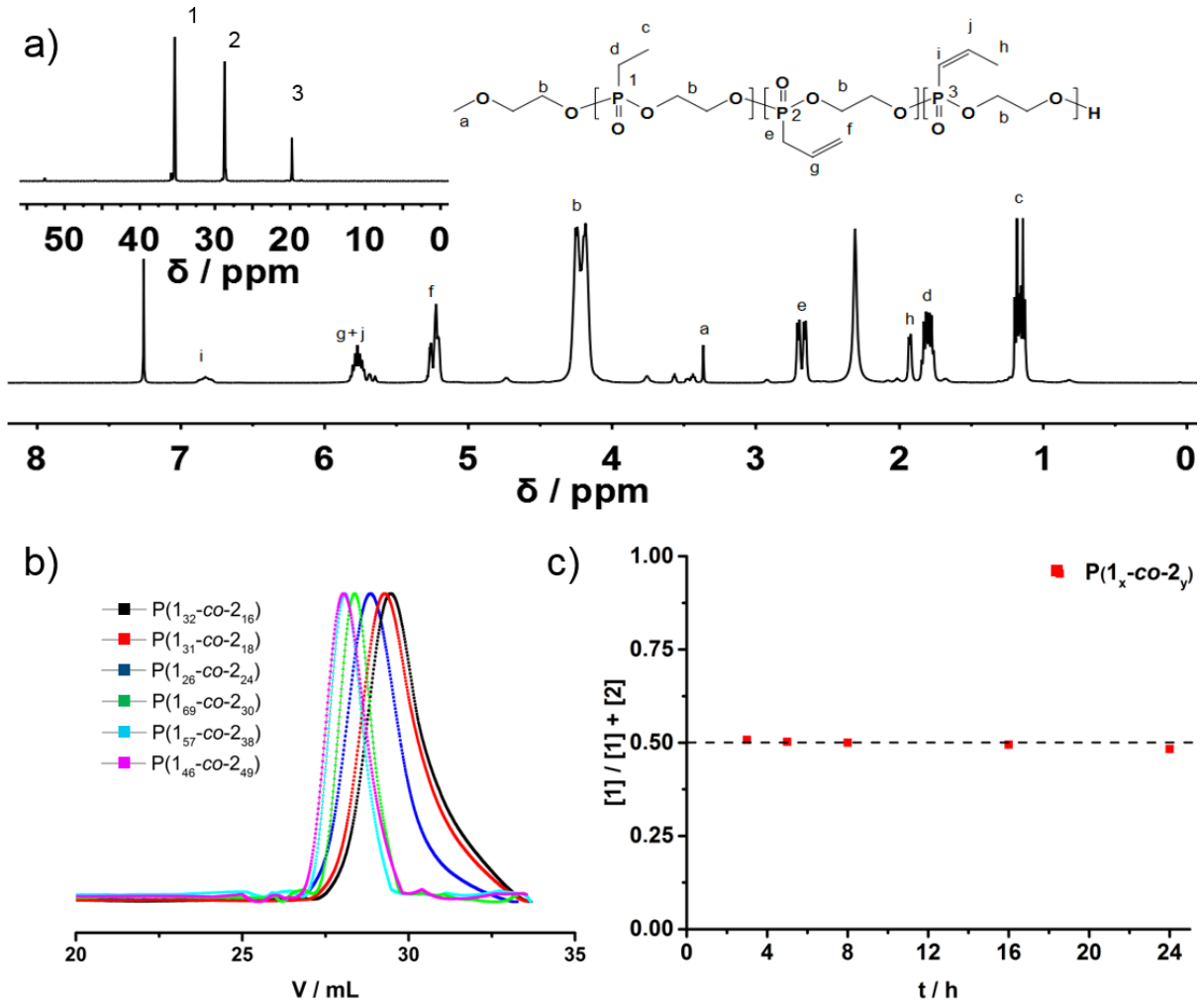

Figure 7.1: Analytical data of the synthesized polymers P(1$_x$-*co*-2$_y$): a) ^{1}H NMR (500 MHz) and ^{31}P NMR (201 MHz, inset) of P(1$_{25}$-*co*-2$_{25}$) in CDCl$_3$ at 298K. b) SEC elugrams of P(1$_x$-*co*-2$_y$) in DMF (RI detection, 1 g L^{-1} LiBr) at 333K. c) ^{31}P NMR spectroscopy assisted copolymerization kinetics.

^{1}H DOSY NMR spectroscopy shows that all previously assigned protons have the same diffusion coefficient and are part of the same molecule. (Figure 7.2)

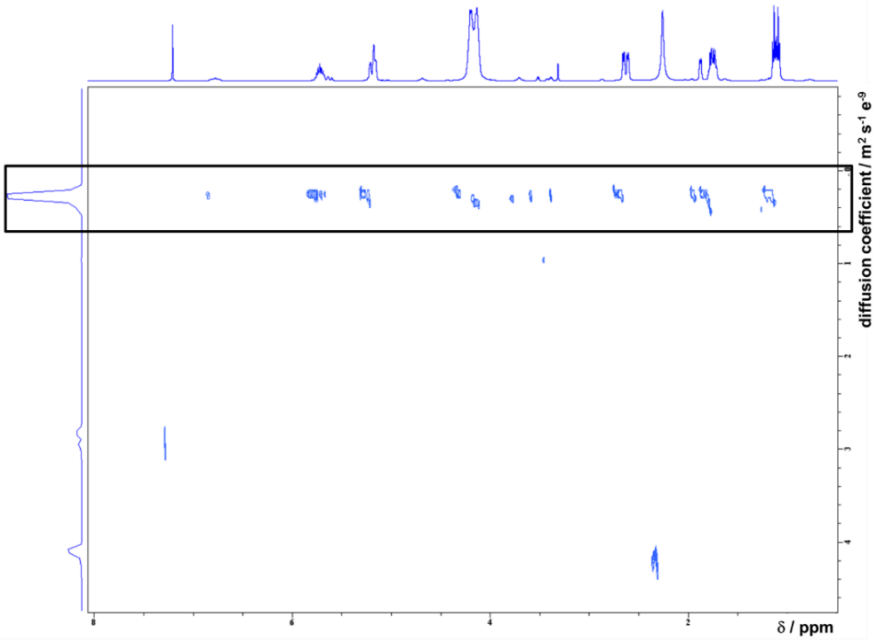

Figure 7.2: ^{1}H DOSY (500 MHz) NMR spectrum of P(1_x-*co*-2_y) in $CDCl_3$ at 298K.

All copolymers obtained under these conditions showed a monomodal and narrow molecular weight distribution (1.06 < *Đ* < 1.25) with *Đ* decreasing with increasing molecular weight (Figure 7.1, b. Thermal analysis via DSC showed that all polymers were completely amorphous and had low glass transition temperature (T_g) in the range of -50 to -40 °C similar to other poly(phosphoester)s (Figure 7.3).[44,45]

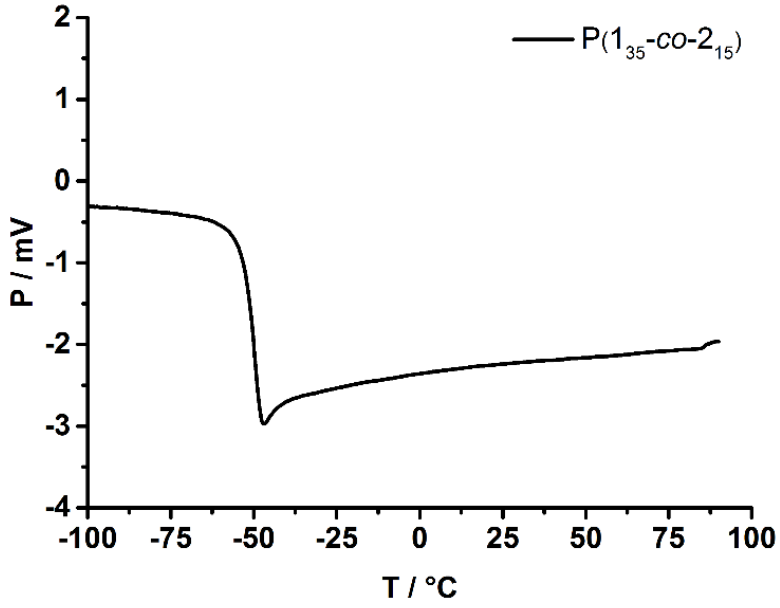

Figure 7.3: Representative DSC thermogram of P(1_{35}-*co*-2_{15}) from -100 °C to 100 °C at a heating rate of 1 °C min^{-1}.

All copolymers prepared were water-soluble without any phase separation behavior up to a concentration of at least 10 g L^{-1}, similar to previously reported homopolymers of **(1)**.[41] No cell toxicity was observed towards macrophages even at concentrations of up to 1,000 µg mL^{-1} (Figure 7.4). Analytical data of all polymers are shown in Table 7.1.

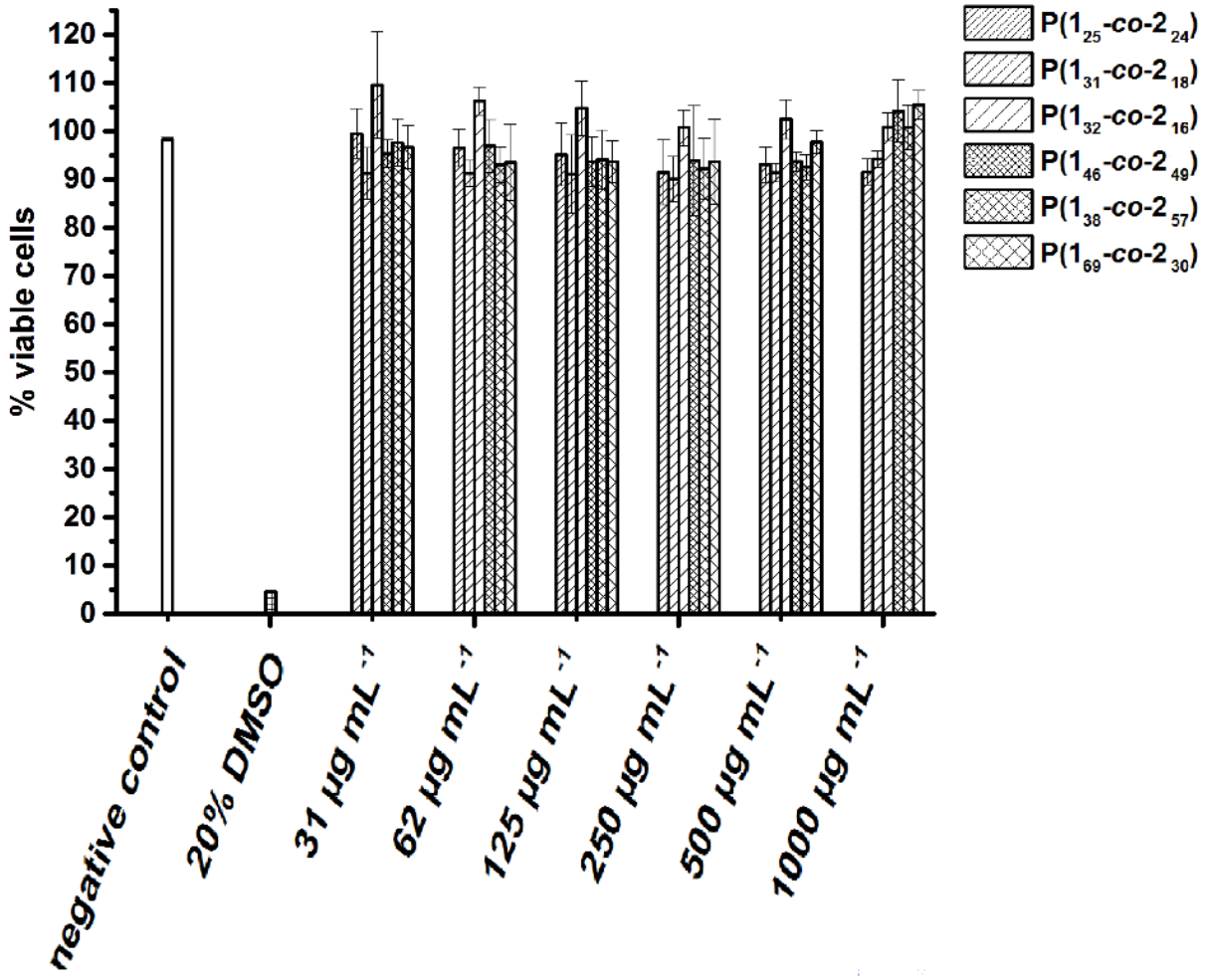

Figure 7.4: Cell-viability assay of P(1_x-*co*-2_y) against the macrophage cell-line RAW 264.7 after 48h of incubation (performed by Johanna Simon).

Table 7.1: Analytical data of all synthesized polymers.

sample	theoretical composition (1) / (2)[a]	copolymer composition (1) / (2) / propenyl [b]	M_n / g mol^{-1} [b]	Đ [c]	T_g / °C [d]
P(2)$_{42}$	-	-	6,000	1.30	-49.5
P(1$_{17}$-*co*-2$_{24}$)	18 / 25	17 / 24 / 1	5,300	1.18	-49.7
P(1$_{26}$-*co*-2$_{24}$)	25 / 25	26 / 24 / 3	7,000	1.20	-54.8
P(1$_{31}$-*co*-2$_{18}$)	30 / 20	31 / 18 / 1	6,200	1.22	-57.2
P(1$_{32}$-*co*-2$_{16}$)	35 / 15	32 / 16 / 1	6,200	1.25	-50.7
P(1$_{46}$-*co*-2$_{49}$)	50 / 50	46 / 49 / 1	14,000	1.11	-48.0
P(1$_{57}$-*co*-2$_{38}$)	60 / 40	57 / 38 / 3	13,700	1.10	-50.7
P(1$_{69}$-*co*-2$_{30}$)	70 / 30	69 / 30 / 2	14,000	1.13	-51.1

a) Monomer feed ratio. b) Determined via ^{1}H NMR spectroscopy. c) Determined via SEC in DMF (1 g L^{-1} LiBr) at 333K (vs. PEG calibration). d) Determined via DSC measurements.

Post-polymerization modification

The pendant double bonds allowed for further adjustment of the copolymers properties. In order to introduce an UCST-type phase separation, 3-mercaptopropionic acid was attached to the side-chains to induce hydrogen-bonding in analogy to PAA. As a secondary effect, this increased the hydrophobicity of the side-chain due to the incorporation of hydrophobic thioether segments, thus potentially inducing LCST behavior. The photochemical thiol-ene reaction, catalyzed with 2,2-dimethoxy-2-phenyl acetophenone (DMPA) was used to produce the modified copolymers **P(1$_x$-*co*-2$^{COOH}_y$)** as shown in Figure 7.1, c.

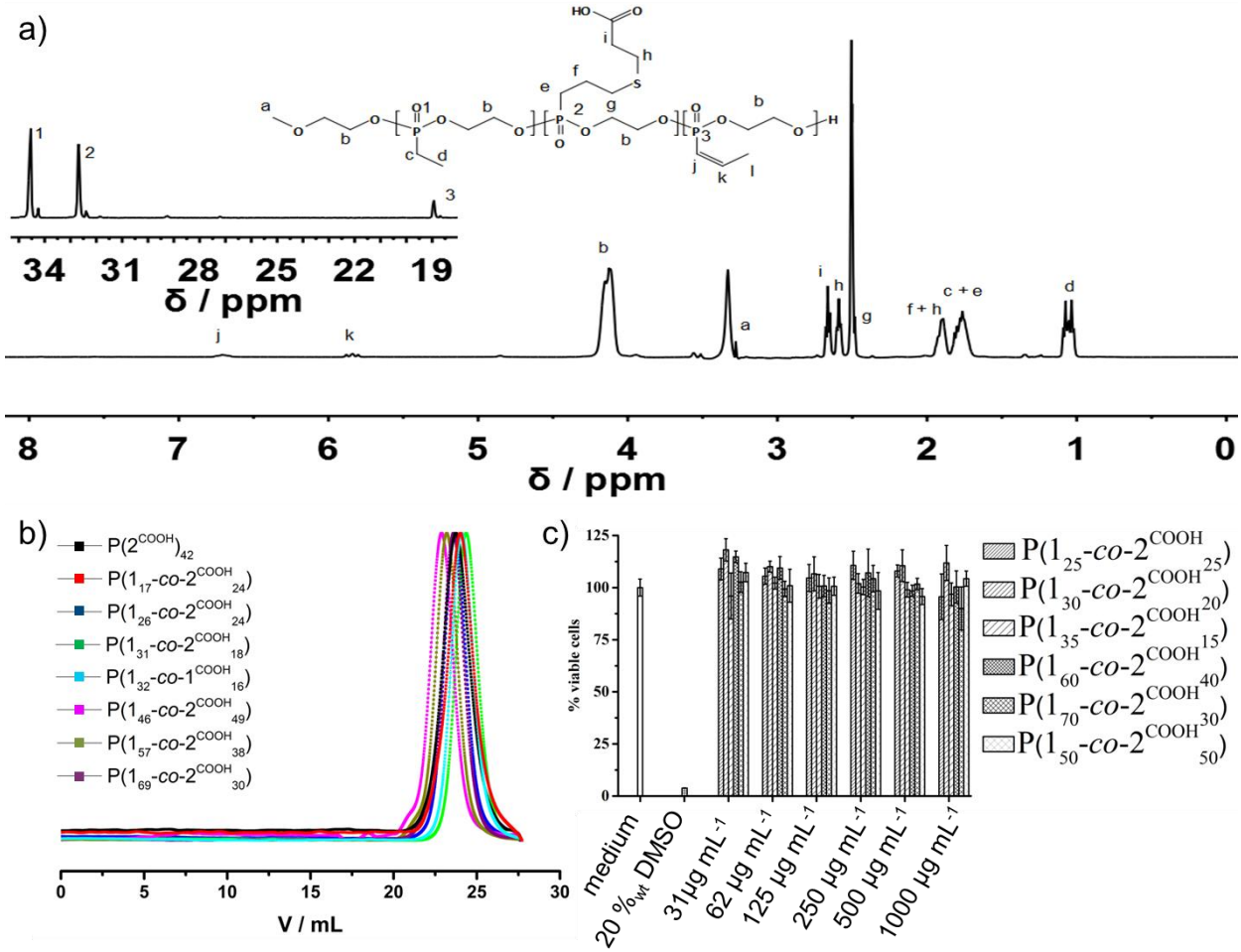

Figure 7.5: Analytical data of the modified polymers P(1_x-*co*-2^{COOH}_y): a) ^{1}H NMR (500 MHz) and ^{31}P NMR (201 MHz, inset) NMR spectra of P(1_x-*co*-2^{COOH}_y) in DMSO-d_6 at 298K. b) SEC trace of P(1_x-*co*-2^{COOH}_y) in 0.1 M PBS at pH 6.5 at 298K (RI detection). c) Cell-viability assay of P(1_x-*co*-2^{COOH}_y) against the macrophage cell-line RAW264.7 at different concentrations. The pure cell-culture medium used as a negative control and 20%$_{wt}$ DMSO used as a positive control (performed by Johanna Simon).

^{1}H NMR spectroscopy was used to analyze the modified polymers (Figure 7.5, a). The resonances of the double bonds at 5.85 - 5.70 ppm and 5.28 - 5.18 ppm (corresponding to the allylic protons) vanished, proving successful post modification. The resonances at 6.79 - 6.65 ppm and 5.90 - 5.77 ppm of the propenyl protons, however, did not change as these double bonds are inert under the reaction conditions. Furthermore, new resonances belonging to the 3-mercaptopropionic acid side-chains emerged in the spectrum at 2.70 - 2.64 ppm (-CH_2-COOH) and 2.63 - 2.55 ppm (-S-CH_2-), respectively.

The resonance of the allyl-phosphorus in the ^{31}P NMR (Figure 7.5, a, inset) spectrum at 28.59 ppm vanished almost entirely, and a new signal at 32.70 ppm emerged, which corresponded to the functionalized comonomer units. The resonances of the propenyl-phosphorus at 19.65 ppm remained unchanged. Residual Allyl-^{31}P resonance signals were used to determine the conversion. In all cases, > 98% conversion was reached after 60 min of irradiation. The covalent attachment of the carboxylic acid moieties to the polymer was further proven via 2D NMR spectroscopy: ^{1}H DOSY NMR spectroscopy showed that all proton signals had the same diffusion coefficient and were hence part of the same molecule (Figure 7.6).

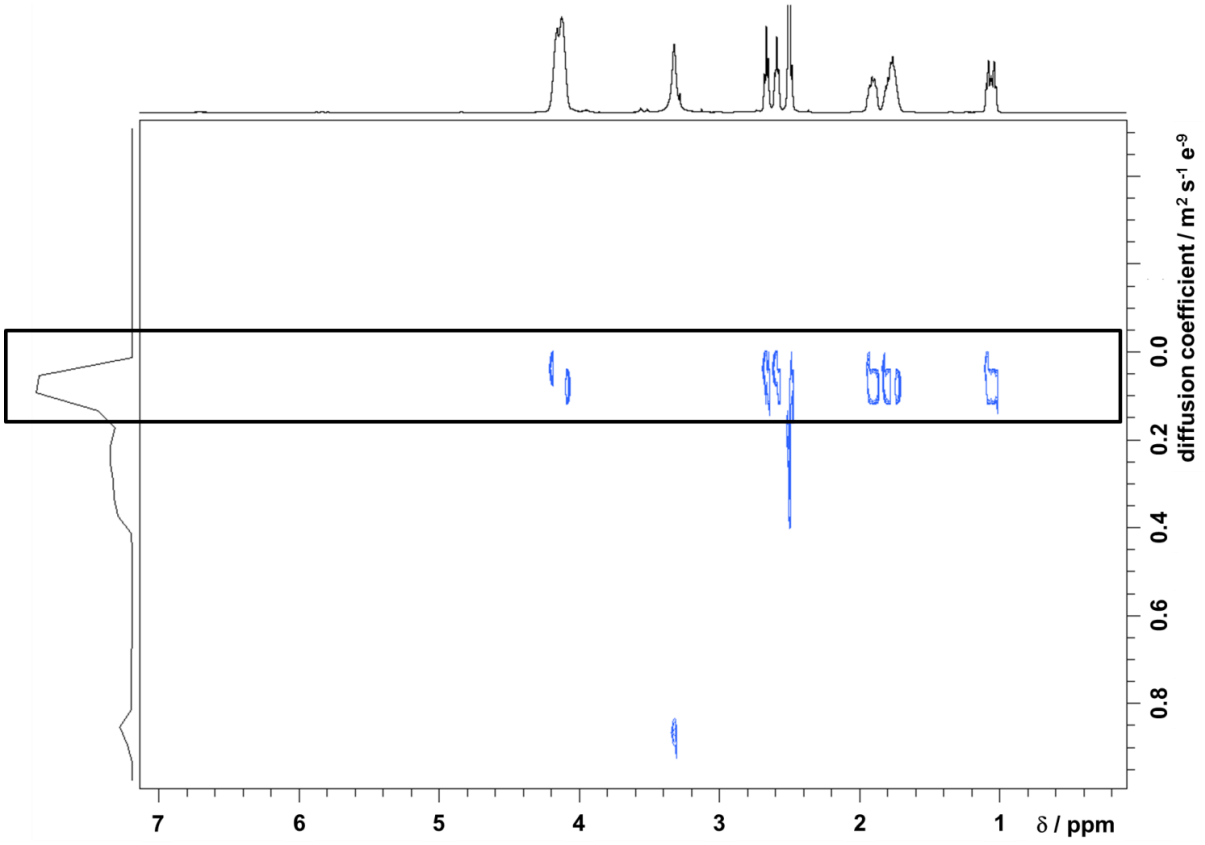

Figure 7.6: ^{1}H DOSY (500 MHz) NMR spectrum of P(1_x-*co*-2^{COOH}_y) in DMSO-d_6 at 298K.

^{1}H TOCSY NMR measurements showed a through bond correlation of the protons adjacent to the sulfur with the protons adjacent to the phosphorus. Both measurements proved the covalent attachment of the carboxylic acid moieties to the polymer (Figure 7.7).

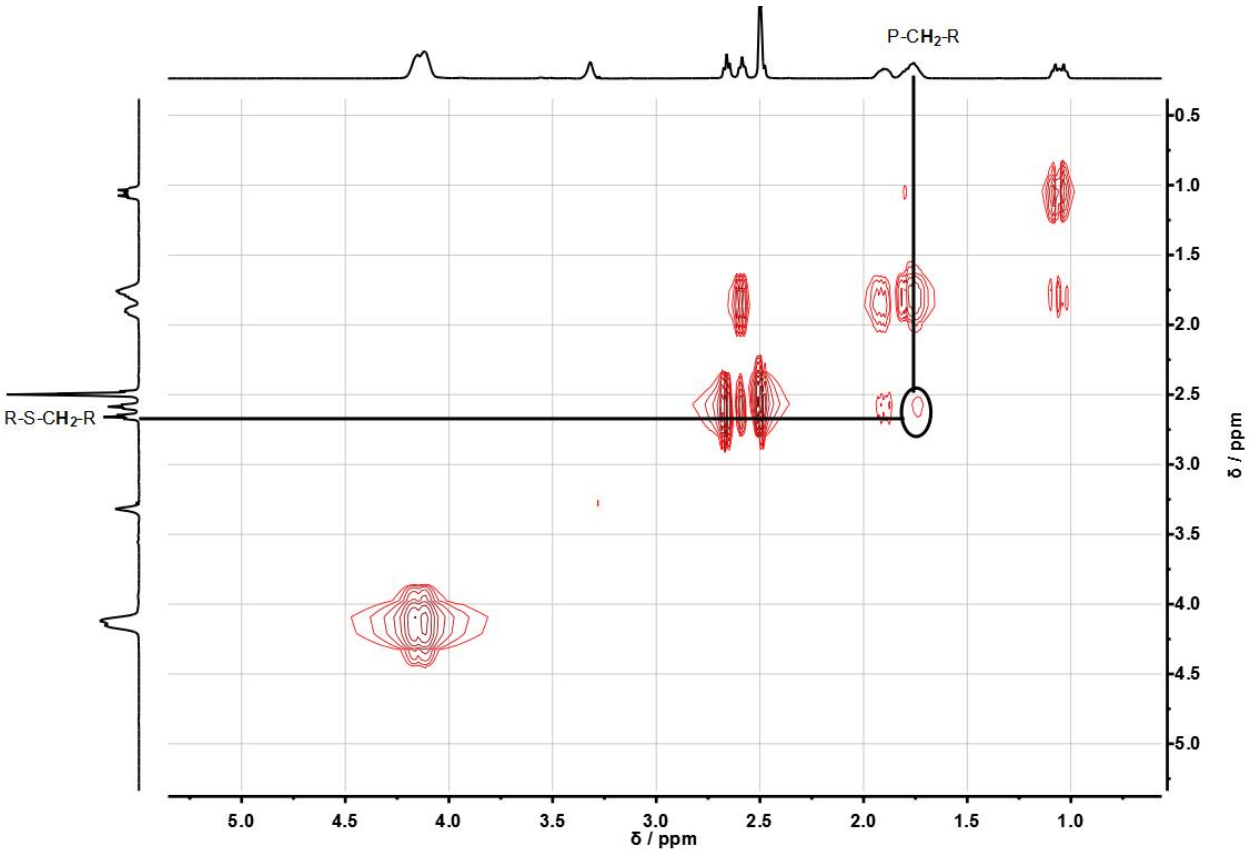

Figure 7.7: $^{1}H^{1}H$ TOCSY (500 MHz) NMR spectrum of P(1_x-*co*-2^{COOH}_y) in DMSO-d_6 at 298K.

SEC was performed in 0.1 mol L^{-1} PBS at pH 6.5. All polymers showed a monomodal and narrow molecular weight distribution (Figure 7.5, b). Comparison with the unmodified polymer under the same conditions showed a shift to lower elution volumes after the modification and no significant change in the traces shape indicating no backbone degradation under the reaction conditions (Figure 7.8). Again, a cell-viability assay against the macrophage cell line RAW264.7 was performed to evaluate the cell-toxicity of the modified polymers for future applications. The pure cell-culture medium was used as a negative control and 20%wt DMSO as a positive control. All modified polymers regardless of copolymer composition or molecular weight (polymers fully soluble under the conditions of the cell experiments) showed excellent cell-viability even up to concentrations as high as 1,000 µg mL^{-1} (Figure 7.5, c).

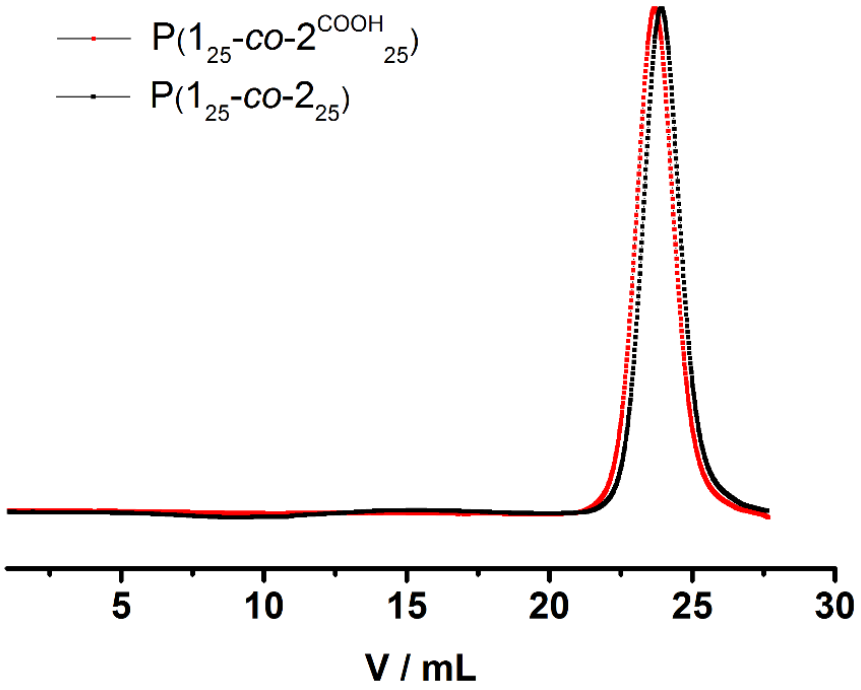

Figure 7.8: Representative overlay of SEC traces of P(1_{25}-*co*-2_{25}) (black) and P(1_{25}-*co*-2^{COOH}_{25}) (red) in 0.1 M PBS at pH 6.5 at 298K (RI detection).

Thermal analysis in bulk via DSC showed an increase of the glass transition temperature for all polymers of 30 °C as a result of the incorporated carboxylic acid (Figure 7.9).

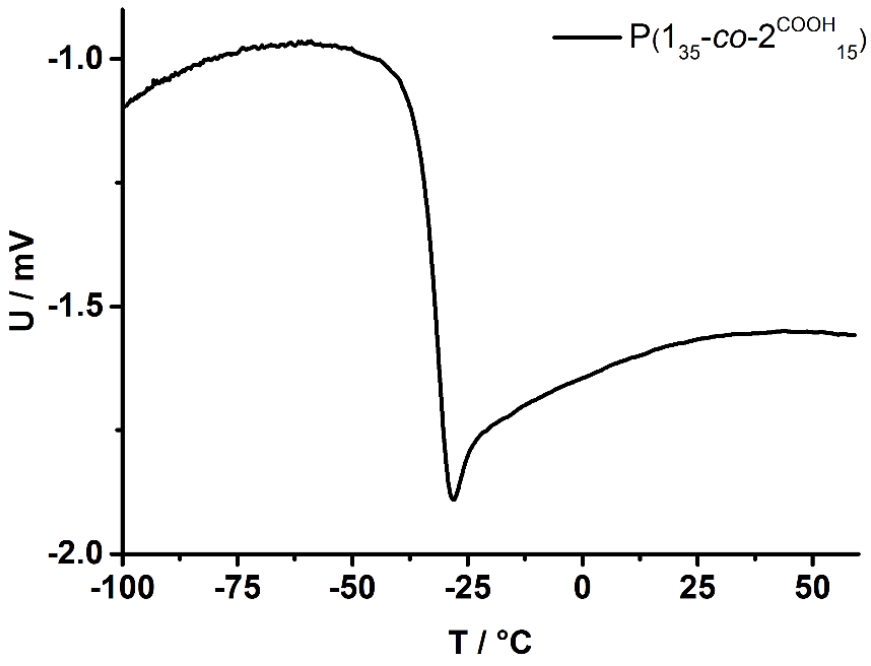

Figure 7.9: DSC thermogram of P(1_{35}-*co*-2^{COOH}_{15}) from -100 °C to 60 °C at a heating rate of 1 °C min^{-1}.

Analytical data of all polymers are shown in Table 7.2.

Table 7.2: Analytical data of all modified polymers

sample	copolymer composition 1 / COOH / propenyl [a]	M_n / g mol^{-1} [a]	Đ [b]	T_g / °C [c]	T_m / °C [c]	T_c / °C [c]
P(2$^{COOH}_{42}$)	-	11,000	1.25	-14.6	-	-
P(1$_{17}$-*co*-2$^{COOH}_{24}$)	17 / 24 / 1	8,400	1.24	-29.7	-	-
P(1$_{26}$-*co*-2$^{COOH}_{24}$)	26 / 24 / 3	10,000	1.14	-27.9	-	-
P(1$_{31}$-*co*-2 $^{COOH}_{18}$)	31 / 18 / 1	7,700	1.17	-45.0	-	-
P(1$_{32}$-*co*-2 $^{COOH}_{16}$)	32 / 16 / 1	7,800	1.15	-32.5	-	-
P(1$_{46}$-*co*-2 $^{COOH}_{49}$)	46 / 49 / 1	19,500	1.07	-18.4	-	-
P(1$_{57}$-*co*-2 $^{COOH}_{38}$)	57 / 38 / 3	17,800	1.06	-20.6	-	-
P(1$_{69}$-*co*-2 $^{COOH}_{30}$)	69 / 30 / 2	17,300	1.08	-32.1	-	-
***m*-PEG$_{113}$-*b*-P(1$_2$-*co*-2$^{COOH}_3$)**	2 / 3 / 1	6,200	1.10	-40.3	58.9	36.7
***m*-PEG$_{113}$-*b*-P(1$_7$-*co*-2$^{COOH}_7$)**	7 / 7 / 1	7,700	1.16	-22.3	55.2	33.7
***m*-PEG$_{113}$-*b*-P(1$_{30}$-*co*-2$^{COOH}_{30}$)**	30 / 30 / 1	17,700	1.15	-27.5	53.6	14.5
***m*-PEG$_{113}$-*b*-P(1$_{56}$-*co*-2$^{COOH}_{57}$)**	56 / 57 / 1	27,000	1.14	-15.9	51.2	32.0
***m*-PEG$_{113}$-*b*-P(1$_{23}$-*co*-2$^{COOH}_{36}$)**	23 / 36 / 2	13,700	1.19	-20.1	54.5	-10.1
***m*-PEG$_{113}$-*b*-P(1$_{17}$-*co*-2$^{COOH}_{38}$)**	17 / 38 / 1	13,200	1.18	-36.5	52.1	33.5

a) Determined via ^{1}H NMR spectroscopy. b) Determined via SEC in 0.1 M PBS at pH 6.5 at 298K (vs. PEG calibration). c) Determined via DSC measurements (heating, cooling at 10 °C min^{-1}).

Polymer Degradation

Several studies already showed that PPEs can be degraded either hydrolytically or enzymatically by, e.g., phosphodiesterase I.[41,46,47] Furthermore, phosphonic acid derivatives are known to be metabolically digested by microorganisms via the radical cleavage of the P-C bond, resulting in the formation of phosphate derivatives to be used in metabolism.[48] Furthermore, just recently, we demonstrated the enhanced degradation rate of PPn's in (bacteria-rich) sea water under aerobic conditions compared to sterile water.[39, 48] Still, to ensure hydrolysis of our carboxylated polymers, degradation of the modified polymers were investigated in water at two different pH values at 37 °C and analyzed via SEC and ^{31}P NMR spectroscopy. At pH 6.1, as expected, the polymers were stable and did not show any signs of degradation until the end of the experiment (42 days). Neither the SEC elugram nor the ^{31}P NMR spectrum changed during this time (Figures 7.10 and 7.11).

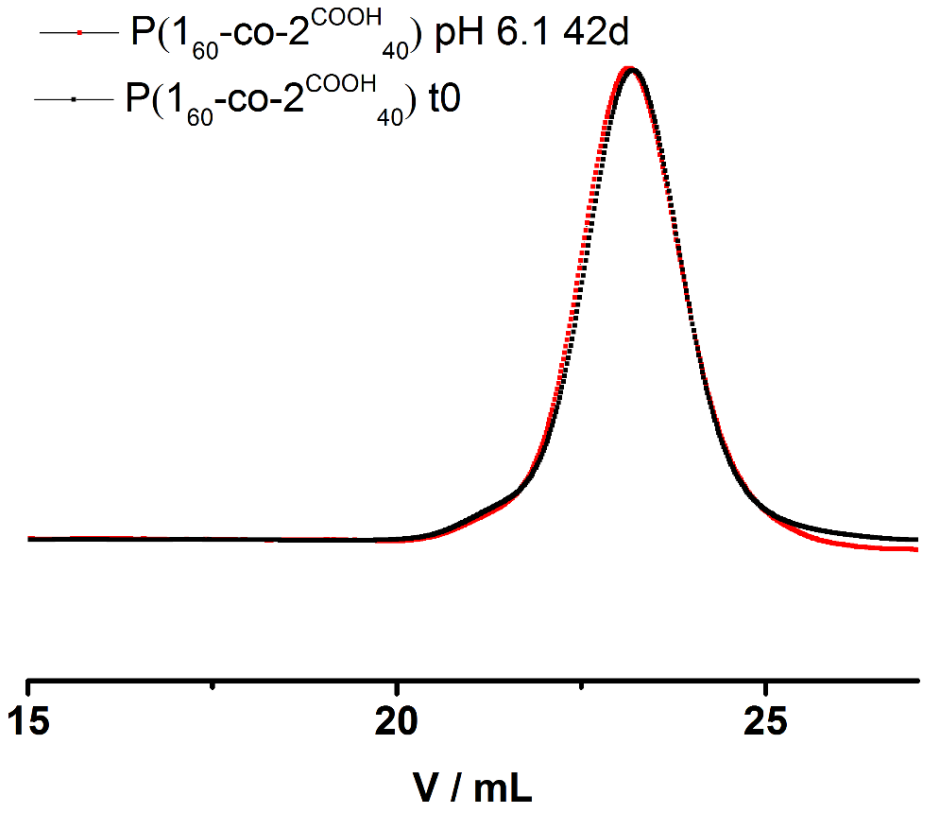

Figure 7.10: SEC trace of P(1_{60}-*co*-2^{COOH}_{40}) (RI detection) in 0.1 M PBS at pH 6.5 at 298K before (black) and after (red) incubation at pH 6.

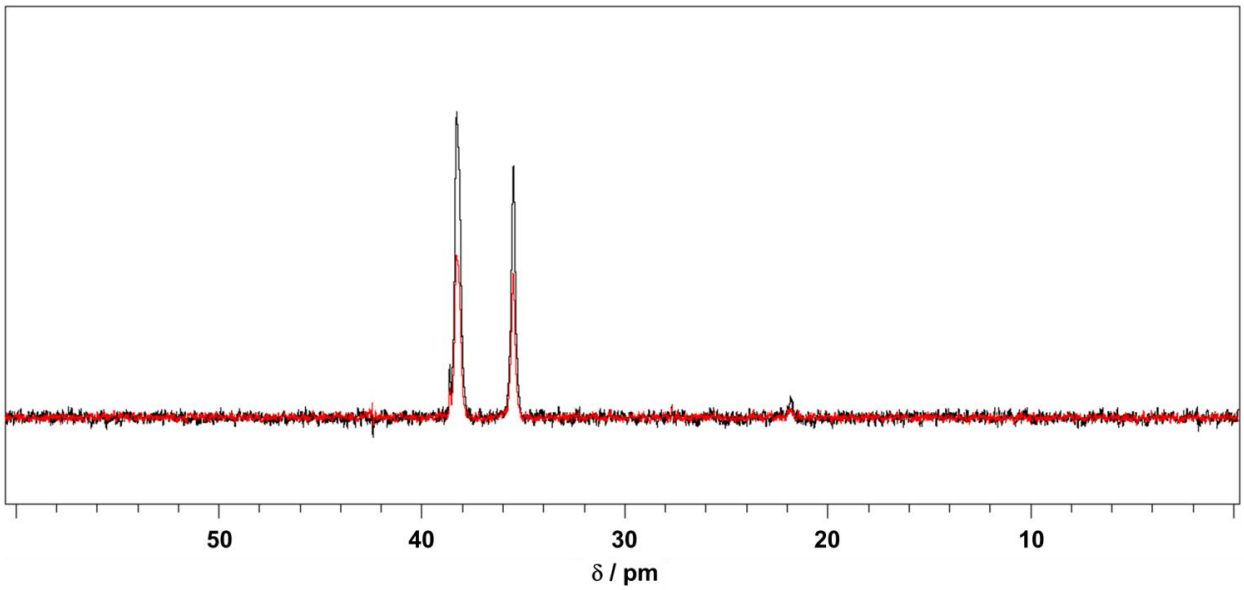

Figure 7.11: ^{31}P NMR (201 MHz) spectra of P(1_{60}-*co*-2^{COOH}_{40}) in 10% D_2O and 90% H_2O at 298K before (black) and after (red) incubation at pH 6.

Under basic conditions (pH 13), however, complete degradation was observed within 1h of incubation. A complete loss of polymeric material was shown by the SEC elugram (RI detection, Figure 7.12). A shift towards high-field of the ^{31}P NMR resonances proved the complete ester hydrolysis (Figure 7.13).

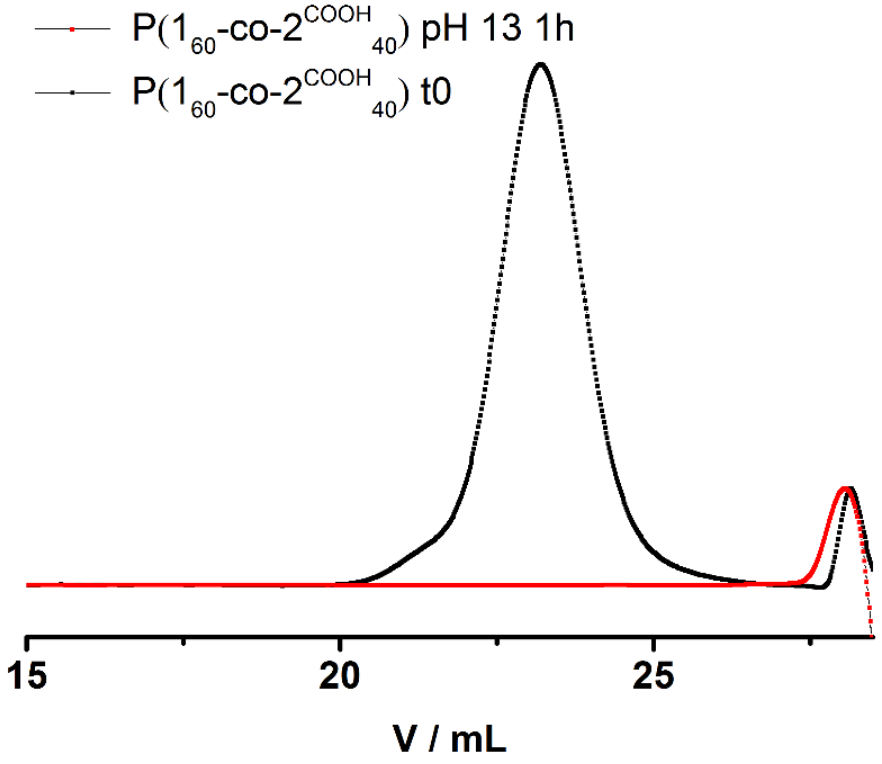

Figure 7.12: SEC trace of P(1_{60}-*co*-2^{COOH}_{40}) (RI detection) in 0.1 M PBS at pH 6.5 at 298K before (black) and after (red) incubation at pH 13.

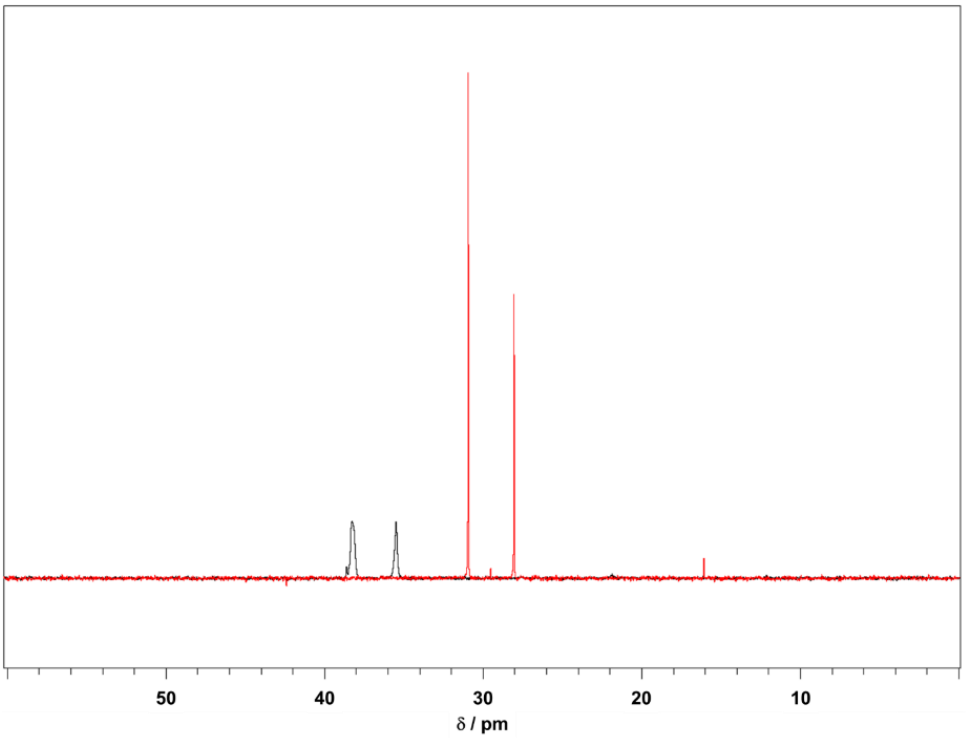

Figure 7.13: ^{31}P NMR (201 MHz) spectra of P(1_{60}-*co*-2^{COOH}_{40}) in 10% D_2O and 90% H_2O at 298K before (black) and after (red) incubation at pH 13.

Thermoresponsive behavior of random copolymers

After modification with the hydrogen bonding side-chains, the solubility profile of the random copolymers was significantly altered. **P(1_x-*co*-2^{COOH}_y)** copolymers showed the desired UCST behavior: high solubility at elevated and precipitation at low temperatures.

As a result of carboxylic acid induced H-bonding, the phase separation temperature was expected to be dependent on the concentration, pH, copolymer composition and salt concentration of the solution. Therefore, a thorough investigation of these parameters on the thermal behavior was conducted.

At low pH, all carboxylic acids were protonated and formed intra- and intermolecular hydrogen bonds. Under these conditions, the concentration of **P(1_{25}-*co*-2^{COOH}_{25})** strongly influenced the phase separation temperature (Figure 7.14, a). At a concentration of 5 g L^{-1} the polymer showed both an LCST phase separation at 37 °C and an additional UCST phase separation at 75 °C.

The occurrence of such a schizophrenic behavior was a result of the decreased overall polymer hydrophilicity due to the thioether side-chains. The UCST phase separation

temperature dropped to 71 °C and 46 °C for concentrations of 3.75 and 2.50 g L^{-1}, respectively with no detectable LCST phase separation under these conditions as it presumably shifted below 0 °C. At a concentration of 1 g L^{-1} and below, no macroscopic phase separation was observed, and the polymer remained soluble over the whole temperature range.

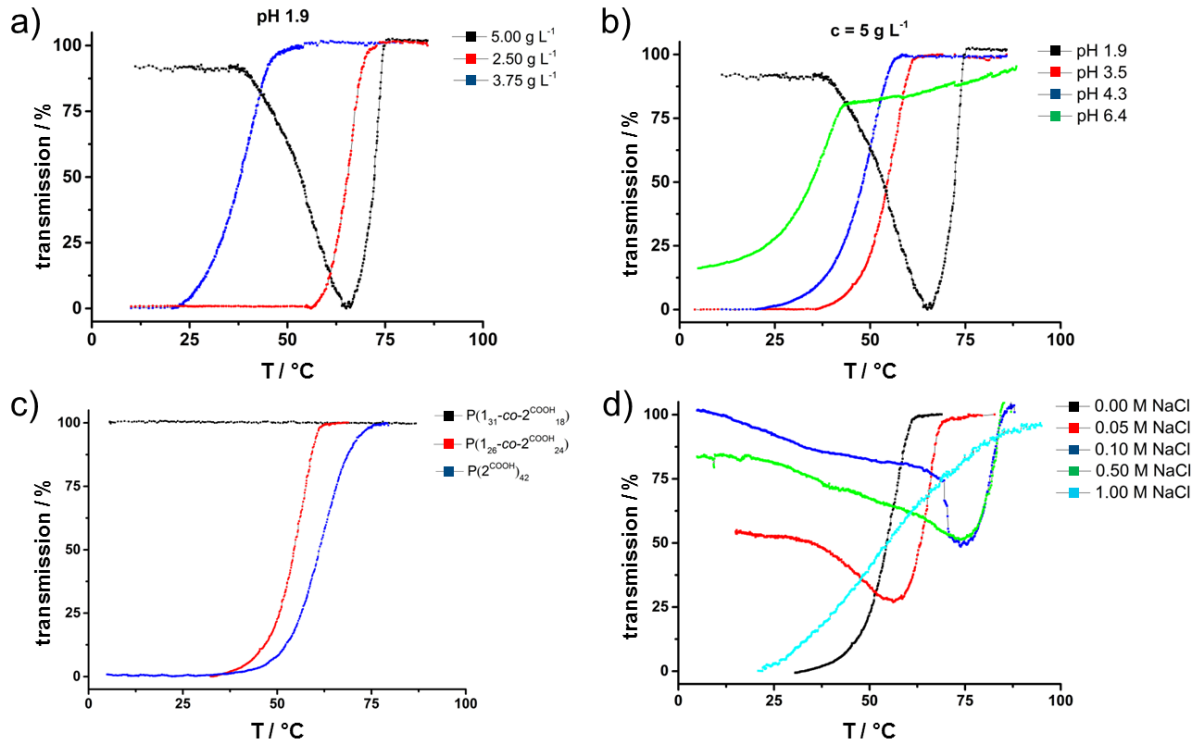

Figure 7.14: Turbidity measurements of P(1_x-*co*-2^{COOH}_y) at a cooling rate of 1 °C min^{-1} at different conditions. The Transmission was measured at 500 nm. a) Concentration dependency of UCST cloud points of P(1_{26}-*co*-2^{COOH}_{24}) at pH 1.9. b) pH dependency of UCST cloud points of P(1_{26}-*co*-2^{COOH}_{24}) at 5 g L^{-1}. c) Copolymer composition dependency of P(1_x-*co*-2^{COOH}_y) on UCST behavior at pH 3.5 and 5 g L^{-1}. d) Salt concentration dependency of UCST of P(1_{26}-*co*-2^{COOH}_{24}).

The degree of protonation of the carboxylic acid groups had a strong influence on the phase transition behavior of the polymers as it influenced the overall hydrophilicity and the H-bonding capacity of the polymer. Figure 7.14, b shows the pH-dependent turbidity measurements of **P(1_{25}-*co*-2^{COOH}_{25})** at a fixed concentration of 5 g L^{-1}. By increasing the pH value from 1.9 over 3.5 and 4.3 to 6.4, a reduction of the UCST phase transition temperature from 75 °C to 43 °C and broadening of the transition range was observed. Similar results were observed for pH-dependent measurements of poly(acrylic acid).[15] These were attributed to a decrease in inter- and intramolecular H-bonding in addition to an increased overall hydrophilicity of the polymer by partial deprotonation of the acid. Interestingly, the LCST behavior observed at pH 1.9 dropped below the measured temperature range (5 - 90 °C) at elevated pH values.

This was a result of the increasing hydrophilicity of the polymer chain as LCST is typically observed for polar polymers with hydrophobic side-chains.

By variation of the copolymer composition, i.e., the amount of H-bonding groups, the phase separation temperature can be adjusted as well (Figure 7.14, c): the homopolymer **P(2^{COOH})$_{42}$** exhibited a UCST phase separation at 75 °C in water (ph = 4.3, c = 5 g L^{-1}). Decreasing the amount of carboxylic acid groups to 50% (**P(1$_{26}$-*co*-2^{COOH}$_{24}$)**) reduced this value to 51 °C as a result of the decreased H-bonding. Further reduction of the –COOH amount below this threshold value (e.g., in **P(1$_{31}$-*co*-2^{COOH}$_{18}$)** with 40% comonomer content) resulted in the loss of UCST behavior under these conditions.

UCST and LCST polymers, in general, are influenced by the presence of salts in solution as a result of charge shielding effects and salt solvation. Different concentrations of sodium chloride were added to a solution of **P(1$_{26}$-*co*-2^{COOH}$_{24}$)** at pH 3.5 o investigate the influence of salt on the phase separation temperature (Figure 7.14, d). According to sodium's and chloride's position in the Hofmeister series as weakly kosmotropic cations /anions, sodium chloride was expected to increase the UCST and decrease the LCST phase separation temperature.[49]

In accordance, even at concentrations as low as 0.05 mol L^{-1}, the UCST phase separation onset shifted towards higher temperatures in a concentration-dependent manner, whereas high concentrations induced a strong broadening of the phase separation range due to efficient shielding effects. However, due to the reemerging of the LCST behavior, the thermogram got significantly more complicated. The addition of salt-induced an LCST behavior where the polymer partly dissolved below 50 °C. Increasing the salt concentration increased the LCST phase transition temperature as well as the fraction of the dissolved polymer. At the highest concentration, however, this effect vanished again. This behavior at first seemed contradictory to results found for, e.g., P(NIPAM), where the LCST values decreased with increasing sodium chloride concentrations.[49]

A possible explanation might be an interaction between the sodium cations and the carboxylic acid side-chains as well as phosphonic acid groups in the backbone. The overall hydration of the backbone would increase and thus shift the LCST values towards higher temperatures.

SEC of **P(1_{25}-*co*-2^{COOH}_{25})** before and after turbidity measurement (pH 1.9 shown exemplarily as harshest conditions) shows that no degradation occurred during the time of the measurement (Figure 7.15). All cloud points mentioned in this manuscript were determined at the onset temperature of transmission change in the cooling curve.

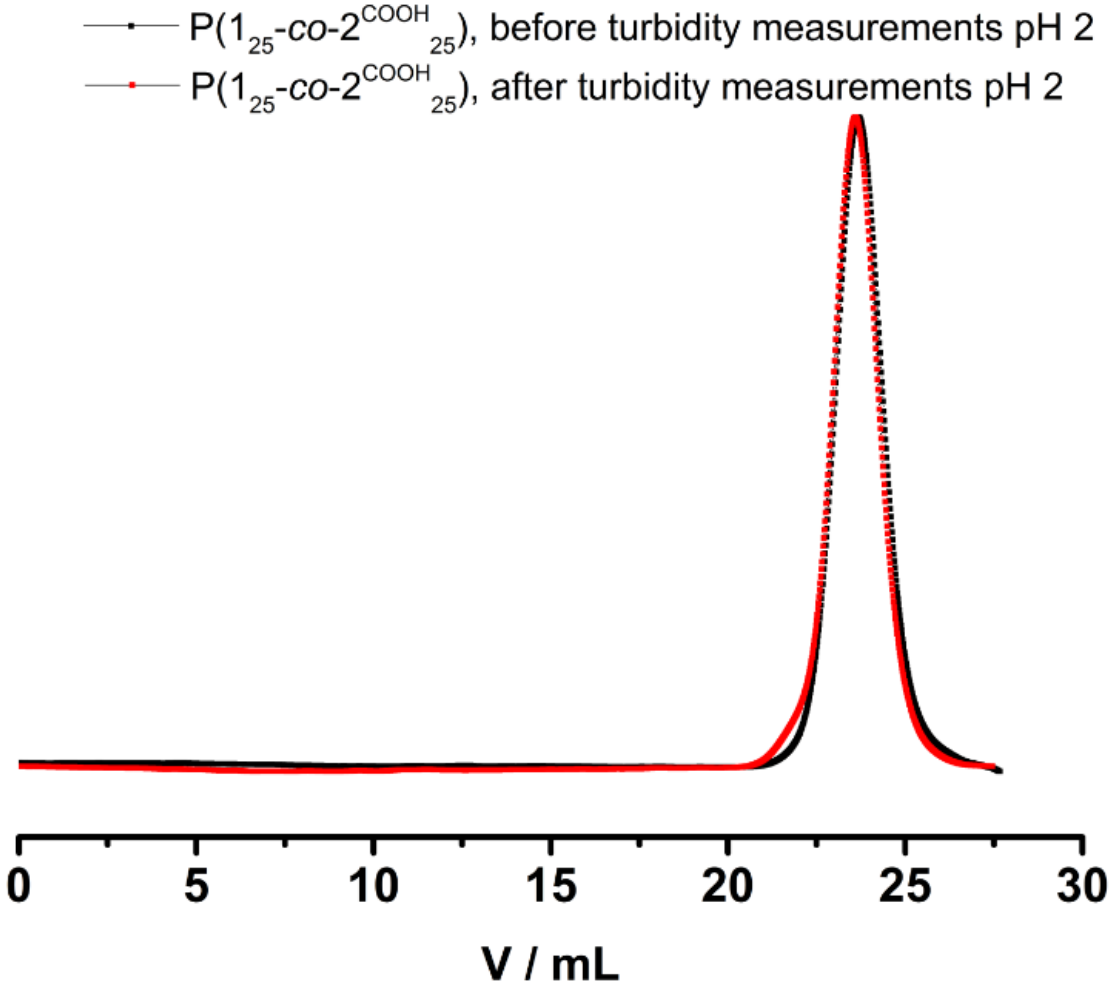

Figure 7.15: SEC trace (RI detection) of P(1_{25}-*co*-2^{COOH}_{27}) before (black) and after (red) turbidity measurements at pH 2 in 0.1 M PBS at pH 6.5 at 298K to ensure polymer integrity.

Preparation of block copolymers and self-assembly into polymersomes.

As a proof of concept application of these degradable UCST-PPEs, we used them as thermo-responsive switches for block copolymer self-assembly. Block copolymers were synthesized that should be amphiphilic at low temperatures and hydrophilic at elevated temperatures. Commercially available, water-soluble poly(ethylene glycol) (**m-PEG$_{113}$-OH**) served as a macroinitiator for the polymerization, and different amounts of the thermoresponsive units were placed in the PPE-block to generate diblock copolymers with adjustable UCST. Polymerization of the phosphonate block and post-modification proceeded under the same conditions as previously stated. All previously discussed resonances in ^{1}H and ^{31}P NMR spectra were present and could be assigned (Figure 7.16). The **m-PEG$_{113}$** backbone resonance (3.51 ppm), as well as the methoxy moiety of **m-PEG** (3.24 ppm) in the ^{1}H NMR spectrum, were used to determine the degree of polymerization of the poly(phosphonate) segment.

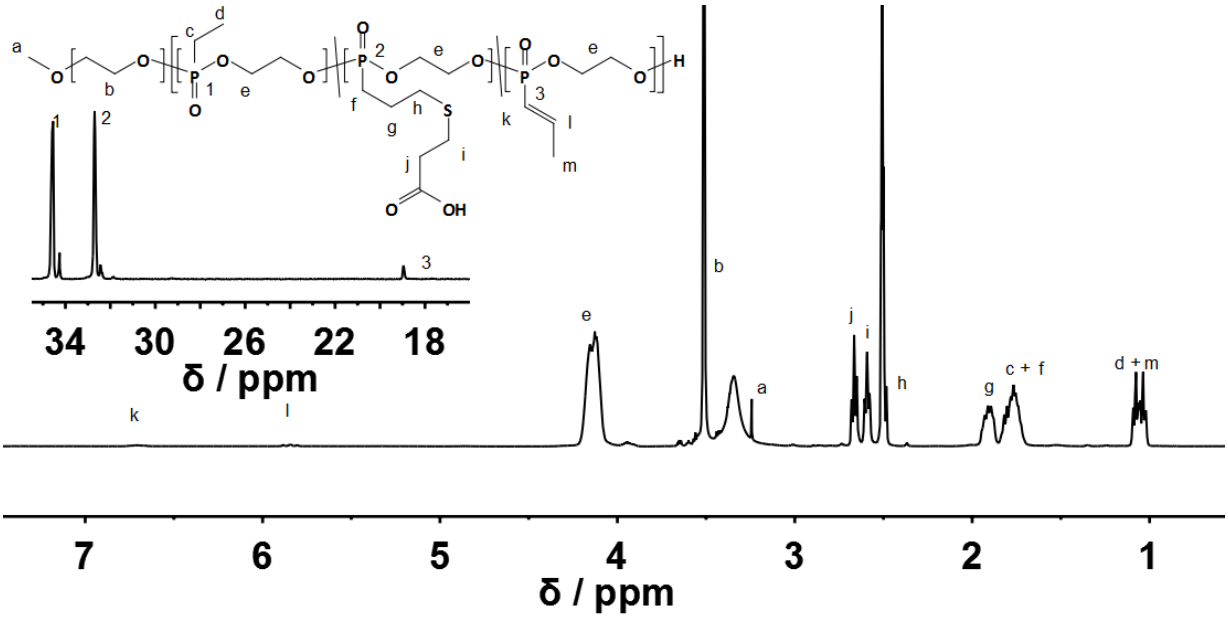

Figure 7.16: ^{1}H (500 MHz) NMR spectrum of *m*-PEG$_{113}$-*b*-P(1$_x$-*co*-2$^{COOH}_y$) in DMSO-*d*$_6$ at 298K.

^{1}H DOSY NMR spectroscopy further showed that the resonances of **m-PEG** and the poly(phosphonate) have the same diffusion coefficient and hence are part of the same molecule. A decrease of the diffusion coefficient compared to ***m*-PEG$_{113}$-OH** (Figure 7.17) as well as a shift towards lower elution volumes of the copolymer compared to the macroinitiator in aqueous SEC further proved the formation of the block copolymer and full initiator efficiency (Figure 7.18).

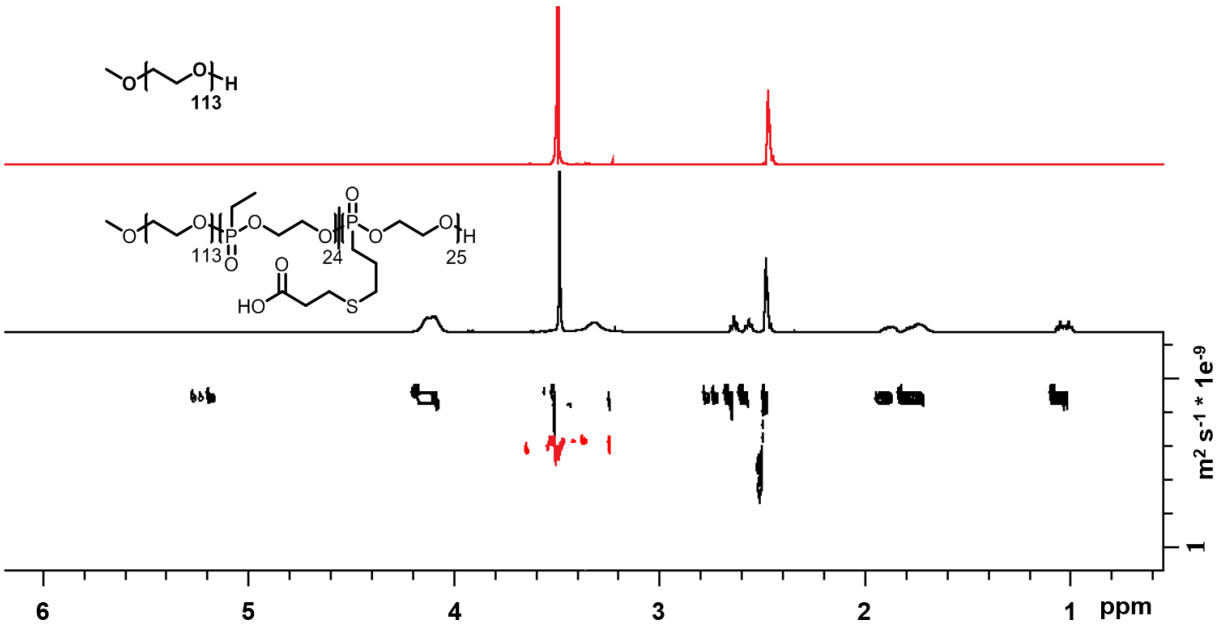

Figure 7.17: ^{1}H DOSY NMR (500MHz) and respective ^{1}H NMR (500 MHz) NMR spectra of m-PEG$_{113}$-*b*-P(1$_{30}$-*co*-2$^{COOH}_{30}$) (black) and macroinitiator m-PEG$_{113}$ (red) in DMSO-d_6 at 298K.

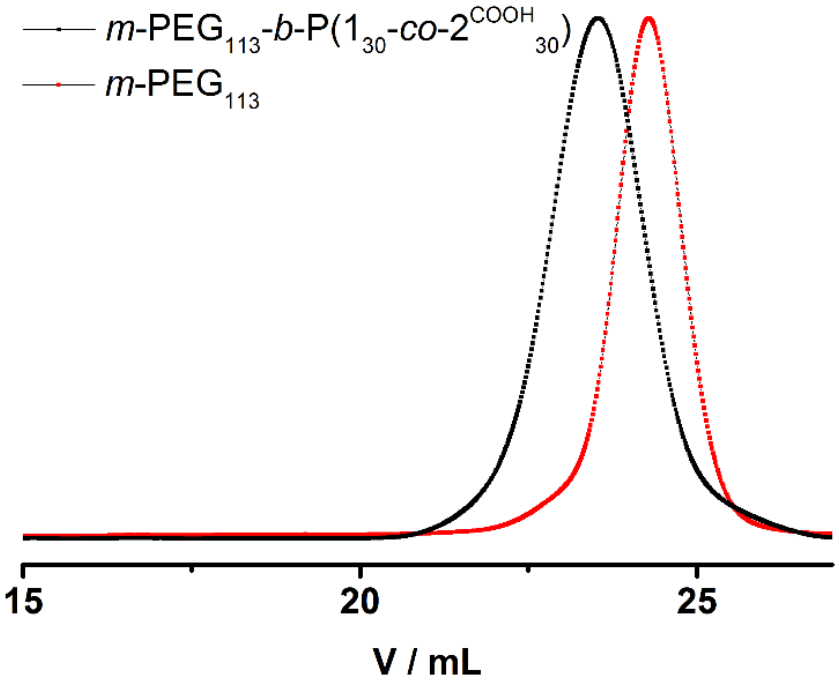

Figure 7.18: SEC trace (RI detection) of macroinitiator m-PEG$_{113}$OH (black) and block copolymer *m*-PEG113-*b*-P(1$_{30}$-*co*-2$^{COOH}_{30}$) (red) in 0.1 M PBS at pH 6.5 at 298K.

Thermal analysis in bulk showed a melting point at 53.6 °C (from ***m*-PEG$_{113}$OH**) and a glass transition at -27.5 °C (from the poly(phosphonate) segment). The T_g of ***m*-PEG$_{113}$OH** was hardly detectable under these conditions, however, due to the distinct crystallization peak of PEG phase separation of the two blocks is expected (Figure 7.19). Analytical data of all polymers are shown in Table 7.2.

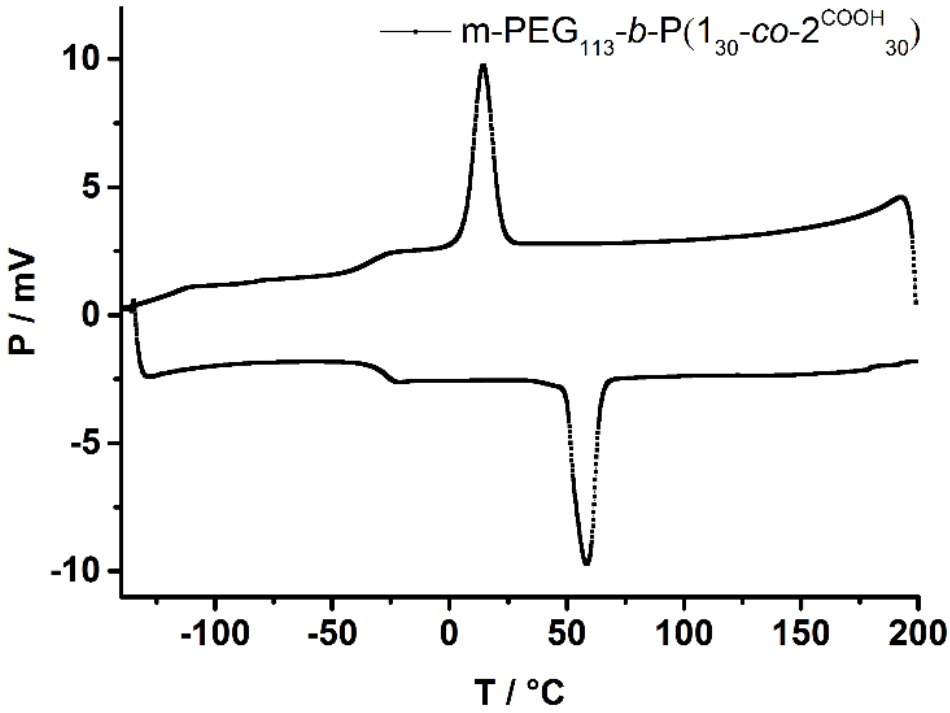

Figure 7.19: DSC thermogram of *m*-PEG-*b*-P(1$_{30}$-*co*-2$^{COOH}_{30}$) from -140 °C to 200 °C at a heating rate of 1 °C min^{-1}.

Self-assembly- and thermal behavior of block copolymers

The self-assembly in aqueous solution of these block copolymers was investigated to elucidate the potential in drug delivery applications. The ***m*-PEG-*b*-poly(phosphonate)** block copolymers dissolved in water macroscopically at room temperature, but self-assembled on the nanoscale (Scheme 7.1, c). For further investigation, 1%$_{v/v}$ DMSO was used to pre-dissolve the polymers to decrease the initial size distribution. ***m*-PEG$_{113}$-*b*-P(1$_{23}$-*co*-2$^{COOH}_{36}$)**, a block copolymer with 60% of the phosphonate block being carboxylated, formed narrowly distributed structures with a hydrodynamic diameter of 140 nm (obtained from DLS, Figure 7.20).

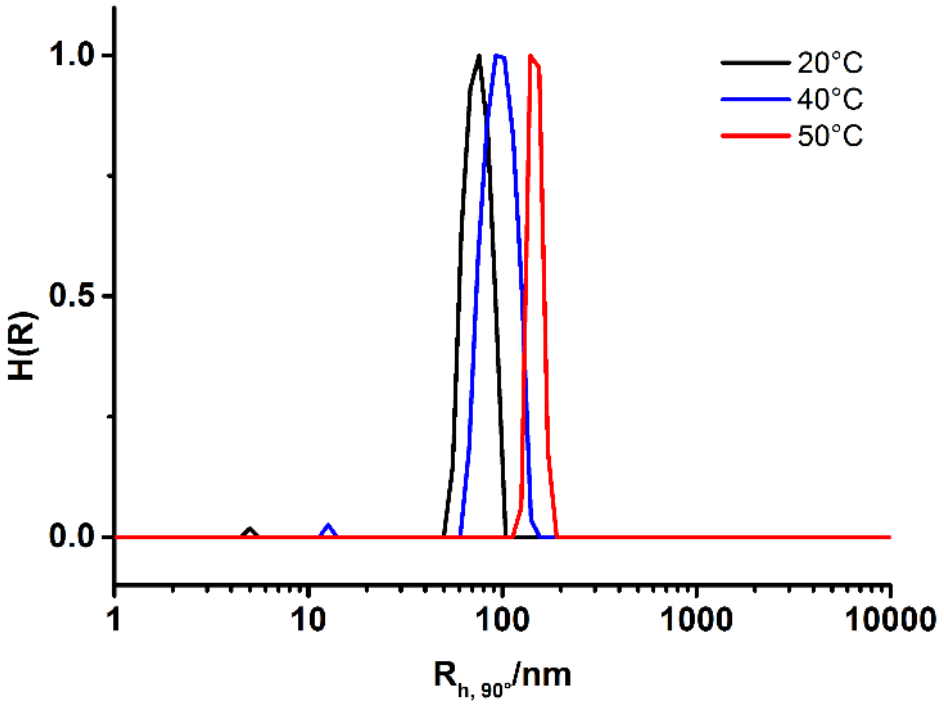

Figure 7.20: Temperature dependence of intensity weighed size distribution of polymersomes produced from *m*-PEG-*b*-P(1_{23}-*co*-2^{COOH}_{36}) at a concentration of 10 g L^{-1}. Increasing temperature induces an increase of R_h without broadening of size-distribution, indicating a swelling of the polymersome.

Transmission electron microscopy of a sample embedded in a trehalose matrix (to retain the native structure as much as possible) confirmed the presence of vesicular structures with diameters between 100 and 200 nm (Figure 7.21, left). These polymersomes were very bright compared to the uranyl acetate stained background indicating a low permeability for the contrast agent. Upon heating these polymersomes, an irreversible growth in size due to the hydrophobic to hydrophilic transition of the phosphonate block resulting in an overall increased hydrophilicity of the polymer occurred (Figure 7.20).

The size-distribution remained narrow, indicating a swelling rather than precipitation of the polymer. At a temperature of 40 °C, a size increase of 30% was observed in temperature-dependent DLS measurements. A similar, though reversible, behavior was presented by Dong *et al.* and Yan *et al*., who demonstrated the synthesis of "breathing" polymersomes for stimuli-responsive payload release or growing compartments.[50,51] The temperature dependent growth was further visualized by TEM.

At room temperature, vesicular structures with diameters between 100 and 200 nm were observed. By preparation and fixation of the sample at elevated temperatures (40 °C), however, in accordance with DLS results, the observed vesicles were considerably larger. This was accompanied by a substantial accumulation of contrast agent inside the vesicle, indicating an increased permeability of the membrane (Figure 7.21, right).

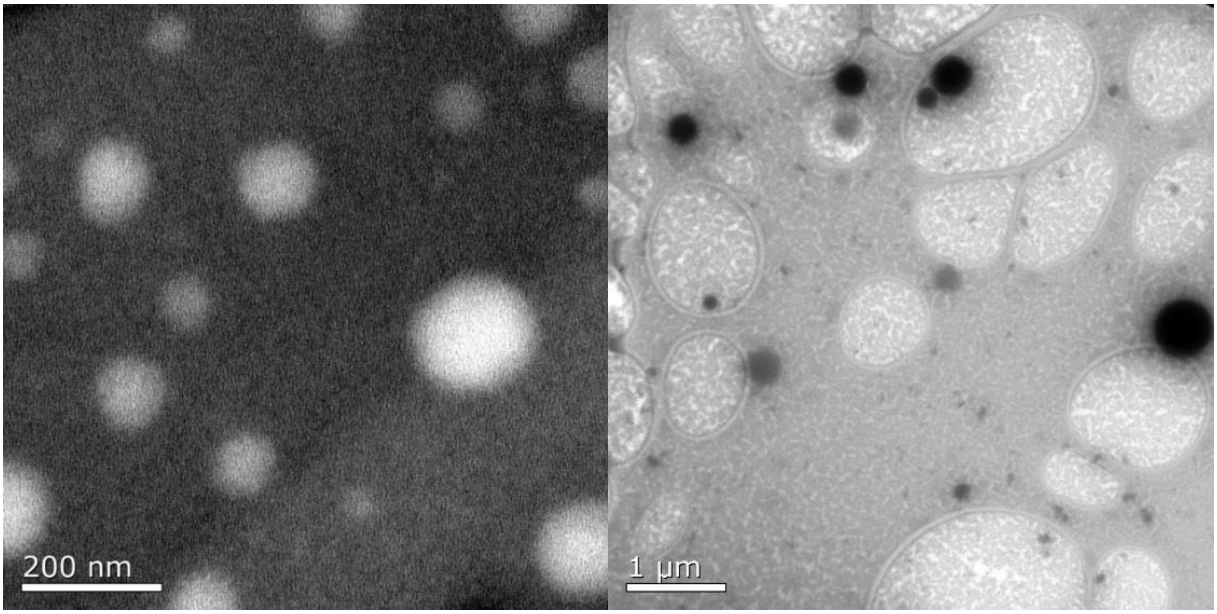

Figure 7.21: Transmission electron microscopy (TEM) image (in trehalose matrix, stained with uranyl acetate) of *m*-PEG-*b*-P(1_{23}-*co*-2^{COOH}_{36}) after self-assembly into polymersomes in water at room temperature (left) and 40 °C (right).

Upon decreasing the amount of –COOH groups in the phosphonate block to 50%, thus decreasing the H-bonding capacities of the hydrophobic block and the amount of hydrophobic thioether side-chains, the temperature behavior changed. **m-PEG$_{113}$-*b*-P(1$_{30}$-*co*-2$^{COOH}_{30}$)**, self-assembled into polymersomes with a hydrodynamic diameter of D_h = 250 nm. TEM was again used to visualize these structures. Well-defined polymersomes with an aqueous core and a membrane of ~ 20 nm thickness were observed (Figure 7.22, a).

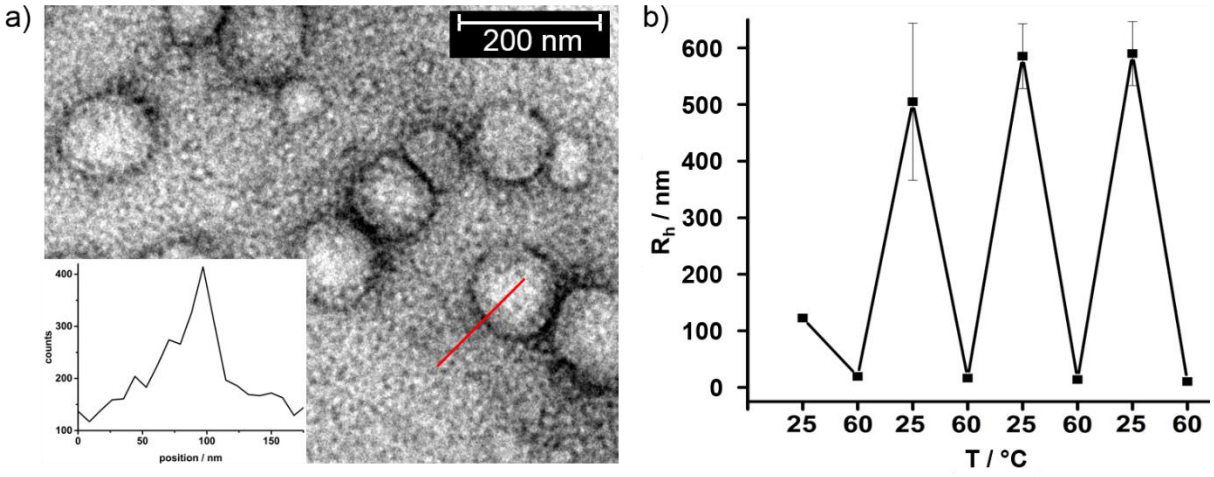

Figure 7.22: Analytical data of thermoresponsive block copolymer m-PEG$_{113}$-*b*-P(1$_{30}$-*co*-2$^{COOH}_{30}$): a) Transmission electron microscopy (TEM) image (in trehalose matrix, stained with uranyl acetate) of block copolymers after self-assembly into polymersomes in water at room temperature. Inset: EDX phosphorus signal of line-scan (red). Scale bar 200 nm. b) Temperature-dependent DLS measurements of m-PEG$_{113}$-*b*-P(1$_{30}$-*co*-2$^{COOH}_{30}$) in water (10 g L^{-1}). Hydrodynamic radius (number average weighing) plotted against temperature after several heating-cooling cycles.

The mean diameter of 170 nm was smaller than the diameter determined from DLS measurements as a result of shrinkage during the TEM measurement in the saccharide matrix. Elemental analysis via EDX-line scanning measurements showed a high enrichment of phosphorus in the vesicle membrane compared to the external and internal medium (see inset in Figure 7.22, a). Again, a low contrast as a consequence of low uranyl acetate concentration inside the polymersome implies little permeability of the membrane.

Upon heating, however, the polymersomes of **m-PEG$_{113}$-*b*-P(1$_{30}$-*co*-2$^{COOH}_{30}$)** completely disassembled due to the hydrophobic-hydrophilic change of the poly(phosphonate) block and the lower amount of hydrophobic side-chains. This disintegration was again observed via temperature DLS measurements. Figure 7.22, b shows the hydrodynamic radius plotted against the temperature after several heating-cooling cycles. The radius decreased from the initial 127 nm (polymersomes “as prepared” after sonication) at 25 °C to 17 nm at 60 °C, proving the disintegration of the polymersomes. This process was reversible as the polymersomes reformed at lower temperatures and disintegrated again at elevated temperature. The size of these temperature-induced self-assembled structures leveled at R_h of ca. 600 nm after several heating-cooling cycles, after which their size became fully reversible.

The vesicular structure after the temperature-induced self-assembly was visualized by TEM (Figure 7.23).

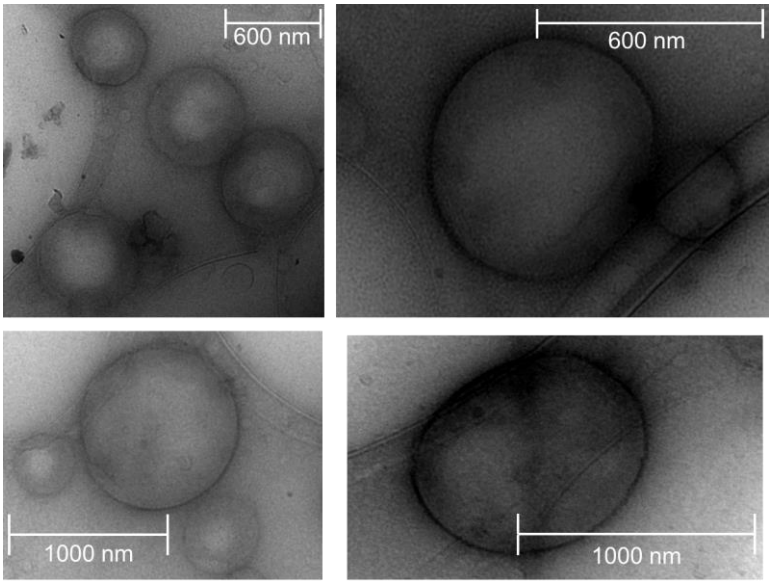

Figure 7.23: Transmission electron microscopy (TEM) image (in trehalose matrix, stained with uranyl acetate) of large block copolymer vesicles of *m*-PEG-*b*-P(1_{30}-*co*-2^{COOH}_{30}) after one (top row) and three (bottom row) heating-cooling cycles.

Summary and Conclusion

To conclude, we were able to synthesize poly(ethylene alkyl phosphonate) copolymers exhibiting adjustable UCST phase separation in water. Synthesis proceeded via the AROP of cyclic monomers and produced copolymers with excellent control over molecular weight, copolymer composition, and narrow molecular weight distributions. Attachment of carboxylic acid groups onto the reactive allyl-side chains via photochemical thiol-ene reaction provided H-bonding moieties to induce the UCST thermoresponsiveness. The polymers were hydrolytically degradable at basic pH values and non-cell-toxic in *in-vitro* tests. The concentration-, pH-, and composition-dependencies of the thermo-responsive phase separation were thoroughly investigated and discussed. These polymers were used as thermo-responsive switches to control self-assembly and disassembly of block copolymers in water. PEG-b-PPEs with variable transition temperatures assembled into polymersomes at room temperature that changed their solubility profile at elevated temperatures. Depending on the amount of carboxylic acid groups in the thermo-responsive block, upon heating an increased membrane permeability and swelling, or a reversible assembly/disassembly of the polymersomes at lower temperatures was achieved. In contrast to well-established block copolymers with LCST-segments and their

temperature-responsive self-assembly,[52-54] the use of UCST block copolymers to form vesicles is investigated to a much lesser extent.[55] Even though the complete disintegration of the polymersomes only occurs at non-physiological temperatures, we believe that the swelling occurring at temperatures around 40 °C makes them a promising platform for future research for stimuli-responsive compartmentalization, heat therapy, or delivery applications towards areas of increased temperature, such as inflamed or cancerous tissue.

Acknowledgement

The authors thank Prof. Dr. K. Landfester for continuous support, C. Rosenauer (MPIP) for DLS measurements, Dr. I. Lieberwirth, Dr. M. Kokkinopoulou, and K. Kirchhoff (MPIP) for TEM measurements and discussion and Dr. M. Wagner (MPIP) for NMR measurements. The authors acknowledge support from the "Deutsche Forschungsgemeinschaft" (DFG WU 750/6-1).

References

1. Anastase-Ravion, S.; Ding, Z.; Pelle, A.; Hoffman, A. S.; Letourneur, D., *J. Chromatogr. B,* **2001,***761*, 247-254.
2. Kanazawa, H.; Yamamoto, K.; Matsushima, Y.; Takai, N.; Kikuchi, A.; Sakurai, Y.; Okano, T., *Anal. Chem.,* **1996,** *68*, 100-5.
3. Karimi, M.; Sahandi Zangabad, P.; Ghasemi, A.; Amiri, M.; Bahrami, M.; Malekzad, H.; Ghahramanzadeh Asl, H.; Mahdieh, Z.; Bozorgomid, M.; Ghasemi, A.; Rahmani Taji Boyuk, M. R.; Hamblin, M. R., *ACS Appl. Mater., Interfaces,* **2016,** *8,* 21107-33.
4. Yamato, M.; Akiyama, Y.; Kobayashi, J.; Yang, J.; Kikuchi, A.; Okano, T., *Prog. Polym. Sci.,* **2007,** *32*, 1123-1133.
5. Nayak, S.; Lee, H.; Chmielewski, J.; Lyon, L. A., *J. Am. Chem. Soc.,* **2004,** *126*, 10258-9.
6. Hoogenboom, R., *Angew. Chem.,* **2009,** *48*, 7978-94.
7. Sahn, M.; Yildirim, T.; Dirauf, M.; Weber, C.; Sungur, P.; Hoeppener, S.; Schubert, U. S., *Macromolecules,* **2016,** *49*, 7257-7267.
8. Jia, Z.; Chen, H.; Zhu, X.; Yan, D., *J. Am. Chem. Soc.,* **2006,** *128*, 8144-5.
9. Pasparakis, G.; Cockayne, A.; Alexander, C., *J. Am. Chem. Soc.,* **2007,** *129*, 11014-11015.
10. Stefanadis, C.; Chrysochoou, C.; Markou, D.; Petraki, K.; Panagiotakos, D. B.; Fasoulakis, C.; Kyriakidis, A.; Papadimitriou, C.; Toutouzas, P. K., *J. Clin. Oncol.,* **2001,** *19*, 676-81.
11. Nurkhamidah, S.; Woo, E. M., *Macromolecules,* **2012,** *45*, 3094-3103.
12. Li, S.-H.; Woo, E. M., *J. Polym. Sci. B Polym. Phys.,* **2008,** *46*, 2355-2369.
13. Seuring, J.; Agarwal, S., *Macromol. Rapid Commun.,* **2012,** *33*, 1898-920.
14. Schulz, D. N.; Peiffer, D. G.; Agarwal, P. K.; Larabee, J.; Kaladas, J. J.; Soni, L.; Handwerker, B.; Garner, R. T., *Polymer,* **1986,** *27*, 1734-1742.

15. Buscall, R.; Corner, T., *Eur. Polym. J.,* **1982,** *18*, 967-974.
16. Bulmus, V.; Patir, S.; Tuncel, S. A.; Piskin, E., *J. Control. Release, 76*, 265-274.
17. Aoki, T.; Nakamura, K.; Sanui, K.; Kikuchi, A.; Okano, T.; Sakurai, Y.; Ogata, N., *Polymer Journal,* **1999,** *31*, 1185-1188.
18. Plamper, F. A.; Schmalz, A.; Ballauff, M.; Muller, A. H., *J. Am. Chem. Soc.,* **2007,** *129*, 14538-9.
19. Seuring, J.; Agarwal, S., *Macromol. Chem. Phys.,* **2010,** *211*, 2109-2117.
20. Seuring, J.; Bayer, F. M.; Huber, K.; Agarwal, S., *Macromolecules,* **2012,** *45*, 374-384.
21. Amemori, S.; Kokado, K.; Sada, K., *J. Am. Chem. Soc., 134*, **2012,** 8344-8347.
22. Liu, F.; Seuring, J.; Agarwal, S., *Macromol. Chem. Phys.,* **2014,** *215*, 1466-1472.
23. Seuring, J.; Agarwal, S., *Acs Macro Lett.,* **2013,** *2*, 597-600.
24. Käfer, F.; Lerch, A.; Agarwal, S., *J. Polym. Sci. A Polym. Chem.,* **2017,** *55*, 274-279.
25. Zhang, G.; Wang, Y.; Liu, G., *Polym. Chem.,* **2016,** *7*, 6645-6654.
26. Di, Y.; Ma, X.; Li, C.; Liu, H.; Fan, X.; Wang, M.; Deng, H.; Jiang, T.; Yin, Z.; Deng, K., *Macromol. Chem. Phys.,* **2014,** *215*, 365-371.
27. Boustta, M.; Colombo, P. E.; Lenglet, S.; Poujol, S.; Vert, M., *J. Control. Release,* **2014,** *174*, 1-6.
28. Flory, P. J.; Osterheld, J. E., *J. Phys. Chem.,* **1954,** *58*, 653-661.
29. Bokias, G.; Staikos, G.; Iliopoulos, I., *Polymer,* **2000,** *41*, 7399-7405.
30. Sun, H.; Chen, X.; Han, X.; Liu, H., *Langmuir,* **2017,** *33*, 2646-2654.
31. Cummings, C.; Murata, H.; Koepsel, R.; Russell, A. J., *Biomacromolecules,* **2014,** *15*, 763-71.
32. Zhang, Y.; Chen, S.; Pang, M.; Zhang, W., *Polym. Chem.,* **2016,** *7*, 6880-6884.
33. Ye, H.; Owh, C.; Loh, X. J., *RSC Adv.,* **2015,** *5*, 48720-48728.
34. Wu, G.; Chen, S.-C.; Zhan, Q.; Wang, Y.-Z., *Macromolecules,* **2011,** *44*, 999-1008.
35. Fujihara, A.; Shimada, N.; Maruyama, A.; Ishihara, K.; Nakai, K.; Yusa, S., *Soft Matter,* **2015,** *11*, 5204-13.
36. Shih, Y. J.; Chang, Y.; Deratani, A.; Quemener, D., *Biomacromolecules,* **2012,** *13*, 2849-58.
37. Yuan, W.; Zou, H.; Guo, W.; Wang, A.; Ren, J., *J. Mater. Chem. B,* **2012,** *22*, 24783.
38. Steinbach, T.; Wurm, F. R., *Angew. Chem.,* **2015,** *54*, 6098-108.
39. Lin, H.; Wolf, T.; Wurm, F. R.; Kelland, M. A., *Energy Fuels,* **2017,** *31*, 3843-3848.
40. Steinbach, T.; Ritz, S.; Wurm, F. R., *Acs Macro Lett.,* **2014,** *3*, 244-248.
41. Wolf, T.; Steinbach, T.; Wurm, F. R., *Macromolecules,* **2015,** *48*, 3853-3863.
42. Wolf, T.; Nass, J.; Wurm, F. R., *Polym. Chem.,* **2016,** *7*, 2934-2937.
43. Uysal, B. B.; Gunay, U. S.; Hizal, G.; Tunca, U., *J. Polym. Sci. A Polym. Chem.,* **2016,** *52*, 1581-1587.
44. Steinbach, T.; Alexandrino, E. M.; Wahlen, C.; Landfester, K.; Wurm, F. R., *Macromolecules,* **2014,** *47*, 4884-4893.
45. Bauer, K. N.; Tee, H. T.; Lieberwirth, I.; Wurm, F. R., *Macromolecules,* **2016,** *49*, 3761-3768.
46. Wang, Y. C.; Tang, L. Y.; Sun, T. M.; Li, C. H.; Xiong, M. H.; Wang, J., *Biomacromolecules,* **2008,** *9*, 388-95.
47. Bender, A. T.; Beavo, J. A., *Pharmacol. Rev.,* **2006,** *58*, 488-520.
48. Horsman, G. P.; Zechel, D. L., *Chem. Rev.,* **2017,***117*, 5704-5783.

49. Zhang, Y.; Furyk, S.; Bergbreiter, D. E.; Cremer, P. S., J*. Am. Chem. Soc.,* **2005,** *127*, 14505-10.
50. Yan, Q.; Wang, J.; Yin, Y.; Yuan, J., *Angew. Chem.,* **2013,** *52*, 5070-3.
51. Dong, R.; Zhu, B.; Zhou, Y.; Yan, D.; Zhu, X., *Angew. Chem.,* **2012,** *51*, 11633-7.
52. Lee, J. S.; Zhou, W.; Meng, F.; Zhang, D.; Otto, C.; Feijen, J., *J. Control. Release,* **2010,** *146*, 400-8.
53. Agut, W.; Brulet, A.; Schatz, C.; Taton, D.; Lecommandoux, S., *Langmuir,* **2010,** *26*, 10546-54.
54. Qin, S.; Geng, Y.; Discher, D. E.; Yang, S., *Adv. Mater.,* **2006,** *18*, 2905-2909.
55. Yoshimitsu, H.; Korchagina, E.; Kanazawa, A.; Kanaoka, S.; Winnik, F. M.; Aoshima, S., *Polym. Chem.,* **2016,** *7*, 2062-2068.

Supporting Information for

Degradable Polymersomes with Upper Critical Solution Temperature - Induced Disassembly in Water

Materials

Solvents and chemicals were purchased from Acros Organics, Sigma Aldrich or Fluka and used as received unless otherwise stated. All chemicals were purchased in highest purities, dry and stored over molecular sieve (4Å), if possible. 2-(Methoxy)ethanol and DBU were distilled from calcium hydride and stored over molecular sieve (4Å) under argon before use. Deuterated solvents were purchased from Deutero GmbH (Kastellaun, Germany) and used as received. Ultrapure water with a resistivity of 18.2 MΩ cm^{-1} (Milli-Q, Millipore®) was used to prepare buffers. Dulbecco's Modified Eagle Medium (DMEM), fetal bovine albumin (FBS) penicillin and streptomycin were purchased from Invitrogen, Germany.

Instrumentation and Characterization Techniques

Size exclusion chromatography (SEC) measurements were performed on two different setups: In DMF (1 g L^{-1} LiBr added) at 60 °C and a flow rate of 1 mL min^{-1} with a PSS SECcurity as an integrated instrument, including a PSS GRAM 100-1000 column and a refractive index (RI) detector. Calibration was carried out using poly(ethylene glycol) standards provided by Polymer Standards Service. In phosphate buffered saline (100 mM phosphate, 50 mM sodium chloride, pH 6.5 at 25 °C and a flow rate of 1 mL min^{-1} with a set of HEMA-Bio columns (40/100/1000) with 10 µm particles with a length of 300 mm and an internal diameter of 8 mm from MZ-Analysentechnik. A refractive index (RI) detector (Agilent 1260) was used for detection. Calibration was carried out using poly(ethylene glycol) standards provided by Polymer Standards Service. All NMR experiments were acquired on a Bruker 500 AMX system. The temperature was kept at 298.3K and calibrated with a standard ^{1}H methanol NMR sample using the topspin 3.0 software (Bruker). $^{13}C\{H\}$ NMR spectra were referenced internally to solvent signals. $^{31}P\{H\}$ NMR spectra were referenced externally to phosphoric acid. The $^{13}C\{H\}$ NMR (125 MHz) and $^{31}P\{H\}$ NMR (201 MHz) measurements were obtained with a 1H powergate decoupling method using 30 °

degree flip angle. 1D and $^{1}H^{1}H$ TOCSY (total correlation spectroscopy) NMR spectra were processed with the MestReNova 9.0.1-13254 software whereas ^{1}H DOSY (diffusion orientated spectroscopy) NMR spectra were processed with the TopSpin 3.0 software. Differential Scanning Calorimetry (DSC) measurements were performed using a Mettler-Toledo DSC823 thermal analysis system in the temperature range from -100 to 100 °C under nitrogen with a heating rate of 10 °C min^{-1}. Cloud points were determined either in ultrapure water with a resistivity of 18.2 MΩ cm^{-1} (Milli-Q, Millipore®) or in otherwise stated salt solutions and detected by the optical transmittance of a light beam (λ = 500 nm) through a 1 cm sample cell. The measurements were performed on a Jasco V-630 photo spectrometer with a Jasco ETC-717 Peltier element. The intensity of the transmitted light was recorded versus the temperature of the sample cell. The temperature ramp was 1 °C min^{-1} and values were recorded every 0.1 °C. Dynamic light scattering (DLS) measurements were performed on an ALV spectrometer consisting of a goniometer and an ALV-5004 multiple-tau full-digital correlator (320 channels) which allows measurements over an angular range from 30° to 150. A He-Ne Laser (wavelength of 632.8 nm) is used as light source. For temperature controlled measurements the light scattering instrument is equipped with a thermostat from Julabo. Measurements were performed at 90° angle (5 measurements, 30 seconds averaged) Temperature was increased from 25 °C to 60 °C (step 5 °C). After reaching the desired temperatures, samples were tempered for 15 minutes before continuing. Transmission electron microscopy (TEM) measurements were performed on a Tecnai F20 electron microscope (FEI, Thermo Fisher Scientific) at a voltage of 200KV. Samples were prepared on a lacey grid as a 1 to 1 mixture of the dispersion and an aqueous trehalose solution ($1\%_{wt}$) for fixation to retain the natural conformation and stained with uranyl acetate solution ($4\%_{wt}$). Murine macrophage-like cells (RAW 264.7) were cultivated in DMEM supplemented with 10% FBS, 100 units of penicillin, and 100 mg mL^{-1} streptomycin. Cells were grown in a humidified incubator at 37 °C and 5% CO_2. The effect of **P(1_n-*co*-2_m)** and **P(1_n-*co*-2^{COOH}_m)** on cell viability of RAW 264.7 cells was measured by CellTiter-Glo Luminescent Cell Viability Assay (Promega) according to the manufacturer. Luminescent signals were measured with a Tecan infinite M1000. RAW 264.7 cells were seeded at a density of 15,000 cells cm^{-2} in 96-well plates (100 µL per well). The polymers were dissolved in DMEM (stock concentration: 1 mg mL^{-1}) and further diluted

to the indicated concentrations. After 24h of incubation, the cell culture medium was replaced by the polymer supplemented medium, and cells were incubated for 48h.

Experimental

***O, O*-diethyl allyl phosphonic acid diester:** Triethylphosphite (194.50 g, 1.17 mol) and allyl bromide (173.00 g, 1,43 mol) were heated at 71 °C for 23h in a round-bottom flask equipped with a dean-stark receiver to collect the formed bromoethane. Fractionated distillation of the mixture yielded the desired phosphonic acid diester as a colorless liquid. (192.37 g, 1.08 mol, yield: 93%, bp 60-62 °C / 4 mbar). ^{1}H NMR ($CDCl_3$, 500 MHz, 298K, ppm): δ = 5.82 – 5.66 (m, 1H, -C**H**=CH_2), 5.22 – 5.08 (m, 1H, -CH=C**H$_2$**), 4.13 – 43.97 (m, 4H, -P-O-C**H$_2$**-), 2.55 (ddt, 2H, $^{2}J_{HP}$ = 21.9 Hz, $^{2}J_{HH}$ = 7.4 Hz, $^{3}J_{HH}$ = 1.3 Hz, -P-C**H$_2$**-), 1.26 (t, 6H, $^{3}J_{HH}$ = 7.1 Hz, -O-CH_2-C**H$_3$**). ^{13}C{H} NMR ($CDCl_3$, 125 MHz, 298K, ppm): δ = 127.49 (s, -C=**C**), 119.73 (d, $^{2}J_{CP}$ = 16.5 Hz)-**C**=C), 61.79 (s, -P-O-**C**-), 31.66 (d, $^{1}J_{CP}$ = 137.5 Hz, P-**C**-), 16.27 (s, -O-C-**C**). ^{31}P{H} NMR ($CDCl_3$, 201 MHz, 298K, ppm): δ = 26.90

Allyl phosphonic acid dichloride: *O, O*-diethyl allyl phosphonic acid diester (50.00 g, 0.30 mol) was dissolved in acetonitrile (400 mL) in a flame-dried 100 mL Schlenk-flask under argon. Dry sodium iodide (84.00 g, 0.60 mol) was added. The Schlenk-flask was equipped with a dropping funnel, and chlorotrimethylsilane (136.00 g, 1.20 mol) was added dropwise at room temperature. After complete addition, the reaction was heated to 40 °C for 2h. ^{31}P{H} NMR analysis of the crude reaction mixture confirmed the formation of *O, O*-bis(trimethyl)silyl allyl phosphonic acid diester. ^{31}P{H} NMR ($CDCl_3$, ppm): δ = 22.07. Excess of chlorotrimethylsilane and solvent were evaporated *in vacuo*. The crude ester was used without further purification. It was dissolved in dry dichloromethane (100 mL), and DMF (0.5 mL) was added. Oxalyl chloride (102.00 g, 1.20 mol) was added drop-wise at room temperature. After complete addition, the reaction was stirred for 16h. Fractionated distillation yielded the desired product as a colorless liquid (56.5 g, yield: 60% over two steps, b.p. 100 °C / 40 mbar). ^{1}H NMR ($CDCl_3$, ppm): δ 5.29 - 5.73 (m, 1H, -C**H**=CH_2), 5.53 - 5.37 (m, 2H, -CH=C**H$_2$**), 3.37 (ddt, $^{2}J_{HP}$ = 19.0 Hz, $^{3}J_{HH}$ = 7.3 Hz, $^{4}J_{HH}$ = 1.1 Hz, 2H, P-C**H$_2$**-). ^{13}C{H} NMR

($CDCl_3$, ppm): δ 124.57 (d, $^2J_{CP}$ = 19.5 Hz, -C=**C**), 124.02 (d, $^3J_{CP}$ = 14.7 Hz, -**C**=C), 47.58 (d, $^1J_{CP}$ = 97.5 Hz, P-**C**-). $^{31}P\{H\}$ NMR ($CDCl_3$, ppm): δ 46.02.

2-Allyl-2-oxo-1,3,2-dioxaphospholane (2): The cyclic monomer was synthesized according to a modified literature procedure.[1] A flame-dried three-necked round-bottom flask, equipped with a magnetic stirring bar and two dropping funnels, was charged with 250 mL dry THF and cooled to -21 °C. Allyl phosphonic acid dichloride (29.2 g, 0.20 mol) was dissolved in dry THF (250 mL) and transferred into one dropping funnel via a flame-dried stainless steel capillary. A solution of dry ethylene glycol (11.0 g, 0.20 mol) and dry pyridine (29.0 g, 0.40 mol) in THF (250 mL) was transferred into the second dropping funnel via a flame-dried stainless steel capillary. Dropping speed was adjusted to be approximately equal for both mixtures, and the reaction temperature kept at -21 °C. After complete addition the solution was stirred for 5h and kept over-night at -28 °C to facilitate the precipitation of the pyridinium hydrochloride byproduct. The precipitate was removed by filtration via a flame-dried Schlenk funnel, and the solvent was removed *in vacuo*. Fractionated distillation yielded the desired product as colorless oil (14.1 g, yield: 51%, b.p. 86 °C / 1x10^{-3} mbar). ^1H NMR ($CDCl_3$, ppm): δ 5.81 - 5.65 (m, 1H, -C**H**=CH_2), 5.33 - 5.17 (m, 2H, -CH=C**H₂**), 4.52 - 4.37 (m, 2, H-P-O-C**H₂**-), 4.30 - 4.11 (m, 2H, -P-O-C**H₂**-), 2.82 (ddt, $^2J_{HP}$ = 22.0 Hz, $^3J_{HH}$ = 7.4 Hz, $^4J_{HH}$ = 1.2 Hz, 2H, -P-C**H₂**-). $^{13}C\{H\}$ NMR ($CDCl_3$, ppm): δ 126.46 (d, $^2J_{CP}$ = 12.1 Hz, -**C**=C), 121.02 (d, $^3J_{CP}$ = 14.3 Hz, -C=**C**), 66.72 (s, -P-O-**C**-), 31.15 (d, $^1J_{CP}$ = 129.5 Hz, -P-**C**-). $^{31}P\{H\}$ NMR ($CDCl_3$, ppm): δ 45.91.

Representative procedure for the copolymerization of dioxaphospholanes: The monomers were weighed into a flame-dried Schlenk-tube, dissolved in dry benzene and dried by repeated lyophilization. The monomers were dissolved in dry dichloromethane at a total concentration of 4 mol L^{-1}. A stock solution of initiator in dry dichloromethane was prepared with a concentration 0.2 mol L^{-1}, and the calculated amount was added to the monomer solution via a gas-tight syringe (Hamilton®). A stock solution of DBU in dry dichloromethane was prepared with a concentration of 0.2 mol L^{-1}. The monomer solution and the catalyst solution were adjusted to 0 °C. The polymerization was initiated by the quick addition of the calculated volume of the

catalyst solution containing 3.0 equivalents of DBU with respect to the initiator. Polymerization was terminated after 16h by the rapid addition of an excess of formic acid dissolved in dichloromethane with a concentration of 20 mg mL^{-1}. The colorless, amorphous polymers were purified by precipitation in cold diethyl ether dialyzed against Milli-Q (Millipore®) water overnight and dried at reduced pressure.

Representative NMR data of P($\mathbf{1_{25}}$-*co*-$\mathbf{2_{25}}$): ^{1}H NMR ($CDCl_3$, 500 MHz, 298K, ppm): δ = 5.82 – 5.62 (m, side-chain, -C**H**=CH_2), 5.30 – 5.11 (m, side-chain, -CH=C$\mathbf{H_2}$), 3.36 (s, initiator, C$\mathbf{H_3}$-O-), 4.22 - 4.01 (m, backbone, -C$\mathbf{H_2}$-C$\mathbf{H_2}$-), 2.84 – 2.62 (dd, side-chain, -P-C$\mathbf{H_2}$-C=, $^{2}J_{HP}$ = 22.0 Hz, $^{3}J_{HH}$ = 7.4 Hz), 1.83 - 1.69 (m, side-chain -P-C$\mathbf{H_2}$-), 1.05 (dt, side-chain -P-CH_2-C$\mathbf{H_3}$, $^{2}J_{HP}$ = 20.1 Hz, $^{3}J_{HH}$ = 7.6 Hz). ^{13}C{H} NMR ($CDCl_3$, 125 MHz, 298K, ppm): δ = 127.05 (s, side-chain, P-C-**C**=C), 120.88 (s, side-chain, P-C-C=**C**), 64.56 (s, broad, backbone -**C**-), 30.99 (d, side-chain, P-**C**-C=C, $^{1}J_{CP}$ = 171,2 Hz), 18.89 (d, side-chain, P-**C**-C, $^{1}J_{CP}$ = 147,5 Hz), 6.31 (s, side-chain, P-C-**C**). ^{31}P{H} NMR ($CDCl_3$, 201 MHz, 298K, ppm): δ = 35.28 (**P**-CH_2-CH_3), 28.59 (**P**-CH_2-CH=CH_2).

Photochemical thiol-ene post-polymerization reaction with 3-mercaptopropionic acid: P($\mathbf{1_n}$-*co*-$\mathbf{2_m}$), 3-mercaptopropionic acid (2.5 eq relative to the amount of allyl groups) and 2,2-dimethoxy-2-phenyl acetophenone (10 mol%, relative to the amount of allyl groups) were dissolved in 0.25 mL DMF. The solution was degassed by three freeze-pump-thaw cycles and transferred into a quartz glass cuvette equipped with a stirring bar. The solution was irradiated at 365 nm for 1h. Afterwards, the polymer was precipitated from cold diethyl ether and dialyzed against water to yield **P($\mathbf{1_n}$-*co*-$\mathbf{2^{COOH}_m}$)**.

Representative NMR data of P($\mathbf{1_n}$-*co*-$\mathbf{2^{COOH}_m}$): ^{1}H NMR (DMSO-d_6, 500 MHz, 298K, ppm): δ = 4.22 - 4.01 (m, backbone, -C$\mathbf{H_2}$-C$\mathbf{H_2}$-), 3.12 (s, initiator, C$\mathbf{H_3}$-O-), 2.66 (t, side-chain, -S-C$\mathbf{H_2}$-, $^{3}J_{HH}$ = 5 Hz), 2.59 (t, side-chain, -C$\mathbf{H_2}$-S-, $^{3}J_{HH}$ = 5 Hz), 2.49 (t, side-chain, -C$\mathbf{H_2}$-COOH, $^{3}J_{HH}$ = 5 Hz), 1.95 – 1.86 (m, side-chain, -C$\mathbf{H_2}$-CH_2-S-), 1.84 – 1.71 (m, side-chain, P-CH_2-), 1.05 (dt, side-chain -P-CH_2-C$\mathbf{H_3}$, $^{2}J_{HP}$ = 20.1 Hz, $^{3}J_{HH}$ = 7.6 Hz), ^{13}C{H} NMR (DMSO-d_6, 125 MHz, 298K, ppm): δ = 173.37 (s, side-chain, -

COOH), 64.76 (s, broad, backbone, -**C**-), 34.87 (s, side-chain, -S-**C**-), 26.81 (s, side-chain, -P-C-C-**C**-S-), 24.14 (d, side-chain, -P-**C**-, $^{1}J_{CP}$ = 138,7 Hz), 22.68 (d, side-chain, -P-C-**C**-, $^{2}J_{CP}$ = 3.7 Hz), 18.23 (d, side-chain, -P-**C**-, $^{1}J_{CP}$ = 140.0 Hz), 6.71 (d, side-chain, -P-C-C, $^{2}J_{CP}$ = 6.2 Hz).^{31}P{H} NMR (DMSO-d_6, 201 MHz, 298K, ppm): δ = 34.52 (**P**-CH_2-CH_3), 32,70 (**P**-CH_2-CH_2-CH_2-S-).

Representative NMR data of m-PEG-*b*-P(1$_n$-*co*-2$^{COOH}_m$): ^{1}H NMR (DMSO-d_6, 500 MHz, 298K, ppm): δ = 4.22 - 4.01 (m, backbone, -C**H$_2$**-C**H$_2$**-), 3.50 (s, backbone PEG, -O-C**H$_2$**-C**H$_2$**-), 3.24 (s, initiator, C**H$_3$**-O-), 2.66 (t, side-chain, -S-C**H$_2$**-, $^{3}J_{HH}$ = 5 Hz), 2.59 (t, side-chain, -C**H$_2$**-S-, $^{3}J_{HH}$ = 5 Hz), 2.49 (t, side-chain, -C**H$_2$**-COOH, $^{3}J_{HH}$ = 5 Hz), 1.95 – 1.86 (m, side-chain, -C**H$_2$**-CH_2-S-), 1.84 – 1.71 (m, side-chain, P-CH_2-), 1.05 (dt, side-chain -P-CH_2-C**H$_3$**, $^{2}J_{HP}$ = 20.1 Hz, $^{3}J_{HH}$ = 7.6 Hz), ^{13}C{H} NMR (DMSO-d_6, 125 MHz, 298K, ppm): δ = 173.37 (s, side-chain, -**C**OOH), 70.21 (s, backbone PEG -O-**C**-), 64.76 (s, broad, backbone, -**C**-), 34.87 (s, side-chain, -S-**C**-), 26.81 (s, side-chain, -P-C-C-**C**-S-), 24.14 (d, side-chain, -P-**C**-, $^{1}J_{CP}$ = 138,7 Hz), 22.68 (d, side-chain, -P-C-**C**-, $^{2}J_{CP}$ = 3.7 Hz), 18.23 (d, side-chain, -P-**C**-, $^{1}J_{CP}$ = 140.0 Hz), 6.71 (d, side-chain, -P-C-C, $^{2}J_{CP}$ = 6.2 Hz).^{31}P{H} NMR (DMSO-d_6, 201 MHz, 298K, ppm): δ = 34.52 (**P**-CH_2-CH_3), 32,70 (**P**-CH_2-CH_2-CH_2-S-).

Polymersome preparation: For a typical polymersome preparation, the respective block-copolymer (10 mg) was dissolved in DMSO (10 µL) and diluted in ultrapure water (990 µL) to a concentration of 10 g L^{-1} in a sonication bath.

Supporting figures

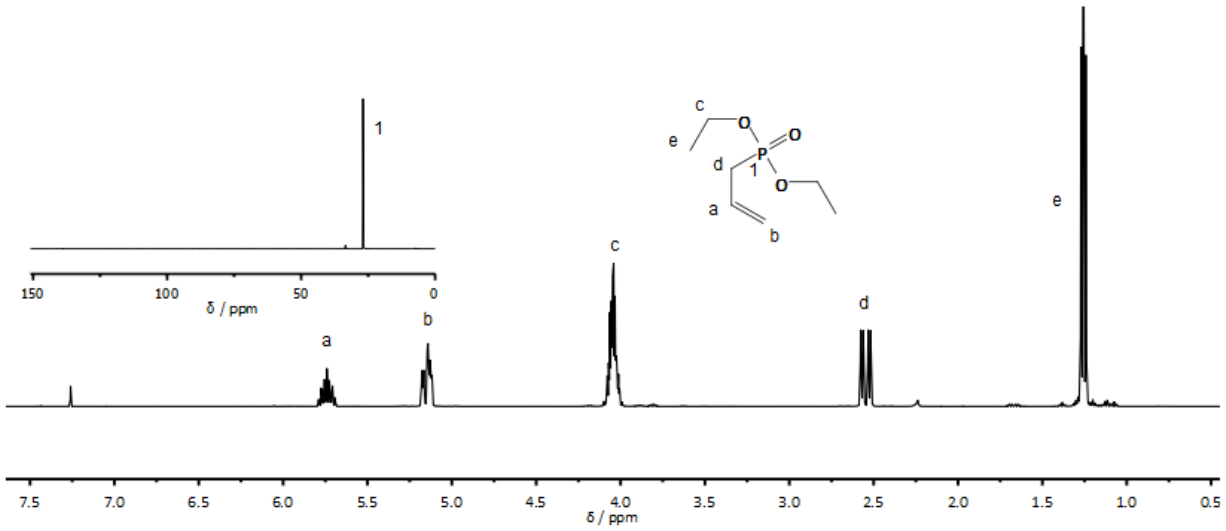

Figure S7.1: ^{1}H (500 MHz) and ^{31}P (201 MHz) NMR spectra of O, O-diethyl allyl phosphonate in $CDCl_3$ at 298K.

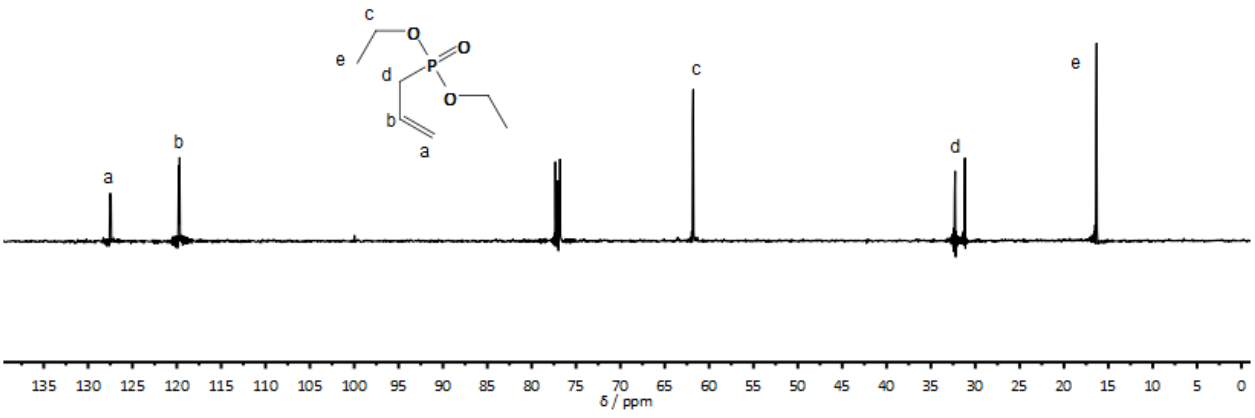

Figure S7.2: ^{13}C (125 MHz) NMR spectrum O, O-diethyl allyl phosphonate in $CDCl_3$ at 298K.

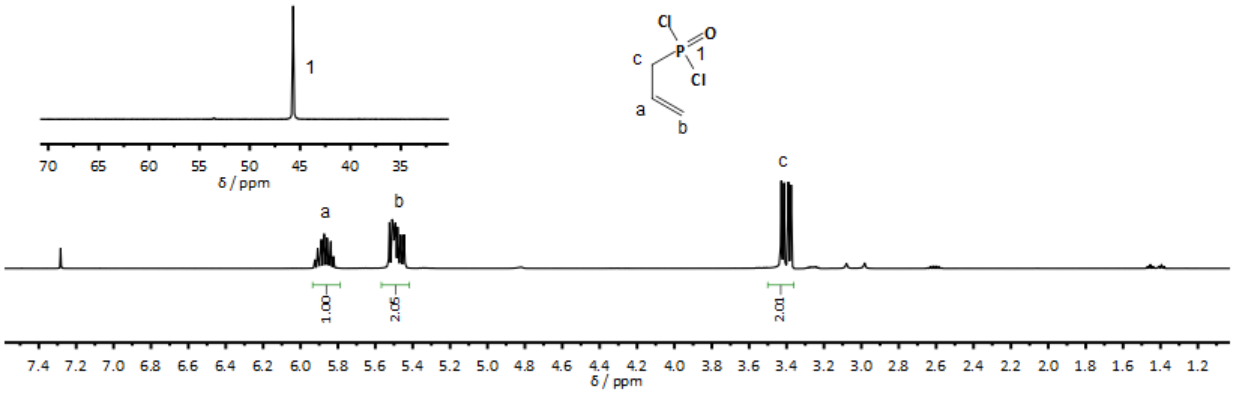

Figure S7.3: ^{1}H (500 MHz) and ^{31}P (201 MHz) NMR spectra of allyl phosphonic acid dichloride in $CDCl_3$ at 298K.

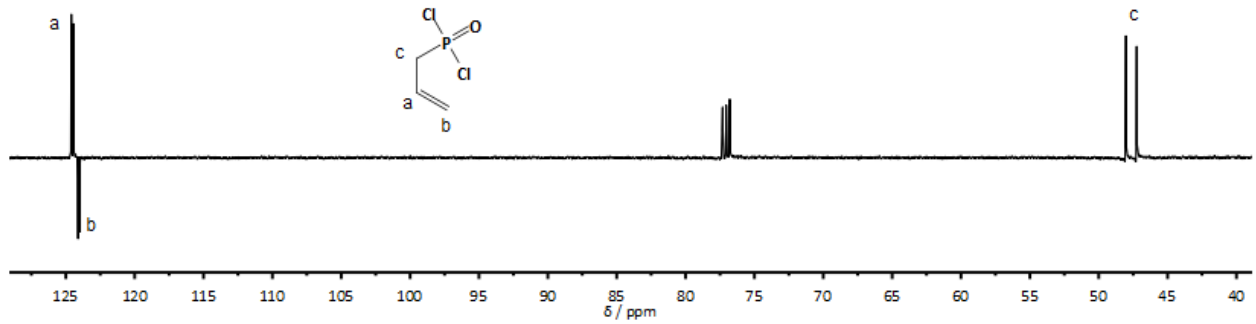

Figure S7.4: ^{13}C (125 MHz) NMR spectrum of allyl phosphonic acid dichloride in $CDCl_3$ at 298K.

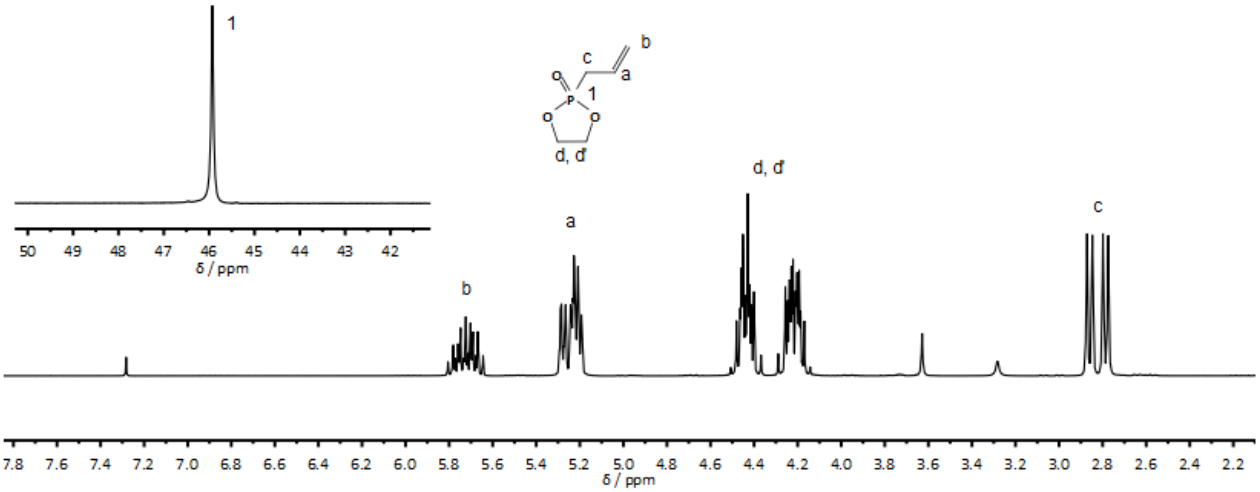

Figure S7.5: ^{1}H (500 MHz) and ^{31}P (201 MHz) NMR spectra of 2-allyl-2-oxo-1,3,2-dioxaphospholane (2) in $CDCl_3$ at 298K.

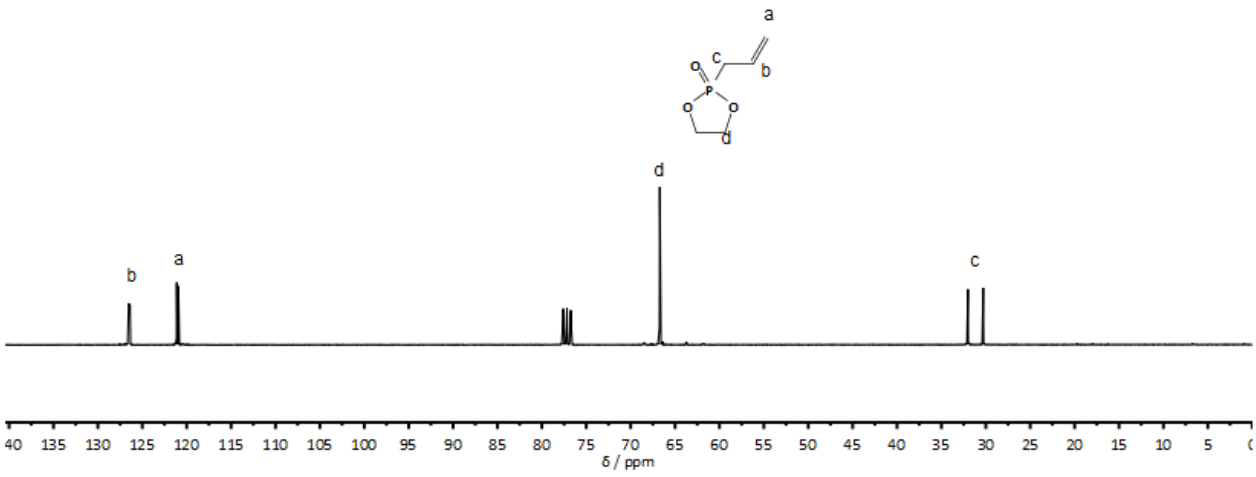

Figure S7.6: ^{13}C (125 MHz) NMR spectrum of 2-allyl-2-oxo-1,3,2-dioxaphospholane (2) in $CDCl_3$ at 298K.

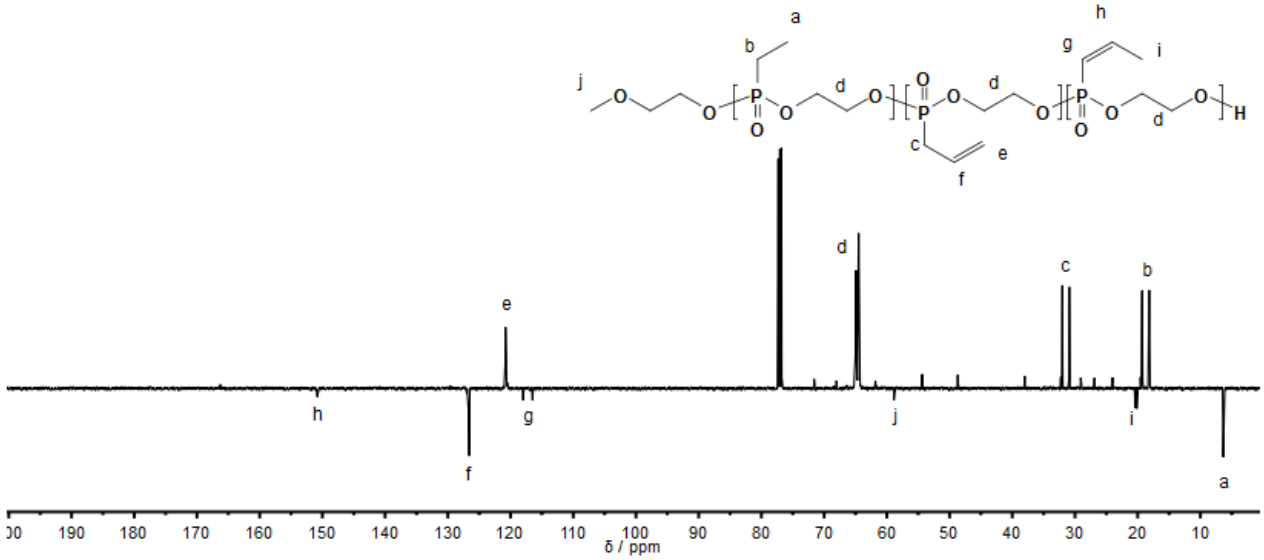

Figure S7.7: ^{13}C (125 MHz) NMR spectrum of P(1_n-*co*-2_m) in $CDCl_3$ at 298K.

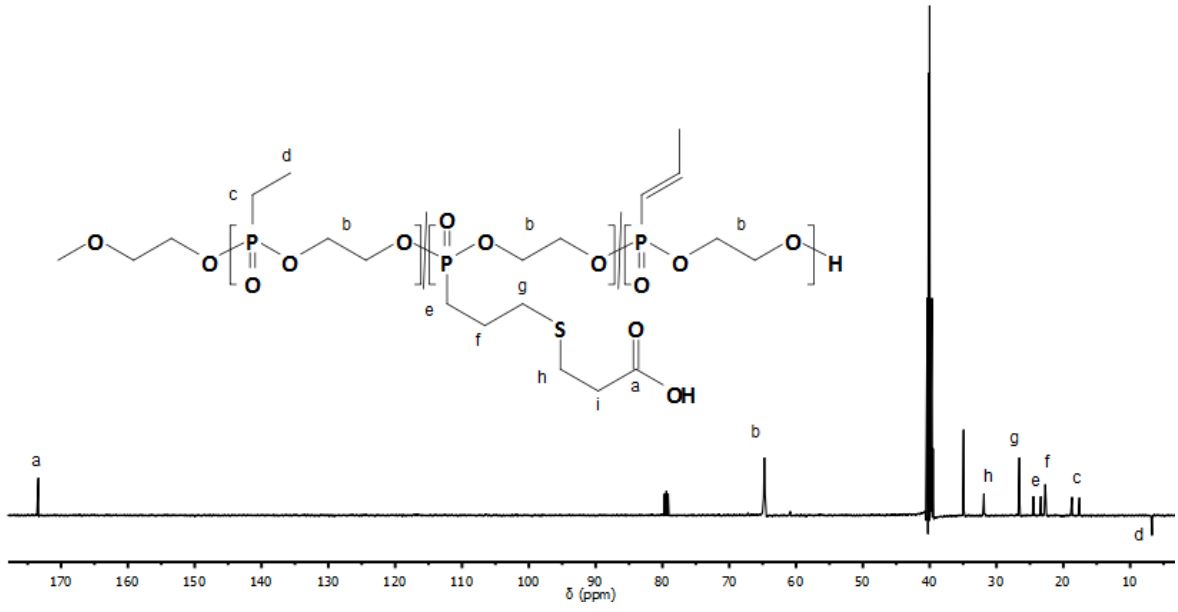

Figure S7.8: ^{13}C (125 MHz) NMR spectrum of P(1_n-*co*-2^{COOH}_m) in DMSO-d_6 at 298K.

1. Steinbach, T.; Ritz, S.; Wurm, F. R., *ACS macro letters* **2014,** *3* (3), 244-248.

Chapter 7: Degradable Polymersomes with Upper Critical Solution Temperature Induces Disassembly in Water.

All previously presented chapters discussed the synthesis, characterization, degradation, and temperature dependent solubility behavior of PPn homo-, co-, and terpolymers. In most cases, a direct comparison with poly(ethylene glycol), the gold standard for polymers in biomedical applications, was made with the emphasis on PPns being more chemically versatile and degradable.

One major asset of PEG, however, is the fact that PEGylated surfaces and drugs are less prone to degradation and significantly less likely to be recognized by the cells of the immune system. Both result in an increased residence time in the bloodstream and beneficial effect on the overall pharmacokinetics of the drug. The decreased immune system recognition, the “stealth effect”, is already clinically used to prolong the plasma halftime of several drugs. Therefore, in order to seriously be considered as a complementary to PEG, every potential PEG alternative needs to show similar degrees of “stealth”.

Chapter 8 presents the cooperation work with Johanna Simon from our group. The interactions of PPnylated (poly(phosphonate) modified) model nanocarriers with human blood components and cells of the immune system under *in vitro* conditions are investigated. We first show that PPnylated carriers show a similar behavior as PEGylated carriers, both regarding the amount and nature of the surface adsorbed proteins, as well as in their “stealth” behavior towards macrophages and Hela cells.

Afterwards, we utilize the chemical versatility of poly(phosphonate)s mentioned above to change the hydrophilicity of the polymers on the surface by copolymerization already discussed in **Chapter 4**. This enables us to investigate the influence of the polymer hydrophilicity on the “stealth” behavior of the respective surface polymers.

Chapter 8: Hydrophilicity Regulates Specific Protein Adsorption on Poly(phosphoester) Coated Nanocarriers Controlling Uptake in Immune Cells.

Johanna Simon[1‡], Thomas Wolf[1‡], Katja Klein[1], Katharina Landfester[1], Frederik R. Wurm[1], and Volker Mailänder[1,2]*

[1]Max-Planck-Institut für Polymerforschung, Ackermannweg 10, 55128 Mainz, Germany

[2]Dermatology Clinic, University Medical Center of the Johannes Gutenberg-University Mainz

‡Shared first author

Manuscript in preparation.

Thomas Wolf performed the polymer synthesis, characterization, nanoparticle surface modification, and colloidal analysis. **Johanna Simon** performed all biological experiments. This includes the cell-toxicity and cell-uptake studies, the confocal laser scanning microscopy, and the protein analysis (quantitative and qualitative).

Keywords: anionic ring-opening polymerization, random copolymerization, poly(phosphoester)s, poly(ethylene alkyl phosphonate)s, mini-emulsion polymerization, grafting-onto, protein corona, polymer-protein interactions, “stealth” effect

Abstract

Increasing the plasma half-time is an essential goal in the development and improvement of drugs and drug carriers. Attachment of polymer chains, especially poly(ethylene glycol) (PEG), the so-called PEGylation, is a well-established and effective method to increase the plasma half-time. However, the reasons for PEG's success are still widely unknown and were speculated to be a result of a decreased overall protein adsorption on the hydrophilic surface. We investigate the influence of surface properties of poly(phosphoester)-coated nanocarriers, focusing primarily on the surface hydrophilicity and on the protein adsorption behavior to control the stealth properties. We combine the precision of anionic ring-opening co-polymerization to poly(ethylene alkyl phosphonate)s with the grafting-onto process onto model polymer nanocarriers to control the surface hydrophilicity precisely. We found that the overall protein amount is unchanged despite the hydrophilicity of the investigated nanocarriers. However, the protein type is dramatically altered which eventually mediates the interaction with immune cells.

Introduction

Rapid clearance from the bloodstream and degradation are two major barriers foreign materials, such as nanocarriers, must face when entering the body. This results in a reduced plasma half-time which, together with high toxicity of many drugs, limits the pharmaceutical efficacy of many drug carriers.[1,2,3]

An efficient method to decrease the body clearance and the toxicity is the attachment of so-called "stealth" polymers (such as PEG),[4,5] which reduces the uptake of the "stealthed" carrier into immune cells (e.g., macrophages) and protect it from enzymatic degradation.[5] However, since PEG's initial discovery as a "stealth" polymer in 1977 several drawbacks of PEGylation have been revealed. These include the lack of chemical modification, the formation of toxic degradation products under oxidative conditions, and the rising amount of patients showing anti-PEG antibodies.[6,7,8]

Consequently, PEG alternatives have been developed, with similar "stealth" behavior, but potentially fewer side-effects and more chemical versatility. The most promising ones are polysaccharides[9,10], poly(2-oxazolines)[11,12] and poly(phosphoester)s

(PPEs).[13,14] It is noticeable, that all these "stealth" polymers differ significantly in their chemical structure and properties, but all reduce protein binding significantly.

However, recent studies proved that reducing the protein adsorption alone is not sufficient to induce "stealth" properties, but rather the specific adsorption of certain blood proteins is necessary for a reduced cellular uptake.[13] Upon exposure of nanocarriers to blood plasma, proteins adsorb on the nanocarrier's surface forming the so-called "protein corona".[15] This protein layer highly alters the properties such as size, charge or aggregation behavior of nanocarriers and affects the body distribution, toxicity, and especially cellular interactions.[16,17] Therefore, controlling the protein corona is crucial to design therapeutic effective nanocarriers. Corona proteins enhancing the interactions with phagocytic cells are called opsonins. Typical examples are immunoglobulins and complement proteins. Also, few proteins with the opposite effect are known, prolonging the blood circulation and preventing cellular interactions.[18] From these dysopsonins, albumin is the most prominent, while also apolipoprotein J (clusterin) was identified as a dysopsonin and was detected in high amounts on PEGylated, poly(phosphate) modified, and polysaccharide stealth nanocarriers.[9,13]

However, despite these new insights, an understanding of the stealth effect on the molecular level is still missing. Several studies cover the influence of surface charge[19,20] or hydrophilicity[21,22,23], particle size[21], and grafting density[24,25]. However, many of these studies lack detailed and quantitative investigation of the protein corona and only describe the cellular uptake behavior.

In this study, we investigated the interaction of PPn grafted model nanocarriers (NC) of different hydrophilicity and correlate their uptake into immune- and cancer cells and their "stealth" behavior with a detailed analysis of the protein adsorption pattern. Well-defined and degradable PPns with adjustable hydrophilicity were prepared by the organocatalytic anionic ring-opening polymerization (oAROP) of cyclic phosphonates and grafted onto model nanocarriers. The cell-uptake of these nanocarriers into a macrophage cell-line was investigated and correlated with the adsorption pattern of human blood proteins. We observed an increased cellular uptake of the NC's upon falling below a certain hydrophilicity threshold. Quantitative analysis of the protein amount adsorbed onto the NC's proved no increase in protein adsorption even above this threshold, but a distinct change in the protein adsorption pattern.

Results and Discussion

Copolymer Synthesis

A well-defined system is essential to investigate the relationship between surface hydrophilicity and stealth behavior of nanocarriers. Amino-functionalized, fluorescent poly(styrene) nanoparticles prepared by radical mini-emulsion polymerization were used as precise model nanocarriers to anchor the stealth polymers. Poly(ethylene alkyl phosphonate)s were synthesized via the living ring-opening copolymerization of 2-alkyl-2-oxo-1,3,2-dioxaphospholanes.[13] Well-defined, random copolymers with excellent control over the degree of polymerization and copolymer composition, as well as narrow molecular weight distributions were prepared.[24] To adjust the hydrophilicity of the polymers, 2-ethyl-2-oxo-1,3,2-dioxaphospholane **(1)**, leading to hydrophilic polymers comparable to PEG, was copolymerized with 2-*n*-butyl-2-oxo-1,3,2-dioxaphospholane **(2)**, providing hydrophobic side-chains. The respective homopolymer properties, as well as detailed synthetic protocols for the oAROP, have been reported previously.[26-28] Commercial 4-(maleinimido)phenyl isocyanate was used for ω-functionalization of the copolymers to introduce maleimide groups for *aza-Michael* addition with the surface amine groups (Figure 8.1, a). This combines the high control of polymer properties of oAROP with the isotropic surface coverage of the grafting-onto process.[24]

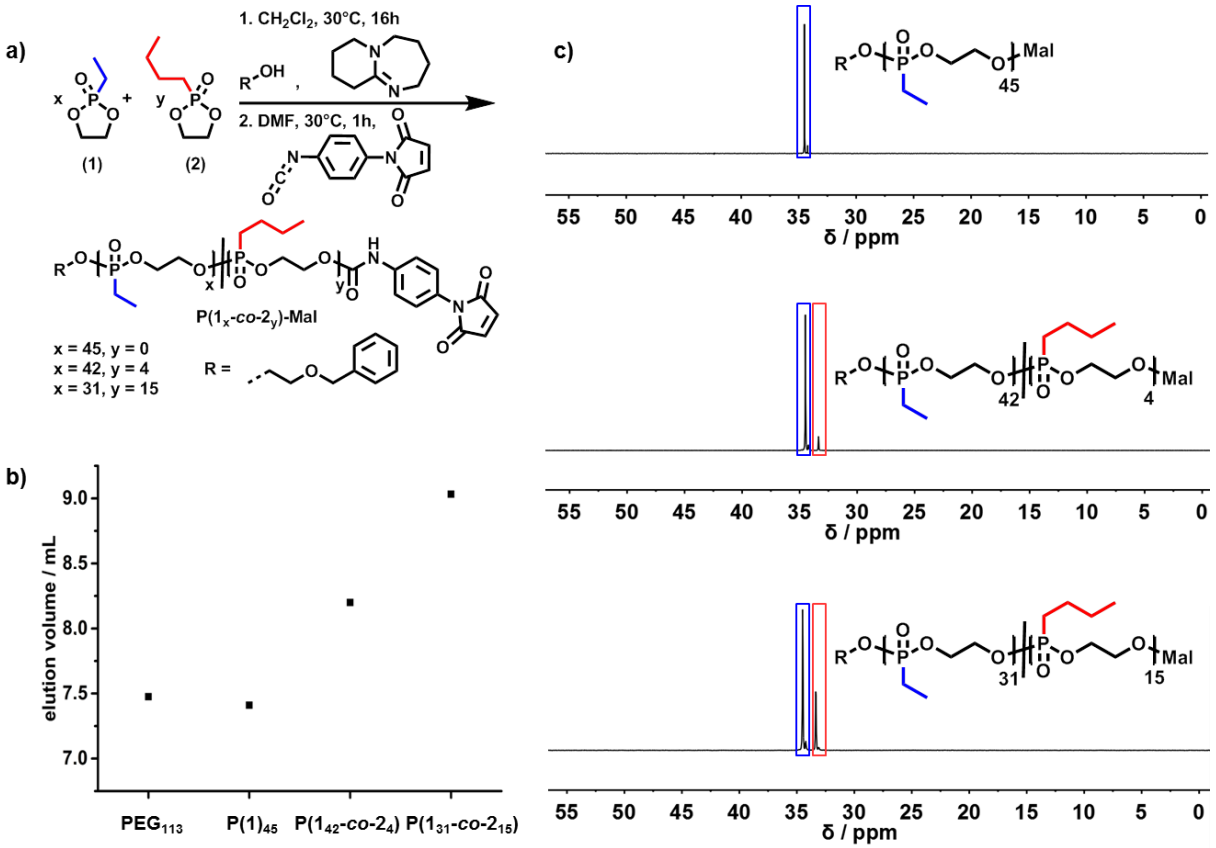

Figure 8.1 a) Schematic presentation of the oAROP of (1) and (2) followed by *ω*-functionalization to produce random copolymers P(1_x-*co*-2_y)-Mal. b) Elution volume of the investigated (co)polymers on rpHPLC to evaluate their hydrophilicity.[24] c) ^{31}P NMR spectra (DMSO-d_6, 298K) of the produced (co)polymers.

The SEC elugrams of all polymers were monomodal and showed narrow molecular weight distributions (*Đ* < 1.19) (Figure 8.2). ^{1}H DOSY NMR spectroscopy assured attachment of the maleimide groups and copolymer formation. All ^{1}H NMR resonances possess the same diffusion coefficient and are part of the same molecule (Figures S8.7 and S8.9).

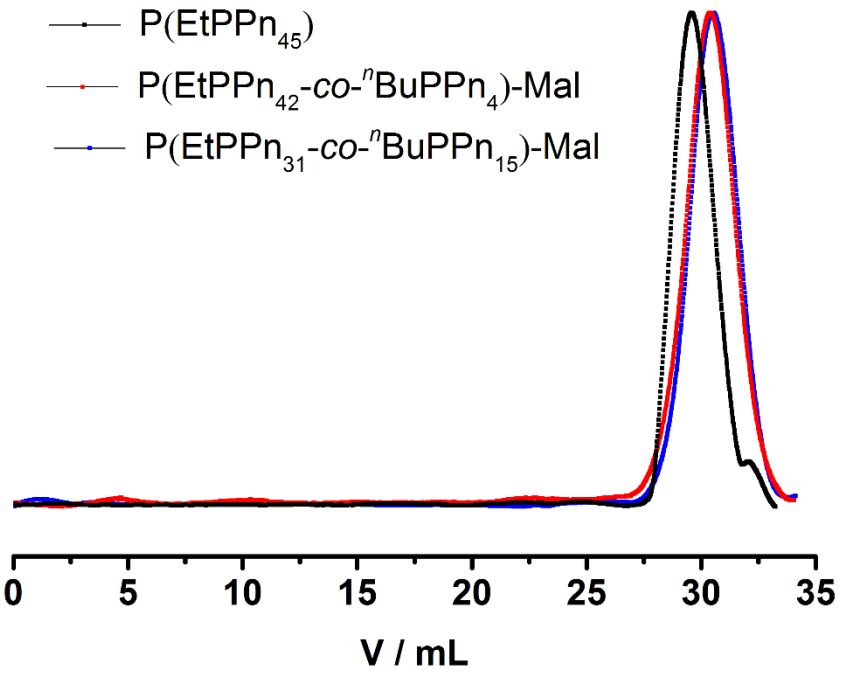

Figure 8.2: SEC trace (RI detection) of poly(ethylene alkyl phosphonate) (co)polymers used in this study in DMF (0.1 g L^{-1} LiBr) at 333K.

Quantification of molecular weights, the degree of ω-functionalization and the copolymer compositions were determined by ^{1}H NMR spectroscopy via end-group analysis (Figures 8.3, S5, S6, and S8). Briefly, the resonances of the maleimide signals (6.96 - 6.46 ppm), as well as aromatic proton resonances (7.76 - 7.20 ppm), were compared with the initiator's resonances (4.52 ppm) and the polymer backbone resonances (4.31 - 3.98 ppm). In all cases ω-functionalities of > 97% were achieved. The relative ^{1}H NMR resonances of the side-chain methylene groups at 1.05 ppm (ethyl -C**H$_3$**) and 0.87 ppm (*n*-butyl -C**H$_3$**) were compared to obtain the copolymer composition. The results were further confirmed by comparing the ^{31}P NMR resonances of **P(1)** at 34.5 ppm and **P(2)** at 33.4 ppm (Figure 8.1, c). The final copolymers contained 0, 8.6, and 32 mol% of hydrophobic *n*-butyl side-chains.

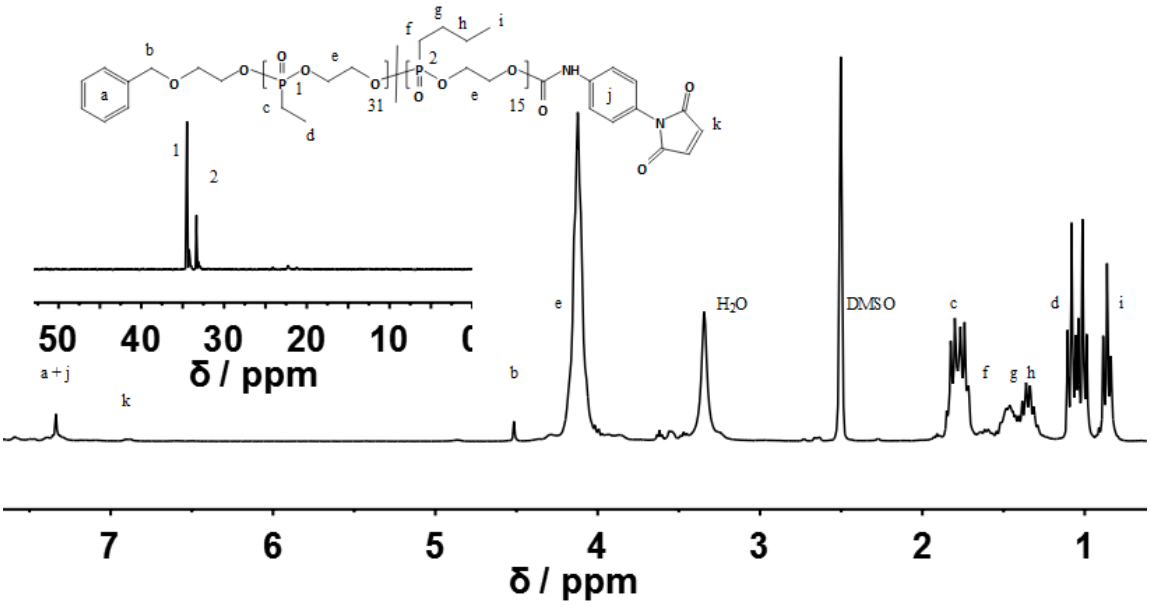

Figure 8.3: Exemplary ^{1}H (500 MHz) and ^{31}P (201 MHz) NMR spectra of maleimide terminated poly(ethylene ethyl-*co*-*n*-butyl phosphonate) P(1_{31}-co-2_{15}) in DMSO-d_6 at 298K.

The hydrophilicity of the copolymers was evaluated via reverse phase HPLC (rpHPLC). The elution volume of the hydrophobic column was used to gauge the macroscopic hydrophilicity of the polymer, as polymers of higher hydrophobicity elute later from the column due to stronger interactions. With an elution volume of 7.1 mL **P(1)$_{45}$-Mal** exhibits a similar hydrophilicity to the *benchmark*, ***m*-PEG$_{113}$-Mal** that elutes at 7.45 mL (chosen due to comparable M_n values). Higher amounts of *n*-butyl side chains resulted in lower hydrophilicity, with the elution volumes rising to 8.19 mL for **P(1_{42}-*co*-2_4)-Mal** and 9.03 mL for **P(1_{31}-*co*-2_{15})-Mal** as shown in Figure 8.1, b. These values correlate well with the calculated logP values of the respective polymers (Table 8.1).

To exclude the formation of pronounced hydrophobic patches in the form of gradients or block copolymer structures, ^{31}P NMR spectroscopy assisted copolymerization kinetics were conducted according to previous studies (Figure S8.10).[24] The ratio of repetition unit **(1)** and **(2)** incorporated into the polymer backbone during the polymerization was observed. This ratio (initial monomer feed ratio 1:1 for better visualization) stayed constant during the polymerization, proving the random incorporation of both monomers into the backbone (polymer characteristics are summarized in Table 8.1).

Table 8.1: Analytical data of maleimide functionalized polymers.

sample	(1) / (2) theo[a)]	(1) / (2) exp.[b)]	P_n[b)]	M_n[b)]	$Đ$[c)]	f / %[b)]	V / mL[d)]	logP[e)]
m-PEG$_{113}$-Mal	-	-	113	5,000	1.03	97	4.45	-2.27
P(1)$_{45}$-Mal	-	-	45	6,100	1.19	99	7.10	-3.89
P(1$_{42}$-*co*-2$_4$)-Mal	0,90 / 0,10	0,91 / 0,09	42 / 4	6,300	1.17	99	8.19	-1.73
P(1$_{31}$-*co*-2$_{15}$)-Mal	0,70 / 0,30	0,67 / 0,33	31 / 15	6,700	1.18	97	9.03	+0.35

a) Monomer feed ratio. b) Determined via ^{1}H NMR (500 MHz) spectroscopy. c) Determined via SEC in DMF (RI detection, 333K, vs. PEG). d) Elution volume on rpHPLC. e) logP value calculated from www.molinspiration.com

Surface Modification

To evaluate the effect of the copolymer hydrophilicity on the stealth properties of nanocarriers, model NCs based on poly(styrene nanoparticles (D_h = 107 nm ± 9 nm) were prepared via free radical terpolymerization of styrene, 2-aminoethyl methacrylate and BODIPY-methacrylate in a cetyl trimethyl ammonium chloride (CTMA-Cl) stabilized mini-emlusion process.[29] The maleimide-modified polymers were coupled to the amino groups on the NCs via the *aza-Michael* addition reaction in aqueous dispersion. (Figures S11 - S15) In addition, according to the protocol from Schöttler *et al*., the average number of polymer chains per NC was determined from the ratio between the PS backbone resonances in ^{1}H NMR spectroscopy (7.14 - 6.17 ppm) and the **PEG** or **PPn** resonances (3.60 - 3.55 ppm and 4.44 - 4.03 ppm), respectively.[13] On average, 5,300-6,300 chains were attached to each NC. In combination with the surface area obtained from the DLS diameter, a distance of 6 - 7 nm between two polymer chains was calculated (Figure 8.4). According to Perry *et al*., the polymers should take a mushroom conformation under these conditions and hence provide a dense enough layer to induce stealth behavior.[25]

The size of the nanocarriers remained relatively constant before and after coupling of the different polymers (Figure 8.4). The ζ-potential however, changed from + 47 mV to + 7 mV for ***m*-PEG** and ~ - 20 mV for all **PPn** modifications. Furthermore, the functionalized NC stayed colloidal stable in NaCl solution (9 g L^{-1}) as opposed to the unmodified NC, indicating a shift from electrostatic, CTMA-Cl, to a steric stabilization by the polymer grafts and a successful conjugation.

Finally, the ζ-potential of all NC after incubation in human plasma equilibrated to ~ -30 mV because of protein adsorption, similar to other reported nanocarriers in plasma.[13]

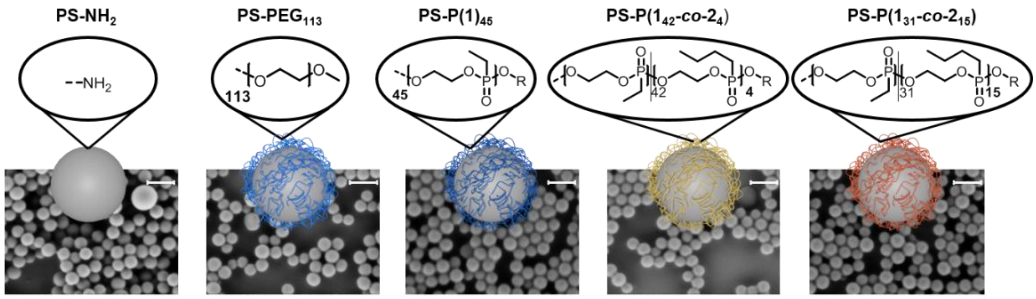

modification	-	*m*-PEG$_{113}$	P(1)$_{45}$	P(1$_{42}$-co-2$_4$)	P(1$_{31}$-co-2$_{15}$)
chains / particle	-	5300	5500	6300	5400
D_h (H_2O) / nm	107 ± 9	124 ± 36	127 ± 28	105 ± 13	105 +61
D_h (NaCl 9 g L^{-1}) / nm	-	115 ± 27	111 ± 17	106 ± 24	155 ± 16
ζ-potential / mV	+47 ± 9	+ 7 ± 7	- 24 ± 5	- 16 ± 7	- 22 ± 4
ζ-potential in plasma / mV	-28 ± 9	-33 ± 7	-30 ± 19	-30 ± 5	-31 ± 7

Figure 8.4: Analytical data of model nanocarriers used herein. Scale bar in SEM images 200 nm.

Cellular internalization behavior of nanoparticles

The main feature of stealth nanocarriers is the prolonged blood circulation time which is caused by reduced interactions with immune cells (e.g., phagocytic cells). Therefore, we study the cellular internalization of the here described nanocarriers towards the murine macrophage cell line, RAW 264.7 by flow cytometry and confocal laser scanning microscopy (cLSM).

The nanocarriers were incubated in human plasma before cell uptake experiments to allow the formation of the protein corona and mimic *in vivo* conditions. Flow cytometry analysis indicates a high internalization rate of pristine NC (Figure 8.5). Additionally, high colocalization of the negatively charged cell membrane and positively charged nanocarriers is observed in cLSM images (Figure 8.5, b-c). For nanocarriers coated with PEG and the hydrophilic P1, the cellular uptake is strongly diminished. Interestingly, for nanocarriers coated with **P(1$_{42}$-*co*-2$_{4}$)** containing low amounts of hydrophobic *n*-butyl side chains, the cellular uptake behavior remained unchanged (Figure 8.5, a). However, with increasing the hydrophobicity to (**P(1$_{31}$-*co*-2$_{15}$)**, we observed an increase in the cellular uptake. These first results indicate that a defined surface hydrophilicity enables controlled cellular interaction. Comparable results were obtained for HeLa cells (Figure S8.17). Additional, there is no unspecific binding or cell adhesion for polymer-coated nanocarriers compared to pristine NCs (Figures S18-19).

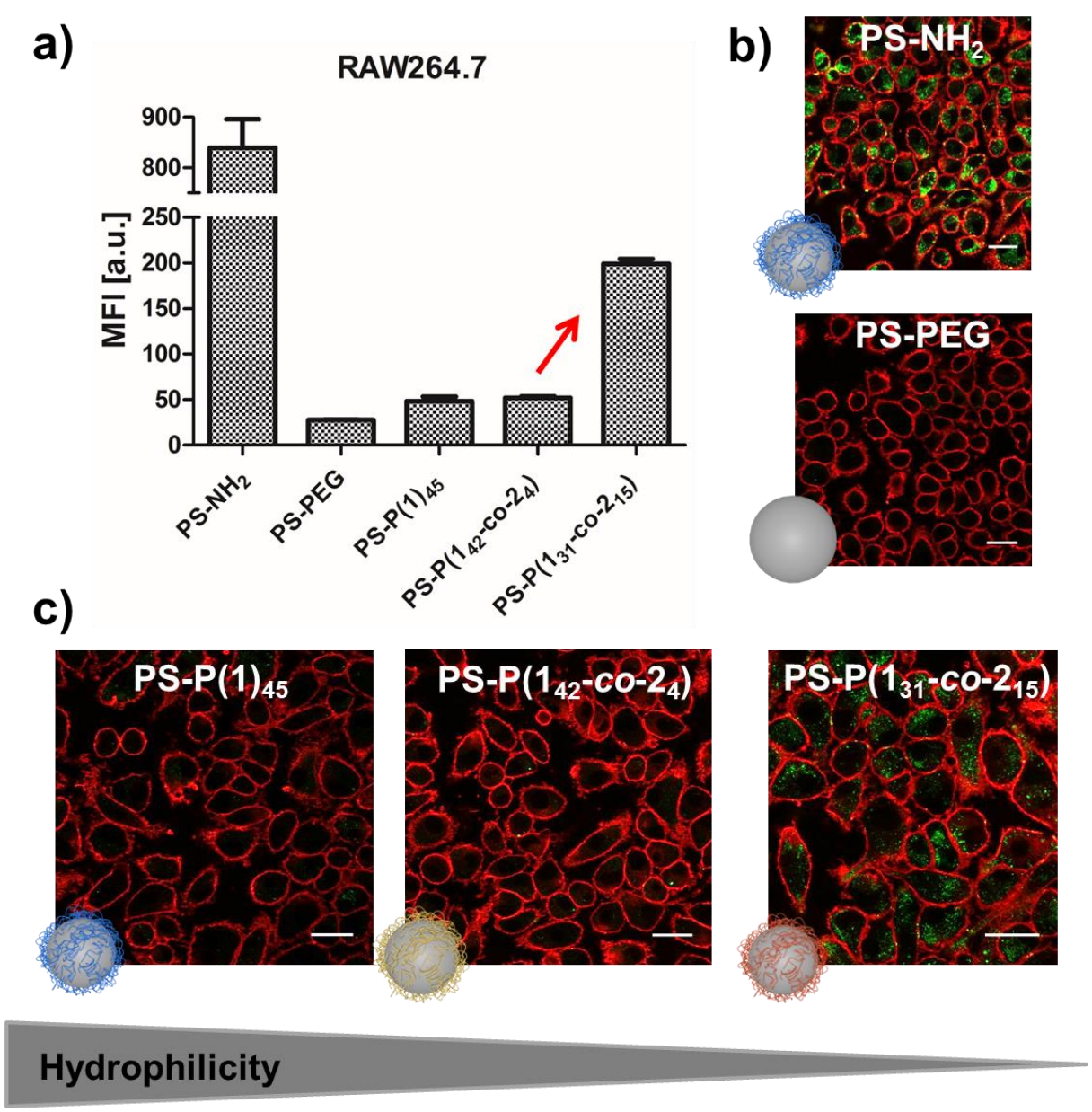

Figure 8.5: Cellular interaction studies of pristine and polymer coated PS-NP after plasma incubation: a) Flow cytometry analysis b-c) Confocal laser scanning microscopy images. Values are expressed as mean ± SD of triplicates. The cell membrane is stained with CellMask Orange and pseudocolored in red and PS-NCs are pseudocolored in green. Scale bar:10 µm. (All experiments were performed by Johanna Simon.)

Qualitative and quantitative protein adsorption behavior

In general, a reduced protein adsorption has been reported for hydrophilic surfaces, and with increasing hydrophobicity, the amount of protein adsorption also increases. All model nanocarriers were incubated with human plasma at 37°C for 1h, and the hard corona proteins were isolated and quantified by the Pierce Assay (Figure 8.6, a). Compared to PS-NH_2, a strongly reduced amount of proteins adsorbed to **PEG**ylated and **P(1)$_{45}$** modified NCs (Figure 8.6, a). However, increasing the hydrophobicity of the polymer shield on the nanocarriers did not influence the amount of protein adsorbed on the NCs (~ 0.5 mg per 0.05 m^2 surface area NC).

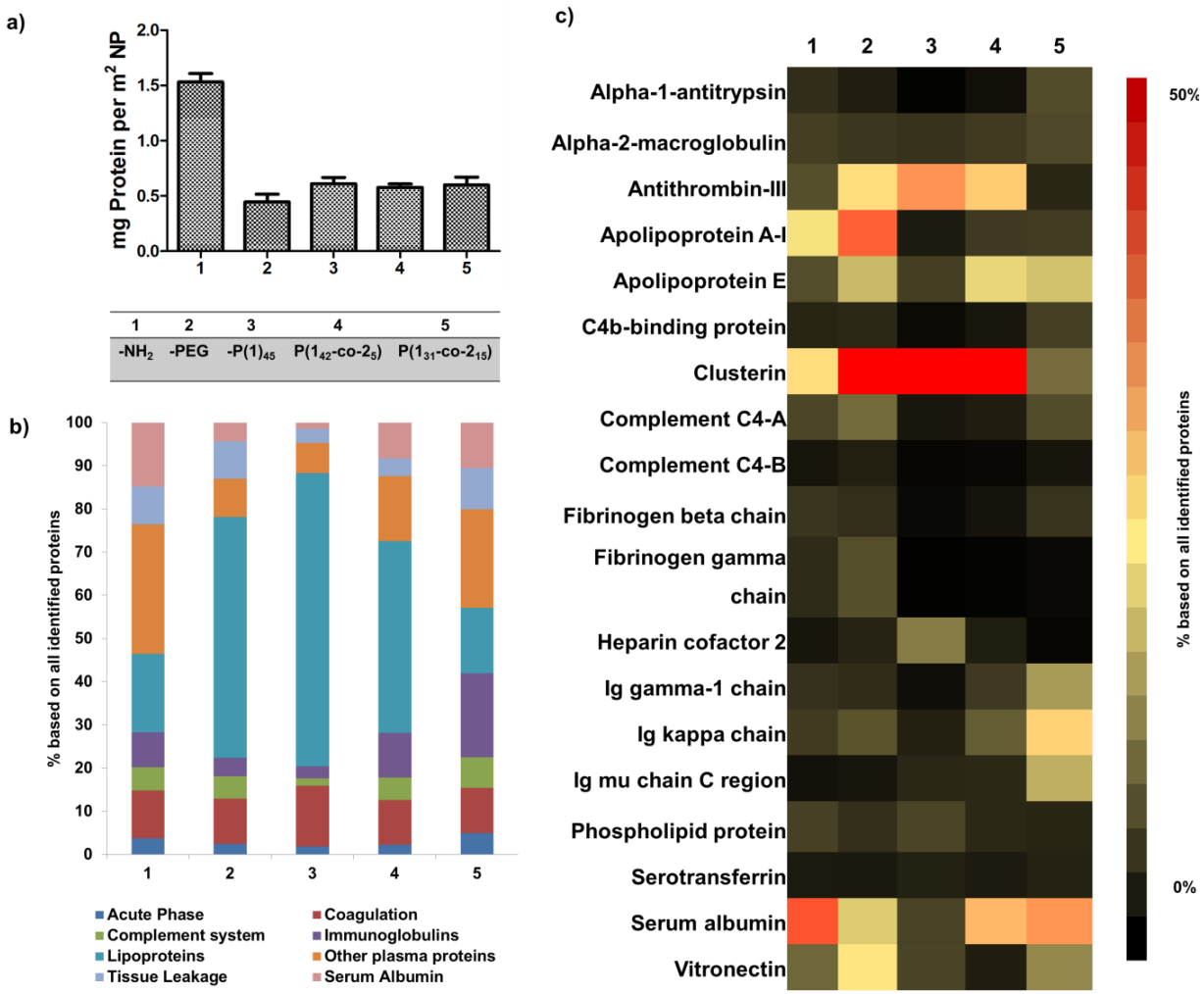

Figure 8.6: Qualitative and quantitative protein corona analysis of pristine and polymer coated PS-NC a) Pierce Assay b) LCMS Protein Classification c) LCMS Protein Identification. Values are expressed as mean ± SD triplicates. (All experiments were performed by Johanna Simon.)

Moving on, we analyzed the protein corona via SDS-PAGE (Figure S8.20) and liquid chromatography coupled to mass spectrometry (LC-MS) to assess the biological identity of the NC, i.e., after incubation in human plasma. In line with previous reports, the protein adsorption pattern of PS-NH_2 is dominated by albumin which is the most abundant plasma protein. On NCs coated with the hydrophilic polymers (**PEG** and **P(1)$_{45}$**) a substantial enrichment of apolipoproteins, e.g., clusterin and ApoAI (Figure 8.6, c) was found. When the more hydrophobic **P(1$_{42}$-*co*-2$_4$)** is coupled to the nanocarriers, no influence on the cellular uptake was found (Figure 8.5) and also no significant differences in the protein corona pattern compared to **P(1)$_{45}$** is measured (Figure 8.6, b). However, a significantly different protein pattern adsorbs on nanocarriers with the most hydrophobic polymer (**P(1$_{31}$-*co*-2$_{15}$)**) (Figure 8.6, b). Especially immunoglobulins, fibrinogen, and albumin were identified in substantial amounts, which are less pronounced on the other "stealth" nanocarriers (Figure 8.6, c)

Summary and Conclusion

The NC covered with hydrophilic poly(phosphonates)s exhibit stealth behavior comparable to that of PEGylated NC under *in vitro* conditions. We proved that NC coated either with hydrophilic or hydrophobic polymers exhibit an overall low protein binding. However, a clear correlation between polymer hydrophilicity as determined via rpHPLC, the protein adsorption pattern, and the resulting cellular interactions was shown. Upon surpassing a certain threshold of hydrophilicity, the protein adsorption pattern changes from being dysopsonin dominated (clusterin) towards an opsonin coverage (e.g., IgG). This is an essential step towards understanding the stealth effect as it is the first study correlating well-controlled surface hydrophilicity with quantitative high-resolution protein corona analysis and the phenomenological observation of "stealth". This important knowledge is needed to improve the properties of the nanocarriers for therapeutic application.

Acknowledgement

The authors thank C. Rosenauer (MPIP) for DLS measurements, Dr. I. Lieberwirth and C. Sieber (MPIP) for TEM measurements and discussion and Dr. M. Wagner (MPIP) for NMR measurements. The authors acknowledge support from the “Deutsche Forschungsgemeinschaft” (DFG WU 750/6-1).

References

1. Yoo, J. W.; Chambers, E.; Mitragotri, S., *Curr. Pharm. Design.* **2010,** *16*, 2298-2307.
2. Dawidczyk, C. M.; Kim, C.; Park, J. H.; Russell, L. M.; Lee, K. H.; Pomper, M. G.; Searson, P. C., *J. Contr.Relea.,* **2014,** *187*, 133-44.
3. Owens, D. E., 3rd; Peppas, N. A., *Int. J. Pharm.,* **2006,** *307*, 93-102.
4. Suk, J. S.; Xu, Q.; Kim, N.; Hanes, J.; Ensign, L. M., *Adv. Drug. Deliv. Rev.,* **2016,** *99*, 28-51.
5. Knop, K.; Hoogenboom, R.; Fischer, D.; Schubert, U. S., *Angew. Chem. Int. Ed.,* **2010,** *49*, 6288-308.
6. A. Abuchowski; J.R.McCoy; N.C.Palczuk; T. van Es; F.F.Davis, *J. Biol. Chem.,* **1977,** *252*, 3582–3586.
7. Kawai, F.; Kimura, T.; Fukaya, M.; Tani, Y.; Ogata, K.; Ueno, T.; Fukami, H., *Appl. environ. microbiol.,* **1978,** *35*, 679-684.
8. Tagami, T.; Uehara, Y.; Moriyoshi, N.; Ishida, T.; Kiwada, H., *J. Contr. Relea.,* **2011,** *151*, 149-154.
9. Kang, B.; Okwieka, P.; Schöttler, S.; Winzen, S.; Langhanki, J.; Mohr, K.; Opatz, T.; Mailander, V.; Landfester, K.; Wurm, F. R., *Angew. Chem. Int. Ed.,* **2015,** *54*, 7436-40.
10. Baier, G.; Baumann, D.; Siebert, J. M.; Musyanovych, A.; Mailander, V.; Landfester, K., *Biomacromolecules,* **2012,** *13*, 2704-15.
11. Bauer, M.; Lautenschlaeger, C.; Kempe, K.; Tauhardt, L.; Schubert, U. S.; Fischer, D., *Macromol. Biosci.,* **2012,** *12*, 986-98.
12. Bludau, H.; Czapar, A. E.; Pitek, A. S.; Shukla, S.; Jordan, R.; Steinmetz, N. F., *Eur. Polym. J.,* **2017,** *88*, 679-688.
13. Schöttler, S.; Becker, G.; Winzen, S.; Steinbach, T.; Mohr, K.; Landfester, K.; Mailander, V.; Wurm, F. R., *Nat. Nanotechnol.,* **2016,** *11*, 372-7.
14. Bauer, K. N.; Tee, H. T.; Velencoso, M. M.; Wurm, F. R., *Progr. Polym. Sci.,* **2017**.
15. Lynch, I.; Salvati, A.; Dawson, K. A., *Nat. Nanotechnol.,* **2009,** *4*, 546-7.
16. Lee, Y. K.; Choi, E. J.; Webster, T. J.; Kim, S. H.; Khang, D., *Int. J. Nanomed.,* **2015,** *10*, 97-113.
17. Ritz, S.; Schöttler, S.; Kotman, N.; Baier, G.; Musyanovych, A.; Kuharev, J.; Landfester, K.; Schild, H.; Jahn, O.; Tenzer, S.; Mailander, V., *Biomacromolecules* **2015,** *16*, 1311-21.
18. Takeuchi, T.; Kitayama, Y.; Sasao, R.; Yamada, T.; Toh, K.; Matsumoto, Y.; Kataoka, K., *Angew. Chem. Int. Ed.,* **2017,** *56*, 7088-7092.
19. Bewersdorff, T.; Vonnemann, J.; Kanik, A.; Haag, R.; Haase, A., *Int. J. Nanomed.,* **2017,** *12*, 2001-2019.
20. Yoon, J.-Y.; Kim, J.-H.; Kim, W.-S., *Colloids Surf. B,* **1998,** *12*, 15-22.

21. Lindman, S.; Lynch, I.; Thulin, E.; Nilsson, H.; Dawson, K. A.; Linse, S., *Nano. Lett.,* **2007,** *7*, 914-20.
22. Cedervall, T.; Lynch, I.; Foy, M.; Berggard, T.; Donnelly, S. C.; Cagney, G.; Linse, S.; Dawson, K. A., *Angew. Chem. Int. Ed.,* **2007,** *46*, 5754-6.
23. Gessner, A.; Waicz, R.; Lieske, A.; Paulke, B. R.; Mäder, K.; Müller, R. H., *Int. J. Pharm.,* **2000,** *196*, 245-249.
24. Asai, M.; Zhao, D.; Kumar, S. K., *ACS Nano,* **2017**.
25. Perry, J. L.; Reuter, K. G.; Kai, M. P.; Herlihy, K. P.; Jones, S. W.; Luft, J. C.; Napier, M.; Bear, J. E.; DeSimone, J. M., *Nano. Lett.,* **2012,** *12*, 5304-10.
26. Steinbach, T.; Ritz, S.; Wurm, F. R., *Acs Macro Lett.,* **2014,** *3*, 244-248.
27. Wolf, T.; Steinbach, T.; Wurm, F. R., *Macromolecules* **2015,** *48*, 3853-3863.
28. Wolf, T.; Rheinberger, T.; Wurm, F. R., *Europ. Polym. J.,* **2017**.
29. Holzapfel, V.; Musyanovych, A.; Landfester, K.; Lorenz, M. R.; Mailander, V., *Macromol. Chem. Phys.,* **2005,** *206*, 2440-2449.

Supporting Information for

Hydrophilicity Regulates Specific Protein Adsorption on Poly(phosphoester) Coated Nanocarriers Controlling Uptake in Immune Cells.

Materials

Solvents and chemicals were purchased from Acros Organics, Sigma Aldrich or Fluka and used as received unless otherwise stated. 4-(Maleinimido) phenyl isocyanate was purchased from Fisher Scientific. All chemicals were purchased in highest purities, dry and stored over molecular sieve (4Å), if possible. 2-(Benzyloxy) ethanol and DBU were distilled from calcium hydride and stored over molecular sieve (4Å) under argon before use. Deuterated solvents were purchased from Deutero GmbH (Kastellaun, Germany) and used as received. Dulbecco's Modified Eagle Medium (DMEM), fetal bovine albumin (FBS) penicillin and streptomycin were purchased from Invitrogen, Germany.

Blood was taken from the Department of Transfusion Medicine Mainz from ten healthy donors. Citrate was used as an anticoagulant, and the obtained human citrate plasma was pooled. Human citrate plasma was stored at -80 °C and centrifuged for 30 mins at 20,000 g prior using to remove aggregated proteins from the plasma pool.

Instrumentation and Characterization Techniques

Size exclusion chromatography (SEC) measurements were performed in DMF (1 g L^{-1} LiBr added) at 60°C and a flow rate of 1 mL min^{-1} with a PSS SECcurity as an integrated instrument, including a PSS GRAM 100-1000 column and a refractive index (RI) detector. Calibration was carried out using poly(ethylene glycol) standards provided by Polymer Standards Service. A refractive index (RI) detector (Agilent 1260) was used for detection. Calibration was carried out using poly(ethylene glycol) or poly(styrene) standards both provided by Polymer Standards Service. All NMR experiments were acquired on a Bruker 500 AMX system.

The temperature was kept at 298.3K and calibrated with a standard ^{1}H methanol NMR sample using the topspin 3.5 software (Bruker). ^{13}C{H} NMR spectra were referenced internally to solvent signals. ^{31}P{H} NMR spectra were referenced externally to phosphoric acid. The ^{13}C{H} NMR (125 MHz) and ^{31}P{H} NMR (201 MHz) measurements were obtained with a 1H powergate decoupling method using 30 ° degree flip angle. ^{1}D NMR spectra were processed with the MestReNova 9.0.1-13254 software whereas ^{1}H DOSY (diffusion orientated spectroscopy) NMR spectra were processed with the TopSpin 3.5 software. Dynamic light scattering (DLS) measurements were performed on an ALV spectrometer consisting of a goniometer and an ALV-5004 multiple-tau full-digital correlator (320 channels) which allows measurements over an angular range from 30° to 150. A He-Ne Laser (wavelength of 632.8 nm) is used as light source. The amount of amino groups was calculated from the results of the titration experiments performed on a particle charge detector PCD 02 (Mütek GmbH, Germany) in combination with a Titrino Automatic Titrator 702 SM (Metrohm AG, Switzerland). The amino groups were titrated against the negatively charged polyelectrolyte standard sodium poly(ethylene sulfonate) (PES-Na), 1 mM, f = 1.22, to determine the point of zero charge. The titration was performed using 10 mL of the dispersion with a solid content of 1 g L^{-1}(0.1 wt%) in an aqueous solution with pH 2. The amount of groups per particle was calculated from the consumed volume (an average of three titrations) of the polyelectrolyte solution using the following equations:

$$\frac{groups}{g_{Polymer}} = \frac{V \cdot f \cdot c_{polyelectrolyte} \cdot N_A}{SC}$$

$$\frac{groups}{particle} = \frac{groups}{g_{Polymer}} \cdot \frac{\rho_{PS} \cdot d_n^3 \cdot \pi}{6}$$

$$\frac{groups}{nm^2} = \frac{groups}{g_{Polymer}} \cdot \frac{\rho_{PS} \cdot d_n \cdot 10^{-18}}{6}$$

V= volume of consumed polyelectrolyte [L]; f= PCD factor (titer); c= concentration of polyelectrolyte [mol L^{-1}]; N_A= Avogadro constant (6.022*10^{23} mol^{-1}); SC= solid content of dispersion [g]; ρ_{PS}= density of polystyrene (1.045*10^{6} g m^{-3}); d_n= average number diameter of particles [m].

The zeta potential of the dispersion was measured diluted in potassium chloride solution ($1*10^{-3}$ M in water) with a Zeta Sizer Nano Series (Malvern Instruments, U.K.) at 20 °C.

SEM images were recorded by using a field emission microscope LEO (Zeiss) 1530 Gemini (Oberkochen, Germany) working at an acceleration voltage of 200 or 400 V. The samples were prepared by diluting the dispersion 1:1,000 in demineralized water. Then, one droplet of the sample was placed onto a silica wafer and dried overnight.

Solid content of the particle dispersion was determined by weighing freeze-dried aliquots of the dispersion under the assumption of ρ_{PS}= density of polystyrene = $1.045*10^{6}$ g m^{-3})

The amount of PPn or PEG chains per particle was approximated via ^{1}H NMR spectroscopy (500 MHz, $CDCl_3$, 298K). To do so, the integrals of the PS backbone (7.23 - 6.27 ppm) were compared with the integrals of the PPn (4.30 - 4.06 ppm) or PEG (3.72 - 3.62 ppm) backbone, respectively.

Synthesis of poly(styrene) nanoparticles: A macro emulsion was prepared with a continuous phase containing cetyl trimethyl ammonium chloride solution (25%wt in water, 527 mg, 1.46 mmol) as surfactant and 2-aminoethyl methacrylate hydrochloride (547 mg, 3.32 mmol, 3%wt to styrene) in 72.0 g sterile Milli-Pore water and a dispersed phase containing distilled styrene (17.1 g, 164 mmol), hexadecane (792 mg, 2.77 mmol) as ultrahydrophobe, BODIPY-methacrylate (17.3 mg, $3.7*10^{-2}$ mmol) as fluorescent dye and 2,2'-azobis(2-methyl butyronitrile) (V59) (301 mg, 1.56 mmol) as oil soluble azo initiator. Both phases were made homogenous by mechanical stirring, and the continuous phase was added slowly to the stirring dispersed phase. The macro-emulsion was stirred for 1 h at highest speed. To produce the mini-emulsion, the macro-emulsion was passed through a microfluidizer (Microfluidics USA, LM10) with a y-chamber 48 times at 103 MPa. The first 12 passes were discarded. The mini-emulsion was directly transferred into a 100 mL flask and stirred in an oil bath at 72 °C. The polymerization was run for 12h. The dispersion was purified by centrifugation (6 x 1.5h, 12,000 rpm), the supernatant always removed and the pellet re-dispersed in sterile Milli-pore water.

D_h (DLS): 106.8 ± 9.1 nm (8.5%); ξ-potential: + 47.4 ± 9.5 mV (20.0%); -NH_2 groups / particle (PCD): 29.000; M_n (SEC, DMF, 0.1 mol LiBr, RI-detection, 333K, PS standard): 107380 g mol^{-1}; Mw: 278004 g mol^{-1}, $Đ$ = 2.59.

Representative procedure for the synthesis of P(1)$_n$ and P(1$_x$-co-2$_y$)-Mal: The monomer(s) were weighed into a flame-dried Schlenk-tube, dissolved in dry benzene and dried by 3 times lyophilization. The monomers were dissolved in dry dichloromethane at a total concentration of 4 mol L^{-1}. A stock solution of initiator 2-(benzyloxy)ethanol in dry dichloromethane was prepared with a concentration 0.2 mol L^{-1}, and the calculated amount was added to the monomer solution via gas-tight syringe (Hamilton®). A stock solution of DBU in dry dichloromethane was prepared with a concentration of 0.2 mol L^{-1}. The monomer solution and the catalyst solution were adjusted to 30 °C. The polymerization was initiated by the addition of the calculated volume of the catalyst solution containing 3.0 equivalents of DBU with respect to the initiator. Polymerization was terminated after 16h by the rapid addition 2.5 equivalents of 4-(maleinimido)phenyl isocyanate in 1 mL dry DMF. The yellow solution rapidly turned red, indicating the successful termination reaction. After 20 min, the amorphous polymers were purified by precipitation in cold diethyl ether, dialyzed against 2 L Milli-Q (Millipore®) water overnight (1,000 g mol^{-1} cut off, regenerated cellulose membrane) and dried at reduced pressure. Yield: 95-97% amorphous solid.

Representative NMR data of P(1)$_n$-Mal: ^{1}H NMR (DMSO-d_6, 500 MHz, 298K, ppm): δ = 7.76 - 7.18 (m, aromatic C**H**), 6.91 (s, Maleimid C), 4.53 (s, aryl-C**H$_2$**-), 4.22 - 4.01 (m, backbone -C**H$_2$**-C**H$_2$**-), 3.63 (t, backbone terminal -C**H$_2$**-OH), 1.79 (dq, side-chain -P-C**H$_2$**-, $^2J_{HP}$ = 15.9 Hz, $^3J_{HP}$ = 7.7 Hz), 1.05 (dt, side-chain -C**H$_3$**, $^2J_{HP}$ = 20.2 Hz, $^3J_{HP}$ = 7.6 Hz).^{13}C NMR (DMSO-d6, 125 MHz, 298K, ppm): δ = 138.78 (s, imide **C**), 133.78, 128.80, 127.97 (aromatic **C**), 64.56 (s, broad, backbone -**C**H$_2$-), 18.31 (d, $^1J_{CP}$ = 139.5 Hz, side-chain -P-**C**-), 6.71 (d, $^2J_{CP}$ = 6.75 Hz, side-chain -P-C-**C**).^{31}P{H} NMR (DMSO-d_6, 201 MHz, 298K, ppm): δ = 34.53 (backbone), 34.26 (terminal).

Representative NMR data of P(1_x-*co*-2_y)-Mal: ^{1}H NMR (DMSO-d_6, 500 MHz, 298K, ppm): δ = 7.76 - 7.18 (m, aromatic C**H**), 6.91 (s, Maleimid C**H**), 4.53 (s, aryl-C**H$_2$**-), 4.22 - 4.01 (m, backbone -C**H$_2$**-C**H$_2$**-), 3.63 (t, backbone terminal -C**H$_2$**-OH), 1.84 - 1.70 (m, side-chain -P-C**H$_2$**-), 1.63 - 1.56 (m, side-chain -P-C**H$_2$**-), 1.54 - 1.41 (m, side-chain -P-CH$_2$-C**H$_2$**-), 1.40 - 1.29 (m, side-chain -P-CH$_2$-CH$_2$-C**H$_2$**-), 1.05 (dt, side-chain -P-CH$_2$-C**H$_3$**, $^3J_{HP}$ = 20.1 Hz, $^3J_{HH}$ = 7.6 Hz), 0.86 (t, side-chain -P-CH$_2$-CH$_2$-CH$_2$-C**H$_3$**, $^3J_{HH}$ = 7.3 Hz). ^{13}C NMR (DMSO-d6, 125 MHz, 298K, ppm): δ = 138.78 (s, imide **C**), 133.78, 128.80, 127.97 (s, aromatic **C**), 64.56 (s, broad, backbone -**C**H$_2$-), 60.85 (s, aryl-**C**-), 24.66 (d, side-chain -P-**C**-, $^1J_{CP}$ = 145.0 Hz), 24.42 (d, side-chain –P-C-**C**-, $^2J_{CP}$ = 5 Hz), 23.41 (d, side-chain -P-C-C-**C**-, $^3J_{CP}$ = 16.3 Hz), 18.06 (d, side-chain -P-**C**-, $^1J_{CP}$ = 138.8 Hz), 13.90 (s, side-chain -P-C-C-C-**C**), 6.68 (d, side-chain -P-C-**C**, $^2J_{CH}$ = 6.3 Hz). ^{31}P{H} NMR (DMSO-d_6, 201 MHz, 298K, ppm): δ = 34.53 (backbone, Et-**P**), 34.26 (terminal, Et-**P**), 33.28 (backbone, ^{n}Bu-**P**), 33.04 (terminal, ^{n}Bu-**P**).

Modification of poly(styrene) nanoparticles via Michael-addition: For a typical Michael-addition 3 mL of particle dispersion (1%$_{wt}$, 4.5*10^{13} particles, 2.1*10^{-6} mol NH$_2$ groups) was basified with 72 µL pyridine (pH 8.5) and stirred for 20 min at room temperature at 500 rpm. Then 2.5 eq of polymer (concerning the –NH$_2$ groups) dissolved in 1 mL sterile Milli-Pore water were added. The reaction was stirred for 24h at room temperature and 500 rpm to ensure full conversion. The dispersion was purified by repeated centrifugation (3 x 1 h, 20,000 rpm). Each time the supernatant was removed and the pellet re-dispersed in sterile Milli-Pore water (2 x 3 mL, 1 x 2 mL). After determination of the solid content, the dispersion was adjusted to 1%$_{wt}$ with sterile Milli-Pore water.

Cell culture: RAW264.7 cells were kept in DMEM, and Hela cells were maintained in EMEM both supplemented with 10% FBS, 100 IU mL^{-1} penicillin and 100 µg mL^{-1} streptomycin.

Flow cytometry: Cells (10^{5}cells) were seeded out in 24-well in cell culture medium and kept overnight at 37 °C. Before cell uptake studies, the cell culture medium was

exchanged to cell culture medium without FBS. Nanocarriers were incubated with human plasma for 1h to allow protein corona formation (details see protein corona analysis). Protein-coated nanocarriers were added to cell culture medium without FBS at a final concentration of 75 µg mL^{-1} and incubated with cells for 2h at 37 °C (internalization) or 4 °C (binding). Cells were washed with PBS to remove free nanoparticles, detached with Trypsin-EDTA, centrifuged (500 g, 5 mins) and resuspended in PBS.

Flow cytometry measurements were performed with a CyFlow ML cytometer (laser: 488 nm laser for Bodipy excitation; emission: 527 nm bandpass filter). FCS Express V4 software was used for data analysis herby selecting cells on a forward/sideward scatter plot, excluding cell debris. The fluorescent signal was expressed in a histogram, and the median intensity was determined. The mean value and standard deviation from triplicates were calculated.

Confocal laser scanning microscopy. To verify the intracellular localization of nanocarriers cell images were taken with a Laser Scanning Confocal Microscope (Leica, LSM SP5 STED) consisting of a multi-laser combination and five detectors (range of 400 - 800 nm). Nanocarriers were detected at 530 - 545 nm (pseudo-colored in green) and the cell membrane was stained with CellMaskOrange (2.5 mg ml^{-1}) detected at 570 - 640 nm (pseudocolored in red). Images were evaluated with LAS AF 3,000 software and Image J. For confocal analysis, cells were seeded out in 8-well ibidi dishes ($8*10^4$ cells), and the experiments were conducted in the same manner as flow cytometry experiments. Before images were taken, cells were fixed with 4% paraformaldehyde for 15 min at room temperature.

Protein corona preparation. As previously described a constant ratio between nanoparticle surface area and plasma was chosen[1-2] (0.05 m^2 PS-NC per 1 mL plasma). The dispersion was incubated at 37 °C, 300 rpm for 1h and subsequently centrifuged (20,000g, 1h, 4 °C). The nanoparticle pellet was washed with PBS (3 times, 1 mL) to remove loosely and unbound proteins. For protein identification, the nanoparticle pellet was resuspended in 100 µL 2% SDS with 62.5 mM Tris hydrochloride solution and incubated for 5 min at 95 °C. The dispersion was centrifuged, and the resulting supernatant contained desorbed corona proteins.

Pierce Assay. The protein concentration was determined by Pierce 660 nm Protein Assay according to the manufacturers´ instruction. Bovine serum albumin was used as a standard. Absorbance was measured with a Tecan infinite plate reader.

SDS-PAGE. Proteins were analyzed by SDS-PAGE using NuPage 10% Bis-Tris Protein Gels. 7 µg of total protein was loaded for Coomassie staining, and 1 µg of protein was applied if gels were stained with Pierce Silver Staining Kit. The protein sample volume was adjusted with water to a volume of 26 µL and mixed with 4 µL of NuPage Sample Reducing Agent and 10 µL of NuPage LDS Sample Buffer. Electrophoresis was carried out for 1.5h at 100 V. Gels were either stained with Simply Blue Safe Stain overnight or Pierce Silver Staining Kit according to the manufacturers´ instruction.

In solution digestion. Proteins were precipitated using ProteoExtract protein precipitation kit according to manufacturers´ instruction, and in solution, digestion was performed as previously reported [1-3]. For LC-MS measurements, samples were diluted with 0.1% formic acid and spiked with 50 fmol μL^{-1} Hi3 E. Coli Standard (Waters Corporation) for absolute peptide quantification.

LC-MS measurements and data analysis. A Synapt G2-Si mass spectrometer coupled with a nanoACQUITY UPLC system was used for proteomic experiments. The system was operated as described in several reports. Data was processed, and peptides were identified with Progenesis QI for Proteomics. Generated peptide masses were searched against a reviewed human protein sequence database downloaded from Uniprot. The database was modified with the sequence information of Hi3 Ecoli standard (Chaperone protein ClpB) for absolute quantification. For peptide identification, at least three assigned fragments are required. For protein identification, at least two assigned peptides and five assigned fragments are needed. Peptides with a score parameter less than four were rejected. Based on the TOP3/Hi3[4] approach, the amount of protein in fmol was generated.

Supporting Figures:

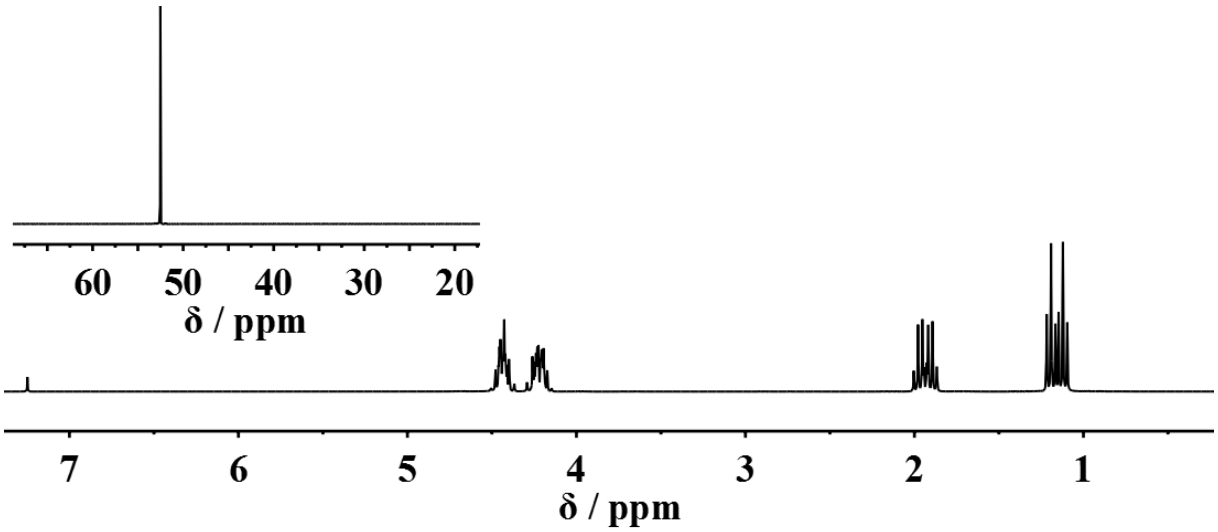

Figure S8.1: ^{1}H (500 MHz) and ^{31}P (201 MHz, inset) NMR spectra of 2-ethyl-2-oxo-1,3,2-dioxaphospholane (1) in DMSO-d_6 at 298K.

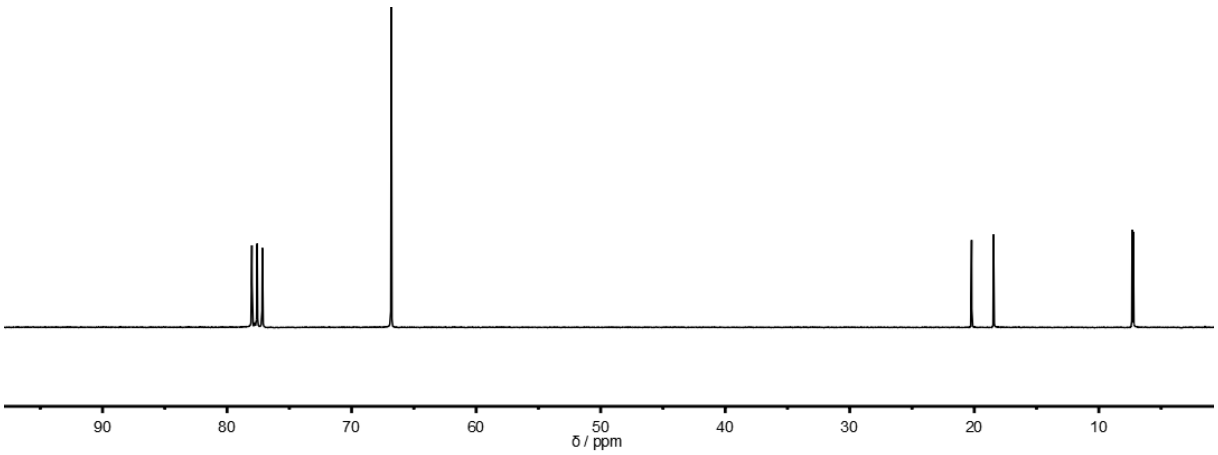

Figure S8.2: ^{13}C (125 MHz) NMR spectrum of 2-ethyl-2-oxo-1,3,2-dioxaphospholane (1) in DMSO-d_6 at 298K.

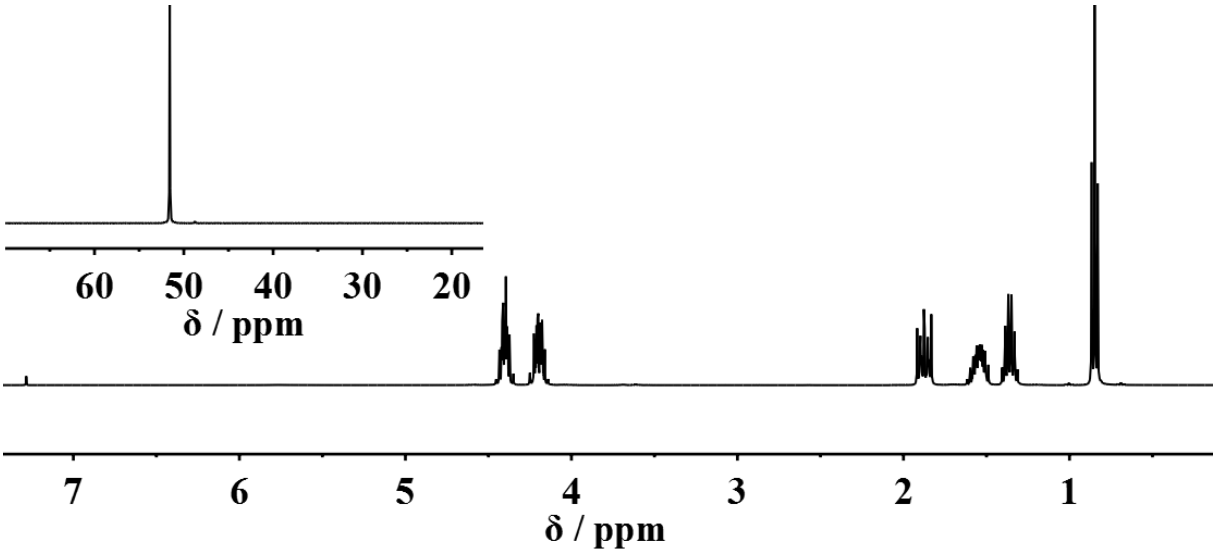

Figure S8.3: ^{1}H (500 MHz) and ^{31}P (210 MHz, inset) NMR spectra of 2-*n*-butyl-2-oxo-1,3,2-dioxaphospholane (2) in DMSO-d_6 at 298K.

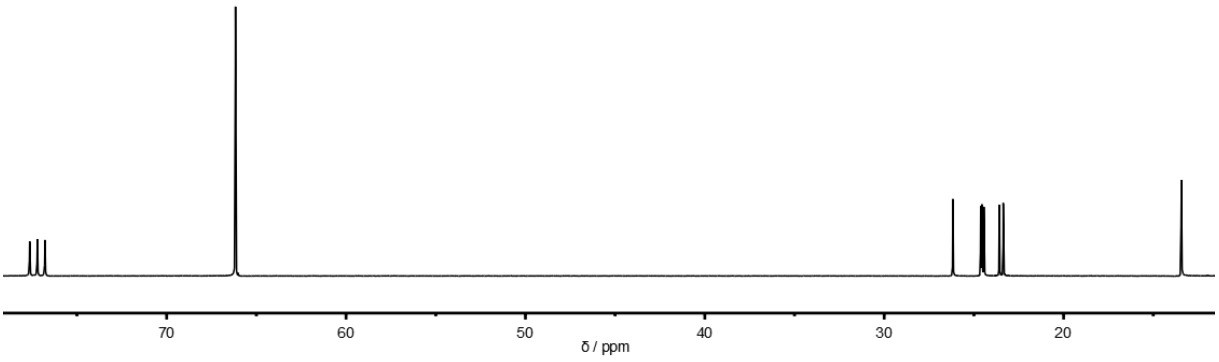

Figure S8.4: ^{13}C (125 MHz) NMR spectrum of 2-*n*-butyl-2-oxo-1,3,2-dioxaphospholane (1) in DMSO-d_6 at 298K.

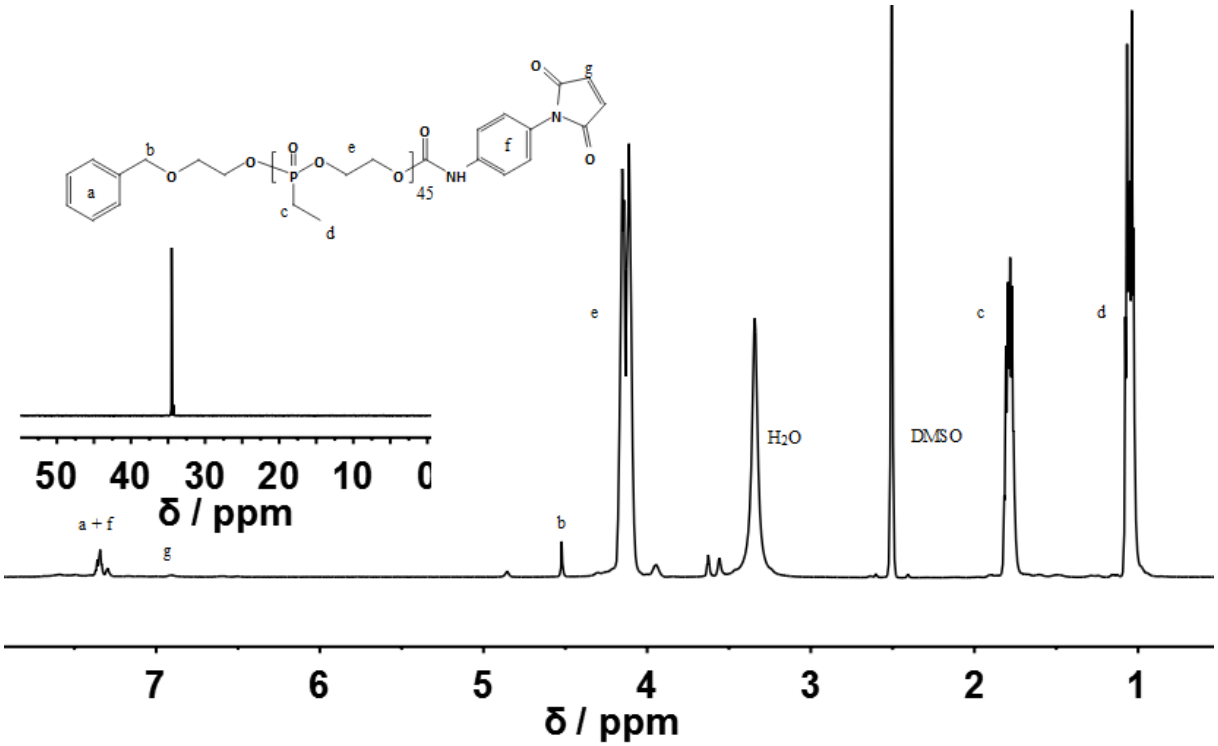

Figure S8.5: ^{1}H (500 MHz) and ^{31}P (210 MHz, inset) NMR spectra of a maleimide terminated poly(ethylene ethyl phosphonate) $P(1)_{45}$ in DMSO-d_6 at 298K.

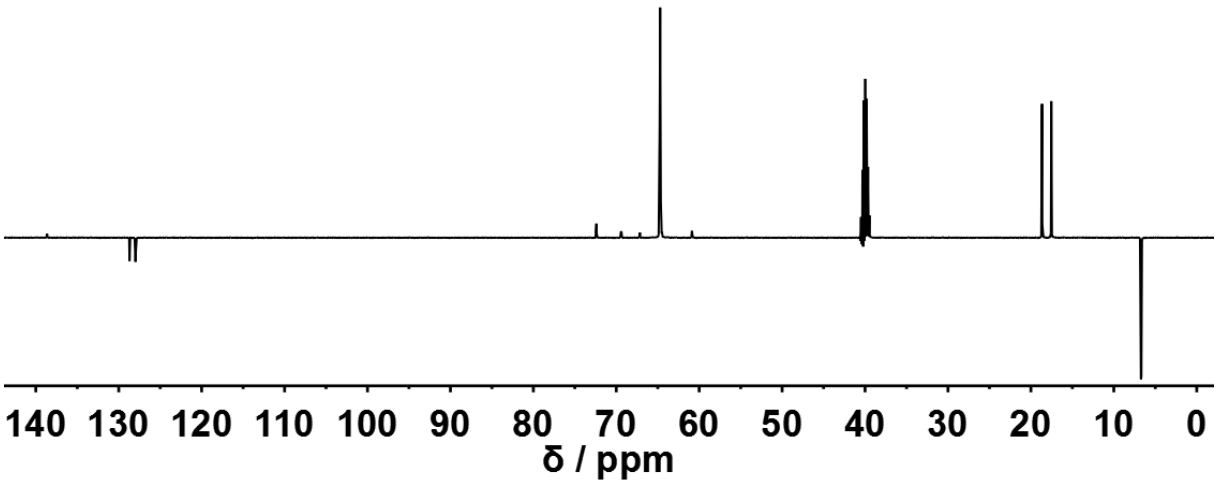

Figure S8.6: ^{13}C (500 MHz) NMR spectrum of maleimide terminated poly(ethylene ethyl phosphonate) $P(1)_{45}$ in DMSO-d_6 at 298K.

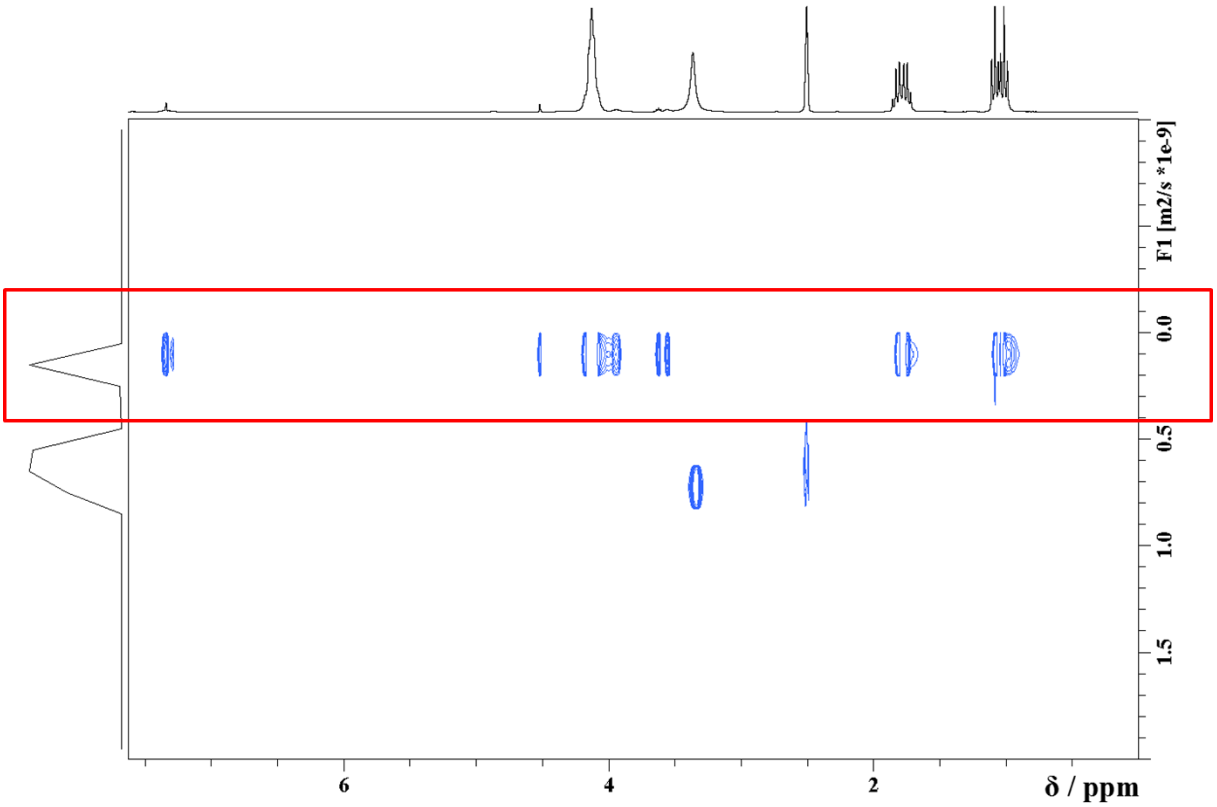

Figure S8.7: ^{1}H DOSY (500 MHz) NMR spectrum of maleimide terminated poly(ethylene ethyl phosphonate) P(1)$_{45}$ in DMSO-d_6 at 298K.

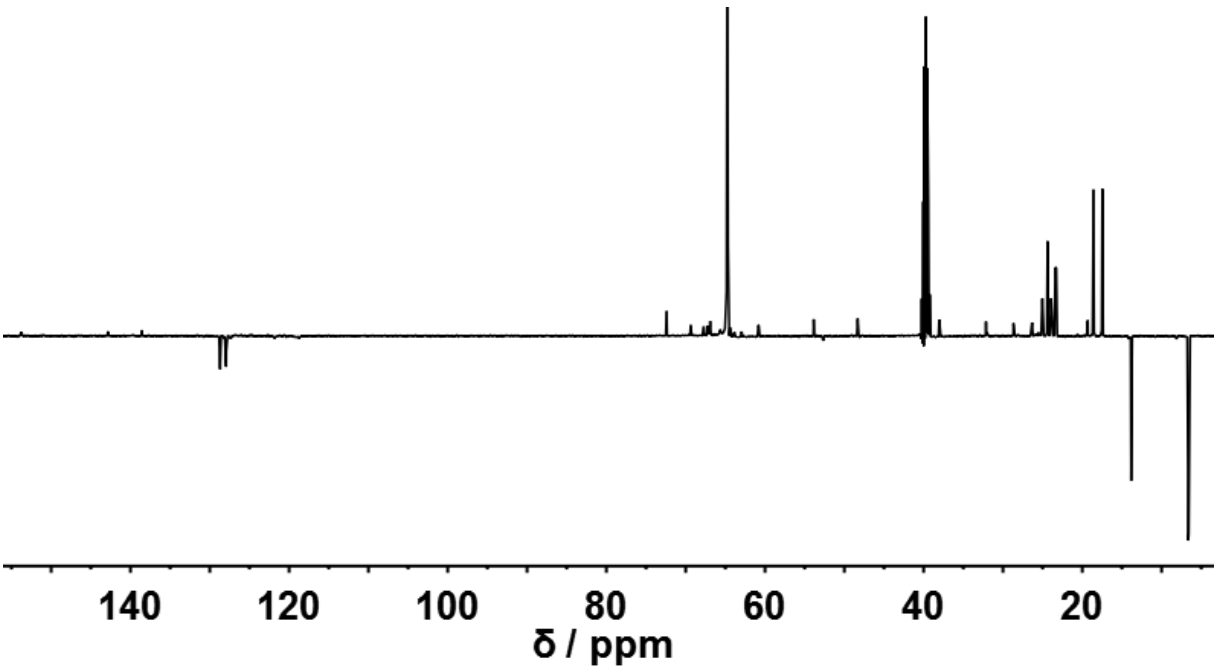

Figure S8.8: ^{13}C (125 MHz) NMR spectrum of maleimide terminated poly(ethylene ethyl-*co*-*n*-butyl phosphonate) P(1$_{31}$-co-2$_{15}$) in DMSO-d_6 at 298K.

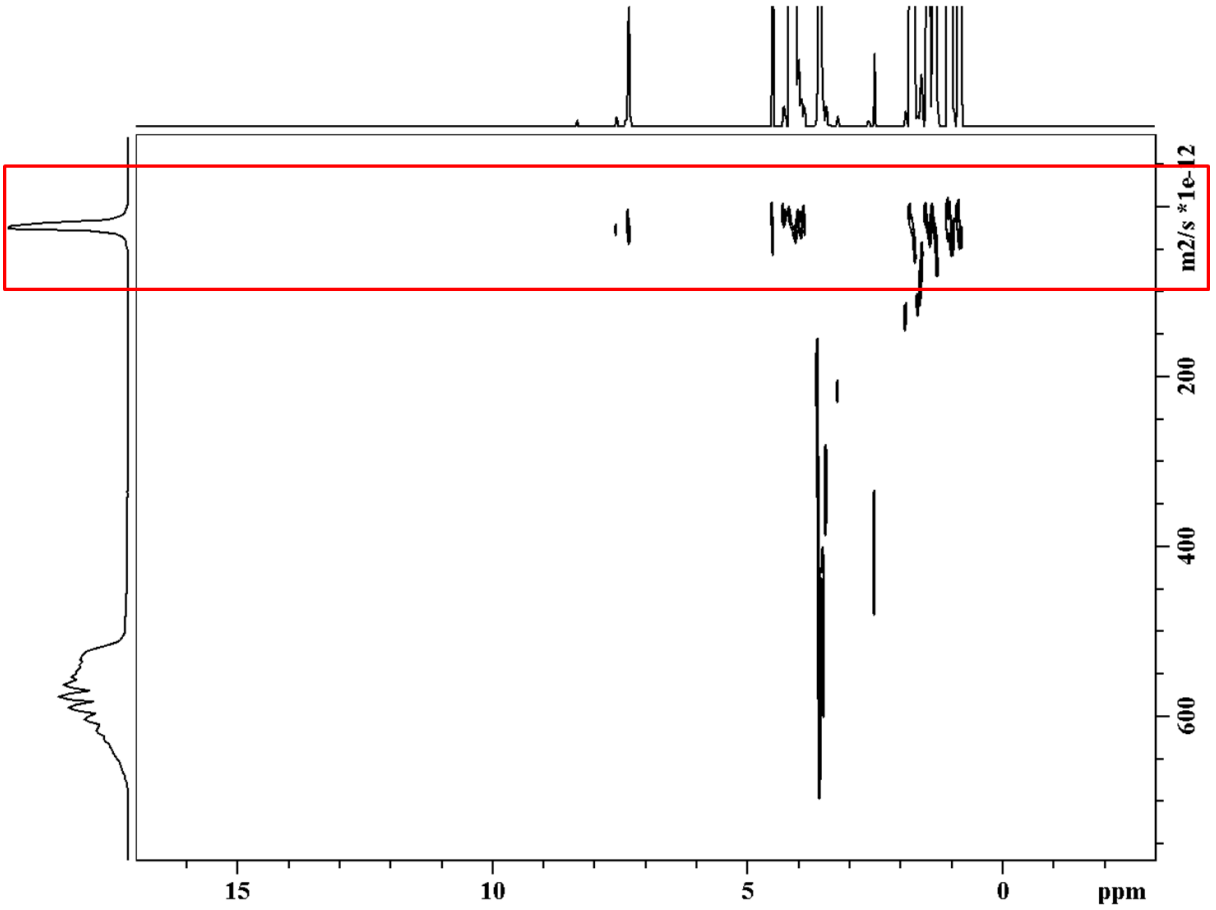

Figure S8.9: ^{1}H DOSY (500 MHz) NMR spectrum of maleimide terminated poly(ethylene ethyl-*co*-*n*-butyl phosphonate) P(1_{31}-co-2_{15}) in DMSO-d_6 at 298K.

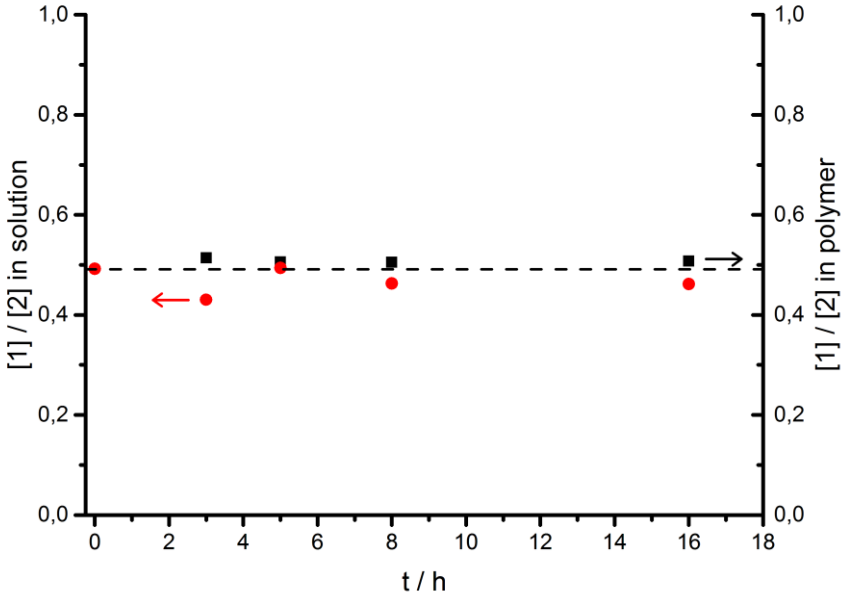

Figure S8.10: ^{31}P NMR (201 MHz) assisted copolymerization kinetics.

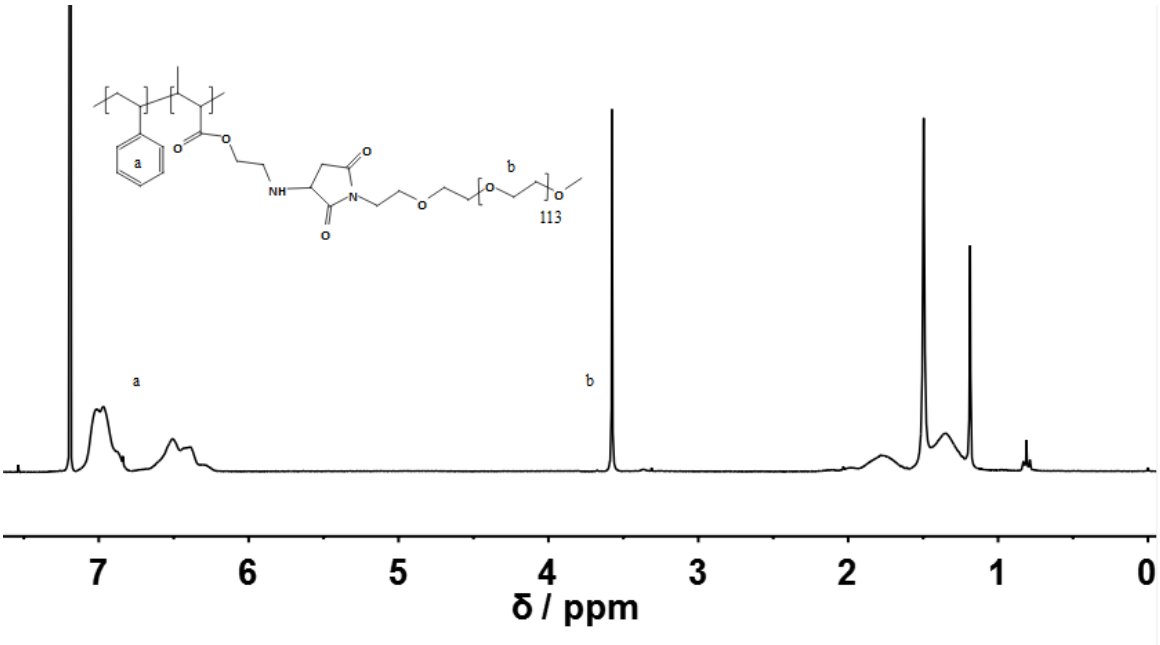

Figure S8.11: ^{1}H (500 MHz) NMR spectrum of polystyrene nanoparticles modified with PEG (PS-PEG) dissolved in $CDCl_3$ at 298K.

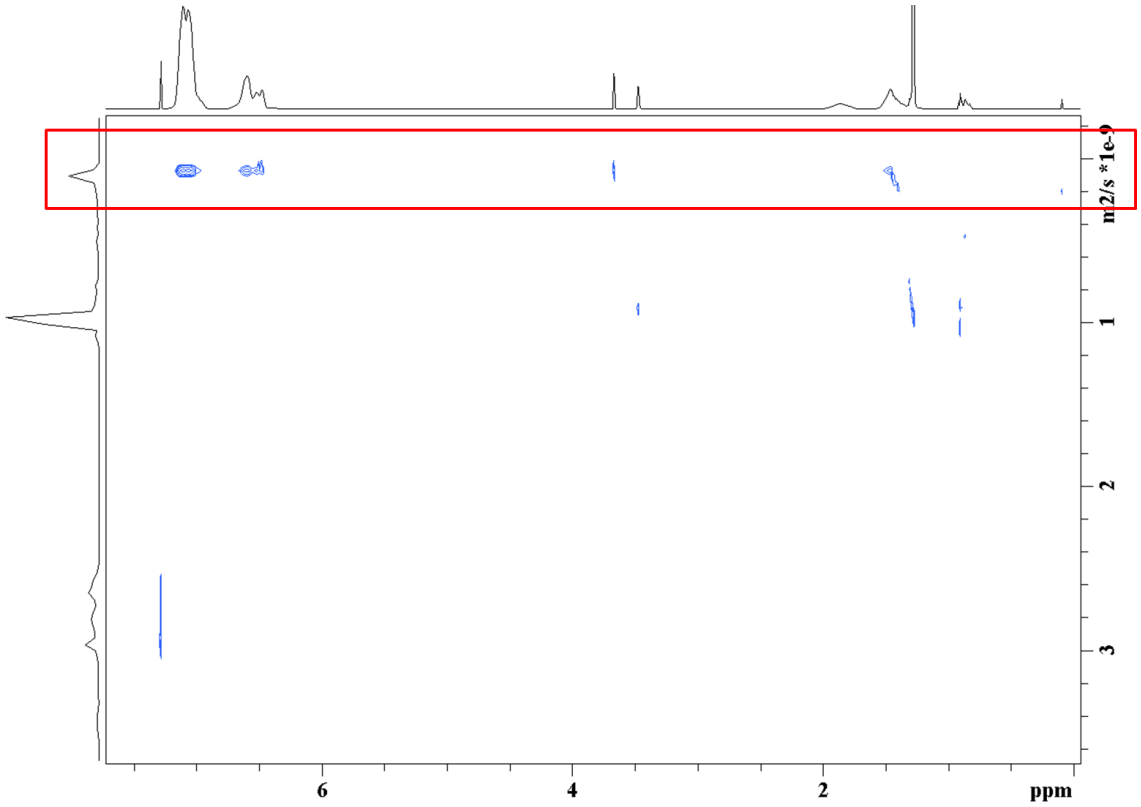

Figure S8.12: ^{1}H DOSY (500 MHz) NMR spectrum of polystyrene nanoparticles modified with PEG (PS-PEG) dissolved in $CDCl_3$ at 298K.

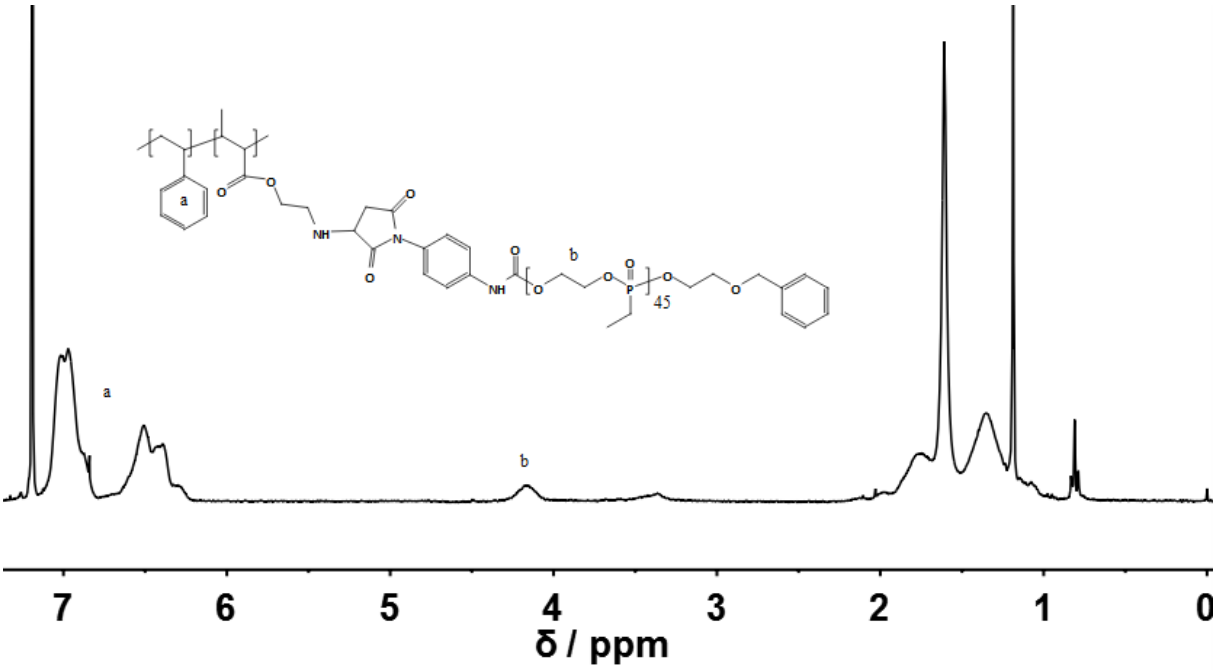

Figure S8.13: ^{1}H (500 MHz) NMR spectrum of polystyrene nanoparticles modified with hydrophilic poly(phosphonate) $P(1)_{45}$ ($PS\text{-}P(1)_{45}$) dissolved in $CDCl_3$ at 298K.

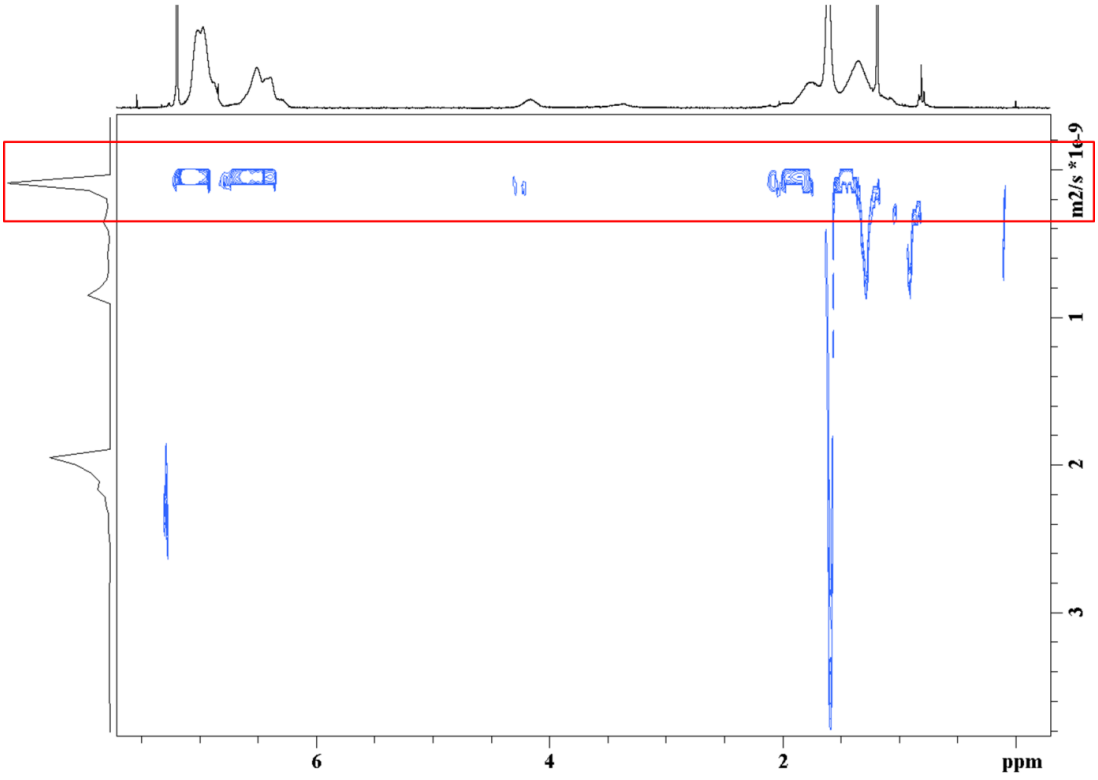

Figure S8.14: ^{1}H DOSY (500 MHz) NMR spectrum of polystyrene nanoparticles modified with hydrophilic poly(phosphonate) $P(1)_{45}$ ($PS\text{-}P(1)_{45}$) dissolved in $CDCl_3$ at 298K.

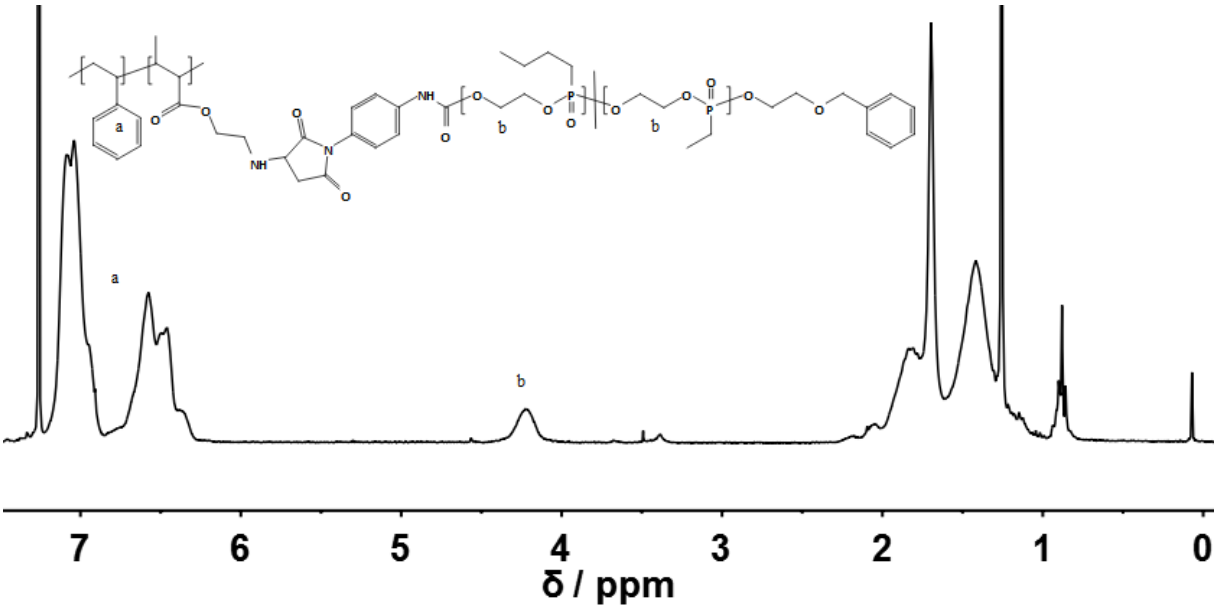

Figure S8.15: ^{1}H (500 MHz) NMR spectrum of polystyrene nanoparticles modified with hydrophobic poly(phosphonate) copolymer P(1_{31}-*co*-2_{15}) (PS-P(1_{31}-*co*-2_{15})) dissolved in $CDCl_3$ at 298K.

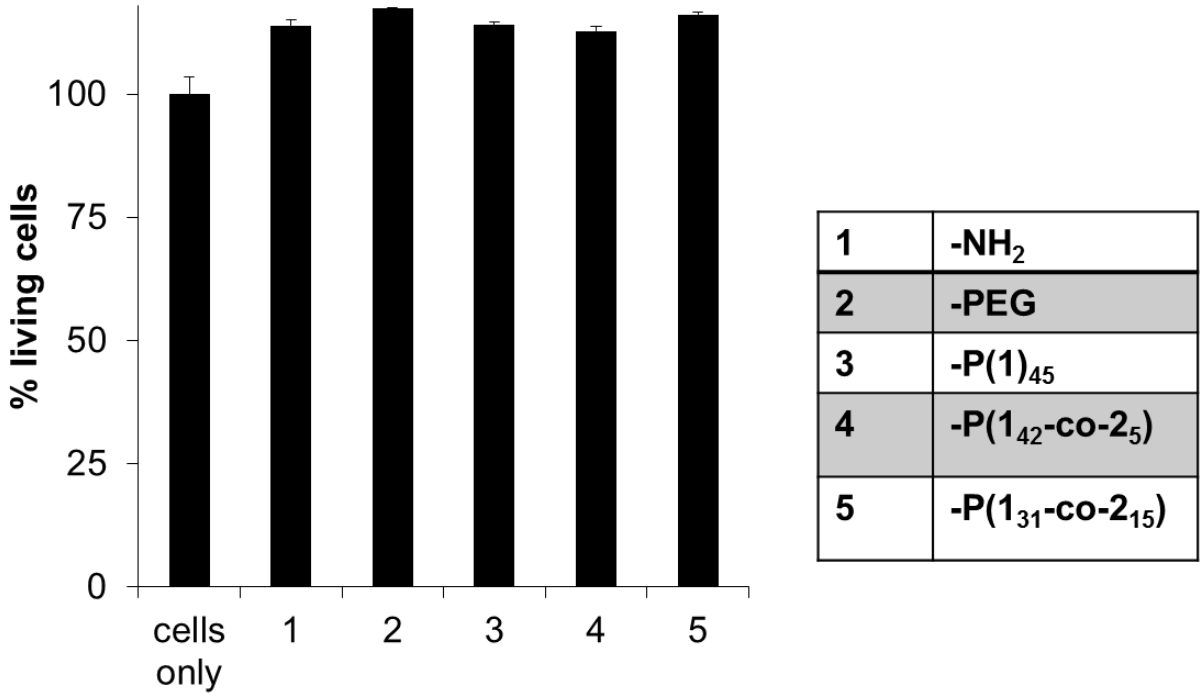

Figure S8.16: Cytotoxicity assay of nanoparticles (75 µg mL^{-1}) incubated with RAW264.7 cells for 2h. Cytotoxicity was determined by PI staining (2 µg ml^{-1}) whereas incubation without nanoparticles was defined as 100% viable. Values are expressed as mean ± SD of triplicates.

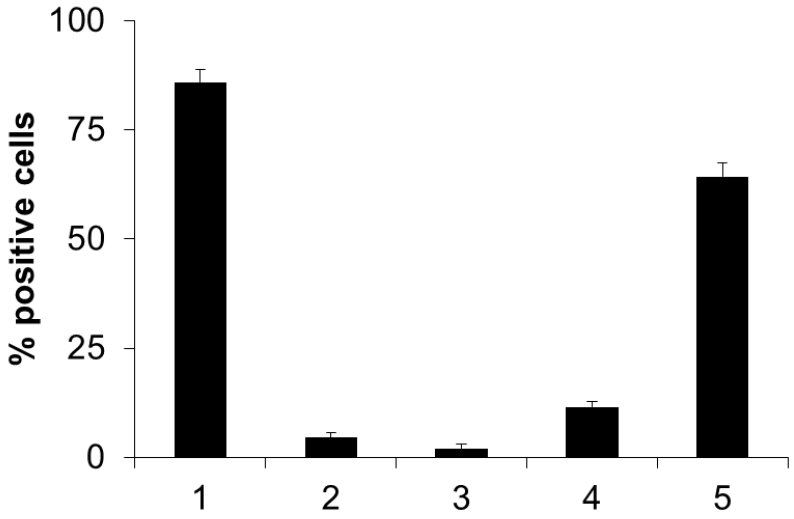

1	-NH_2
2	-PEG
3	-$P(1)_{45}$
4	-$P(1_{42}$-co-$2_5)$
5	-$P(1_{31}$-co-$2_{15})$

Figure S8.17: Flow cytometry analysis of HeLa cells incubated with plasma coated PS-NC (75 µg mL^{-1}) for 3h in serum-free medium. Values (% of fluorescent positive cells) are expressed as mean ± SD of duplicates.

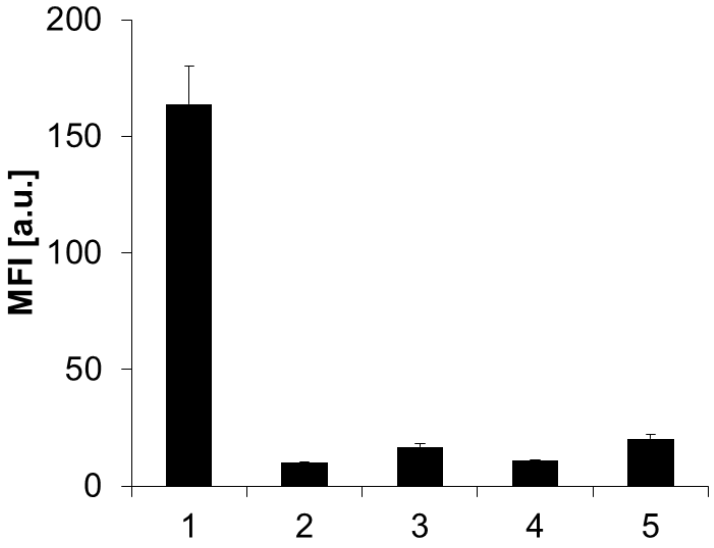

1	-NH_2
2	-PEG
3	-$P(1)_{45}$
4	-$P(1_{42}$-co-$2_5)$
5	-$P(1_{31}$-co-$2_{15})$

Figure S8.18: Flow cytometry analysis of RAW264.7 cells incubated with plasma coated PS-NC (75 µg mL^{-1}) for 2h in serum-free medium at 4 °C. Median Fluorescence intensity values (MFI) are expressed as mean ± SD of triplicates. There is a strong unspecific binding to PS-NH_2 towards the cell membrane.

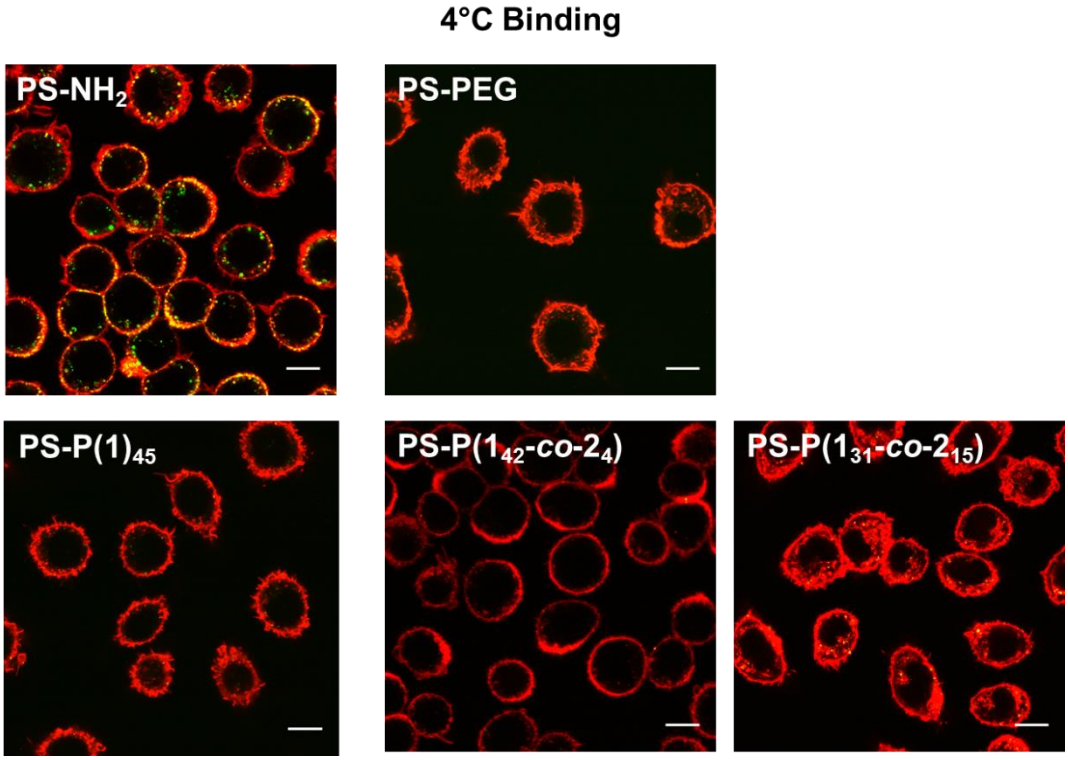

Figure S8.19:1 cLSM images of RAW264.7 cells incubated with plasma coated PS-NC (75µg mL^{-1}) for 2h in serum-free medium. The cell membrane is stained with CellMask Orange and pseudocolored in red, and the PS-NCs are pseudocolored in green. Scale bar: 10 µm.

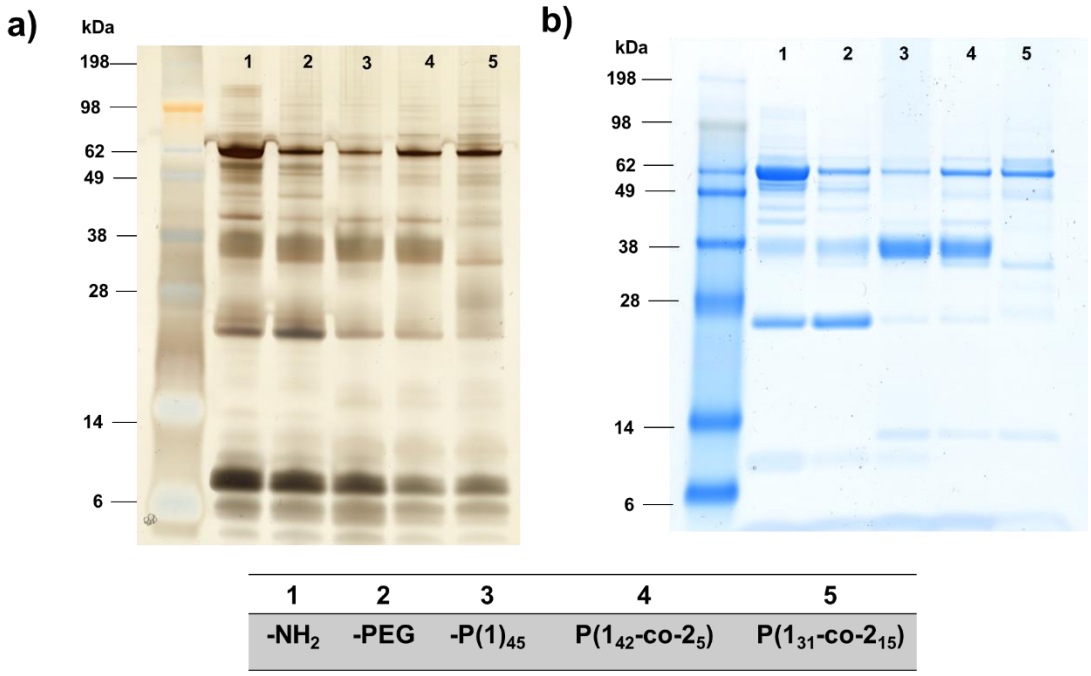

Figure S8.20: SDS PAGE after protein corona analysis of PS-NC incubated with human plasma. Proteins were visualized by Silver Staining (a) or Coomassie blue (b).

Appendix

List of Publications

Organic Catalysis for Polymerization: “Other ROP”
Thomas Wolf and Frederik R. Wurm, book chapter, *under preparation.*

A Library of Well-Defined and Water-Soluble Poly(phosphonate)s with Adjustable Hydrolysis.
Thomas Wolf, Tobias Steinbach, and Frederik R. Wurm*, Macromolecules*, **2015,** 48, 3853-3863.

Adjustable Glass Transition Temperatures of Poly(ethylene alkyl phosphonate) Copolymers.
Thomas Wolf, Johannes Naß, and Frederik R. Wurm*, Polymer Chemistry*, **2016,** 7, 2934-2937.

Temperature-Responsive Poly(phosphonate) Copolymers: from Single Chains to Macroscopic Coacervates
Thomas Wolf, Johannes Hunold, Johanna Simon, Christine Rosenauer, Dariush Hinderberger, and Frederik R. Wurm, *submitted for publication.*

Poly(alkyl ethylene phosphonate)s – A New Class of Non-Amide Kinetic Hydrate Inhibitor Polymers
Hong Lin, **Thomas Wolf**, Frederik R. Wurm, and Malcolm A. Kelland, *Energy&Fuels*, **2017,** 31, 3873-3848.

Thermoresponsive Coacervate Formation of Random Poly(phosphonate) Terpolymers.
Thomas Wolf, Timo Rheinberger, and Frederik R. Wurm*, European Polymer Journal*, **2017,** 10.1016/j.eurpolymj.2017.05.048.

Degradable Polymersomes with Upper Critical Solution Temperature - Induced Disassembly in Water.
Thomas Wolf, Timo Rheinberger, Johanna Simon, and Frederik R. Wurm, *The Journal of the American Chemical Society*, **2017,** 139, 11064-11072.

Hydrophilicity Regulates Specific Protein Adsorption on Poly(phosphoester) Coated Nanocarriers Controlling Uptake in Immune Cells.
Johanna Simon, **Thomas Wolf**, Katja Klein, Katharina Landfester, Frederik R. Wurm, and Volker Mailänder, *under preparation*.

Appendix

Conference Contributions

Conference on Ionic Polymerization, 2015, Bordeaux, France,
Thomas Wolf, Tobias Steinbach, and Frederik R. Wurm, poster presentation,
Poly(ethylene alkyl phosphonate)s: Tailored degradability for water-soluble poly(phosphoester)s.

Makromolekulares Kolloquium Freiburg, 2016, Freiburg, Germany,
Mark Steinmann, Kristin N. Bauer, Alper Cankaya, Greta Becker, Hisaschi Tee, **Thomas Wolf**, Frederik R. Wurm, poster presentation,
The Versatility of Main-Chain Phosphorus-Containing Polymers: Adhesion, Stealth, Degradation.

Makromolekulares Kolloquium Freiburg, 2017, Freiburg, Germany,
Thomas Wolf, Kristin Bauer, Greta Becker, Jens C. Markwart, and Frederik R. Wurm, poster presentation,
Binding Matters Binding-Patterns Control the Properties of Poly(phosphoester / -amide)s.

Conference on Advanced Polymers via Macromolecular Engineering, 2017, Ghent, Belgium,
Thomas Wolf, Timo Rheinberger and Frederik R. Wurm, poster presentation,
Poly(ethylene alkyl phosphonate) copolymers with LCST and UCST.

Conference on Ionic Polymerization, 2017, Durham, United Kingdom,
Thomas Wolf, and Frederik R. Wurm, oral presentation,
Poly(alkylene alkyl phosphonate) Copolymers: LCST and UCST Thermal Response.